UNIVERSITÀ DEGLI STUDI DI PALERMO

Dottorato di Ricerca in Scienze Molecolari e Biomolecolari (Internazionale)-XXXII CICLO
Dipartimento Scienze e Tecnologie Biologiche Chimiche e Farmaceutiche (STEBICEF)
CHIM/08

SYNTHESIS AND BIOLOGICAL EVALUATION OF NEW IMIDAZO[2,1-*b*][1,3,4]THIADIAZOLE DERIVATIVES AS ANTICANCER AND ANTIBIOFILM AGENTS, AND PRECLINICAL INVESTIGATION OF ANTI-LDH-A COMPOUNDS AGAINST MALIGNANT MESOTHELIOMA

IL DOTTORE
Dott.ssa GIOVANNA LI PETRI

IL COORDINATORE
Chiar.ma Prof.ssa PATRIZIA DIANA

I TUTORS
Chiar.ma Prof.ssa PATRIZIA DIANA
Chiar.mo Prof. GODEFRIDUS J PETERS

I CO TUTORS
Chiar.mo Prof. GIROLAMO CIRRINCIONE
Chiar.ma Prof.ssa ELISA GIOVANNETTI

CICLO XXXII
ANNO CONSEGUIMENTO TITOLO 2020

Contents

Chapter 1: Introduction

1. A perspective on drug design approaches

2. An overview on biofilm formation and its role in the persistence of bacterial infections

3. An overview of pancreatic cancer with special focus on Pancreatic Ductal Adenocarcinoma (PDAC)

    3.1 Brief description of pancreatic anatomy

    3.2 General introduction of pancreatic cancer with insights on PDAC

    3.3 Diagnosis: clinical presentation, diagnostic tools and tests, managements

    3.4 Treatments: pros and cons

    3.5 Tumor biology

        3.5.1 Pathogenesis of PDAC

        3.5.2 Genetic abnormalities in primary and metastatic PDAC

        3.5.3 PDAC pharmacogenetics

        3.5.4 Molecular mechanisms underlying invasion and metastasis: Epithelial to mesenchymal transition events

        3.5.5 Role of focal adhesion kinase (FAK) in tumor growth and spread

4. An overview of malignant mesotheliomas

    4.1 Brief description of mesothelium: origin, structure and function

    4.2 Pathological disease of mesothelium: malignant mesothelioma

    4.3 Diagnosis: clinical presentation, diagnostic tests, managements

    4.3 Treatment

    4.4 Correlation between hypoxia and malignant mesothelioma

    4.5 Biomarkers for the diagnostic evaluation

5. Outline of the PhD Thesis

Part I: ***In vitro pharmacological studies as important tools in large-scale drug discovery, and approaches to the combination therapy with special focus on PDAC cancer (chapters 2-4)***

Chapter 2: *A Brief Guide to Performing Pharmacological Studies In Vitro: Reflections from the EORTC-PAMM Course "Preclinical and Early-phase Clinical Pharmacology"*

Capula M, Corno C, El Hassouni B, **Li Petri G**, Aranđelović S; EORTC PAMM Group

Anticancer Research 2019 July;39(7):3413-3418, doi: 10.21873/anticanres.13485

Chapter 3: *To Combine or Not Combine: Drug Interactions and Tools for Their Analysis. Reflections from the EORTC-PAMM Course on Preclinical and Early-phase Clinical Pharmacology*

El Hassouni B, Mantini G, **Li Petri G**, Capula M, Boyd L, Weinstein HNW, Vallés-Marti A, Kouwenhoven MCM, Giovannetti E, Westerman BA, Peters GJ; EORTC PAMM Group

Anticancer Research. 2019 July;39(7):3303-3309, doi: 10.21873/anticanres.13472

Chapter 4: *Pharmacogenetics of treatments for pancreatic cancer*

El Hassouni B, **Li Petri G**, Liu DSK, Cascioferro S, Parrino B, Hassan W, Diana P, Ali A, Frampton AE, Giovannetti E

Expert Opinion on Drug Metabolism & Toxicology 2019 June;15(6):437-447, doi: 10.1080/17425255.2019.1620731

Part II: ***Evaluation of biological activity of the new class of imidazo[2,1-b][1,3,4]thiadiazole compounds as antitumor and their repurposing as antibiofilm agents (chapters 5-8)***

Chapter 5: *Biological Evaluation of the Antiproliferative and Anti-migratory Activity of a Series of 3-(6-Phenylimidazo[2,1-b][1,3,4]thiadiazol-2-yl)-1H-indole Derivatives Against Pancreatic Cancer Cells*

Li Petri G, Cascioferro S, El Hassouni B, Carbone D, Parrino B, Cirrincione G, Peters GJ, Diana P, Giovannetti E

Anticancer Research. 2019 July;39(7):3615-3620, doi: 10.21873/anticanres.13509

Chapter 6: *Development of a new series of 3-(6-phenylimidazo [2,1-b][1,3,4]thiadiazol-2-yl)-1H-indole derivatives for the treatment of pancreatic cancer*

Cascioferro S[a], **Li Petri G[a]**, Parrino B, El Hassouni B[a], Carbone D, Arizza V, Perricone U, Padova A, Funel N, Peters GJ, Cirrincione G, Giovannetti E*****, Diana P*****

[a]equal contributors

[*]Corresponding authors

Molecules 2020, 25(2), 329; https://doi.org/10.3390/molecules25020329

Chapter 7: *Imidazo[2,1-b][1,3,4]thiadiazoles with antiproliferative activity against primary and gemcitabine-resistant pancreatic cancer cells*

Cascioferro S[a], **Li Petri G[a]**, Parrino B, Carbone D, Funel N, Bergonzini C, Mantini G, Dekker H, Daan Geerke, Peters GJ, Cirrincione G, Giovannetti E*****, Diana P*****

[a]equal contributors

*Corresponding authors
Accepted in European Journal of Medicinal Chemistry
Available online 25 January 2020, 112088. doi: https://doi.org/10.1016/j.ejmech.2020.112088

Chapter 8: *2,6-Disubstituted imidazo[2,1-b][1,3,4]thiadiazole derivatives as potent staphylococcal biofilm inhibitors*
Cascioferro S, Parrino B, **Li Petri G**, Cusimano MG, Schillaci D, Di Sarno V, Musella S, Giovannetti E, Cirrincione G, Diana P
European Journal Medicinal Chemistry. 2019 Apr 1;167:200-210, doi: 10.1016/j.ejmech.2019.02.007. Epub 2019 Feb 10

Part III: ***In vitro and in vivo studies on Malignant Mesothelioma (chapters 9-11)***

Chapter 9: *Proton-coupled folate transporter as a biomarker of outcome to treatment for pleural mesothelioma*
Li Petri G, Cascioferro S, Parrino B, Peters GJ, Diana P, Giovannetti E
Pharmacogenomics. 2018 July 1;19(10): 811-814, doi: 10.2217/pgs-2018-0071. Epub 2018 June 19

Chapter 10: *Impact of hypoxia on chemoresistance of mesothelioma mediated by proton-coupled folate transporter, and preclinical activity of new anti-LDH-A compounds*
Li Petri G*, El Hassouni B*, Sciarrillo R*, Funel N, Mantini G, Zeeuw van der Laan EA, Cascioferro S, Avan A, Zaffaroni N, LagerweiJ T, Parrino B, Deraco M, Granchi C, Bulinska A, Smolenski RT, Jansen G, Assaraf Y, Diana P, Cloos J, Peters GJ, Minutolo F, Giovannetti E
*equal contributors
Provisionally accepted in British Journal of Cancer

Chapter 11: *2-(1H-indol-3-yl)-6-(thiophen-3-yl)imidazo[2,1-b][1,3,4]thiadiazole for the treatment of Diffuse Malignant Peritoneal Mesothelioma*
Li Petri G, El Hassouni B, Zoppi S, Cascioferro S, Zaffaroni N, Peters GJ, Cirrincione G, Diana P, Giovannetti E
Unpublished results

Chapter 12: Discussion and conclusions

Chapter 13: English Summary

Chapter 14: CV and list of publications

Chapter 1

Introduction and outline of the Thesis

1. A perspective on drug design approaches

Despite the synergistic work between chemists, computational chemists, biologists, bioinformatics and surgeons, the treatment of tumors is far from providing satisfactory clinical results. Medicinal chemistry is making enormous efforts to search for powerful anticancer agents, thanks also to the *in silico* studies which provide a lot of information about selectivity and affinity between ligands and specific targets, thus accelerating the drug discovery processes.[1] Over the years, the design of biologically active agents has evolved from the traditional strategy of "one-molecule one-target one-disease", proposed by Paul Ehrlich over 150 years ago, to "cocktail therapy", and the recent "multi-target direct ligand" (MTDL) approach. These three approaches can be summarized in the well-known 'key' and 'lock' models (Figure 1) which describe the interaction of the ligand (the key) with the substrate (the lock).[2] In table 1 the advantages and disadvantages of each approach are summarized. The aim of 'one-compound one-target one-disease' strategy is to design a single small chemical entity that specifically recognizes one target, considered fully responsible of the disease. As a result, the treatment should be better tolerated due to the absence of adverse side-effects. Unfortunately, this strategy often fails because a poor correlation between *in vitro* effects and *in vivo* efficacies is found. Indeed, *-omics* studies suggest the huge complexity of tumor environment correlated with its pathogenesis. This means that the multifactorial nature of tumors usually requires the modulation of different biological targets that can be achieved through the poly-pharmacological practices, with the combination of drugs (also known as cocktail therapy) or a single MTDL.[2–4] The first real effect of the combination drugs was published in 1965 when Emil Frei, James F. Holland and Emil J. Freireich reported the efficacy of combination treatment of paediatric patients suffering from acute lymphocytic leukemia, with the POMP regimen, i.e. a combination of methotrexate, 6-mercaptopurine, vincristine and prednisone.[5] The combination of two or more agents has several advantages. First of all, the outcome of the treatments is improved by obtaining additive or synergistic effects, thus reducing the doses administered and consequently the toxicity. In addition, combination therapy might prevent the emergence of chemoresistance, because cancer cells are usually unable to adapt to the toxic effects of different therapeutic agents simultaneously administered.[6] Unluckily, several drawbacks limit its clinical use:

- **i)** the unwanted side effects that can be synergistically or additively produced, and thereby the difficulty to identify the responsible agent;
- **ii)** the unpredictable pharmacodynamic and pharmacokinetic profiles of the components, which favour the well-known drug-drug interaction (DDI) (for instance, one drug may

inhibits the metabolic activity of the secondary or tertiary agent, thus increasing the toxicity or reducing the efficacy of therapy);[7]

iii) the polypharmacy reduces patience compliance.[6]

The concept of MTDL is more recent. It was introduced at the beginning of 2000 by Morphy and Roncovik and today is the hottest topics in drug discovery. MTDLs are rationally designed through the pharmacophore-based approach, which consists of combining two or more scaffolds with specific biological activities already known, in a single final hybrid structure. In order to prevent that the final molecule is characterized by a high molecular weight (MW) or other pitfalls, for instance the steric effects that influence the link with the targets, the way by which the pharmacophores are combined, must be well studied. Therefore, MTDLs are classified into linked, fused or merged types. Linked MTDLs are characterized by a linker that separates pharmacophores and sometimes, itself can act as pharmacophore. The linker can be cleavable or non-cleavable, in fact it should be stable *in vivo* or suitably designed to be degraded after the administration, for instance by plasma esterase or preferably in the tumor. Finally, based on the degree of overlap of the pharmacophores, the MTDLs can be classified as fused or merged. In the fused MTDLs the pharmacophores partly share the structure, while the merged MTDLs have the highest degree of overlap, allowing to obtain molecules with low MW and better physicochemical profiles.[8] MTDLs recognize unrelated targets thanks to the presence of different scaffolds in the same molecule, or isoforms of the same protein or different proteins belong to the same signalling pathway. In addition, MTDLs have clear advantages in terms of pharmacokinetic and pharmacodynamic, better patience compliance, reduced risk of drug interactions, and display additive or synergistic effects.[2] Ramsey et al., performed an analysis on the new molecules entities (NMEs) approved by US Food and Drug Administration (FDA) from 2015 to September 2017 which includes all therapeutic areas. Over this triennium, 101 new NMEs were approved and classified into categories, as follows: small molecules subdivided into single-target and multi-target drugs, biologics, therapeutic combinations and diagnostics. The number of multi-target drugs approved is increased (21%, from 2015 to September 2017) compared to previous analysis (16%, from January 2000 to December 2015) conducted by Lin et al.,[9] over the period of sixteen years. Adding together the 21% of MTDLs and the newly approved therapeutic combination (10%), this analysis supported the advancement of poly-pharmacological strategies.[4]

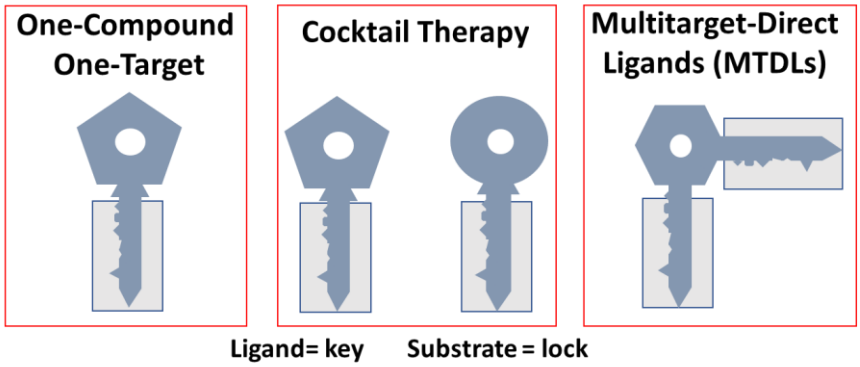

Figure 1. Representative image of the key and lock models.

Table 1. Dis- and advantages of the use of different approaches to the treatments of the disease.

	Advantages	***Disadvantages***
Single-molecule single-target	• Ideally absence of off-target side effects • High target specificity	• Often poor correlation between *in vitro* effects and *in vivo* efficacy • Multi-drug resistance (mediated by MDR1 or P-gp)
Combination therapies	• Minimize drug resistance • Synergistic or additive interaction • Target to the heterogeneous nature of tumors • Multiple drugs can more easily bypass MDR (e.g. by PgP or BCRP)	• Combination can produce unwanted side-effects • Drug-drug interactions (DDI) • Reduced patient-compliance • Lower drug dose may lead to decrease efficacy
Multitarget-Direct Ligands (MTDLs)	• Ligand acts on several isoforms of the same protein • Different members of a given biochemical pathway might share ligand specificity • A ligand might display affinity to two or more unrelated targets • More predictive pharmacokinetics, better patient compliance, and reduced risk of drug interactions • Therapeutic efficacy may increase through inhibition of more targets, which might enhance each other	• The ratio of each pharmacophore in the molecular structure usually cannot be changed • Difficult to achieve sequenced administration at the targets • Achieving balanced and multi-selective potency toward multiple targets is challenging • Multi-drug resistance (mediated by MDR1 or P-gp)

Indole scaffold, one of the most abundant bi-heterocycle in nature, is widely used in medicinal chemistry for the targeted-based design and development of new anticancer agents. It is an important moiety in many natural products such as alkaloids, and others potential drugs isolated from plant, animal and microbial hormones. Since the nineteenth century when Fischer discovered its synthesis,[10] the indole scaffold became the main part in many marketed pharmaceutical bioactive drugs. Natural compounds bearing indole nucleus displayed versatile pharmacological activity including antibacterial[11] and antifungal,[11–13] anti-inflammatory,[14] antihistamine,[15] antioxidant,[16] antidiabetic,[17] antiviral,[18] anticholinesterase[19] and anticancer.[20–25] For instance, Vinblastine and its oxidised form Vincristine, two potent antimitotic agents isolated from *Catharanthus roseus*, have been used for the treatment of various cancer diseases among which Hodgkin's disease, non-Hodgkin's lymphoma, Kaposi's sarcoma, and breast or testicular cancers.[26] Many other natural alkaloids indole-analogues have shown anticancer activity; these include mitomycin C, isolated from *Streptomyces caespitosus*, that is widely used for the treatment of metastatic bladder, breast, cervix, colorectal and anal, gastric, head and neck, non-small-cell lung and pancreatic cancers.[27] Bis-indole alkaloids such as dragmacidin, hyrtinadine A, nortopsentin D, topsentin and hyrtiosins B that exhibited cytotoxic activity against different cancer cell lines.[28] Interestingly, these products have always been a source of inspiration for synthetic indole derivatives with anticancer activity able to bind multiple receptors with high affinity.[29] More in depth investigation on mechanism of action underling antitumor activity revealed that most indole-based molecules act as tubulin polymerization inhibitors with potential of interacting with colchicine binding site, and on other targets such as histone deacetylases (HDACs), sirtuins, PIM kinases, DNA topoisomerases, and δ-receptors.[30,31]

The imidazo[2,1-*b*][1,3,4]thiadiazole nucleus has been considered as an important scaffold for the design of molecules with various biological activities including anticancer,[32] analgesic,[33] anti-leishmanial,[34] antioxidant,[35] antitubercular,[36] anticonvulsant,[37] and antibacterial.[38-39]

Based on these knowledge, one of the aims of this Thesis was to synthesize new molecules through a structure-based molecular hybridization approach. They were designed with the imidazo[2,1-*b*][1,3,4]thiadiazole scaffold bearing the indole-based moiety. Finally, antitumor and antibiofilm of these compounds were evaluated.

In the chapters 5,6,7,8 and 11 we report the synthesis and the biological activities, as antibiofilm and antitumor, of the new imidazo[2,1-*b*][1,3,4]thiadiazole derivatives.

2. An overview of biofilm formation and its role in the persistence of bacterial infections

By definition, biofilm is a *consortium* of one or more types of microorganisms immersed in a matrix of acellular components.[40] The morphology of each biofilm depends on the microorganisms that compose it including bacteria, fungi and protists, capable of growing on many different surfaces. The acellular component is constitute by one or more extracellular polysaccharides, proteins, lipids and extracellular DNA (e-DNA) as well as molecules originating from the host, such as mucus and DNA, together called extracellular polymeric substances (EPS). These components are secreted into the environment by the cells themselves, and nourishing, air and water are guaranteed through microchannel. There are several reasons behind the transition from planktonic status to the biofilm, among which:

i) biofilm protects microorganisms from environmental condition, for instance the blood stream;[41]

ii) EPS guarantees resistance to the bactericide, limiting drug delivery and encouraging the exchange of plasmid DNA between cells by horizontal gene transfer, for instance genes involved in drug resistance.[41]

Biofilm formation occurs gradually: the first step is the attachment of some cells onto a surface or tissue. Specifically, this step can be divided into two sub-steps processes which consist of an initial reversible attack followed by the irreversible attack of the cells on the surface. After that, other cells of the same species or not are recruited in the biofilm from the bulk fluid, thus creating multi-layers colonies into which cells are able to distribute themselves based on oxygen demand for their metabolism and acquire specialized functions. This step is called maturation. Therefore, when the biofilm has matured, the last step consisting of dispersion of the biofilm, begins which is critical for the biofilm life cycle.[41] Various human diseases are linked to biofilms including the bacterial one. For example, gastrointestinal, oral and respiratory, urinary tracts and chronic wounds, are typically sites to growth.[42] In addition, devises such as catheters, heart valves, and prostheses are also common sites for biofilm development, thus inducing the nosocomial chronic infections which are difficult to treat with conventional antibiotics.[43] Bacteria in a biofilm are more resistant to antibiotics than planktonic. This was first observed in 1985 when *P. aeruginosa* cells in a biofilm or in planktonic form had a different response to the treatment with tobramycin, 50 μg/mL *versus* 1 mg/mL, respectively to reduce the survival.[44] Drug resistance of biofilm is due to:

- limited drug delivery because EPS matrix provides physical protection and reduces the penetration;

- exchange of mutated genetic material carrying information of resistance;
- reduced growth rate of persister cells, a subpopulation of cells defined as dormant, which form spontaneously within a biofilm and acquire stubborn resistance to the antibiotics;
- cells that live in the part of biofilm with low oxygen rate and metabolism with consequently low cell division. Therefore, all drug which act in the splitting step of cells do not work;
- finally, overexpression of efflux pump that throws the drugs out of cells.[41]

According to current estimates by the National Institute of Health, from 65 to 80% of all bacterial infections are biofilm-mediated,[45] therefore, it is a priority to search for new agents able to overcome drug resistance, hitting one or more mechanisms of formation or of maintenance of biofilms, including Sortase A (SrtA), the transpeptidase involved in the process of bacterial adhesion, or autoinducing peptides (AIPs), autoinducer-2 (AI-2), bacterial second messengers, such as c-di-GMP and c-di-AMP.[46]

3. An overview of pancreatic cancer with special focus on Pancreatic Ductal Adenocarcinoma (PDAC)

3.1 Brief description of pancreatic anatomy

The pancreas is an elongated (12-15 cm; 6 inches) and tapered glandular organ placed in the upper abdomen, behind the stomach. The wider portion, close to the duodenum, is called the head of the pancreas, while the middle and the rest of the organ are called body and tail, respectively. Actually, it is a heterocrine gland, namely two glands intimately mixed together into one organ. For this reason, it has a dual function: digestive exocrine and hormone-producing endocrine.

The first one consists in the secretion of pancreatic juice produced by the acinar tissue, consisting of cells called ‘acini’. The juice is composed of inactive digestive or lytic enzymes, to break down the proteins, fats, carbohydrates, and nucleic acids of food in small components that must be absorbed by the intestine; these enzymes are released in a system of many small ducts and thus, conveyed into the larger central pancreatic duct, from which they are drained into the bile duct to reach the duodenum where finally, they are activated. In addition, the pancreatic juice contains bicarbonate, secreted by ductal cells, to neutralize gastric acid in the duodenum and ensuring a neutral/alkaline environment necessary for the activity of enzymes.

The second function of the gland is to release hormones into the bloodstream. They are produced by the endocrine pancreas, composed of small islands of cells, called the islets of Langerhans. In particular, five different cells make up the islets: α- and β-cells that produce

insulin and glucagon, respectively, which regulate the level of glucose in the blood; δ-cells that release somatostatin, which controls the secretory activities of the first two cells before mentioned; ε- cells that produce ghrelin, involved in regulating the body's energy balance; finally, PP- cells that regulate the exocrine and endocrine secretion of the pancreas through the production of pancreatic polypeptide.[47,48] (Figure 2)

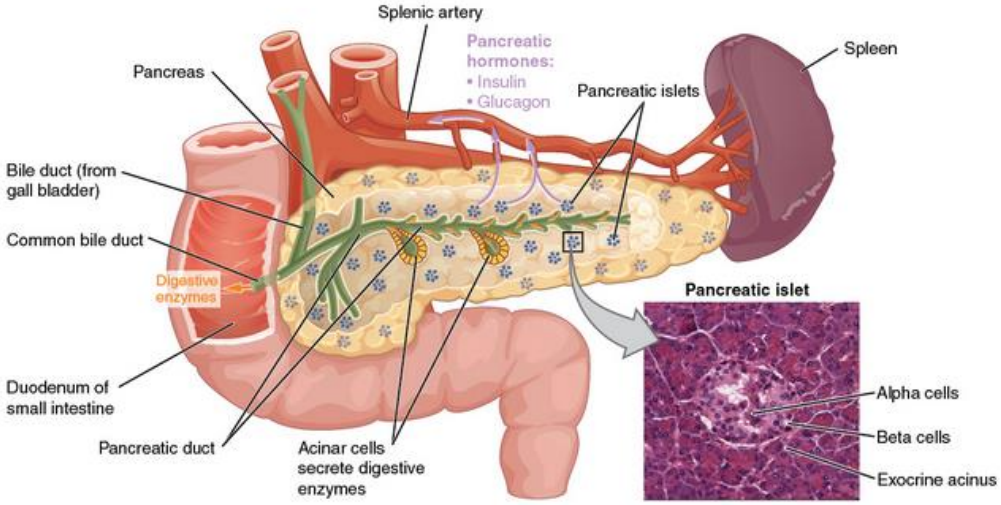

Figure 2. Representative image of the pancreas anatomy.[49]

3.2 General introduction of pancreatic cancer with insights on PDAC

Pancreatic cancer is a highly malignant disease and, despite the low incidence rate of approximately 3% of all cancer cases, pancreatic cancer represents the seventh leading cause of cancer related-deaths worldwide; Europe, North America and Australia/New Zealand are the most affected countries.[50] In 2019, the American Cancer Society estimated 1,762,450 new cancer cases and 606,880 cancer deaths in the United States (US). Among these, 56,770 new cases and 45,750 new deaths of pancreatic cancer were estimated in both sexes, thus representing the third cause of cancer death in the US.[51]

The numerous types of malignant pancreatic neoplasms reflect the different types of cells that make up the organ.[52] Currently, they are classified based on their cellular differentiation (ductal, acinar or neuroendocrine), and on macroscopic appearances (solid or cystic). Most of these tumors are of the exocrine type because they start in cells that produce the digestive juice of the pancreas. Among these, 75-80% of pancreatic cancer are adenocarcinomas and begin in the cells lining the pancreatic duct. Conversely, pancreatic neuroendocrine tumors (PanNETs), arising from endocrine cells, occurring for the 15-20% of cases. Other less commons are colloid carcinomas (2%), solid-pseudopapillary tumors (2%), acinar cell carcinomas (1%), pancreatoblastomas (0.5%), adenosquamous, hepatoid, medullary, signet ring cell and undifferentiated carcinoma.[52–54]

Pancreatic ductal adenocarcinoma (PDAC) is the most common type of pancreatic malignancy and one of the most aggressive solid tumors. Usually, it develops in the head of the pancreas (60-70%), rarely in the tail (5-10%) and body (10-20%).[55] The 5-years survival rate in patients with early-stage of PDAC is achieved only in 25%, after surgical resection. However, most PDAC patients are diagnosed at advanced stage (locally-advanced or metastatic) with non-resectable tumor, therefore, the overall 5-years survival is only 8%. Despite numerous efforts in pancreatic cancer research, mortality rates related to the incidence remain high and relatively unchanged over the years, both for men and women, thus planning to become the second most common cause of cancer death by 2030, overcoming breast, prostate, and colorectal cancers.[56] There are many risk factors associated with the disease, many of which are related to eating habits and reduced physical activity, as well as high consumption of alcohol and tobacco smoke, the latter associated with a risk 2-3 times greater than development of the disease compared to non-smokers. Other risk factors are diabetes mellitus and chronic pancreatitis,[54,57] or Hereditary Pancreatitis (HP) and hereditary genetic syndromes.[58]

PDAC has a very poor prognosis and several factors contribute to this. First of all, it is diagnosed at an advanced stage due to the absence of specific symptoms which, together with the lack of adequate screening tools for diagnosis, make it difficult to diagnose PDAC in the early stage. Further, poor clinical outcome is due to the high aggressiveness of PDAC characterized by rapid growth, lymph-nodes and vasculatures infiltration, as well as metastasis to distant organs, particularly liver, lung and peritoneum. In fact, typical TNM status at diagnosis is T3N1, in which T3 indicates that the tumor has grown outside the pancreas into surrounding tissues, but not yet into major blood vessels or nerves, while N1 indicates the presence of metastasis in regional lymph nodes. Consequently, only 10-20% of patients are eligible to surgical resection of tumor. Finally, genetic and epigenetic alterations and the complex microenvironment of PDAC, as well as the inherent and/or acquired resistance to conventional treatment modalities, contribute to the high malignancy of tumors.[53,59]

3.3 Diagnosis: clinical presentation, diagnostic tools and test, management

Clinical signs and symptoms of PDAC rely on the localization of the tumor. Notably, the tumors that occur in the head of the pancreas are typically associated with abdominal pain, jaundice (also known as icterus, a yellowish pigmentation of the skin and whites of the eyes due to high bilirubin levels), pruritus, dark urine, and acholic stools as a result of obstruction within the biliary tree. While, for the minority of cases, the symptoms associated with the development of cancer in the body and tail of the pancreas, defined as "non-specific", include

unexplained weight loss, anorexia, early sense of satisfaction of the appetite, dyspepsia, nausea, and depression.[60]

Several diagnostic imaging tools are available for the diagnosis of PDAC, although not specific and often unable to identify patients with early-stage disease. Ultrasound (US) is generally used for an initial diagnosis in patient with the most common symptoms of pancreatic cancer. Unfortunately, this technique is not sensitive and makes no distinction between PDAC and inflammatory diseases such as pancreatitis. Endoscopic Ultrasound (EUS) can give information about staging of the tumor and to complete the diagnosis obtaining tissue fragments by fine-needle aspiration. This test can be associated with US. Computed Tomography (CT) is a high accuracy test for determining the extent of primary tumor, but also locoregional extension, vascular invasion, distant metastases and to establish the resectability of the tumor. For patients that show allergy to contrast media, other opportunity is the use of the Magnetic Resonance Imaging (MRI), whose sensitivity and specificity are comparable to CT (approximately 80-90%). MRI detects the infiltration of lymph-nodes and distant metastases. Finally, Positron Emission Tomography (PET), similarly to CT and MRI, allows whole body imaging to staging of diseases; this is the most sensitive and specific among the diagnostic tests available. In fact, this technique uses the amount of glucose consumed by the tumor compared to the healthy tissue. Therefore, through the [^{18}F]-2-fluoro-2-deoxy-glucose (^{18}F-FDG) uptake in cells, tumor volume is predicted and, consequently, the efficacy of the treatment. The only disadvantage of the technique is the false-positive result between inflammatory tissue and tumor, due to the similar appearance of pancreatitis and PDAC.[61]

The image techniques described above can also be complemented with evaluation of cancer antigen 19-9 (CA 19-9). However, CA 19-9, is not only expressed in pancreatic tumor, but also in chronic pancreatitis or inflammatory disease. As a result, it is not a predictive factor of the present tumor alone. It can be used to confirm the diagnosis and predict prognosis and recurrence after resection.[60]

In order to establish the best route for the treatment of PDAC, as well as speculate on patient prognosis, a careful staging of the tumor is necessary. The staging TNM (Tumor Node Metastasis) system of the American Joint Committee on Cancer (AJCC) 8th edition, is the widely used. Particularly, this system takes into account three factors: the size of the tumor (T) (T1, Maximum tumor diameter ≤ 2 cm; T2, Maximum tumor diameter > 2 cm, but ≤ 4 cm; T3, Maximum tumor diameter > 4 cm; T4, Tumor unresectable primary tumor), whether or not the lymph-nodes are involved (N) (N0, No regional LN metastasis; N1, Metastasis in 1-3 regional LNs; N2, Metastasis in > 4 regional LNs), and finally, presence of metastasis (M) (M0, No

distant metastasis; M1, Distant metastasis). Of note, the AJCC 8th edition optimized the division of tumor stages compared to the previous, in order to improve clinical management and increase the survival time. In fact, unlike the older system, in this last edition, stage III is subdivided into IIIA (Tany N2 M0) and IIIB (T4 AnyN M0).[62]

3.4 Treatment: pros and cons

Several clinical managements of PDAC are available, such as surgery, radiation, conventional chemotherapy, immunotherapy, the use of targeted and multi-targeted drug, while miRNA-targeting is still experimental. The choice of one or more treatment options depends on the extent of the tumor. For this reason, PDAC is classified into 4 categories: resectable, borderline resectable, which exhibit venous involvement of superior mesenteric vein/portal-vein (SMV/PV) and gastroduodenal artery encasement, locally advanced and metastatic. The option of surgery depends mainly on the extent of the tumor (resectable or resectable borderline) and location. Only 5-20% of patients have a resectable disease at the time of diagnosis and, in most cases, it relapses within a year. In patients that underwent to surgical resection, the overall 5-year survival rate is in the range between 15 and 40%, for other patients the overall 5-year survival rate is less than 5%. However, surgical options consist in pancreaticoduodenectomy (removal of head/body of the pancreas and nearby organs), distal pancreatectomy (tail, body and spleen), total pancreatectomy (whole pancreas and nearby organs) or palliative surgery (stent or bypass), which may alleviate symptoms of biliary and gastric outlet obstruction.[63]

Radiotherapy (RT) is generally used as adjuvant after surgical resection, in fact, on its own, it has shown no benefit in terms of survival compared to chemotherapy. Kamarajiah et al., reported a study of a big retrospective cohort in which the adjuvant RT after R0 PDAC resection was associated with a survival benefit in patients with node-positive disease.[64] Instead, combination of RT and chemotherapy (called chemoradiotherapy) has rarely provided tumor downstaging and conversion to resectability, and often has false positive results.[63]

Immunotherapy can be executed through checkpoint inhibitors, vaccines, monoclonal antibodies, adoptive cell transfer, viruses, and use of cytokines. The use of the immunotherapy has shown conflicting results and several efforts must be made in order to improve the effectiveness and patient's applicability.[63]

Another route in the treatment of PDAC could be the targeted-therapy. Several signalling pathway are involved in the growth, invasion and metastasis of the tumor, and consequently, there are many opportunities to target. Unfortunately, because PDAC has a heterogeneous nature, most of target-therapies fail. Only in one phase III trial, the use of erlotinib, a specific epidermal growth factor receptor (EFGR) inhibitor, in combination with gemcitabine, showed

two weeks improvement of patient's' survival with advanced stage disease, compared gemcitabine alone, but for its limited benefits, it has been rarely used in the clinic.[63,65]

Different genetic aberration occur in PDAC, therefore, the use of multitarget drugs could be a new approach in the treatment of this disease. Fifty-one patients with metastatic PDAC, have been enrolled in a clinical study of phase II for the clinical evaluation of dasatinib, an oral multitarget tyrosine kinase inhibitor that targets BCR-ABL, c-Src, c-KIT, platelet-derived growth factor receptor β, and EphA2, all dysregulated in PDAC. Unfortunately, dasatinib had no clinical activity in metastatic PDAC, in fact, the median OS (4.7 months) and the median progression-free survival (2.1 months) were lower than to the chemotherapy approaches described below.[66] This may be related to the limited tumor penetration of dasatinib, since it is an excellent substrate for efflux pumps.[67]

miRNAs are a class of endogenous small non-coding RNAs mainly active in the regulation of gene expression at the transcriptional and post-transcriptional levels. They are involved in control of several cellular processes such as proliferation, apoptosis and cellular differentiation by mRNA degradation. However, their altered expression is correlated to the development and progression of cancer. Aberrant expressions of miRNAs have been found in PDAC and several preclinical studies have argued that their management could represent the recent and emerging landscape. For instance, a nanoparticle-based miR-150 delivery system was developed and tested against PDAC cells. miR-150 is a tumor suppressor and its ability to decrease the growth, motility, and invasion of PDAC is associated with down-regulation of the expression of its target gene, MUC4.[68] Furthermore, in a study conducted on mouse model, the combination of gemcitabine and miR-205 prevented tumor growth and induced apoptosis of MIA PaCa cells, typically resistant to gemcitabine.[69]

To date, conventional chemotherapy, in particular combination of drugs, is the best option for the treatments of PDAC. Gemcitabine, a deoxycytidine nucleoside analogue, also known as dFdC: 2′,2′-difluorodeoxycytidine, was the first agent approved by the FDA for the treatment of advanced and metastatic pancreatic cancer, based on clinical improvement in comparison with 5-fluorouracil (5-FU). Unfortunately, the clinical effects are limited by chemoresistance, partly due to the extensive dense fibrous stroma and consequently, to the poor penetration of drug in it.[70] Multiple phase II and III studies evaluated the additional use of other agents associated with gemcitabine, for instance the combination with 5-FU, capecitabine, oxaliplatin, and cisplatin, which however, did not improve survival compared with gemcitabine alone.[71–77] The first moderate benefit has been the combination of gemcitabine with erlotinib.[65] However, in 2013, addition of nab-paclitaxel to gemcitabine showed benefits in overall survival (about 2-

months) compared to gemcitabine alone. In fact, nanomolecular albumin-bound (nab)-paclitaxel was formulated with the aim to have greater plasma and tumor delivery, impact on the stroma, and higher cytotoxic activity of paclitaxel and other drugs in combination, i.e. gemcitabine. In a phase III trials conducted with metastatic patients, the median overall survival was 8.5 months in the *nab*-paclitaxel-gemcitabine group compared to 6.7 months in the gemcitabine group, and the survival rate was 35% *versus* 22%, respectively, at 1 year, and 9% *versus* 4% at 2 years.[78] Unfortunately, this regimen has increased toxicity compared with single agent gemcitabine. In 2011, Conroy et al., reported the results of a highly effective combination of fluorouracil, leucovorin, irinotecan and oxaliplatin (FOLFIRINOX) treatment in patients with metastatic pancreatic cancer.[79] Despite the numerous adverse side effects, the objective response rate was 31.6% in FOLFIRINOX group *versus* 9.4% in the gemcitabine group ($P < 0.001$), thus becoming the first-line treatment option. Instead, a retrospective analysis conducted on 83 patients with advanced pancreatic cancer treated with FOLFIRINOX plus (nab)-paclitaxel and gemcitabine showed the same overall survival outcome.[80]

3.5 Tumor biology

3.5.1 Pathogenesis of PDAC

PDAC gradually develops from non-malignant ductal lesions to invasive ductal adenocarcinoma and different precursor lesions have been recognized. These include the pancreatic intraepithelial neoplasia (PanIN) and cystic neoplastic lesions, the latter classified in intraductal papillary mucinous neoplasm (IPMN) and mucinous cystic neoplasms (MCN). According to the recent classification system and recommendations from the Baltimore consensus meeting, neoplastic precursor lesions can be classified in low- and high- grade.[81] Briefly, PanIN is defined as a *microscopic, flat or papillary, non-invasive epithelial neoplasm characterized by varying amounts of mucin and degrees of cytologic and architectural atypia.*[81] PanIN lesions (divided in PanIN-1, -2, -3) are accompanied by specific genetic alterations; for instance, mutations in codon 12 of the *KRAS2* gene and inactivating mutations in *p16/CDKN2A* gene have been found in low-grade lesions (PanIN-1 and -2), while other additional mutations, in particular inactivating mutations in *SMAD4*, *TP53* and *BRCA2*, occur in high-grade lesions (PanIN-3).[82] IPMN is defined as *a grossly visible, predominantly papillary or rarely flat, non-invasive mucin-producing epithelial neoplasm arising in the main pancreatic duct or branch ducts.* PanINs and IPMN share several characteristics: they are composed of columnar mucinous cells with papillary configuration, have various degrees of atypia and can involve both smaller and main ducts. The only characteristic that help to distinguish these two lesions

is the size; PanIN lesions are usually < 0.5 cm, while IPMN lesions have a diameter ≥ 1.0 cm.[81] Cells of IPMN lesions are also characterized by gene alterations, in particular, *SMAD4* gene is inactivated, whereas *STK11/LKB1* is lost. Finally, MCN is distinguished from the other IPMN cystic lesions by the presence of a single ovarian-type stroma. Between these two cystic neoplastic lesions there are crucial differences regarding the pathogenesis. While MCN arises from ovarian rests in the pancreas, IPMN appears to arise from the pancreatic duct. In addition, MCN lesions do not recur after complete resection, while at least 10% of patients with IPMN who undergo to partial pancreatic resection have a recurrent frequency.[82,83] Common gene alterations between cystic neoplastic lesions have been found in *RNF43*, gene encoding for a protein with intrinsic E3 ubiquitin ligase activity.

PDAC tumor microenvironment (TME) is characterized by a dense stroma, known as desmoplasia or desmoplastic reaction, which is comprised of cellular components, predominantly cancer-associated fibroblasts (CAFs), immune cells, stellate cells, and acellular components such as collagen, fibronectin, cytokines and growth factors that are localized in the extracellular matrix (ECM). Several studies highlighted the ability of stroma components to promote tumor progression, invasion, metastasis and chemoresistance, the latter also due to the physical barrier created by the desmoplastic reaction. Physiologically, cellular components of the stroma ensure tissue repair following damage. Particularly, acinar cells secrete pro-inflammatory and pro-angiogenic growth factors/cytokines, and activate immune cells (adaptive and innate), PSCs/fibroblasts, and vascular cells to restore normal pancreatic function. Conversely, after oncogenic mutations, epithelial cells transform into cancer cells and the control of the activity of cellular components of stroma fails, with the subsequent uncontrolled secretion of pro-inflammatory growth factors/cytokines, including transforming growth factor beta-1 (TGF-β1), fibroblast growth factor-2 (FGF2), interleukin 1 and 6 (IL-1/6), sonic hedgehog (SHH), platelet-derived growth factor (PDGF) that activate fibroblast/PSCs proliferation and ECM deposition. Therefore, targeting tumor-stromal components becomes the new strategy in pancreatic treatment.[84,85]

3.5.2 Genetic abnormalities in primary and metastatic PDAC

Several genes are somatically mutated in primary PDAC. Four out of these genes GTPase Kirsten RAS (*KRAS*), cyclin dependent kinase inhibitor 2A (*P16/CDKN2A*), *TP53* and *SMAD4* are frequently altered and their activating or inactivating mutation progressively occurs. In fact, in the early stages of PDAC the activating mutation of the *KRAS* gene occurs, followed by inactivating mutation in the *CDKN2A* gene and finally, in the latest stages of pancreatic carcinogenesis, the inactivating mutations of the *TP53* and *SMAD4* genes, which are

responsible of progression and invasion. *KRAS* and *CDKN2A* genes are found in approximately 90% of PDAC, *TP53* gene in 75%, and *SMAD4* gene in 30-50%. *KRAS* mutation determines a constitutively activation of RAS protein and as result, the activation of cellular proliferation, while the inactivation of *CDKN2A* gene, and consequently the loss of *p16,* encourages the proliferation activity, because there is not the control of the transition from G1 to S phase of the cell cycle. The inactivation of *TP53* gene activity causes the loss of control in the processes of DNA repair and apoptosis events and finally, the loss *SMAD4* gene activity results in aberration of TGF-β signalling pathway.[52] Other genes such as DNA repair genes *BRCA1*, *BRCA2* and *PALB2* and histone-modifying genes *KDM6A*, *MLL2* and *MLL3*, are lower frequency mutated.[59] Yachida and collaborators showed that, in patients who underwent an autopsy, the four mutated genes described before, *KRAS, P16/CDKN2A, TP53* and *SMAD4,* are coexistent in primary PDAC as well as in metastasis. In addition, they observed that only in 37% of patients all these four genes were mutated, and that the disease free survival and overall survival were correlated to the number of altered genes.[86]

3.5.3 PDAC pharmacogenetics

The individual variability of pharmacological responses to the same anticancer treatments has pushed the international interest in personalized treatment, that by definition is "the management of a patient's disease or disposition by utilizing the best molecular knowledge to accomplish the best medical result for that individual".[87] This variability is due to various factors including age, sex, liver and kidney functions, comorbidities and co-drugs, all linked to cancer genetics. Pharmacogenetics is the branch of science that deals with the study of the inherited genetic differences in drug metabolic pathways which affect individual responses to drugs, both in therapeutic terms and in terms of adverse effects. Therefore, it aims to provide the best knowledge on the genetic variants of the single patient, as well as on other factors that involve the activity of the drug as transporters, receptors and enzymes; in other words, pharmacogenetics intends to identify the gene polymorphisms and drug activity.[88] The treatment of PDAC with gemcitabine, FOLFIRINOX and nab-paclitaxel/gemcitabine combinations, may be affected by genetic dysregulation. In chapter 4 we focused on PDAC pharmacogenetics and the correlation between polymorphism and -omics profiles with the response to gemcitabine, FOLFIRINOX and nab-paclitaxel combinations.

3.5.4 Molecular mechanisms underlying invasion and metastasis: Epithelial mesenchymal transition events

PDAC is one of the most aggressive malignancies, largely for its tendency to metastasize, that together with the resistance to currently available therapeutic interventions, is the main

cause of PDAC-related mortality. Metastasis is an extremely controlled set of processes involving distinct signalling pathways of cellular and non-cellular components of TME. This process occurs in multiple steps in which cancer cells acquire the ability to spread from the primary tumor to the distant organs. They consist in the *invasion* by the tumor cells of surrounding tissue, then *intravasation* into lymphatic circulatory systems and transport of the cells through them, followed by *extravasation* in the distant capillaries, by the development of micro-metastases, and finally, by macro-metastatic colonizations.[89] Most patients at diagnosis have advanced disease, characterized by infiltration of lymph nodes and vascularization, as well as by metastases to distant organs, such as the liver, lungs and peritoneum.[59] In addition, patients who underwent surgical resection that subsequently had a recurrent metastasis in different sites, had different clinical outcomes. For instance, Sahin and collaborators, observed that patients with first site of lung recurrence had a more favourable outcome compared to patients who recurred with liver metastasis as the first site of recurrence (median Time from relapse to death of 15 *versus* 9 months respectively, P = 0.02).[90]

A lot of studies suggested that epithelial-to-mesenchymal transition (EMT) contributes to early-stage dissemination of cancer cells and is pivotal for invasion and metastasis of PDAC.[91] EMT and mesenchymal-to-epithelial transition (MET) are physiological events that play key roles in the differentiation of multiple tissues and organs, particularly during embryonic development. Further, EMT events also occur in the physiological response to injuries in which keratinocytes reprogram their EMT processes. The conversion from epithelial to mesenchymal cells involves phenotypic changes like the loss of cell-cell or cell-extracellular adhesion and cell polarity, and acquisition of migratory and invasive properties.[92] The activation of this program depends on microenvironmental signals and is coordinated by the EMT-inducing transcription factors (EMT-TFs) that interact with epigenetic regulators to control the expression of proteins involved in cell polarity, cell-cell contact, cytoskeleton structure and extracellular matrix degradation. Because the hallmark of EMT is the loss of E-cadherin expression, EMT-TFs can be classified based on their ability to repress E-cadherin directly or indirectly. The most representative are the direct repressors that include: zinc-finger proteins belong to the SNAILs superfamily, such as SNAIL1, SNAIL2 (also known as SLUG) and SNAIL3 (SMUC), and zinc-finger and E-box binding proteins of the ZEB family, such as ZEB1 (TCF8) and ZEB2 (SIP1). The factors such as TWIST proteins (TWIST1 and TWIST2) repress E-cadherin transcription indirectly. Although EMT is fundamental for the physiological responses to the injuries as well as for the formation of internal organs, pathological EMT features are observed during the development of cancer and tissue fibrosis, due to the

dysregulations of protein expressions of the EMT regulators.[93] In chapter 7 we studied the ability of new imidazothiadiazole derivatives to influence the expression of the key regulators of EMTs. In particular, we focused the studies on the expression of zinc-finger protein SNAIL1 and SNAIL2, E-cadherin (CDH1) and N-cadherin (CDH2), VIM (vimentin) and matrix metalloproteinases -2 and -9 (MMP2 and MMP9), both at mRNA and protein expression levels.

3.5.5 Role of focal adhesion kinase (FAK) in tumor growth and spread

Focal adhesion kinase (FAK), also known as protein tyrosine kinase 2 (PTK2), is a non-receptor protein tyrosine kinase that plays its biological function in the regulation of several cellular processes such as proliferation, motility, migration, invasion and cell survival. Notably, it coordinates single or complex signals, working as a linker for the communication between extracellular matrix and intracellular cell compartments, through the phosphorylation of the downstream substrates. It is activated by different receptors including integrins, growth factor receptors, G protein coupled-receptors and cytokine receptors, and then it binds the downstream signalling molecules such as Src, p130Cas, Grb2, PI3K and paxillin.[94] Structurally, it is composed by four domains that have been widely characterized. From the N- to C-*terminus* sites there are: the FERM (band 4.1, Ezrin, Radixin, Moesin) domain followed by a kinase domain, a region proline-enriched, and finally, FAT (Focal Adhesion Targeting). FAK is characterized by different phosphorylation sites. Among these, the major involved for the activation of the kinase is the tyrosine residue Y-397, which is located in the linker between FERM and kinase domains.

Dysregulation of FAK is found in many cancers, both at early and in advanced stages of the tumors; in addition, its overexpression could give information about the prognosis.[95] As many other cancers, also in PDAC FAK is overexpressed. Begum and collaborators showed that in MIA PaCa-2 and Capan-1 cancer cells, in which the overexpression of FAK was induced, the levels of activated pFAK-Y397 were increased, as well as in colony formation,[96] while another study showed the antitumor activity of a specific FAK inhibitor on different pancreatic cancer cells in which FAK was overexpressed.[97] Therefore, the development of molecules targeting FAK could be a good strategy for PDAC treatment. In chapter 7 we demonstrated the ability of our imidazothiadiazole compounds to inhibit the phosphorylation of 45 tyrosine kinases substrates, whose visualization on Cytoscape highlighted PTK2/FAK as an important hub between those proteins. This was validated by the ELISA assay, demonstrating the reduction of the phosphorylation of residue Y-397.

4. An overview of Malignant Mesothelioma

4.1 Brief description of mesothelium: origin, structure and function

The discovery of the existence of the mesothelium dates back to two centuries ago when Bichat observed a single line of flat cells, that line the body serous membranes, which Minot subsequently called mesothelial cells. Embryologically, it develops from mesodermal tissue around 14 days of gestation, in humans.[98] The mesothelium forms a monolayer of flattened squamous-like mesothelial cells resting on a thin basement membrane supported by a dense irregular connective tissue. Exceptionally, in specific areas, including the milky spots of the *omentum*, the parenchymal organs (liver, spleen), the peritoneal side of the diaphragm overlaying the lymphatic lacunae, the septal folds of the mediastinal pleura, and areas of injury, mesothelium consists of cuboidal cells.

Although a long time has passed from discovery of the mesothelium, as well as from its description, its true function has been clarified only in the last 20 years. In addition to the "static" role as a protective layer covering the peritoneal, pleural and pericardial cavities and most of the internal organs to prevent adhesion and to provide a slippery non-adhesive surface that facilitates movements, its "dynamic" role has also been described which consists in the defense against microorganisms, lesions and invasion of tumor cells.[98,99] These functions are supported to the metabolic activity of mesothelial cells and by the secretion of glycocalyx, a fluid film composed of lipoproteins, phospholipids, proteoglycans, and hyaluronan.[100]

4.2 Pathological disease of mesothelium: malignant mesothelioma

Malignant mesotheliomas are rare and aggressive tumors that occur mostly in the pleura and peritoneum sites, with the frequency rate of 80-90% and 10-15%, respectively, while pericardium and *tunica vaginalis testis* are infrequently involved (about 1% for both sites).[101] The prognosis after diagnosis is poor with a median survival from 4 to 10 months, depending to subtype of cells that characterized the tumor.[102] The incidence of malignant mesotheliomas is associated with exposure to asbestos, that collectively refers to six different mineral fibres present in nature (crocidolite, actinolite, tremolite, anthophyllite, amosite and chrysotile). Recent epidemiological data in the US showed 1 case for 100,000 persons not exposed to asbestos against 2 or 3 cases for 100,000 persons exposed, due to occupational exposure or living in industrialized countries.[103] However, constant exposure to asbestos triggers inflammatory reaction, toxicity and mutagenic response with the result to have alterations in the expression of redox dependent enzymes and other etiological factors.[104] Approximately, 12% of mesotheliomas occur in carriers of genetic mutations and they can be triggered by

asbestos exposure. Mostly the germline mutations in BRCA1-associated protein 1 (*BAP1*) or in genes that regulate DNA repair, such as *MLH1*, *MLH3*, *TP53* and *BRCA2* are associated with the disease. Other risk factors include therapeutic ionizing radiation to the chest, the exposure to the simian virus 40 (SV40), immune deficiency, chronic inflammation and others.[104,105]

4.3 Diagnosis: clinical presentation, diagnostic tests, management

Several clinical signs and symptoms indicate the presence of malignant mesotheliomas. The first symptom that occurs in patients affected with pleural mesothelioma is the dyspnea, associated with dry cough, chest pain, fatigue, weight loss and fever. Early satiety and inability to lean forward are also observed in patients with ascites, and these clinical symptoms are also associated with peritoneal mesothelioma. Pleural or peritoneal effusions are fundamental for early diagnosis.

Primary mesothelioma tumors may spread to give metastasis. In 55.4% of patients post-mortem metastases were found, while lymph-node infiltration was identified in 53.3% of cases. Liver (31.9%), spleen (10.8%), thyroid (6.9%), and brain (3.0%) organs are the most involved in metastases. Mesothelial cells, called also mesodermal in prenatally state, maintain the pluripotential ability and therefore, can arising tumors with an epithelioid, sarcomatoid, or biphasic histology. [105]

Diagnostic tools reveal the presence of mesotheliomas and in addition, histologically differentiate the tumor. Cytological analysis helps pathologists to detect pleural mesothelioma through detection of epithelial cells in pleural fluid, while immunohistochemistry (IHC) analysis can discern epithelial cells from mesothelial and inflammatory cells. In addition, thoracoscopy and laparoscopy biopsy are useful tools to definitely detect pleural and peritoneal mesothelioma and to identify the subtypes of mesothelioma cells. Moreover, diagnostic images are essential to reveal staging of tumor. CT is mainly used as first imaging modality to delineate tumor invasion of the chest wall and diaphragm. PET coupled with CT helps to identify additional sites of tumor and to understand the course of therapy. Magnetic resonance imaging (MRI), laparoscopy, endobronchial ultrasound (EBUS) with lymph node biopsies, or mediastinoscopy are additional methods that revealed the extent of disease.

Knowing the staging of the tumor is necessary in order to assess the anatomical extent, the potential efficacy of the treatments, and to decide whether the tumor can be resected. The recent AJCC TNM system, applied starting from January 2018, is used only for malignant pleural mesothelioma, in fact, other kind of mesotheliomas are less common and do not have formal staging systems. Malignant pleural mesothelioma may be classified into four stages. Stage I

and III are divided in A and B, based on the size of tumor for the stage I, and size of the tumor and involvement of lymph-nodes for the stage III.[106]

4.3 Treatment

The 'classic' modalities of intervention (chemotherapy, radiotherapy and surgery) to treat patients with malignant mesothelioma are strongly influenced by tumor extension (TNM) that is determined by imaging techniques, though often these are not precise enough to determine the "T" and "N" staging. Concerning surgical resection of the tumor, the goal of extra-pleural pneumonectomy (EPP), pleurectomy/decortication (P/D), and P/D that also involves resection of the pericardium (called EPD), is to give a curative options treatment but the results are disappointing. Patients affected by malignant peritoneal mesothelioma experience benefit in term of overall survival by the regional chemotherapy with hyperthermic intraperitoneal chemotherapy (HIPEC) and normothermic intraperitoneal chemotherapy long-term (NIPEC-LT).[107] However, full resection (macro-and microscopic) of mesothelioma is impossible, irrespective of the surgical technique used and in addition, only patients with an epithelioid histological subtype may benefit. Mesothelioma with sarcomatous or biphasic types are worse candidates for any type of surgery.[108] Therefore, surgery is usually performed with chemotherapy and radiotherapy (RT), performing multimodal treatment. RT is used mainly to prevent metastasis after surgery, to reduce the tumor mass that compromises closely organs, and finally, in the form of high dose hemithoracic radiation, to control tumor growth and improve the survival.[109]

Combination of cisplatin and pemetrexed or raltitrexed is the current standard first-line therapy for the treatment of malignant pleural mesothelioma. In fact, this combination has shown a longer survival compared with cisplatin alone in randomised phase III trials (OS, 12.1 vs 9.3 months; respectively).[110] For patients that do not tolerate cisplatin, the alternative is the substitution with carboplatin.[111] The efficacy of this combination therapy was also observed in another retrospective study, in which the OS from diagnosis to death of patients who received second-line gemcitabine-based chemotherapy after treatment with pemetrexed plus platinum, was 13.1 months compared to patients that received first-line pemetrexed-based plus platinum regimens (20.8 months).[112]

4.4 Correlation between hypoxia and malignant mesothelioma

It is well established that solid tumors are typically characterized by hypoxic microenvironment and low pH, thus representing prognostic factors. These features are due to the rapid proliferation of cells that overcome the ability to supply with new vascularization. Cancer cells can easily adapt to the low oxygen gradients in which overexpression of the

hypoxia-inducible factor-1 (HIF-1), a master regulator of oxygen homeostasis, plays a critical role. For instance, it induces genes primarily involved in anaerobic glycolysis, angiogenesis, apoptosis, invasion and metastasis, as well as aggressiveness and chemoresistance to several treatments.[113] Together with HIF-1 overexpression, other factors contribute to the chemoresistance, including acidosis, nutrient starvation, increased interstitial fluid pressure, and low drug concentrations.[114]

Malignant mesothelioma is a highly hypoxic tumor and it was demonstrated by the overexpression of HIF-1.[115] Raz and collaborators postulated that hypoxia was the main cause of resistance to the antifolate by the suppression of key genes involved in folate homeostasis, including the influx transporters reduced folate carrier (RFC) and proton-coupled folate transporter (PCFT). In addition, the high serum level of the human isoform-5 of lactate dehydrogenase (LDH-A), the major check-point for the switch from aerobic to anaerobic glycolysis in carcinomas, has a prognostic value in tumor progression, and should be considered as a new target for mesothelioma treatment, also together with routine treatment.

4.5 Biomarkers for diagnostic evaluation

The search for biomarkers for the diagnosis of the disease as well as for the response to chemotherapy is extremely important for oncologists both to select suitable patients for specific chemotherapy and to observe the progress or regression of the tumor during treatment.

In mesothelioma, different biomarkers have been associated both in malignant and in benign conditions. Therefore, it is usually convenient to monitor a group of biomarkers, although none has been validated in clinical trials. Anyway, glycoproteins such as soluble mesothelin and osteopontin are the most valuable biomarkers overexpressed in mesothelioma, and others such as hyaluronic acid, fibulin-3, pan-VEGR in the blood and pleural fluid were found as indicators of tumor.[116] The research for novel and reliable biomarkers continues. We described in chapters 9 and 10, the prognostic value of LDH-A and PCFT, as promising predictors of pemetrexed's efficacy or chemoresistance, but also potential useful target to overcome such chemoresistance.

5. Outline of the PhD Thesis

The study in the current Thesis is mainly based on the search for the new therapeutics in the treatment of pancreatic and mesothelioma cancer. In the introductory chapter we briefly introduced a perspective on drug design approaches over the years which introduces the design of a novel class of imidazo[2,1-*b*][1,3,4]thiadiazole derivatives with antitumor and antibiofilm activity. Therefore, the molecular biology of pancreatic ductal adenocarcinoma (PDAC) and malignant mesotheliomas were described, as well as a brief introduction on biofilm formation and its role in the persistence of bacterial infections.

Overall the Thesis is devided in three main parts:

Part I: *In vitro* pharmacological studies as important tools in large-scale drug discovery, and the use of combination therapies with special focus on PDAC cancer (**chapters 2-4**).

Part II: Preclinical evaluation of the antitumor activity of a new class of imidazo[2,1-*b*][1,3,4]thiadiazole derivatives and their repurposing as antibiofilm agents (**chapters 5-8**).

Part III: *In vitro* and *in vivo* studies on malignant mesotheliomas (**chapters 9-11**).

Part I:

In **chapter 2** we discuss the *in vitro* cytotoxic tests available for the high-throughput screening in drug-discovery.

In **chapter 3** we summarize the main mathematical equations to evaluate the synergistic, additive or antagonistic effects of drug combinations and the computational approach to evaluate these interactions.

In **chapter 4** we describe the main findings on PDAC polymorphisms and *-omics* profiles correlated to the response to gemcitabine, FOLFIRINOX and *nab*-paclitaxel combinations, as well as limitations of targeted therapy.

Part II:

In **chapters 5** and **6** we describe the antitumor activity of the derivatives of type *2-(6-phenylimidazo[2,1-b][1,3,4]thiadiazol-2-yl)-1H-indoles* against three PDAC cell lines (SUIT-2, Capan-1 and Panc-1).

In **chapter 7** we describe on the antitumor activity of the derivatives of type *2-(1H-indol-3-yl)-6-(thiophen-3-yl)imidazo[2,1-b][1,3,4]thiadiazole* and *2-(1H-indol-3-yl)-6-phenylimidazo[2,1-b][1,3,4]thiadiazole-5-carbaldehyde* on a panel of PDAC cells (SUIT-2, Capan-1, Panc-1, Panc-1R and PDAC-3).

In **chapter 8** we describe the antibiofilm properties of compounds reported in **chapter 5** and **6** against Gram-positive bacterial (reference strains *Staphylococcus aureus* ATCC 25923,

Staphylococcus aureus ATCC 6538 and *Staphylococcus epidermidis* ATCC 12228) and Gram negative (strains *Pseudomonas aeruginosa* ATCC 15442 and *Escherichia coli* ATCC 25922).

Part III:

In **chapter 9** we speculate on the role of PCFT as biomarker to predict the efficacy of the treatment with pemetrexed of malignant mesotheliomas, as well as new target to overcome drug resistance.

In **chapter 10** we identify the correlation of hypoxia and PCFT silencing with higher LDH-A expression and the research for new LDH-A inhibitors against mesothelioma.

In **chapter 11** we describe the *in vitro* antitumor activity of ten *2-(1H-indol-3-yl)-6-(thiophen-3-yl)imidazo[2,1-b][1,3,4]thiadiazole* derivatives against two DMPM primary cell lines, MesoII and STO.

References

(1) Ma, X. H.; Shi, Z.; Tan, C.; Jiang, Y.; Go, M. L.; Low, B. C.; Chen, Y. Z. In-Silico Approaches to Multi-Target Drug Discovery : Computer Aided Multi-Target Drug Design, Multi-Target Virtual Screening. *Pharm. Res.* **2010**, *27* (5), 739–749. https://doi.org/10.1007/s11095-010-0065-2.

(2) Talevi, A. Multi-Target Pharmacology: Possibilities and Limitations of the "Skeleton Key Approach" from a Medicinal Chemist Perspective. *Front Pharmacol* **2015**, *6*. https://doi.org/10.3389/fphar.2015.00205.

(3) Alcaro, S.; Bolognesi, M. L.; García-Sosa, A. T.; Rapposelli, S. Editorial: Multi-Target-Directed Ligands (MTDL) as Challenging Research Tools in Drug Discovery: From Design to Pharmacological Evaluation. *Front Chem* **2019**, *7*. https://doi.org/10.3389/fchem.2019.00071.

(4) Ramsay, R. R.; Popovic-Nikolic, M. R.; Nikolic, K.; Uliassi, E.; Bolognesi, M. L. A Perspective on Multi-Target Drug Discovery and Design for Complex Diseases. *Clin Transl Med* **2018**, *7* (1), 3. https://doi.org/10.1186/s40169-017-0181-2.

(5) Frei, E.; Karon, M.; Levin, R. H.; Freireich, E. J.; Taylor, R. J.; Hananian, J.; Selawry, O.; Holland, J. F.; Hoogstraten, B.; Wolman, I. J.; et al. The Effectiveness of Combinations of Antileukemic Agents in Inducing and Maintaining Remission in Children with Acute Leukemia. *Blood* **1965**, *26* (5), 642–656.

(6) Mokhtari, R. B.; Homayouni, T. S.; Baluch, N.; Morgatskaya, E.; Kumar, S.; Das, B.; Yeger, H. Combination Therapy in Combating Cancer. *Oncotarget* **2017**, *8* (23), 38022–38043. https://doi.org/10.18632/oncotarget.16723.

(7) Palleria, C.; Di Paolo, A.; Giofrè, C.; Caglioti, C.; Leuzzi, G.; Siniscalchi, A.; De Sarro, G.; Gallelli, L. Pharmacokinetic Drug-Drug Interaction and Their Implication in Clinical Management. *J Res Med Sci* **2013**, *18* (7), 601–610.

(8) Zhou, J.; Jiang, X.; He, S.; Jiang, H.; Feng, F.; Liu, W.; Qu, W.; Sun, H. Rational Design of Multitarget-Directed Ligands: Strategies and Emerging Paradigms. *J. Med. Chem.* **2019**. https://doi.org/10.1021/acs.jmedchem.9b00017.

(9) Lin, H.-H.; Zhang, L.-L.; Yan, R.; Lu, J.-J.; Hu, Y. Network Analysis of Drug–Target Interactions: A Study on FDA-Approved New Molecular Entities Between 2000 to 2015. *Scientific Reports* **2017**, *7* (1), 1–9. https://doi.org/10.1038/s41598-017-12061-8.

(10) Fischer, E.; Jourdan, F. Ueber Die Hydrazine Der Brenztraubensäure. *Berichte der deutschen chemischen Gesellschaft* **1883**, *16* (2), 2241–2245. https://doi.org/10.1002/cber.188301602141.

(11) Sayed, M.; El-Dean, A. M. K.; Ahmed, M.; Hassanien, R. Synthesis of Some Heterocyclic Compounds Derived from Indole as Antimicrobial Agents. *Synthetic Communications* **2018**, *48* (4), 413–421. https://doi.org/10.1080/00397911.2017.1403627.

(12) Sivaprasad, G.; Perumal, P. T.; Prabavathy, V. R.; Mathivanan, N. Synthesis and Anti-Microbial Activity of Pyrazolylbisindoles--Promising Anti-Fungal Compounds. *Bioorg. Med. Chem. Lett.* **2006**, *16* (24), 6302–6305. https://doi.org/10.1016/j.bmcl.2006.09.019.

(13) Donawade, D. S.; Raghu, A. V.; Gadaginamath, G. S. Synthesis and Antimicrobial Activity of Some New 1-Substituted-3-Pyrrolyl Aminocarbonyl/Oxadiazolyl/Triazolyl/5-Methoxy-2-Methylindoles and Benz[g]Indoles. *Indian Journal of Chemistry - Section B Organic and Medicinal Chemistry* **2006**, *45* (3), 689–696.

(14) Kuduk, S. D.; Chang, R. K.; Wai, J. M.-C.; Di Marco, C. N.; Cofre, V.; DiPardo, R. M.; Cook, S. P.; Cato, M. J.; Jovanovska, A.; Urban, M. O.; et al. Amidine Derived Inhibitors of Acid-Sensing Ion Channel-3 (ASIC3). *Bioorg. Med. Chem. Lett.* **2009**, *19* (15), 4059–4063. https://doi.org/10.1016/j.bmcl.2009.06.021.

(15) Rahaman, S. A.; Ragjendra Prasad, Y.; Bhuvaneswari, K.; Kumar, P. Synthesis and Antihistaminic Activity of Novel Pyrazoline Derivatives. *International Journal of ChemTech Research* **2010**, *2* (1), 16–20.

(16) Mohamed, M. S.; Youns, M. M.; Ahmed, N. M. Novel Indolyl-Pyrimidine Derivatives: Synthesis, Antimicrobial, and Antioxidant Evaluations. *Med Chem Res* **2014**, *23* (7), 3374–3388. https://doi.org/10.1007/s00044-014-0916-1.

(17) Li, Y.-Y.; Wu, H.-S.; Tang, L.; Feng, C.-R.; Yu, J.-H.; Li, Y.; Yang, Y.-S.; Yang, B.; He, Q.-J. The Potential Insulin Sensitizing and Glucose Lowering Effects of a Novel Indole Derivative in Vitro and in Vivo. *Pharmacological Research* **2007**, *56* (4), 335–343. https://doi.org/10.1016/j.phrs.2007.08.002.

(18) Abdel-Gawad, H.; Mohamed, H. A.; Dawood, K. M.; Badria, F. A.-R. Synthesis and Antiviral Activity of New Indole-Based Heterocycles. *Chemical and Pharmaceutical Bulletin* **2010**, *58* (11), 1529–1531. https://doi.org/10.1248/cpb.58.1529.

(19) Ghanei-Nasab, S.; Khoobi, M.; Hadizadeh, F.; Marjani, A.; Moradi, A.; Nadri, H.; Emami, S.; Foroumadi, A.; Shafiee, A. Synthesis and Anticholinesterase Activity of Coumarin-3-Carboxamides Bearing Tryptamine Moiety. *European Journal of Medicinal Chemistry* **2016**, *121*, 40–46. https://doi.org/10.1016/j.ejmech.2016.05.014.

(20) MacDonough, M. T.; Strecker, T. E.; Hamel, E.; Hall, J. J.; Chaplin, D. J.; Trawick, M. L.; Pinney, K. G. Synthesis and Biological Evaluation of Indole-Based, Anti-Cancer Agents Inspired by the Vascular Disrupting Agent 2-(3′-Hydroxy-4′-Methoxyphenyl)-3-(3″,4″,5″-Trimethoxybenzoyl)-6-Methoxyindole (OXi8006). *Bioorganic & Medicinal Chemistry* **2013**, *21* (21), 6831–6843. https://doi.org/10.1016/j.bmc.2013.07.028.

(21) Akkoç, M. K.; Yüksel, M. Y.; Durmaz, I.; Atalay, R. E. Design, Synthesis, and Biological Evaluation of Indole-Based 1,4-Disubstituted Piperazines as Cytotoxic Agents. *Turkish Journal of Chemistry* **2012**, *36* (4), 515–525. https://doi.org/10.3906/kim-1111-5.

(22) Kumar, D.; Kumar, N. M.; Noel, B.; Shah, K. A Series of 2-Arylamino-5-(Indolyl)-1,3,4-Thiadiazoles as Potent Cytotoxic Agents. *European Journal of Medicinal Chemistry* **2012**, *55*, 432–438. https://doi.org/10.1016/j.ejmech.2012.06.047.

(23) Queiroz, M.-J. R. P.; Abreu, A. S.; Carvalho, M. S. D.; Ferreira, P. M. T.; Nazareth, N.; São-José Nascimento, M. Synthesis of New Heteroaryl and Heteroannulated Indoles from Dehydrophenylalanines: Antitumor Evaluation. *Bioorganic & Medicinal Chemistry* **2008**, *16* (10), 5584–5589. https://doi.org/10.1016/j.bmc.2008.04.004.

(24) Zhang, F.; Zhao, Y.; Sun, L.; Ding, L.; Gu, Y.; Gong, P. Synthesis and Anti-Tumor Activity of 2-Amino-3-Cyano-6-(1H-Indol-3-Yl)-4-Phenylpyridine Derivatives in Vitro. *European Journal of Medicinal Chemistry* **2011**, *46* (7), 3149–3157. https://doi.org/10.1016/j.ejmech.2011.03.055.

(25) Ahmad, A.; Rahman, W. A. S. and K. W. Anticancer Properties of Indole Compounds: Mechanism of Apoptosis Induction and Role in Chemotherapy http://www.eurekaselect.com/71540/article (accessed Oct 4, 2019).

(26) Almagro, L.; Fernández-Pérez, F.; Pedreño, M. A. Indole Alkaloids from Catharanthus Roseus: Bioproduction and Their Effect on Human Health. *Molecules* **2015**, *20* (2), 2973–3000. https://doi.org/10.3390/molecules20022973.

(27) Bradner, W. T. Mitomycin C: A Clinical Update. *Cancer Treat. Rev.* **2001**, *27* (1), 35–50. https://doi.org/10.1053/ctrv.2000.0202.

(28) Cytotoxic Bisindole Alkaloids from a Marine Sponge Spongosorites sp. - Journal of Natural Products (ACS Publications) https://pubs.acs.org/doi/abs/10.1021/np049577a (accessed Apr 29, 2018).

(29) Kaushik, N. K.; Kaushik, N.; Attri, P.; Kumar, N.; Kim, C. H.; Verma, A. K.; Choi, E. H. Biomedical Importance of Indoles. *Molecules* **2013**, *18* (6), 6620–6662. https://doi.org/10.3390/molecules18066620.

(30) Mirzaei, H.; Shokrzadeh, M.; Modanloo, M.; Ziar, A.; Riazi, G. H.; Emami, S. New Indole-Based Chalconoids as Tubulin-Targeting Antiproliferative Agents. *Bioorganic Chemistry* **2017**, *75*, 86–98. https://doi.org/10.1016/j.bioorg.2017.09.005.

(31) Dadashpour, S.; Emami, S. Indole in the Target-Based Design of Anticancer Agents: A Versatile Scaffold with Diverse Mechanisms. *European Journal of Medicinal Chemistry* **2018**, *150*, 9–29. https://doi.org/10.1016/j.ejmech.2018.02.065.

(32) Romagnoli, R.; Baraldi, P. G.; Prencipe, F.; Balzarini, J.; Liekens, S.; Estévez, F. Design, Synthesis and Antiproliferative Activity of Novel Heterobivalent Hybrids Based on Imidazo[2,1-b][1,3,4]Thiadiazole and Imidazo[2,1-b][1,3]Thiazole Scaffolds. *Eur J Med Chem* **2015**, *101*, 205–217. https://doi.org/10.1016/j.ejmech.2015.06.042.

(33) Jadhav, V. B.; Kulkarni, M. V.; Rasal, V. P.; Biradar, S. S.; Vinay, M. D. Synthesis and Anti-Inflammatory Evaluation of Methylene Bridged Benzofuranyl Imidazo[2,1-b][1,3,4]Thiadiazoles. *Eur J Med Chem* **2008**, *43* (8), 1721–1729. https://doi.org/10.1016/j.ejmech.2007.06.023.

(34) Tahghighi, A.; Razmi, S.; Mahdavi, M.; Foroumadi, P.; Ardestani, S. K.; Emami, S.; Kobarfard, F.; Dastmalchi, S.; Shafiee, A.; Foroumadi, A. Synthesis and Anti-Leishmanial Activity of 5-(5-Nitrofuran-2-Yl)-1,3,4-Thiadiazol-2-Amines Containing N-[(1-Benzyl-1H-1,2,3-Triazol-4-Yl)Methyl] Moieties. *Eur J Med Chem* **2012**, *50*, 124–128. https://doi.org/10.1016/j.ejmech.2012.01.046.

(35) Jakovljević, K.; Matić, I. Z.; Stanojković, T.; Krivokuća, A.; Marković, V.; Joksović, M. D.; Mihailović, N.; Nićiforović, M.; Joksović, L. Synthesis, Antioxidant and Antiproliferative Activities of 1,3,4-Thiadiazoles Derived from Phenolic Acids. *Bioorg. Med. Chem. Lett.* **2017**, *27* (16), 3709–3715. https://doi.org/10.1016/j.bmcl.2017.07.003.

(36) Alegaon, S. G.; Alagawadi, K. R.; Sonkusare, P. V.; Chaudhary, S. M.; Dadwe, D. H.; Shah, A. S. Novel Imidazo[2,1-b][1,3,4]Thiadiazole Carrying Rhodanine-3-Acetic Acid as Potential Antitubercular Agents. *Bioorg. Med. Chem. Lett.* **2012**, *22* (5), 1917–1921. https://doi.org/10.1016/j.bmcl.2012.01.052.

(37) Bhongade, B. A.; Talath, S.; Gadad, R. A.; Gadad, A. K. Biological Activities of Imidazo[2,1-b][1,3,4]Thiadiazole Derivatives: A Review. *Journal of Saudi Chemical*

Society **2016**, *20* (Supplement 1), S463–S475. https://doi.org/10.1016/j.jscs.2013.01.010.

(38) Schillaci, D.; Spanò, V.; Parrino, B.; Carbone, A.; Montalbano, A.; Barraja, P.; Diana, P.; Cirrincione, G.; Cascioferro, S. Pharmaceutical Approaches to Target Antibiotic Resistance Mechanisms. *J. Med. Chem.* **2017**, *60* (20), 8268–8297. https://doi.org/10.1021/acs.jmedchem.7b00215.

(39) Cascioferro, S.; Parrino, B.; Petri, G. L.; Cusimano, M. G.; Schillaci, D.; Di Sarno, V.; Musella, S.; Giovannetti, E.; Cirrincione, G.; Diana, P. 2,6-Disubstituted Imidazo[2,1-b][1,3,4]Thiadiazole Derivatives as Potent Staphylococcal Biofilm Inhibitors. *European Journal of Medicinal Chemistry* **2019**, *167*, 200–210. https://doi.org/10.1016/j.ejmech.2019.02.007.

(40) Vasudevan, R. Biofilms: Microbial Cities of Scientific Significance. *JMEN* **2014**, *1* (3). https://doi.org/10.15406/jmen.2014.01.00014.

(41) Rabin, N.; Zheng, Y.; Opoku-Temeng, C.; Du, Y.; Bonsu, E.; Sintim, H. O. Biofilm Formation Mechanisms and Targets for Developing Antibiofilm Agents. *Future Med Chem* **2015**, *7* (4), 493–512. https://doi.org/10.4155/fmc.15.6.

(42) Hall, M. R.; McGillicuddy, E.; Kaplan, L. J. Biofilm: Basic Principles, Pathophysiology, and Implications for Clinicians. *Surg Infect (Larchmt)* **2014**, *15* (1), 1–7. https://doi.org/10.1089/sur.2012.129.

(43) Parrino, B.; Diana, P.; Cirrincione, G.; Cascioferro, S. Bacterial Biofilm Inhibition in the Development of Effective Anti-Virulence Strategy. *Open Med Chem J* **2018**, *12*, 84–87. https://doi.org/10.2174/1874104501812010084.

(44) Nickel, J. C.; Ruseska, I.; Wright, J. B.; Costerton, J. W. Tobramycin Resistance of Pseudomonas Aeruginosa Cells Growing as a Biofilm on Urinary Catheter Material. *Antimicrob. Agents Chemother.* **1985**, *27* (4), 619–624. https://doi.org/10.1128/aac.27.4.619.

(45) Jamal, M.; Ahmad, W.; Andleeb, S.; Jalil, F.; Imran, M.; Nawaz, M. A.; Hussain, T.; Ali, M.; Rafiq, M.; Kamil, M. A. Bacterial Biofilm and Associated Infections. *J Chin Med Assoc* **2018**, *81* (1), 7–11. https://doi.org/10.1016/j.jcma.2017.07.012.

(46) Parrino, B.; Schillaci, D.; Carnevale, I.; Giovannetti, E.; Diana, P.; Cirrincione, G.; Cascioferro, S. Synthetic Small Molecules as Anti-Biofilm Agents in the Struggle against Antibiotic Resistance. *Eur J Med Chem* **2019**, *161*, 154–178. https://doi.org/10.1016/j.ejmech.2018.10.036.

(47) El Sayed, S. A.; Mukherjee, S. Physiology, Pancreas. In *StatPearls*; StatPearls Publishing: Treasure Island (FL), 2019.

(48) The Pancreas https://www.hopkinsmedicine.org/health/conditions-and-diseases/the-pancreas (accessed Sep 5, 2019).

(49) 17.9 The Endocrine Pancreas – Anatomy and Physiology https://opentextbc.ca/anatomyandphysiology/chapter/17-9-the-endocrine-pancreas/ (accessed Oct 31, 2019).

(50) Bray, F.; Ferlay, J.; Soerjomataram, I.; Siegel, R. L.; Torre, L. A.; Jemal, A. Global Cancer Statistics 2018: GLOBOCAN Estimates of Incidence and Mortality Worldwide for 36 Cancers in 185 Countries. *CA Cancer J Clin* **2018**, *68* (6), 394–424. https://doi.org/10.3322/caac.21492.

(51) Siegel, R. L.; Miller, K. D.; Jemal, A. Cancer Statistics, 2019. *CA: A Cancer Journal for Clinicians* **2019**, *69* (1), 7–34. https://doi.org/10.3322/caac.21551.

(52) Pelosi, E.; Castelli, G.; Testa, U. Pancreatic Cancer: Molecular Characterization, Clonal Evolution and Cancer Stem Cells. *Biomedicines* **2017**, *5* (4). https://doi.org/10.3390/biomedicines5040065.

(53) Kleeff, J.; Korc, M.; Apte, M.; La Vecchia, C.; Johnson, C. D.; Biankin, A. V.; Neale, R. E.; Tempero, M.; Tuveson, D. A.; Hruban, R. H.; et al. Pancreatic Cancer. *Nature Reviews Disease Primers* **2016**, *2*, 16022. https://doi.org/10.1038/nrdp.2016.22.

(54) Luchini, C.; Capelli, P.; Scarpa, A. Pancreatic Ductal Adenocarcinoma and Its Variants. *Surg Pathol Clin* **2016**, *9* (4), 547–560. https://doi.org/10.1016/j.path.2016.05.003.

(55) Scialpi, M.; Reginelli, A.; D'Andrea, A.; Gravante, S.; Falcone, G.; Baccari, P.; Manganaro, L.; Palumbo, B.; Cappabianca, S. Pancreatic Tumors Imaging: An Update. *International Journal of Surgery* **2016**, *28*, S142–S155. https://doi.org/10.1016/j.ijsu.2015.12.053.

(56) Rahib, L.; Smith, B. D.; Aizenberg, R.; Rosenzweig, A. B.; Fleshman, J. M.; Matrisian, L. M. Projecting Cancer Incidence and Deaths to 2030: The Unexpected Burden of Thyroid, Liver, and Pancreas Cancers in the United States. *Cancer Res* **2014**, *74* (11), 2913–2921. https://doi.org/10.1158/0008-5472.CAN-14-0155.

(57) Rawla, P.; Sunkara, T.; Gaduputi, V. Epidemiology of Pancreatic Cancer: Global Trends, Etiology and Risk Factors. *World J Oncol* **2019**, *10* (1), 10–27. https://doi.org/10.14740/wjon1166.

(58) pubmeddev; al, N. C., et. Demographic, clinical, and pathological features of early onset pancreatic cancer patients. - PubMed - NCBI https://www.ncbi.nlm.nih.gov/pubmed/30208959 (accessed Sep 8, 2019).

(59) Giovannetti, E.; van der Borden, C. L.; Frampton, A. E.; Ali, A.; Firuzi, O.; Peters, G. J. Never Let It Go: Stopping Key Mechanisms Underlying Metastasis to Fight Pancreatic Cancer. *Semin. Cancer Biol.* **2017**, *44*, 43–59. https://doi.org/10.1016/j.semcancer.2017.04.006.

(60) De La Cruz, M. S. D.; Young, A. P.; Ruffin, M. T. Diagnosis and Management of Pancreatic Cancer. *Am Fam Physician* **2014**, *89* (8), 626–632.

(61) Tummers, W. S.; Willmann, J. K.; Bonsing, B. A.; Vahrmeijer, A. L.; Gambhir, S. S.; Swijnenburg, R.-J. Advances in Diagnostic and Intraoperative Molecular Imaging of Pancreatic Cancer. *Pancreas* **2018**, *47* (6), 675–689. https://doi.org/10.1097/MPA.0000000000001075.

(62) Shin, D. W.; Lee, J.-C.; Kim, J.; Woo, S. M.; Lee, W. J.; Han, S.-S.; Park, S.-J.; Choi, K. S.; Cha, H. S.; Yoon, Y.-S.; et al. Validation of the American Joint Committee on Cancer 8th Edition Staging System for the Pancreatic Ductal Adenocarcinoma. *Eur J Surg Oncol* **2019**. https://doi.org/10.1016/j.ejso.2019.06.002.

(63) Adamska, A.; Domenichini, A.; Falasca, M. Pancreatic Ductal Adenocarcinoma: Current and Evolving Therapies. *International Journal of Molecular Sciences* **2017**, *18* (7), 1338. https://doi.org/10.3390/ijms18071338.

(64) Kamarajah, S. K.; Sonnenday, C. J.; Cho, C. S.; Frankel, T. L.; Bednar, F.; Lawrence, T. S.; Nathan, H. Association of Adjuvant Radiotherapy With Survival After Margin-Negative Resection of Pancreatic Ductal Adenocarcinoma: A Propensity-Matched National Cancer Database (NCDB) Analysis. *Ann. Surg.* **2019**. https://doi.org/10.1097/SLA.0000000000003242.

(65) Erlotinib plus gemcitabine compared with gemcitabine alone in patients with advanced pancreatic cancer: a phase III trial of the National Cancer In... - PubMed - NCBI https://www.ncbi.nlm.nih.gov/pubmed/17452677 (accessed Sep 10, 2019).

(66) Chee, C. E.; Krishnamurthi, S.; Nock, C. J.; Meropol, N. J.; Gibbons, J.; Fu, P.; Bokar, J.; Teston, L.; O'Brien, T.; Gudena, V.; et al. Phase II Study of Dasatinib (BMS-354825) in Patients with Metastatic Adenocarcinoma of the Pancreas. *Oncologist* **2013**, *18* (10), 1091–1092. https://doi.org/10.1634/theoncologist.2013-0255.

(67) De Klerk, D. J.; Honeywell, R. J.; Jansen, G.; Peters, G. J. Transporter and Lysosomal Mediated (Multi)Drug Resistance to Tyrosine Kinase Inhibitors and Potential Strategies

to Overcome Resistance. *Cancers* **2018**, *10* (12), 503. https://doi.org/10.3390/cancers10120503.

(68) Arora, S.; Swaminathan, S. K.; Kirtane, A.; Srivastava, S. K.; Bhardwaj, A.; Singh, S.; Panyam, J.; Singh, A. P. Synthesis, Characterization, and Evaluation of Poly (D,L-Lactide-Co-Glycolide)-Based Nanoformulation of MiRNA-150: Potential Implications for Pancreatic Cancer Therapy. *Int J Nanomedicine* **2014**, *9*, 2933–2942. https://doi.org/10.2147/IJN.S61949.

(69) Mittal, A.; Chitkara, D.; Behrman, S. W.; Mahato, R. I. Efficacy of Gemcitabine Conjugated and MiRNA-205 Complexed Micelles for Treatment of Advanced Pancreatic Cancer. *Biomaterials* **2014**, *35* (25), 7077–7087. https://doi.org/10.1016/j.biomaterials.2014.04.053.

(70) Amrutkar, M.; Gladhaug, I. P. Pancreatic Cancer Chemoresistance to Gemcitabine. *Cancers* **2017**, *9* (11), 157. https://doi.org/10.3390/cancers9110157.

(71) Berlin, J. D.; Catalano, P.; Thomas, J. P.; Kugler, J. W.; Haller, D. G.; Benson, A. B. Phase III Study of Gemcitabine in Combination with Fluorouracil versus Gemcitabine Alone in Patients with Advanced Pancreatic Carcinoma: Eastern Cooperative Oncology Group Trial E2297. *J. Clin. Oncol.* **2002**, *20* (15), 3270–3275. https://doi.org/10.1200/JCO.2002.11.149.

(72) Herrmann, R.; Bodoky, G.; Ruhstaller, T.; Glimelius, B.; Bajetta, E.; Schüller, J.; Saletti, P.; Bauer, J.; Figer, A.; Pestalozzi, B.; et al. Gemcitabine plus Capecitabine Compared with Gemcitabine Alone in Advanced Pancreatic Cancer: A Randomized, Multicenter, Phase III Trial of the Swiss Group for Clinical Cancer Research and the Central European Cooperative Oncology Group. *J. Clin. Oncol.* **2007**, *25* (16), 2212–2217. https://doi.org/10.1200/JCO.2006.09.0886.

(73) Cunningham, D.; Chau, I.; Stocken, D. D.; Valle, J. W.; Smith, D.; Steward, W.; Harper, P. G.; Dunn, J.; Tudur-Smith, C.; West, J.; et al. Phase III Randomized Comparison of Gemcitabine versus Gemcitabine plus Capecitabine in Patients with Advanced Pancreatic Cancer. *J. Clin. Oncol.* **2009**, *27* (33), 5513–5518. https://doi.org/10.1200/JCO.2009.24.2446.

(74) Louvet, C.; Labianca, R.; Hammel, P.; Lledo, G.; Zampino, M. G.; André, T.; Zaniboni, A.; Ducreux, M.; Aitini, E.; Taïeb, J.; et al. Gemcitabine in Combination with Oxaliplatin Compared with Gemcitabine Alone in Locally Advanced or Metastatic Pancreatic Cancer: Results of a GERCOR and GISCAD Phase III Trial. *J. Clin. Oncol.* **2005**, *23* (15), 3509–3516. https://doi.org/10.1200/JCO.2005.06.023.

(75) Poplin, E.; Feng, Y.; Berlin, J.; Rothenberg, M. L.; Hochster, H.; Mitchell, E.; Alberts, S.; O'Dwyer, P.; Haller, D.; Catalano, P.; et al. Phase III, Randomized Study of Gemcitabine and Oxaliplatin versus Gemcitabine (Fixed-Dose Rate Infusion) Compared with Gemcitabine (30-Minute Infusion) in Patients with Pancreatic Carcinoma E6201: A Trial of the Eastern Cooperative Oncology Group. *J. Clin. Oncol.* **2009**, *27* (23), 3778–3785. https://doi.org/10.1200/JCO.2008.20.9007.

(76) Colucci, G.; Labianca, R.; Di Costanzo, F.; Gebbia, V.; Cartenì, G.; Massidda, B.; Dapretto, E.; Manzione, L.; Piazza, E.; Sannicolò, M.; et al. Randomized Phase III Trial of Gemcitabine plus Cisplatin Compared with Single-Agent Gemcitabine as First-Line Treatment of Patients with Advanced Pancreatic Cancer: The GIP-1 Study. *J. Clin. Oncol.* **2010**, *28* (10), 1645–1651. https://doi.org/10.1200/JCO.2009.25.4433.

(77) Heinemann, V.; Quietzsch, D.; Gieseler, F.; Gonnermann, M.; Schönekäs, H.; Rost, A.; Neuhaus, H.; Haag, C.; Clemens, M.; Heinrich, B.; et al. Randomized Phase III Trial of Gemcitabine plus Cisplatin Compared with Gemcitabine Alone in Advanced Pancreatic Cancer. *J. Clin. Oncol.* **2006**, *24* (24), 3946–3952. https://doi.org/10.1200/JCO.2005.05.1490.

(78) Von Hoff, D. D.; Ervin, T.; Arena, F. P.; Chiorean, E. G.; Infante, J.; Moore, M.; Seay, T.; Tjulandin, S. A.; Ma, W. W.; Saleh, M. N.; et al. Increased Survival in Pancreatic Cancer with Nab-Paclitaxel plus Gemcitabine. *N. Engl. J. Med.* **2013**, *369* (18), 1691–1703. https://doi.org/10.1056/NEJMoa1304369.

(79) Conroy, T.; Desseigne, F.; Ychou, M.; Bouché, O.; Guimbaud, R.; Bécouarn, Y.; Adenis, A.; Raoul, J.-L.; Gourgou-Bourgade, S.; de la Fouchardière, C.; et al. FOLFIRINOX versus Gemcitabine for Metastatic Pancreatic Cancer. *N. Engl. J. Med.* **2011**, *364* (19), 1817–1825. https://doi.org/10.1056/NEJMoa1011923.

(80) Vogl, U. M.; Andalibi, H.; Klaus, A.; Vormittag, L.; Schima, W.; Heinrich, B.; Kafka, A.; Winkler, T.; Öhler, L. Nab-Paclitaxel and Gemcitabine or FOLFIRINOX as First-Line Treatment in Patients with Unresectable Adenocarcinoma of the Pancreas: Does Sequence Matter? *BMC Cancer* **2019**, *19*. https://doi.org/10.1186/s12885-018-5240-6.

(81) Basturk, O.; Hong, S.-M.; Wood, L. D.; Adsay, N. V.; Albores-Saavedra, J.; Biankin, A. V.; Brosens, L. A. A.; Fukushima, N.; Goggins, M.; Hruban, R. H.; et al. A Revised Classification System and Recommendations From the Baltimore Consensus Meeting for Neoplastic Precursor Lesions in the Pancreas: *The American Journal of Surgical Pathology* **2015**, *39* (12), 1730–1741. https://doi.org/10.1097/PAS.0000000000000533.

(82) Maitra, A.; Hruban, R. H. Pancreatic Cancer. *Annu Rev Pathol* **2008**, *3*, 157–188. https://doi.org/10.1146/annurev.pathmechdis.3.121806.154305.

(83) Tanaka, M.; Chari, S.; Adsay, V.; Carlos Castillo, F.-D.; Falconi, M.; Shimizu, M.; Yamaguchi, K.; Yamao, K.; Matsuno, S. International Consensus Guidelines for Management of Intraductal Papillary Mucinous Neoplasms and Mucinous Cystic Neoplasms of the Pancreas. *Pancreatology* **2006**, *6* (1), 17–32. https://doi.org/10.1159/000090023.

(84) Kota, J.; Hancock, J.; Kwon, J.; Korc, M. Pancreatic Cancer: Stroma and Its Current and Emerging Targeted Therapies. *Cancer Letters* **2017**, *391*, 38–49. https://doi.org/10.1016/j.canlet.2016.12.035.

(85) von Ahrens, D.; Bhagat, T. D.; Nagrath, D.; Maitra, A.; Verma, A. The Role of Stromal Cancer-Associated Fibroblasts in Pancreatic Cancer. *Journal of Hematology & Oncology* **2017**, *10* (1), 76. https://doi.org/10.1186/s13045-017-0448-5.

(86) Yachida, S.; White, C. M.; Naito, Y.; Zhong, Y.; Brosnan, J. A.; Macgregor-Das, A. M.; Morgan, R. A.; Saunders, T.; Laheru, D. A.; Herman, J. M.; et al. Clinical Significance of the Genetic Landscape of Pancreatic Cancer and Implications for Identification of Potential Long-Term Survivors. *Clin Cancer Res* **2012**, *18* (22), 6339–6347. https://doi.org/10.1158/1078-0432.CCR-12-1215.

(87) Mirsadeghi, S.; Larijani, B. Personalized Medicine: Pharmacogenomics and Drug Development. *Acta Med Iran* **2017**, *55* (3), 150–165.

(88) Robert, J.; Le Morvan, V.; Giovannetti, E.; Peters, G. J. On the Use of Pharmacogenetics in Cancer Treatment and Clinical Trials. *European Journal of Cancer* **2014**, *50* (15), 2532–2543. https://doi.org/10.1016/j.ejca.2014.07.013.

(89) Steeg, P. S. Tumor Metastasis: Mechanistic Insights and Clinical Challenges. *Nat. Med.* **2006**, *12* (8), 895–904. https://doi.org/10.1038/nm1469.

(90) Sahin, I. H.; Elias, H.; Chou, J. F.; Capanu, M.; O'Reilly, E. M. Pancreatic Adenocarcinoma: Insights into Patterns of Recurrence and Disease Behavior. *BMC Cancer* **2018**, *18* (1), 769. https://doi.org/10.1186/s12885-018-4679-9.

(91) Wang, S.; Huang, S.; Sun, Y. L. Epithelial-Mesenchymal Transition in Pancreatic Cancer: A Review. *Biomed Res Int* **2017**, *2017*. https://doi.org/10.1155/2017/2646148.

(92) Thiery, J. P.; Acloque, H.; Huang, R. Y. J.; Nieto, M. A. Epithelial-Mesenchymal Transitions in Development and Disease. *Cell* **2009**, *139* (5), 871–890. https://doi.org/10.1016/j.cell.2009.11.007.

(93) Puisieux, A.; Brabletz, T.; Caramel, J. Oncogenic Roles of EMT-Inducing Transcription Factors. *Nat. Cell Biol.* **2014**, *16* (6), 488–494. https://doi.org/10.1038/ncb2976.

(94) Peng, X.; Guan, J.-L. Focal Adhesion Kinase: From in Vitro Studies to Functional Analyses in Vivo. *Curr. Protein Pept. Sci.* **2011**, *12* (1), 52–67.

(95) Hall, J. E.; Fu, W.; Schaller, M. D. Chapter Five - Focal Adhesion Kinase: Exploring FAK Structure to Gain Insight into Function. In *International Review of Cell and Molecular Biology*; Jeon, K. W., Ed.; Academic Press, 2011; Vol. 288, pp 185–225. https://doi.org/10.1016/B978-0-12-386041-5.00005-4.

(96) Begum, A.; Ewachiw, T.; Jung, C.; Huang, A.; Norberg, K. J.; Marchionni, L.; McMillan, R.; Penchev, V.; Rajeshkumar, N. V.; Maitra, A.; et al. The Extracellular Matrix and Focal Adhesion Kinase Signaling Regulate Cancer Stem Cell Function in Pancreatic Ductal Adenocarcinoma. *PLOS ONE* **2017**, *12* (7), e0180181. https://doi.org/10.1371/journal.pone.0180181.

(97) Kanteti, R.; Mirzapoiazova, T.; Riehm, J. J.; Dhanasingh, I.; Mambetsariev, B.; Wang, J.; Kulkarni, P.; Kaushik, G.; Seshacharyulu, P.; Ponnusamy, M. P.; et al. Focal Adhesion Kinase a Potential Therapeutic Target for Pancreatic Cancer and Malignant Pleural Mesothelioma. *Cancer Biology & Therapy* **2018**, *19* (4), 316–327. https://doi.org/10.1080/15384047.2017.1416937.

(98) Mutsaers, S. Mesothelial Cells: Their Structure, Function and Role in Serosal Repair. *Respirology (Carlton, Vic.)* **2002**, *7*, 171–191. https://doi.org/10.1046/j.1440-1843.2002.00404.x.

(99) Mutsaers, S. E.; Prêle, C. M.-A.; Pengelly, S.; Herrick, S. E. Mesothelial Cells and Peritoneal Homeostasis. *Fertility and Sterility* **2016**, *106* (5), 1018–1024. https://doi.org/10.1016/j.fertnstert.2016.09.005.

(100) Yung, S.; Chan, T. M. Pathophysiological Changes to the Peritoneal Membrane during PD-Related Peritonitis: The Role of Mesothelial Cells. *Mediators Inflamm* **2012**, *2012*. https://doi.org/10.1155/2012/484167.

(101) Tischoff, I.; Neid, M.; Neumann, V.; Tannapfel, A. Pathohistological Diagnosis and Differential Diagnosis. In *Malignant Mesothelioma*; Tannapfel, A., Ed.; Springer Berlin Heidelberg: Berlin, Heidelberg, 2011; Vol. 189, pp 57–78. https://doi.org/10.1007/978-3-642-10862-4_5.

(102) Factors associated with survival in a large series of patients with malignant pleural mesothelioma in New South Wales https://www.ncbi.nlm.nih.gov/pmc/articles/PMC4453733/ (accessed Sep 19, 2019).

(103) Baumann, F.; Carbone, M. Environmental Risk of Mesothelioma in the United States: An Emerging Concern-Epidemiological Issues. *J Toxicol Environ Health B Crit Rev* **2016**, *19* (5–6), 231–249. https://doi.org/10.1080/10937404.2016.1195322.

(104) Nabavi, N.; Bennewith, K. L.; Churg, A.; Wang, Y.; Collins, C. C.; Mutti, L. Switching off Malignant Mesothelioma: Exploiting the Hypoxic Microenvironment. *Genes Cancer* **2016**, *7* (11–12), 340–354. https://doi.org/10.18632/genesandcancer.124.

(105) Carbone, M.; Adusumilli, P. S.; Alexander, H. R.; Baas, P.; Bardelli, F.; Bononi, A.; Bueno, R.; Felley-Bosco, E.; Galateau-Salle, F.; Jablons, D.; et al. Mesothelioma: Scientific Clues for Prevention, Diagnosis, and Therapy. *CA Cancer J Clin* **2019**. https://doi.org/10.3322/caac.21572.

(106) Malignant Mesothelioma Stages https://www.cancer.org/cancer/malignant-mesothelioma/detection-diagnosis-staging/staging.html (accessed Sep 22, 2019).

(107) Sugarbaker, P. H. Update on the Management of Malignant Peritoneal Mesothelioma. *Transl Lung Cancer Res* **2018**, *7* (5), 599–608. https://doi.org/10.21037/tlcr.2018.08.03.

(108) Rusch, V. W.; Giroux, D.; Kennedy, C.; Ruffini, E.; Cangir, A. K.; Rice, D.; Pass, H.; Asamura, H.; Waller, D.; Edwards, J.; et al. Initial Analysis of the International Association For the Study of Lung Cancer Mesothelioma Database. *Journal of Thoracic Oncology* **2012**, *7* (11), 1631–1639. https://doi.org/10.1097/JTO.0b013e31826915f1.

(109) Mutti, L.; Peikert, T.; Robinson, B. W. S.; Scherpereel, A.; Tsao, A. S.; de Perrot, M.; Woodard, G. A.; Jablons, D. M.; Wiens, J.; Hirsch, F. R.; et al. Scientific Advances and New Frontiers in Mesothelioma Therapeutics. *J Thorac Oncol* **2018**, *13* (9), 1269–1283. https://doi.org/10.1016/j.jtho.2018.06.011.

(110) Vogelzang, N. J.; Rusthoven, J. J.; Symanowski, J.; Denham, C.; Kaukel, E.; Ruffie, P.; Gatzemeier, U.; Boyer, M.; Emri, S.; Manegold, C.; et al. Phase III Study of Pemetrexed in Combination with Cisplatin versus Cisplatin Alone in Patients with Malignant Pleural Mesothelioma. *J. Clin. Oncol.* **2003**, *21* (14), 2636–2644. https://doi.org/10.1200/JCO.2003.11.136.

(111) Ceresoli, G. L.; Castagneto, B.; Zucali, P. A.; Favaretto, A.; Mencoboni, M.; Grossi, F.; Cortinovis, D.; Del Conte, G.; Ceribelli, A.; Bearz, A.; et al. Pemetrexed plus Carboplatin in Elderly Patients with Malignant Pleural Mesothelioma: Combined

Analysis of Two Phase II Trials. *Br. J. Cancer* **2008**, *99* (1), 51–56. https://doi.org/10.1038/sj.bjc.6604442.

(112) Mutlu, H.; Gündüz, S.; Karaca, H.; Büyükçelik, A.; Cihan, Y. B.; Erden, A.; Akca, Z.; Coşkun, H. S. Second-Line Gemcitabine-Based Chemotherapy Regimens Improve Overall 3-Year Survival Rate in Patients with Malignant Pleural Mesothelioma: A Multicenter Retrospective Study. *Med. Oncol.* **2014**, *31* (8), 74. https://doi.org/10.1007/s12032-014-0074-9.

(113) Ruan, K.; Song, G.; Ouyang, G. Role of Hypoxia in the Hallmarks of Human Cancer. *J. Cell. Biochem.* **2009**, *107* (6), 1053–1062. https://doi.org/10.1002/jcb.22214.

(114) Doktorova, H.; Hrabeta, J.; Khalil, M. A.; Eckschlager, T. Hypoxia-Induced Chemoresistance in Cancer Cells: The Role of Not Only HIF-1. *Biomed Pap Med Fac Univ Palacky Olomouc Czech Repub* **2015**, *159* (2), 166–177. https://doi.org/10.5507/bp.2015.025.

(115) Klabatsa, A.; Sheaff, M. T.; Steele, J. P. C.; Evans, M. T.; Rudd, R. M.; Fennell, D. A. Expression and Prognostic Significance of Hypoxia-Inducible Factor 1α (HIF-1α) in Malignant Pleural Mesothelioma (MPM). *Lung Cancer* **2006**, *51* (1), 53–59. https://doi.org/10.1016/j.lungcan.2005.07.010.

(116) Arnold, D. T.; Maskell, N. A. Biomarkers in Mesothelioma. *Ann Clin Biochem* **2018**, *55* (1), 49–58. https://doi.org/10.1177/0004563217741145.

Part I

In vitro pharmacological studies as important tools in large-scale drug discovery, and approaches to the combination therapy with special focus on PDAC cancer

(chapters 2-4)

Chapter 2

A Brief Guide to Performing Pharmacological Studies In Vitro: Reflections from the EORTC-PAMM Course "Preclinical and Early-phase Clinical Pharmacology"

Capula M[1], Corno C[2], El Hassouni B[3], **Li Petri G[3,4]**, Aranđelović S[5]; EORTC PAMM Group

1. *Fondazione Pisana per la Scienza-ONLUS, Pisa, Italy*
2. *Molecular Pharmacology Unit, Department of Applied Research and Technological Development, Fondazione IRCCS, Istituto Nazionale dei Tumori, Milan, Italy*
3. *Amsterdam UMC, VU University of Amsterdam, Medical Oncology, Cancer Center Amsterdam, Amsterdam, the Netherlands*
4. *Department of Biological, Chemical and Pharmaceutical Sciences and Technologies (STEBICEF), University of Palermo, Palermo, Italy*
5. *Laboratory of Pharmacology, Department of Experimental Oncology, Institute for Oncology and Radiology of Serbia, Belgrade, Serbia*

Anticancer Research 2019 July;39(7):3413-3418

doi: 10.21873/anticanres.13485

A Brief Guide to Performing Pharmacological Studies In Vitro: Reflections from the EORTC-PAMM Course "Preclinical and Early-phase Clinical Pharmacology"

Abstract

One aim of cell-based *in vitro* assays is to identify the best drug candidate to develop using the best tumor cell model. This is challenging in every anticancer drug discovery process. Briefly, we summarize the parameters to be taken into account when performing *in vitro* cell assays, in order to obtain reliable and reproducible results, which was fundamentally discussed by lecturers at the educational course on preclinical and early-phase clinical pharmacology studies, at the 40th Winter Meeting of the Pharmacology and Molecular Mechanisms Group of the European Organization for Research and Treatment of Cancer. Moreover, specific cellular sensitivity tests are described. In addition to monolayer *in vitro* cell models for the screening of new potential candidate drugs, three-dimensional tumor/cell tissue models are emerging as new pre-clinical tools that more closely reflect the *in vivo* microenvironment. Therefore, the use of different *in vitro* models for drug screening can enhance the predictability and reliability of pre-clinical drug-discovery phases and target validation.

Keywords: *In vitro*; anticancer drugs; cell-sensitivity assays; review; tumor cells

Introduction

Over the past decades conventional approaches to anticancer drug discovery have largely relied on screening for determining biological activity and deriving structure–activity relationships, with testing for improved drug efficacy, based on assays in immortalized cancer cell lines as the first preclinical step, which is simple and reliable.[1–5] Mechanism-of-action studies of drug candidates are performed *in vitro*, using a wide variety of time- and cost-effective techniques in order to define which compounds should progress to the next stage in the drug development process. Monolayer cultures are the easiest and most 'controllable' models for the evaluation of drug potency for most cytotoxic agents. However, this simple model does not capture the complexity of the physiological microenvironment. It is becoming more and more evident that the tumor microenvironment is highly complex and heterogeneous, and that it plays a critical role in tumor cell dissemination and multi-drug resistance.[6,7] Availability of high-throughput screening approaches and advances in genomics and proteomics are shifting standards of preclinical drug testing from empirical to target-based approaches, aimed at identifying genetic, transcriptional, and protein biomarkers of drug sensitivity and resistance.[8,9] Discovery of important signaling pathways and mutations that drive cancerous transformation lead to the development of more selective drugs to combat cancer, such as tyrosine kinase inhibitors (gefitinib, erlotinib, osimertinib), poly (ADP-ribose) polymerase inhibitors (olaparib), proteasome inhibitors (bortezomib) and many monoclonal antibodies (trastuzumab, ramucirumab).[10–15]

New knowledge has led investigators to incorporate a variety of cell lines and tumor cell-tissue models into the screening protocols of potential anticancer drug candidates, including cell lines harboring specific mutations, human tumor stem cells and endothelial cells lines.[16,17] There is a need for a better understanding of the complex interplay between cancer cells and neighboring cells, including stromal and immune system cells that lead to restructuration of the extracellular matrix and formation of chaotic vascularization structures, which eventually leads to metastasis. How tumor cells modulate their environment is of utmost relevance in defining efficient therapy strategies, as well as appropriate *in vitro* systems for drug evaluation.[18,19]

At the 40th Winter Meeting of The Pharmacology and Molecular Mechanisms (PAMM) group within European Organization for Research and Treatment of Cancer (EORTC), 2019, in Verona, Italy, the topics of the educational course on preclinical and early-phase clinical pharmacology studies addressed the new emerging concepts and current needs and challenges in preclinical drug investigation and therapeutics development. Utilization of

in vitro, *ex vivo*, and *in silico* approaches in preclinical drug testing was thoroughly discussed by the presenters of the EORTC-PAMM Group (http://www.eortc.org/researchfield/pharmacology-molecular-mechanisms). Here, we briefly summarize the main criteria to be used in planning *in vitro* studies. The knowledge of basic concepts and awareness of troubleshooting in performing preclinical pharmacological studies *in vitro* are fundamental to producing reliable results.

How to Perform Preclinical Pharmacological Studies *In Vitro*

The measurement of drug dose–response in cultured cells is the cornerstone of preclinical assessment of anticancer drugs. High-throughput experimentation in multi-well plates, such as that carried out in the context of the NCI-60 program in which a panel of 60 different human tumor cell lines from nine different types of cancer were tested, is the most representative example of *in vitro* drug screening on a large-scale, with improved reproducibility (http://www.lincsproject.org/).[20]

Considering that most research laboratories evaluate the activity of new compounds using few cell lines, utilization of suitable cellular models and appropriate chemosensitivity assay are of critical importance in achieving major goals, specifically in order to: a) identify new potential agents; b) determine their mechanism of action; c) understand the cellular response to the investigated drug.[3,21] Suggestions are to use cell lines with specific biological characteristics that match the rationale of compound design. More specifically, authenticated cell lines should be used to ensure the validity of the data. Authentication may be provided by short tandem repeat profiling, which is the analysis of microsatellite regions of DNA that have variable numbers of repeats and are located throughout the genome.

In many types of cancer, such as pancreatic, the subpopulation of cancer stem cells (CSCs) is highly enriched. CSCs are resistant to current chemotherapeutic drugs and therefore are thought to promote tumour recurrence.[22,23] CSCs are self-renewing tumor-initiating cells; in principle, they are good experimental models, but they need to be well characterized with appropriate markers. Immortalized human umbilical vein endothelial cells, which express integrin subunits consistent with an endothelial origin, and transformed human umbilical vein endothelial cells (EA.hy 926) provide valuable *in vitro* models for studying molecular mechanisms underlying endothelial cell proliferation and migration during tumor metastasis.[17,24] Among the basic conditions related to the investigated tumor cell lines that should be predetermined and recorded as part of the dose–response measurement are plating density, and the proliferative rate/cell-doubling time.

The impact of the type and volume of medium used, should be determined empirically for each cell line prior to study and should be set so as to have as little effect as possible, on growth rate over the incubation period.

Performing Reliable Cell-survival and Cell Growth-inhibition Assays

Although simple in principle, cell-based assays are subject to a variety of factors that can affect the results, making data unreliable (examples are listed in table I). Thus, basics principles have to be followed when designing and performing cell-based assays *in vitro*.[3]

Table I. Factors influencing the reliability and reproducibility of in vitro experiments.

Drug solvent	• Incorrect solvent can influence drug stability, leading to inaccurate concentration determination • Final concentration of solvent should be non-toxic to cells
Drug concentration	• Pharmacologically/clinically relevant concentrations should be used for established drugs • Broad ranges can be used for initial screening with novel compounds, followed by a narrow range around concentrations leading to response
Drug exposure duration	• Duration of drug exposure should match the *in vivo* situation • Metabolism of the drug should be taken into account
Seeding density and assay timing	• Cell density and assay timing are cell line-dependent and should be optimized accordingly

Performing reliable cell-survival assays requires careful control over key pharmacological parameters that affect the proliferative rate of tumor cells *in vitro*. Suggestions are to carefully account for **a)** an appropriate drug solvent; **b)** pharmacologically relevant drug concentrations for established drugs and novel compounds; **c)** duration of drug exposure that would match the *in vivo* situation (*e.g.* reflecting time of plasma peaks and drug persistence); **d)** optimization of cell-seeding density and assay timing to the particular cell-doubling time.

Choosing an appropriate drug solvent is critical in that a solvent may influence the stability of the drug. Attention should be paid so that solvents are used at concentrations that are non-toxic for the cells. If the compound is stable once dissolved, it can be stocked at low temperature (−20°C, −80°C), otherwise it has to be freshly dissolved prior to use. It is also important to know if a compound shows protein binding and if this is reversible. Dimethyl sulfoxide [DMSO, $O=S(CH_3)_2$], is viewed as a 'universal' solvent able to solubilize most small molecules at high concentrations (up to 100 mmol/L). However, using DMSO as a solvent might be inappropriate.[25] It should also be recognized whether the tested compound is a pro-drug and whether it can be substituted for the active metabolite. For metal-based drugs such as Pt(II) or Ru(II) complexes, in aqueous solution exchange of the anionic (halide) ligands is considered as a part of complex activation.[26] Activation of organometallic ruthenium pro-drugs by substitution reactions under physiological (intracellular) conditions enhances their reactivity with nucleophilic targets

in cells, such as DNA. However, the drug needs to be stable throughout storage and the experiment, particularly as continuous exposure may lead to drug (chemical) breakdown. Stability in a particular solvent (DMSO, saline) may be determined by nuclear magnetic resonance (NMR) spectroscopy in order to confirm that structures of complexes in solution do not change over time, for example, that coordinated ligands remain at the same position around the metal center.[26,27]

In order to determine the approximate range of drug sensitivity for the cell lines under study, it is often advisable to run a preliminary experiment. When no prior information is available, the standard approach should be to perform cell-sensitivity assays, using serial dilutions of the tested drug, at concentrations ranging from 10 nM to 100 μM, with half-$\log_{10}$ steps.[28] Dose–response studies should be followed by analysis of more narrowly spaced concentrations around the responsive range. The process of reliably and accurately treating cells with drug is not inconsequential. It is highly recommended to carry out the relevant experiments, using clinically meaningful concentrations with a standard agent as reference, and comparative activity against non-cancer cells is desirable. High drug concentrations should only be used for a short treatment duration.

In Vitro Cell-Sensitivity Assays

Two key pharmacological parameters that determine cellular response are the concentration (C) of a drug and the duration of drug exposure (T).[3,20] For conventional cytotoxic agents, cell proliferation and survival in monolayer (2D) cultures are usually proportional to the product of C × T, with the exception of drugs that are cell-cycle phase-specific, where cellular response above a threshold concentration is typically proportional to exposure.[29]

Time-dependent measurement that reveal changes in response over time, adapted to plate-based experiments, can be performed using various approaches. The achievement of reliable, relevant and reproducible results depends on the selection of an appropriate assay, and experimental design. The choice of the specific cell-sensitivity assay should be made so that the endpoint of the assay addresses the experimental question correctly.

The colony-forming assay, in which the clonogenic capability of cells is evaluated, represents the gold standard of cell-sensitivity assays. Cells are considered clonogenic if they maintain the capacity to proliferate indefinitely and to form a clone or colony (Figure 1A).[16] Untreated cells plated as a single-cell suspension at low densities (2–50 cells/cm^2) can generate colonies. The loss of reproductive integrity can be related to the antitumor activity of compounds by a curve where survival is expressed as a function of drug

concentration. Critical parameters for this type of assay are: Plating efficiency (PE) = ratio of the number of colonies to the number of cells seeded; surviving fraction (SF) = number of colonies after treatment of cells expressed in terms of PE.

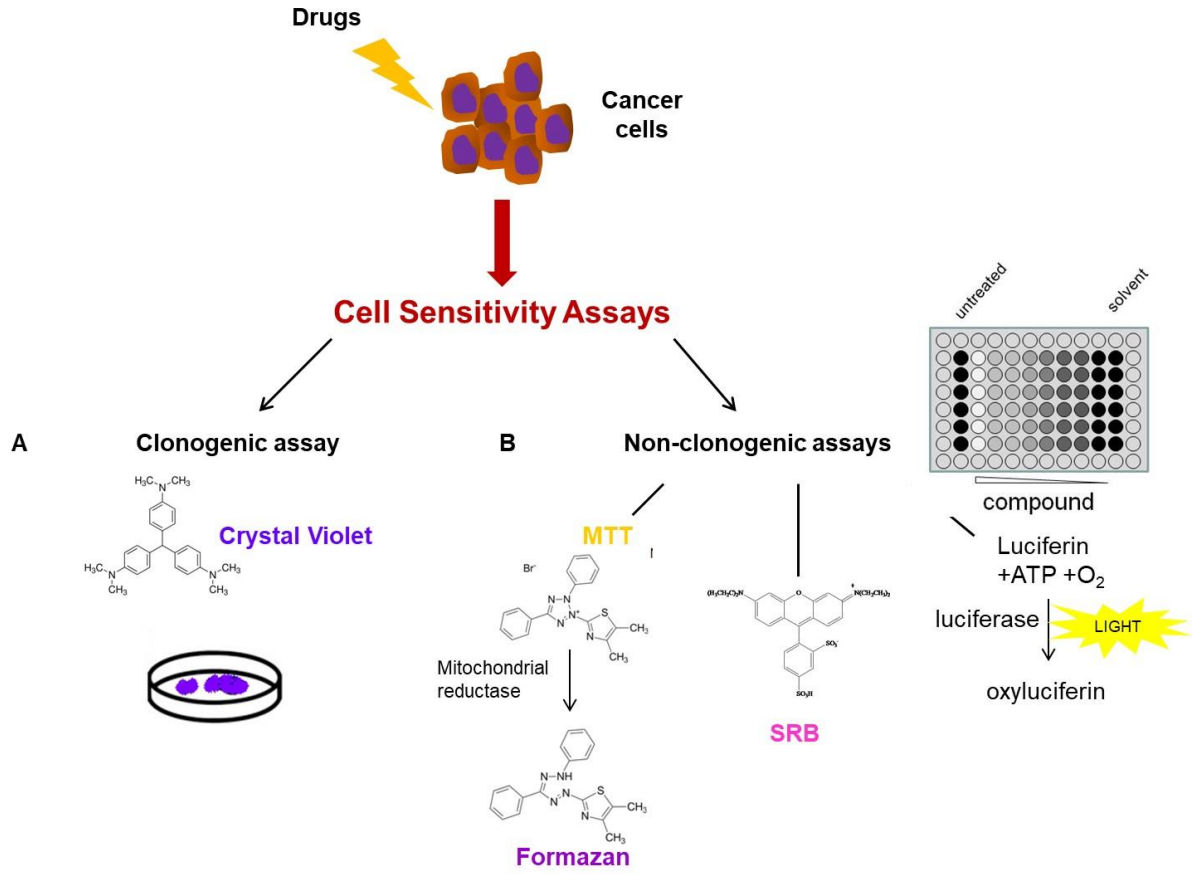

Figure 1. Schematic representation of cell-sensitivity assays. The most common assays used to evaluate the sensitivity of tumor cells to anticancer drugs are shown. Clonogenic assays comprise the analysis of the ability of a compound to inhibit the formation of cell colonies on plastic or agar (A). Non-clonogenic assays are the most commonly employed cell-sensitivity assays with an endpoint different from clonogenic capability (B).

There are multiple methods for determining cell sensitivity to drugs based on cell ability to either bind, exclude or metabolize certain dyes, such as those in assays using trypan blue exclusion, sulforhodamine B (SRB), tetrazolium or resazurine reduction, and ATP content.

(i) In the tetrazolium reduction assay, [3-(4,5-dimethylthiazol-2-yl)-2,5 diphenyltetrazolium bromide] (**MTT**), the most commonly utilized of the tetrazolium family, is added to cultures in which the viable cells (metabolically active), are able to convert these compounds into colored formazan products, that can be colorimetrically detected at 570 nm, with a microplate reader (Figure 1B).[30] Assay

conditions need to be standardized for each cell line, as formazan production varies depending on the cell line and on cell number.

(ii) The SRB assay is a rapid and sensitive method utilizing a bright pink anionic dye that binds electrostatically to the basic amino acids of trichloroacetic acid (TCA)-fixed cells (Figure 1B).[31] The protein-bound dye is extracted with Tris base [tris (hydroxymethyl) aminomethane], after washing off the unbound dye, and the protein content can be quantified colorimetrically at 550 nm with a microplate reader. The endpoint of SRB assay is nondestructive, not time critical (stable) and comparable with those of other assays. Although labor-intensive with several washing steps, it offers a practical advantage of high-throughput screening of anticancer drugs, and the results obtained with SRB assay are not significantly different from those obtained with the MTT assay.[30]

(iii) The ATP content assay is based on the key role of ATP in cellular biological processes as the main carrier of energy in cells and on the relationship between ATP concentration in all living cells and cell biomass. When the cellular membrane loses its integrity, the ability to produce ATP is also lost and the remaining ATP is quickly consumed by endogenous ATP-ases. Therefore, the ATP assay is used to assess cell viability through high-throughput screening platforms using an ATP detection kit. When these assays are used, the following parameters can be obtained:

- IC_{50}: Concentration of agent that inhibits cell growth/survival (in the case of colony-forming assay) by 50%;
- GI_{50}: agent concentration which inhibits growth by 50%;
- TGI: total growth inhibition;
- LC_{50}: concentration leading to death of 50% initially seeded cells, the lethal concentration (see https://dtp.cancer.gov/discovery_development/nci-60/methodology.htlm) (Figure 2).

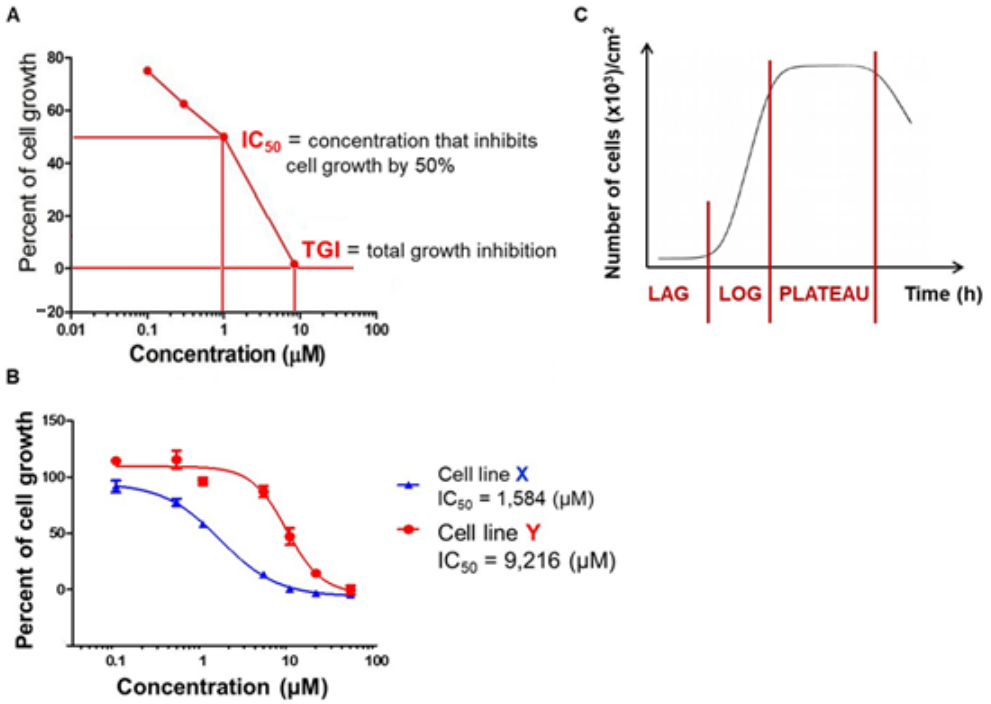

Figure 2. Graphical representation of relevant cell-pharmacological parameters.

A: Representative plot from a cell-sensitivity assay where cell growth inhibition is measured. Concentration that inhibits cell growth by 50 % (IC_{50}), and Total Growth Inhibition (TGB) values are determined from the plot. **B:** Plots of drug concentration-dependent decrease of cell growth (%) for two different tumor cell lines (X, Y). **C:** The different phases of tumor cell growth in monolayer culture and drug-free medium are shown.

Quality Control of Cell Culture

The most frequent type of contamination of cell cultures *in vitro* is Mycoplasma, representing over 20% among culture contaminants.[32] These bacteria belong to the order of Mollicutes, characterized by the lack of a cell wall, and affect cellular physiology. Mycoplasma can pass through filters (220 nm pores), the source of contamination most often other cultures, serum, feeder layers, and infected personnel. A few techniques are available to detect Mycoplasma contamination such as growth in broth, staining, (*e.g.*, 4′,6-diamidino-2-phenylindole, DAPI), polymerase chain reaction, and ATP luminometry. As well as cell line authentication by short tandem repeat analysis, detection of Mycoplasma contamination should be a routine test when running cell pharmacology assays.[33]

The use of 2D cell-culture systems for the discovery of new anticancer drugs represents a simple, reliable and economical approach in pre-clinical phases, and provides important information about drug activity, in terms of growth inhibition potency and cytotoxicity. However, these kind of assays do not consider the complexity of the tumor microenvironment, often inducing different responses to the same treatment in *in vitro* and

in vivo tests. Through the cooperative work of cell biologists and bioengineers, new scaffolds for 3D tumor cell/tissue growth have been generated. Multicellular spheroids and organoids also represent valuable models for use in cellular pharmacology studies, exploitable even in co-culture approaches. They mimic the *in vivo* cellular microenvironment, taking into account the influence of specific parameters on drug response, including the physical and mechanical properties of the extracellular matrix, the oxygen gradient, extracellular pH and gradient of nutrients, as well as drug transport. Although some obstacles must be overcome, such as the use of suitable coating matrices, 3D cultures are considered useful future tools for obtaining more reliable results in pre-clinical trials for high-throughput screening in the drug discovery and target validation.

Acknowledgements

This review article was prepared on behalf of the EORTC-PAMM Group, the organizing committee of the EORT-PAMM winter meeting and the educational course on Pre-clinical Pharmacology of Anticancer Drugs 2019,Verona, Italy

Conflicts of Interest

The authors wish to confirm that there are no known conflicts of interest associated with this publication and there has been no significant financial support for this work that could have influenced its outcome.

Authors' contributions

All authors made equal and substantial contributions to conception, design and writing of the paper.

References

(1) Kelland, L. R. Preclinical Perspectives on Platinum Resistance. *Drugs* **2000**, *59 Suppl 4*, 1–8; discussion 37-38. https://doi.org/10.2165/00003495-200059004-00001.

(2) Ziegler, C. J.; Silverman, A. P.; Lippard, S. J. High-Throughput Synthesis and Screening of Platinum Drug Candidates. *J. Biol. Inorg. Chem.* **2000**, *5* (6), 774–783.

(3) Perego, P.; Hempel, G.; Linder, S.; Bradshaw, T. D.; Larsen, A. K.; Peters, G. J.; Phillips, R. M.; EORTC PAMM Group. Cellular Pharmacology Studies of Anticancer Agents: Recommendations from the EORTC-PAMM Group. *Cancer Chemother. Pharmacol.* **2018**, *81* (3), 427–441. https://doi.org/10.1007/s00280-017-3502-7.

(4) Giovannetti, E.; Zucali, P. A.; Assaraf, Y. G.; Leon, L. G.; Smid, K.; Alecci, C.; Giancola, F.; Destro, A.; Gianoncelli, L.; Lorenzi, E.; et al. Preclinical Emergence of Vandetanib as a Potent Antitumour Agent in Mesothelioma: Molecular Mechanisms Underlying Its Synergistic Interaction with Pemetrexed and Carboplatin. *Br J Cancer* **2011**, *105* (10), 1542–1553. https://doi.org/10.1038/bjc.2011.400.

(5) Massihnia, D.; Avan, A.; Funel, N.; Maftouh, M.; van Krieken, A.; Granchi, C.; Raktoe, R.; Boggi, U.; Aicher, B.; Minutolo, F.; et al. Phospho-Akt Overexpression Is Prognostic and Can Be Used to Tailor the Synergistic Interaction of Akt Inhibitors with Gemcitabine in Pancreatic Cancer. *Journal of Hematology & Oncology* **2017**, *10* (1), 9. https://doi.org/10.1186/s13045-016-0371-1.

(6) van Beijnum, J. R.; Giovannetti, E.; Poel, D.; Nowak-Sliwinska, P.; Griffioen, A. W. MiRNAs: Micro-Managers of Anticancer Combination Therapies. *Angiogenesis* **2017**, *20* (2), 269–285. https://doi.org/10.1007/s10456-017-9545-x.

(7) Phillips, R. M. Targeting the Hypoxic Fraction of Tumours Using Hypoxia-Activated Prodrugs. *Cancer Chemother. Pharmacol.* **2016**, *77* (3), 441–457. https://doi.org/10.1007/s00280-015-2920-7.

(8) Roma-Rodrigues, C.; Mendes, R.; Baptista, P. V.; Fernandes, A. R. Targeting Tumor Microenvironment for Cancer Therapy. *Int J Mol Sci* **2019**, *20* (4). https://doi.org/10.3390/ijms20040840.

(9) Castagna, A.; Antonioli, P.; Astner, H.; Hamdan, M.; Righetti, S. C.; Perego, P.; Zunino, F.; Righetti, P. G. A Proteomic Approach to Cisplatin Resistance in the Cervix Squamous Cell Carcinoma Cell Line A431. *Proteomics* **2004**, *4* (10), 3246–3267. https://doi.org/10.1002/pmic.200400835.

(10) Burger, A. M. Highlights in Experimental Therapeutics. *Cancer Lett.* **2007**, *245* (1–2), 11–21. https://doi.org/10.1016/j.canlet.2006.03.012.

(11) Erdem, L.; Giovannetti, E.; Leon, L. G.; Honeywell, R.; Peters, G. J. Polymorphisms to Predict Outcome to the Tyrosine Kinase Inhibitors Gefitinib, Erlotinib, Sorafenib and Sunitinib. *Curr Top Med Chem* **2012**, *12* (15), 1649–1659. https://doi.org/10.2174/156802612803531333.

(12) Lamb, Y. N.; Scott, L. J. Osimertinib: A Review in T790M-Positive Advanced Non-Small Cell Lung Cancer. *Target Oncol* **2017**, *12* (4), 555–562. https://doi.org/10.1007/s11523-017-0519-0.

(13) Evers, B.; Schut, E.; van der Burg, E.; Braumuller, T. M.; Egan, D. A.; Holstege, H.; Edser, P.; Adams, D. J.; Wade-Martins, R.; Bouwman, P.; et al. A High-Throughput Pharmaceutical Screen Identifies Compounds with Specific Toxicity against BRCA2-Deficient Tumors. *Clin. Cancer Res.* **2010**, *16* (1), 99–108. https://doi.org/10.1158/1078-0432.CCR-09-2434.

(14) Gatti, L.; Zuco, V.; Zaffaroni, N.; Perego, P. Drug Combinations with Proteasome Inhibitors in Antitumor Therapy. *Curr. Pharm. Des.* **2013**, *19* (22), 4094–4114. https://doi.org/10.2174/1381612811319220015.

(15) Gatti, L.; Benedetti, V.; De Cesare, M.; Corna, E.; Cincinelli, R.; Zaffaroni, N.; Zunino, F.; Perego, P. Synergistic Interaction between the Novel Histone Deacetylase Inhibitor ST2782 and the Proteasome Inhibitor Bortezomib in Platinum-Sensitive and Resistant Ovarian Carcinoma Cells. *J. Inorg. Biochem.* **2012**, *113*, 94–101. https://doi.org/10.1016/j.jinorgbio.2012.04.007.

(16) Hamburger, A. W.; Salmon, S. E. Primary Bioassay of Human Tumor Stem Cells. *Science* **1977**, *197* (4302), 461–463. https://doi.org/10.1126/science.560061.

(17) Rhim, J. S.; Tsai, W. P.; Chen, Z. Q.; Chen, Z.; Van Waes, C.; Burger, A. M.; Lautenberger, J. A. A Human Vascular Endothelial Cell Model to Study Angiogenesis and Tumorigenesis. *Carcinogenesis* **1998**, *19* (4), 673–681. https://doi.org/10.1093/carcin/19.4.673.

(18) Langhans, S. A. Three-Dimensional in Vitro Cell Culture Models in Drug Discovery and Drug Repositioning. *Front. Pharmacol.* **2018**, *9*. https://doi.org/10.3389/fphar.2018.00006.

(19) Mebarki, M.; Bennaceur, A.; Bonhomme-Faivre, L. Human-Cell-Derived Organoids as a New Ex Vivo Model for Drug Assays in Oncology. *Drug Discovery Today* **2018**, *23* (4), 857–863. https://doi.org/10.1016/j.drudis.2018.02.003.

(20) Su, G.; Burant, C. F.; Beecher, C. W.; Athey, B. D.; Meng, F. Integrated Metabolome and Transcriptome Analysis of the NCI60 Dataset. *BMC Bioinformatics* **2011**, *12 Suppl 1*, S36. https://doi.org/10.1186/1471-2105-12-S1-S36.

(21) Kumar, S.; Bajaj, S.; Bodla, R. B. Preclinical Screening Methods in Cancer. *Indian J Pharmacol* **2016**, *48* (5), 481–486. https://doi.org/10.4103/0253-7613.190716.

(22) Avan, A.; Quint, K.; Nicolini, F.; Funel, N.; Frampton, A. E.; Maftouh, M.; Pelliccioni, S.; Schuurhuis, G. J.; Peters, G. J.; Giovannetti, E. Enhancement of the Antiproliferative Activity of Gemcitabine by Modulation of C-Met Pathway in Pancreatic Cancer. *Curr. Pharm. Des.* **2013**, *19* (5), 940–950.

(23) Bertolini, G.; D'Amico, L.; Moro, M.; Landoni, E.; Perego, P.; Miceli, R.; Gatti, L.; Andriani, F.; Wong, D.; Caserini, R.; et al. Microenvironment-Modulated Metastatic CD133+/CXCR4+/EpCAM- Lung Cancer-Initiating Cells Sustain Tumor Dissemination and Correlate with Poor Prognosis. *Cancer Res.* **2015**, *75* (17), 3636–3649. https://doi.org/10.1158/0008-5472.CAN-14-3781.

(24) Lana, F.; Sandra, A.; Ana, K.; Radmila, J.; Biljana, D.; Siniša, R. Trans-Platinum(II)/(IV) Complexes with Acetylpyridine Ligands as Antivascular Agents in Vitro: Cytotoxic and Antiangiogenic Potential. *Anticancer Agents Med Chem* **2016**, *16* (12), 1628–1639.

(25) Hall, M. D.; Telma, K. A.; Chang, K.-E.; Lee, T. D.; Madigan, J. P.; Lloyd, J. R.; Goldlust, I. S.; Hoeschele, J. D.; Gottesman, M. M. Say No to DMSO: Dimethylsulfoxide Inactivates Cisplatin, Carboplatin, and Other Platinum Complexes. *Cancer Res.* **2014**, *74* (14), 3913–3922. https://doi.org/10.1158/0008-5472.CAN-14-0247.

(26) Patra, M.; Joshi, T.; Pierroz, V.; Ingram, K.; Kaiser, M.; Ferrari, S.; Spingler, B.; Keiser, J.; Gasser, G. DMSO-Mediated Ligand Dissociation: Renaissance for Biological Activity of N-Heterocyclic-[Ru(H6-Arene)Cl2] Drug Candidates. *Chemistry* **2013**, *19* (44), 14768–14772. https://doi.org/10.1002/chem.201303341.

(27) Strong in Vitro Cytotoxic Potential of New Ruthenium–Cymene Complexes | Organometallics https://pubs.acs.org/doi/abs/10.1021/acs.organomet.5b00041 (accessed Sep 28, 2019).

(28) Boyd, M. R. The NCI Human Tumor Cell Line (60-Cell) Screen. In *Anticancer Drug Development Guide: Preclinical Screening, Clinical Trials, and Approval*; Teicher, B. A., Andrews, P. A., Eds.; Cancer Drug Discovery and Development; Humana Press: Totowa, NJ, 2004; pp 41–61. https://doi.org/10.1007/978-1-59259-739-0_3.

(29) Kavallaris, M. Microtubules and Resistance to Tubulin-Binding Agents. *Nat. Rev. Cancer* **2010**, *10* (3), 194–204. https://doi.org/10.1038/nrc2803.

(30) Supino, R. MTT Assays. *Methods Mol. Biol.* **1995**, *43*, 137–149. https://doi.org/10.1385/0-89603-282-5:137.

(31) Skehan, P.; Storeng, R.; Scudiero, D.; Monks, A.; McMahon, J.; Vistica, D.; Warren, J. T.; Bokesch, H.; Kenney, S.; Boyd, M. R. New Colorimetric Cytotoxicity Assay for Anticancer-Drug Screening. *J. Natl. Cancer Inst.* **1990**, *82* (13), 1107–1112. https://doi.org/10.1093/jnci/82.13.1107.

(32) Drexler, H. G.; Uphoff, C. C. Mycoplasma Contamination of Cell Cultures: Incidence, Sources, Effects, Detection, Elimination, Prevention. *Cytotechnology* **2002**, *39* (2), 75–90. https://doi.org/10.1023/A:1022913015916.

(33) Molla Kazemiha, V.; Amanzadeh, A.; Memarnejadian, A.; Azari, S.; Shokrgozar, M. A.; Mahdian, R.; Bonakdar, S. Sensitivity of Biochemical Test in Comparison with Other Methods for the Detection of Mycoplasma Contamination in Human and Animal Cell Lines Stored in the National Cell Bank of Iran. *Cytotechnology* **2014**, *66* (5), 861–873. https://doi.org/10.1007/s10616-013-9640-9.

Chapter 3

To combine or not to combine: drug interactions and tools for their analysis. Reflections from the EORTC-PAMM Course on "Preclinical and Early-phase Clinical Pharmacology

El Hassouni B[1], Mantini G[1], **Li Petri G[1]**, Capula M[2], Boyd L[1], Weinstein HNW[1], Vallés-Marti A[1], Kouwenhoven MCM[3], Giovannetti E[1], Westerman BA[4], Peters GJ[1]; EORTC PAMM Group

1. *Department of Medical Oncology, Cancer Center Amsterdam, Amsterdam UMC, VU University Medical Center (VUmc), Amsterdam, The Netherlands*
2. *Fondazione Pisana per la Scienza, Pisa, Italy*
3. *Department of Neurology, Brain Tumor Center Amsterdam, Amsterdam University Medical Center (VUmc), Amsterdam, The Netherlands*
4. *Department of Neurosurgery, Amsterdam UMC, VU University Medical Center, Amsterdam, the Netherlands*

Anticancer Research. 2019 July;39(7):3303-3309

doi: 10.21873/anticanres.13472

To combine or not to combine: drug interactions and tools for their analysis. Reflections from the EORTC-PAMM Course on "Preclinical and Early-phase Clinical Pharmacology

Abstract

Combination therapies are used in the clinic to achieve cure, better efficacy and to circumvent resistant disease in patients. Initial assessment of the effect of such combinations, usually of two agents, is frequently performed using *in vitro* assays. In this review, we give a short summary of the types of analyses that were presented during the Preclinical and Early-phase Clinical Pharmacology Course of the Pharmacology and Molecular Mechanisms Group, European Organization for Research and Treatment on Cancer, that can be used to determine the efficacy of drug combinations. The effect of a combination treatment can be calculated using mathematical equations based on either the Loewe additivity or Bliss independence model, or a combination of both, such as Chou and Talalay's median drug effect model. Interactions can be additive, synergistic (more than additive), or antagonistic (less than additive). Software packages CalcuSyn (also available as CompuSyn) and Combenefit are designed to calculate the extent of the combined effects. Interestingly, the application of machine learning methods in the prediction of combination treatments, which can include pharmacogenomic, genetic, metabolomic and proteomic profiles, might contribute to further refinement of combination regimens. However, more research is needed to apply appropriate rules of machine learning methods to ensure correct predictive models.

Keywords: Combination treatment, synergy, Calcusyn, Compusyn, review.

Introduction

Even as early as the 1960s, the majority of clinical treatments consisted of combination regimens. Combinations such as mechlorethamine, vincristine, procarbazine and prednisone (MOPP), and cyclophosphamide, hydroxydaunorubicin and oncovin with prednisone (CHOP) represented a breakthrough in the cure of lymphoma, while other combinations led to a high curation rate in childhood leukaemia.[1] Depending on the type of combination used, the treatment rationale is to **i)** increase the efficacy of each separate drug without increasing toxicity, **ii)** add a drug which offers protection against toxicity, **iii)** bypass resistance development, or **iv)** target different subpopulations in a heterogeneous tumour. The initial clinical rationale was to achieve a better therapeutic effect (*e.g.* a complete response) than accomplished by each drug separately (*e.g.* only a partial response).[2] Historically, the selection of drugs to apply in combination therapies was based on the observation that each of the drugs showed antitumor activity against a certain tumour type, preferably with different toxicities of the two drugs. Doses and schedules were determined by trial and error. Soon thereafter, a complementary scientific approach was used to select combinations based on the mechanisms of action of each drug.[3] An excellent example is the gemcitabine–cisplatin combination, which was initially developed by our group[4] (with the aim of preventing repair of DNA–platinum adducts) and is now standard therapy for tumours such as non-small cell lung cancer and bladder cancer. Another combination is 5-fluorouracil (5-FU) and leucovorin (folinic acid) for which we demonstrated in model systems (cell lines, experimental tumours and in tumours of patients) that leucovorin increased and prolonged the inhibition of the 5-FU target, thymidylate synthase.[5] 5-FU and leucovorin are part of the standard combination of drugs used in regimens of folinic acid, 5-FU and oxaliplatin (FOLFOX), folinic acid, 5-FU and irinotecan (FOLFIRI) (colon cancer) and FOLFIRI with oxaliplatin (FOLFIRINOX) (pancreatic cancer). The increased toxicity which is often observed with these combinations is usually controlled by combinations with anti-emetics or a corticosteroid such as dexamethasone. The latter may also have (or influence) antitumor effects.[6]

Currently most combinations are established using various *in vitro* assays either focusing on the interaction of drugs on a specific target in a cell-free system, or using a pharmacological assay as summarized previously.[7–9] However, an often observed mistake is the lack of proper controls (simply testing the effect of the single agent and combined effect over the whole tested concentration range on cells).

The effect of combination treatment compared to monotherapies can be described as synergistic, additive or antagonistic. The definition is dependent on the mathematical model used, but in general it can be stated that additivity means that the predicted effect of the combination is equivalent to either the sum or the product of each separate effect. Synergism is better than the expected theoretical effect (higher than the sum or lower than the product) and antagonism is worse than the expected theoretical effect (lower than the sum or higher than the product).

In this review, we give a short summary of the types of analyses that can be used to determine the efficacy of drug combinations. Furthermore, we summarize the advantages and disadvantages of these methods and lastly discuss emerging computational approaches.

Methods for Determining the Effect of Drug Combinations

Several mathematical models were initially used to evaluate drug interactions in cell-free systems, in which the definition of the reference state (meaning no interaction) was the basis. In the Loewe additivity model,[10] it was hypothesized that when drug A is combined with itself, the effect would be the sum of: A+A=2A. When another drug was used, the reference state would be A+B=2A. In the Bliss independence model,[11] which is most commonly used, the reference state (additivity) is a product of the fractional response, in which 0.5×0.5=0.25. Almost all current models are either a modified use of the Bliss and Loewe models, or are predominantly based on the Bliss model. Application of cell free models to cellular systems assumes a sigmoidal dose-response curve based on the Hill equation allowing (a) fractional-effect analysis, (b) isobolograms, (c) the response surface area model, based on a mixed Loewe-Bliss; and (d) median effect analysis (Figure 1).

Fractional-effect Analysis

Fractional-effect analysis determines the theoretical additive effect of a combination by multiplying the effect of each drug alone.[12] When drugs A and B are combined at an equitoxic concentration, *e.g.* achieving 50% growth inhibition (IC_{50}), the theoretical fractional effect is 0.5 for each drug, and additivity is 0.5×0.5=0.25. When drug C has a moderate effect, *e.g.* 25% growth inhibition at a specific concentration (IC_{25}), the fractional effect (*fa*) is calculated as: (*fa*)=(1-g Growth inhibition in %)/100 resulting in a value of 0.75. When treatment with drug D has only a minor effect *e.g.* 2% growth inhibition, the fractional effect is 0.98. The additivity of the combination of drugs C (fa=0.75) and A (fa=0.5) is equal to their product, *i.e.* 0.375, and that for drugs D (fa=0.98) and A (fa=0.5) is similarly computed to give 0.49. Synergism is achieved for these combinations when the experimentally determined fractional effect is lower than 0.25 (A combined with B), 0.375

(A combined with C) or (A combined with D) 0.49, respectively. Antagonism is achieved when these values are higher than 0.25, 0.375 or 0.49, respectively. This method is rather straightforward, but a linear concentration–effect relationship is assumed with sigmoidal dose–response curves. The model does not allow calculation of the variation (confidence interval) within each experiment, only between experiments, and cell kill (a negative fraction) cannot be evaluated.

Isobologram

The first isobolograms were designed in the 1950s by Nobel laureates Elion and Hitchings,[13] in which, for each given level of toxicity, the dose of one drug is plotted on the x-axis and that of the second drug on the y-axis (Figure 1B), *e.g.* equitoxic doses of the single drugs. When there is additivity, there should be a straight line connecting the plotted IC_{50} values and when the effect of the combination treatment is synergistic, the plotted line falls to the left of this line and when antagonistic, to the right of this line.[14] Subsequently Chou and Talalay,[15] computerized the model applying the CalcuSyn program (Biosoft, Cambridge, UK) (see below). Despite the simplicity and accuracy of this method, the extent of synergism or antagonism cannot be quantified, nor is it possible to calculate the variation between experiments, in contrast to fractional-effect analysis. Cell kill cannot be evaluated either. However, this model proved very valuable to move the first combinations into the clinic.

The Response Surface Area Approach

According to several mathematicians,[14–16] the response surface area model is to be preferred, since this method allows calculation of the extent of synergism/antagonism (called the envelop of synergism), a confidence interval, and the evaluation of more than two drugs. The results of such analysis are presented in various forms, and usually include a 3-D plot or a contour plot. In the 3-D plot, the concentration of the drugs is plotted on two corresponding horizontal axes and the effect of the combination (response) on the vertical axis (Figure 1C, left). In the initial presentations, synergism was considered a combination index (CI) value > 0 and antagonism as less than 0. Later presentations of the 3-D plots used different units for the response (*i.e.* synergy/antagonism), such as a ratio, percentage change or % relative to the control. Synergism is usually presented as a different colour/peak. An alternative presentation is a contour plot, in which the concentration of a drug is on one of the axes and synergism is shown as a ‘contour’ of a different colour, either white in black/white presentation, or red or blue according to the preference of the mathematician (Figure 1C, right). Despite ready-to-use mathematical models, evaluation

of response surface area plots requires a considerable insight into mathematics. Moreover, the presentation of the plots does not allow for determination of whether synergism is observed under clinically relevant conditions, since the extent of growth inhibition is often not shown and also cell kill is often not considered in the calculation. However, in more recent applications, the so-called Bliss index (a measure for synergy) can be given for each effect of a combination. However, in order to optimally predict the efficacy of the combination, experience with the model and sufficient statistical knowledge is essential.

Median Drug-effect Analysis

In order to provide a pragmatic and easy-to-use method to evaluate combinations, Chou and Talalay[15] developed the median-effect principle based on the first models of Loewe[10] and Bliss.[11] However, the median-effect principle is based on the mass-action law and not on statistics, and provides a diagnostic plot, including an isobologram. The median drug-effect equation is based on the four equations of Henderson-Hasselbach,[17] Michaelis-Menten,[18] Hill[19] and Scatchard,[20] and therefore the dose-response curves of the single drug and combinations should be sigmoidal. Curves are plotted based on the doses of a drug (D1 and D2), and the effect of a drug, expressed as fraction affected (Fa) and fraction unaffected (Fu). An Fa of 0.5 means 50% growth inhibition, and Fa of 0.75 means 75% growth inhibition (or 25% growth); this means that Fa+Fu=1. The effect of a drug can be described as the ratio between Fa/Fu=(D/Dm)m. Log transformation yields the median-effect equation: log(Fa/Fu)=m log(D) – m log(Dm), in which D is the dose, m the sigmoidicity of the curve and Dm equals the dose that results in an Fa of 0.5 (*i.e.* IC_{50}). By transforming Fa+Fu=1 to Fu=(1−Fa), the formula can be transformed into Fa/(1−Fa)=(D/Dm)m, and assuming m=1 to Fa=[1+(Dm/D)]−1. When the effects for two drugs are combined and the formula for the CI is derived: CI=[(D)1/(D1-Fa)1]+[(D)2/(D1-Fa)2]+[α(D)1(D)2/(D1-Fa)1(D1-Fa)2], in which (D)1 and (D)2 are doses used for combination, (D1−Fa)1 and (D1−Fa)2 are the doses of the individual drugs resulting in 1−Fa; the slope is m, while α=1 for mutually nonexclusive drugs. A CI above 1.2 is considered to be antagonistic, between 0.8 and 1.2 additive, and below 0.8 synergistic.

The usual presentation of the results requires a normal growth-inhibition curve and a plot of CI *versus* Fa (Figure 1D). The growth-inhibition curves are essential for proper evaluation, since it should be determined whether the curves are sigmoidal or hyperbolic, whether there are outliers, and whether sigmoidicity is similar for each drug. A simple quality check includes the comparison of the Dm value calculated by the program with the IC_{50} value from the curve, which should be similar. The CI–Fa plot evaluates synergism

over the whole Fa range from 0-1. However, CI values above an Fa of 0.95 are usually not reliable, while CI values obtained at Fa<0.5 can be considered as not relevant, since Fa<0.5 represent minor, clinically not relevant growth inhibition. In order to combine the data of more experiments, it is recommended to calculate the average of the CI values at Fa of 0.5, 0.75 and 0.90 for each separate experiment. Subsequently, the averages of each experiment can be used to calculate the means and SEM for the experiments. In this model, it should be specified whether the combined drugs act on a common target or have a similar mechanism of action, *i.e.* are mutually exclusive, where one agent may prevent the action of the other. The agents may have different mechanisms of action or targets and therefore act in a mutually nonexclusive manner.

In order to digitalize the median-effect method, the CalcuSyn software was designed based on the formulas given above by Chou and Talalay, allowing the user to plot the dose-response curves of the single agents and the combination treatment to determine the CI. CalcuSyn can be downloaded from http://www.biosoft.com/w/calcusyn.htm, however a fee dependent on the intended number of users is required. In 2005, Chou published another software program based on the median-effect of the mass-action law, CompuSyn, which can be downloaded free of charge from www.combosyn.com. The program does not allow values above 1 or below 0 to be entered, which can be solved by plotting these values all at either 0.95 or 0.05, respectively. Although this limitation does not allow evaluation of cell kill, this can be solved by using a modified calculation of Fa as described by Bijnsdorp *et al.*[8] Even though the program advises combining drugs at a fixed ratio based on the IC_{50}, the current version also allows evaluation of non-fixed ratios. Loewe synergy using surface area models can be calculated using Combenefit, which can be downloaded for free from https://sourceforge.net/projects/combenefit/.

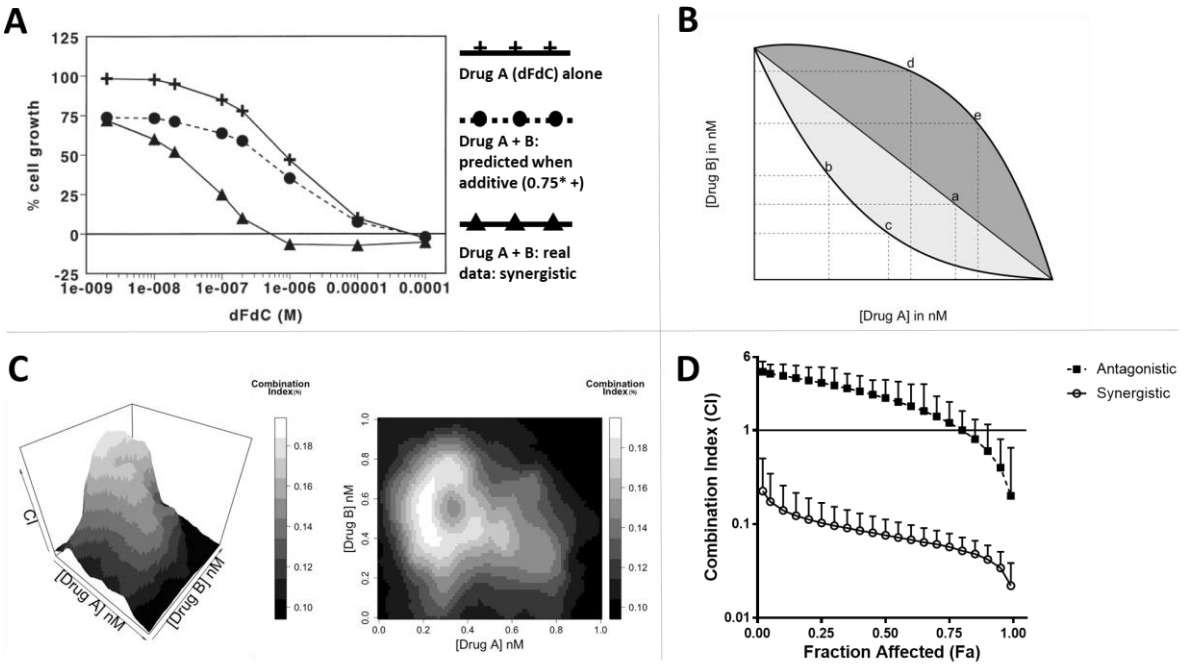

Figure 1. Examples of plots to determine the effect of combination treatments. **A:** Fractional effect analysis, reprinted with permission from (3). **B:** Isobologram. **C:** The response surface area model (left) and a contour plot (right). **D:** Median-effect analysis. CI: Combination index.

Models evaluating the effect of two agents combined are valuable in the development of novel treatment strategies. Nevertheless, researchers should be aware of the limitations and pitfalls that these models carry. A concise summary of the advantages and disadvantages of the aforementioned methods are listed in table I.

Method	Advantages	Disadvantages
Fractional effect analysis	• Straightforward method for mutually nonexclusive drugs	• Model assumes linear concentration-effect curve in contrast to reality (sigmoidal) • No confidence interval quantification
Isobologram	• Simple and accurate method	• Level of synergy or antagonism cannot be determined • The isobole based on the dose pair is often curvilinear instead of linear due to variability in drug potency • No experimental variation quantification
The response surface approach	• Model assumes sigmoidal concentration-effect relationship	• Output interpretation requires expertise since it is aggregated • Sufficient statistical knowledge essential
Median-drug effect analysis	• A distinction between mutually exclusive and non-exclusive acting agents can be made	• Synergy evaluation can be complicated • Fa values < 0 or > 1 cannot be included in calculations, but by adapting the model this can still be achieved[8]

Fa: Fraction affected.

How Should Novel Tyrosine Kinase-directed Drugs Be Combined?

The models described above were developed primarily to evaluate combinations of two or more conventional anticancer chemotherapeutics. This raises the question of whether the model can also be used to evaluate combinations of conventional chemotherapy agents with novel chemotherapeutics drugs, such as tyrosine kinase inhibitors (TKI) or combinations of TKIs. There is sufficient evidence in literature that Calcusyn can be used to evaluate combinations of drugs such as pemetrexed or gemcitabine with a TKI, such as erlotinib or crizotinib, respectively.[21,22] However, for these studies, it is even more evident that genetic properties of the cells should be taken into account, while the concentration of a TKI should be chosen in a range high enough to modulate its target. For instance, in the

case of erlotinib, it is not sensible to combine these drugs for tumours that have a *RAS* mutation,[21] while for crizotinib, either a MET proto-oncogene receptor tyrosine kinase (*c-MET*) amplification or mutation is required to achieve an effect.[23] This also means that the drugs can better be combined at a non-fixed ratio, for which the current version of CalcuSyn has a separate option.

Similarly, combinations of one or more TKIs can be evaluated using the above-mentioned programs on the condition that genetic and biochemical properties are taken into account when combining these drugs. An example is the combination of erlotinib, an epidermal growth factor receptor (EGFR) inhibitor, with crizotinib, which inhibits c-MET. Resistance to erlotinib can be due to increased c-MET signalling, which can be inhibited by crizotinib. This combination appeared to be synergistic in cells with active EGFR and c-Met signalling, and additive when one of the pathways was active. Antagonism was observed in a cell line lacking these properties.[24]

These considerations indicate that a lower concentration of one drug may be sufficient for modulating cellular signalling. This has led some investigators to use ultra-low concentrations in the 'homeopathic' range, arguing that patient toxicity might also be reduced. However, when no clear effect on signalling is observed in mechanistic experiments, such combinations should be considered with care.

Translation of Combinations to *In Vivo* Models

When combining drugs *in vivo*, additional aspects should be taken care of. Ideally a synergistic effect on the tumour would be associated with an antagonistic effect on normal tissues. Unfortunately, this is not often observed and initial dosing *in vivo* (usually mice) should be done with care; moreover, the outcome often cannot be predicted with current *in vitro* alternative models, including organoids, since the whole *in vivo* mechanism of drug absorption, distribution, metabolism and excretion is not present therein. Usually one of these aspects can be investigated in a proper model (*e.g.* cytochrome p450 (CYP)-mediated metabolism or glucuronidation and other phase I and II metabolic pathways or ATP-binding cassette transporter-mediated efflux) and can be used to adapt the *in vivo* scheduling. Therefore, it is advised to start with a lower dose of at least one of the drugs. Usually it is advised to give one drug at the maximal tolerated dose (MTD) of the single agent and the other at its 0.66×MTD, although most investigators start with each drug at its 0.66×MTD. Serial two-fold dilutions can be tested before an efficacy experiment in case severe toxicity is expected. *In vitro* experiments can provide guidelines on the scheduling for animal experiments, but toxicity might also be synergistic, necessitating

alternative scheduling. Mechanistic pharmacological studies in animals will provide essential information on proper dosing and scheduling *in vivo*. The above-mentioned example of gemcitabine and cisplatin showed pre-treatment of cell lines with gemcitabine would increase the formation of DNA-platinum adducts and prevent repair of these adducts. However, dosing for both drugs had to be reduced, but the combined effect was superior to that of each drug alone at its MTD.[25] The same principle was applied to the combination of gemcitabine and crizotinib in mice, in which the combination was based on *in vitro* synergism in a pancreatic cancer cell line with a *c-MET* amplification. It was decided to give gemcitabine at its 0.83×MTD. The combination of gemcitabine and crizotinib was superior to that of each drug separately, while crizotinib increased the accumulation of the active metabolite of gemcitabine by inhibition of gemcitabine degradation.[23] In short, it can be concluded that for *in vivo* combinations, the schedule can often be deduced from *in vitro* data, while dosing should be reduced slightly.

New Computational-based Approaches for Capturing Cellular and Signalling Complexity

The rapid development and application of machine-learning methods is now also being applied in biomedical sciences. The utilisation of several machine-learning methods for assessment of combination drug therapy for HIV, hypertension, infectious diseases and cancer is described elaborately by Tsigelny.[26] For example, machine-learning networks can implement various parameters, such as **i)** compound-specific physical and chemical properties; **ii)** biochemical response of target molecule(s); **iii)** cellular response; and **iv)** patient characteristics, including genomic, proteomic and metabolomic profiles, which sounds promising.

Current predictive models for drug-combination effects are commonly based on high-throughput testing of drug combinations for each cell line. These data are then used to identify the molecular features that predict therapy response.[27] A pan-cancer DREAM community challenge, the AstraZeneca Drug Combination Prediction Challenge, showed such findings on a pan-cancer scale.[28] Synergy prediction based on models of drug interactions are appearing.

Given that most therapy combination approaches are based on an aggregated index of synergy, the analytical methods that exist today might need additional refinements to capture intercellular (cell identity) as well as intracellular heterogeneity (signalling activity) and their combined effects on efficacy of drug combinations. Single-cell tracing methods, such as single-cell genetic/mRNA profiling, fluorescent reporter systems and

cell-tracing barcode technologies can provide relevant insight into population changes as well as fluctuations in the mechanism of action that result in therapy efficacy. These computational models should provide sufficient complexity to predict the effect of combination therapies on a cellular/signalling level accurately. Given this high complexity, more advanced machine-learning methods, such as deep learning, might be needed to enable adequate modelling.

Conclusion

Drug combinations have been used for decades in the clinic to enhance the treatment of patients, and are therefore not a novelty in the field of pharmacology. Various *in vitro* models together with mathematical equations based on the Bliss independence model, Loewe additivity model or a combination of both, *i.e.* the median drug effect, enable the prediction of the effect of two agents combined. Nonetheless, application of these models should be tailored to the context of each study and with awareness of the limitations and advantages of each method. Considering the increment in the development of novel therapeutics, the number of combinations that can be made is substantial. Aside from more complex single-cell assay read-outs that are able to capture cellular and signalling heterogeneity, more advanced computational models might be needed, including deep learning methodologies. Therefore, we anticipate that refinements of the classical synergy models with emerging artificial intelligence-based models will benefit the investigation of new combination treatments in the near future.

Conflicts of Interest

The Authors have no conflicts of interest to declare in regard to this study.

Authors' Contributions

BEH, GJ, BW and EG wrote the article. GM provided the figures and GLP the table. MJ, LB, HNW, AVM and MCMK revised the article.

Acknowledgements

This work was partially supported by the following grants: CCA Foundation 2012 and 2015 grants (GJP, EG), Fondazione Pisana per la Scienza (EG), KWF Dutch Cancer Society grants (KWF project#10401 and #11957, EG) and AIRC/Start-Up grant (EG).

References

(1) DeVita, V. T.; Chu, E. A History of Cancer Chemotherapy. *Cancer Res.* **2008**, *68* (21), 8643–8653. https://doi.org/10.1158/0008-5472.CAN-07-6611.

(2) Bertino JR and Chou T-C. Chemotherapy: synergism and antagonism. In Encyclopedia of Cancer. Vol 1. Academic Press, Inc., **1997**, 368-379.

(3) Peters, G. J.; van der Wilt, C. L.; van Moorsel, C. J.; Kroep, J. R.; Bergman, A. M.; Ackland, S. P. Basis for Effective Combination Cancer Chemotherapy with Antimetabolites. *Pharmacol. Ther.* **2000**, *87* (2–3), 227–253. https://doi.org/10.1016/s0163-7258(00)00086-3.

(4) Bergman, A. M.; Ruiz van Haperen, V. W.; Veerman, G.; Kuiper, C. M.; Peters, G. J. Synergistic Interaction between Cisplatin and Gemcitabine in Vitro. *Clin. Cancer Res.* **1996**, *2* (3), 521–530.

(5) Peters, G. J.; Backus, H. H. J.; Freemantle, S.; van Triest, B.; Codacci-Pisanelli, G.; van der Wilt, C. L.; Smid, K.; Lunec, J.; Calvert, A. H.; Marsh, S.; et al. Induction of Thymidylate Synthase as a 5-Fluorouracil Resistance Mechanism. *Biochim. Biophys. Acta* **2002**, *1587* (2–3), 194–205. https://doi.org/10.1016/s0925-4439(02)00082-0.

(6) Bergman, A. M.; Pinedo, H. M.; Peters, G. J. Steroids Affect Collateral Sensitivity to Gemcitabine of Multidrug-Resistant Human Lung Cancer Cells. *Eur. J. Pharmacol.* **2001**, *416* (1–2), 19–24. https://doi.org/10.1016/s0014-2999(01)00858-5.

(7) Perego, P.; Hempel, G.; Linder, S.; Bradshaw, T. D.; Larsen, A. K.; Peters, G. J.; Phillips, R. M.; EORTC PAMM Group. Cellular Pharmacology Studies of Anticancer Agents: Recommendations from the EORTC-PAMM Group. *Cancer Chemother. Pharmacol.* **2018**, *81* (3), 427–441. https://doi.org/10.1007/s00280-017-3502-7.

(8) Bijnsdorp, I. V.; Giovannetti, E.; Peters, G. J. Analysis of Drug Interactions. *Methods Mol. Biol.* **2011**, *731*, 421–434. https://doi.org/10.1007/978-1-61779-080-5_34.

(9) Peters, G. J.; Chatelut, E.; Larsen, A. K.; Zaffaroni, N. EORTC-Related New Drug Discovery and Development Activities: Role of the Pharmacology and Molecular Mechanisms Group. *European Journal of Cancer Supplements* **2012**, *10* (1), 128–140. https://doi.org/10.1016/S1359-6349(12)70022-8.

(10) Loewe S and Muischnek H. Effect of combinations: mathematical basis of problem. *Arch Exp Pathol Pharmacol* **1926**, *114*, 313-326.

(11) Bliss, C. I. The Toxicity of Poisons Applied Jointly1. *Annals of Applied Biology* **1939**, *26* (3), 585–615. https://doi.org/10.1111/j.1744-7348.1939.tb06990.x.

(12) Webb J. Effect of more than one inhibitor. *Enzymes Metabol Inh* **1963**, *1*, 66-79.

(13) Elion, G. B.; Singer, S.; Hitchings, G. H. Antagonists of Nucleic Acid Derivatives. VIII. Synergism in Combinations of Biochemically Related Antimetabolites. *J. Biol. Chem.* **1954**, *208* (2), 477–488.

(14) Steel, G. G.; Peckham, M. J. Exploitable Mechanisms in Combined Radiotherapy-Chemotherapy: The Concept of Additivity. *Int. J. Radiat. Oncol. Biol. Phys.* **1979**, *5* (1), 85–91. https://doi.org/10.1016/0360-3016(79)90044-0.

(15) Chou, T. C.; Talalay, P. Quantitative Analysis of Dose-Effect Relationships: The Combined Effects of Multiple Drugs or Enzyme Inhibitors. *Adv. Enzyme Regul.* **1984**, *22*, 27–55.

(16) Berenbaum, M. C. What Is Synergy? *Pharmacol. Rev.* **1989**, *41* (2), 93–141.

(17) Haring, M. M. The Determination of Hydrogen Ions. Third Edition (Clark, W. Mansfield). *J. Chem. Educ.* **1928**, *5* (10), 1362. https://doi.org/10.1021/ed005p1362.2.

(18) Michaelis L and Menten ML. Die Kinetik der Invertinwirkung. *Biochem Z* **1913**, *49*, 333-369.

(19) Hill, A. V. The Combinations of Haemoglobin with Oxygen and with Carbon Monoxide. I. *Biochem J* **1913**, *7* (5), 471–480.

(20) Scatchard, G. THE ATTRACTIONS OF PROTEINS FOR SMALL MOLECULES AND IONS. *Annals of the New York Academy of Sciences* **1949**, *51* (4), 660–672. https://doi.org/10.1111/j.1749-6632.1949.tb27297.x.

(21) Giovannetti, E.; Lemos, C.; Tekle, C.; Smid, K.; Nannizzi, S.; Rodriguez, J. A.; Ricciardi, S.; Danesi, R.; Giaccone, G.; Peters, G. J. Molecular Mechanisms Underlying the Synergistic Interaction of Erlotinib, an Epidermal Growth Factor Receptor Tyrosine Kinase Inhibitor, with the Multitargeted Antifolate Pemetrexed in Non-Small-Cell Lung Cancer Cells. *Mol. Pharmacol.* **2008**, *73* (4), 1290–1300. https://doi.org/10.1124/mol.107.042382.

(22) Avan, A.; Caretti, V.; Funel, N.; Galvani, E.; Maftouh, M.; Honeywell, R. J.; Lagerweij, T.; Van Tellingen, O.; Campani, D.; Fuchs, D.; et al. Crizotinib Inhibits Metabolic Inactivation of Gemcitabine in C-Met-Driven Pancreatic Carcinoma. *Cancer Res.* **2013**, *73* (22), 6745–6756. https://doi.org/10.1158/0008-5472.CAN-13-0837.

(23) Avan, A.; Caretti, V.; Funel, N.; Galvani, E.; Maftouh, M.; Honeywell, R. J.; Lagerweij, T.; Van Tellingen, O.; Campani, D.; Fuchs, D.; et al. Crizotinib Inhibits Metabolic Inactivation of Gemcitabine in C-Met-Driven Pancreatic Carcinoma. *Cancer Res.* **2013**, *73* (22), 6745–6756. https://doi.org/10.1158/0008-5472.CAN-13-0837.

(24) Van Der Steen, N.; Leonetti, A.; Keller, K.; Dekker, H.; Funel, N.; Lardon, F.; Ruijtenbeek, R.; Tiseo, M.; Rolfo, C.; Pauwels, P.; et al. Decrease in Phospho-PRAS40 Plays a Role in the Synergy between Erlotinib and Crizotinib in an EGFR and CMET Wild-Type Squamous Non-Small Cell Lung Cancer Cell Line. *Biochem. Pharmacol.* **2019**, *166*, 128–138. https://doi.org/10.1016/j.bcp.2019.05.014.

(25) van Moorsel, C. J.; Pinedo, H. M.; Smid, K.; Comijn, E. M.; Voorn, D. A.; Veerman, G.; Lakerveld, B.; Van der Vijgh, W. J.; Giaccone, G.; Postmus, P. E.; et al. Schedule-Dependent Pharmacodynamic Effects of Gemcitabine and Cisplatin in Mice Bearing Lewis Lung Murine Non-Small Cell Lung Tumours. *Eur. J. Cancer* **2000**, *36* (18), 2420–2429. https://doi.org/10.1016/s0959-8049(00)00345-2.

(26) Tsigelny, I. F. Artificial Intelligence in Drug Combination Therapy. *Brief. Bioinformatics* **2018**. https://doi.org/10.1093/bib/bby004.

(27) Bansal, M.; Yang, J.; Karan, C.; Menden, M. P.; Costello, J. C.; Tang, H.; Xiao, G.; Li, Y.; Allen, J.; Zhong, R.; et al. A Community Computational Challenge to Predict the Activity of Pairs of Compounds. *Nat. Biotechnol.* **2014**, *32* (12), 1213–1222. https://doi.org/10.1038/nbt.3052.

(28) Menden, M. P.; Casale, F. P.; Stephan, J.; Bignell, G. R.; Iorio, F.; McDermott, U.; Garnett, M. J.; Saez-Rodriguez, J.; Stegle, O. The Germline Genetic Component of Drug Sensitivity in Cancer Cell Lines. *Nat Commun* **2018**, *9* (1), 3385. https://doi.org/10.1038/s41467-018-05811-3.

Chapter 4

Pharmacogenetics of treatments for pancreatic cancer

El Hassouni B[1], **Li Petri G[1,2]**, Liu DSK[3], Cascioferro S[2], Parrino B[2], Hassan W[1], Diana P[2], Ali A[4,5], Frampton AE[3], Giovannetti E[1,6]

1. *Department of Medical Oncology, Cancer Center Amsterdam, Amsterdam UMC, VU University Medical Center (VUmc), Amsterdam, The Netherlands*
2. *Department of Biological, Chemical and Pharmaceutical Sciences and Technologies (STEBICEF), University of Palermo, Palermo, Italy*
3. *Department of Surgery and Cancer, Imperial College, London, UK*
4. *Institute of Cancer Sciences, College of Medical, Veterinary and Life Sciences, University of Glasgow, Glasgow UK*
5. *Institute of Basic Medical Sciences, Khyber Medical University, Peshawar, Pakistan*
6. *Cancer Pharmacology Lab, AIRC Start Up Unit, Fondazione Pisana per la Scienza, Pisa, Italy*

Expert Opinion on Drug Metabolism & Toxicology 2019 June;15(6):437-447

doi: 10.1080/17425255.2019.1620731

Pharmacogenetics of treatments for pancreatic cancer

Abstract

Introduction: Despite clinical efforts, pancreatic ductal adenocarcinoma (PDAC) has a dismal prognosis. The scarcity of effective therapies can be reflected by the lack of reliable biomarkers to adapt anticancer drugs prescription to tumors' and patients' features.

Areas covered: Pharmacogenetics should provide the way to select patients who may benefit from a specific therapy that best matches individual and tumor genetic profile, but it has not yet led to gains in outcome. This review describes PDAC pharmacogenetics findings, critically reappraising studies on polymorphisms and -omics profiles correlated to response to gemcitabine, FOLFIRINOX, and nab-paclitaxel combinations, as well as limitations of targeted therapies. Further, we question whether personalized approaches will benefit patients to any significant degree, supporting the need of new strategies within well-designed trials and validated genomic tests for treatment decision-making.

Expert opinion: A major challenge in PDAC is the identification of subgroups of patients who will benefit from treatments. Minimally-invasive tests to analyze biomarkers of drug sensitivity/toxicity should be developed alongside anticancer treatments. However, progress might fall below expectations because of tumor heterogeneity and clonal evolution. Whole-genome sequencing and liquid biopsies, as well as prospective validation in selected cohorts, should overcome the limitations of traditional pharmacogenetic approaches.

Keywords: Pancreatic cancer; pharmacogenetic studies; gemcitabine; FOLFIRINOX; nab-paclitaxel; promises and pitfalls of pharmacogenetic approaches; validated tests and clinical trials.

Article Highlights

- Improving survival in pancreatic ductal adenocarcinoma (PDAC) is a critical unmet need.
- Over the last years, patients have slightly benefitted from new combinations of conventional chemotherapy agents, improved surgical outcomes, and advancements in diagnostics, such as refinement of endoscopy.
- However, late-stage diagnosis and resistance to chemotherapy remain the biggest hurdles for PDAC treatment.
- Immunotherapy and targeted therapies lack effectiveness in treatment of PDAC due to its complex tumor microenvironment.
- Pharmacogenetics of standard treatments modalities has suggested several candidate biomarkers, but most studies showed conflicting results that are difficult to translate in the clinical setting.
- New technologies should improve pharmacogenetic approaches by moving from candidate gene methods toward genome-wide studies.
- In the future, oncologists should strive for biomarker-driven clinical trials, improving selection of clinical trial participants and more standardized protocols in biomedical research data processing.
- Liquid biopsies have the potential to pair with genomic tests and new trials, establishing more effective clinical management strategies for PDAC patients.

Introduction

Pancreatic cancer is a highly malignant disease with a rising incidence and is currently amongst the top five of the leading causes of cancer-related deaths.[1,2] Pancreatic ductal adeno-carcinoma (PDAC) is an exocrine tumor that arises from the cells of the pancreatic duct or ductules and comprises the majority of pancreatic cancers.[3] However, because of onco-genic insults or different environmental stress factors, pancreatic acinar cells can differentiate into ductal-like cells, in the so-called acinar-to-ductal metaplasia (ADM) of the pancreas. This ADM may lead to pancreatic intraepithelial neoplasia, which is the most common precancerous lesion that drives PDAC formation and progression.[4]

PDAC is a highly fatal malignancy with neither a limited number of known risk factors nor effective screening modalities. At the time of diagnosis, more than 80% of PDAC patients present with unresectable disease, which translates into a very poor prognosis, and a five-year overall survival (OS) of 3% in patients with metastatic disease at onset.[5]

Accumulating genetic and molecular data has defined sub-groups of PDAC with distinct biology and potential subtype-specific therapeutic vulnerabilities, as recently reviewed by Collisson and collaborators.[6] However, this has not yet been translated in the development of effective therapeutic strategies to overcome PDAC chemoresistance. One main contributor to this poor prognosis is indeed the inherent and/or acquired resistance of PDAC to conventional treatment modalities.[7]

Although research has been conducted to establish new chemotherapy regimens as well as innovative treatment modalities acting on specific molecular pathways, new strategies to target this disease are urgently warranted in order to achieve significant clinical improvement.[8,9] Therefore, in addition to overcoming the challenges of chemotherapy options by the development of new anticancer drugs, novel pharmacogenetic strategies are also needed.

Pharmacogenetics of standard treatment modalities

By definition, pharmacogenetics is the study of the inherited genetic differences in drug metabolic pathways (as well as other determinants in pharmacological activity, such as transporters, receptors, and enzymes), which affect individual responses to drugs, both in terms of therapeutic as well as adverse effects. The terms pharmacogenetics and pharmacogenomics tend to be used interchangeably and a consensus remains equivocal.[10]

In clinical oncology, pharmacogenetic studies typically evaluate the correlation of drug activity with individual patients' features, focusing on one or a few genes, whereas pharmacogenomics considers the whole genome of the tumor, through the application of

new -omic technologies. In this review, we describe dysregulations at germinal and tumor level that potentially affect the activity of standard treatment modalities in PDAC, such as gemcitabine, FOLFIRINOX, and nab-paclitaxel/gemcitabine combinations. Figure 1 summarizes the most important candidate bio-markers in the intake, mechanism of action, and metabolism/catabolism of the drugs in the FOLFIRINOX and nab-paclitaxel-gemcitabine regimens. In addition, several studies showed the potential role of dysregulation of apoptosis in the chemoresistance to all these regimens. Apoptosis can occur via two signaling pathways, the extrinsic pathway that is activated via the death receptor or the intrinsic (mitochondrial) pathway that both lead to the activation of caspases.[11] PDAC cells predominantly rely on the mitochondrial-enhanced apoptosis pathway dependent on the Bcl-2 family members.[12] The Bcl-2 family can be divided into antiapoptotic proteins (Bcl-xL and Bcl-2) and proapoptotic proteins (Bax, Bak, and Bad), which interact with other molecules to regulate apoptosis. Interestingly, unlike Bcl-2, Bcl-xL is overexpressed in Fas and TRIAL-mediated apoptosis-resistant PDAC cells. Moreover, proapoptotic protein Bax overexpression increased the sensitivity to5-fluorouracil (5-FU) in ASPC-1 cells.[13] However, in orthotopic SCID mice growing Colo357-blc-xl tumors, the tumor regression was higher compared to Colo357-wildtype tumors, contradicting previous *in vitro* data,[14] and suggesting that other pathways can play an important role in mediating gemcitabine effects and resistance. For instance, in PANC-1 cells, gemcitabine treatment caused a downregulation of antiapoptotic pancreatitis-associated protein and upregulation of proapoptotic TP53INP1 and p-GSK-3β.[15]

However, none of these pro- or antiapoptotic proteins has been validated as a reliable biomarker of drug activity or resistance in PDAC.

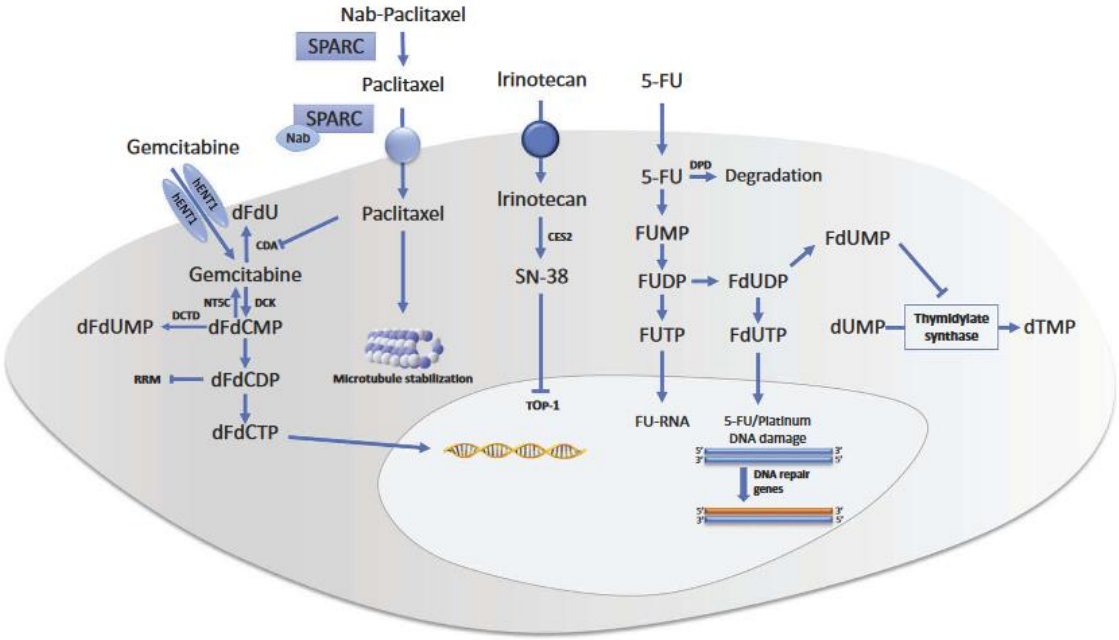

Figure 1. Main determinants in the mechanism of action of current PDAC treatments modalities. Gemcitabine uptake is predominantly facilitated by human equilibrative transporter 1, followed by cytidine deaminase (CDA) inactivation or activation by deoxycytidine kinase (DCK), resulting after various phosphorylation steps in DNA synthesis inhibition. Paclitaxel uptake is enhanced by secreted protein acidic and rich in cysteine (SPARC) that binds to albumin and therefore produces free paclitaxel. Prodrug irinotecan is activated by carboxyl esterase-2 (CES2) to its active metabolite SN-38 that inhibits topoisomerase-1 (TOP1). 5-Fluorouracilmetabolite FdUTP results in DNA damage, whereas FdUMP inhibits thymidylate synthase.

Gemcitabine (2′,2′-difluorodeoxycytidine, dFdC; Gemzar®) is a pyrimidine analogue widely prescribed to treat a variety of solid tumors such as pancreatic, breast, ovarian, bladder, or non-small-cell lung cancers (NSCLCs).[16] It has been used for decades as the first-line treatment for metastatic pancreatic cancer, as it showed a better response compared to 5-FU treatment.[17] However, the median OS witnessed with gemcitabine was not very promising. Besides, gemcitabine has a low response rate. In order to improve PDAC patients' prognosis, gemcitabine was used in combination with other treatment modalities such as capecitabine, but there was only a marginal improvement in terms of OS. Similar results were also obtained with a combination of cisplatin and gemcitabine.[18] These results were confirmed by a meta-analysis, including more than 25 studies and 8000 patients, which showed only a trend and no statistically significant differences when comparing all the combinations with both platinum and fluoropyrimidine compounds to gemcitabine monotherapy.[19]

Clinical trials were also conducted to test the combination of Epidermal Growth Factor Receptor (EGFR) tyrosine kinase inhibitor erlotinib with gemcitabine, but the very short improvement in terms of survival benefit, though significant, was not considered clinically relevant.[20] Of note, EGFR mutations that are used to guide the treatment of NSCLC with EGFR tyrosine kinase inhibitors[21] are rare in PDAC samples.[22] Skin rash and EGFR expression were initially proposed as surrogate markers of efficacy for the erlotinib-gemcitabine combination, but they both failed to identify patients with clinical benefit in a following randomized phase III trial.[23] Therefore, no predictive factor of clinical response to erlotinib has yet been found in PDAC patients. Several studies have tried to identify molecular or genetic determinants of response to gemcitabine mostly in PDAC and NSCLC patients at both the somatic and the constitutional levels.[24,25]

Because of its hydrophilic nature, gemcitabine requires facilitated transport for cellular uptake, and it is transported into the cells by membrane nucleoside transporters, including the human equilibrative nucleoside transporter-1 (hENT1) and human concentrative nucleoside transporter-3 (hCNT3).[26] After uptake, it is monophosphorylated by rate-limiting enzyme deoxycytidine kinase (DCK) to dFdC-MP. Kinases CMP/UMP kinase (CMPK1) and nucleoside-diphosphate kinase (NDPK, NME) are responsible for production of the subsequent metabolites dFdC-DP and dFdC-TP, respectively. Metabolite dFdC-DP depletes deoxynucleotide pools via inhibition of ribonucleotide reductase 1 (RRM1), whereas dFdC-TP is incorporated into DNA leading to DNA synthesis inhibition. Conversely, inactivation of over 90% of prodrug dFdC to difluorodeoxyuridine is catalyzed by cytidine deaminase (CDA), whereas dFdC-MP is dephosphorylated by 5′-nucleotidase. Deoxycytidylate(DCMP) deaminase produces dFdUMP from dFdC-MP, which inhibits thymidylate synthase (TS). Of note, the genes coding for hENT1 (SLC29A1) and hCNT3 (SLC28A3) are characterized by several poly-morphisms, which might affect protein expression. However, studies on the clinical significance of these polymorphisms showed controversial results,[27] and the most studied pharmacogenetic biomarker for gemcitabine activity in PDAC is tumor expression ofhENT1. The higher activity and uptake in cancer cells, using both *in vitro* and *in vivo* models associated with significantly higher expression levels of both transporters,[28] could explain the marked increase in OS observed in pancreatic cancer patients treated with gemcitabine. In particular, analyses of hENT1 mRNA and protein expression with PCR and immunohistochemical approaches demonstrated that high levels of hENT1 correlated with a statistically significantly longer survival, both in the adjuvant and in the metastatic setting, though the number of patients

in the latter cohort was extremely small.[29,30] In addition, the retrospective analysis of the phase III clinical trials RTOG-9704 and ESPAC-1/3 supported the role of hENT1 as a predictive biomarker of adjuvant gemcitabine efficacy: patients with tumors characterized by high hENT1 expression had significantly longer OS com-pared to patients with low hENT1 expression.[31,32] Of note, this association was missing in patients treated with 5-FU, suggesting a predictive and not prognostic role for hENT1. However, a recent study in hepatocarcinoma patients is challenging this concept, since hENT1 overexpression was associated with a high proliferation rate and a worse survival in resected intrahepatic cholangiocarcinoma patients who did not receive adjuvant treatments. These findings suggest the potential prognostic role of hENT1 in this set of patients.[33] Moreover, the role of hENT1 expression as a biomarker could not be identified when a comparison of gemcitabine with its lipophilic analog CO-101 was carried out within the prospective biomarker stratified trial LEAP, in the metastatic setting.[34] Similarly, the immunohistochemical study of hENT1 expression using the rabbit monoclonal antibody SP120 in the samples from the patients enrolled in the phase III CONKO-001 trial, which compared gemcitabine *versus* observation in the adjuvant setting, showed no correlation between hENT1 levels and OS.[35]

These conflicting results might either be due to the use of different types of hENT1 antibodies between studies or to changes in the expression pattern related to the disease-stage, since PDAC genomic landscapes seem highly dynamic during cancer progression, which might also explain the metastatic behavior of this tumor type.[36,37] Finally, another key determinant in the low response rate to gemcitabine is the particularly complex microenvironment of PDAC, comprising several cellular components (fibroblasts, stellate, endothelial, and immune cells) and a dense extracellular matrix (ECM) that makes up nearly 80% of the tumor mass.[38] In particular, PDAC stroma can contribute to hypoperfusion and hypoxia, reducing gemcitabine delivery and activity.[39,40] Moreover, recent studies demonstrated the inter- and intra-tumoral heterogeneity in cancer-associated fibroblasts, which might also play an important role in PDAC chemoresistance and lack of correlation of clinical outcome with tumor pharmacogenetic biomarkers.[41,42]

Other studies evaluated polymorphisms and expression of potential pharmacogenetic biomarkers for gemcitabine activity, such as the metabolizing and catabolizing enzymes DCK and CDA, respectively, as reviewed previously.[27] A recent computational study identified three single nucleotide polymorphisms (SNPs) ABCG2 Q141K (rs2231142), hENT3(SLC29A3 S158F [rs780668]), and POLR2A N764K (rs2228130) that significantly

correlated with patient outcome ($p< 0.05$) in a Singaporean NSCLC patient cohort treated with gemcitabine-based chemotherapy.[43] However, more research is needed to prove the value of these SNPs and to determine the presence of these SNPs in other ethnic populations.

NDPK NME5 downregulation in the gemcitabine-resistant pancreatic cancer cell line PAXC002 resensitized the cells to gemcitabine.[44] Remarkably, PAXC002 was obtained from a patient who was not treated with chemotherapy prior to tumor resection, enabling the study of the innate gemcitabine-resistance mechanism. Yet, NME5 overexpression induced gemcitabine resistance also in the gemcitabine-sensitive BxPC-3 cells. However, most of these studies were retrospective, with small sample size, without appropriate statistical correction or further prospective studies in larger populations. Moreover, these studies used different methodologies, without appropriate validation,[45] as well as evaluation of tumor clonal heterogeneity and evolution of tumor cells and microenvironment after relapse.[46] In conclusion, after more than 20 years of use in the clinical practice, currently no prognostic biomarkers are available to stratify survival outcomes for PDAC patients receiving gemcitabine.

Pharmacogenetics of FOLFIRINOX

FOLFIRINOX is a combination of a number of chemotherapeutic drugs which includes 5-FU, leucovorin, irinotecan, and oxaliplatin. The antimetabolite 5-FU is activated in the cells, producing its mono-, di-, and tri-phosphate metabolites, fluorouridine monophosphate (FUMP), fluorouridine diphosphate(FUDP), and fluorouridine triphosphate (FUTP). Diphosphorylated 5-FU (FUDP) is converted to FdUDP and subsequently FdUMP, which inhibits TS. Furthermore, FUDP can be converted to FUTP, that is incorporated into RNA leading to toxicity. Triphosphorylated metabolite FdUTP exerts its cytotoxic effect by incorporating into the DNA.[47] Carboxylesterase 2 (CES2) predominantly activates prodrug irinotecan to its active metabolite SN-38, which inhibits topoisomerase-1 (TOP1) leading to cell death.[48] Inactivation of irinotecan and SN-38 is carried out by CYP3A and a variety of UDP-glycoronosyltransferases (UGTs). The pharmacogenomics of SN-38, such as the correlation of downregulation of well-studied UGT1A1 variant UGT1A1*28 to dose and regimen-dependent toxicity in patients and ABCB1 polymorphisms, are well described by Marsh and collaborators.[48]

Similar to cisplatin and carboplatin, oxaliplatin is a DNA adduct forming agent, but with a less toxic profile.[49] Polymorphisms in DNA repair and metabolic enzymes are responsible

for the differences in drug response and toxicity. The effects of the various polymorphisms associated with clinical outcome are summarized by Kweekel and collaborators.[49]

The FOLFIRINOX regimen has been first introduced as a standard treatment for metastatic PDAC after the phase III clinical trial PRODIGE 4/ACCORD 11, which showed a better OS and progression-free survival (PFS) as compared to gemcitabine monotherapy.[50] A more recent study on adjuvant therapy has demonstrated that a modified FOLFIRINOX regimen is also associated with a significantly longer survival than gemcitabine among patients with resected PDAC.[50] A retrospective study by a single institution found that the presence of mutations in 5 genes involved in DNA damage repair (i.e. BRCA1 [N= 7], BRCA2 [N= 5], PALB2 [N= 3], MSH2[N= 1], and FANCF [N= 1]) was associated with improved OS in a total of 36 patients with metastatic PDAC treated with FOLFIRINOX.[51] Interestingly, a previous study on the analysis of coding exons of 12 genes (ATM, ATR, BAP1, BRCA1,BRCA2, BLM, CHEK1, CHEK2, FANCA, MRE11A, PALB2, andRAD51) related to homologous recombination repair (HRR) showed exceptional responses with respect to PFS of more than 2 years in two patients with inactivating HRR-related gene mutations that received FOLFIRINOX as a first-line treatment.[52] Moreover, a recent study on both tissue and plasma samples showed that microRNA-181a-5p was significantly downregulated in nonprogressive patients after FOLFIRINOX treatment, and these results were linked to the modulation of ATM expression and DNA repair both in tissues and in PDAC cell lines.[53] These results suggest the potential role of genes involved in DNA repair as biomarkers of FOLFIRINOX activity, and should prompt further studies, that might also consider well-known polymorphisms of the nucleotide excision repair system, such as XPD-Lys751Gln. The XPD-Gln751Gln variant has indeed been associated with greater resistance to cisplatin-induced damage and had an impact on the outcome of metastatic PDAC patients treated with gemcitabine-cisplatin-based polychemotherapy.[54] However, a recent study did not find a significant association between the safety or efficacy of FOLFIRINOX and the tumor expression of excision repair cross-complementing (ERCC) proteins (ERCC1, ERCC2, ERCC4),and glutathione S-transferase Pi in 34 patients with unresectable pancreatic cancer.[55]

Other studies evaluated enzymes that have been suggested to be the key determinants and thus potential predictive biomarkers of 5-FU activity, such as DPYD, which causes the degradation of 5-FU, and TS, the main target inhibited by 5-FU.[56] In a preclinical study in 15 PDAC cell lines and 2 5-FU-resistant subclones,[57] a higher resistance to 5-FU correlated with higher Dihydropyrimidine dehydrogenase (DPD) and TS mRNA expression levels.

These findings suggest that PDAC cells with low TS and/or DPD levels are more sensitive to 5-FU.

In a study on 68 resected pancreatic cancer tissues treated with adjuvant 5-FU liver perfusion chemotherapy, the immunohistochemical analysis of DPD protein expression showed a significantly shorter OS in patients with high DPD levels.[58] Similarly, immunohistochemistry on tumor cores of 238 patients enrolled in the ESPAC-3 trial, randomized to either postoperative gemcitabine or 5-fluorouracil/folinic acid (5FU/FA), showed that DPD was associated with reduced OS inpatients treated in the 5FU/FA arm, but not in the gemcitabine arm. Furthermore, in patients with low hENT1 expression, high DPD expression was associated with a shorter survival in the 5FU/FA arm, but not in the gemcitabine arm. Thus, together with the evaluation of the expression of hENT1, DPD expression might identify subgroups of patients who benefit from either postoperative 5FU/FA or gemcitabine.[59]

However, further data on correlation between TS protein expression and outcome of PDAC patients treated with 5-FU are controversial. In resected patients, high TS expression levels were significantly associated with longer OS, but high TS expression was not correlated to OS in patients with advanced PDAC.[60] Moreover, no data have yet been provided from the AFUGEM GERCOR trial, a randomized phase II study of FOLFIRINOX or nab-paclitaxel plus gemcitabine first-line therapy in metastatic patients, involving the assessment of TS as a potential 5-FU efficacy marker.[61]

Finally, only a few studies analyzed potential biomarkers for the activity of irinotecan.

Resistant pancreatic cells showed decreased mRNA levels of TOP1, which is the main target of irinotecan.[62] Of note,TOP1 gene copy numbers are increased in cancers of the bile duct and pancreas,[63] but TOP1 expression was not associated with irinotecan sensitivity in a more comprehensive study including a wider panel of PDAC cell lines. Pharmacological analyses of these cells did not show a correlation of irinotecan activity with either the expression of catabolic enzymes (CYP3A4, CYP3A5, UGT1A10) or the expression of the export transporters (ABCB1, ABCC2).[64] However, further analysis of *in vivo* models genetic databases, proteomics, and tissue microarrays showed that high expression of CES2, which activates irinotecan, was associated with a better prognosis in 22 resectable and borderline resectable patients treated with FOLFIRINOX in the neoadjuvant setting. These results prompt further studies on patients in the metastatic setting, as well as on new potential biomarkers for the FOLFIRINOX regimen.

Pharmacogenetics of nab-paclitaxel and gemcitabine combination

Following the positive results of the phase III MPACT trial, the combination of nab-paclitaxel (Abraxane®) with gemcitabine represents another first-line option for patients with advanced or metastatic PDAC.[65]

Nab-paclitaxel is a 130-nm, nanoparticle formulation com-posed by paclitaxel bound to albumin. The reduced diameter of these particles and the transcytosis mediated by albumin enhance intracellular paclitaxel delivery. Furthermore, these molecules have a greater distribution volume, and a faster clearance than conventional paclitaxel, resulting in accumulation at a much higher concentration in tumor tissues.[66] Paclitaxel is predominantly taken up into hepatic cell by the organic anion transporting polypeptide 1B3 (OATP1B), where inactivation catalyzed by cytochrome P450's CYP2C8, CYP3A4, and CYP3A5 leading to metabolites 6α-hydroxypaclitaxel,p-hydroxy-C3′-paclitaxel, and dihydroxypaclitaxel occurs.[67] In addition, P-glycoprotein (Pgp) is responsible for paclitaxel efflux. A study on polymorphisms in these genes revealed that the allele causing increased paclitaxel metabolism was associated within creased neurotoxicity, emphasizing the role of hydroxylated paclitaxel metabolites.[68] However, these variants, as well as polymorphisms in Pgp, are highly dependent on ethnic populations and have shown contradicting results between studies reviewed previously.[69]

The secreted protein acidic and rich in cysteine (SPARC) has been studied as a biomarker of nab-paclitaxel activity because it binds albumin, potentially enhancing the selective uptake of this drug in tumor cells.[70] In addition, this protein has been correlated to PDAC cell proliferation and metastasis.[71] An initial immunohistochemical study in 36 patients showed that a higher level of SPARC expression is correlated with a higher OS.[72] However, preclinical studies in both engineered mouse (i.e. KPC models) and patient-derived xenografts demonstrated that SPARC does not play a role in nab-paclitaxel internalization in cancer cells.[73,74] Consistently, following immunohistochemical studies showed that the expression of SPARC did not correlate with OS.[75] These controversial findings might be explained by another study in preclinical models of PDAC, including models with SPARC nullizygosity, showing that nab-paclitaxel accumulates and acts in a dose-dependent manner. The interaction of plasma SPARC and albumin-bound drugs was reported at low doses but was saturated at therapeutic doses in mouse tumors.[73] Nab-paclitaxel has also been found to cause the inactivation of CDA, which in turn results in inhibition of gemcitabine catabolism, leading to higher levels of gemcitabine and a higher response rate in KPC models.[76] Of note, reduction of CDA levels by increased activity of

reactive oxygen species also correlated with the synergistic interaction with the c-Met inhibitor crizotinib.[77] However, a chemical inhibitor of CDA which stabilized and thereby artificially increased gemcitabine levels in murine PDAC did not enhance cancer cell death, suggesting that other factors, such as microenvironmental factors, including the pleiotropic matricellular signaling protein connective tissue growth factor[78] may play a more important role in treatment responses of PDAC.

Since paclitaxel is essentially a spindle poison that induces cell death through its ability to disrupt mitosis by binding to the microtubule protein beta-tubulin (TUBB3), several studies investigated the role of tubulin as a biomarker in different tumor types, such metastatic gastric cancer patients receiving taxane-based first-line palliative chemotherapy.[79] A more recent immunohistochemical study evaluated TUBB3 expression in tumor samples obtained by endoscopic ultrasound-guided fine needle aspiration from 75 patients with unresectable PDAC who received the nab-paclitaxel–gemcitabine regimen. Remarkably, patients withoutTUBB3 expression showed a significantly higher disease control rate and a longer PFS. These findings support the use of TUBB3 as an innovative biomarker for treatment optimization.[80] Previous studies showed similar results when evaluating TUBB3 expression levels in lung cancer patients treated with paclitaxel. In a study on 91 NSCLC patients, it was found that low levels of tubulin expression were associated with a higher response to paclitaxel-based treatment and a higher survival rate, whereas tubulin expression was not predictive in patients receiving regimens without paclitaxel.[81] Moreover, the prognostic effect of tubulin was confirmed by the recent LACE-Bio project that included immunohistochemistry biomarkers tested for correlation with OS in four trials (International Adjuvant Lung Cancer Trial, Adjuvant Navelbine International Trialist Association, JBR10, and Cancer and Leukemia Group B-9633) and showed that the majority of the promising biomarkers could not be validated, suggesting the different tissue fixation methods, storage, and varying reagent/antibody batches as potential causes for the controversial results.[82]

Interestingly, a preclinical study in cancer cells resistant to paclitaxel demonstrated a feedback activation of TUBB3 triggered by the FOXO3a-dependent regulation of ABCB1, which resulted in the accentuation of resistance as well as in acquired cross-resistance to a number of drugs such as 5-FU, docetaxel, and cisplatin.[83] It has been reported that ABC multidrug transporters are involved in drug resistance, drug disposition, and chemotherapy toxicity.[84] For example, in the case of irinotecan, ABCB1 contributes to the cellular uptake of this prodrug and its active metabolite SN-38. Yet, the ABCB1 1236 C>T variant

decreased the clearance of irinotecan significantly, ABCC2 3972T>C was associated with toxicity, and ABCG2 overexpressing cells were resistant to irinotecan and SN-38.[85] However, despite many studies on ABC transporters and their complex pharmacogenetics, clinical trials evaluating the prognostic/predictive role of ABC transporters as well as the activity of inhibitors of these proteins did not translate in successful clinical application. Future studies should therefore be aimed at combining the present knowledge of clinically relevant ABC transporters in the field of pharmacogenetics (including several polymorphic variants),biochemistry, and computational biology, which in conjunction with state-of-the-art medicinal chemistry can generate novel inhibitors for future clinical trials to overcome multidrug resistance. Such an integrated approach may also help to guide personalized therapy in cancer patients to achieve the most optimal treatment outcome.[86]

Failure of molecularly targeted treatments and lack of (pharmacogenetic) biomarkers for personalized medicine approaches

The increased understanding of tumor biology and genetics, together with the development of more sophisticated methodologies for the molecular diagnostics of cancer, led to the development of effective targeted therapies in different tumor types such as lung and breast cancer. These drugs target signaling oncoproteins that have acquired tumor-driving functions through genetic aberrancies, such as overexpression or mutations, and provide new treatment opportunities to patients who could not receive suitable conventional chemotherapy.[87] Moreover, large-scale cancer genomic studies have defined subtypes in many cancer types, often providing insights that might lead to clinically relevant approaches to improving patient care.[88] Similar studies, including complex bioinformatics approaches, have been performed in PDAC, unravelling key mechanisms of pathogenesis, as recently reviewed.[89]

Unfortunately, this improved knowledge in the underlying genetics of PDAC has not yet been translated into the identification of ‘actionable’ therapeutic targets and systemic treatments with molecularly targeted agents.[90]

Several studies showed that the microenvironment plays a central role in PDAC development and metastasis, suggesting that its exploitation is required to develop more powerful treatment strategies.[91,92] As mentioned before, approximately 80% of PDAC tumor mass is constituted by stroma comprising cellular components (stellate cells, fibroblasts, endothelial, and immune cells) and an ECM. The ECM consists of proteoglycans, hyaluronic acid (HA), and collagen, which influence interstitial fluid pressure and blood

vessels distribution which contribute to hypoperfusion, hypoxia, and altered cancer cell metabolism, and thus reducing drug delivery and activity.[93,94]

Several studies showed the key role of tumor-associated macrophages in inducing chemoresistance of PDAC cells by secreting insulin-like growth factors (IGF) 1 and 2, which activate insulin/IGF receptors and reduce sensitivity to gemcitabine, as well as by releasing pyrimidines, such as deoxycytidine, which inhibit gemcitabine by competition at the level of drug uptake and metabolism.[95,96]

Other components that might affect aggressive behaviour and therapy response include the cancer-associated fibroblasts and the inflammatory cells that modulate cancer-directed immune mechanisms and contribute to epithelial-to-mesenchymal transition (EMT).[97] Of note, EMT has typically been related to chemoresistance, but its influence on the aggressive metastatic behavior of PDAC is less clear[98]. This might explain the clinical failure of drugs targeting critical pathways in EMT, such as Notch, which gives rise to CD44-positive pancreatic cancer stem cells and facilitates EMT in preclinical PDAC models.[99] Unfortunately, in phase I/II clinical trials, a monoclonal antibody against Notch2/Notch3(Tarextumab) did not improve the OS when combined with gemcitabine and nab-paclitaxel, while the gamma-secretase inhibitor MK0752 combined with gemcitabine had severe adverse effects leading to high patient withdrawal.[100,101] Similarly, the stromal targeting approaches had unsatisfactory clinical results, both when targeting the Hedgehog pathway by IPI-926[102] and when using a recombinant pegylated hyaluronidase enzyme PEGPH20 to target tumor stromal HA. In particular, for the latter approach, a randomized phase II trial of PEGPH20 combined with gemcitabine and nab-paclitaxel in patients with high levels of HA (evaluated by a immunohistochemistry) met only the secondary end point of PFS and underwent a temporary hold due to increased thrombosis. High-risk patients for thromboembolism were then excluded and all the patients were placed on heparin primary prophylaxis. However, a randomized phase II of frontline PEGPH20 combined to FOLFIRINOX in a non-biomarker selected population was terminated for futility at the interim analysis.[103] Disappointing results have also been obtained with inhibitors of the JAK2/STAT3 pathway, such as ruxolitinib, which progressed up to a phase III study, in combination with capecitabine, which was stopped when interim analysis demonstrated futility,[104,105] as well as with inhibitors of MEK/ERK/MAPK and/or PI3K/AKT/mTOR. These negative results might be ascribed, at least in part, to the lack of biomarkers predictive of drug activity as well as to poor clinical design and patient selection criteria. Incorporating effective biomarkers and utilizing better

endpoints should improve therapeutic potential, as demonstrated across multiple malignancies by the analysis performed by Jardim and collaborators, who found that 57% of successful studies utilized biomarker-driven patient selection, compared to 16% of failed drug programs.[106] Moreover, as reported in a systematic review on 32 phase III studies between 1997 and 2015 in PDAC, showing a sobering overall success rate of 15% in phase III trials, half of the studies advanced to phase III despite a negative phase II outcome.[107] Consideration must then also be given to the needed caution when utilizing surrogate markers in clinical trials. Response rate and PFS have indeed often failed to correlate with increased OS in PDAC.

Expert opinion

Immunotherapy and targeted therapies have revolutionized the treatment of a number of solid malignancies, including metastatic melanoma and NSCLC, but such therapies are not effective for PDAC, despite the increased knowledge of the genomic land-scape and of the complex tumor microenvironment. As a result, this disease is one of the most aggressive tumors, and all the scientific and clinical efforts have not yet produced a meaningful impact on the prognosis PDAC patients-

The causes of this grim clinical scenario are multiple.[108] Because of the lack of validated screening tests for early diagnosis and of the retroperitoneal location of PDAC, which determines insidious clinical symptoms, this tumor is rarely diagnosed when surgical resection would be feasible. Chemotherapy provides only a small benefit, and most efforts to improve the current regimens failed in advanced clinical trials. Still, despite these limited results, considering the scarce efficacy of currently approved treatment options, it would be recommended that most PDAC patients enroll in clinical trials with the hope of improving both fundamental and clinical understanding of the disease and drive promising leads for novel therapeutic strategies. Indeed, the investments of the last 20 years clearly established that the advent of multidisciplinary centers specializing in the care of PDAC patients is improving the outcome and quality of life of these patients. In particular, high volume centers have improved surgical outcomes.[109,110] The expertise in endoscopy is also likely to improve patient care, as demonstrated by the diagnostic advantages of direct histological processing of fine needle aspiration samples compared to the use of cytology.[111]

Remarkably, the introduction of endoscopic core biopsy needles has also improved the ability to acquire samples for both diagnostic and experimental purposes. This is extremely important in order to improve the rational use of innovative cancer therapeutics, as well as

of the conventional chemotherapeutic drugs, through the histopathological assessment of tumor samples, which should be associated with a refined pharmacogenetic evaluation. Until now, most clinical trials in PDAC patients have not been biomarker driven.[1] However, the oncologists have to face relevant interindividual variability in drug activity, and several studies demonstrated that both heterogeneous genetic and microenvironmental features underlay the different levels of therapeutic resistance in this tumor.[7]

Further basic and translational studies are therefore war-ranted in order to identify critical pathways that distinguish the unique drug-sensitive PDAC subtypes, which should lead to personalized therapies. Importantly, the Pancreatic Cancer Action Network has recently launched the Precision Promise trial initiative, in which patients will undergo biomarker analysis with pathologic evaluation, genomic sequencing, and transcriptome analysis to determine assignment in treatment arms focused on stromal disruption, DNA damage repair, or immunotherapy.[112] Of note, this trial is designed to be dynamic, by incorporating promising novel drugs/targets while eliminating failing ones. The identification of biomarkers and key chemoresistance mechanisms and the dynamic targeting of these targets in a personalized manner should yield a more safe and consistent clinical benefit. This new trial will hopefully provide useful results about the correlation of specific pharmacogenetic markers, overcoming the problems of the previous studies, such as the small number of patients/samples, the intra-tumor heterogeneity as well as other complex factors, including reversible epigenetic factors, such as microRNA and factors affecting DNA methylation.

However, despite the great potential of next-generation sequencing to exponentially accelerate the acquisition of data for biomedical research including pharmacogenetics biomarkers, these technologies are still limited by the lack of standardized protocols and bioinformatics infrastructures that can integrate different information and extract clinically useful data.[113] Thus, a standardization of these methodologies will be essential to perform studies on larger cohorts of patients. This standardization will also greatly impact sharing data through common‘ virtual multicenter trials’ and building innovative mathematic modeling for molecular markers predicting drug activity.

A recent article has critically reviewed the challenges associated with personalized medicine in cancer patients, suggesting that‘ the clinical benefit of personalized medicine as it is currently practiced will be limited’.[114] Tumor cells have indeed the ability to develop resistance to single molecular targeted agents by means of overexpression/mutation of the target or activation of alternative pathways, and even the combinations of several

molecular targets have effects which are limited by signaling plasticity. These abilities challenge the idea that the pharmacogenetic studies will allow the selection of more effective drugs. However, the authors of the same article do not suggest abandoning personalized medicine but rather evaluating it in a small number of well-designed collaborative studies, always within well-planned prospective clinical trials in which a direct comparison is performed between patient treatments selected on the basis of standard criteria *versus* treatment selection based on patient/cancergenetic characteristics.

Of note, several pharmacogenetic studies showed association between candidate polymorphisms or other genetic aberrations and clinical outcome or toxicity in PDAC, but most of these studies were retrospective, monocentric, without multiple correction and validation in broader populations. Hopefully, novel pharmacogenetic biomarkers will be validated in prospective studies, including information combining together pharmacological studies on appropriate preclinical models and pharmacokinetics/pharmacodynamics studies, and used to select cancer patients to be treated with differential systemic treatment of PDAC in the near future. For instance, the parallel, integrated analysis of the expression of CES2, hENT1, and TUBB3 expression might guide the choice between FOLFIRINOX and gemcitabine monotherapy or gemcitabine combined with nab-paclitaxel.

Finally, liquid biopsies are adding an extremely important toll for the advancement of these approaches, allowing to better evaluate heterogeneity and possible evolution of cancer cells, also through multiple and repeated sampling.[115] For instance, a recent statement paper has declared that the isolation and analysis of circulating cell-free tumor DNA in plasma is a powerful tool with considerable potential to tailor the clinical management and to improve clinical outcomes in NSCLC.[116] Further studies collecting similar evidences across different tumor types, including PDAC, are warranted.

Funding

This work was partially supported in the collection and analysis of data by the following grants to Elisa Giovannetti: AIRC/Start-Up grant, CCA Foundation 2015 and 2016 grants, Fondazione Pisana per la Scienza grant, and KWF Dutch Cancer Society grants (KWF project #10401 and#11957).

Declaration of interest

The authors have no relevant affiliations or financial involvement with any organization or entity with a financial interest in or financial conflict with the subject matter or materials

discussed in the manuscript. This includes employment, consultancies, honoraria, stock ownership or options, expert testimony, grants or patents received or pending, or royalties.

Reviewer disclosures

Peer reviewers on this manuscript have no relevant financial or other relationships to disclose.

References

(1) Rahib, L.; Smith, B. D.; Aizenberg, R.; Rosenzweig, A. B.; Fleshman, J. M.; Matrisian, L. M. Projecting Cancer Incidence and Deaths to 2030: The Unexpected Burden of Thyroid, Liver, and Pancreas Cancers in the United States. *Cancer Res* **2014**, *74* (11), 2913–2921. https://doi.org/10.1158/0008-5472.CAN-14-0155.

(2) Siegel, R. L.; Miller, K. D.; Jemal, A. Cancer Statistics, 2019. *CA: A Cancer Journal for Clinicians* **2019**, *69* (1), 7–34. https://doi.org/10.3322/caac.21551.

(3) Ying, H.; Dey, P.; Yao, W.; Kimmelman, A. C.; Draetta, G. F.; Maitra, A.; DePinho, R. A. Genetics and Biology of Pancreatic Ductal Adenocarcinoma. *Genes Dev.* **2016**, *30* (4), 355–385. https://doi.org/10.1101/gad.275776.115.

(4) Origin of pancreatic ductal adenocarcinoma from atypical flat lesions: a comparative study in transgenic mice and human tissues. - PubMed - NCBI https://www.ncbi.nlm.nih.gov/pubmed/21984419 (accessed Sep 30, 2019).

(5) Kleeff, J.; Korc, M.; Apte, M.; La Vecchia, C.; Johnson, C. D.; Biankin, A. V.; Neale, R. E.; Tempero, M.; Tuveson, D. A.; Hruban, R. H.; et al. Pancreatic Cancer. *Nature Reviews Disease Primers* **2016**, *2*, 16022. https://doi.org/10.1038/nrdp.2016.22.

(6) Collisson, E. A.; Bailey, P.; Chang, D. K.; Biankin, A. V. Molecular Subtypes of Pancreatic Cancer. *Nat Rev Gastroenterol Hepatol* **2019**, *16* (4), 207–220. https://doi.org/10.1038/s41575-019-0109-y.

(7) Collisson, E. A.; Olive, K. P. Pancreatic Cancer: Progress and Challenges in a Rapidly Moving Field. *Cancer Res.* **2017**, *77* (5), 1060–1062. https://doi.org/10.1158/0008-5472.CAN-16-2452.

(8) Garrido-Laguna, I.; Hidalgo, M. Pancreatic Cancer: From State-of-the-Art Treatments to Promising Novel Therapies. *Nat Rev Clin Oncol* **2015**, *12* (6), 319–334. https://doi.org/10.1038/nrclinonc.2015.53.

(9) Neoptolemos, J. P.; Kleeff, J.; Michl, P.; Costello, E.; Greenhalf, W.; Palmer, D. H. Therapeutic Developments in Pancreatic Cancer: Current and Future Perspectives. *Nat Rev Gastroenterol Hepatol* **2018**, *15* (6), 333–348. https://doi.org/10.1038/s41575-018-0005-x.

(10) Robert, J.; Le Morvan, V.; Giovannetti, E.; Peters, G. J.; PAMM Group of EORTC. On the Use of Pharmacogenetics in Cancer Treatment and Clinical Trials. *Eur. J. Cancer* **2014**, *50* (15), 2532–2543. https://doi.org/10.1016/j.ejca.2014.07.013.

(11) Hengartner, M. O. The Biochemistry of Apoptosis. *Nature* **2000**, *407* (6805), 770–776. https://doi.org/10.1038/35037710.

(12) Westphal, S.; Kalthoff, H. Apoptosis: Targets in Pancreatic Cancer. *Mol. Cancer* **2003**, *2*, 6.

(13) Overexpression of Bax sensitizes human pancreatic cancer cells to apoptosis induced by chemotherapeutic agents | SpringerLink https://link.springer.com/article/10.1007/s00280-002-0435-5 (accessed Sep 30, 2019).

(14) Resistance of pancreatic cancer to gemcitabine treatment is dependent on mitochondria-mediated apoptosis - Schniewind - 2004 - International Journal of Cancer - Wiley Online Library https://onlinelibrary.wiley.com/doi/full/10.1002/ijc.11679 (accessed Sep 30, 2019).

(15) Jiang, P.-H.; Motoo, Y.; Sawabu, N.; Minamoto, T. Effect of Gemcitabine on the Expression of Apoptosis-Related Genes in Human Pancreatic Cancer Cells. *World J Gastroenterol* **2006**, *12* (10), 1597–1602. https://doi.org/10.3748/wjg.v12.i10.1597.

(16) Ciccolini, J.; Serdjebi, C.; Peters, G. J.; Giovannetti, E. Pharmacokinetics and Pharmacogenetics of Gemcitabine as a Mainstay in Adult and Pediatric Oncology: An EORTC-PAMM Perspective. *Cancer Chemother. Pharmacol.* **2016**, *78* (1), 1–12. https://doi.org/10.1007/s00280-016-3003-0.

(17) Burris, H. A.; Moore, M. J.; Andersen, J.; Green, M. R.; Rothenberg, M. L.; Modiano, M. R.; Cripps, M. C.; Portenoy, R. K.; Storniolo, A. M.; Tarassoff, P.; et al. Improvements in Survival and Clinical Benefit with Gemcitabine as First-Line Therapy for Patients with Advanced Pancreas Cancer: A Randomized Trial. *J. Clin. Oncol.* **1997**, *15* (6), 2403–2413. https://doi.org/10.1200/JCO.1997.15.6.2403.

(18) Heinemann, V.; Quietzsch, D.; Gieseler, F.; Gonnermann, M.; Schönekäs, H.; Rost, A.; Neuhaus, H.; Haag, C.; Clemens, M.; Heinrich, B.; et al. Randomized Phase III Trial of Gemcitabine plus Cisplatin Compared with Gemcitabine Alone in Advanced Pancreatic Cancer. *J. Clin. Oncol.* **2006**, *24* (24), 3946–3952. https://doi.org/10.1200/JCO.2005.05.1490.

(19) Sun, C.; Ansari, D.; Andersson, R.; Wu, D.-Q. Does Gemcitabine-Based Combination Therapy Improve the Prognosis of Unresectable Pancreatic Cancer? *World J Gastroenterol* **2012**, *18* (35), 4944–4958. https://doi.org/10.3748/wjg.v18.i35.4944.

(20) Erlotinib plus gemcitabine compared with gemcitabine alone in patients with advanced pancreatic cancer: a phase III trial of the National Cancer In... - PubMed - NCBI https://www.ncbi.nlm.nih.gov/pubmed/17452677 (accessed Sep 10, 2019).

(21) Santarpia, M.; Rolfo, C.; Peters, G. J.; Leon, L. G.; Giovannetti, E. On the Pharmacogenetics of Non-Small Cell Lung Cancer Treatment. *Expert Opin Drug Metab Toxicol* **2016**, *12* (3), 307–317. https://doi.org/10.1517/17425255.2016.1141894.

(22) Propper, D.; Davidenko, I.; Bridgewater, J.; Kupcinskas, L.; Fittipaldo, A.; Hillenbach, C.; Klughammer, B.; Ducreux, M. Phase II, Randomized, Biomarker Identification Trial (MARK) for Erlotinib in Patients with Advanced Pancreatic Carcinoma. *Ann. Oncol.* **2014**, *25* (7), 1384–1390. https://doi.org/10.1093/annonc/mdu176.

(23) Van Cutsem, E.; Li, C.-P.; Nowara, E.; Aprile, G.; Moore, M.; Federowicz, I.; Van Laethem, J.-L.; Hsu, C.; Tham, C. K.; Stemmer, S. M.; et al. Dose Escalation to Rash for Erlotinib plus Gemcitabine for Metastatic Pancreatic Cancer: The Phase II RACHEL Study. *Br J Cancer* **2014**, *111* (11), 2067–2075. https://doi.org/10.1038/bjc.2014.494.

(24) Ciccolini, J.; Mercier, C.; Dahan, L.; André, N. Integrating Pharmacogenetics into Gemcitabine Dosing--Time for a Change? *Nat Rev Clin Oncol* **2011**, *8* (7), 439–444. https://doi.org/10.1038/nrclinonc.2011.1.

(25) Toffalorio, F.; Santarpia, M.; Radice, D.; Jaramillo, C. A.; Spitaleri, G.; Manzotti, M.; Catania, C.; Jordheim, L. P.; Pelosi, G.; Peters, G. J.; et al. 5'-Nucleotidase CN-II Emerges as a New Predictive Biomarker of Response to Gemcitabine/Platinum Combination Chemotherapy in Non-Small Cell Lung Cancer. *Oncotarget* **2018**, *9* (23), 16437–16450. https://doi.org/10.18632/oncotarget.24505.

(26) de Sousa Cavalcante, L.; Monteiro, G. Gemcitabine: Metabolism and Molecular Mechanisms of Action, Sensitivity and Chemoresistance in Pancreatic Cancer. *Eur. J. Pharmacol.* **2014**, *741*, 8–16. https://doi.org/10.1016/j.ejphar.2014.07.041.

(27) Elnaggar, M.; Giovannetti, E.; Peters, G. J. Molecular Targets of Gemcitabine Action: Rationale for Development of Novel Drugs and Drug Combinations. *Curr. Pharm. Des.* **2012**, *18* (19), 2811–2829. https://doi.org/10.2174/138161212800626175.

(28) Mackey, J. R.; Mani, R. S.; Selner, M.; Mowles, D.; Young, J. D.; Belt, J. A.; Crawford, C. R.; Cass, C. E. Functional Nucleoside Transporters Are Required for Gemcitabine Influx and Manifestation of Toxicity in Cancer Cell Lines. *Cancer Res.* **1998**, *58* (19), 4349–4357.

(29) Spratlin, J.; Sangha, R.; Glubrecht, D.; Dabbagh, L.; Young, J. D.; Dumontet, C.; Cass, C.; Lai, R.; Mackey, J. R. The Absence of Human Equilibrative Nucleoside Transporter 1 Is Associated with Reduced Survival in Patients with Gemcitabine-Treated Pancreas Adenocarcinoma. *Clin. Cancer Res.* **2004**, *10* (20), 6956–6961. https://doi.org/10.1158/1078-0432.CCR-04-0224.

(30) Giovannetti, E.; Del Tacca, M.; Mey, V.; Funel, N.; Nannizzi, S.; Ricci, S.; Orlandini, C.; Boggi, U.; Campani, D.; Del Chiaro, M.; et al. Transcription Analysis of Human Equilibrative Nucleoside Transporter-1 Predicts Survival in Pancreas Cancer Patients Treated with Gemcitabine. *Cancer Res.* **2006**, *66* (7), 3928–3935. https://doi.org/10.1158/0008-5472.CAN-05-4203.

(31) Farrell, J. J.; Elsaleh, H.; Garcia, M.; Lai, R.; Ammar, A.; Regine, W. F.; Abrams, R.; Benson, A. B.; Macdonald, J.; Cass, C. E.; et al. Human Equilibrative Nucleoside Transporter 1 Levels Predict Response to Gemcitabine in Patients with Pancreatic Cancer. *Gastroenterology* **2009**, *136* (1), 187–195. https://doi.org/10.1053/j.gastro.2008.09.067.

(32) Greenhalf, W.; Ghaneh, P.; Neoptolemos, J. P.; Palmer, D. H.; Cox, T. F.; Lamb, R. F.; Garner, E.; Campbell, F.; Mackey, J. R.; Costello, E.; et al. Pancreatic Cancer HENT1 Expression and Survival from Gemcitabine in Patients from the ESPAC-3 Trial. *J. Natl. Cancer Inst.* **2014**, *106* (1), djt347. https://doi.org/10.1093/jnci/djt347.

(33) Tavolari, S.; Deserti, M.; Vasuri, F.; Curti, S.; Palloni, A.; Pinna, A. D.; Cescon, M.; Frega, G.; De Lorenzo, S.; Barbera, M. A.; et al. Membrane Human Equilibrative Nucleoside Transporter 1 Is Associated with a High Proliferation Rate and Worse Survival in Resected Intrahepatic Cholangiocarcinoma Patients Not Receiving Adjuvant Treatments. *Eur. J. Cancer* **2019**, *106*, 160–170. https://doi.org/10.1016/j.ejca.2018.11.005.

(34) Poplin, E.; Feng, Y.; Berlin, J.; Rothenberg, M. L.; Hochster, H.; Mitchell, E.; Alberts, S.; O'Dwyer, P.; Haller, D.; Catalano, P.; et al. Phase III, Randomized Study of Gemcitabine and Oxaliplatin versus Gemcitabine (Fixed-Dose Rate Infusion) Compared with Gemcitabine (30-Minute Infusion) in Patients with Pancreatic Carcinoma E6201: A Trial of the Eastern Cooperative Oncology Group. *J. Clin. Oncol.* **2009**, *27* (23), 3778–3785. https://doi.org/10.1200/JCO.2008.20.9007.

(35) Sinn, M.; Riess, H.; Sinn, B. V.; Stieler, J. M.; Pelzer, U.; Striefler, J. K.; Oettle, H.; Bahra, M.; Denkert, C.; Bläker, H.; et al. Human Equilibrative Nucleoside Transporter 1 Expression Analysed by the Clone SP 120 Rabbit Antibody Is Not Predictive in Patients with Pancreatic Cancer Treated with Adjuvant Gemcitabine - Results from the CONKO-001 Trial. *Eur. J. Cancer* **2015**, *51* (12), 1546–1554. https://doi.org/10.1016/j.ejca.2015.05.005.

(36) Notta, F.; Chan-Seng-Yue, M.; Lemire, M.; Li, Y.; Wilson, G. W.; Connor, A. A.; Denroche, R. E.; Liang, S.-B.; Brown, A. M. K.; Kim, J. C.; et al. A Renewed Model of

Pancreatic Cancer Evolution Based on Genomic Rearrangement Patterns. *Nature* **2016**, *538* (7625), 378–382. https://doi.org/10.1038/nature19823.

- **An interesting research on a new model of PDAC evolution based on genomic rearrangement**

(37) Giovannetti, E.; van der Borden, C. L.; Frampton, A. E.; Ali, A.; Firuzi, O.; Peters, G. J. Never Let It Go: Stopping Key Mechanisms Underlying Metastasis to Fight Pancreatic Cancer. *Semin. Cancer Biol.* **2017**, *44*, 43–59. https://doi.org/10.1016/j.semcancer.2017.04.006.

(38) Erkan, M.; Reiser-Erkan, C.; Michalski, C. W.; Kong, B.; Esposito, I.; Friess, H.; Kleeff, J. The Impact of the Activated Stroma on Pancreatic Ductal Adenocarcinoma Biology and Therapy Resistance. *Curr. Mol. Med.* **2012**, *12* (3), 288–303. https://doi.org/10.2174/156652412799218921.

(39) Olive, K. P.; Jacobetz, M. A.; Davidson, C. J.; Gopinathan, A.; McIntyre, D.; Honess, D.; Madhu, B.; Goldgraben, M. A.; Caldwell, M. E.; Allard, D.; et al. Inhibition of Hedgehog Signaling Enhances Delivery of Chemotherapy in a Mouse Model of Pancreatic Cancer. *Science* **2009**, *324* (5933), 1457–1461. https://doi.org/10.1126/science.1171362.

(40) Maftouh, M.; Avan, A.; Sciarrillo, R.; Granchi, C.; Leon, L. G.; Rani, R.; Funel, N.; Smid, K.; Honeywell, R.; Boggi, U.; et al. Synergistic Interaction of Novel Lactate Dehydrogenase Inhibitors with Gemcitabine against Pancreatic Cancer Cells in Hypoxia. *Br. J. Cancer* **2014**, *110* (1), 172–182. https://doi.org/10.1038/bjc.2013.681.

(41) Neuzillet, C.; Tijeras-Raballand, A.; Ragulan, C.; Cros, J.; Patil, Y.; Martinet, M.; Erkan, M.; Kleeff, J.; Wilson, J.; Apte, M.; et al. Inter- and Intra-Tumoural Heterogeneity in Cancer-Associated Fibroblasts of Human Pancreatic Ductal Adenocarcinoma. *J. Pathol.* **2019**, *248* (1), 51–65. https://doi.org/10.1002/path.5224.

(42) Öhlund, D.; Handly-Santana, A.; Biffi, G.; Elyada, E.; Almeida, A. S.; Ponz-Sarvise, M.; Corbo, V.; Oni, T. E.; Hearn, S. A.; Lee, E. J.; et al. Distinct Populations of Inflammatory Fibroblasts and Myofibroblasts in Pancreatic Cancer. *J. Exp. Med.* **2017**, *214* (3), 579–596. https://doi.org/10.1084/jem.20162024.

(43) Limviphuvadh, V.; Tan, C. S.; Konishi, F.; Jenjaroenpun, P.; Xiang, J. S.; Kremenska, Y.; Mu, Y. S.; Syn, N.; Lee, S. C.; Soo, R. A.; et al. Discovering Novel SNPs That Are Correlated with Patient Outcome in a Singaporean Cancer Patient Cohort Treated with Gemcitabine-Based Chemotherapy. *BMC Cancer* **2018**, *18* (1), 555. https://doi.org/10.1186/s12885-018-4471-x.

(44) Li, F.; Hu, G.; Jiang, Z.; Guo, J.; Wang, K.; Ouyang, K.; Wen, D.; Zhu, M.; Liang, J.; Qin, X.; et al. Identification of NME5 as a Contributor to Innate Resistance to Gemcitabine in Pancreatic Cancer Cells. *FEBS J.* **2012**, *279* (7), 1261–1273. https://doi.org/10.1111/j.1742-4658.2012.08521.x.

(45) Lunenburg, C. A. T. C.; Guchelaar, H.-J.; van Schaik, R. H. N.; Neumaier, M.; Swen, J. J. Confirmation Practice in Pharmacogenetic Testing; How Good Is Good Enough? *Clin. Chim. Acta* **2019**, *490*, 77–80. https://doi.org/10.1016/j.cca.2018.12.023.

(46) Caiado, F.; Silva-Santos, B.; Norell, H. Intra-Tumour Heterogeneity - Going beyond Genetics. *FEBS J.* **2016**, *283* (12), 2245–2258. https://doi.org/10.1111/febs.13705.

(47) Longley, D. B.; Harkin, D. P.; Johnston, P. G. 5-Fluorouracil: Mechanisms of Action and Clinical Strategies. *Nat. Rev. Cancer* **2003**, *3* (5), 330–338. https://doi.org/10.1038/nrc1074.

(48) Marsh, S.; Hoskins, J. M. Irinotecan Pharmacogenomics. *Pharmacogenomics* **2010**, *11* (7), 1003–1010. https://doi.org/10.2217/pgs.10.95.

(49) Kweekel, D. M.; Gelderblom, H.; Guchelaar, H.-J. Pharmacology of Oxaliplatin and the Use of Pharmacogenomics to Individualize Therapy. *Cancer Treat. Rev.* **2005**, *31* (2), 90–105. https://doi.org/10.1016/j.ctrv.2004.12.006.

(50) Conroy, T.; Desseigne, F.; Ychou, M.; Bouché, O.; Guimbaud, R.; Bécouarn, Y.; Adenis, A.; Raoul, J.-L.; Gourgou-Bourgade, S.; de la Fouchardière, C.; et al. FOLFIRINOX versus Gemcitabine for Metastatic Pancreatic Cancer. *N. Engl. J. Med.* **2011**, *364* (19), 1817–1825. https://doi.org/10.1056/NEJMoa1011923.

(51) Sehdev, A.; Gbolahan, O.; Hancock, B. A.; Stanley, M.; Shahda, S.; Wan, J.; Wu, H. H.; Radovich, M.; O'Neil, B. H. Germline and Somatic DNA Damage Repair Gene Mutations and Overall Survival in Metastatic Pancreatic Adenocarcinoma Patients Treated with FOLFIRINOX. *Clin. Cancer Res.* **2018**, *24* (24), 6204–6211. https://doi.org/10.1158/1078-0432.CCR-18-1472.

(52) Kondo, T.; Kanai, M.; Kou, T.; Sakuma, T.; Mochizuki, H.; Kamada, M.; Nakatsui, M.; Uza, N.; Kodama, Y.; Masui, T.; et al. Association between Homologous Recombination Repair Gene Mutations and Response to Oxaliplatin in Pancreatic Cancer. *Oncotarget* **2018**, *9* (28), 19817–19825. https://doi.org/10.18632/oncotarget.24865.

(53) Meijer, L. L.; Garajová, I.; Caparello, C.; Le Large, T. Y. S.; Frampton, A. E.; Vasile, E.; Funel, N.; Kazemier, G.; Giovannetti, E. Plasma MiR-181a-5p Downregulation Predicts Response and Improved Survival After FOLFIRINOX in Pancreatic Ductal Adenocarcinoma. *Ann. Surg.* **2018**. https://doi.org/10.1097/SLA.0000000000003084.

(54) Avan, A.; Pacetti, P.; Reni, M.; Milella, M.; Vasile, E.; Mambrini, A.; Vaccaro, V.; Caponi, S.; Cereda, S.; Peters, G. J.; et al. Prognostic Factors in Gemcitabine-Cisplatin Polychemotherapy Regimens in Pancreatic Cancer: XPD-Lys751Gln Polymorphism Strikes Back. *Int. J. Cancer* **2013**, *133* (4), 1016–1022. https://doi.org/10.1002/ijc.28078.

(55) Tezuka, S.; Ueno, M.; Kobayashi, S.; Morimoto, M.; Ohkawa, S.; Hirotani, A.; Tozuka, Y.; Moriya, S.; Nakamura, Y.; Miyagi, Y.; et al. Predictive Value of ERCC1, ERCC2, ERCC4, and Glutathione S-Transferase Pi Expression for the Efficacy and Safety of FOLFIRINOX in Patients with Unresectable Pancreatic Cancer. *Am J Cancer Res* **2018**, *8* (10), 2096–2105.

(56) Wang, W.-B.; Yang, Y.; Zhao, Y.-P.; Zhang, T.-P.; Liao, Q.; Shu, H. Recent Studies of 5-Fluorouracil Resistance in Pancreatic Cancer. *World J Gastroenterol* **2014**, *20* (42), 15682–15690. https://doi.org/10.3748/wjg.v20.i42.15682.

(57) Kurata, N.; Fujita, H.; Ohuchida, K.; Mizumoto, K.; Mahawithitwong, P.; Sakai, H.; Onimaru, M.; Manabe, T.; Ohtsuka, T.; Tanaka, M. Predicting the Chemosensitivity of Pancreatic Cancer Cells by Quantifying the Expression Levels of Genes Associated with the Metabolism of Gemcitabine and 5-Fluorouracil. *Int. J. Oncol.* **2011**, *39* (2), 473–482. https://doi.org/10.3892/ijo.2011.1058.

(58) Nakayama, S.; Takeda, S.; Kawase, Y.; Inoue, S.; Kaneko, T.; Nakao, A. Clinical Significance of Dihydropyrimidine Dehydrogenase in Adjuvant 5-Fluorouracil Liver Perfusion Chemotherapy for Pancreatic Cancer. *Ann Surg* **2004**, *240* (5), 840–844. https://doi.org/10.1097/01.sla.0000143300.49878.51.

(59) Elander, N. O.; Aughton, K.; Ghaneh, P.; Neoptolemos, J. P.; Palmer, D. H.; Cox, T. F.; Campbell, F.; Costello, E.; Halloran, C. M.; Mackey, J. R.; et al. Expression of Dihydropyrimidine Dehydrogenase (DPD) and HENT1 Predicts Survival in Pancreatic Cancer. *Br. J. Cancer* **2018**, *118* (7), 947–954. https://doi.org/10.1038/s41416-018-0004-2.

(60) Zandomeni, R.; Mittleman, B.; Bunick, D.; Ackerman, S.; Weinmann, R. Mechanism of Action of Dichloro-Beta-D-Ribofuranosylbenzimidazole: Effect on in Vitro Transcription. *PNAS* **1982**, *79* (10), 3167–3170. https://doi.org/10.1073/pnas.79.10.3167.

(61) Bachet, J.-B.; Chibaudel, B.; Bonnetain, F.; Validire, P.; Hammel, P.; André, T.; Louvet, C.; GERCOR group. A Randomized Phase II Study of Weekly Nab-Paclitaxel plus Gemcitabine or Simplified LV5FU2 as First-Line Therapy in Patients with Metastatic

Pancreatic Cancer: The AFUGEM GERCOR Trial. *BMC Cancer* **2015**, *15*, 653. https://doi.org/10.1186/s12885-015-1656-4.

(62) Takeda, S.; Shimazoe, T.; Sato, K.; Sugimoto, Y.; Tsuruo, T.; Kono, A. Differential Expression of DNA Topoisomerase I Gene between CPT-11 Acquired- and Native-Resistant Human Pancreatic Tumor Cell Lines: Detected by RNA/PCR-Based Quantitation Assay. *Biochem. Biophys. Res. Commun.* **1992**, *184* (2), 618–625. https://doi.org/10.1016/0006-291x(92)90634-w.

(63) Grunnet, M.; Calatayud, D.; Schultz, N. A. A.; Hasselby, J. P.; Mau-Sørensen, M.; Brünner, N.; Stenvang, J. TOP1 Gene Copy Numbers Are Increased in Cancers of the Bile Duct and Pancreas. *Scand. J. Gastroenterol.* **2015**, *50* (4), 485–494. https://doi.org/10.3109/00365521.2014.980318.

(64) Capello, M.; Lee, M.; Wang, H.; Babel, I.; Katz, M. H.; Fleming, J. B.; Maitra, A.; Wang, H.; Tian, W.; Taguchi, A.; et al. Carboxylesterase 2 as a Determinant of Response to Irinotecan and Neoadjuvant FOLFIRINOX Therapy in Pancreatic Ductal Adenocarcinoma. *J. Natl. Cancer Inst.* **2015**, *107* (8). https://doi.org/10.1093/jnci/djv132.

- **An important study on candidate biomarkers in outcome of PDAC patients treated with FOLFIRINOX**

(65) Von Hoff, D. D.; Ervin, T.; Arena, F. P.; Chiorean, E. G.; Infante, J.; Moore, M.; Seay, T.; Tjulandin, S. A.; Ma, W. W.; Saleh, M. N.; et al. Increased Survival in Pancreatic Cancer with Nab-Paclitaxel plus Gemcitabine. *N. Engl. J. Med.* **2013**, *369* (18), 1691–1703. https://doi.org/10.1056/NEJMoa1304369.

- **The clinical study leading to approval of the combination ofgemcitabine and nab-paclitaxel in first-line treatment ofadvanced PDAC**

(66) Desai, N.; Trieu, V.; Yao, Z.; Louie, L.; Ci, S.; Yang, A.; Tao, C.; De, T.; Beals, B.; Dykes, D.; et al. Increased Antitumor Activity, Intratumor Paclitaxel Concentrations, and Endothelial Cell Transport of Cremophor-Free, Albumin-Bound Paclitaxel, ABI-007, Compared with Cremophor-Based Paclitaxel. *Clin. Cancer Res.* **2006**, *12* (4), 1317–1324. https://doi.org/10.1158/1078-0432.CCR-05-1634.

(67) Rodríguez-Antona, C. Pharmacogenomics of Paclitaxel. *Pharmacogenomics* **2010**, *11* (5), 621–623. https://doi.org/10.2217/pgs.10.32.

(68) Leskelä, S.; Jara, C.; Leandro-García, L. J.; Martínez, A.; García-Donas, J.; Hernando, S.; Hurtado, A.; Vicario, J. C. C.; Montero-Conde, C.; Landa, I.; et al. Polymorphisms

in Cytochromes P450 2C8 and 3A5 Are Associated with Paclitaxel Neurotoxicity. *Pharmacogenomics J.* **2011**, *11* (2), 121–129. https://doi.org/10.1038/tpj.2010.13.

(69) Rodriguez-Antona, C.; Ingelman-Sundberg, M. Cytochrome P450 Pharmacogenetics and Cancer. *Oncogene* **2006**, *25* (11), 1679–1691. https://doi.org/10.1038/sj.onc.1209377.

(70) Desai, N.; Pnsldent, V. Nab Technology : A Drug Delivery Platform Utilising Endothelial Gp 60 Receptor-Based Transport and Tumour-Derived SPARC for Targeting I; 2009.

(71) Neuzillet, C.; Tijeras-Raballand, A.; Cros, J.; Faivre, S.; Hammel, P.; Raymond, E. Stromal Expression of SPARC in Pancreatic Adenocarcinoma. *Cancer Metastasis Rev.* **2013**, *32* (3–4), 585–602. https://doi.org/10.1007/s10555-013-9439-3.

(72) Von Hoff, D. D.; Ramanathan, R. K.; Borad, M. J.; Laheru, D. A.; Smith, L. S.; Wood, T. E.; Korn, R. L.; Desai, N.; Trieu, V.; Iglesias, J. L.; et al. Gemcitabine plus Nab-Paclitaxel Is an Active Regimen in Patients with Advanced Pancreatic Cancer: A Phase I/II Trial. *J. Clin. Oncol.* **2011**, *29* (34), 4548–4554. https://doi.org/10.1200/JCO.2011.36.5742.

(73) Neesse, A.; Frese, K. K.; Chan, D. S.; Bapiro, T. E.; Howat, W. J.; Richards, F. M.; Ellenrieder, V.; Jodrell, D. I.; Tuveson, D. A. SPARC Independent Drug Delivery and Antitumour Effects of Nab-Paclitaxel in Genetically Engineered Mice. *Gut* **2014**, *63* (6), 974–983. https://doi.org/10.1136/gutjnl-2013-305559.

(74) Kim, H.; Samuel, S.; Lopez-Casas, P.; Grizzle, W.; Hidalgo, M.; Kovar, J.; Oelschlager, D.; Zinn, K.; Warram, J.; Buchsbaum, D. SPARC-Independent Delivery of Nab-Paclitaxel without Depleting Tumor Stroma in Patient-Derived Pancreatic Cancer Xenografts. *Mol. Cancer Ther.* **2016**, *15* (4), 680–688. https://doi.org/10.1158/1535-7163.MCT-15-0764.

(75) Hidalgo, M.; Plaza, C.; Musteanu, M.; Illei, P.; Brachmann, C. B.; Heise, C.; Pierce, D.; Lopez-Casas, P. P.; Menendez, C.; Tabernero, J.; et al. SPARC Expression Did Not Predict Efficacy of Nab-Paclitaxel plus Gemcitabine or Gemcitabine Alone for Metastatic Pancreatic Cancer in an Exploratory Analysis of the Phase III MPACT Trial. *Clin. Cancer Res.* **2015**, *21* (21), 4811–4818. https://doi.org/10.1158/1078-0432.CCR-14-3222.

(76) Frese, K. K.; Neesse, A.; Cook, N.; Bapiro, T. E.; Lolkema, M. P.; Jodrell, D. I.; Tuveson, D. A. Nab-Paclitaxel Potentiates Gemcitabine Activity by Reducing Cytidine Deaminase

Levels in a Mouse Model of Pancreatic Cancer. *Cancer Discov* **2012**, *2* (3), 260–269. https://doi.org/10.1158/2159-8290.CD-11-0242.

(77) Avan, A.; Caretti, V.; Funel, N.; Galvani, E.; Maftouh, M.; Honeywell, R. J.; Lagerweij, T.; Van Tellingen, O.; Campani, D.; Fuchs, D.; et al. Crizotinib Inhibits Metabolic Inactivation of Gemcitabine in C-Met-Driven Pancreatic Carcinoma. *Cancer Res.* **2013**, *73* (22), 6745–6756. https://doi.org/10.1158/0008-5472.CAN-13-0837.

(78) Neesse, A.; Frese, K. K.; Bapiro, T. E.; Nakagawa, T.; Sternlicht, M. D.; Seeley, T. W.; Pilarsky, C.; Jodrell, D. I.; Spong, S. M.; Tuveson, D. A. CTGF Antagonism with MAb FG-3019 Enhances Chemotherapy Response without Increasing Drug Delivery in Murine Ductal Pancreas Cancer. *Proc Natl Acad Sci U S A* **2013**, *110* (30), 12325–12330. https://doi.org/10.1073/pnas.1300415110.

(79) Hwang, J.-E.; Hong, J.-Y.; Kim, K.; Kim, S.-H.; Choi, W.-Y.; Kim, M.-J.; Jung, S.-H.; Shim, H.-J.; Bae, W.-K.; Hwang, E.-C.; et al. Class III β-Tubulin Is a Predictive Marker for Taxane-Based Chemotherapy in Recurrent and Metastatic Gastric Cancer. *BMC Cancer* **2013**, *13*, 431. https://doi.org/10.1186/1471-2407-13-431.

(80) Kato, A.; Naiki-Ito, A.; Naitoh, I.; Hayashi, K.; Nakazawa, T.; Shimizu, S.; Nishi, Y.; Okumura, F.; Inoue, T.; Takada, H.; et al. The Absence of Class III β-Tubulin Is Predictive of a Favorable Response to Nab-Paclitaxel and Gemcitabine in Patients with Unresectable Pancreatic Ductal Adenocarcinoma. *Hum. Pathol.* **2018**, *74*, 92–98. https://doi.org/10.1016/j.humpath.2018.01.009.

(81) Sève, P.; Mackey, J.; Isaac, S.; Trédan, O.; Souquet, P.-J.; Pérol, M.; Lai, R.; Voloch, A.; Dumontet, C. Class III Beta-Tubulin Expression in Tumor Cells Predicts Response and Outcome in Patients with Non-Small Cell Lung Cancer Receiving Paclitaxel. *Mol. Cancer Ther.* **2005**, *4* (12), 2001–2007. https://doi.org/10.1158/1535-7163.MCT-05-0244.

(82) Seymour, L.; Le Teuff, G.; Brambilla, E.; Shepherd, F. A.; Soria, J.-C.; Kratzke, R.; Graziano, S.; Douillard, J.-Y.; Rosell, R.; Reiman, A.; et al. LACE-Bio: Validation of Predictive and/or Prognostic Immunohistochemistry/Histochemistry-Based Biomarkers in Resected Non-Small-Cell Lung Cancer. *Clin Lung Cancer* **2019**, *20* (2), 66-73.e6. https://doi.org/10.1016/j.cllc.2018.10.001.

(83) Aldonza, M. B. D.; Hong, J.-Y.; Alinsug, M. V.; Song, J.; Lee, S. K. Multiplicity of Acquired Cross-Resistance in Paclitaxel-Resistant Cancer Cells Is Associated with Feedback Control of TUBB3 via FOXO3a-Mediated ABCB1 Regulation. *Oncotarget* **2016**, *7* (23), 34395–34419. https://doi.org/10.18632/oncotarget.9118.

(84) Lockhart, A. C.; Tirona, R. G.; Kim, R. B. Pharmacogenetics of ATP-Binding Cassette Transporters in Cancer and Chemotherapy. *Mol. Cancer Ther.* **2003**, *2* (7), 685–698.

(85) Mathijssen, R. H. J.; Marsh, S.; Karlsson, M. O.; Xie, R.; Baker, S. D.; Verweij, J.; Sparreboom, A.; McLeod, H. L. Irinotecan Pathway Genotype Analysis to Predict Pharmacokinetics. *Clin. Cancer Res.* **2003**, *9* (9), 3246–3253.

(86) Jaramillo, A.; Saig, F.; Cloos, J.; Jansen, G.; Peters, G. How to Overcome ATP-Binding Cassette Drug Efflux Transporter-Mediated Drug Resistance? *Cancer Drug Resistance* **2018**, *1*, 6–29. https://doi.org/10.20517/cdr.2018.02.

(87) Codacci-Pisanelli, G.; Frati, L.; Mini, E. Three Cheers for Targeted Therapy in Non-Small Cell Lung Cancer... When We Hit the Target! *J Chemother* **2011**, *23* (4), 245–246. https://doi.org/10.1179/joc.2011.23.4.245.

(88) Moscow, J. A.; Fojo, T.; Schilsky, R. L. The Evidence Framework for Precision Cancer Medicine. *Nat Rev Clin Oncol* **2018**, *15* (3), 183–192. https://doi.org/10.1038/nrclinonc.2017.186.

(89) Le Large, T. Y. S.; Mato Prado, M.; Krell, J.; Bijlsma, M. F.; Meijer, L. L.; Kazemier, G.; Frampton, A. E.; Giovannetti, E. Bioinformatic Analysis Reveals Pancreatic Cancer Molecular Subtypes Specific to the Tumor and the Microenvironment. *Expert Rev. Mol. Diagn.* **2016**, *16* (7), 733–736. https://doi.org/10.1080/14737159.2016.1175940.

(90) Caparello, C.; Meijer, L. L.; Garajova, I.; Falcone, A.; Le Large, T. Y.; Funel, N.; Kazemier, G.; Peters, G. J.; Vasile, E.; Giovannetti, E. FOLFIRINOX and Translational Studies: Towards Personalized Therapy in Pancreatic Cancer. *World J. Gastroenterol.* **2016**, *22* (31), 6987–7005. https://doi.org/10.3748/wjg.v22.i31.6987.

(91) McAllister, S. S.; Weinberg, R. A. The Tumour-Induced Systemic Environment as a Critical Regulator of Cancer Progression and Metastasis. *Nat. Cell Biol.* **2014**, *16* (8), 717–727. https://doi.org/10.1038/ncb3015.

(92) Neesse, A.; Bauer, C. A.; Öhlund, D.; Lauth, M.; Buchholz, M.; Michl, P.; Tuveson, D. A.; Gress, T. M. Stromal Biology and Therapy in Pancreatic Cancer: Ready for Clinical Translation? *Gut* **2019**, *68* (1), 159–171. https://doi.org/10.1136/gutjnl-2018-316451.

- **A state-of-the-art review on new potential anti-stromal approaches in PDAC**

(93) Neesse, A.; Algül, H.; Tuveson, D. A.; Gress, T. M. Stromal Biology and Therapy in Pancreatic Cancer: A Changing Paradigm. *Gut* **2015**, *64* (9), 1476–1484. https://doi.org/10.1136/gutjnl-2015-309304.

(94) Grasso, C.; Jansen, G.; Giovannetti, E. Drug Resistance in Pancreatic Cancer: Impact of Altered Energy Metabolism. *Crit. Rev. Oncol. Hematol.* **2017**, *114*, 139–152. https://doi.org/10.1016/j.critrevonc.2017.03.026.

(95) Ireland, L.; Santos, A.; Ahmed, M. S.; Rainer, C.; Nielsen, S. R.; Quaranta, V.; Weyer-Czernilofsky, U.; Engle, D. D.; Perez-Mancera, P. A.; Coupland, S. E.; et al. Chemoresistance in Pancreatic Cancer Is Driven by Stroma-Derived Insulin-Like Growth Factors. *Cancer Res.* **2016**, *76* (23), 6851–6863. https://doi.org/10.1158/0008-5472.CAN-16-1201.

(96) Halbrook, C. J.; Pontious, C.; Kovalenko, I.; Lapienyte, L.; Dreyer, S.; Lee, H.-J.; Thurston, G.; Zhang, Y.; Lazarus, J.; Sajjakulnukit, P.; et al. Macrophage-Released Pyrimidines Inhibit Gemcitabine Therapy in Pancreatic Cancer. *Cell Metab.* **2019**. https://doi.org/10.1016/j.cmet.2019.02.001.

(97) Özdemir, B. C.; Pentcheva-Hoang, T.; Carstens, J. L.; Zheng, X.; Wu, C.-C.; Simpson, T. R.; Laklai, H.; Sugimoto, H.; Kahlert, C.; Novitskiy, S. V.; et al. Depletion of Carcinoma-Associated Fibroblasts and Fibrosis Induces Immunosuppression and Accelerates Pancreas Cancer with Reduced Survival. *Cancer Cell* **2014**, *25* (6), 719–734. https://doi.org/10.1016/j.ccr.2014.04.005.

(98) Zheng, X.; Carstens, J. L.; Kim, J.; Scheible, M.; Kaye, J.; Sugimoto, H.; Wu, C.-C.; LeBleu, V. S.; Kalluri, R. Epithelial-to-Mesenchymal Transition Is Dispensable for Metastasis but Induces Chemoresistance in Pancreatic Cancer. *Nature* **2015**, *527* (7579), 525–530. https://doi.org/10.1038/nature16064.

(99) Yen, W.-C.; Fischer, M. M.; Axelrod, F.; Bond, C.; Cain, J.; Cancilla, B.; Henner, W. R.; Meisner, R.; Sato, A.; Shah, J.; et al. Targeting Notch Signaling with a Notch2/Notch3 Antagonist (Tarextumab) Inhibits Tumor Growth and Decreases Tumor-Initiating Cell Frequency. *Clin. Cancer Res.* **2015**, *21* (9), 2084–2095. https://doi.org/10.1158/1078-0432.CCR-14-2808.

(100) Results of a randomized phase II trial of an anti-notch 2/3, tarextumab (OMP-59R5, TRXT, anti-Notch2/3), in combination with nab-paclitaxel and gemcitabine (Nab-P+Gem) in patients (pts) with untreated metastatic pancreatic cancer (mPC). | Journal of Clinical Oncology https://ascopubs.org/doi/abs/10.1200/JCO.2017.35.4_suppl.279 (accessed Oct 1, 2019).

(101) Cook, N.; Basu, B.; Smith, D.-M.; Gopinathan, A.; Evans, J.; Steward, W. P.; Palmer, D.; Propper, D.; Venugopal, B.; Hategan, M.; et al. A Phase I Trial of the γ-Secretase Inhibitor MK-0752 in Combination with Gemcitabine in Patients with Pancreatic Ductal

Adenocarcinoma. *Br. J. Cancer* **2018**, *118* (6), 793–801. https://doi.org/10.1038/bjc.2017.495.

(102) Rhim, A. D.; Oberstein, P. E.; Thomas, D. H.; Mirek, E. T.; Palermo, C. F.; Sastra, S. A.; Dekleva, E. N.; Saunders, T.; Becerra, C. P.; Tattersall, I. W.; et al. Stromal Elements Act to Restrain, Rather than Support, Pancreatic Ductal Adenocarcinoma. *Cancer Cell* **2014**, *25* (6), 735–747. https://doi.org/10.1016/j.ccr.2014.04.021.

(103) Krantz, B. A.; Yu, K. H.; O'Reilly, E. M. Pancreas Adenocarcinoma: Novel Therapeutics. *Chin Clin Oncol* **2017**, *6* (3), 30. https://doi.org/10.21037/cco.2017.06.14.

(104) Hurwitz, H. I.; Uppal, N.; Wagner, S. A.; Bendell, J. C.; Beck, J. T.; Wade, S. M.; Nemunaitis, J. J.; Stella, P. J.; Pipas, J. M.; Wainberg, Z. A.; et al. Randomized, Double-Blind, Phase II Study of Ruxolitinib or Placebo in Combination With Capecitabine in Patients With Metastatic Pancreatic Cancer for Whom Therapy With Gemcitabine Has Failed. *J. Clin. Oncol.* **2015**, *33* (34), 4039–4047. https://doi.org/10.1200/JCO.2015.61.4578.

(105) Hurwitz, H.; Van Cutsem, E.; Bendell, J.; Hidalgo, M.; Li, C.-P.; Salvo, M. G.; Macarulla, T.; Sahai, V.; Sama, A.; Greeno, E.; et al. Ruxolitinib + Capecitabine in Advanced/Metastatic Pancreatic Cancer after Disease Progression/Intolerance to First-Line Therapy: JANUS 1 and 2 Randomized Phase III Studies. *Invest New Drugs* **2018**, *36* (4), 683–695. https://doi.org/10.1007/s10637-018-0580-2.

(106) Jardim, D. L.; Groves, E. S.; Breitfeld, P. P.; Kurzrock, R. Factors Associated with Failure of Oncology Drugs in Late-Stage Clinical Development: A Systematic Review. *Cancer Treat. Rev.* **2017**, *52*, 12–21. https://doi.org/10.1016/j.ctrv.2016.10.009.

(107) Rahib, L.; Fleshman, J. M.; Matrisian, L. M.; Berlin, J. D. Evaluation of Pancreatic Cancer Clinical Trials and Benchmarks for Clinically Meaningful Future Trials: A Systematic Review. *JAMA Oncol* **2016**, *2* (9), 1209–1216. https://doi.org/10.1001/jamaoncol.2016.0585.

- **An important systematic review describing the evolution of clinical trials and potential causes of their failure in PDAC patients.**

(108) Oberstein, P. E.; Olive, K. P. Pancreatic Cancer: Why Is It so Hard to Treat? *Therap Adv Gastroenterol* **2013**, *6* (4), 321–337. https://doi.org/10.1177/1756283X13478680.

(109) Lidsky, M. E.; Sun, Z.; Nussbaum, D. P.; Adam, M. A.; Speicher, P. J.; Blazer, D. G. Going the Extra Mile: Improved Survival for Pancreatic Cancer Patients Traveling to High-Volume Centers. *Ann. Surg.* **2017**, *266* (2), 333–338. https://doi.org/10.1097/SLA.0000000000001924.

(110) Birkmeyer, J. D.; Siewers, A. E.; Finlayson, E. V. A.; Stukel, T. A.; Lucas, F. L.; Batista, I.; Welch, H. G.; Wennberg, D. E. Hospital Volume and Surgical Mortality in the United States. *N. Engl. J. Med.* **2002**, *346* (15), 1128–1137. https://doi.org/10.1056/NEJMsa012337.

(111) Brais, R. J.; Davies, S. E.; O'Donovan, M.; Simpson, B. W.; Cook, N.; Darbonne, W. C.; Chilcott, S.; Lolkema, M. P.; Neesse, A.; Lockley, M.; et al. Direct Histological Processing of EUS Biopsies Enables Rapid Molecular Biomarker Analysis for Interventional Pancreatic Cancer Trials. *Pancreatology* **2012**, *12* (1), 8–15. https://doi.org/10.1016/j.pan.2011.12.009.

(112) Precision PromiseSM Clinical Trial Consortium Sites - Pancreatic Cancer Action Network/. *Pancreatic Cancer Action Network*.

(113) Guchelaar, H.-J.; Gelderblom, H.; van der Straaten, T.; Schellens, J. H. M.; Swen, J. J. Pharmacogenetics in the Cancer Clinic: From Candidate Gene Studies to next-Generation Sequencing. *Clin. Pharmacol. Ther.* **2014**, *95* (4), 383–385. https://doi.org/10.1038/clpt.2014.13.

(114) Tannock, I. F.; Hickman, J. A. Limits to Personalized Cancer Medicine. *N. Engl. J. Med.* **2016**, *375* (13), 1289–1294. https://doi.org/10.1056/NEJMsb1607705.

(115) Karachaliou, N.; Mayo-de-Las-Casas, C.; Molina-Vila, M. A.; Rosell, R. Real-Time Liquid Biopsies Become a Reality in Cancer Treatment. *Ann Transl Med* **2015**, *3* (3), 36. https://doi.org/10.3978/j.issn.2305-5839.2015.01.16.

(116) Rolfo, C.; Mack, P. C.; Scagliotti, G. V.; Baas, P.; Barlesi, F.; Bivona, T. G.; Herbst, R. S.; Mok, T. S.; Peled, N.; Pirker, R.; et al. Liquid Biopsy for Advanced Non-Small Cell Lung Cancer (NSCLC): A Statement Paper from the IASLC. *J Thorac Oncol* **2018**, *13* (9), 1248–1268. https://doi.org/10.1016/j.jtho.2018.05.030.

Part II

Evaluation of biological activity of the new class of imidazo[2,1-b][1,3,4]thiadiazole compounds as antitumor and their repurposing as antibiofilm agents

(chapters 5-8)

Chapter 5

Biological Evaluation of the Antiproliferative and Anti-migratory Activity of a Series of 3-(6-Phenylimidazo[2,1-b][1,3,4]thiadiazol-2-yl)-1H-indole Derivatives Against Pancreatic Cancer Cells

Li Petri G[1,2], Cascioferro S[2], El Hassouni B[1], Carbone D[2], Parrino B[2], Cirrincione G[2], Peters GJ[1], Diana P[2], Giovannetti E[1,3]

1. *Department of Medical Oncology, Cancer Center Amsterdam, Amsterdam UMC, VU University Medical Center (VUmc), Amsterdam, The Netherlands*
2. *Department of Biological, Chemical and Pharmaceutical Sciences and Technologies (STEBICEF), University of Palermo, Palermo, Italy*
3. *Cancer Pharmacology Laboratory, AIRC Start-Up Unit, Fondazione Pisana per la Scienza, Pisa, Italy*

Anticancer Research. 2019 July;39(7):3615-3620

doi: 10.21873/anticanres.13509

Biological Evaluation of the Antiproliferative and Anti-migratory Activity of a Series of 3-(6-Phenylimidazo[2,1-b][1,3,4]thiadiazol-2-yl)-1H-indole Derivatives Against Pancreatic Cancer Cells

Abstract

Heterocyclic rings have been recognized as a key component of many natural, semi-synthetic and synthetic molecules with a broad spectrum of biological activities. Among these molecules, the indole and imidazo[2,1-*b*][1,3,4]thiadiazole systems have recently been described as useful scaffolds for the design of anticancer agents. Here we assessed the antitumor activity of a series of 3-(6-phenylimidazo[2,1-*b*][1,3,4]thiadiazol-2-yl)-1*H*-indoles, designed as hybrid structures. Seven out of ten compounds (**1a-g**) were submitted to the National Cancer Institute (NCI) screening. Remarkably, compound **1g** showed anti-proliferative activity on the full panel of sixty human cancer lines, with GI_{50}s between 1.67 and 10.3 µM. Further studies showed antitumor activity of **1g**, **1h, 1i** and **1l** in 3 pancreatic cancer cell lines. In particular, derivatives **1g** and **1h** inhibited both proliferation and migration of SUIT-2 cells at concentrations lower than 10 µM. In conclusion, new indole derivatives are characterized by *in vitro* antitumor activity, supporting future mechanistic studies.

Keywords: imidazo[2,1-*b*][1,3,4]thiadiazole derivatives, indole system, anti-proliferative activity, anti-migratory activity, pancreatic cancer.

Introduction

The use of the heterocyclic ring systems containing oxygen, nitrogen or sulphur heteroatom(s), is attracting much attention in the field of medicinal chemistry for the design and development of new potential therapeutic agents.[1] The incorporation of heterocyclic rings makes it possible to modify some important pharmaceutical parameters such as lipophilicity, polarity and aqueous solubility, in order to obtain lead compounds with ideal biological and physical-chemical features. These characteristics are essential to predict the selectivity and potency of a candidate drug.[2] The indole nucleus has recently emerged as one of the most relevant heterocyclic rings, endorsed by the unique ability to mimic peptide derivatives and reversibly bind proteins.[3] Many indole derivatives endowed with significant biological activities including anti-inflammatory, analgesic,[4] antiviral,[5] anticancer[6–10] and antibacterial agents[11] were reported in the last decade. Additionally, the imidazo[2,1-*b*][1,3,4]thiadiazole ring system has been described as an important scaffold for the design and the synthesis of compounds with different therapeutic properties such as anti-tubercular,[12] antibacterial,[13] anticonvulsant and analgesic,[14] antifungal[15] and anticancer.[16,17]

On the basis of these findings as well as on the concept of the "One-Compound-Multi-Target",[18,19] we synthesized a series of hybrid structures, 3-(6-phenylimidazo[2,-1-*b*][1,3,4]thiadiazol-2-yl)-1*H*-indoles, in order to obtain active analogues with different biological activities. Interestingly, these compounds were able to inhibit the biofilm formation of the Gram-positive bacterial reference strains *Staphylococcus aureus* ATCC 25923, *S. aureus* ATCC 6538 and *Staphylococcus epidermidis* ATCC 12228 at low micromolar concentration.[20] Since previous studies reported that several compounds bearing the imidazo[2,1-*b*][1,3,4]thiadiazole ring system showed potent anticancer activity[17] we decided to assay ten imidazo[2,1-*b*][1,3,4]thiadiazole compounds (Figure 1) also for their antiproliferative activity. For this purpose, seven out of these compounds, **1a-g**, (Figure 1) were submitted to the National Cancer Institute (NCI) screening.[21] This screening is performed for the evaluation of their antitumor activity on a panel of 60 human cancer cell lines derived from 9 cancer types grouped into disease subpanels including leukemia, non-small cell lung, colon, central nervous system, melanoma, ovarian, renal, prostate, and breast tumors. Furthermore, we investigated the antiproliferative activity of the imidazo[2,1-*b*][1,3,4]thiadiazoles **1a-l** on three pre-clinical models of pancreatic ductal adenocarcinoma (PDAC), including SUIT-2, Capan-1 and Panc-1. PDAC is a deadly disease with poor prognosis and high mortality rate. According to Rahib and collaborators,

PDAC will become the second leading cause of cancer death in the United States in the next ten years.[22] Nowadays, there are no effective treatments for patients with advanced PDAC. Therefore, new drugs to treat this aggressive tumor are urgently needed.

Materials and methods

Drugs and chemical

The imidazo[2,1-*b*][1,3,4]thiadiazole compounds were synthesised as previously described.[20] The drugs were dissolved in dimethyl sulfoxide (DMSO). The medium, foetal bovine serum (FBS), penicillin (50 IU mL^{-1}) and streptomycin (50 µg mL^{-1}) were from Gibco (Gaithersburg, MD, USA). All other chemicals were from Sigma (Zwijndrecht, the Netherlands).

Cell culture

Capan-1 and Panc-1 cell lines, were purchased at the ATCC (Manassas, VA, USA), while SUIT-2 cells were a generous gift from Dr. Adam Frampton (Imperial College, London, UK), The cell lines were tested for their authentication by STR–PCR, performed by BaseClear (Leiden, the Netherlands). The cells were cultured in RPMI-1640 (Roswell Park Memorial Institute 1640) supplemented with 10% heat-inactivated FBS, 1% penicillin/streptomycin, or in DMEM (Dulbecco's Modified Eagle's Medium), supplemented with 10% heat-inactivated FBS, 1% HEPES. The cells were kept in a humidified atmosphere of 5% CO_2 and 95% air at 37 °C and harvested with trypsin-EDTA.

Cell growth inhibition

The *in vitro* antiproliferative activity of imidazothiadiazole compounds **1a-g** was evaluated by the NCI on a panel of human cancer cells including cells derived from different tumor types, using the NCI validated protocol: https://dtp.cancer.gov/discovery_development/nci-60/methodology.htm. Furthermore, the in vitro antiproliferative activity of imidazothiadiazole compounds **1a-l** was assessed on the PDAC cells SUIT-2, Capan-1 and Panc-1, by the sulforhodamine-B (SRB) assay, as previously described.[23] In short, cells were seeded into 96-well flat-bottom plates in a volume of 100 µL at a density of $3x10^3$ cells/well for SUIT-2 and Panc-1, while $5x10^3$ cells/well were seeded for Capan-1. Cells were incubated for 24 hours at 37 °C to create a monolayer and then they were treated with 100 µL of the compounds dissolved in DMSO at different concentrations in the nano- and micro-molar range. After 72 hours treatment the cells were fixed with 25 µL of 50% cold trichloroacetic acid (TCA) and kept for at least 60 minutes at 4°C. Then, the plates were washed gently with deionized water, dried

at room temperature (RT) overnight and stained with 50 μL of 0.4% SRB solution in 1% acetic acid for 15 minutes at RT. The excess of SRB was removed on dried tissues and the plates were washed with a 1% acetic acid solution and dried at RT overnight. The SRB was dissolved in 150 μL of tris(hydroxymethyl)aminomethane solution pH= 8.8 (TRIS base), and the optical density (OD) was measured at wavelengths of 490 nm and 540 nm. Cell growth inhibition was calculated as the percentage of drug treated cells *versus* vehicle-treated cells ("negative control") OD (corrected for OD before drug addiction, "day-0"). Finally, the half maximal inhibitory concentration (IC_{50}) was calculated with GraphPad Prism 7 (Intuitive Software for Science). The 50% inhibitory concentration of cell growth (IC_{50}) was calculated by non-linear least squares curve fitting (GraphPad PRISM, Intuitive Software for Science, San Diego, CA). In the NCI protocol IC_{50} is denoted as GI_{50} (50% growth inhibitory concentration).

Wound-healing assay

The *in vitro* scratch wound-healing assay was performed as previously described.[24] SUIT-2 cells were seeded in 96-well flat-bottom plates at a density of $5x10^4$ cells/well in 100 μL. After 24 hours of pre-incubation at 37 °C, 5% CO_2 and 100% humidity, the cell monolayer was scratched with a specific scratch tool to create a scratch of constant width. After removal of the detached cells by washing with phosphate buffered saline (PBS), medium containing the compounds of interest was added to the experimental wells. The wound confluence was monitored by phase-contrast microscopy using a Universal Grab 6.3 software (Digital Cell Imaging Labs, Keerbergen, Belgium) integrated to the Leica DMI300B migration station (Leica Microsystems, Eindhoven, Netherlands) and the pictures were captured immediately after scratch and treatment (T = 0, and 4, 8, 20 and 24). The results were analyzed with the Scratch Assay 6.2 software (Digital Cell Imaging Labs).

Statistical analysis

All SRB assays were carried out in triplicate and repeated at least three times, whereas the percentages of cell migration were calculated taking into account at least six scratch areas. The data was evaluated using the GraphPad Prism version 7 software (GraphPad Software, San Diego, CA, USA). Data is expressed as mean values ± SEM and analyzed by the Student t test.

Table I. Concentrations leading to 50% growth inhibition (GI_{50}) and total growth inhibition (TGI) by compound **1g** against cell lines of the National Cancer Institute panel.

Panel/cell line	**Compound 1g**		**Panel/cell line**	**Compound 1g**	
	GI_{50}	**TGI**		**GI_{50}**	**TGI**
Leukemia			**Melanoma**		
CCRF-CEM	3.73	>1.00	MALME-3M	2.25	4.93
HL-60(TB)	9.21	>1.00	M14	2.10	4.75
K-562	2.51	-	MDA-MB-435	2.42	5.82
RPMI-8226	3.19	20.4	SK-MEL-2	3.33	13.4
Non-Small			SK-MEL-28	3.29	11.7
Cell					
Lung Cancer					
A549/ATCC	2.31	5.31	SK-MEL-5	3.86	15.2
EKVX	2.83	11.4	UACC-257	7.45	30.7
HOP-62	2.70	13.3	UACC-62	3.15	13.2
HOP-92	2.01	5.68	**Ovarian**		
			Cancer		
NCI-H226	10.3	39.8	IGROV1	2.27	11.5
NCI-H23	1.99	4.82	OVCAR-3	1.96	4.32
NCI-H322M	3.17	20.0	OVCAR-4	1.80	3.80
NCI-H460	2.04	4.17	OVCAR-5	3.52	15.6
NCI-H522	1.98	4.81	OVCAR-8	3.01	9.30
Colon Cancer			NCI/ADR-RES	3.38	10.9
HCC-2998	2.67	54.9	SK-OV-3	9.01	22.8
HCT-116	1.67	64.3	**Renal Cancer**		
HCT-15	2.11	>1.00	786-0	2.16	4.57
HT29	2.28	9.90	A498	10.2	24.6
KM12	2.19	>1.00	ACHN	2.02	6.49
SW-620	2.26	>1.00	CAKI-1	2.04	6.22
CSN Cancer			RXF 393	3.19	8.82
SF-268	2.70	7.60	SN12C	2.74	10.0
SF-295	4.70	1.63	TK-10	3.18	6.55
SF-539	1.78	3.41	UO-31	1.67	11.2
SNB-19	4.51	18.6	**Breast Cancer**		
SNB-75	3.72	24.3	MCF7	1.77	5.13
U251	2.02	4.09	MDA-MB-	1.73	4.05
			231/ATCC		
Prostate			HS 578T	2.87	14.5
Cancer					
PC-3	1.87	4.66	BT-549	2.90	11.2
DU-145	2.80	7.71	MDA-MB-468	2.94	8.41

Results and discussion

Antiproliferative activity of the imidazo[2,1-b][1,3,4]thiadiazole derivatives 1a-l.

Compounds **1a-g** were submitted to the National Cancer Institute (NCI, Bethesda MD) and pre-screened, according to the NCI protocol, at one concentration (10 μM) in a full panel of 60 human cancer cell lines. The derivative **1g** satisfied the threshold inhibition criteria established by the NCI and was further selected for full evaluation at five concentration levels (10^{-4}-10^{-8} M). Remarkably, its GI_{50s} were in the range from 1.67 to 10.3 μM (**Table 1**). The antiproliferative effect of the compound **1g** was then evaluated on PDAC cells, using eight increasing concentrations (from 0.125 nM to 20 μM). The PDAC cells were also used to explore the activity of the compounds **1h-l** in order to investigate the specific role of a different halogen on the indole moiety (compound **1l**) as well as the effects of *N*-methyl-indole (compound **1h**) or by different substituents on the phenyl ring (compounds **1i-l**). As shown in the table and in the lower panel of the Table II the compounds **1a-h** showed a relevant anti-proliferative activity, mostly on SUIT-2 cells, with IC_{50} values in the range of 4.3 to 10.7 μM. In particular, the lowest IC_{50s} were observed in SUIT-2 cells exposed to **1e** and **1f** (4.3-5.0 μM). Conversely, the IC_{50} of the **1i** compound was above 20 μM in all cell lines. Capan-1 and Panc-1 cells were more resistant to all the compounds, with IC_{50}s>20 μM, except to compound **1l,** which was more active in Capan-1 cells (with IC_{50} of 13.8 μM compared to >20 μM in both SUIT-2 and Panc-1 cells). Compound **1g** was active both in SUIT-2 and Panc-1 cells**,** with IC_{50}s between 8.4 and 9.8 μM, respectively. Notably, compound **1d** showed anti-proliferative activity against SUIT-2 cells with IC_{50} of 5.16 μM. Instead, in Capan-1 and Panc-1 cells, it displayed moderate antiproliferative activity with IC_{50s} of 9.73 and 10.56 μM, respectively.

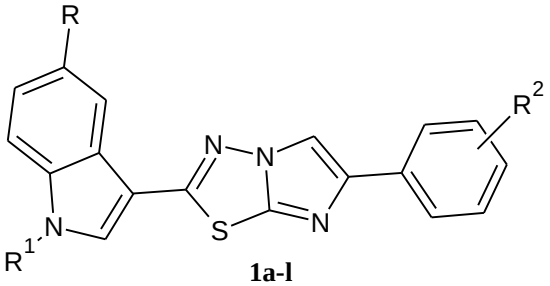

1a-l

	Substituents			Cell lines and [a]IC_{50} (μM) ± SEM[b]		
Compound	**R**	**R^1**	**R^2**	**SUIT-2**	**Capan-1**	**Panc-1**
1a	H	H	H	10.7 ± 0.23	>20	>20
1b	H	H	3-OCH_3	9.57 ± 0.54	>20	>20
1c	H	H	4-CF_3	5.90 ± 0.46	>20	>20
1d	H	CH_3	H	5.16 ± 0.10	9.73 ± 0.82	10.56 ± 0.11
1e	H	CH_3	3-OCH_3	4.30 ± 0.29	>20	>20
1f	H	CH_3	2,5-OCH_3	5.00 ± 0.38	>20	>20
1g	Br	H	2,5-OCH_3	8.40 ± 0.16	>20	9.84 ± 0.24
1h	Br	CH_3	2,5-OCH_3	5.96 ± 0.28	>20	>20
1i	Br	CH_3	4-CF_3	>20	>20	>20
1l	Cl	H	4-F	>20	13.75 ± 0.84	>20

[a]The values are reported as means ± SEM of three separate experiments.

[b]SEM: Standard Error of the Mean

Table II. Anti-proliferative activity of the compounds 1a-l on SUIT-2, Capan-1 and Panc-1 cells. (*Upper panel*) Chemical structure of the compound **1a-l**. (*Lower panel - table*) List of the compounds, reporting the information on the chemical structure of the R, R^1 and R^2 components and the IC_{50} values ± SEM in the PDAC cell lines.

Antimigratory activity of the compounds 1c-f, and 1g,h on SUIT-2 cells.

Cell migration and invasion are essential for spreading cells from the primary tumor to distant sites and creating metastatic outbreaks. This is a relevant aspect that contributes to the poor prognosis of many cancers. In particular, PDAC is an aggressive metastatic disease and to date, the molecular mechanisms that drive the metastatic events are still unknown. Certainly, a key role is played by the stroma components that maintain cell growth and facilitate the acquisition of aggressive and invasive features.[25] The human cell line SUIT-2 was derived from a metastatic lesion in the liver of a PDAC patient and we selected these cells as an optimal model for studying the anti-migratory activity of our new compounds.[26] Considering the interesting *in vitro* antiproliferative activities of the compounds **1c-f** and **h**, together with the NCI results of the compound **1g**, we selected

these compounds for the analysis of the inhibition of the migration rate using a high-throughput screening scratch wound healing assay. The SUIT-2 cells were treated with the compounds **1c-f,** and **1h** at 3x IC_{50}, whereas compound **1g** was used at its IC_{50} value. The percentage of migration was monitored over time through a series of pictures captured immediately after scratch and treatment (T=0) and after 4, 8, 20 and 24 hours. As shown in the Figure 2A, unexpectedly, compounds **1c** and **1f** supported cell migration. Previous studies, showed the ability of indoles to reduce migration in cancer cells,[27] but a seminal study on the oral oxindole multitargeted kinase inhibitor sunitinib reported metastatic acceleration depending on treatment schedule and tumor models.[28] However, compounds **1d**, **1e**, **1g** and **1h** slowed the migratory effect of the cells compared to the controls (Figure 2A,B). In particular, compared to untreated cells (set at 100%), the percentages of migration in cells treated for 24 hours with the compounds **1d**, **1e**, **1g** and **1h** were 72.7%, 84.1%, 61.3% and 68.2%, respectively.

These anti-migratory effects were more evident at 20 and 24 hours from the start of the treatment, and statistical analyses showed that the inhibition of migration compared to control was significant for the compounds **1f** and **1h**.

Importantly, in order to optimize the experimental conditions for the wound-healing assay, we determined the duplication time of SUIT-2 cells, which were above 24 hours. Moreover, we measured the area of the wound track (as shown in representative pictures in Figure 2C), which was approximately 10^6 μm^2. This is too large to be covered by only cell proliferation in 24 hours, since the average tumor adherent cell surface is around 100-150 μm^2. Ultimately, we did not observe detached cells after 24-hour drug treatment, which proves that drug exposure did not cause cell death at that timepoint.

Finally, these results were comparable to previous data showing that indole-3-carbinol and indole[3,2-*b*]carbazole suppress EMT and migration of breast cancer cells through the repression of focal adhesion kinase,[29] and will prompt future studies on molecular mechanisms underlying the anti-migratory activity of our new compounds.

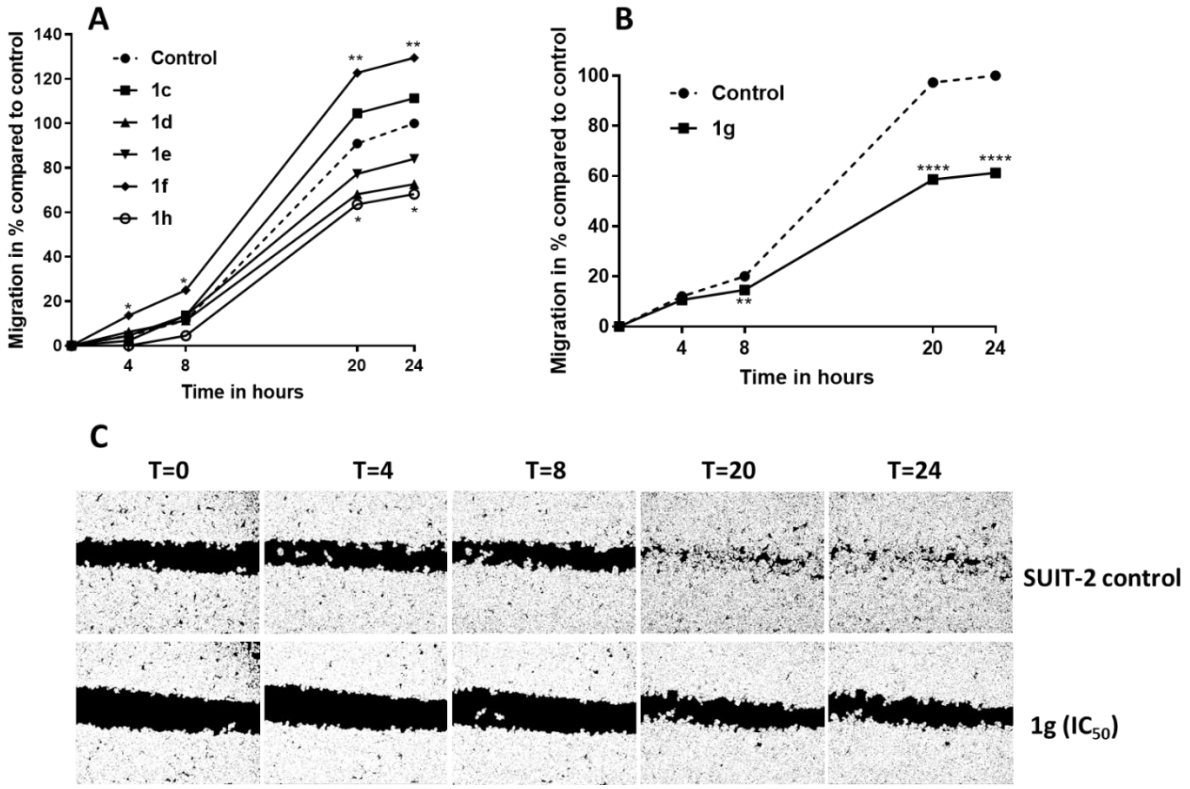

Figure 2. Modulation of migration rate in SUIT-2 cells treated with imidazo[2,1-*b*][1,3,4]thiadiazole derivatives 1c-f and 1g,h. The modulation of migration rate was monitored over time (0, 4, 8, 20 and 24 hours) in SUIT-2 cells treated with the compounds **1c-f** and **1h** (**A**) at concentrations of 3x IC_{50} values, and **1g** (**B**) at its IC_{50}. Points represent the means of at least six different scratch areas. SEMs were always below 10%. All the P values were calculated with Student's t-test. ****p<0.0001, **p<0.01, *p<0.05. **C:** Representative images of the scratch areas of SUIT-2 cells monitored over time (T=0 and at 4, 8, 20, and 24 hours from the start of the treatment). (*Upper panels*) untreated cells; (*lower panels*) cells treated with compound **1g**. Original magnification 5X.

Conclusion

The imidazo[2,1-*b*][1,3,4]thiadiazole derivatives **1a-l** endowed with antibiofilm activity[20] also showed anti-proliferative activity. Among the seven 3-(6-phenylimidazo[2,-1-*b*][1,3,4]thiadiazol-2-yl)-1*H*-indole derivatives, **1a-g,** screened on a panel of sixty human cancer cells by the NCI at the concentration of 10 µM, compound **1g** displayed relevant anti-proliferative activity with GI_{50} values ranging from 1.67 to 10.3 µM. However, compounds **1a-h** showed interesting *in vitro* anti-proliferative activity against the PDAC cells SUIT-2, whereas the compound **1d** was active on the other two PDAC preclinical models, Capan-1 and Panc-1. Finally, a wound healing assay demonstrated the anti-migratory ability of the compounds **1d**, **1e**, **1g** and **1h,** which reduced cell migration by 20 to 40%, compared to the control.

Overall, the results of cytotoxicity and cell migration will prompt further studies on the imidazo[2,1-*b*][1,3,4]thiadiazole derivatives **1d**, **e**, **g** and **h,** that could be used as interesting hit compounds to implement the drug discovery process of indole derivatives.

Conflicts of Interest

The Authors have declared that no conflict of interest exists in regard to this study.

Authors' Contributions

GLP was the principal investigator and takes primary responsibility for the article; SC, BEH, DC, and BP provided essential material and participated in the research design; GLP, SC, and EG wrote the article; GJP, GC and PD edited the paper. All Authors read and approved the final article.

Acknowledgements

This work was partly supported by Fondazione Associazione Italiana per la Ricerca sul Cancro (AIRC Start-Up Grant 2013; EG), the Dutch Cancer Society (KWF#10401 and #; EG) and VUMC Cancer Center Amsterdam Foundation (CCA grant 2015, 2016, 2018).

References

(1) Cascioferro, S.; Parrino, B.; Spanò, V.; Carbone, A.; Montalbano, A.; Barraja, P.; Diana, P.; Cirrincione, G. 1,3,5-Triazines: A Promising Scaffold for Anticancer Drugs Development. *Eur J Med Chem* **2017**, *142*, 523–549. https://doi.org/10.1016/j.ejmech.2017.09.035.

(2) Gomtsyan, A. Heterocycles in Drugs and Drug Discovery. *Chem Heterocycl Comp* **2012**, *48* (1), 7–10. https://doi.org/10.1007/s10593-012-0960-z.

(3) de Sá Alves, F. R.; Barreiro, E. J.; Fraga, C. A. M. From Nature to Drug Discovery: The Indole Scaffold as a "Privileged Structure." *Mini Rev Med Chem* **2009**, *9* (7), 782–793.

(4) Radwan, M. A. A.; Ragab, E. A.; Sabry, N. M.; El-Shenawy, S. M. Synthesis and Biological Evaluation of New 3-Substituted Indole Derivatives as Potential Anti-Inflammatory and Analgesic Agents. *Bioorganic & Medicinal Chemistry* **2007**, *15* (11), 3832–3841. https://doi.org/10.1016/j.bmc.2007.03.024.

(5) Giampieri, M.; Balbi, A.; Mazzei, M.; La Colla, P.; Ibba, C.; Loddo, R. Antiviral Activity of Indole Derivatives. *Antiviral Research* **2009**, *83* (2), 179–185. https://doi.org/10.1016/j.antiviral.2009.05.001.

(6) Spanò, V.; Attanzio, A.; Cascioferro, S.; Carbone, A.; Montalbano, A.; Barraja, P.; Tesoriere, L.; Cirrincione, G.; Diana, P.; Parrino, B. Synthesis and Antitumor Activity of New Thiazole Nortopsentin Analogs. *Mar Drugs* **2016**, *14* (12). https://doi.org/10.3390/md14120226.

(7) Parrino, B.; Attanzio, A.; Spanò, V.; Cascioferro, S.; Montalbano, A.; Barraja, P.; Tesoriere, L.; Diana, P.; Cirrincione, G.; Carbone, A. Synthesis, Antitumor Activity and CDK1 Inhibiton of New Thiazole Nortopsentin Analogues. *Eur J Med Chem* **2017**, *138*, 371–383. https://doi.org/10.1016/j.ejmech.2017.06.052.

(8) Cascioferro, S.; Attanzio, A.; Di Sarno, V.; Musella, S.; Tesoriere, L.; Cirrincione, G.; Diana, P.; Parrino, B. New 1,2,4-Oxadiazole Nortopsentin Derivatives with Cytotoxic Activity. *Mar Drugs* **2019**, *17* (1). https://doi.org/10.3390/md17010035.

(9) Parrino, B.; Carbone, A.; Ciancimino, C.; Spanò, V.; Montalbano, A.; Barraja, P.; Cirrincione, G.; Diana, P.; Sissi, C.; Palumbo, M.; et al. Water-Soluble Isoindolo[2,1-a]Quinoxalin-6-Imines: In Vitro Antiproliferative Activity and Molecular Mechanism(s) of Action. *Eur J Med Chem* **2015**, *94*, 149–162. https://doi.org/10.1016/j.ejmech.2015.03.005.

(10) Parrino, B.; Carbone, A.; Spanò, V.; Montalbano, A.; Giallombardo, D.; Barraja, P.; Attanzio, A.; Tesoriere, L.; Sissi, C.; Palumbo, M.; et al. Aza-Isoindolo and Isoindolo-

Azaquinoxaline Derivatives with Antiproliferative Activity. *Eur J Med Chem* **2015**, *94*, 367–377. https://doi.org/10.1016/j.ejmech.2015.03.009.

(11) Carbone, A.; Parrino, B.; Cusimano, M. G.; Spanò, V.; Montalbano, A.; Barraja, P.; Schillaci, D.; Cirrincione, G.; Diana, P.; Cascioferro, S. New Thiazole Nortopsentin Analogues Inhibit Bacterial Biofilm Formation. *Mar Drugs* **2018**, *16* (8). https://doi.org/10.3390/md16080274.

(12) Gadad, A. K.; Noolvi, M. N.; Karpoormath, R. V. Synthesis and Anti-Tubercular Activity of a Series of 2-Sulfonamido/Trifluoromethyl-6-Substituted Imidazo[2,1-b]-1,3,4-Thiadiazole Derivatives. *Bioorg. Med. Chem.* **2004**, *12* (21), 5651–5659. https://doi.org/10.1016/j.bmc.2004.07.060.

(13) Gadad, A. K.; Mahajanshetti, C. S.; Nimbalkar, S.; Raichurkar, A. Synthesis and Antibacterial Activity of Some 5-Guanylhydrazone/Thiocyanato-6-Arylimidazo[2,1-b]-1,3, 4-Thiadiazole-2-Sulfonamide Derivatives. *Eur J Med Chem* **2000**, *35* (9), 853–857.

(14) Khazi, I. A. M.; Mahajanshetti, C. S.; Gadad, A. K.; Tarnalli, A. D.; Sultanpur, C. M. Synthesis, Anticonvulsant and Analgesic Activities of Some 6-Substituted Imidazo(2,1-b)-1,3,4-Thiadiazole-2-Sulfonamides and Their 5-Bromo Derivatives. *Arzneimittel-Forschung/Drug Research* **1996**, *46* (10), 949–952.

(15) Andotra, C. S.; Langer, T. C.; Kotha, A. Synthesis and Antifungal Activity of Some Substituted 1,3,4-Thiadiazolo[3,2-a]-s-Triazin-5-Phenyl-7-Thiones and Imidazo-[2,1-b]-1,3,4-Thiadiazol-5-Ones. *Journal of the Indian Chemical Society* **1997**, *74* (2), 125–127.

(16) Terzioglu, N.; Gürsoy, A. Synthesis and Anticancer Evaluation of Some New Hydrazone Derivatives of 2,6-Dimethylimidazo[2,1-b][1,3,4]Thiadiazole-5-Carbohydrazide. *European Journal of Medicinal Chemistry* **2003**, *38* (7–8), 781–786. https://doi.org/10.1016/S0223-5234(03)00138-7.

(17) Romagnoli, R.; Baraldi, P. G.; Prencipe, F.; Balzarini, J.; Liekens, S.; Estévez, F. Design, Synthesis and Antiproliferative Activity of Novel Heterobivalent Hybrids Based on Imidazo[2,1-b][1,3,4]Thiadiazole and Imidazo[2,1-b][1,3]Thiazole Scaffolds. *Eur J Med Chem* **2015**, *101*, 205–217. https://doi.org/10.1016/j.ejmech.2015.06.042.

(18) Singh, H.; Kinarivala, N.; Sharma, S. Multi-Targeting Anticancer Agents: Rational Approaches, Synthetic Routes and Structure Activity Relationship. *Anticancer Agents Med Chem* **2019**. https://doi.org/10.2174/1871520619666190118120708.

(19) Tao, X.; Yin, L.; Xu, L.; Peng, J. Dioscin: A Diverse Acting Natural Compound with Therapeutic Potential in Metabolic Diseases, Cancer, Inflammation and Infections. *Pharmacol. Res.* **2018**, *137*, 259–269. https://doi.org/10.1016/j.phrs.2018.09.022.

(20) Cascioferro, S.; Parrino, B.; Petri, G. L.; Cusimano, M. G.; Schillaci, D.; Di Sarno, V.; Musella, S.; Giovannetti, E.; Cirrincione, G.; Diana, P. 2,6-Disubstituted Imidazo[2,1-b][1,3,4]Thiadiazole Derivatives as Potent Staphylococcal Biofilm Inhibitors. *European Journal of Medicinal Chemistry* **2019**, *167*, 200–210. https://doi.org/10.1016/j.ejmech.2019.02.007.

(21) Holbeck, S. L. Update on NCI in Vitro Drug Screen Utilities. *Eur. J. Cancer* **2004**, *40* (6), 785–793. https://doi.org/10.1016/j.ejca.2003.11.022.

(22) Rahib, L.; Smith, B. D.; Aizenberg, R.; Rosenzweig, A. B.; Fleshman, J. M.; Matrisian, L. M. Projecting Cancer Incidence and Deaths to 2030: The Unexpected Burden of Thyroid, Liver, and Pancreas Cancers in the United States. *Cancer Res* **2014**, *74* (11), 2913–2921. https://doi.org/10.1158/0008-5472.CAN-14-0155.

(23) Sciarrillo, R.; Wojtuszkiewicz, A.; Kooi, I. E.; Gómez, V. E.; Boggi, U.; Jansen, G.; Kaspers, G.-J.; Cloos, J.; Giovannetti, E. Using RNA-Sequencing to Detect Novel Splice Variants Related to Drug Resistance in In Vitro Cancer Models. *J Vis Exp* **2016**, No. 118. https://doi.org/10.3791/54714.

(24) Massihnia, D.; Avan, A.; Funel, N.; Maftouh, M.; van Krieken, A.; Granchi, C.; Raktoe, R.; Boggi, U.; Aicher, B.; Minutolo, F.; et al. Phospho-Akt Overexpression Is Prognostic and Can Be Used to Tailor the Synergistic Interaction of Akt Inhibitors with Gemcitabine in Pancreatic Cancer. *Journal of Hematology & Oncology* **2017**, *10* (1), 9. https://doi.org/10.1186/s13045-016-0371-1.

(25) Giovannetti, E.; van der Borden, C. L.; Frampton, A. E.; Ali, A.; Firuzi, O.; Peters, G. J. Never Let It Go: Stopping Key Mechanisms Underlying Metastasis to Fight Pancreatic Cancer. *Semin. Cancer Biol.* **2017**, *44*, 43–59. https://doi.org/10.1016/j.semcancer.2017.04.006.

(26) Iwamura, T.; Caffrey, T. C.; Kitamura, N.; Yamanari, H.; Setoguchi, T.; Hollingsworth, M. A. P-Selectin Expression in a Metastatic Pancreatic Tumor Cell Line (SUIT-2). *Cancer Res.* **1997**, *57* (6), 1206–1212.

(27) Weng, J.-R.; Tsai, C.-H.; Kulp, S. K.; Chen, C.-S. Indole-3-Carbinol as a Chemopreventive and Anti-Cancer Agent. *Cancer Lett.* **2008**, *262* (2), 153–163. https://doi.org/10.1016/j.canlet.2008.01.033.

(28) Ebos, J. M. L.; Lee, C. R.; Cruz-Munoz, W.; Bjarnason, G. A.; Christensen, J. G.; Kerbel, R. S. Accelerated Metastasis after Short-Term Treatment with a Potent Inhibitor of Tumor Angiogenesis. *Cancer Cell* **2009**, *15* (3), 232–239. https://doi.org/10.1016/j.ccr.2009.01.021.

(29) Ho, J.-N.; Jun, W.; Choue, R.; Lee, J. I3C and ICZ Inhibit Migration by Suppressing the EMT Process and FAK Expression in Breast Cancer Cells. *Mol Med Rep* **2013**, *7* (2), 384–388. https://doi.org/10.3892/mmr.2012.1198.

Chapter 6

3-(6-Phenylimidazo [2,1-b][1,3,4]thiadiazol-2-yl)-1H-Indole Derivatives as New Anticancer Agents in the Treatment of Pancreatic Ductal Adenocarcinoma

Stella Cascioferro[1,a], **Giovanna Li Petri[1,2,a]**, Barbara Parrino[1], Btissame El Hassouni[2,a], Daniela Carbone[1], Vincenzo Arizza[1], Ugo Perricone[3], Alessandro Padova[3], Niccola Funel[4], Godefridus J. Peters[2], Girolamo Cirrincione[1], Elisa Giovannetti[2,4*], Patrizia Diana[1*]

1. *Department of Biological, Chemical and Pharmaceutical Sciences and Technologies (STEBICEF), University of Palermo, Palermo, Italy*
2. *Department of Medical Oncology, Cancer Center Amsterdam, Amsterdam UMC, VU University Medical Center (VUmc), Amsterdam, The Netherlands*
3. *Fondazione RI.MED. Via Bandiera 11, 90133 Palermo, Italy;*
4. *Cancer Pharmacology Lab, AIRC Start Up Unit, Fondazione Pisana per la Scienza, Pisa, Italy*

[a]Equally contributed

[*]Corresponding authors

***Molecules*. 2020, *25*(2), 329;**

doi.org/10.3390/molecules25020329

3-(6-Phenylimidazo [2,1-b][1,3,4]thiadiazol-2-yl)-1H-Indole Derivatives as New Anticancer Agents in the Treatment of Pancreatic Ductal Adenocarcinoma

Abstract

Abstract: A new series of imidazo[2,1-*b*][1,3,4]thiadiazole derivatives was efficiently synthesized and screened for their *in vitro* antiproliferative activity on a panel of pancreatic ductal adenocarcinoma (PDAC) cells, including SUIT-2, Capan-1 and Panc-1. Compounds **9c** and **9l**, showed relevant *in vitro* antiproliferative activity on all three pre-clinical models with half maximal inhibitory concentration (IC_{50}) ranging from 5.11 to 10.8 μM, while the compounds **9e** and **9n** were active in at least one cell line. In addition, compound **9c** significantly inhibited the migration rate of SUIT-2 and Capan-1 cells in the scratch wound-healing assay. In conclusion, our results will support further studies to increase the library of imidazo [2,1-*b*][1,3,4] thiadiazole derivatives for deeper understanding of the relationship between biological activity of the compounds and their structures in the development of new antitumor compounds against pancreatic diseases.

Keywords: imidazo[2,1-*b*][1,3,4]thiadiazole derivatives; antiproliferative activity; migration assay; indole compounds; pancreatic cancer; resistance

Introduction

Pancreatic ductal adenocarcinoma (PDAC) is a fatal disease with an increased incidence also in young adults and a mortality/incidence ratio around 98%,[1,2] therefore new therapeutic strategies to counteract this malignancy are urgently needed. [1,3,4]Thiadiazole, both uncondensed or annealed to other heterocyclic moieties, particularly with imidazole ring, has been recognized as valuable scaffold for the development of pharmacologically active derivatives as it is present in many molecules with biological properties including anti-inflammatory,[3] anti-Alzheimer's disease,[4] anti-leishmanial,[5] antioxidant,[6] antitubercular,[7] anticonvulsant,[8] antibacterial and antibiofilm.[9–11] In particular, this ring system showed interesting antitumor activity with different mechanisms of action.[12–14] Among the imidazo[2,1-*b*][1,3,4]thiadiazole derivatives endowed with antiproliferative properties, the 2,6-disubstituted and the 2,5,6-trisubstituted showed the most interesting activity. Romagnoli et al. reported a series of 2-substituted-6-[*m*-(*α*-bromoacryloylamido)phenyl]imidazo[2,1-*b*][1,3,4]thiadiazoles **1** (Figure 1) with significant antiproliferative activity against murine leukaemia (L1210), murine mammary carcinoma (FM3A), human T-lymphocyte leukemia(CEM) and human cervix carcinoma (HeLa) cells, showing IC_{50} values in the submicromolar and nanomolar range.[15] Compound **2** (Figure 1) showed potent cytotoxic activity against the full NCI-60 cell panel eliciting GI_{50} values ranging from 1.4 to 4.2 μM.[16] Another representative example of imidazo[2,1-*b*][1,3,4]thiadiazole derivatives endowed with anticancer activity was reported by Patel and coworkers, who described the impressive inhibitory activity (IC_{50} = 1.2 nM) of compound **3** (Figure 1) against transforming growth factor-β type I receptor also known as activin receptor-like kinase 5.[17]

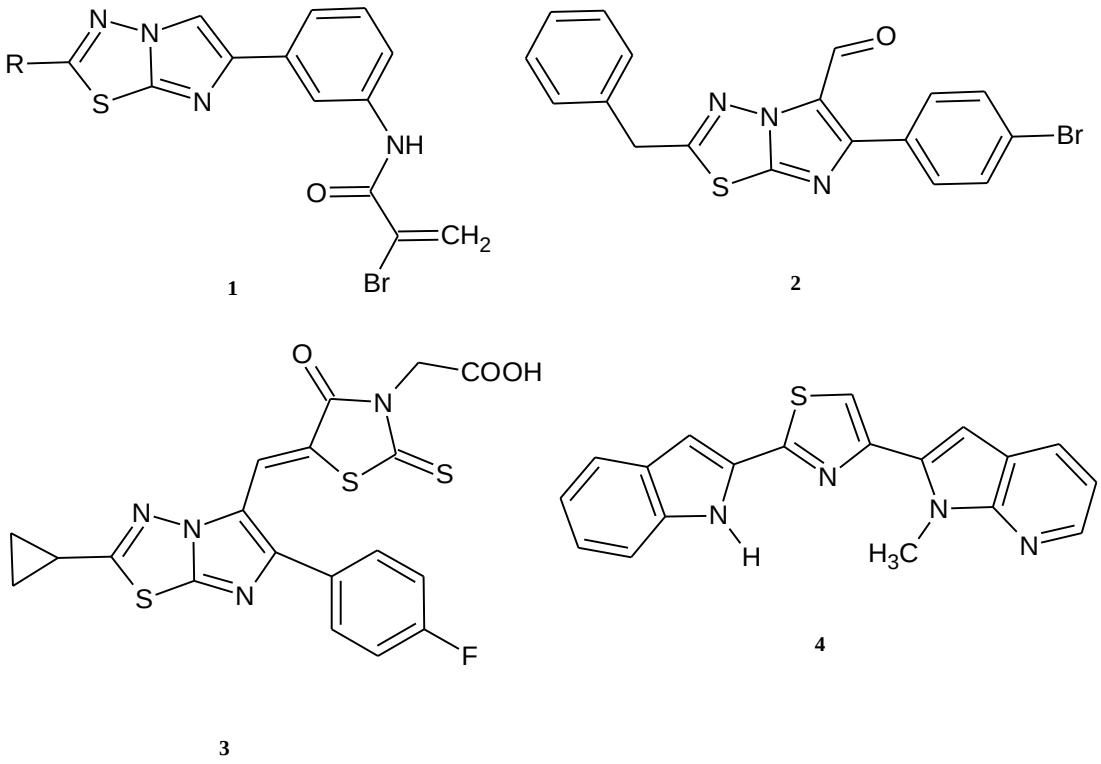

Figure 1. Chemical structures of the imidazo[2,1-*b*][1,3,4]thiadiazole compounds **1**–**3** and of the indole derivative **4**.

Our previous studies on nitrogen heterocyclic systems with anticancer properties[18–28] and the interesting antiproliferative activity described for the imidazo[2,1-*b*][1,3,4]thiadiazole scaffold encouraged us to continue this approach. Moreover, indole compounds were widely described for their anticancer properties. Among them, the bisindole derivative **4** was reported as a potent antitumor compound, which was able to inhibit CDK1 with an IC_{50} value of 0.86 µM. Therefore, on the basis of the significant antiproliferative activities described for the imidazo[2,1-*b*][1,3,4]thiadiazole and the indole scaffolds, we decided to synthesize and evaluate the cytotoxic activity of a new series of 3-(6-phenylimidazo[2,1-*b*][1,3,4]thiadiazol-2-yl)-1*H*-indole derivatives.

Results and Discussion

Chemistry

A series of new 16 imidazo[2,1-*b*][1,3,4]thiadiazole derivatives **9a-p** was synthesized as described in Scheme 1.

The indole-3-carbonitrile **5** was prepared by the reaction of the commercially available 1*H*-indoles **4** with chlorosulfonyl isocyanate (CSI) in anhydrous acetonitrile under stirring at 0 °C (yield 98%). The methylation of compounds **5** with dimethyl carbonate in anhydrous DMF at 130 °C afforded the derivatives **6** (yield 98%). The key intermediates

5-(1*H*-indol-3-yl)-1,3,4-thiadiazol-2-amines **7** were prepared in excellent yields (98%) by heating at 60 °C under stirring derivatives **5** or **6** with thiosemicarbazide in trifluoroacetic acid (TFA) for 3.5 h. Finally, by refluxing in anhydrous ethanol the 5-(1*H*-indol-3-yl)-1,3,4-thiadiazol-2-amines **7** with the suitable α-bromoacetyl derivatives **8,** the desired compounds **9** were obtained as hydrobromide salts in good yields (60-81%).

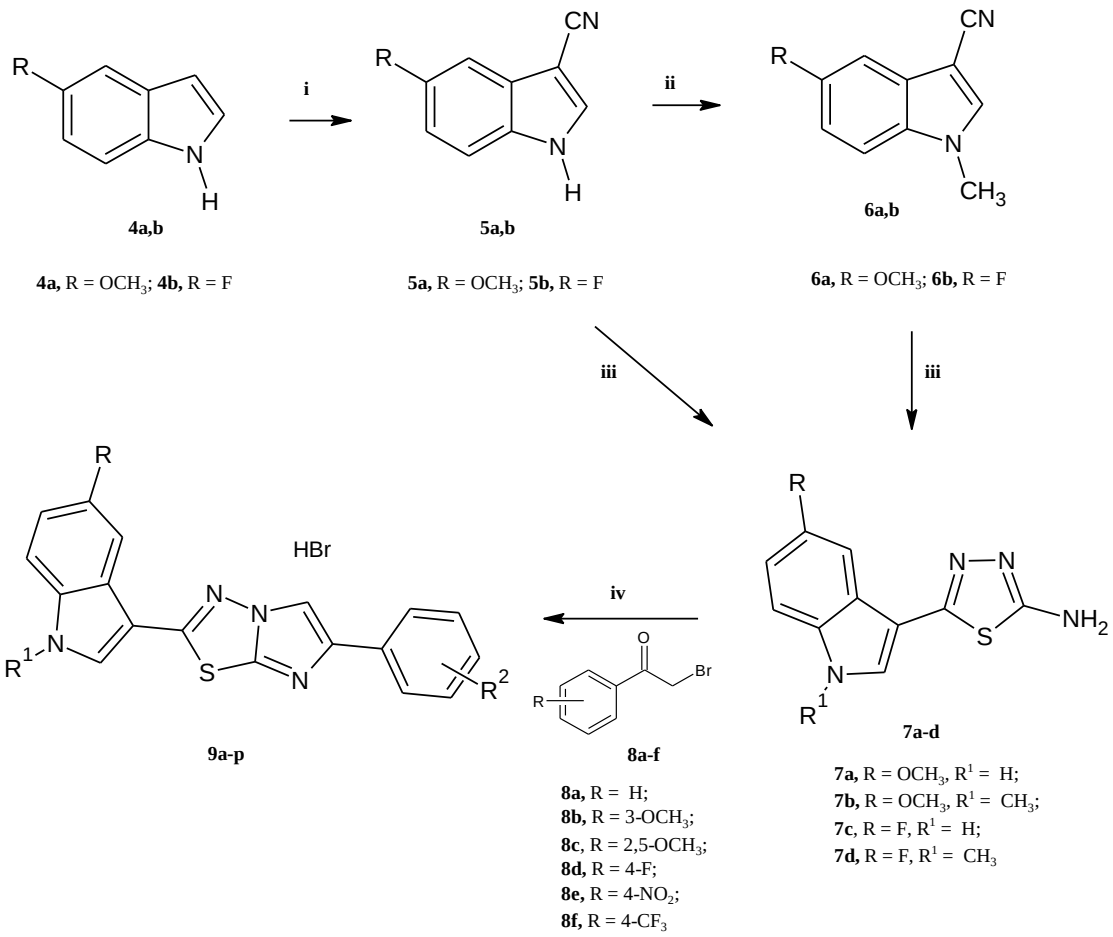

Scheme 1. Synthesis of the 3-(6-phenylimidazo[2,1-*b*][1,3,4]thiadiazol-2-yl)-1*H*-indole derivatives **9a-p**. Reagents and conditions: i) CH_3CN, CSI, 0 °C, 2 h, then DMF, 0 °C, 1.5 h (98%); ii) DMF, $(CH_3O)_2CO$, K_2CO_3, 130 °C, 3.5 h (98%); iii) trifluoroacetic acid, thiosemicarbazide, 60 °C, 3.5 h (98%); iv) anhydrous ethanol, reflux, 24 h (60-81%)

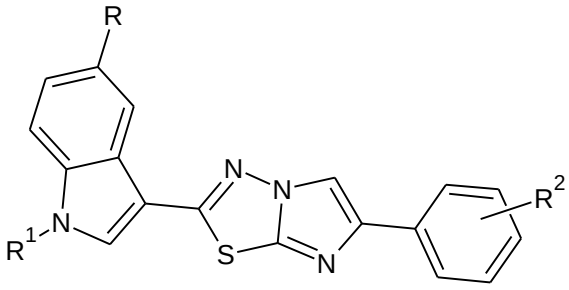

9a-p

Compound	R	R1	R2	Yield (%)
9a	OCH_3	H	H	80%
9b	OCH_3	H	4-F	75%
9c	OCH_3	H	4-NO_2	73%
9d	OCH_3	H	3-OCH_3	78%
9e	OCH_3	H	2,5-OCH_3	78%
9f	OCH_3	H	4-CF_3	68%
9g	OCH_3	CH_3	H	81%
9h	OCH_3	CH_3	4-F	72%
9i	OCH_3	CH_3	3-OCH_3	60%
9j	OCH_3	CH_3	2,5-OCH_3	65%
9k	OCH_3	CH_3	4-CF_3	67%
9l	F	H	H	72%
9m	F	H	3-OCH_3	74%
9n	F	H	4-CF_3	68%
9o	F	H	2,5-OCH_3	76%
9p	F	CH_3	4-CF_3	78%

Figure 2. *Upper panel***:** Chemical backbone structure of compounds **9a–p**. *Lower panel:* Table listing the chemical structure of the R, R1 and R2 components

Biological studies

Antiproliferative activity of the new imidazothiadiazole compounds 9a-p on SUIT-2, Capan-1 and Panc-1 pancreatic cancer cells.

The *in vitro* antiproliferative activity of a new library of imidazo[2,1-*b*][1,3,4]thiadiazole compounds **9a-p** was evaluated by Sulforhodamine-B assay (SRB) on a panel of PDAC cells, including SUIT-2, Capan-1 and Panc-1. These cells have been used in a number of pharmacological studies and are representative of the typical inherent resistance of pancreatic cancer cells to most chemotherapeutic agents.[29,30]

All compounds (**9a–p**) were initially screened at three different concentration (0.1, 1 and 16 μM) in all cell lines. The compounds **9c**, **9e**, **9l** and **9n** emerged for their ability to inhibit the growth rate in one or more cell lines. Therefore, these compounds were selected for further screening using eight different increasing concentrations (in the range between 0.125 and 16 μM) in order to evaluate the half maximal inhibitory concentration (IC_{50}) values. **Table 1** summarizes the IC_{50s} reported as means ± SEM of three independent experiments.

Table 1. IC_{50s} of SUIT-2, Capan-1 and Panc-1 cells treated with compounds **9a-p**.

	IC_{50}[a] (μM) ± SEM[b]		
	Cell lines		
Comp	**SUIT-2**	**Capan-1**	**Panc-1**
9a	>16	>16	>16
9b	>16	>16	>16
9c	5.5 ± 0.19	5.11 ± 0.29	5.18 ± 0.12
9d	>16	>16	>16
9e	>16	>16	10.26 ± 0.20
9f	>16	>16	>16
9g	>16	>16	>16
9h	>16	>16	>16
9i	>16	>16	>16
9j	>16	>16	>16
9k	>16	>16	>16
9l	10.4 ± 0.07	8.57 ± 0.51	10.8 ± 0.13
9m	>16	>16	>16
9n	11.8 ± 0.54	10.49 ±0.16	>16
9o	>16	>16	>16
9p	>16	>16	>16

[a]The values are reported as means ± SEM of three separated experiments.

[b]SEM: Standard Error Media.

The compounds **9c** and **9l** showed relevant antiproliferative activities in all the three preclinical *in vitro* models, with IC_{50s} ranging from 5.11 to 10.8 μM. Between these two derivatives, the compound **9c** induced the most relevant inhibition of cell growth, showing similar activities in SUIT-2, Capan-1 and Panc-1 cells, with IC_{50s} of 5.5, 5.11 and 5.18 μM, respectively (Figure 3).

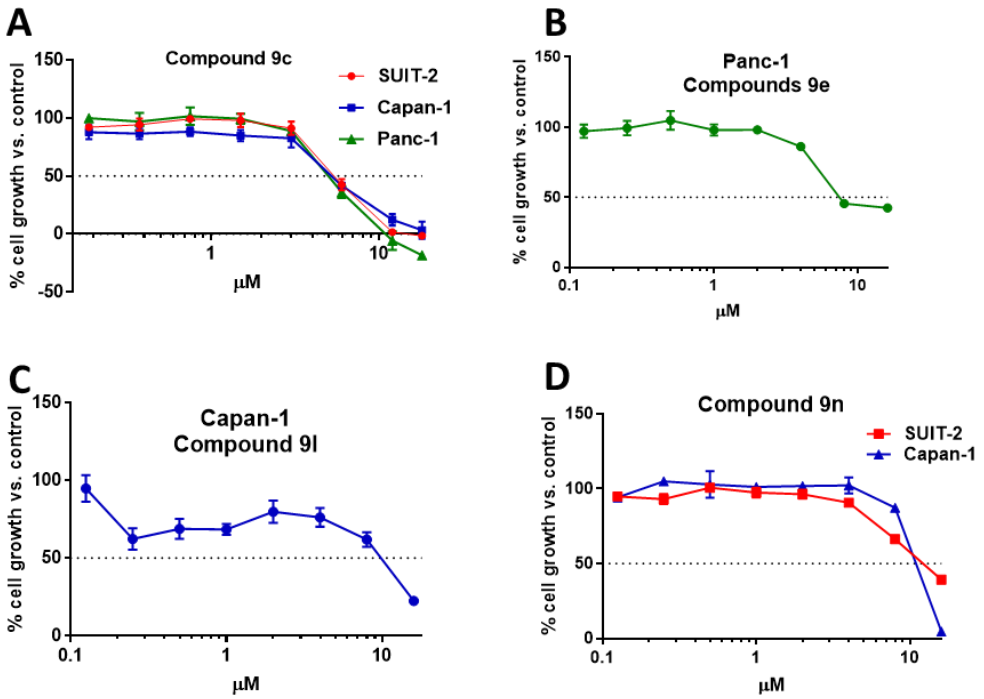

Figure 3. Representative growth inhibition curves of pancreatic ductal adenocarcinoma (PDAC) cells, SUIT-2 (red line), Capan-1 (blue line) and Panc-1 (green line) treated for 72 h with the compound **9c (A), 9e (B), 9l (C)** and **9n (D)** . Points, mean values obtained from three independent experiments; bars, SEM.

The compound **9e** was more active in Panc-1 cells, with IC_{50} value of 10.26 µM, whereas SUIT-2 and Capan-1 cells were resistant to the same treatment and showed IC_{50s} > 16 µM. Conversely, the IC_{50} of the compound **9n** was above 16 µM in Panc-1 cells, while SUIT-2 and Capan-1 cells were more sensitive, with IC_{50s} of 11.8 and 10.49 µM, respectively.

In parallel experiments we evaluated the IC_{50}s of the conventional anticancer drugs gemcitabine and 5-fluorouracil, which were below 1 µM. These results were in agreement with previous studies.[29,31] However, because of PDAC chemoresistant nature, these drugs have very limited clinical activity, prompting studies on novel compounds.

Results highlighted that the introduction of a methyl group on the nitrogen atom of the indole moiety was detrimental for the antiproliferative activity against the three cancer cell lines, whereas, substitutions on the phenyl ring as well as the presence of a fluorine atom or a methoxy group on the indole scaffold were not relevant for the activity.

Compound 9c inhibited the migration rate in SUIT-2, Capan-1 and Panc-1 cells.

It is well known that the poor prognosis of PDAC is caused by its early metastatic behaviour. Although many efforts have been made in the multi-omic fields to study the promoters of metastatic events and identify new drug targets, the key drivers of the

metastatic properties of PDAC remain unclear.[32,33] However, new therapeutic agents are needed to overcome PDAC aggressiveness and combat PDAC metastasis. Therefore, considering the metastatic nature of SUIT-2, Capan-1 and Panc-1 cells,[34,35] we assessed whether or not the most promising compound **9c** was able to affect cell migration. To this goal, the inhibition of cell migration was examined through a high-throughput screening using the scratch wound healing assay, as described previously.[36] SUIT-2, Capan-1 and Panc-1 cells were treated with the compound **9c** at concentration of $3xIC_{50}$ and the migration rate was monitored over time within 24 hours. Images of the wound closure were taken immediately after scratch (T = 0) and at 4, 8, 20 and 24 hours from the treatment. As shown in the Figure 4, the compound **9c** led to a net reduction of the migration in SUIT-2 and Capan-1 cells, whose the percentages of migration compared to the control (set to 100%) were 59.09% and 27.71%, respectively. Of note these results showed that this compound was able to inhibit migration more than gemcitabine, which in parallel experiments marginally (i.e., less than 15% inhibition) affected PDAC cell migration, as also reported in our previous studies in Panc-1 cells.[37] Conversely, the compound **9c** accelerated migration up to 142.85% in Panc-1 cells. The latter, unexpected results, might be explained by the tendency of PANC-1 cells to clump, a feature which might affect the analysis of the scratch after 24 h. Moreover, though most previous studies, including ours, showed the ability of tyrosine kinase inhibitors (TKIs) to reduce migration in different PDAC cancer cell line,[38] a seminal study on sunitinib and other TKIs reported metastatic acceleration depending on treatment schedule and tumor models.[39]

Statistical analyses showed that the inhibition of cell migration in cells treated was significant in all three pre-clinical models, compared to untreated cells. Importantly, to exclude that the wound areas were covered by cell proliferation, we determined the doubling time of each cell lines used, which were above 24 hours and we measured the area of the wound track which was approximately 10^6 μm^2, too large to be covered by only cell proliferation in 24 hours, since the average tumor adherent cell surface is around 100-150 μm^2. Finally, we used concentrations of the compound **9c** that did not induce cell death during 24 hours of exposure to the treatments, in fact, we did not observe detached cells after 24-hour drug treatment.

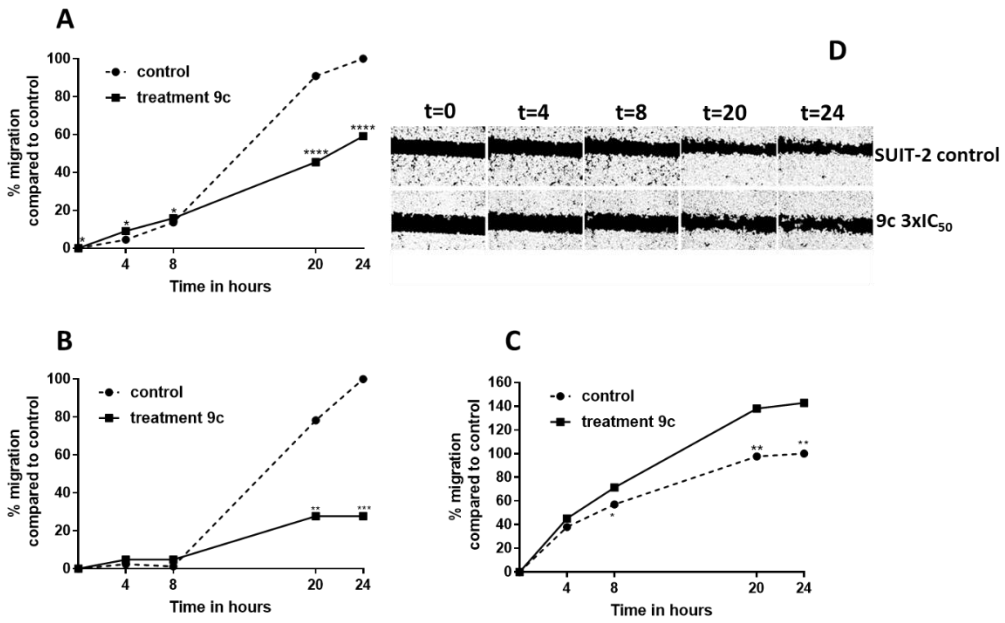

Figure 4. Modulation of migration rate in SUIT-2, Capan-1 and Panc-1 cells treated with imidazo[2,1-*b*][1,3,4]thiadiazole compound **9c**. The percentages of migration were monitored over time at 0, 4, 8, 20, 24 hours in SUIT-2 (A), Capan-1 (B) and Panc-1 (C) cells treated with compound **9c** at concentration of 3x IC_{50} values. Points represent the means of at least six different scratch areas. SEM were always below 10%. All the P values were calculated with Student's t-test. ****p<0.0001, ***p<0.001 **p<0.01, *p<0.05. (D) Representative images of the scratch areas of SUIT-2 cells monitored over time (T=0 and at 4, 8, 20, and 24 hours from the start of the treatment). (*Upper panels*) untreated cells; (*lower panels*) cells treated with compound **9c**. Original magnification 5X.

Materials and Methods

Chemistry

All melting points were taken on a Büchi-Tottoly capillary apparatus and are uncorrected. IR spectra were determined in bromoform with a Shimadzu FT/IR 8400S spectrophotometer. ^{1}H and ^{13}C NMR spectra were measured at 200 and 50.0 MHz, respectively, in DMSO-d_6 solution, using a Bruker Avance II series 200 MHz spectrometer. Column chromatography was performed with Merck silica gel 230-400 mesh ASTM or with Büchi Sepacor chromatography module (prepacked cartridge system). Elemental analyses (C, H, N) were within ±0.4% of theoretical values and were performed with a VARIO EL III elemental analyser. Purity of all the tested compounds was greater than 95%, determined by HPLC (Agilent 1100 Series).

Synthesis of 1H-indole-3-carbonitriles (**5a,b**)

A solution of the indole **4a,b** (5.10 mmol) in anhydrous acetonitrile (4.5 ml) was treating by adding dropwise chlorosulfonyl isocyanate (CSI) (0.44 ml, 5.10 mmol). The reaction mixture was stirred at 0 °C for 2 h, then, anhydrous dimethylformamide (DMF) (2.8 ml, 36.39 mmol) was slowly added and the mixture was stirred at 0 °C for 1.5 h. The resulting solution was poured into crushed ice. The solid obtained was filtered and dried (yields 98%).

Analytical and spectroscopic data for compounds **5a,b** are in agreement with those reported in literature.[40]

Synthesis of 1-methylindole-3-carbonitriles (**6a,b**)

To a solution of the suitable 3-cyanoindole **5a,b** (7.03 mmol) in anhydrous DMF (10 ml) 3.61 mmol of K_2CO_3 and dimethyl carbonate (1.8 ml, 21.4 mmol) were added and the mixture was heated at 130 °C for 3.5 h. After cooling (3 °C), water and ice (25 ml) was slowly added under stirring. The suspension obtained was extracted with diethyl ether (3x10 ml) and the organic phase was washed with water and brine, was dried over Na_2SO_4 and the solvent evaporated at reduced pressure to obtain the 3-cyano-1-methylindole **6a,b** in excellent yields.

Analytical and spectroscopic data are in accordance to those reported in literature.[41]

Synthesis of 5-(1H-indol-3-yl)-1,3,4-thiadiazol-2-amines (**7a-d**)

A mixture of the suitable indole-3-carbonitrile **5a,b** or **6a,b** (5 mmol), thiosemicarbazide 5mmol) and trifluoroacetic acid (5 ml) was heated at 60 °C for 3.5 h. The reaction mixture was then poured into ice and neutralized with $NaHCO_3$ saturated solution. The solid obtained was filtered off, washed with water, cyclohexane and diethyl ether.

5-(5-Methoxy-1H-indol-3-yl)-1,3,4-thiadiazol-2-amine (**7a**)

Orange powder. Yield: 98%, m.p. 216-217°C, IR cm^{-1}: 3604 (NH), 3558 (NH_2), ^{1}HNMR (200MHz, DMSO-d_6) δ: 3.79 (3H, s, OCH_3), 6.85-6.91 (1H, m, Ar-H), 7.39 (1H, d, J = 8.8 Hz, Ar-H), 7.53 (1H, s, Ar-H), 8.02 (1H, s, Ar-H), 8.58 (2H, bs, NH_2), 11.80 (1H, s, NH). ^{13}C NMR (50 MHz, DMSO-d_6) δ: 55.23 (q), 101.9 (d), 105.7 (s), 112.9 (d), 113.0 (d), 124.3 (s), 128.7 (d), 131.4 (s), 152.1 (s), 154.7 (s), 166.5 (s). Anal. Calcd for $C_{11}H_{10}N_4OS$ (MW: 246.29): C, 53.64%; H, 4.09%; N, 22.75%. Found: C, 53.82%; H, 4.28%; N, 22.53%.

5-(5-Methoxy-1-methyl-1H-indol-3-yl)-1,3,4-thiadiazol-2-amine (**7b**)

Orange powder. Yield: 98%, m.p. 206-207 °C, IR cm^{-1}: 3381 (NH_2), ^{1}HNMR (200MHz, DMSO-d_6) δ: 3.80 (6H, s, OCH_3, CH_3), 6.9 (1H, dd, J = 2.4, 2.5 Hz, Ar-H), 7.13 (2H, s, NH_2), 7.41 (1H, d, J = 8.9 Hz, Ar-H), 7.61 (1H, d, J = 2.3 Hz, Ar-H), 7.81 (1H, s, Ar-H). ^{13}C NMR (50 MHz, DMSO-d_6) δ: 32.8 (q), 55.2 (q), 102.3 (d), 106.0 (s), 111.1 (d), 112.5 (d), 124.9 (s), 130.6 (d), 132.0 (s), 152.2 (s), 154.6 (s), 165.4 (s). Anal. Calcd for $C_{12}H_{12}N_4OS$ (MW: 260.31): C, 55.37%; H, 4.65%; N, 21.52%. Found: C, 55.58%; H, 4.81%; N, 21.63%.

5-(5-Fluoro-1H-indol-3-yl)-1,3,4-thiadiazol-2-amine (**7c**)

Orange powder. Yield: 98%, m.p. 257-258 °C IR cm^{-1}: 3558 (NH), 3461 (NH_2), ^{1}HNMR (200MHz, DMSO-d_6) δ: 7.03-7.12 (1H, m, Ar-H), 7.33-7.50 (3H, m, Ar-H, NH_2), 7.80 (1H, dd, J = 2.4, 2.4 Hz, Ar-H), 7.95 (1H, s, Ar-H), 11.79 (1H, s, NH). ^{13}C NMR (50 MHz, DMSO-d_6) δ: 105.4 (d, J_F = 24.0 Hz), 107.3 (s), 110.7 (d, J_F = 25.5 Hz), 113.1 (d, J_F = 10.0 Hz), 124.2 (s), 128.5 (d), 133.0 (s), 152.0 (s), 159.9 (s), 165.8 (s). Anal. Calcd for $C_{10}H_7FN_4S$ (MW: 234.25): C, 51.27%; H, 3.01%; N, 23.92%. Found: C, 51.42%; H, 3.28%; N, 24.05%.

5-(5-Fluoro-1-methyl-1H-indol-3-yl)-1,3,4-thiadiazol-2-amine (**7d**)

Light orange powder. Yield: 98%, m.p. 183-184 °C IR cm^{-1}: 3450 (NH_2) ^{1}HNMR (200MHz, DMSO-d_6) δ: 3.85 (3H, s, CH_3), 7.12-7.21 (1H, m, Ar-H), 7.55-7.62 (1H, m, Ar-H), 7.76 (1H, dd, J = 2.5, 2.5 Hz, Ar-H), 8.10 (3H, s, Ar-H, NH_2). ^{13}C NMR (50 MHz, DMSO-d_6) δ: 33.1 (q), 105.35 (s), 105.5 (d, J_F = 24.0 Hz), 111.1 (d, J_F = 26.0 Hz), 112.0 (d, J_F = 9.5 Hz), 124.3 (s), 124.5 (s), 133.0 (d), 133.7 (s), 151.3 (s), 155.7 (s). Anal. Calcd for $C_{11}H_9FN_4S$ (MW: 248.28): C, 53.21%; H, 3.65%; N, 22.57%. Found: C, 53.50%; H, 3.78%; N, 22.69%.

3.1.4 Synthesis of 3-(6-phenylimidazo[2,1-b][1,3,4]thiadiazol-2-yl)-1H-indole hydrobromides (**9a-p**)

A mixture of 5-(1*H*-indol-3-yl)-1,3,4-thiadiazol-2-amine **7a-d** (0.92 mmol) and the 2-bromoethanone **8a-f** (0.92 mmol) in 40 ml of anhydrous ethanol was stirred at reflux for 24 h. After cooling at room temperature the obtained solid was filtered off and washed with cold ethanol. Derivative **9p** was characterized only by ^{1}HNMR spectra due to its poor solubility.

5-Methoxy-3-(6-phenylimidazo[2,1-b][1,3,4]thiadiazol-2-yl)-1H-indole hydrobromide **9a**

Light brown solid. Yield: 80%, m.p. 234-235 °C. IR cm^{-1}: 3592 (NH), 3433 (NH); ^{1}HNMR (200MHz, DMSO-d_6) δ: 3.85 (3H, s, OCH_3), 6.94 (1H, dd, J = 2.1, 2.2 Hz, Ar-H), 7.32-7.49 (4H, m, Ar-H), 7.63 (1H, s, Ar-H), 7.88 (2H, d, J = 7.6 Hz, Ar-H), 8.33 (1H, d, J = 7.6 Hz, Ar-H), 8.84 (1H, s, Ar-H), 12.10 (1H, s, NH). ^{13}C NMR (50 MHz, DMSO-d_6) δ: 55.3 (q), 102.2 (d), 105.8 (s), 110.9 (d), 113.1 (d), 113.4 (d), 124.3 (s), 124.6 (2xd), 127.7 (d), 128.8 (2xd), 130.2 (d), 131.6 (s), 132.3 (s), 142.6 (s), 142.7 (s), 155.2 (s), 158.3 (s). Anal. Calcd for $C_{19}H_{15}BrN_4OS$ (MW: 427.3): C, 53.40 %; H, 3.54%; N, 13.11%. Found: C, 53.62 %; H, 3.70%; N, 13.05%.

5-Methoxy-3-[6-(4-fluorophenyl)imidazo[2,1-b][1,3,4]thiadiazol-2-yl]-5-methoxy-1H-indole hydrobromide **9b**

Light grey solid. Yield: 75%, m.p. 277-278 °C. IR cm^{-1}: 3615 (NH), 3392 (NH); ^{1}HNMR (200MHz, DMSO-d_6) δ: 3.85 (3H, s, OCH_3), 6.48 (1H, bs, NH), 6.92-6.96 (2H, d, J = 8.7 Hz, Ar-H), 7.24-7.33 (2H, d, J = 2.3 Hz, Ar-H), 7.43-7.44 (1H, d, J = 8.8 Hz, Ar-H), 7.62 (1H, s, Ar-H), 7.88-7.94 (2H, m, Ar-H), 8.29-8.31 (1H, d, J = 2.29 Hz, Ar-H), 8.77 (1H, s, Ar-H), 12.08 (1H, bs, NH). ^{13}C NMR (50 MHz, DMSO-d_6) δ: 55.3 (q), 102.2

(d), 106.6 (s), 110.6 (d), 113.1 (d), 113.3 (d), 115.4 (d), 115.8 (d), 124.3 (s), 126.4 (d), 126.6 (2xd), 129.5 (s), 130.0 (s), 131.6 (s), 142.4 (s), 142.8 (s), 155.1 (s), 157.9 (s). Anal. Calcd for $C_{19}H_{14}BrFN_4OS$ (MW: 445.31): C, 51.25%; H, 3.17%; N, 12.58%. Found: C, 51.45%; H, 3.33%; N, 12.65%.

5-Methoxy-3-[6-(4-nitrophenyl)imidazo[2,1-b][1,3,4]thiadiazol-2-yl]-1H-indole **9c**

Dark yellow solid. Yield: 73%, m.p. 291-292 °C. IR cm $^{-1}$: 3609 (NH); ^{1}HNMR (200MHz, DMSO-d_6) δ: 3.86 (3H, s, OCH_3), 6.91-6.96 (1H, dd, *J* = 2.3, 2.3, Ar-H), 7.41-7.45 (1H, d, *J* = 8.8 Hz, Ar-H), 7.62 (1H, d, *J* = 2.2 Hz, Ar-H), 8.06 (1H, s, Ar-H), 8.11 (1H, s, Ar-H), 8.21 (1H, s, Ar-H), 8.25 (2H, d, *J* = 2.2, Ar-H), 8.96 (1H, s, Ar-H), 12.03 (1H, bs, NH). ^{13}C NMR (50 MHz, DMSO-d_6) δ: 55.3 (q), 102.2 (d), 106.2 (s), 113.0 (d), 113.3 (d), 124.1 (3xd), 124.3 (s), 124.8 (2xd), 130.0 (d), 131.6 (s), 140.6 (s), 142.4 (s), 144.0 (s), 145.6 (s), 155.1 (s), 158.1 (s). Anal. Calcd for $C_{19}H_{13}N_5O_3S$ (MW: 391.40): C, 58.30%; H, 3.35%; N, 17.89%. Found: C, 58.46%; H, 3.48%; N, 18.02%.

5-Methoxy-3-[6-(3-methoxyphenyl)imidazo[2,1-b][1,3,4]thiadiazol-2-yl]-1H-indole hydrobromide **9d**

Light brown solid. Yield: 78%, m.p. 272-273 °C. IR cm $^{-1}$: 3604 (NH), 3142 (NH); ^{1}HNMR (200MHz, DMSO-d_6) δ: 3.83 (3H, s, OCH_3), 3.85 (3H, s, OCH_3), 6.87-6.98 (2H, m, Ar-H), 7.32-7.48 (4H, m, Ar-H), 7.63 (1H, d, *J* = 2.28 Hz, Ar-H), 8.33 (1H, d, *J* = 2.9 Hz, Ar-H), 8.61 (1H, s, NH), 8.86 (1H, s, Ar-H), 12.09 (1H, bs, NH). ^{13}C NMR (50 MHz, DMSO-d_6) δ: 55.1 (q), 55.3 (q), 102.1 (d), 106.0 (s), 109.8 (2xd), 111.1 (d), 113.1 (s), 113.4 (2xd), 116.9 (d), 124.3 (s), 129.9 (2xd), 131.6 (s), 134.2 (s), 140.3 (s), 155.1 (s), 159.3 (s), 159.6 (s). Anal. Calcd for $C_{20}H_{17}BrN_4O_2S$ (MW: 457.34): C, 52.52%; H, 3.75%; N, 12.25%. Found: C, 52.69%; H, 3.82%; N, 12.36%.

5-Methoxy-3-[6-(2,5-dimethoxyphenyl)imidazo[2,1-b][1,3,4]thiadiazol-2-yl]-5-methoxy-1H-indole **9e**

Yellow solid. Yield: 78%, m.p. 261-262 °C. IR cm $^{-1}$: 3604 (NH); ^{1}HNMR (200MHz, DMSO-d_6) δ: 3.78 (3H, s, OCH_3), 3.85 (3H, s, OCH_3), 3.94 (3H, s, OCH_3), 6.88-6.96 (2H, m, Ar-H), 7.07 (1H, d, *J* = 9.0 Hz, Ar-H), 7.43-7.65 (3H, m, Ar-H), 8.36 (1H, d, *J* = 3.0 Hz, Ar-H), 8.71 (1H, s, NH), 12.12 (1H, bs, NH). ^{13}C NMR (50 MHz, DMSO-d_6) δ: 55.4 (2xq), 55.9 (q), 102.3 (d), 105.7 (s), 111.6 (3xd), 112.8 (s), 113.1 (d), 113.4 (d), 113.6 (d) 124.3 (s), 130.5 (d), 131.6 (s), 137.3 (s), 141.8 (s), 149.8 (s), 153.2 (s), 155.2 (s),

158.8 (s). Anal. Calcd for $C_{21}H_{18}N_4O_3S$ (MW: 406.57): C, 62.05%; H, 4.46%; N, 13.78%. Found: C, 62.58%; H, 4.58%; N, 13.86%.

5-Methoxy-3-{6-[4-(trifluoromethyl)phenyl]imidazo[2,1-b][1,3,4]thiadiazol-2-yl}-1H-indole hydrobromide **9f**

White solid. Yield: 68%, m.p. 198-199 °C. IR cm $^{-1}$: 3609 (NH), 3228 (NH); ^{1}HNMR (200MHz, DMSO-d_6) δ: 3.86 (3H, s, OCH_3), 6.43 (1H, bs, NH), 6.92 (1H, d, *J* = 8.8 Hz, Ar-H), 7.42-7.48 (1H, m, Ar-H), 7.64 (1H, s, Ar-H), 7.75-8.11 (4H, dd, *J* = 7.5, 7.7 Hz, Ar-H), 8.28 (1H, s, Ar-H), 8.91 (1H, s, Ar-H), 12.06 (1H, bs, NH). ^{13}C NMR (50 MHz, DMSO-d6) δ: 55.3 (q), 102.2 (d), 106.1 (s), 112.1 (d), 113.0 (d), 113.3 (d), 124.3 (s), 124.8 (3xd) 125.6 (d), 130.0 (d), 131.6 (2xs), 137.8 (s), 142.7 (s), 143.5 (s), 155.1 (2xs), 157.9 (s). Anal. Calcd for $C_{20}H_{14}BrF_3N_4OS$ (MW: 495.31): C, 48.50%; H, 2.85%; N, 11.31%. Found: C, 48.69%; H, 2.98%; N, 11.26%.

5-Methoxy-1-methyl-3-(6-phenylimidazo[2,1-b][1,3,4]thiadiazol-2-yl)-1H-indole hydrobromide **9g**

Light grey solid. Yield: 81%, m.p. 252-253 °C. IR cm $^{-1}$: 3592 (NH); ^{1}HNMR (200MHz, DMSO-d_6) δ: 3.85 (6H, s, OCH_3, CH_3), 6.96-7.01 (1H, dd, *J* = 2.4, 2.4 Hz, Ar-H), 7.28-7.60 (5H, m, Ar-H), 7.84 (2H, d, *J* = 7.1 Hz, Ar-H), 8.33 (1H, s, Ar-H), 8.52 (1H, bs, NH), 8.81 (1H, s, Ar-H). ^{13}C NMR (50 MHz, DMSO-d_6) δ: 33.3 (q, CH_3), 55.3 (q, OCH_3), 102.4 (d), 104.5 (s), 110.9 (d), 111.9 (s), 112.9 (d), 124.6 (2xd), 127.7 (d) 128.8 (2xd), 132.1 (s), 132.3 (s), 133.6 (d), 142.6 (s), 142.5 (s), 155.5 (s), 157.8 (s). Anal. Calcd for $C_{20}H_{17}BrN_4OS$ (MW: 441.34): C, 54.43%; H, 3.88%; N, 12.69%. Found: C, 54.59%; H, 4.00%; N, 12.96%.

5-Methoxy-3-[6-(4-fluorophenyl)imidazo[2,1-b][1,3,4]thiadiazol-2-yl]-5-methoxy-1-methyl-1H-indole hydrobromide **9h**

Light yellow solid. Yield: 72%, m.p. 278-279 °C. IR cm $^{-1}$: 3609 (NH); ^{1}HNMR (200MHz, DMSO-d_6) δ: 3.84 (6H, s, OCH_3, CH_3), 6.95-7.01 (1H, dd, *J* = 1.6, 1.56 Hz, Ar-H), 7.22-7.31 (2H, m, Ar-H), 7.48-7.52 (1H, d, *J* = 8.9 Hz, Ar-H), 7.58 (1H, d, *J* = 2.0 Hz, Ar-H), 7.95-7.82 (2H, m, Ar-H), 8.29 (1H, s, Ar-H), 8.74 (1H, s, Ar-H), 9.66 (1H, bs, NH). ^{13}C NMR (50 MHz, DMSO-d_6) δ: 33.2 (q), 55.4 (q), 102.3 (d), 104.7 (s), 110.6 (d), 111.9 (d), 112.9 (d), 115.4 (d), 115.8 (d), 124.6 (s), 126.4 (d) 126.5 (d), 129.6 (s), 132.3 (s), 133.4

(d), 142.6 (2xs), 155.4 (2xs), 157.3 (s). Anal. Calcd for $C_{20}H_{16}BrN_4OS$ (MW: 459.33): C, 52.30%; H, 3.51%; N, 12.20%. Found: C, 52.50%; H, 4.67%N, 12.35%.

5-Methoxy-1-methyl-3-[6-(3-methoxyphenyl)imidazo[2,1-b][1,3,4]thiadiazol-2-yl]-1H-indole hydrobromide **9i**

Brown solid. Yield: 60%, m.p. 260-261 °C. IR cm $^{-1}$: 3461 (NH); ^{1}HNMR (200MHz, DMSO-d_6) δ: 3.82 (3H, s, CH_3), 3.85 (6H, s, OCH_3), 5.99 (1H, bs, NH), 6.86 (H, d, *J* = 7.3 Hz, Ar-H), 6.96-7.02 (1H, dd, *J* = 2.4, 2.3 Hz, Ar-H), 7.30-7.61 (5H, m, Ar-H), 8.32 (1H, s, Ar-H), 8.81 (1H, s, Ar-H). ^{13}C NMR (50 MHz, DMSO-d_6) δ: 33.3 (q), 55.0 (q), 55.3 (q, OCH_3), 102.3 (d), 104.7 (s), 109.7 (2xd), 111.9 (d), 112.9 (d), 113.2 (s), 116.8 (d), 124.6 (s), 129.8 (2xd), 130.5 (d), 132.3 (s), 134.0 (s), 142.5 (s), 142.9 (s), 155.4 (s), 157.6 (s), 159.6 (s). Anal. Calcd for $C_{21}H_{19}BrN_4O_2S$ (MW: 471.46): C, 53.51%; H, 4.06%; N, 11.89%. Found: C, 53.68%; H, 4.15%; N, 11.99%.

5-Methoxy-3-[6-(2,5-dimethoxyphenyl)imidazo[2,1-b][1,3,4]thiadiazol-2-yl]-5-methoxy-1-methyl-1H-indole **9j**

White solid. Yield: 65%, m.p. 277-278 °C. ^{1}HNMR (200MHz, DMSO-d_6) δ: 3.77 (3H, s, CH_3), 3.85 (6H, dd, *J* = 1.6 Hz, OCH_3), 3.93 (3H, s, CH_3), 6.86 - 7.09 (3H, m, Ar-H), 7.50 - 7.56 (4H, m, Ar-H), 8.34 (1H, s, Ar-H). ^{13}C NMR (50 MHz, DMSO-d_6) δ: 33.3 (q), 55.2 (q), 55.4 (q), 55.9 (q), 99.4 (s), 102.4 (d), 104.4 (s), 111.5 (2xd), 112.6 (s), 112.8 (2xd), 112.9 (d), 114.2 (d), 124.6 (s), 132.3 (2xs), 133.8 (d), 141.6 (s), 149.8 (s), 153.1 (s), 155.5 (s). Anal. Calcd for $C_{22}H_{10}BrN_4O_3S$ (MW: 420.48): C, 62.84%; H, 4.79%; N, 13.32%. Found: C, 62.95%; H, 4.89%; N, 13.39%.

5-Methoxy-1-methyl-3-{6-[4-(trifluoromethyl)phenyl]imidazo[2,1-b][1,3,4]thiadiazol-2-yl}-1H-indole **9k**

Light grey solid. Yield: 67%, m.p. 216°C. ^{1}HNMR (200MHz, DMSO-d_6) δ: 3.85(6H, s, CH_3, OCH_3), 6.96-7.02 (1H, dd, *J* = 2.4, 2.4 Hz, Ar-H), 7.48 (1H, d, *J* = 8.9 Hz, Ar-H), 7.61 (1H, d, *J* = 2.3 Hz, Ar-H), 7.72-8.08 (4H, dd, *J* = 8.0, 8.1 Hz, Ar-H), 8.24 (1H, s, Ar-H), 8.85 (1H, s, Ar-H). ^{13}C NMR (50 MHz, DMSO-d_6) δ: 33.2 (q), 55.3 (q), 99.4 (s), 102.4 (d), 104.9 (2xs), 111.9 (d), 112.1 (s), 112.9 (d), 124.7 (4xd), 125.5 (d), 132.3 (s), 133.2 (d), 138.0 (s), 143.0 (s), 155.4 (2xs), 157.3 (s). Anal. Calcd for $C_{21}H_{15}F_3N_4OS$ (MW: 428.43): C, 58.87%; H, 3.53%; N, 13.08%. Found: C, 59.01%; H, 3.62%; N, 13.14%.

5-Fluoro-3-(6-phenylimidazo[2,1-b][1,3,4]thiadiazol-2-yl)-1H-indole hydrobromide **9l**

White solid. Yield: 72%, m.p. 278-279°C. IR cm $^{-1}$: 3145 (NH) 2890 (NH).; ^{1}HNMR (200MHz, DMSO-d_6) δ: 7.03 (1H, bs, NH), 7.11-7.47(4H, m, Ar-H), 7.53-7.60 (1H, m, Ar-H), 7.82-7.90 (3H, m, Ar-H), 8.41 (1H, d, Ar-H), 8.75 (1H, s, Ar-H) 12.28 (1H, bs, NH). ^{13}C NMR (50 MHz, DMSO-d6) δ: 105.0 (d), 106.5 (s), 110.0 (d), 110.6 (s), 111.2 (d), 111.7 (d), 123.9 (s), 124.5 (2xd), 127.3 (d), 128.7 (2xd), 131.3 (d), 133.3 (2xs), 142.8 (s), 143.9 (s), 157.2 (s). Anal. Calcd for $C_{18}H_{12}BrFN_4S$ (MW: 415.28): C, 52.06%; H, 2.91%; N, 13.49%. Found: C, 52.16%; H, 3.02%; N, 13.59%.

5-Fluoro-3-[6-(3-methoxyphenyl)imidazo[2,1-b][1,3,4]thiadiazol-2-yl]-1H-indole hydrobromide **9m**

White solid. Yield: 74%, m.p. 282-283°C. IR cm $^{-1}$: 3153 (NH), 3658 (NH); ^{1}HNMR (200MHz, DMSO-d_6) δ: 3.82 (3H, s, OCH_3), 6.87-7.62 (6H, m, Ar-H), 7.80-7.86 (1H, dd, *J* = 2.3, 2.3 Hz, Ar-H), 8.44 (1H, d, *J* = 3 Hz, Ar-H), 8.81 (1H, s, Ar-H), 9.01 (1H, bs, NH), 12.30 (1H, bs, NH). ^{13}C NMR (50 MHz, DMSO-d_6) δ: 55.0 (q), 99.4 (s), 105.0 (d), 109.8 (2xd), 110.4 (s), 111.0 (s), 111.3 (d), 113.2 (d), 113.8 (s), 114.0 (d), 116.9 (d), 118.7 (s), 124.1 (s), 129.8 (d), 131.4 (d), 133.3 (s), 142.7 (s), 143.2 (s), 151.6 (2xs). Anal. Calcd for $C_{19}H_{14}BrFN_4OS$ (MW: 445.30): C, 51.25%; H, 3.17%; N, 12.58%. Found: C, 51.39%; H, 3.25%; N, 12.64%.

5-Fluoro-3-{6-[4-(trifluoromethyl)phenyl]imidazo[2,1-b][1,3,4]thiadiazol-2-yl}-1H-indole hydrobromide **9n**

White solid. Yield: 68%, m.p. 259-260 °C. IR cm $^{-1}$: 3155 (NH), 2925 (NH); ^{1}HNMR (200MHz, DMSO-d_6) δ: 6.16 (1H, bs, NH), 7.10-7.20 (1H, m, Ar-H), 7.52-7.58 (1H, dd, *J* = 4.5, 4.6 Hz, Ar-H), 7.73-7.86 (3H, m, Ar-H), 8.05 (2H, dd, *J* = 8.1 Hz, Ar-H), 8.41 (1H, d, *J* = 2.9 Hz, Ar-H), 8.88 (1H, s, Ar-H), 12.27 (1H, bs, NH). ^{13}C NMR (50 MHz, DMSO-d_6) δ: 105.6 (d), 112.1 (d), 113.2 (d), 113.9 (d), 114.0 (s), 123.9 (s), 124.1 (s), 124.7 (4xd), 125.6 (d), 126.7 (s), 131.3 (d), 133.3 (s), 137.9(s), 143.0 (s), 143.5 (s), 157.4 (s). Anal. Calcd for $C_{19}H_{11}BrF_4N_4S$ (MW: 483.27): C, 47.22%; H, 2.29%; N, 11.59%. Found: C, 47.36%; H, 2.36%; N, 11.65%.

5-Fluoro-3-[6-(2,5-dimethoxyphenyl)imidazo[2,1-b][1,3,4]thiadiazol-2-yl]-1H-indole hydrobromide **9o**

White solid. Yield: 76%, m.p. 266 °C. IR cm $^{-1}$: 3427 (NH), 3093 (NH); ^{1}HNMR (200MHz, DMSO-d_6) δ: 3.77 (3H, s, OCH_3), 3.92 (3H, s, OCH_3), 4.25 (1H, bs, NH), 6.82-6.87 (1H, dd, *J* = 2.9, 2.84 Hz, Ar-H), 7.02-7.20 (2H, m, 2xAr-H), 7.52-7.59 (1H, dd, *J* = 4.32, 4.52 Hz, Ar-H), 7.70 (1H, d, *J* = 2.86 Hz, Ar-H), 7.87 (1H, d, *J* = 89.6 Hz, Ar-H), 8.41 (1H, s, Ar-H), 8.55 (1H, s, Ar-H), 12.24 (1H, bs, NH). ^{13}C NMR (50 MHz, DMSO-d6) δ: 55.3 (q), 55.7 (q), 105.1 (d), 105.6 (d), 106.6 (s), 111.5 (2xd), 112.5 (2xd), 113.8 (d), 122.2 (s), 124.0 (s), 131.1 (d), 133.3 (s), 139.7 (s), 142.0 (s), 149.8 (s), 153.1 (s), 156.9 (s). Anal. Calcd for $C_{20}H_{16}BrFN_4O_2S$ (MW: 475.33): C, 50.54%; H, 3.39%; N, 11.79%. Found: C, 50.68%; H, 3.52%; N, 11.86%.

5-Fluoro-1-methyl-3-{6-[4-(trifluoromethyl)phenyl]imidazo[2,1-b][1,3,4]thiadiazol-2-yl}-1H-indole hydrobromide **9p**

Grey solid. Yield: 78%, m.p 281°C. IR cm^{-1}: 3501 (NH); ^{1}HNMR (200MHz, DMSO-d_6) δ: 3.85 (3H, s, CH_3), 7.18-7.28 (1H, m, Ar-H), 7.57-7.81 (5H, m, Ar-H, NH), 8.02 (2H, d, *J* = 8.0 Hz, Ar-H), 8.36 (1H, s, Ar-H), 8.81 (1H, s, Ar-H). Anal. Calcd for $C_{20}H_{13}BrF_4N_4S$ (MW: 497.30): C, 48.30%; H, 2.63%; N, 11.27%. Found: C, 48.50%; H, 2.75%; N, 11.36%.

Biology

Drugs and chemical

The 3-(6-phenylimidazo[2,1-*b*][1,3,4]thiadiazol-2-yl)-1*H*-indolecompounds **9a-p** were synthesised at the Department of Pharmacy, University of Palermo (Palermo, Italy). The drugs were dissolved in DMSO. The medium, foetal bovine serum (FBS), penicillin (50 IU ml^{-1}) and streptomycin (50 µg ml^{-1}) were from Gibco (Gaithersburg, MD, USA). All other chemicals were from Sigma (Zwijndrecht, the Netherlands).

Cell cultures

Capan-1 and Panc-1 cell lines were purchased at the ATCC(American Type Culture Collection) (Manassas, VA, USA), while SUIT-2 cells were a generous gift from Dr. Adam Frampton (Imperial College, London, UK). The cell lines were tested for their authentication by STR–PCR (Short Tandem Repeat- Polymerase Chain Reaction), performed by BaseClear (Leiden, the Netherlands). The cells were cultured in RPMI-1640 (Roswell Park Memorial Institute 1640) supplemented with 10% heat-inactivated FBS, 1% penicillin/streptomycin, or in DMEM (Dulbecco's Modified Eagle's Medium),

supplemented with 10% heat-inactivated FBS, 1% HEPES (4-(2-hydroxyethyl)-*1*-piperazineethanesulfonic acid). The cells were kept in a humidified atmosphere of 5% CO_2 and 95% air at 37 °C and harvested with trypsin-EDTA (Ethylenediaminetetraacetic acid).

Cell growth inhibition

To evaluate the inhibitory effects of the imidazo[2,1-*b*][1,3,4]thiadiazole compounds **9a-p** on cell growth, we performed the Sulforhodamine-B (SRB) assay, as previously described.[42] Cells were seeded into 96-well flat-bottom plates in triplicate at a density of 3 x 10^3 cells/well for SUIT-2 and Panc-1, while 5 x 10^3 cells/well were used for Capan-1. Cells were incubated at 37 °C for 24 hours to create a confluent monolayer and then they were treated with 100 µL of increasing concentrations of the compounds dissolved in DMSO.

After 72 hours of treatment, the cells were fixed with 25 µL of 50% cold trichloroacetic acid (TCA) and kept for at least 60 minutes at 4°C. Then, the plates were washed gently with deionized water, dried at room temperature (RT) overnight and stained with 50 µL of 0.4% SRB solution in 1% acetic acid for 15 minutes at RT. The excess of SRB stain was removed on dried tissues and the plates were washed with 1% acetic acid and let dry at RT overnight. The SRB was dissolved in 150 µL of tris(hydroxymethyl)aminomethane solution pH= 8.8 (TRIS base), and the optical density (OD) was detected at a wavelength of 490 nm and 540 nm. Cell growth inhibition was calculated as the percentage versus vehicle-treated cells ("negative control") OD (corrected for OD before drug addiction). Finally, the half maximal inhibitory concentration (IC_{50}) was calculated by non-linear least squares curve fitting (GraphPad Prism 7, Intuitive Software for Science, San Diego, CA).

Wound-healing assays

The *in vitro* scratch wound-healing assay was performed as previously described.[43] SUIT-2, Capan-1 and Panc-1 cells were seeded into a 96-well plates at a density of 5 x 10^4 cells/well and incubated for 24 hours at 37 °C, 5% CO_2 and 100% humidity. Then, cell monolayer was scratched through a specific needle to create a scratch of constant width. After removal of the detached cells by washing with phosphate buffered saline (PBS), we added only medium in the control wells and medium with the compounds of interest in the experimental wells. The wound closure was monitored by phase-contrast microscopy using a Universal Grab 6.3 software (Digital Cell Imaging Labs, Keerbergen, Belgium) integrated to the Leica DMI300B migration station (Leica Microsystems, Eindhoven,

Netherlands) and the pictures were captured immediately after scratch (T = 0), and at 4, 8, 20 and 24 hours from the treatment. The results were analyzed with the Scratch Assay 6.2 software (Digital Cell Imaging Labs).

Statistical analysis

All SRB assays were carried out in triplicate and repeated at least three times, whereas the percentages of cell migration were calculated taking into account at least six scratch areas. The data were evaluated using GraphPad Prism (GraphPad Software, San Diego, CA, USA). Data were expressed as mean values ± SEM and analyzed by the Student's t-test.

Conclusion

PDAC is one of the deadliest cancer types and despite enormous efforts in pancreatic cancer research, in 2019, the American Cancer Society estimated 1,762,450 new cancer cases and 606,880 cancer deaths in the United States (US).[44] Due to the lack of clinical signs and symptoms, most patients are diagnosed at an advanced/unresectable stage of the disease and regimens with combinations of conventional chemotherapy drugs are the best option for the treatment of PDAC patients.[45] However, PDACs are characterized by common inherent or acquired resistance to conventional treatment modalities and new therapeutic strategies are warranted.[33,46] A new series of imidazo[2,1-*b*][1,3,4]thiadiazole derivatives **9a**–**p** were efficiently synthesized and tested for their *in vitro* antiproliferative properties on a panel of PDAC cell lines, including SUIT-2, Capan-1 and Panc-1. Four out of sixteen compounds (**9c**, **9e**, **9l** and **9n**), showed interesting *in vitro* antiproliferative activity. In particular, the compounds **9c** and **9l** were active in all three preclinical models with IC_{50s} ranging from 5.1 to 10.8 µM. Notably, the IC_{50s} of the compound **9c** in SUIT-2, Capan-1 and Panc-1 cells were the lowest (around 5 µM). The compound **9e** was active only in Panc-1 cells. Conversely, the compound **9n** inhibited cell proliferation in SUIT-2 and Capan-1 cells, with IC_{50s} of 11.8 ± 0.54 and 10.49 ± 0.16 µM, respectively. Finally, using the scratch wound-healing assay, we demonstrated a relevant anti-migratory activity of the compound **9c** in SUIT-2 and Capan-1 cells. Overall, the results of cytotoxicity and cell migration obtained with compound **9c** could suggest its role as an interesting hit compound to create a library of new derivatives and study in deep the structure–activity relationship (SAR). This could indeed be extremely useful to guide the synthesis of future analogues. In particular, we focused our research on derivatives bearing at position 5 of

indole scaffold a group (-OCH3) or atom (-F) with electron-withdrawing properties. Furthermore, we investigated how the N-methyl indole, as well as the effect of different substitutions on the phenyl ring, could influence activity. As reported in the Table 1, some of the compounds 1*H*-indole showed antiproliferative activity in one or more cell lines, unlike the 1-methyl-1*H*-indole analogues. Probably, this is due to the ability to create hydrogen bonds with the target. Concerning the substitution on phenyl ring, we did not observe differences between the presence or absence of electron-withdrawing groups, with the exception of nitro group (-NO_2) that, thanks to the delocalization of negative and positive charges, increased the cytotoxicity activity in all the cell lines.

Author Contributions: Stella Cascioferro, Giovanna Li Petri, Barbara Parrino, Daniela Carbone, Ugo Perricone performed chemical research and analyzed the data. Giovanna Li Petri, Btissame El Hassouni, Vincenzo Arizza, Niccola Funel, performed biological research and analyzed the data. Godefridus J. Peters, Girolamo Cirrincione, Alessandro Padova, Patrizia Diana, and Elisa Giovannetti participated in the design of the research and the writing of the manuscript. All authors read and approved the final manuscript.

Funding: This project was supported by a 2014–2020 PON Ricerca e Innovazione grant from the Italian Ministry of Education, University and Research, entitled “PROGEMA - Processi Green per l'Estrazione di Principi Attivi e la Depurazione di Matrici di Scarto e Non” (ARS01_00432) to P.D. and by the AIRC Start-up grant to E.G.

Conflicts of Interest: The authors declare no conflict of interest

References

(1) Torre, L. A.; Siegel, R. L.; Ward, E. M.; Jemal, A. Global Cancer Incidence and Mortality Rates and Trends--An Update. *Cancer Epidemiol. Biomarkers Prev.* **2016**, *25* (1), 16–27. https://doi.org/10.1158/1055-9965.EPI-15-0578.

(2) Sung, H.; Siegel, R. L.; Rosenberg, P. S.; Jemal, A. Emerging Cancer Trends among Young Adults in the USA: Analysis of a Population-Based Cancer Registry. *The Lancet Public Health* **2019**, *4* (3), e137–e147. https://doi.org/10.1016/S2468-2667(18)30267-6.

(3) Jadhav, V. B.; Kulkarni, M. V.; Rasal, V. P.; Biradar, S. S.; Vinay, M. D. Synthesis and Anti-Inflammatory Evaluation of Methylene Bridged Benzofuranyl Imidazo[2,1-b][1,3,4]Thiadiazoles. *Eur J Med Chem* **2008**, *43* (8), 1721–1729. https://doi.org/10.1016/j.ejmech.2007.06.023.

(4) Agatonovic-Kustrin, S.; Kettle, C.; Morton, D. W. A Molecular Approach in Drug Development for Alzheimer's Disease. *Biomed. Pharmacother.* **2018**, *106*, 553–565. https://doi.org/10.1016/j.biopha.2018.06.147.

(5) Tahghighi, A.; Razmi, S.; Mahdavi, M.; Foroumadi, P.; Ardestani, S. K.; Emami, S.; Kobarfard, F.; Dastmalchi, S.; Shafiee, A.; Foroumadi, A. Synthesis and Anti-Leishmanial Activity of 5-(5-Nitrofuran-2-Yl)-1,3,4-Thiadiazol-2-Amines Containing N-[(1-Benzyl-1H-1,2,3-Triazol-4-Yl)Methyl] Moieties. *Eur J Med Chem* **2012**, *50*, 124–128. https://doi.org/10.1016/j.ejmech.2012.01.046.

(6) Jakovljević, K.; Matić, I. Z.; Stanojković, T.; Krivokuća, A.; Marković, V.; Joksović, M. D.; Mihailović, N.; Nićiforović, M.; Joksović, L. Synthesis, Antioxidant and Antiproliferative Activities of 1,3,4-Thiadiazoles Derived from Phenolic Acids. *Bioorg. Med. Chem. Lett.* **2017**, *27* (16), 3709–3715. https://doi.org/10.1016/j.bmcl.2017.07.003.

(7) Alegaon, S. G.; Alagawadi, K. R.; Sonkusare, P. V.; Chaudhary, S. M.; Dadwe, D. H.; Shah, A. S. Novel Imidazo[2,1-b][1,3,4]Thiadiazole Carrying Rhodanine-3-Acetic Acid as Potential Antitubercular Agents. *Bioorg. Med. Chem. Lett.* **2012**, *22* (5), 1917–1921. https://doi.org/10.1016/j.bmcl.2012.01.052.

(8) Bhongade, B. A.; Talath, S.; Gadad, R. A.; Gadad, A. K. Biological Activities of Imidazo[2,1-b][1,3,4]Thiadiazole Derivatives: A Review. *Journal of Saudi Chemical Society* **2016**, *20*, S463–S475. https://doi.org/10.1016/j.jscs.2013.01.010.

(9) Schillaci, D.; Spanò, V.; Parrino, B.; Carbone, A.; Montalbano, A.; Barraja, P.; Diana, P.; Cirrincione, G.; Cascioferro, S. Pharmaceutical Approaches to Target Antibiotic Resistance Mechanisms. *J. Med. Chem.* **2017**, *60* (20), 8268–8297. https://doi.org/10.1021/acs.jmedchem.7b00215.

(10) Cascioferro, S.; Parrino, B.; Petri, G. L.; Cusimano, M. G.; Schillaci, D.; Di Sarno, V.; Musella, S.; Giovannetti, E.; Cirrincione, G.; Diana, P. 2,6-Disubstituted Imidazo[2,1-b][1,3,4]Thiadiazole Derivatives as Potent Staphylococcal Biofilm Inhibitors. *European Journal of Medicinal Chemistry* **2019**, *167*, 200–210. https://doi.org/10.1016/j.ejmech.2019.02.007.

(11) Parrino, B.; Schillaci, D.; Carnevale, I.; Giovannetti, E.; Diana, P.; Cirrincione, G.; Cascioferro, S. Synthetic Small Molecules as Anti-Biofilm Agents in the Struggle against Antibiotic Resistance. *Eur J Med Chem* **2019**, *161*, 154–178. https://doi.org/10.1016/j.ejmech.2018.10.036.

(12) Karki, S. S.; Panjamurthy, K.; Kumar, S.; Nambiar, M.; Ramareddy, S. A.; Chiruvella, K. K.; Raghavan, S. C. Synthesis and Biological Evaluation of Novel 2-Aralkyl-5-Substituted-6-(4'-Fluorophenyl)-Imidazo[2,1-b][1,3,4]Thiadiazole Derivatives as Potent Anticancer Agents. *Eur J Med Chem* **2011**, *46* (6), 2109–2116. https://doi.org/10.1016/j.ejmech.2011.02.064.

(13) Kumar, S.; Hegde, M.; Gopalakrishnan, V.; Renuka, V. K.; Ramareddy, S. A.; De Clercq, E.; Schols, D.; Gudibabande Narasimhamurthy, A. K.; Raghavan, S. C.; Karki, S. S. 2-(4-Chlorobenzyl)-6-Arylimidazo[2,1-b][1,3,4]Thiadiazoles: Synthesis, Cytotoxic Activity and Mechanism of Action. *Eur J Med Chem* **2014**, *84*, 687–697. https://doi.org/10.1016/j.ejmech.2014.07.054.

(14) Arjomandi, O. K.; Hussein, W. M.; Vella, P.; Yusof, Y.; Sidjabat, H. E.; Schenk, G.; McGeary, R. P. Design, Synthesis, and in Vitro and Biological Evaluation of Potent Amino Acid-Derived Thiol Inhibitors of the Metallo-β-Lactamase IMP-1. *Eur J Med Chem* **2016**, *114*, 318–327. https://doi.org/10.1016/j.ejmech.2016.03.017.

(15) Romagnoli, R.; Baraldi, P. G.; Prencipe, F.; Balzarini, J.; Liekens, S.; Estévez, F. Design, Synthesis and Antiproliferative Activity of Novel Heterobivalent Hybrids Based on Imidazo[2,1-b][1,3,4]Thiadiazole and Imidazo[2,1-b][1,3]Thiazole Scaffolds. *Eur J Med Chem* **2015**, *101*, 205–217. https://doi.org/10.1016/j.ejmech.2015.06.042.

(16) Kumar, S.; Gopalakrishnan, V.; Hegde, M.; Rana, V.; Dhepe, S. S.; Ramareddy, S. A.; Leoni, A.; Locatelli, A.; Morigi, R.; Rambaldi, M.; et al. Synthesis and Antiproliferative Activity of Imidazo[2,1-b][1,3,4]Thiadiazole Derivatives. *Bioorg. Med. Chem. Lett.* **2014**, *24* (19), 4682–4688. https://doi.org/10.1016/j.bmcl.2014.08.032.

(17) Patel, H. M.; Sing, B.; Bhardwaj, V.; Palkar, M.; Shaikh, M. S.; Rane, R.; Alwan, W. S.; Gadad, A. K.; Noolvi, M. N.; Karpoormath, R. Design, Synthesis and Evaluation of Small Molecule Imidazo[2,1-b][1,3,4]Thiadiazoles as Inhibitors of Transforming

Growth Factor-β Type-I Receptor Kinase (ALK5). *Eur J Med Chem* **2015**, *93*, 599–613. https://doi.org/10.1016/j.ejmech.2014.09.002.

(18) Parrino, B.; Carbone, A.; Ciancimino, C.; Spanò, V.; Montalbano, A.; Barraja, P.; Cirrincione, G.; Diana, P.; Sissi, C.; Palumbo, M.; et al. Water-Soluble Isoindolo[2,1-a]Quinoxalin-6-Imines: In Vitro Antiproliferative Activity and Molecular Mechanism(s) of Action. *Eur J Med Chem* **2015**, *94*, 149–162. https://doi.org/10.1016/j.ejmech.2015.03.005.

(19) Parrino, B.; Ullo, S.; Attanzio, A.; Cascioferro, S.; Spanò, V.; Carbone, A.; Montalbano, A.; Barraja, P.; Cirrincione, G.; Tesoriere, L.; et al. Synthesis of 5H-Pyrido[3,2-b]Pyrrolizin-5-One Tripentone Analogs with Antitumor Activity. *Eur J Med Chem* **2018**, *158*, 236–246. https://doi.org/10.1016/j.ejmech.2018.09.017.

(20) Diana, P.; Stagno, A.; Barraja, P.; Montalbano, A.; Carbone, A.; Parrino, B.; Cirrincione, G. Synthesis of the New Ring System Pyrrolizino[2,3-b]Indol-4(5H)-One. *Tetrahedron* **2011**, *67*, 3374–3379. https://doi.org/10.1016/j.tet.2011.03.060.

(21) Parrino, B.; Carbone, A.; Spanò, V.; Montalbano, A.; Giallombardo, D.; Barraja, P.; Attanzio, A.; Tesoriere, L.; Sissi, C.; Palumbo, M.; et al. Aza-Isoindolo and Isoindolo-Azaquinoxaline Derivatives with Antiproliferative Activity. *Eur J Med Chem* **2015**, *94*, 367–377. https://doi.org/10.1016/j.ejmech.2015.03.009.

(22) Diana, P.; Stagno, A.; Barraja, P.; Carbone, A.; Parrino, B.; Dall'Acqua, F.; Vedaldi, D.; Salvador, A.; Brun, P.; Castagliuolo, I.; et al. Synthesis of Triazenoazaindoles: A New Class of Triazenes with Antitumor Activity. *ChemMedChem* **2011**, *6* (7), 1291–1299. https://doi.org/10.1002/cmdc.201100027.

(23) Parrino, B.; Ciancimino, C.; Carbone, A.; Spano', V.; Montalbano, A.; Barraja, P.; Cirrincione, G.; Diana, P. Synthesis of Isoindolo[1,4]Benzoxazinone and Isoindolo[1,5]Benzoxazepine: Two New Ring Systems of Pharmaceutical Interest. **2015**, *71* (39), 7332–7338. https://doi.org/10.1016/j.tet.2015.04.083.

(24) Cascioferro, S.; Attanzio, A.; Di Sarno, V.; Musella, S.; Tesoriere, L.; Cirrincione, G.; Diana, P.; Parrino, B. New 1,2,4-Oxadiazole Nortopsentin Derivatives with Cytotoxic Activity. *Mar Drugs* **2019**, *17* (1). https://doi.org/10.3390/md17010035.

(25) Parrino, B.; Attanzio, A.; Spanò, V.; Cascioferro, S.; Montalbano, A.; Barraja, P.; Tesoriere, L.; Diana, P.; Cirrincione, G.; Carbone, A. Synthesis, Antitumor Activity and CDK1 Inhibiton of New Thiazole Nortopsentin Analogues. *Eur J Med Chem* **2017**, *138*, 371–383. https://doi.org/10.1016/j.ejmech.2017.06.052.

(26) Spanò, V.; Attanzio, A.; Cascioferro, S.; Carbone, A.; Montalbano, A.; Barraja, P.; Tesoriere, L.; Cirrincione, G.; Diana, P.; Parrino, B. Synthesis and Antitumor Activity of New Thiazole Nortopsentin Analogs. *Mar Drugs* **2016**, *14* (12). https://doi.org/10.3390/md14120226.

(27) Carbone, A.; Parrino, B.; Di Vita, G.; Attanzio, A.; Spanò, V.; Montalbano, A.; Barraja, P.; Tesoriere, L.; Livrea, M. A.; Diana, P.; et al. Synthesis and Antiproliferative Activity of Thiazolyl-Bis-Pyrrolo[2,3-b]Pyridines and Indolyl-Thiazolyl-Pyrrolo[2,3-c]Pyridines, Nortopsentin Analogues. *Mar Drugs* **2015**, *13* (1), 460–492. https://doi.org/10.3390/md13010460.

(28) Parrino, B.; Carbone, A.; Di Vita, G.; Ciancimino, C.; Attanzio, A.; Spanò, V.; Montalbano, A.; Barraja, P.; Tesoriere, L.; Livrea, M. A.; et al. 3-[4-(1H-Indol-3-Yl)-1,3-Thiazol-2-Yl]-1H-Pyrrolo[2,3-b]Pyridines, Nortopsentin Analogues with Antiproliferative Activity. *Mar Drugs* **2015**, *13* (4), 1901–1924. https://doi.org/10.3390/md13041901.

(29) Meijer, L. L.; Garajová, I.; Caparello, C.; Le Large, T. Y. S.; Frampton, A. E.; Vasile, E.; Funel, N.; Kazemier, G.; Giovannetti, E. Plasma MiR-181a-5p Downregulation Predicts Response and Improved Survival After FOLFIRINOX in Pancreatic Ductal Adenocarcinoma. *Ann. Surg.* **2018**. https://doi.org/10.1097/SLA.0000000000003084.

(30) El Hassouni, B.; Li Petri, G.; Liu, D. S. K.; Cascioferro, S.; Parrino, B.; Hassan, W.; Diana, P.; Ali, A.; Frampton, A. E.; Giovannetti, E. Pharmacogenetics of Treatments for Pancreatic Cancer. *Expert Opin Drug Metab Toxicol* **2019**, *15* (6), 437–447. https://doi.org/10.1080/17425255.2019.1620731.

(31) Le Large, T. Y. S.; El Hassouni, B.; Funel, N.; Kok, B.; Piersma, S. R.; Pham, T. V.; Olive, K. P.; Kazemier, G.; van Laarhoven, H. W. M.; Jimenez, C. R.; et al. Proteomic Analysis of Gemcitabine-Resistant Pancreatic Cancer Cells Reveals That Microtubule-Associated Protein 2 Upregulation Associates with Taxane Treatment. *Ther Adv Med Oncol* **2019**, *11*, 1758835919841233. https://doi.org/10.1177/1758835919841233.

(32) Giovannetti, E.; van der Borden, C. L.; Frampton, A. E.; Ali, A.; Firuzi, O.; Peters, G. J. Never Let It Go: Stopping Key Mechanisms Underlying Metastasis to Fight Pancreatic Cancer. *Semin. Cancer Biol.* **2017**, *44*, 43–59. https://doi.org/10.1016/j.semcancer.2017.04.006.

(33) Le Large, T. Y. S.; Bijlsma, M. F.; Kazemier, G.; van Laarhoven, H. W. M.; Giovannetti, E.; Jimenez, C. R. Key Biological Processes Driving Metastatic Spread of Pancreatic

Cancer as Identified by Multi-Omics Studies. *Seminars in Cancer Biology* **2017**, *44*, 153–169. https://doi.org/10.1016/j.semcancer.2017.03.008.

(34) Iwamura, T.; Caffrey, T. C.; Kitamura, N.; Yamanari, H.; Setoguchi, T.; Hollingsworth, M. A. P-Selectin Expression in a Metastatic Pancreatic Tumor Cell Line (SUIT-2). *Cancer Res.* **1997**, *57* (6), 1206–1212.

(35) Deer, E. L.; Gonzalez-Hernandez, J.; Coursen, J. D.; Shea, J. E.; Ngatia, J.; Scaife, C. L.; Firpo, M. A.; Mulvihill, S. J. Phenotype and Genotype of Pancreatic Cancer Cell Lines. *Pancreas* **2010**, *39* (4), 425–435. https://doi.org/10.1097/MPA.0b013e3181c15963.

(36) Maftouh, M.; Avan, A.; Funel, N.; Frampton, A. E.; Fiuji, H.; Pelliccioni, S.; Castellano, L.; Galla, V.; Peters, G. J.; Giovannetti, E. MiR-211 Modulates Gemcitabine Activity through Downregulation of Ribonucleotide Reductase and Inhibits the Invasive Behavior of Pancreatic Cancer Cells. *Nucleosides Nucleotides Nucleic Acids* **2014**, *33* (4–6), 384–393. https://doi.org/10.1080/15257770.2014.891741.

(37) Avan, A.; Crea, F.; Paolicchi, E.; Funel, N.; Galvani, E.; Marquez, V. E.; Honeywell, R. J.; Danesi, R.; Peters, G. J.; Giovannetti, E. Molecular Mechanisms Involved in the Synergistic Interaction of the EZH2 Inhibitor 3-Deazaneplanocin A with Gemcitabine in Pancreatic Cancer Cells. *Mol. Cancer Ther.* **2012**, *11* (8), 1735–1746. https://doi.org/10.1158/1535-7163.MCT-12-0037.

(38) Avan, A.; Caretti, V.; Funel, N.; Galvani, E.; Maftouh, M.; Honeywell, R. J.; Lagerweij, T.; Van Tellingen, O.; Campani, D.; Fuchs, D.; et al. Crizotinib Inhibits Metabolic Inactivation of Gemcitabine in C-Met-Driven Pancreatic Carcinoma. *Cancer Res.* **2013**, *73* (22), 6745–6756. https://doi.org/10.1158/0008-5472.CAN-13-0837.

(39) Ebos, J. M. L.; Lee, C. R.; Cruz-Munoz, W.; Bjarnason, G. A.; Christensen, J. G.; Kerbel, R. S. Accelerated Metastasis after Short-Term Treatment with a Potent Inhibitor of Tumor Angiogenesis. *Cancer Cell* **2009**, *15* (3), 232–239. https://doi.org/10.1016/j.ccr.2009.01.021.

(40) Carbone, A.; Parrino, B.; Cusimano, M. G.; Spanò, V.; Montalbano, A.; Barraja, P.; Schillaci, D.; Cirrincione, G.; Diana, P.; Cascioferro, S. New Thiazole Nortopsentin Analogues Inhibit Bacterial Biofilm Formation. *Mar Drugs* **2018**, *16* (8). https://doi.org/10.3390/md16080274.

(41) Boosa, V.; Bilakanti, V.; Velisoju, V. K.; Gutta, N.; Inkollu, S.; Akula, V. An Insight on the Influence of Surface Lewis Acid Sites for Regioselective CH Bond C3-Cyanation of Indole Using NH4I and DMF as Combined Cyanide Source over Cu/SBA-15 Catalyst. *Molecular Catalysis* **2018**, *445*, 43–51. https://doi.org/10.1016/j.mcat.2017.11.007.

(42) Sciarrillo, R.; Wojtuszkiewicz, A.; Kooi, I. E.; Gómez, V. E.; Boggi, U.; Jansen, G.; Kaspers, G.-J.; Cloos, J.; Giovannetti, E. Using RNA-Sequencing to Detect Novel Splice Variants Related to Drug Resistance in In Vitro Cancer Models. *J Vis Exp* **2016**, No. 118. https://doi.org/10.3791/54714.

(43) Massihnia, D.; Avan, A.; Funel, N.; Maftouh, M.; van Krieken, A.; Granchi, C.; Raktoe, R.; Boggi, U.; Aicher, B.; Minutolo, F.; et al. Phospho-Akt Overexpression Is Prognostic and Can Be Used to Tailor the Synergistic Interaction of Akt Inhibitors with Gemcitabine in Pancreatic Cancer. *Journal of Hematology & Oncology* **2017**, *10* (1), 9. https://doi.org/10.1186/s13045-016-0371-1.

(44) Bray, F.; Ferlay, J.; Soerjomataram, I.; Siegel, R. L.; Torre, L. A.; Jemal, A. Global Cancer Statistics 2018: GLOBOCAN Estimates of Incidence and Mortality Worldwide for 36 Cancers in 185 Countries. *CA Cancer J Clin* **2018**, *68* (6), 394–424. https://doi.org/10.3322/caac.21492.

(45) Caparello, C.; Meijer, L. L.; Garajova, I.; Falcone, A.; Le Large, T. Y.; Funel, N.; Kazemier, G.; Peters, G. J.; Vasile, E.; Giovannetti, E. FOLFIRINOX and Translational Studies: Towards Personalized Therapy in Pancreatic Cancer. *World J. Gastroenterol.* **2016**, *22* (31), 6987–7005. https://doi.org/10.3748/wjg.v22.i31.6987.

(46) Kleeff, J.; Korc, M.; Apte, M.; La Vecchia, C.; Johnson, C. D.; Biankin, A. V.; Neale, R. E.; Tempero, M.; Tuveson, D. A.; Hruban, R. H.; et al. Pancreatic Cancer. *Nature Reviews Disease Primers* **2016**, *2*, 16022. https://doi.org/10.1038/nrdp.2016.22.

Chapter 7

Imidazo[2,1-b][1,3,4]thiadiazoles with antiproliferative activity against primary and gemcitabine-resistant pancreatic cancer cells

Cascioferro S[1a], **Li Petri G[1,2a]**, Parrino B[1], Carbone D[1], Funel N[3], Bergonzini C[2], Mantini G[2], Dekker H[2], Daan Geerke[4], Peters GJ[2], Cirrincione G[1], Giovannetti E[2,3]*, Diana P[1]*

[a]equal contributors

*Corresponding authors

1. *Department of Biological, Chemical and Pharmaceutical Sciences and Technologies (STEBICEF), University of Palermo, Palermo, Italy*
2. *Department of Medical Oncology, Cancer Center Amsterdam, Amsterdam UMC, VU University Medical Center (VUmc), Amsterdam, The Netherlands*
3. *Cancer Pharmacology Lab, AIRC Start Up Unit, Fondazione Pisana per la Scienza, Pisa, Italy*
4. *AIMMS Division of Molecular Toxicology, Department of Chemistry and Pharmaceutical Sciences, Faculty of Sciences, VU University Amsterdam, De Boelelaan 1108, 1081 HZ Amsterdam, The Netherlands*

European Journal of Medicinal Chemistry

Available online 25 January 2020, 112088.

doi: https://doi.org/10.1016/j.ejmech.2020.112088

Imidazo[2,1-b][1,3,4]thiadiazoles with antiproliferative activity against primary and gemcitabine-resistant pancreatic cancer cells

Abstract

A new series of eighteen imidazo[2,1-*b*][1,3,4]thiadiazole derivatives was efficiently synthesized and screened for antiproliferative activity against the National Cancer Institute (NCI-60) cell lines panel. Two out of eighteen derivatives, compounds **12a** and **12h**, showed remarkably cytotoxic activity with the half maximal inhibitory concentration values (IC_{50}) ranging from 0.23 to 11.4 µM, and 0.29 to 12.2 µM, respectively. However, two additional compounds, **12b** and **13g**, displayed remarkable *in vitro* antiproliferative activity against pancreatic ductal adenocarcinoma (PDAC) cell lines, including immortalized (SUIT-2, Capan-1, Panc-1), primary (PDAC-3) and gemcitabine-resistant (Panc-1R), eliciting IC_{50} values ranging from micromolar to sub-micromolar level, associated with significant reduction of cell-migration and spheroid shrinkage. These remarkable results might be explained by modulation of key regulators of epithelial-to-mesenchymal transition (EMT), including E-cadherin and vimentin, and inhibition of metalloproteinase-2/-9. High-throughput arrays revealed a significant inhibition of the phosphorylation of 45 tyrosine kinases substrates, whose visualization on Cytoscape highlighted PTK2/FAK as an important hub. Inhibition of phosphorylation of PTK2/FAK was validated as one of the possible mechanisms of action, using a specific ELISA. In conclusion, novel imidazothiadiazoles show potent antiproliferative activity, mediated by modulation of EMT and PTK2/FAK.

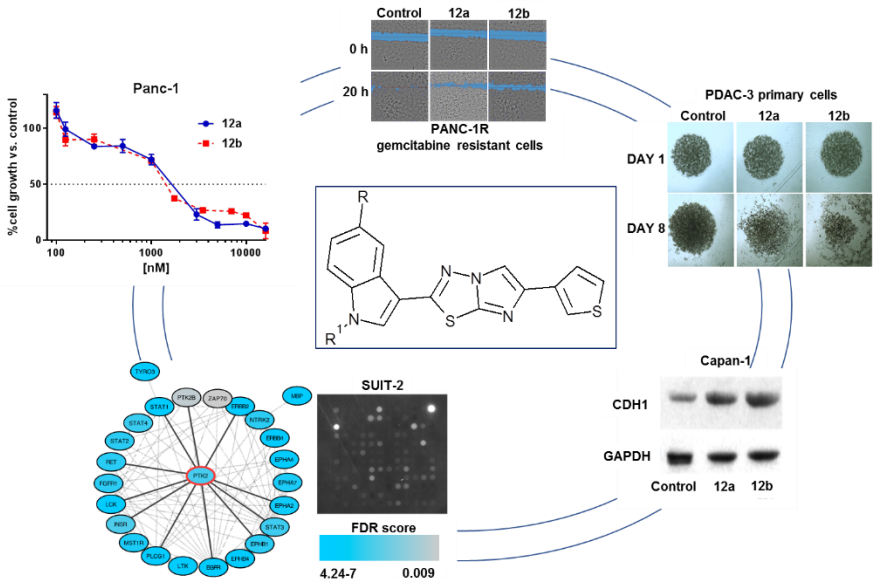

Keywords: imidazo[2,1-*b*][1,3,4]thiadiazole derivatives, pancreatic ductal adenocarcinoma, antiproliferative activity, inhibition of migration, spheroids shrinkage, modulation of EMT, PTK2/FAK

Introduction

The synthesis of hybrid molecules, bearing two or more different biologically active scaffolds in a single structure, is regarded as one of the most valuable approaches in drug development in order to obtain new therapeutic strategies to treat oncological diseases.[1–3] The design of anticancer drugs characterized by two moieties with antitumor activity led to the development of a number of molecules with improved biological potential compared to the parent compounds. In particular, hybrid anticancer drugs showed improved specificity, a greater ability to overcome drug-resistance mechanisms, better patient compliance and lower side effects.[4,5]

The simultaneous presence of two pharmacophores often led to a synergism of the biological activities and therefore to the capability to act towards more than one target. Many examples of hybrid compounds with promising cytotoxic properties have been reported in the latest years. Singla and collaborators described remarkable antiproliferative activity against the NCI-60 cell lines panel of benzimidazole-triazine hybrids **1** (Fig. 1) which showed IC_{50} values from the low micromolar to the nanomolar range.[6] The pyrimidine-triazole hybrids **2** (Fig. 1) exhibited potent anticancer activity against the B16-F10 murine melanoma cancer cell line due to their ability in reducing the pro-caspase3 level while increasing the p53 and active-caspase 3 levels.[7] Pyrazole-benzofuran hybrids **3** (Fig. 1) emerged as promising anticancer compounds against human pancreatic (Panc-1 and PaCa-2 cells), lung (A549 and H-460), breast (MCF-7), colon (HT-29) and prostate (PC-3) cancer, with IC_{50} values in the range of 0.9-2.2 μM (Fig. 1).[8]

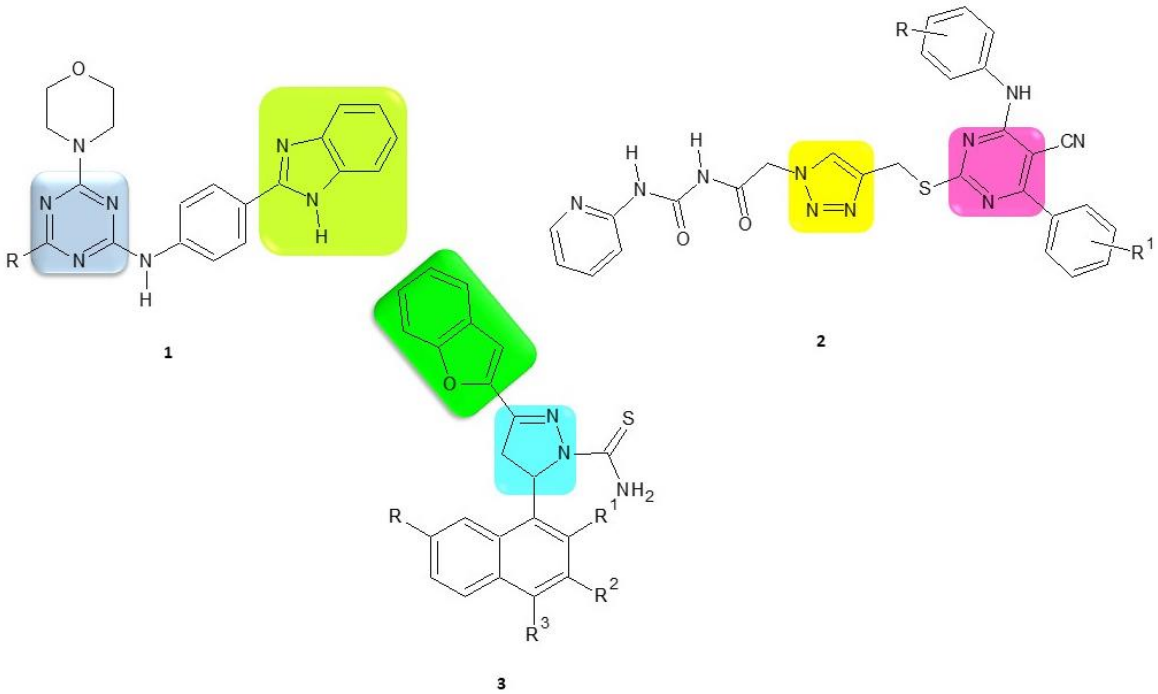

Figure 1. Chemical structures of benzimidazole-triazine hybrids **1**, pyrimidine-triazole hybrids **2**, pyrazole-benzofuran hybrids **3**.

The imidazo[2,1-*b*][1,3,4]thiadiazole nucleus has been considered a privileged scaffold for the development of molecules with various pharmacological activities, such as anticancer,[9] analgesic,[10] anti-leishmanial,[11] antioxidant,[12] antitubercular,[13] anticonvulsant,[14] and antibacterial.[15,16]

Concerning the antitumor activity, many imidazo[2,1-*b*][1,3,4]thiadiazole derivatives have been described as potent anticancer molecules acting on several targets against different tumor models. Compound **4** (Fig. 2) showed potent inhibitory activity (IC_{50} = 1.2 nM) against the activin receptor-like kinase 5 (ALK5) proving to be selective toward the P38α kinase.[17] The imidazo[2,1-*b*][1,3,4]thiadiazole-5-carbaldehyde **5** (Fig. 2) was three fold more potent than melphalan, used as reference drug, against murine (L1210) and human (CEM) leukemia cells as well as against immortalized cervical cancer (HeLa) cells, eliciting IC_{50} values of 0.89 µM, 0.75 µM and 0.90 µM, respectively.[18]

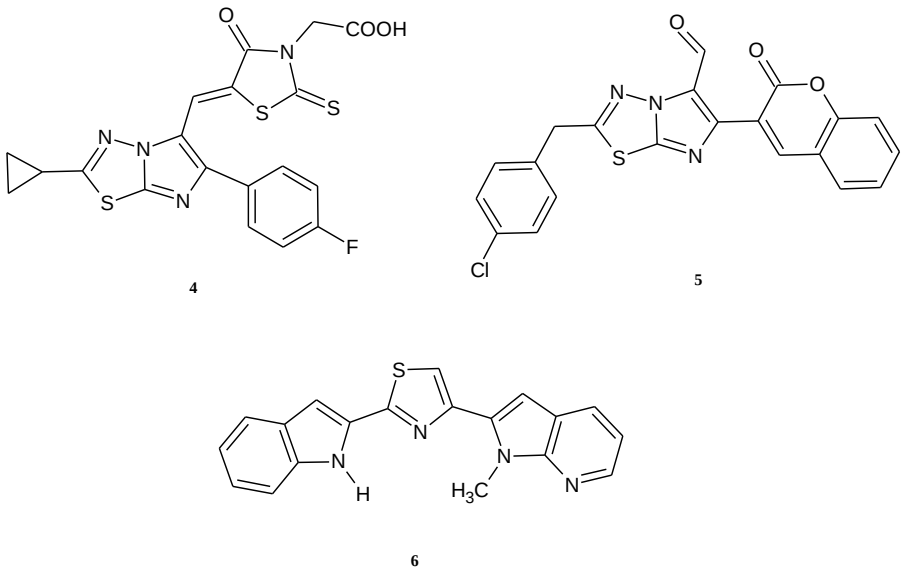

Fig. 2. Chemical structures of the anticancer compounds **4-6**.

In the last decade the indole ring has emerged among the scaffolds recognized as privileged pharmacophores for the development of new antitumor compounds.[19–26]

The indole derivative **6** was described for its potent antiproliferative activity against diffuse malignant peritoneal mesothelioma (DMPM) cell. Nortopsentin analogue **6** potently inhibited CDK1 activity eliciting an IC_{50} value of 0.86 μM and consequently induced a marked cell cycle arrest at the G2/M phase, which was paralleled by an increase in the apoptotic rate.[27]

Therefore, on the basis of the interesting anticancer properties described for imidazo[2,1-*b*][1,3,4]thiadiazole and indole scaffolds, we decided to evaluate the cytotoxic activity of a library of thirty-six 3-(6-phenylimidazo[2,1-*b*][1,3,4]thiadiazol-2-yl)-1*H*-indole derivatives. In particular derivative **7** (Fig. 3) was effective against all the tested cancer cell lines showing GI_{50} values ranging from 1.02 to 9.21 μM.[28]

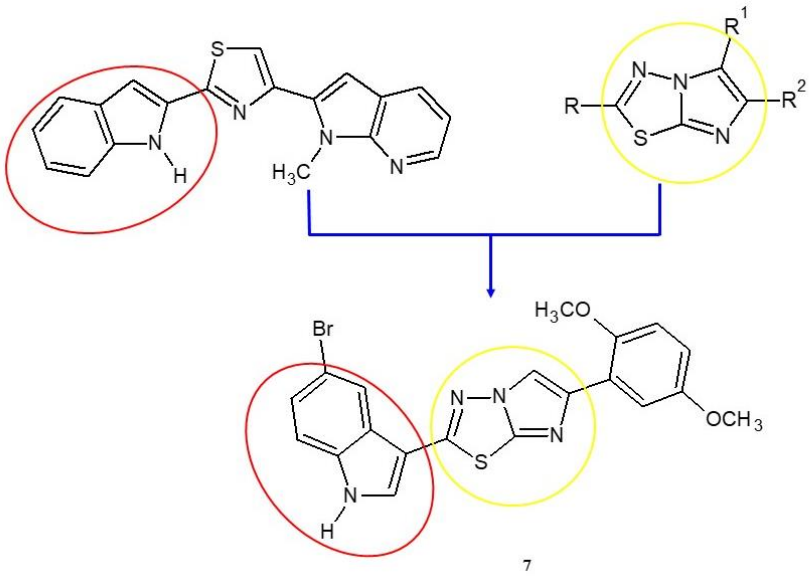

Figure 3. Hybrid compound **7** obtained by combining the two bioactive scaffolds indole and imidazothiadiazole.

These preliminary results prompted further studies on nitrogen heterocyclic systems endowed with antitumor activity,[29–35] and we synthesized eighteen new 3-(imidazo[2,1-*b*][1,3,4]thiadiazol-2-yl)-1*H* indole analogues in order to evaluate how structural modifications on the indole nucleus, introduction of an aldehyde group at the position 5 of the imidazothiadiazole scaffold or the replacement of the phenyl ring at the position 6 with a thiophene ring could influence the anticancer activity of this class of compounds.

We decided to test our new compounds on clinically-relevant models of pancreatic ductal adenocarcinoma (PDAC). This tumor is an extremely aggressive neoplasm, predicted to become the second leading cause of cancer-related deaths before 2030.[36] Cytotoxic chemotherapy remains the mainstay of treatment for most PDAC patients. Treatment with 5-fluorouracil, leucovorin, irinotecan and oxaliplatin (FOLFIRINOX) or with a combination of gemcitabine and nab-paclitaxel, represent the standard-of-care for unresectable patients, and recent data support the use of FOLFIRINOX as adjuvant therapy after surgical resection.[37] However, PDAC is broadly chemoresistant, with a 5-year survival rate below 9%, and novel, more effective therapeutics for PDAC remain an important unmet need.[38–40]

Chemistry

The new imidazothiadiazole derivatives **12-14** were efficiently synthesized following the synthetic route described in Scheme 1.

The commercially available indole-3-carbonitrile **9a** and the derivatives **9b-e**, prepared by reaction of the appropriate 1*H*-indole with chlorosulfonyl isocyanate (CSI), were subjected to a methylation for obtaining the corresponding 1-methyl-1*H*-indole-3-carbonitriles **10a-e**.[16] The 5-(1*H*-indol-3-yl)-1,3,4-thiadiazol-2-amines **11a-j** were obtained in excellent yields (92-100%) by treating the proper derivatives **9a-e** or **10a-e** with thiosemicarbazide.

The 1,3,4-thiadiazol-2-amines **11a-j** underwent a reaction with the appropriate α-bromoacetyl compounds in refluxing ethanol to give the hydrobromide derivatives **12a-r**. Some of such hydrobromides, **12a**,**b**,**d**,**e**,**f**,**h**, were isolated as pure compounds (yields 55-68%) and were characterized without further purifications. Instead, hydrobromides **12c**,**g**,**i**,**j** were treated with saturated aqueous $NaHCO_3$ solution producing the corresponding free bases **13** which were purified by column chromatography providing specimens with suitable analytical and spectral data (yields 58-80%).

Finally, the free bases **13k-r,** prepared through the treatment of the corresponding hydrobromides **12** with saturated aqueous $NaHCO_3$ solution, were subjected to a reaction of formylation using standard Vilsmeier conditions to give the imidazo[2,1-*b*][1,3,4]thiadiazole derivatives **14k-r** (yields 70-90%).

Data on physicochemical properties of the compounds are reported in the Supplementary results and Supplementary Tables 1-2.

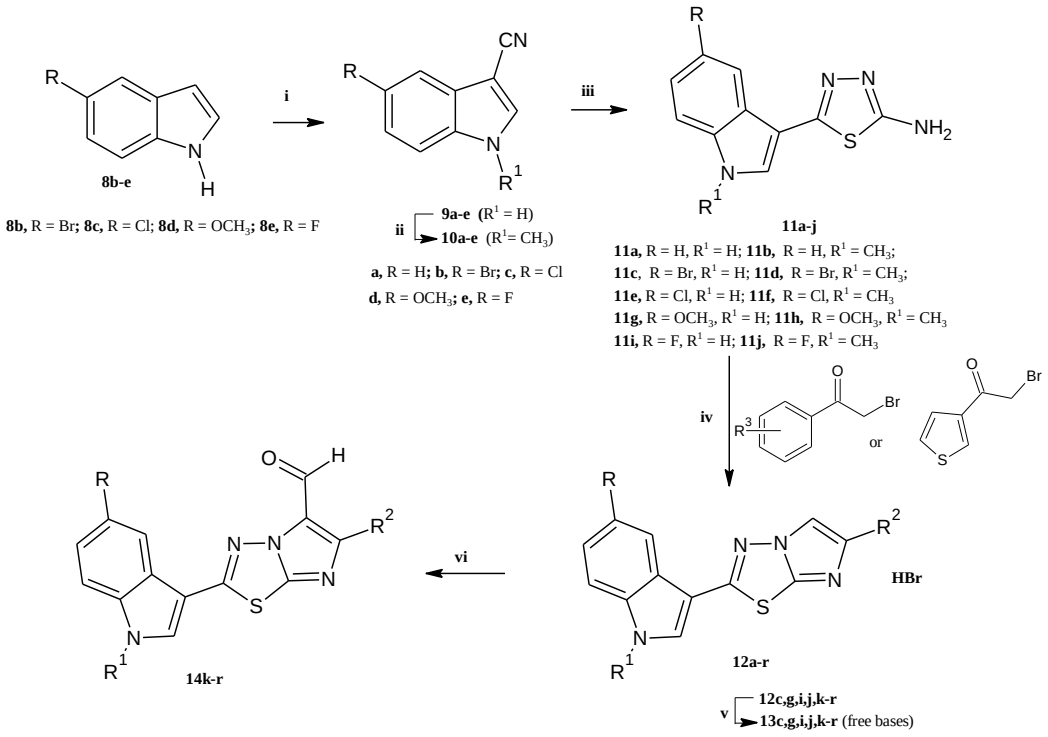

8b, R = Br; 8c, R = Cl; 8d, R = OCH_3; 8e, R = F

a, R = H; b, R = Br; c, R = Cl
d, R = OCH_3; e, R = F

11a, R = H, R^1 = H; 11b, R = H, R^1 = CH_3;
11c, R = Br, R^1 = H; 11d, R = Br, R^1 = CH_3;
11e, R = Cl, R^1 = H; 11f, R = Cl, R^1 = CH_3
11g, R = OCH_3, R^1 = H; 11h, R = OCH_3, R^1 = CH_3
11i, R = F, R^1 = H; 11j, R = F, R^1 = CH_3

Scheme 1. Synthesis of 3-(imidazo[2,1-*b*][1,3,4]thiadiazol-2-yl)-1*H*-indole derivatives **12-14.**

Reagents and conditions: i) CH_3CN, CSI, 0 °C, 2 h, then DMF, 0 °C, 1.5 h (98-100%); ii) DMF, $(CH_3O)_2CO$, K_2CO_3, 130 °C, 3.5 h (98-100%); iii) trifluoroacetic acid, thiosemicarbazide, 60 °C, 3.5 h (98-100%); iv) anhydrous ethanol, reflux, 24 h (42-80%); v) $NaHCO_3$ saturated aqueous solution (58-80 %); vi) $POCl_3$, DMF, 0 - 5 °C, then compound **13**, DMF, 70 °C, 5 h.

Table 1. New 3-(imidazo[2,1-*b*][1,3,4]thiadiazol-2-yl)-1*H*-indole derivatives **12-14**

Comp	R	R^1	R^2	Yield
12a	H	H	tiophen-3-yl	57%
12b	H	CH_3	tiophen-3-yl	55%
12d	Br	CH_3	tiophen-3-yl	68%
12e	Cl	H	tiophen-3-yl	63%
12f	Cl	CH_3	tiophen-3-yl	68%
12h	F	CH_3	tiophen-3-yl	58%
13c	Br	H	tiophen-3-yl	58%
13g	F	H	tiophen-3-yl	80%
13i	OCH_3	H	tiophen-3-yl	58%
13j	OCH_3	CH_3	tiophen-3-yl	70%
14k	H	H	C_6H_5	71%
14l	H	CH_3	C_6H_5	91%
14m	H	H	4-F-C_6H_4	81%
14n	H	H	3OCH_3-C_6H_4	60%
14o	H	H	2,5-OCH_3-C_6H_3	82%
14p	H	CH_3	2,5-OCH_3-C_6H_3	70%
14q	H	H	4-NO_2-C_6H_4	75%
14r	Br	H	2,5-OCH_3-C_6H_3	90%

Results and discussion

Antiproliferative activity

The newly synthesized imidazo[2,1-*b*][1,3,4]thiadiazoles **12a,b,d,e,f,h, 13c,g,i,j** and **14k,l,n,o,p** were submitted to the National Cancer Institute (NCI; Bethesda, MD) for the pharmacological evaluation of their antitumor activity. They were initially pre-screened according to the NCI protocol at one-dose of 10 µM on the full panel of 60 human cancer cell lines derived from 9 cancer cell types and grouped into disease subpanels including leukemia, non-small cell lung, colon, central nervous system, melanoma, ovarian, renal, prostate, and breast cancers. The **12a** and **12h** derivatives were selected for further screening at five concentrations at 10-fold dilution (10^{-4}-10^{-8} M) on the full panel. As shown in Table 2, both derivatives have interesting *in vitro* anticancer activity with GI_{50} values ranging from micromolar to sub-micromolar level, i.e., 0.23-11.4 µM, and 0.29-12.2 µM, respectively (Table 2).

In order to expand the NCI panel, we evaluated the *in vitro* antiproliferative activity of the compounds **12a,b,d,e,f,h**, **13c,g,i,j** and **14k-r** on a panel of PDAC cells, including SUIT-

2, Capan-1 and Panc-1, by Sulforhodamine-B (SRB) assay. PDAC is indeed broadly chemoresistant tumor, with a 5-year survival rate below 9%, and novel, more effective therapeutics for PDAC remain an important unmet need.

A pre-screening assay was initially performed at concentrations of 0.1, 1 and 16 μM. We then expanded the cytotoxicity test, using at least 8 different concentrations (from 125 nM to 16 μM) on the most promising compounds, in order to define more accurate half-maximal inhibitory concentration (IC_{50}) values. The compounds **12a**,**b**,**h** and **13g** exhibited remarkable antiproliferative activity on all the preclinical models with IC_{50} values in the range from 0.85 to 4.86 μM (Table 3).

Table 2. GI_{50} and TGI of the compounds **12a** and **12h**[a]

Panel/Cell line	**12a**		**12h**	
	GI_{50} (μM)	**TGI** (μM)	**GI_{50}** (μM)	**TGI** (μM)
Leukemia				
CCRF-CEM	2.19	27.2	2.54	> 100
HL-60(TB)	0.76	20.9	1.34	15.5
K-562	0.38	39.9	0.45	> 100
RPMI-8226	1.47	15.4	3.01	27
Non-Small Cell Lung Cancer				
A549/ATCC	1.72	> 100	2.85	99.5
EKVX	1.99	> 100	2.51	> 100
HOP-62	1.58	39.9	1.92	23.1
HOP-92	5.46	> 100	12.2	76.9
NCI-H226	9.94	> 100	4.56	35.8
NCI-H23	4.47	> 100	3.82	> 100
NCI-H322M	4.85	52.7	4.71	> 100
NCI-H460	0.57	> 100	1.73	17.1
NCI-H522	0.75	> 100	1.62	24.5
Colon Cancer				
HCC-2998	2.99	26.7	5.64	33.9
HCT-116	0.63	70.6	2.04	26.4
HCT-15	0.49	15.6	0.61	> 100
HT29	0.41	10.2	0.48	14.8
KM12	0.50	10.5	1.04	> 100
SW-620	0.43	> 100	0.48	> 100
CSN Cancer				
SF-268	3.84	> 100	6.58	> 100
SF-295	1.74	6.44	2.24	9.39
SF-539	1.49	4.60	2.18	7.54
SNB-19	2.56	> 100	3.44	> 100
SNB-75	0.45	8.09	1.29	6.45
U251	1.21	17	2.76	17.9
Melanoma				
MALME-3M	10.4	36.9	1.81	31.6
M14	0.75	15.8	1.05	> 100
MDA-MB-435	0.23	0.68	0.29	1.13
SK-MEL-2	1.08	23.8	1.59	7.29
SK-MEL-28	4.74	44.0	7.23	> 100
SK-MEL-5	0.71	15.1	1.80	12.9
UACC-257	11.4	98.3	7.90	> 100
UACC-62	0.74	18.7	1.93	> 100
Ovarian Cancer				
IGROV1	1.79	> 100	1.93	> 100
OVCAR-3	0.92	9.02	2.06	9.67
OVCAR-4	4.42	> 100	5.77	> 100

OVCAR-5	4.27	76.4	8.24	84.4
OVCAR-8	2.72	> 100	4.53	> 100
NCI/ADR-RES	0.56	> 100	0.99	19.1
SK-OV-3	2.80	82.7	3.47	70.9
Renal Cancer				
786-0	3.06	> 100	7.62	52.3
A498	5.97	23.6	4.09	50.0
ACHN	3.23	52.5	3.39	86.8
CAKI-1	1.00	> 100	2.42	57.4
RXF 393	2.05	50.0	1.59	5.73
SN12C	1.15	> 100	4.71	> 100
TK-10	5.21	33.5	4.92	19.4
UO-31	1.71	> 100	1.72	> 100
Prostate Cancer				
PC-3	2.07	> 100	3.19	> 100
DU-145	2.86	> 100	3.67	31.6
Breast Cancer				
MCF7	1.17	20.2	0.83	30.0
MDA-MB-231/ATCC	1.08	7.88	3.23	30.6
HS 578T	2.65	> 100	2.34	13.4
BT-549	2.87	31.7	5.54	77.4
MDA-MB-468	2.92	27.8	1.44	5.47

[a] Data obtained from the NCI in vitro disease-oriented human tumor cell line screen. [b] GI_{50}: concentration that inhibit 50% net cell growth. [c] TGI total growth inhibition

PDAC is notoriously resistant to chemotherapy or radiotherapy. For several decades, gemcitabine monotherapy has been used as a first-line treatment for metastatic PDAC and is still a cornerstone of PDAC treatment in all stages of this disease. However, this drug has limited clinical effects caused by primary PDAC resistance, as well as by the development of resistance within a few weeks from treatment initiation.[41] Therefore, new therapeutic agents should be tested for their ability to circumvent gemcitabine chemoresistance. For this reason, we assessed the cytotoxic activity of the compounds **12a**,**b**,**h** and **13g** in the Panc-1R cells, a gemcitabine-resistant sub-clone obtained by continuous incubation of Panc-1 with 1 μM of the drug.[41] Notably, all these compounds showed antiproliferative activity against Panc-1R, with IC_{50} ranging from 2.2 ± 0.37 μM (compound **12b**) to 3.9 ± 0.25 μM (compound **13g)** as reported in the Fig. 4A and Table 4.

Table 3. Antiproliferative activity of compounds **12a,b,d,e,f,h**, **13c,g,i,j** and **14k-r** on SUIT-2, Capan-1 and Panc-1 cell lines.

IC_{50}[a] (μM) ± SEM[b]			
	Cell lines		
Comp	**SUIT-2**	**Capan-1**	**Panc-1**
12a	**0.85 ± 0.018**	**1.19 ± 0.06**	**1.70 ± 0.20**
12b	**0.99 ± 0.078**	**1.35 ± 0.04**	**1.69 ± 0.10**
12d	>16	>16	>16
12e	>16	>16	>16
12f	>16	>16	>16
12h	**1.78 ± 0.017**	**1.93 ± 0.25**	**2.37 ± 0.028**
13c	>16	>16	>16
13g	**2.16 ± 0.039**	**4.52 ± 0.48**	**4.86 ± 0.5**
13i	>16	>16	>16
13j	>16	>16	>16
14k	9.56 ± 0.34	10.5 ± 0.21	12.41 ± 0.16
14l	>16	>16	>16
14m	7.93 ± 0.23	8.83 ± 0.17	10.53 ± 037
14n	11.49 ± 0.36	>16	>16
14o	13 ± 1.13	>16	>16
14p	12.49 ± 0.18	5.73 ± 0.086	>16
14q	5.32 ± 0.29	6.1 ± 0.019	3.61 ± 0.4
14r	8.7 ± 0.20	8.24 ± 0.08	10.56 ± 0.11
gemcitabine	0.01 ± 0.001	0.02 ± 0.001	0.15 ± 0.01
5-fluorouracil	0.91 ± 0.15	0.47 ± 0.13	4.3 ± 0.42

[a]The values are means ± SEM of three separate experiments.
[b]SEM: Standard Error of the Mean.

Our previous studies showed different genetic and epigenetic modifications, including splicing and phosphoproteomics aberrations,[42,43] underlying the molecular mechanisms of gemcitabine-resistance, and further studies will be carried out to identify how our new compounds counteract these mechanisms. Moreover, the compounds **12a**,**b**,**h** and **13g** were tested on a primary patient-derived PDAC cell culture, PDAC-3 (Fig. 4B-C). This cellular model was chosen since our previous studies showed that its genetic and histological features were similar to the original tumor.[44] In order to maintain the original characteristics of the primary tumor, particularly from the genetic point of view, these cells have been kept in culture only for a few passages. As shown in Fig. 4B the new imidazothiadiazoles maintained their antiproliferative activity on PDAC-3 cells, with IC_{50} values slightly higher in comparison to the values reported on the previously mentioned cancer cell lines. The phase contrast microscopy images in the Fig. 4C highlighted the antiproliferative activity of

compounds **12a** and **12b** (central and right panel, respectively) compared to untreated cells (left picture) after 72 hours of the treatment.

Because of their remarkable antiproliferative activity the compounds **12a**,**b**,**h** and **13g** were selected for following mechanistic studies, in order to unravel the mechanisms underlying their anticancer activity.

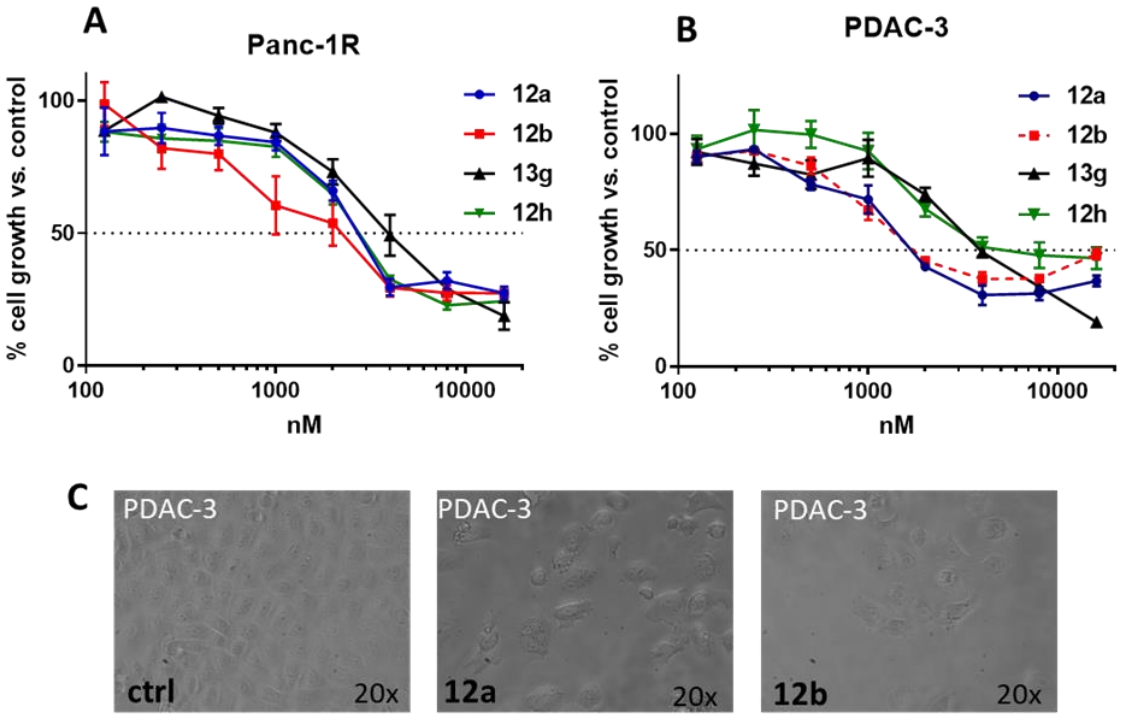

D

Cell line	12a	12b	12h	13g	Gemcitabine	5-fluorouracil
PDAC-3	1.7 ± 0.39	1.7 ± 0.27	5.1 ± 0.37	3.9 ± 0.18	0.03 ± 0.01	0.56 ± 0.32
Panc-1R	2.7 ± 0.25	2.2 ± 0.37	2.8 ± 0.3	3.9 ± 0.8	>10	4.5 ± 0.54

Figure 4. Representative growth curves of Panc-1R (**A**) and PDAC-3 (**B**) cells treated with the compounds **12a,b,h** and **13g** (from 0.125 to 16 µM). *Points*, mean values obtained from three independent experiments; *bars*, SEM. (**C**) Representative pictures of PDAC-3 cells after 72 h from the treatment at concentration of IC_{50} value. *Left panel*: untreated cells; *central panel*: cells treated with compound **12a**; *right panel:* cells treated with compound **12b**. Original magnification 20X. (**D**) IC_{50} values of compounds **12a,b,h** and **13g** on gemcitabine-resistant and primary PDAC-3 cells ([a]The values are means of three separated experiments. [b]SEM: Standard Error Mean).

Despite compound **7** has shown interesting GI_{50} values against all the tested cancer cell lines in the NCI screening, preliminary biological evaluations of analogues **13k,l,n,p,r** showed limited antiproliferative activity.[28] We evaluated the citotoxicity of the compounds **13m, 13o** and **13q** on SUIT-2, Capan-1 and Panc-1 but the IC_{50} values were above 16 µM.

Finally, we performed additional experiments to evaluate the *in vitro* cytotoxicity of the new compounds **12a** and **12b** against the normal fibroblasts Hs27. The results of these experiments allowed us to calculate the selectivity index (SI, IC_{50} non-tumor cell line/IC_{50} tumor cell line), which was 4.5 and 7.2 for compounds 12a and 12b, respectively, and therefore our compounds have SI similar to Gemcitabine and 5-fluorouracil and were regarded as highly cancer selective compared to the primary pancreatic cells PDAC3 (Supplementary Table 3).

Volume reduction of PDAC-3-derived tumor spheres

Two-dimensional cytotoxicity assay obviously provide a useful method to screen libraries of compounds with high-throughput efficiency, but they are not capable of resembling the complex architecture and biology of solid tumors, which grow in three-dimensions (3D).[45] For this reason we evaluated two of our most promising compounds (emerging from monolayer assay) on 3D spheroids of PDAC-3 cells. These primary cultures are indeed able to form spheroids that are more representative of the aggregation of tumor cells *in vivo*, as also reported in our previous studies.[46]

We treated spheroids with compounds **12a** and **12b** after 3 days of growth, at 5-times the IC_{50}, and we took a picture which represent the Day 1. Then the treatment was repeated every four days (Day 5 and Day 8) and pictures were taken immediately before that (Fig. 5A).

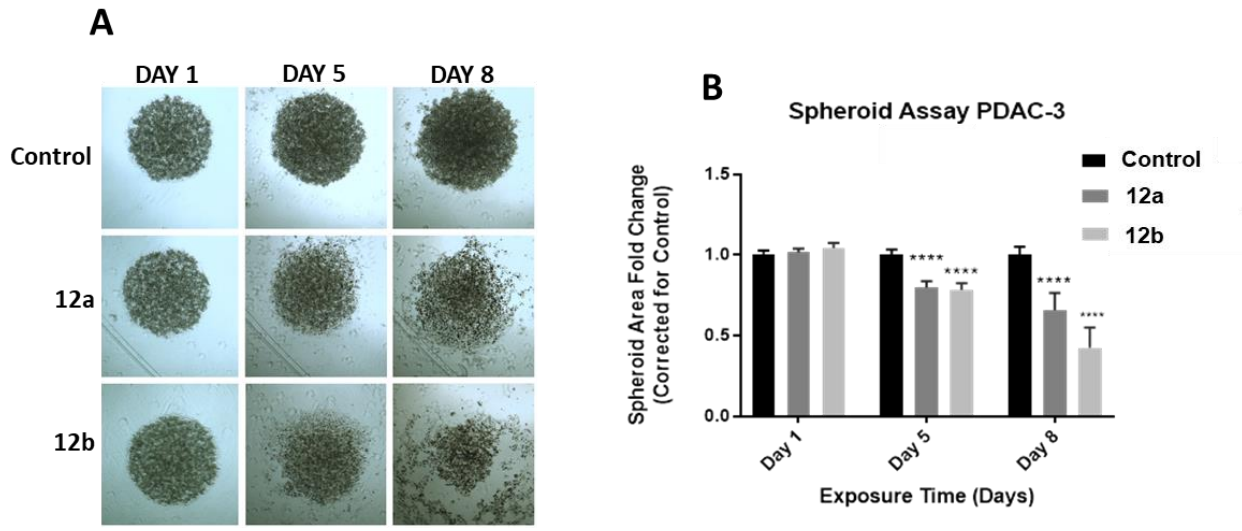

Figure 5. Size reduction of PDAC-3 spheroids treated with compounds **12a** and **12b** at 5-times the IC_{50} (i.e. 8.5 μM). (**A**) Representative pictures of PDAC-3 spheroids exposed to **12a** and **12b**, taken at day 1 of treatment, and after 5 and 8 days with an automated phase-contrast microscope. (**B**) Fold-change, corrected for control, of the spheroids size, at Day 1, Day 5 and Day 8. p-values were determined by Two-way ANOVA followed by Tukey's multiple comparisons test, **** = $p<0.0001$. The values were obtained taking into account the mean values of the areas of at least ten different spheroids.

Reduction of the size of spheroids was calculated by measuring their area with ImageJ. As shown in Fig. 5B, after five, but considerably more after eight days, both compounds clearly showed their ability to hinder the spheroids formation. This reduction is shown as the fold-change between treated spheroids compared to the controls and was statistically significant (p-value < 0.0001). Therefore, these two compounds retained their activity in a 3D model.

Reduction of cell migration

Next to the lack of clinically relevant improvement in effective treatments, the high metastatic potential of PDAC is one of the main causes for the poor outcome of this disease.[36] The ability of the compounds **12a** and **12b** to inhibit the migratory behaviour of PDAC cells was investigated by scratch wound-healing assays on SUIT-2, Capan-1, Panc-1, Panc-1R and PDAC-3 cell lines.

Briefly, $5x10^4$ cells/well were seeded into 96-well flat-bottom plates in a volume of 100 µL and incubated for 24 h to create a monolayer. The scratches in the middle of the wells were created by scraping with a specific tool with needles. The cells were then treated with the compounds using 4x IC_{50} concentrations. These concentrations were chosen after preliminary experiments demonstrating that the exposure for 24 h did not result in pro-apoptotic or necrotic effects. The wound closure was monitored by phase-contrast microscopy and the pictures were captured immediately after scratch (T = 0), and at 4, 8, 20 and 24 h from the treatment. As shown in the Fig. 6A-D, the compounds **12a** and **12b** induced a remarkable reduction of cell migration rate in Panc-1R and SUIT-2 cell lines. The scratch area (μm^2) was already wider in the treated cells compared to the untreated Panc-1R cells after 8 h of treatment. After 24 h from the beginning of the treatment we observed a reduction of the cell migration with a fold-change value of approximately 4 in both cell lines, SUIT-2 and Panc-1, treated with compounds **12a** and **12b** (Fig. 6A,B). Statistical analyses revealed that these differences were significant, compared to the respective controls (i.e., untreated cells) in both cell lines.

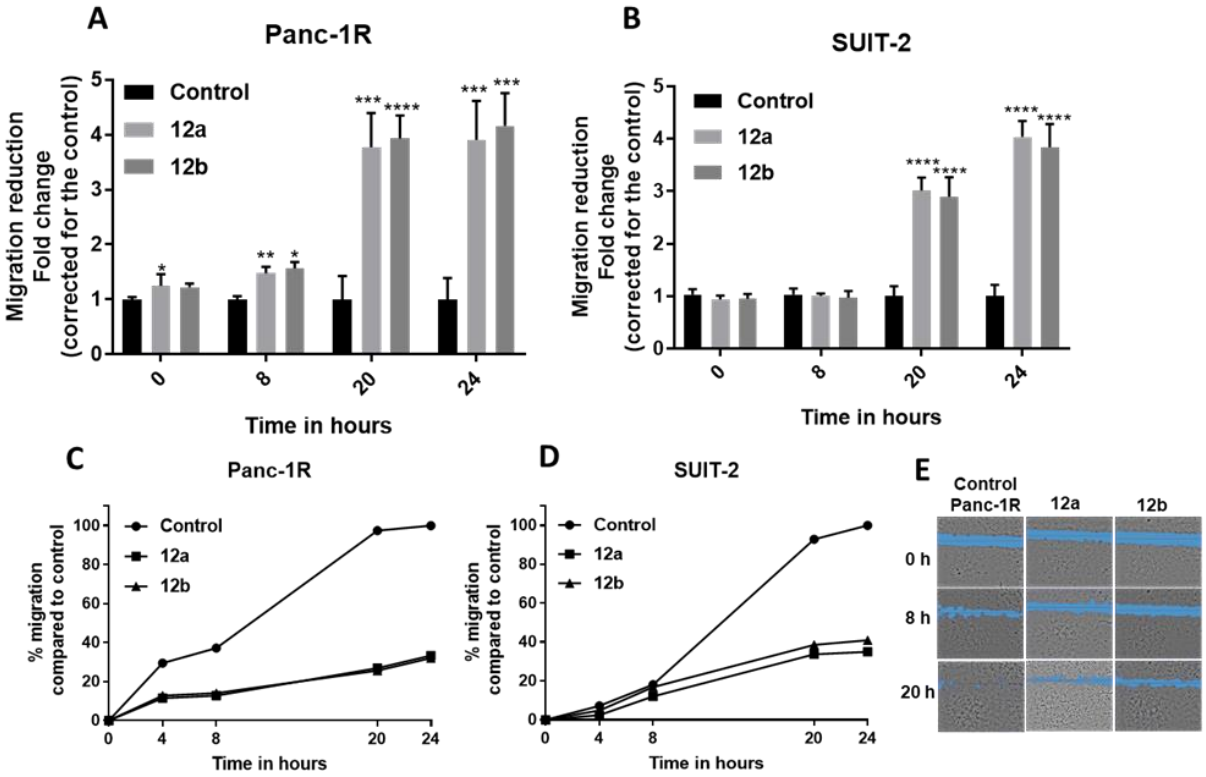

Figure 6. Modulation of the migration rate in Panc-1R and SUIT-2 cells treated with the compounds **12a** and **12b** at concentration of 4x IC_{50}. (**A-B**) Fold-changes in Panc-1R (**A**) and SUIT-2 (**B**) cells were determined by taking into consideration at least four scratch areas. All the *P* values were calculated with Student's t-test. ****p<0.0001, ***p<0.001, **p<0.01, *p<0.05. (**C-D**) Percentages of migration monitored over time (0, 4, 8, 20 and 24 h) of Panc-1R (**C**) and SUIT-2 (**D**) cells treated with compound **12a** and **12b** at concentration 4x IC_{50}. *Points*, mean values obtained from the means of at least three different scratch areas. (**E**) Representative images of the wounds closure captured with the microscope at 0, 8 and 20 h on Panc-1R cells. Original magnification 5X.

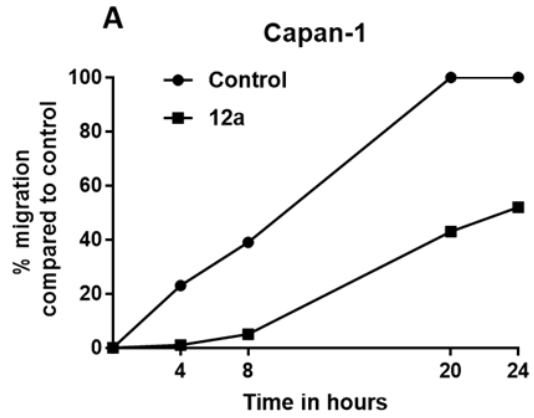

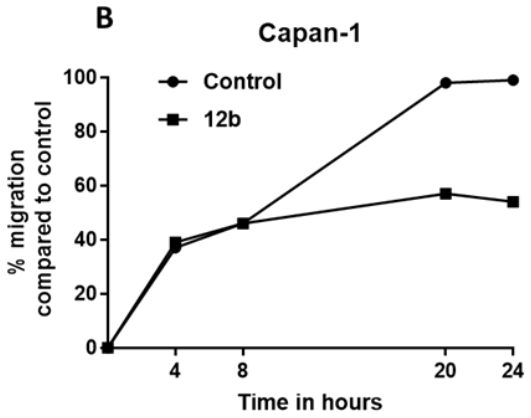

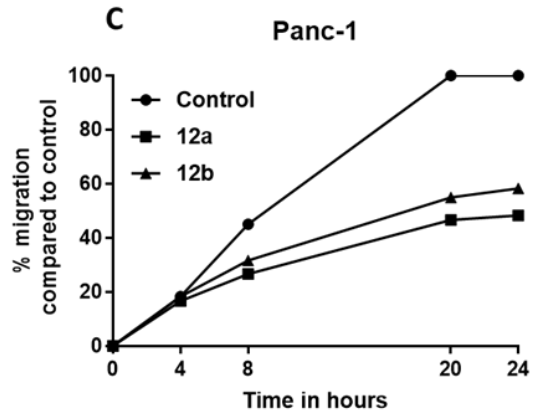

D

Comp	12a	12b	12a	12b
Time (h)	Capan-1		Panc-1	
0	ns	ns	*	ns
4	ns	ns	*	ns
8	**	ns	**	ns
20	****	****	****	***
24	****	****	****	*

ns= not significant
****p<0.0001, ***p<0.001, **p<0.01, *p<0.05

Figure 7. (**A-D**) Percentage of migration monitored over time (0, 4, 8, 20 and 24 h) of Capan-1 (**A-B**) and Panc-1 (**C**) cells treated with the compounds **12a** and **12b** at concentrations of 4x IC_{50}. *Points*, mean values obtained from the means of at least three different scratch areas. (**D**) *(Table)* List of *P* values that were calculated with Student's t-test. ****p<0.0001, ***p<0.001, **p<0.01, *p<0.05, ns= not significant.

In particular, compared to untreated cells (set at 100%), the percentages of migration in cells treated with the compounds **12a** and **12b** were of 33.3% and 32%, respectively, in Panc-1R (Fig. 6C), and 34.9% and 41%, respectively, in SUIT-2 (Fig. 6D) after 24 h from the start of the treatment. The anti-migratory activity was also evident in Capan-1 and Panc-1 cells for which we observed similar statistically significant results, with migration rates between 50% and 60% (Fig. 7A-C and Fig.-table 6D). Finally, as shown in the Supplementary data Fig. 1A, we detected lower migration rates (64% and 71%, respectively) compared to the control (set at 100%) also in the primary PDAC-3 cells treated with the compounds **12a** and **12b**. Overall, these data highlighted the ability of our compounds to significantly reduce the rate of cell migration on all the PDAC preclinical models.

Modulation of Epithelial Mesenchymal transition events as assessed by qRT-PCR, Western blot and gelatine zymography

It is well known that epithelial-to-mesenchymal transition (EMT) events are essential for embryonic development and other physiological events, such as the response to several injuries. During EMT, epithelial cells undergo changes in their phenotypic tracts through the loss of polarity, cell-cell adhesion and extracellular matrix, and they acquire mesenchymal features including motility and invasiveness.[47] Several transcription factors within the cellular microenvironment regulate the expression of epithelial and mesenchymal marker genes, among which the most important include the zinc finger transcription factors SNAIL1 and SNAIL2, potent epithelial repressors belonging to the SNAIL superfamily, E-cadherin (CDH1) and N-cadherin (CDH12), calcium-dependent cell adhesion molecules, vimentin (VIM), type III intermediate filament (IF) protein typically expressed in mesenchymal cells, and finally, the matrix metalloproteinases (MMPs), enzymes involved in the breakdown of extracellular matrix.[48] Remarkably, their dysregulation induces a transition from the physiological function to the pathological one, including mechanisms underlying the origin and progression of tumors and tissue fibrosis.[49] The loss of CDH1 expression is considered the hallmark of EMTs in cancer and recently, SNAIL1 and SNAIL2 have been identified as the major determinants for the repression of its transcription through the direct binding to the E-cadherin E-box promoter.[50–52] Simultaneously, the gain of mesenchymal markers, such as VIM, CDH12, MMPs and others occur.[53] In PDAC, these genes contribute to a crucial network of signalling pathways that contribute to the irreversible change of cell phenotype, both in metastasis and resistance to the chemotherapy.[54] Because of their outstanding effects against PDAC cell migration, we assessed the influence of the imidazothiadiazole derivatives **12a** and **12b** on these EMTs key regulator expression, in SUIT-2, Capan-1 and Panc-1 cells, using RT-qPCR, Western blot and gelatine zymography analyses. Capan-1 and SUIT-2 cells were selected for these experiments because preliminary analyses of the housekeeping protein GAPDH showed that using lysates of these cells the Western blot images were not "saturated" and were kept in the linear range (as revealed by exposing blots to increasing times and drawing a plot of intensity and time exposure). RT-qPCR reactions were performed in order to evaluate the modulation of the mRNA expression of SNAIL1, SNAIL2, CDH1, CDH12. Briefly, SUIT-2 and Capan-1 cells (2.5×10^5/well) were seeded into 6-well plates and incubated for 24 h to form a confluent monolayer. Then they were treated with the compounds **12a** and **12b** at concentrations of 5x IC_{50}. After 24 h, the cells were harvested using TRIzol, and we extracted the total RNA, which was used to synthesize,

by reverse transcription, the cDNA for the PCR reactions. The expression levels were normalized to those of the glyceraldehyde-3-phosphate dehydrogenase (GAPDH) housekeeping gene, whose expression was constant in all cells, as described previously.[55] As shown in Fig. 8A-B, the compounds **12a** and **12b** affected the genes leading EMTs. In both cell lines the mRNA levels of SNAIL1 and SNAIL2 were increased from 1.5 to approximately 1.9 fold compared to the GAPDH in the control cells, suggesting a low amount of protein expression and consequently, due to a negative feedback mechanism, CDH1 protein expression was upregulated, as reported in the Western blot analysis (Fig. 8C-D, Fig. 8G and Supplementary data Fig. 2). Instead, the protein expression of VIM and MMP2 were significantly reduced. Finally, CDH12 protein expression did not noticeably change compared to the control.

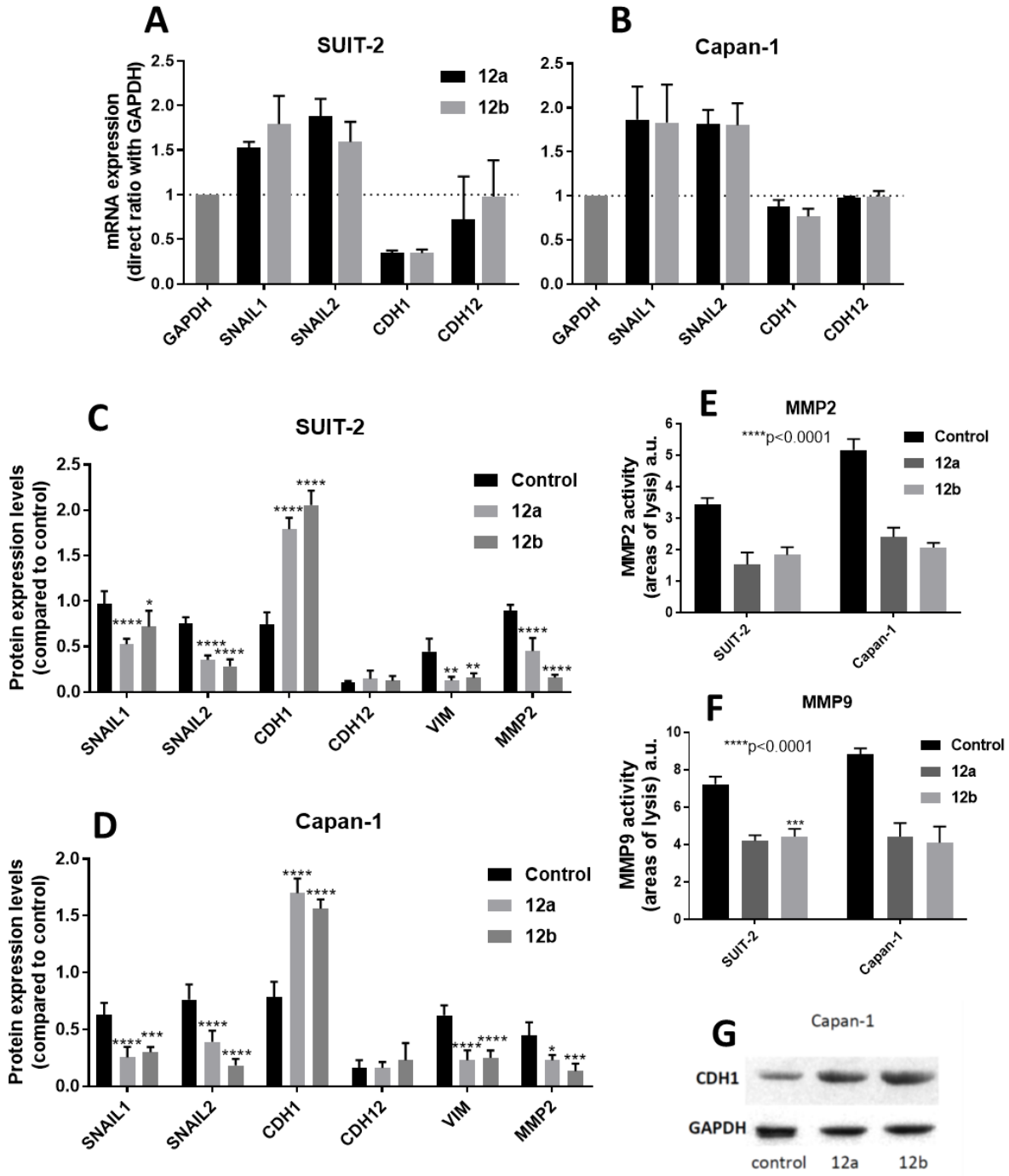

Figure 8. SNAIL1, SNAIL2, CDH1 and CDH12 mRNA expressions in SUIT-2 (**A**) and Capan-1 (**B**) cells treated with the compounds **12a** and **12b** at 5x IC_{50} for 24 h. The expression levels were determined by RT-qPCR and the results were obtained by the delta-delta Ct (cycle threshold) analysis. The experiments were conducted in duplicates and the values are shown as means ± SD. (**C**-**D**) SNAIL1, SNAIL2, CDH1, CDH12, VIM and MMP2 protein levels expression in SUIT-2 (**C**) and Capan-1 (**D**) cells treated with compounds **12a** and **12b**. The protein levels were determined after 24 h of treatment at concentration 5x IC_{50} value by densitometric analysis of the Western Blot performed using ImageJ. All the *P* values were determined by Tukey's multiple comparisons test. ****p<0.0001, ***p<0.001, **p<0.01, *p<0.05. (**E**-**F**) Gelatine zymography analysis of media from

SUIT-2 and Capan-1 cells incubated with serum-free medium for 24 h. The enzymatic activity of MMP2 and MMP9 was determined by densitometric analysis. The cells were treated with the compounds **12a** and **12b** at concentration 5x IC_{50} value for 24 h. ****p<0.0001, ***p<0.001. (**G**) Representative image of CDH1 expression determined by Western blot analysis in Capan-1 cells treated with the compounds **12a** and **12b** at 5x IC_{50} concentrations after 24 h.

Furthermore, considering the pivotal role of MMPs in tumor invasion, through degradation of extracellular matrix components, we evaluated the effect of the compounds **12a** and **12b** on the proteolytic activity of MMP2 and MMP9 by using specific gelatine zymography assays. These assays showed a significant decrease of the activity of MMP2 and MMP9 isolated from SUIT-2 and Capan-1 cells exposed to the compounds. In particular, the activities of the MMP2 and MMP9 enzymes were decreased by about 50% after 24 h of treatment compared to the control (Fig. 8E-F). However, as shown in the Supplementary data Fig. 3, the areas of lysis created by the proteolytic activities of both enzymes isolated from Panc-1 cells treated with compounds **12a** and **12b** were not significantly wider compared to the control.

Profiling of inhibition of kinase activity

To investigate the potential mechanism of action of our compounds, we performed a high-throughput analysis with the Pamgene tyrosine kinase peptide substrate array (PamChip). The PamChip consists of 4 identical arrays, each of which contains 144 peptide sequences immobilized on a porous ceramic membrane (Fig. 9A). Each of these sequences harbours one or more phosphorylation sites, derived from literature or computational predictions. Finally, specific fluorescently labelled anti-phospho antibodies are used to detect the amount of phosphorylated protein by tyrosine kinases from our samples.

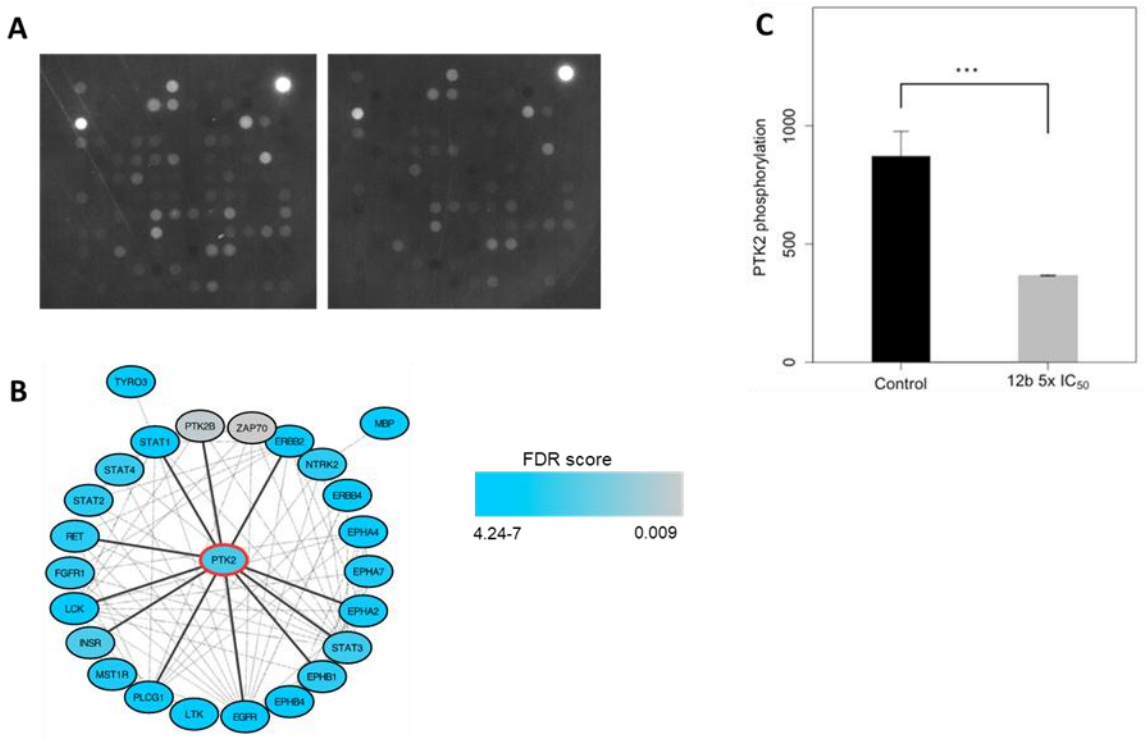

Figure 9. (**A**) Representative images of pictures taken at the end point of the control array (left) and the treated array (right). (**B**) Network visualization obtained with Cytoscape of the significant proteins containing differentially phosphorylated peptides, color legend indicates the significance level of each protein. (**C**) Barplot of PTK2 phosphorylation in the control vs treated with 5x IC_{50} of **12b**.

The compound **12b** significantly inhibited the phosphorylation of 45 peptide substrates in SUIT-2 cells, and we visualized on Cytoscape a network highlighting the interactions between proteins containing the phosphorylated peptides. Notably, PTK2/FAK emerged as an important hub between those proteins (Fig. 9B). In particular, the phosphorylation of PTK2/FAK showed a more than 2-fold inhibition after treatment with compound **12b**, with FDR < 0.01 (Fig. 9C). This result prompted us to validate the inhibition of phosphorylation of PTK2/FAK as one of the possible mechanisms of action of our compound, using a specific ELISA assay, as detailed in the following paragraphs.

Inhibition of PTK2/FAK as assessed by ELISA

The focal adhesion kinase (FAK), also known as protein tyrosine kinase 2 (PTK2), is a downstream non-receptor tyrosine kinase able to mediate information from extracellular matrix into the cytoplasmatic compartment, through a linker with intracellular tails of integrins.[56] FAK controls several cellular processes, including survival, proliferation and motility. However, its overexpression is correlated with many aspects of the tumorigenesis.

For instance, FAK regulates the development of metastasis, driving adhesion, invasion and migration events. Furthermore, the translocation of FAK in the nucleus induces the arrest of p53 activity and its downstream gene transcription.[57] In PDAC, FAK coordinates several signalling pathways involved in growth and metastasis processes.[58] Notably, a recent study reported the ability of the indole-3-carbinol to affect EMTs genes and reduce FAK mRNA expression in MCF-7 cells.[59] Thereby, we conducted a quantitative analysis by the Enzyme-Linked Immunosorbent Assay (ELISA) to investigate whether our imidazothiadiazole compounds could reduce FAK phosphorylation at tyrosine residue 397 (FAK [pY397]), which is essential for the kinase activity of this protein. This assay was carried out on lysates of SUIT-2, Capan-1 and Panc-1 cells treated with compounds **12a** and **12b** at concentrations of 5x IC_{50s} for 24 h. As shown in the Fig. 10, these ELISA experiments showed a reduction of p-FAK in all the PDAC cell lines, with fold-change values ranging from 0.4 to 0.5. Similar results were observed in the Western blot analyses of the same compounds (Supplementary Fig. 4). These results suggest that FAK is a target of our compounds and might explain how they can then suppress FAK-driven migration, and growth in PDAC cells.

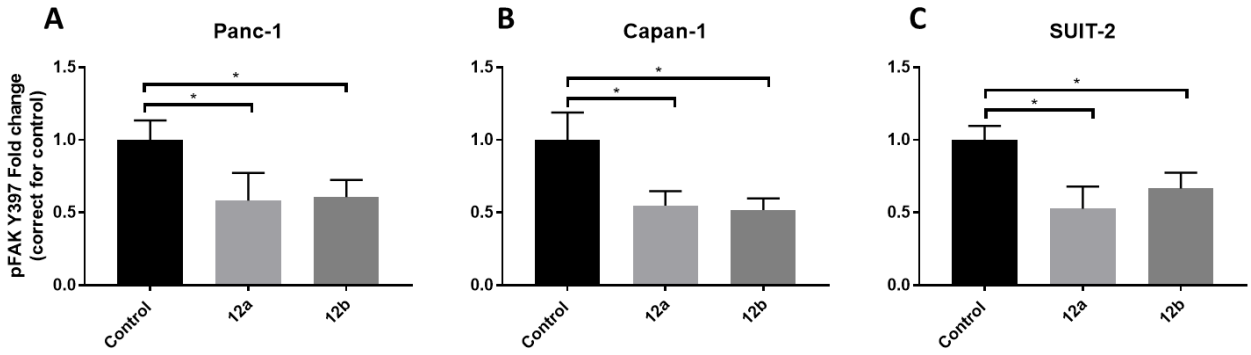

Figure 10. Inhibition of FAK/PTK2 phosphorylation by compounds **12a** and **12b.** Modulation of phosphorylated-FAK (pFAK) at tyrosine residue 397 by compounds **12a** and **12b** on Panc-1 (**A**), Capan-1 (**B**) and SUIT-2 (**C**) cells. The amount of pFAK was measured in cell lysates after 24 h from the treatment with compounds **12a** and **12b** at 5x IC_{50s}. All the *P* values were calculated with Student's t-test, *p<0.05.

Conclusions

A new series of hybrid molecules, **12a,b,d,e,f,h, 13c,g,i,j** and **14k-r** compounds bearing in the same structure the imidazo[2,1-*b*][1,3,4]thiadiazole and indole scaffolds were

efficiently synthesized and evaluated for their antiproliferative activity and mechanism of action on a panel of PDAC cells, namely SUIT-2, Capan-1 and Panc-1.

Among the synthesized imidazothiadiazoles, compounds **12a,b,d,e,f,h, 13c,g,i,j** and **14k,l,n,o,p** were screened by the NCI on the full panel of sixty human cancer cells at concentration of 10 μM. Notably, compounds **12a** and **12h** displayed relevant antiproliferative activity eliciting GI_{50} values in the range from micro- to sub-micromolar levels. In addition, compounds **12b** and **13g** considerably reduced PDAC cell proliferation in SUIT-2, Capan-1, Panc-1, Panc-1R (gemcitabine-resistant) and in the primary cells PDAC-3, growing as monolayers or as spheroids. Noteworthy, compounds **12a,b,h** and **13g** are characterized by a thiophene ring at position 6 of the imidazothiadiazole scaffold, suggesting the importance of this ring for the pharmacological activity. However, in order to confirm the role of aldehyde for the antiproliferative activity future studies in **14a-j** compounds are warranted.

Through wound-healing assays we found remarkably reduction of cell migration in all the PDAC preclinical models when treated with the most promising compounds **12a** and **12b**. These effects might be explained by modulation of key regulators of EMT, including E-cadherin and vimentin, as well as by the inhibition of MMP-2/-9 activities. Finally, high-throughput analysis with kinase arrays revealed a significant inhibition of the phosphorylation of 45 tyrosine kinases substrates, whose visualization on Cytoscape highlighted PTK2/FAK as an important hub between those proteins. These results were validated using a specific ELISA assay, which demonstrated the inhibition of phosphorylation of PTK2/FAK. Altogether these results support the high potential of this type of compounds against EMT and PTK2/FAK, which play a key role in the aggressiveness of pancreatic cancer[55]. In order to support our experimental findings we also investigated the molecular structure of FAK. Unfortunately complete crystal structures of the molecule are not available; e.g. the Tyr397 part is lacking in the published structures, which may be due to the high flexibility of this region of the molecule. This means that proper molecular docking is not yet feasible.

Experimental section

Chemistry

All melting points were taken on a Büchi-Tottoly capillary apparatus and are uncorrected. IR spectra were determined in bromoform with a Shimadzu FT/IR 8400S spectrophotometer. ^{1}H and ^{13}C NMR spectra were measured at 200 and 50.0 MHz, respectively, in DMSO-d_6

solution, using a Bruker Avance II series 200 MHz spectrometer. Column chromatography was performed with Merck silica gel 230-400 mesh ASTM or with Büchi Sepacor chromatography module (prepacked cartridge system). Elemental analyses (C, H, N) were within ±0.4% of theoretical values and were performed with a VARIO EL III elemental analyzer. The LC/HRMS have been obtained on a Thermo Q-Exactive system equipped with a Dionex 3000 chromatographic system.

*Synthesis of 1H-indole-3-carbonitriles (**9b-e**)*

A solution of the suitable indole **8** (5.10 mmol) in anhydrous acetonitrile (4.5 mL) was treated dropwise with chlorosulfonyl isocyanate (CSI) (0.44 mL, 5.10 mmol). The reaction mixture was maintained at 0 °C under stirring for 2 h, then, anhydrous dimethylformamide (DMF) (2.8 mL, 36.39 mmol) was slowly added and the mixture was stirred at 0 °C for 1.5 h. The resulting solution was poured into crushed ice. The solid obtained was filtered and dried (yields 98-100%). Analytical and spectroscopic data for compounds **9b-e** are in agreement with those previously reported.[60]

*Synthesis of 1-methylindole-3-carbonitriles (**10a-e**)*

To a solution of the suitable 3-cyanoindole **9** (7.03 mmol) in anhydrous DMF (10 mL) 3.61 mmol of K_2CO_3 and dimethyl carbonate (1.8 mL, 21.4 mmol) were added and the mixture was heated at 130 °C for 3.5 h. After cooling (0-5 °C), water and ice (25 mL) was slowly added under stirring. The oily suspension obtained was extracted with diethyl ether (3x10 mL), the organic phase was washed with water and brine, dried over Na_2SO_4 and the solvent evaporated at reduced pressure to obtain the 3-cyano-1-methylindoles **10** in excellent yields. Analytical and spectroscopic data are in accordance to those reported in literature.[16]

*Synthesis of 5-(1H-indol-3-yl)-1,3,4-thiadiazol-2-amines (**11a-j**)*

A mixture of the suitable indole-3-carbonitrile **9a-e** or **10a-e** (5 mmol), thiosemicarbazide (5 mmol) and trifluoroacetic acid (5 mL) was heated under stirring at 60 °C for 3.5 h. The reaction mixture was then poured into ice and neutralized with $NaHCO_3$ saturated solution. The solid obtained was filtered off, washed with water, cyclohexane and diethyl ether to give 5-(1*H*-indol-3-yl)-1,3,4-thiadiazol-2-amines **11a-j** in excellent yields. Analytical and spectroscopic data for the derivatives **11a-f** are in accordance to those reported in literature.[16]

*5-(5-Methoxy-1H-indol-3-yl)-1,3,4-thiadiazol-2-amine (**11g**)*

Light yellow solid. Yield: 98%, m.p. 216-217 °C IR: 3604 (NH), 3558 (NH_2) cm $^{-1}$; ^{1}HNMR (200MHz, DMSO-d_6) δ: 3.79 (3H, s, CH_3), 6.88 (1H, dd, J = 2.4, 8.8 Hz, Ar-H), 7.39 (1H, d, J = 8.8 Hz, Ar-H), 7.53 (1H, d, J = 2.3 Hz, Ar-H), 8.02 (1H, s, Ar-H), 8.58 (2H, bs, NH_2), 12.07 (1H, bs, NH). ^{13}C NMR (50 MHz, DMSO-d_6) δ: 55.2 (q), 101.9 (d), 105.7 (s), 112.9 (d), 113.0 (d), 124.4 (s), 128.7 (d), 131.5 (s), 152.2 (s), 154.7 (s), 166.5 (s). Anal. Calcd for $C_{11}H_{10}N_4OS$ (MW: 246.29): C, 53.64; H, 4.09; N, 22.75. Found: C, 53.72; H, 4.16; N, 22.98.

*5-(5-Methoxy-1-methyl-1H-indol-3-yl)-1,3,4-thiadiazol-2-amine (**11h**)*

Light yellow solid. Yield: 99%, m.p. 205-206 °C IR: 3381 (NH_2) cm $^{-1}$; ^{1}HNMR (200MHz, DMSO-d_6) δ: 3.80 (6H, s, CH_3, OCH_3), 6.90 (1H, dd, J = 2.5, 8.8 Hz, Ar-H), 7.13 (2H, s, NH_2), 7.41 (1H, d, J = 8.9 Hz, Ar-H), 7.61 (1H, d, J = 2.4 Hz, Ar-H), 7.81 (1H, s, Ar-H). ^{13}C NMR (50 MHz, DMSO-d_6) δ: 32.8 (q), 55.3 (q), 102.3 (d), 106.0 (s), 111.2 (d), 112.5 (d), 124.9 (s), 130.7 (d), 132.0 (s), 152.2 (s), 154.6 (s), 165.4 (s). Anal. Calcd for $C_{12}H_{12}N_4OS$ (MW: 260.31): C, 55.37; H, 4.65; N, 21.52. Found: C, 55.42; H, 4.80; N, 21.78.

*5-(5-Fluoro-1H-indol-3-yl)-1,3,4-thiadiazol-2-amine (**11i**)*

Light yellow solid. Yield: 98%, m.p. 257°C IR: 3609 (NH), 3461 (NH_2) cm $^{-1}$; ^{1}HNMR (200MHz, DMSO-d_6) δ: 7.03-7.12 (1H, m, Ar-H), 7.33-750 (3H, m, Ar-H, NH_2), 7.80 (1H, dd, J =2.5, 10.0 Hz, Ar-H), 7.95 (1H, s, Ar-H), 11.79 (1H, s, NH). ^{13}C NMR (50 MHz, DMSO-d_6) δ: 105.4 (d, *J* = 24 Hz), 107.4 (s, *J* = 4.5 Hz), 110.7 (d, *J* = 25.5 Hz), 113.1 (d, *J* = 10 Hz), 124.4 (s, *J* = 11 Hz), 128.6 (d), 130.1 (s), 152.0 (s), 159.9 (s), 165.9 (s). Anal. Calcd for $C_{10}H_7FN_4S$ (MW: 234.25): C, 51.27; H, 3.01; N, 23.92. Found: C, 51.38; H, 3.25; N, 24.12.

*5-(5-Fluoro-1-methyl-1H-indol-3-yl)-1,3,4-thiadiazol-2-amine (**11j**)*

Light orange solid. Yield: 98%, m.p. 183°C. IR: 3471 (NH_2) cm $^{-1}$; ^{1}HNMR (200MHz, DMSO-d_6) δ: 3.85 (3H, s, CH_3), 7.12-7.21 (1H, m, Ar-H), 7.59 (1H, dd, J =4.4, 9.9 Hz, Ar-H), 7.76 (2H, dd, J =2.5, 9.8 Hz, Ar-H), 8.10 (2H, s, NH_2). ^{13}C NMR (50 MHz, DMSO-d_6) δ: 33.14 (q), 105.4 (s), 105.5 (d, *J* = 24 Hz), 110.9 (d, *J* = 26 Hz), 112.0 (d, *J* = 9.5 Hz), 124.3 (s), 124.5 (s), 133.1 (d), 151.4 (s), 155.7 (s). Anal. Calcd for $C_{11}H_9FN_4S$ (MW: 248.28): C, 53.21; H, 3.65; N, 22.57. Found: C, 53.38; H, 3.88; N, 22.72.

*General procedure for the synthesis of 3-(6-phenylimidazo[2,1-b][1,3,4]thiadiazol-2-yl)-1H-indole derivatives (**12** and **13**)*

A mixture of 5-(1*H*-indol-3-yl)-1,3,4-thiadiazol-2-amine **11a-j** (0.92 mmol) and the suitable α-bromoacetyl derivative (0.92 mmol) in 40 mL of anhydrous ethanol was stirred at reflux for 24 h. After cooling at room temperature the desired product **12** was filtered off and washed with cold ethanol.

Derivatives **12a**,**b**,**d-f**,**h** were isolated as pure compounds and were characterized without further purifications. Whereas, compounds **12c**,**g**,**i,j** were treated with saturated aqueous $NaHCO_3$ solution to give the corresponding free bases **13** which were purified by silica gel column chromatography eluting by petroleum ether:ethyl acetate, 1:1. Analytical and spectroscopic data for the derivatives **12k-r** are in accordance to those reported in literature.[16]

*3-[6-(Thiophen-3-yl)imidazo[2,1-b][1,3,4]thiadiazol-2-yl]-1H-indole hydrobromide (**12a**)*

White solid, yield: 57%, m.p. 288-289 °C, IR cm^{-1}: 3630 (NH), 3458 (NH). ^{1}HNMR (200 MHz, DMSO-d_6) δ: 7.27-7.34 (2H, m, 2xAr-H), 7.54-7.59 (2H, m, 2xAr-H), 7.68 (1H, dd, *J* = 2.9, 5.0 Hz, Ar-H), 7.89 (1H, dd, *J* = 1.1, 2.8 Hz, Ar-H), 8.16 (1H, dd, *J* = 2.8, 6.2 Hz, Ar-H), 8.42 (1H, d, *J* = 3.0 Hz, Ar-H), 8.71 (1H, s, Ar-H), 10.63 (1H, bs, NH), 12.24 (1H, s, NH). ^{13}C NMR (50 MHz, DMSO-d_6) δ: 106.06 (s), 110.68 (d), 112.62 (d), 120.30 (d), 120.52 (d) , 121.65 (d), 123.31 (d), 123.71 (s), 125.47 (d), 127.24 (d), 130.00 (d), 133.78 (s), 136.70 (s), 139.17 (s), 142.45 (s), 158.13 (s). Anal. Calcd for $C_{16}H_{11}BrN_4S_2$ (MW: 403.32): C, 47.65; H, 2.75; N, 13.89. Found: C, 47.74; H, 2.83; N, 13.95. LC-HRMS: 323.04979 m/z

*1-Methyl-3-[6-(thiophen-3-yl)imidazo[2,1-b][1,3,4]thiadiazol-2-yl]-1H-indole hydrobromide (**12b**)*

Greenish yellow solid, yield: 55%, m.p. 317-318 °C, IR cm^{-1}: 2650 (NH). ^{1}HNMR (200 MHz, DMSO-d_6) δ: 3.91 (3H, s, CH_3), 6.50 (1H, bs, NH), 7.32-7.41 (2H, m, 2xAr-H), 7.55 (1H, d, *J* = 4.9 Hz, Ar-H),7.61-7.66 (2H, m, 3xAr-H), 7.81 (1H, d, *J* = 2.4 Hz, Ar-H), 8.16 (1H, dd, *J* = 2.4, 6.2 Hz, Ar-H), 8.38 (1H, s, Ar-H), 8.60 (1H, s, Ar-H). ^{13}C NMR (50 MHz, DMSO-d_6) δ: 33.14 (q), 99.50 (s), 105.39 (s), 110.30 (d), 111.01 (d), 119.59 (d), 120.44 (s), 121.77 (d), 123.23 (d), 124.06 (s), 125.53 (d), 126.74 (d), 132.95 (s), 133.28 (d), 135.53 (s), 137.25 (s), 141.09 (d). Anal. Calcd for $C_{17}H_{13}BrN_4S_2$ (MW: 417.35): C, 48.92; H, 3.14; N, 13.42. Found: C, 48.85; H, 3.22; N, 13.51. LC-HRMS: 337.05688 m/z.

*5-Bromo-1-methyl-3-[6-(thiophen-3-yl)imidazo[2,1-b][1,3,4]thiadiazol-2-yl]-1H-indole hydrobromide (**12d**)*

Whitish solid, yield: 68%, m.p. 318-319 °C, IR cm^{-1}: 2697-2500 (NH). ^{1}HNMR (200 MHz, DMSO-d_6) δ: 3.87 (3H, s, CH_3), 7.43-7.68 (4H, m, Ar-H), 7.81-7.83 (1H, m, Ar-H), 8.24 (1H, d, *J* = 1.76 Hz, Ar-H), 8.38 (1H, bs, NH), 8.43 (1H, s, Ar-H), 8.69 (1H, s, Ar-H). ^{13}C NMR (50 MHz, DMSO-d_6) δ: 33.39 (q), 104.55 (s), 110.72 (d), 113.26 (d), 114.60 (s), 120.41 (d), 122.63 (d), 125.38 (d), 125.49 (s), 125.80 (d), 127.21 (d), 133.90 (s), 134.58 (d), 136.01 (s), 139.42 (s), 142.21 (s), 157.02 (s). Anal. Calcd for $C_{17}H_{12}Br_2N_4S_2$ (MW: 496.24): C, 41.15 H, 2.44; N, 11.29. Found: C, 41.22; H, 2.52; N, 11.41. LC-HRMS: 416.96634 m/z.

*5-Chloro-3-[6-(thiophen-3-yl)imidazo[2,1-b][1,3,4]thiadiazol-2-yl]-1H-indole hydrobromide (**12e**)*

Whitish solid, yield: 63%, m.p. 276-277 °C, IR cm^{-1}: 3285 (NH), 3168 (NH). ^{1}HNMR (200 MHz, DMSO-d_6) δ: 7.32 (1H, d, *J* = 2.1 Hz, Ar-H), 7.52-7.68 (3H, m, Ar-H), 7.83 (1H, m,, Ar-H), 8.15 (1H, d, *J* = 1.9 Hz, Ar-H), 8.46 (1H, d, *J* = 2.9 Hz, Ar-H), 8.71 (1H, s, Ar-H), 9.19 (1H, bs, NH), 12.37 (1H, s, NH). ^{13}C NMR (50 MHz, DMSO-d_6) δ: 92.15 (s), 99.49 (s), 106.10 (s), 110.43 (d), 114.24 (d), 119.58 (d), 120.27 (d), 121.37 (s), 123.35 (d), 124.74 (s), 125.80 (d), 126.17 (s), 126.67 (d), 131.35 (d), 134.16 (s), 135.22 (s). Anal. Calcd for $C_{16}H_{10}BrClN_4S_2$ (MW: 437.76): C, 43.90; H, 2.30; N, 12.80. Found: C, 43.99; H, 2.41; N, 12.91. LC-HRMS: 357.00452 m/z.

*5-Chloro-1-methyl-3-[6-(thiophen-3-yl)imidazo[2,1-b][1,3,4]thiadiazol-2-yl]-1H-indole hydrobromide (**12f**)*

Whitish solid, yield: 68%, m.p. 324-325°C, IR cm^{-1}: 2625-2496 (NH). ^{1}HNMR (200 MHz, DMSO-d_6) δ: 3.87(3H, s, CH_3), 7.36 (1H, d, *J* = 2.0 Hz Ar-H), 7.51 (1H, m, *J* = 4.5 Hz Ar-H), 7.60-7.68 (2H, m, Ar-H), 7.82 (1H, d, *J* = 1.8 Hz, Ar-H), 8.07 (1H, d, *J* = 1.9 Hz, Ar-H), 8.45 (1H, s, Ar-H), 8.64 (1H, bs, NH), 8.68 (1H, s, Ar-H). ^{13}C NMR (50 MHz, DMSO-d_6) δ: 33.41 (q), 104.61 (s), 110.72 (d), 112.84 (d), 119.60 (d), 120.50 (d), 123.24 (d), 124.87 (s), 125.38 (d), 126.61 (s), 127.23 (d), 133.73 (s), 134.73 (d), 135.75 (s), 139.26 (s), 142.19 (s), 157.10 (s). Anal. Calcd for $C_{17}H_{12}BrClN_4S_2$ (MW: 451.79): C, 45.19; H, 2.68; N, 12.40. Found: C, 45.25; H, 2.74; N, 12.45. LC-HRMS: 371.02017 m/z.

*5-Fluoro-1-methyl-3-[6-(thiophen-3-yl)imidazo[2,1-b][1,3,4]thiadiazol-2-yl]-1H-indole hydro-bromide (**12h**)*

White solid, yield: 58%, m.p. 286-287 °C, IR cm^{-1}: 2713-2485 (NH). ^{1}HNMR (200 MHz, DMSO-d_6) δ: 3.88 (3H, s, CH_3), 7.20 (1H, td, *J* = 2.4, 9.2 Hz, Ar-H), 7.54 (1H, d, *J* = 5.0 Hz, Ar-H), 7.59-7.69 (2H, m, Ar-H), 7.78 (1H, dd, *J* = 2.3, 9.6 Hz, Ar-H), 7.86 (1H, d, *J* = 2.3 Hz, Ar-H), 8.47 (1H, s, Ar-H), 8.67 (1H, s, Ar-H), 10.04 (H, bs, NH). ^{13}C NMR (50 MHz, DMSO-d_6) δ: 33.50 (q), 104.74 (d), 104.83 (s), 105.35 (d, *J* = 6.2 Hz), 110.73 (d), 111.45 (d, *J* = 26.1 Hz), 112.65 (d, *J* = 26.1 Hz), 120.84 (d), 124.15 (s), 124.37 (s), 125.39 (d), 127.36 (s), 133.08 (s), 133.93 (s), 135.03 (d), 140.25 (s, *J* = 180.3 Hz), 157.62 (s). Anal. Calcd for $C_{17}H_{12}BrFN_4S_2$ (MW: 435.33): C, 46.90; H, 2.78; N, 12.87. Found: C, 47.01; H, 2.87; N, 12.95. LC-HRMS: 355.04926 m/z.

*5-Bromo-3-[6-(thiophen-3-yl)imidazo[2,1-b][1,3,4]thiadiazol-2-yl]-1H-indole (**13c**)*

Whitish solid, yield: 58%, m.p. 299-300°C, IR cm^{-1}: 3535-3633 (NH). ^{1}HNMR (200 MHz, DMSO-d_6) δ: 7.39-7.44 (1H, m,, Ar-H), 7.50-7.54 (2H, m, Ar-H), 7.59-7.63 (1H, m, Ar-H), 7.75 (1H, dd, *J* = 1.1, 1.1 Hz, Ar-H), 8.32 (2H, d, *J* = 1.7 Hz, Ar-H), 8.60 (1H, s, Ar-H), 12.29 (1H, s, NH). ^{13}C NMR (50 MHz, DMSO-d_6) δ: 99.49 (s), 106.21 (s), 110.38 (d), 114.03 (s), 114.59 (d), 119.34 (d), 122.61 (d), 125.46 (d), 125.77 (d), 126.72 (d), 130.65 (d), 135.45 (s), 135.98 (s), 141.65 (s), 142.62 (s), 156.42 (s). Anal. Calcd for $C_{16}H_9BrN_4S_2$ (MW: 401.30): C, 47.89; H, 2.26; N, 13.96. Found: C, 47.95; H, 2.31; N, 14.04. LC-HRMS: 402.95081 m/z.

*5-Fluoro-3-[6-(thiophen-3-yl)imidazo[2,1-b][1,3,4]thiadiazol-2-yl]-1H-indole (**13g**)*

Yellow solid, yield: 80%, m.p. 260-261 °C, IR cm^{-1}: 3630 (NH). ^{1}HNMR (200 MHz, DMSO-d_6) δ: 7.16 (1H, td, *J* = 2.5, 9.2 Hz, Ar-H), 7.52-7.63 (3H, m, 3xAr-H), 7.75-7.77 (1H, m, Ar-H), 7.84 (1H, dd, *J*= 2.4, 9.8 Hz, Ar-H), 8.38 (1H, d, *J* = 2.9 Hz, Ar-H), 8.55 (1H, s, Ar-H), 12.24 (1H, s, NH). ^{13}C NMR (50 MHz, DMSO-d_6) δ: 99.40 (s), 104.61 (s), 105.78 (s), 111.36 (d), 113.77 (s), 120.20 (d), 123.70 (s), 123.96 (s), 126.46 (d), 128.11 (d), 131.63 (s), 133.24 (s), 135.45 (d), 138.25 (d), 140.74 (d), 145.68 (d). Anal. Calcd for $C_{16}H_9FN_4S_2$ (MW: 340.4): C, 56.45; H, 2.66; N, 16.46. Found: C, 56.51; H, 2.71; N, 16.56. LC-HRMS: 341.03256 m/z.

*5-Methoxy-3-[6-(thiophen-3-yl)imidazo[2,1-b][1,3,4]thiadiazol-2-yl]-1H-indole (**13i**)*

Yellow solid, yield: 58%, m.p. 255-256 °C, IR cm^{-1}: 3628 (NH). ^{1}HNMR (200 MHz, DMSO-d_6) δ: 3.85 (3H, s, CH_3), 6.95 (1H, dd, *J* = 2.4, 8.8 Hz, Ar-H), 7.44 (1H, d, *J* = 8.8

Hz, Ar-H), 7.52-7.65 (3H, m, Ar-H), 7.75 (1H, dd, *J* = 1.0, 2.8 Hz Ar-H), 8.24 (1H, d, *J* = 3.0 Hz, Ar-H), 8.55 (1H, s, Ar-H), 12.00 (1H, s, NH). ^{13}C NMR (50 MHz, DMSO-d_6) δ: 55.32 (q), 102.18 (d), 106.35 (s), 110.30 (d), 113.09 (d), 113.30 (d), 119.24 (d), 124.34 (s), 125.52 (d), 126.66 (d), 129.59 (d), 131.61 (s), 136.07 (s), 141.49 (s), 142.55 (s), 155.09 (s), 157.08 (s). Anal. Calcd for $C_{17}H_{12}N_4OS_2$ (MW: 352.43): C, 57.93; H, 3.43; N, 15.90. Found: C, 57.88; H, 3.52; N, 15.99. LC-HRMS: 353.05377 m/z.

*5-Methoxy-1-methyl-3-[6-(thiophen-3-yl)imidazo[2,1-b][1,3,4]thiadiazol-2-yl]-1H-indole (**13j**)*

Yellow solid, yield: 60%, m.p. 213-214 °C, ^{1}HNMR (200 MHz, DMSO-d_6) δ: 3.86 (6H, s, OCH_3, CH_3), 6.99 (1H, dd, *J* =2.5, 7.7 Hz, Ar-H), 7.50-7.64 (4H, m, Ar-H), 7.75 (1H, d, *J* = 3.2 Hz, Ar-H), 8.26 (1H, s, Ar-H), 8.55 (1H, s, Ar-H). ^{13}C NMR (50 MHz, DMSO-d_6) δ: 33.24 (q, CH_3), 55.38 (q, CH_3), 99.49 (s), 102.32 (d), 105.06 (s), 110.35 (d), 111.90 (d), 112.96 (d), 119.24 (d), 124.61 (s), 125.52 (d), 126.67 (d), 132.30 (s), 133.03 (d), 136.00 (s), 141.46 (s), 142.43 (s), 155.37 (s), 156.63 (s). Anal. Calcd for $C_{18}H_{14}N_4OS_2$ (MW: 366.46): C, 58.99; H, 3.85; N, 15.29. Found: C, 59.07; H, 3.91; N, 15.37. LC-HRMS: 367.06955 m/z.

*General procedure for the synthesis 2-(1H-indol-3-yl)-6-phenylimidazo[2,1-b][1,3,4]thiadiazole-5-carbaldehydes **14k-r.***

Vilsmeier reagent was prepared at 0 °C by adding dropwise $POCl_3$ (0.11 mL) into a stirred DMF anhydrous (0.08 mL). The appropriate derivative **13** (0.5 mmol) in 2mL of DMF anhydrous was added and the solution was heated at 70 °C under stirring for 5h. The reaction mixture was poured onto ice and the corresponding aldehyde **14** was filtered off and purified by silica gel column chromatography eluting by petroleum ether:ethyl acetate, 3:7.
Derivatives **14l, 14q** were characterized only by ^{1}HNMR spectra due to their poor solubility.

*2-(1H-Indol-3-yl)-6-phenylimidazo[2,1-b][1,3,4]thiadiazole-5-carbaldehyde (**14k**)*

White solid, yield: 70%, m.p. 285-286 °C, IR cm^{-1}: 2918 (NH), 1683 (CO). ^{1}HNMR (200 MHz, DMSO-d_6) δ: 7.30 (1H, m, Ar-H), 7.52 (2H, d, *J* = 6.8 Hz, Ar-H), 8.01 (2H, d, *J* = 5.8 Hz, Ar-H), 8.27-8.30 (3H, m, Ar-H), 8.41 (2H, d, *J* = 3.0 Hz, Ar-H), 10.08 (1H, s, CHO), 12.20 (1H, s, NH). ^{13}C NMR (50 MHz, DMSO-d_6) δ: 106.20 (s), 112.64 (d), 120.65 (d), 121.70 (d), 123.36 (d), 123.47 (s), 123.80 (s), 128.67 (4xd), 129.41 (d), 130.10 (d), 132.38 (s), 136.68 (s), 148.53 (s), 153.45 (s), 159.38 (s), 177.31 (d). Anal. Calcd for $C_{19}H_{12}N_4OS$

(MW: 344.39): C, 66.26; H, 3.51; N, 16.27. Found: C, 66.35; H, 3.59; N, 16.41. LC-HRMS: 345.08148 m/z.

2-(1-Methyl-1H-indol-3-yl)-6-phenylimidazo[2,1-b][1,3,4]thiadiazole-5-carbaldehyde ***(14l)***

White solid, yield: 91%, m.p. 233-234 °C, IR cm^{-1}: 1560 (CO). ^{1}HNMR (200 MHz, DMSO-d_6) δ: 3.90 (3H, s, CH_3), 7.31-7.59 (6H, m, Ar-H), 7.87-8.41(4H, m, Ar-H), 10.07 (1H, s, CHO). Anal. Calcd for $C_{20}H_{14}N_4OS$ (MW: 358.4): Composition: C, 67.02; H, 3.94; N, 15.63. Found: C, 67.28; H, 4.11; N, 15.75. LC-HRMS: 214.09023 m/z.

6-(4-Fluorophenyl)-2-(1H-indol-3-yl)imidazo[2,1-b][1,3,4]thiadiazole-5-carbaldehyde ***(14m)***

White solid, yield: 81%, m.p. 255-256 °C, IR cm^{-1}:3158 (NH), 1560 (CO). ^{1}HNMR (200 MHz, DMSO-d_6) δ: 7.28-7.38 (4H, m, Ar-H), 7.52-7.55 (1H, m, Ar-H), 8.08-8.11 (2H, m, Ar-H), 8.26-8.29 (1H, m, Ar-H), 8.40 (1H, s, Ar-H), 10.09 (1H, s, CHO), 12.19 (1H, s, NH). ^{13}C NMR (50 MHz, DMSO-d_6) δ: 99.5 (s), 106.1 (s), 112.5 (d), 115.3 (d), 115.8 (d), 120.6 (d), 121.7 (d), 123.3 (d), 123.8 (2xs), 128.9 (s), 130.2 (d), 130.7 (d), 130.9 (d), 136.7 (s), 148.2 (s), 151.8 (s), 159.4 (s), 177.3 (d). Anal. Calcd for $C_{19}H_{11}FN_4OS$ (MW: 362.38): C, 62.97; H, 3.06; N, 15.46. Found: C, 63.05; H, 3.11; N, 15.53. LC-HRMS: 363.07043 m/z.

2-(1H-Indol-3-yl)-6-(3-methoxyphenyl)imidazo[2,1-b][1,3,4]thiadiazole-5-carbaldehyde ***(14n)***

White solid, yield: 60%, m.p. 278-279 °C, IR cm^{-1}: 3308 (NH), 1560 (CO). ^{1}HNMR (200 MHz, DMSO-d_6) δ: 3.84 (3H, s, CH_3), 7.06 (1H, d, J = 6.7 Hz, Ar-H), 7.29-7.32 (2H, m, Ar-H), 7.41-7.46 (1H, m, Ar-H), 7.55 (1H, dd, J = 3.1, 5.8 Hz, Ar-H), 7.61 (2H, m, Ar-H), 8.30 (1H, m, Ar-H), 8.42 (1H, d, Ar-H), 10.10 (1H, s, CHO), 12.20 (1H, s, NH). ^{13}C NMR (50 MHz, DMSO-d_6) δ: 55.2 (q), 99.49 (s), 106.2 (s), 113.5 (2xd), 120.7 (d), 121.0 (d), 121.7 (d), 123.3 (d), 123.6 (s), 123.8 (s), 129.7 (2xd), 130.1 (d), 133.7 (s), 136.7 (s), 153.0 (s), 159.3 (s), 159.4 (s), 177.3 (d). Anal. Calcd for $C_{20}H_{14}N_4O_2S$ (MW: 374.42): C, 64.16; H, 3.77; N, 14.96. Found: C, 64.25; H, 3.51; N, 15.13. LC-HRMS: 375.09232 m/z.

6-(2,5-Dimethoxyphenyl)-2-(1H-indol-3-yl)imidazo[2,1-b][1,3,4]thiadiazole-5-carbaldehyde ***(14o)***

Yellow solid, yield: 82%, m.p. 268-269 °C, IR cm^{-1}: 1561 (CO). ^{1}HNMR (200 MHz, DMSO-d_6) δ: 3.75 (3H, s, CH_3), 3.77 (3H, s, CH_3), 7.02-7.18 (3H, m, Ar-H), 7.32 (2H, dd, *J* = 2.9, 5.8 Hz, Ar-H), 7.55-7.58 (1H, m, Ar-H), 8.28 (2H, d, *J* = 5.5 Hz, Ar-H), 8.42 (1H, s, Ar-H), 9.76 (1H, s, CHO), 12.21 (1H, s, NH). ^{13}C NMR (50 MHz, DMSO-d_6) δ: 55.5 (q), 55.9 (q), 99.5 (s), 106.2 (s), 112.5 (d), 113.1 (d), 116.1 (d), 116.3 (2xd), 120.62 (s), 121.7 (d), 122.1 (s), 123.3 (d), 123.8 (s), 130.0 (d), 136.7 (s), 148.7 (s), 150.4 (s), 153.1 (s), 159.2 (s), 177.6 (d). Anal. Calcd for $C_{21}H_{16}N_4O_3S$ (MW: 404.44): C, 62.36; H, 3.99; N, 13.85. Found: C, 62.49; H, 4.05; N, 13.63. LC-HRMS: 405.10297 m/z.

*6-(2,5-Dimethoxyphenyl)-2-(1-methyl-1H-indol-3-yl)imidazo[2,1-b][1,3,4]thiadiazole-5-carbaldehyde (**14p**)*

White solid, yield: 70%, m.p. 216-217 °C, IR cm^{-1}: 1667 (CO). ^{1}HNMR (200 MHz, DMSO-d_6) δ: 3.75 (3H, s, CH_3), 3.77 (3H, s, CH_3), 3.92 (3H, s, CH_3), 7.06 (1H, dd, *J* = 2.9, 5.8 Hz, Ar-H), 7.17 (2H, m, Ar-H), 7.36-7.39 (2H, t, *J* = 4.0 Hz, Ar-H), 7.64 (1H, d, *J* = 8.8 Hz, Ar-H), 8.27 (1H, d, *J* = 10.4 Hz, Ar-H), 8.43 (1H, s, Ar-H), 9.76 (1H, s, CHO). ^{13}C NMR (50 MHz, DMSO-d_6) δ: 33.2 (q), 55.5 (q), 55.97 (q), 99.5 (s), 105.1 (s), 108.5 (d), 111.1 (d), 113.1 (d), 116.1 (s), 116.3 (d), 118.73 (d), 120.68 (d), 122.0 (d), 123.4 (d), 123.9 (s), 124.1 (s),136.2 (s),137.3 (s), 148.6 (s), 150.4 (s), 153.0 (s), 158.8 (s), 177.6 (d). Anal. Calcd for $C_{22}H_{18}N_4O_3S$ (MW: 418.47): C, 63.14; H, 4.34; N, 13.39. Found: C, 63.21; H, 4.43; N, 13.48. LC-HRMS: 419.11682 m/z.

*2-(1H-Indol-3-yl)-6-(4-nitrophenyl)imidazo[2,1-b][1,3,4]thiadiazole-5-carbaldehyde (**14q**)*

Yellow solid, yield: 75%, m.p. 314-315 °C, IR cm^{-1}: 3311 (NH), 1561 (CO). ^{1}HNMR (200 MHz, DMSO-d_6) δ: 7.31 (2H, d, *J* = 2.9 Hz, Ar-H), 7.52 (1H, s, Ar-H), 8.34-8.43 (5H, m, Ar-H), 10.21 (1H, s, CHO), 12.23 (1H, s, NH). Anal. Calcd for $C_{19}H_{11}N_5O_3S$ (MW: 389.39): C, 58.61; H, 2.85; N, 17.99. Found: C, 58.82; H, 2.73; N, 18.09. LC-HRMS: 390.06683 m/z.

*2-(5-Bromo-1H-indol-3-yl)-6-(2,5-dimethoxyphenyl)imidazo[2,1-b][1,3,4]thiadiazole-5-carbaldehyde (**14r**)*

White solid, yield: 90%, m.p. 250-251 °C, IR cm^{-1}: 3268 (NH), 1654 (CO). ^{1}HNMR (200 MHz, DMSO-d_6) δ: 3.76 (6H, d, *J* =3.9 Hz, 2xCH_3), 7.08-7.18 (3H, m, Ar-H), 7.42-7.56 (2H, m, Ar-H), 8.45 (2H, d, *J* =10.3 Hz, Ar-H), 9.76 (1H, s, CHO), 12.38 (1H, bs, NH). ^{13}C

NMR (50 MHz, DMSO-d_6) δ: 55.3 (q), 55.9 (q), 99.5 (s), 105.9 (s), 108.2 (s), 114.3 (s), 116.1 (d), 116.3 (d), 122.0 (s), 122.9 (d), 123.9 (s), 125.5 (s), 126.0 (d), 131.2 (d), 135.5 (s), 141.6 (d), 150.3 (s), 150.7 (d), 153.3 (s), 158.7 (s), 178.6 (d). Anal. Calcd for $C_{21}H_{15}BrN_4O_3S$ (MW: 483.33): C, 52.18; H, 3.13; N, 11.59. Found: C, 52.39; H, 3.21; N, 11.70. LC-HRMS: 485.01031 m/z.

Biology

Drugs and chemicals

The synthesized imidazothiadiazole compounds **12-14** were dissolved in DMSO. The medium, foetal bovine serum (FBS), penicillin (50 IU mL^{-1}) and streptomycin (50 µg mL^{-1}) were from Gibco (Gaithersburg, MD, USA). All other chemicals were from Sigma (Zwijndrecht, the Netherlands).

Cell culture

Capan-1 and Panc-1 cell lines, were purchased at the ATCC (Manassas, VA, USA), while SUIT-2 cells were a generous gift from Dr. Adam Frampton (Imperial College, London, UK). Panc-1R cells, a gemcitabine-resistant sub-clone obtained by continuous incubation of Panc-1 with 1 µM of this drug, were achieved as described previously.[42] The primary PDAC-3 culture was isolated from a patient at Pisa Hospital as described previously.[61] The cell lines were tested for their authentication by STR–PCR, performed by BaseClear (Leiden, the Netherlands). The cells were cultured in RPMI-1640 (Roswell Park Memorial Institute 1640) supplemented with 10% heat-inactivated FBS, 1% penicillin/streptomycin, or in DMEM (Dulbecco's Modified Eagle's Medium), supplemented with 10% heat-inactivated FBS, 1% HEPES. The cells were kept in a humidified atmosphere of 5% CO_2 and 95% air at 37 °C and harvested with trypsin-EDTA. Not all these preclinical models allowed to perform the different experiments to check antitumor properties of new compounds. In particular, PDAC-3 cells were selected to form spheroids which are more representative of the aggregation of tumor cells in vivo, as also reported in our previous studies. All the PDAC cells, i.e., Panc-1R, SUIT-2 and PDAC-3, but also Panc-1 and Capan-1 cells were selected for the wound-healing assay because in all these cells the exposure for 24 h with our compounds did not result in pro-apoptotic or necrotic effects, allowing a reliable analysis of the results. Capan-1 and SUIT-2 cells were selected for Western blot, zymography and PCR assays because preliminary analyses of the housekeeping protein GAPDH at the Western

blot showed that using lysates of these cells the Western blot images were not "saturated" and were kept in the linear range (as revealed by exposing blots to increasing times and drawing a plot of intensity and time exposure). SUIT-2 cells were selected for the PamChip array because of the lowest background noise observed in preliminary experiments.

Cell growth inhibition

The *in vitro* antiproliferative activity of the new imidazothiadiazole compounds **12a,b,d,e,f,h**, **13c,g,i,j** and **14k-r** was evaluated on a panel of pancreatic cancer cells by Sulforhodamine-B (SRB) assay, both for primary cell cultures (PDAC-3) and for the immortalized cell lines (SUIT-2, Capan-1, Panc-1 and Panc-1R), following a previously described protocol.[42] The cytotoxicity of the new compounds **12a** and **12b** was also evaluated in the normal fibroblast cells Hs27. The results of these experiments allowed us to calculate the selectivity index (SI, IC_{50} non-tumor cell line/IC_{50} tumor cell line).

Cells were seeded into a 96-well flat-bottom plates in triplicate in a volume of 100 µL ($3x10^3$ cells/well for SUIT-2, Panc-1, Panc-1R and PDAC-3 cell lines, $5x10^3$ cells/well for Capan-1 cells, and $8x10^3$ cells/well for Hs27 cells) and incubated for 24 h at 37 °C to create a confluent monolayer. Then, the cells were treated with 100 µL of the compounds dissolved in DMSO at different concentration (125-16000 nM) for 72 h at 37 °C, 5% CO_2 and 100% humidity. At the end of incubation period, the cells were fixed with 25 µL of 50% cold trichloroacetic acid (TCA) and kept for at least 60 min at 4°C. Then, the plates were emptied and washed gently with deionized water, dried at room temperature (RT) overnight and stained with 50 µL of 0.4% SRB solution in 1% acetic acid for 15 min at RT. The excess of SRB stain was removed and the plates were washed with a 1% acetic acid solution and let dry at RT overnight. The SRB staining was dissolved in 150 µL of tris(hydroxymethyl)aminomethane solution pH= 8.8 (TRIS base), and the absorbance was measured at wavelengths of 490 nm and 540 nm. Cell growth inhibition was calculated as the percentage of drug treated cells versus vehicle-treated cells ("untreated cells or control") OD (corrected for OD before drug addiction, "day-0"). The 50% inhibitory concentration of cell growth (IC_{50}) was calculated by non-linear least squares curve fitting (GraphPad PRISM, Intuitive Software for Science, San Diego, CA). In the NCI protocol IC_{50} is named GI_{50} (50% growth inhibitory concentration).

Wound-healing assay

The *in vitro* scratch wound-healing assay was performed as previously described.[62] SUIT-2, Capan-1, Panc-1 and Panc-1R cells were seeded in 96-well flat-bottom plates at the density of $5x10^4$ cells/well in 100 µL. After 24 h of pre-incubation at 37 °C, 5% CO_2 and 100% humidity, the cell monolayers were scratched using a specific tool with multiple needles to create scratches of constant width. After removal of the detached cells by washing with phosphate buffered saline (PBS) solution, in the control wells the medium was replaced with only medium while the medium added with the compounds of interest in the experimental wells. The wound confluence was monitored by phase-contrast microscopy (Universal Grab 6.3 software, Digital Cell Imaging Labs, Keerbergen, Belgium) integrated to the Leica DMI300B (Leica Microsystems, Eindhoven, Netherlands) migration station and the pictures were captured immediately after scratch (T = 0), and 4, 8, 20 and 24 h from the treatment. The results were analyzed with the Scratch Assay 6.2 software (Digital Cell Imaging Labs).

Spheroid assay

PDAC-3 spheroids were grown in CELLSTAR®96-well cell repellent U-bottom plates (Greiner Bio-One, Cat No. 650970, Kremsmünster, Austria). Cells were seeded at the density of $2x10^4$ cells per well, and incubated at 37°C, 5% CO_2 for 72 h in order to let the spheroids form.

Before the treatment a picture of the plate was taken with an automated phase-contrast microscope DMI300B (Leica Microsystems, Eindhoven, Netherlands*)*, and the subsequent pictures were taken every two days. After 72 h of incubation the culture medium was replaced with medium added with compounds of interest, which were diluted to the final concentration of 8.5 µM (5x the IC_{50}, obtained with previous growth-inhibition assay). Despite the careful pipetting, tilting the plate and placing the pipette tip on the side of the well, the structure of the spheroid was disturbed so we decided to centrifuge the plate at 200xRCF, for 3 min at RT (Rotixa 500RS, Hettich Zentrifugen Technology, Tuttlingen, Germany*)*. The treatment was repeated after four days, to ensure the availability of nutrients, and so was the centrifuge.

Pictures were analysed with ImageJ Software (U.S. National Institute of Health, Bethesda, Maryland, USA) to determine the area of the spheroids treated and compare it to the area of the untreated spheroids, as described previously.[63]

RNA isolation

RNA was extracted from SUIT-2, Capan-1 and Panc-1 cells according to TRIzol-chloroform protocol as described previously.[64] Cells were seeded in a 6-well plate in a density of 2.5 x 10^5 cells/well and kept at 37° C, with a constant level of CO_2 (5%) and 100% humidity for 24 h. Subsequently, the cells were treated for 24 h with the compounds of interest at concentration 5x IC_{50} and stored for an additional 24 h in the incubator. The cells were then harvested by 250 µL of TRIzol reagent. After precipitation with isopropanol and washing with 70% ethanol, the total RNA appeared as a white gel-like pellet at the bottom of the tube. RNA yields and integrity were determined by measuring optical density at 260 nm with a Thermo Scientific NanoDrop 1000™ Spectrophotometer, controlled by ND1000 software. Instead, the test for detection of contaminations by protein or by organic compounds, thiocyanates and phenolate ions was performed by measuring absorbance at 280 and 230 nm, respectively.

Reverse transcription (RT) and quantitative Real-Time PCR (qRT-PCR)

For qRT-PCR, complementary DNA (cDNA) synthesis was performed according to manufacturer's protocol Thermo Scientific™ First Strand cDNA Synthesis Kit. For the reverse transcriptase reactions, 1.5 µg of mRNA was added to a 1 µL of random hexamer primer and, finally, water nuclease free up to a final volume of 11 µL. Therefore, 5X Reaction Buffer (4 µL), RiboLock RNase Inhibitor (20 U/ µL) (1 µL), 10 nM dNTP Mix (2 µL) and M-MuLV Reverse Transcriptase (20 U/ µL) (2 µL) components were added (all provided by Kit). The mixture was incubated for 5 min at 25° C followed by 60 min at 37° C. Subsequently, the reaction was terminated by heating at 70 ° C for 5 min. The DNA samples obtained (20 µL) were diluted 1:10 and used immediately for the RT-PCR assay. RT-PCR reactions were performed using the commercial TaqMan® Universal PCR Master Mix kit. For the RT-PCR, 25 µL of total mix per well is needed. Therefore, 12.5 µL of Universal Master Mix 2X (AmpliTaq Gold DNA Polymerase, dNTPs with dUTP, passive reference, and optimized buffer components), 1 µL of Primers and TaqMan® probe, 6.5 µL of H_2O and 5 µL of cDNA sample were loaded in duplicate on a 96-well PCR plate and the amplification was carried out in a GeneAmp 5700 Sequence Detection System. Samples were amplified by following the thermal cycle conditions for 40 cycles: an initial incubation at 50°C for 2 min to prevent the reamplification of carry-over PCR products by AmpErase uracil-N-glycosylase, followed by incubation at 95°C for 10 min to suppress AmpErase UNG activity and denature the DNA, followed by annealing and extension at 60 °C for 1 minute. Primers

and probes were obtained from Applied Biosystems Assay-on Demand Gene expression products to amplify the following genes: *SNAIL1* (Hs00195591_m1), *SNAIL2* (Hs00950344_m1), *CDH1* (Hs01023894_m1), *CDH12* (Hs00362037_m1). GAPDH (Hs02758991_g1) has been used as housekeeping gene to normalize the amplifications. All reactions were performed in duplicate using the ABI PRISM7500 sequence detection system instrument (AppliedBiosystems). The cycle threshold (Ct) was determined and gene expression levels relative to that of GAPDH were calculated by the $2^{-\Delta\Delta CT}$ method, as described previously.

Western blot and gelatine zymography

The protein expression of SNAIL1, SNAIL2, CDH1, CDH12, and VIM in SUIT-2, PANC-1 and Capan-1 cells treated with compounds 12a and 12b was evaluated by Western Blot analysis as described previously [65]. All the primary antibodies were from Cell Signaling Technology (Beverly, MA). Additional Western blot analyses were performed in order to evaluate the phosphorylation of FAK, using the Phospho-FAK (Tyr397) Antibody #3283 (Cell Signaling Technology).

The activity of MMP2 and MMP9 was evaluated by gelatine zymography, as described previously.[65] PDAC cells (10^6) were seeded in Petri dishes and incubated with serum-free medium for 24 h, with or without the selected compounds at 5x IC_{50}. Medium was harvested and centrifuged (1500 rpm for 5 min) in order to remove cellular debris. The collected media were then mixed with SDS-PAGE buffer 4X without reducing agent and underwent electrophoresis in 10% polyacrylamide gel containing 1mg/mL gelatine. After 1 hour, the gel was exposed to renaturating buffer (50mM Tris-HCl pH 7, 6.5mM $CaCl_2$, 1μM $ZnCl_2$, 2.5% Triton X-100) for 15 min, washed with washing buffer (50mM Tris-HCl pH 7, 6.5mM $CaCl_2$, 1μM $ZnCl_2$) and finally incubated with developing buffer (50 mM Tris-HCl pH 7, 6.5 mM $CaCl_2$, 1μM $ZnCl_2$, 1% Triton X-100, 0.02% NaN_3) for 16 h at 37°C. The staining was then performed using 0.25% Coomassie Brilliant Blue R-250 solution containing 45% methanol and 10% glacial acetic acid for 4 h, washed with a solution of 10% glacial acetic acid and 45% methanol for 2 h. The areas of protease activity were detected as clear bands and the activity of MMPs was assessed by densitometric scanning and quantitative analysis using ImageJ software (National Institutes of Health, Bethesda, MD, US).

PamChip® kinase activity profiling

A PamChip array with 144 kinase peptides substrates (#86312 PamGene International B.V., 's-Hertogenbosch, The Netherlands) was used to test the change in tyrosine kinase activity when using the **12b** compound. This experiment was performed with SUIT-2 cells in biological duplicates (two untreated samples and two treated samples with **12b** compound), as described previously.[66,67]

Preparation of cell lysates

Cells were grown in 25 cm^2 flasks until they reached 80% of confluence, at 37°C and 5% of CO_2, then SUIT-2 cells were treated with 5 μM of **12b** (5x IC_{50}), and the medium of control cells was replaced with fresh medium. Treatment lasted 24 h, and then cells were lysed with 100μL x 10^6 cells of M-PER lysis buffer containing: M-PER Mammalian Extraction Buffer (Thermo Scientific, Rockford, IL, USA), Halt protease Inhibitor cocktail, EDTA free (Complete Mini EDTA-free Protease Inhibitor Cocktail, Roche #11836170001), Halt Phosphatase Inhibitor Cocktail (Thermo Fisher #78420) both diluted 1:100, for at least 15 min at 4°C. The lysates were collected in 1.5 mL tubes, which were centrifuged (at 4°C, 16000g) for 15 min, and the supernatants were collected and stored at -80°C until use. Protein concentration of the samples was determined using Bio-Rad protein Assay, based on the method of Bradford (Bio-Rad, Hercules, CA).

Tyrosine kinase activity profiling

Lysates for the PamChips were prepared in order to reach a concentration of 10 μg protein/array, and they were added to the MasterMix (PamGene reagent kit 32116) containing: PK buffer 10x, BSA solution 100x, PTK additive 10x, 1 M DTT solution, Complete Mini EDTA-free Protease Inhibitor Cocktail, Halt Phosphatase Inhibitor Cocktail 400x (Thermo Fisher), PY-20-FITC (fluorescent labelled antibody), 4 mM ATP solution. Samples were added to the MasterMix immediately prior to loading on the chip. Before loading the samples, the PamStation®12 instrument performed a blocking step with 25μL of 2% BSA on each array followed by three wash steps with PK buffer, then 40 μL of each sample mix was loaded in duplicate onto the arrays. During incubation at 30°C, the sample mix was pumped up and down through the array once per minute for 60 cycles. Repeated fluorescent imaging of each array was performed with a 12-bit CCD camera, monitoring fluorescence intensities in real time.

PamGene data analysis

The intensity of each spot at the end point was evaluated through an open source software (ScanAnalyze) and subsequently corrected for local background noise. Since the negative control was a negative value, all the intensities were subjected to a minimal shift to have the negative control equal to zero.

One duplicate of the treated samples was excluded from the analysis due to bad quality data ending with two controls and one treated samples. To maintain a balance and statistical power for the differential analysis, one extra sample for the control group was generated using the median of the two samples and adding a constant *k* while 2 extra samples for the treated group were generated adding a different constant *k* to the treated sample.

The differential analysis was performed by a Student t test in R (version 3.6.1) and the p.value was corrected by FDR. The significant peptides were selected applying a cutoff on FDR < 0.01. Visualization of differentially phosphorylated protein was performed in Cytoscape (version 3.5.0) and the barplot for PTK2 phosphorylation was generated in R (version 3.6.1).

Enzyme-Linked Immunosorbent Assay (ELISA) for phosphorylated FAK (pFAK) kinase

The pFAK level at tyrosine residue 397 was detected and quantified using Enzyme-Linked Immunosorbent Assay (ELISA). The assay was conducted using Invitrogen™ FAK[pY397] ELISA Kit (Cat. # KHO0441) according to the manufacturer's protocol. Supernatants from Panc-1, Capan-1 and SUIT-2 cells were collected after 24 h from the treatment with imidazothiadiazole compounds **12a** and **12b** at concentration 5x IC_{50} value. The absorbance was read at 450 nm. We performed a parallel ELISA test using the well-known FAK inhibitor defactinib (5 μM). This drug reduced the FAK/PTK2 phosphorylation of 65%, supporting the use of this method in order to check the inhibition of pFAK.

Statistics

All SRB, PCR, Western blot, and zymography assays were carried out in triplicate and repeated at least three times, whereas the percentages of cell migration were calculated taking into account at least six scratch areas. The data was evaluated using the GraphPad Prism version 7 software (GraphPad Software, San Diego, CA, USA). Data is expressed as mean values ± SEM and analyzed by the Student t test.

AUTHOR INFORMATIONS

Corresponding authors

*Email: patrizia.diana@unipa.it; Phone: (+39)091-23896815

*Email: e.giovannetti@amsterdamumc.nl; Phone: (+31)020-4442633

Acknowledgments

This work was partially supported in the collections and analysis of data by the following grants: CCA Foundation 2015 and 2016 grants, KWF Dutch Cancer Society grants (KWF project#10401 and #11957) and AIRC/Start-Up grant (to E.G.). The Authors would like to thank Btissame El Hassouni, MSc (VUmc, Amsterdam, The Netherlands) for the support with the work on the cell culture experiments.

We thank the members of the Drug Discovery Commitee of the EORTC-PAMM group for the useful discussion and support.

List of abbreviations

CDH1: E-cadherin; CDH12: N-cadherin; CSI: chlorosulfonyl isocyanate; DMF: Dimethylformamide; DMPM: diffuse malignant peritoneal mesothelioma; DMSO: Dimethyl sulfoxide; ELISA: enzyme-linked immunosorbent assay; EMT: epithelial mesenchymal transition; FAK: focal adhesion kinase; FBS: foetal bovine serum; FDR: false discovery rate; GI_{50}: growth inhibition of 50% of cells; IC_{50}: inhibitory concentration 50%; MMP-2/9: matrix metalloproteinases-2/9; NCI: National Cancer Institute; PDAC: pancreatic ductal adenocarcinoma; PTK2: protein tyrosine kinase 2; RT: room temperature; SD: standard deviation; SEM: standard error media; SI, selectivity index; SNAIL-1/2: zinc finger protein-1/2; TGI: total growth inhibition; VIM: vimentin

References

(1) Nepali, K.; Sharma, S.; Sharma, M.; Bedi, P. M. S.; Dhar, K. L. Rational Approaches, Design Strategies, Structure Activity Relationship and Mechanistic Insights for Anticancer Hybrids. *Eur J Med Chem* **2014**, *77*, 422–487. https://doi.org/10.1016/j.ejmech.2014.03.018.

(2) Viegas-Junior, C.; Danuello, A.; da Silva Bolzani, V.; Barreiro, E. J.; Fraga, C. A. M. Molecular Hybridization: A Useful Tool in the Design of New Drug Prototypes. *Curr. Med. Chem.* **2007**, *14* (17), 1829–1852.

(3) Nekkanti, S.; Tokala, R.; Shankaraiah, N. Targeting DNA Minor Groove by Hybrid Molecules as Anticancer Agents. *Curr. Med. Chem.* **2017**, *24* (26), 2887–2907. https://doi.org/10.2174/0929867324666170523102730.

(4) Kerru, N.; Singh, P.; Koorbanally, N.; Raj, R.; Kumar, V. Recent Advances (2015-2016) in Anticancer Hybrids. *Eur J Med Chem* **2017**, *142*, 179–212. https://doi.org/10.1016/j.ejmech.2017.07.033.

(5) Yang, K.; Fu, L. Mechanisms of Resistance to BCR-ABL TKIs and the Therapeutic Strategies: A Review. *Crit. Rev. Oncol. Hematol.* **2015**, *93* (3), 277–292. https://doi.org/10.1016/j.critrevonc.2014.11.001.

(6) Singla, P.; Luxami, V.; Paul, K. Synthesis and in Vitro Evaluation of Novel Triazine Analogues as Anticancer Agents and Their Interaction Studies with Bovine Serum Albumin. *European Journal of Medicinal Chemistry* **2016**, *117*, 59–69. https://doi.org/10.1016/j.ejmech.2016.03.088.

(7) Ma, L.-Y.; Wang, B.; Pang, L.-P.; Zhang, M.; Wang, S.-Q.; Zheng, Y.-C.; Shao, K.-P.; Xue, D.-Q.; Liu, H.-M. Design and Synthesis of Novel 1,2,3-Triazole-Pyrimidine-Urea Hybrids as Potential Anticancer Agents. *Bioorg. Med. Chem. Lett.* **2015**, *25* (5), 1124–1128. https://doi.org/10.1016/j.bmcl.2014.12.087.

(8) Qin, H.-L.; Shang, Z.-P.; Jantan, I.; Tan, O. U.; Hussain, M. A.; Sher, M.; Bukhari, S. N. A. Molecular Docking Studies and Biological Evaluation of Chalcone Based Pyrazolines as Tyrosinase Inhibitors and Potential Anticancer Agents. *RSC Adv.* **2015**, *5* (57), 46330–46338. https://doi.org/10.1039/C5RA02995C.

(9) Romagnoli, R.; Baraldi, P. G.; Prencipe, F.; Balzarini, J.; Liekens, S.; Estévez, F. Design, Synthesis and Antiproliferative Activity of Novel Heterobivalent Hybrids Based on Imidazo[2,1-b][1,3,4]Thiadiazole and Imidazo[2,1-b][1,3]Thiazole Scaffolds. *Eur J Med Chem* **2015**, *101*, 205–217. https://doi.org/10.1016/j.ejmech.2015.06.042.

(10) Jadhav, V. B.; Kulkarni, M. V.; Rasal, V. P.; Biradar, S. S.; Vinay, M. D. Synthesis and Anti-Inflammatory Evaluation of Methylene Bridged Benzofuranyl Imidazo[2,1-b][1,3,4]Thiadiazoles. *Eur J Med Chem* **2008**, *43* (8), 1721–1729. https://doi.org/10.1016/j.ejmech.2007.06.023.

(11) Tahghighi, A.; Razmi, S.; Mahdavi, M.; Foroumadi, P.; Ardestani, S. K.; Emami, S.; Kobarfard, F.; Dastmalchi, S.; Shafiee, A.; Foroumadi, A. Synthesis and Anti-Leishmanial Activity of 5-(5-Nitrofuran-2-Yl)-1,3,4-Thiadiazol-2-Amines Containing N-[(1-Benzyl-1H-1,2,3-Triazol-4-Yl)Methyl] Moieties. *Eur J Med Chem* **2012**, *50*, 124–128. https://doi.org/10.1016/j.ejmech.2012.01.046.

(12) Jakovljević, K.; Matić, I. Z.; Stanojković, T.; Krivokuća, A.; Marković, V.; Joksović, M. D.; Mihailović, N.; Nićiforović, M.; Joksović, L. Synthesis, Antioxidant and Antiproliferative Activities of 1,3,4-Thiadiazoles Derived from Phenolic Acids. *Bioorg. Med. Chem. Lett.* **2017**, *27* (16), 3709–3715. https://doi.org/10.1016/j.bmcl.2017.07.003.

(13) Alegaon, S. G.; Alagawadi, K. R.; Sonkusare, P. V.; Chaudhary, S. M.; Dadwe, D. H.; Shah, A. S. Novel Imidazo[2,1-b][1,3,4]Thiadiazole Carrying Rhodanine-3-Acetic Acid as Potential Antitubercular Agents. *Bioorg. Med. Chem. Lett.* **2012**, *22* (5), 1917–1921. https://doi.org/10.1016/j.bmcl.2012.01.052.

(14) Bhongade, B. A.; Talath, S.; Gadad, R. A.; Gadad, A. K. Biological Activities of Imidazo[2,1-b][1,3,4]Thiadiazole Derivatives: A Review. *Journal of Saudi Chemical Society* **2016**, *20* (Supplement 1), S463–S475. https://doi.org/10.1016/j.jscs.2013.01.010.

(15) Schillaci, D.; Spanò, V.; Parrino, B.; Carbone, A.; Montalbano, A.; Barraja, P.; Diana, P.; Cirrincione, G.; Cascioferro, S. Pharmaceutical Approaches to Target Antibiotic Resistance Mechanisms. *J. Med. Chem.* **2017**, *60* (20), 8268–8297. https://doi.org/10.1021/acs.jmedchem.7b00215.

(16) Cascioferro, S.; Parrino, B.; Petri, G. L.; Cusimano, M. G.; Schillaci, D.; Di Sarno, V.; Musella, S.; Giovannetti, E.; Cirrincione, G.; Diana, P. 2,6-Disubstituted Imidazo[2,1-b][1,3,4]Thiadiazole Derivatives as Potent Staphylococcal Biofilm Inhibitors. *European Journal of Medicinal Chemistry* **2019**, *167*, 200–210. https://doi.org/10.1016/j.ejmech.2019.02.007.

(17) Patel, H. M.; Sing, B.; Bhardwaj, V.; Palkar, M.; Shaikh, M. S.; Rane, R.; Alwan, W. S.; Gadad, A. K.; Noolvi, M. N.; Karpoormath, R. Design, Synthesis and Evaluation of Small Molecule Imidazo[2,1-b][1,3,4]Thiadiazoles as Inhibitors of Transforming

Growth Factor-β Type-I Receptor Kinase (ALK5). *Eur J Med Chem* **2015**, *93*, 599–613. https://doi.org/10.1016/j.ejmech.2014.09.002.

(18) Kumar, S.; Hegde, M.; Gopalakrishnan, V.; Renuka, V. K.; Ramareddy, S. A.; De Clercq, E.; Schols, D.; Gudibabande Narasimhamurthy, A. K.; Raghavan, S. C.; Karki, S. S. 2-(4-Chlorobenzyl)-6-Arylimidazo[2,1-b][1,3,4]Thiadiazoles: Synthesis, Cytotoxic Activity and Mechanism of Action. *Eur J Med Chem* **2014**, *84*, 687–697. https://doi.org/10.1016/j.ejmech.2014.07.054.

(19) Cascioferro, S.; Attanzio, A.; Di Sarno, V.; Musella, S.; Tesoriere, L.; Cirrincione, G.; Diana, P.; Parrino, B. New 1,2,4-Oxadiazole Nortopsentin Derivatives with Cytotoxic Activity. *Mar Drugs* **2019**, *17* (1). https://doi.org/10.3390/md17010035.

(20) Parrino, B.; Attanzio, A.; Spanò, V.; Cascioferro, S.; Montalbano, A.; Barraja, P.; Tesoriere, L.; Diana, P.; Cirrincione, G.; Carbone, A. Synthesis, Antitumor Activity and CDK1 Inhibiton of New Thiazole Nortopsentin Analogues. *Eur J Med Chem* **2017**, *138*, 371–383. https://doi.org/10.1016/j.ejmech.2017.06.052.

(21) Spanò, V.; Attanzio, A.; Cascioferro, S.; Carbone, A.; Montalbano, A.; Barraja, P.; Tesoriere, L.; Cirrincione, G.; Diana, P.; Parrino, B. Synthesis and Antitumor Activity of New Thiazole Nortopsentin Analogs. *Mar Drugs* **2016**, *14* (12). https://doi.org/10.3390/md14120226.

(22) Parrino, B.; Carbone, A.; Di Vita, G.; Ciancimino, C.; Attanzio, A.; Spanò, V.; Montalbano, A.; Barraja, P.; Tesoriere, L.; Livrea, M. A.; et al. 3-[4-(1H-Indol-3-Yl)-1,3-Thiazol-2-Yl]-1H-Pyrrolo[2,3-b]Pyridines, Nortopsentin Analogues with Antiproliferative Activity. *Mar Drugs* **2015**, *13* (4), 1901–1924. https://doi.org/10.3390/md13041901.

(23) Carbone, A.; Parrino, B.; Di Vita, G.; Attanzio, A.; Spanò, V.; Montalbano, A.; Barraja, P.; Tesoriere, L.; Livrea, M. A.; Diana, P.; et al. Synthesis and Antiproliferative Activity of Thiazolyl-Bis-Pyrrolo[2,3-b]Pyridines and Indolyl-Thiazolyl-Pyrrolo[2,3-c]Pyridines, Nortopsentin Analogues. *Mar Drugs* **2015**, *13* (1), 460–492. https://doi.org/10.3390/md13010460.

(24) Diana, P.; Stagno, A.; Barraja, P.; Montalbano, A.; Carbone, A.; Parrino, B.; Cirrincione, G. Synthesis of the New Ring System Pyrrolizino[2,3-b]Indol-4(5H)-One. *Tetrahedron* **2011**, *67*, 3374–3379. https://doi.org/10.1016/j.tet.2011.03.060.

(25) Barraja, P.; Caracausi, L.; Diana, P.; Spanò, V.; Montalbano, A.; Carbone, A.; Parrino, B.; Cirrincione, G. Synthesis and Antiproliferative Activity of the Ring System

[1,2]Oxazolo[4,5-g]Indole. *ChemMedChem* **2012**, *7* (11), 1901–1904. https://doi.org/10.1002/cmdc.201200296.

(26) Diana, P.; Stagno, A.; Barraja, P.; Carbone, A.; Parrino, B.; Dall'Acqua, F.; Vedaldi, D.; Salvador, A.; Brun, P.; Castagliuolo, I.; et al. Synthesis of Triazenoazaindoles: A New Class of Triazenes with Antitumor Activity. *ChemMedChem* **2011**, *6* (7), 1291–1299. https://doi.org/10.1002/cmdc.201100027.

(27) Carbone, A.; Pennati, M.; Parrino, B.; Lopergolo, A.; Barraja, P.; Montalbano, A.; Spanò, V.; Sbarra, S.; Doldi, V.; De Cesare, M.; et al. Novel 1H-Pyrrolo[2,3-b]Pyridine Derivative Nortopsentin Analogues: Synthesis and Antitumor Activity in Peritoneal Mesothelioma Experimental Models. *J. Med. Chem.* **2013**, *56* (17), 7060–7072. https://doi.org/10.1021/jm400842x.

(28) Li Petri, G.; Cascioferro, S.; El Hassouni, B.; Carbone, D.; Parrino, B.; Cirrincione, G.; Peters, G. J.; Diana, P.; Giovannetti, E. Biological Evaluation of the Antiproliferative and Anti-Migratory Activity of a Series of 3-(6-Phenylimidazo[2,1-b][1,3,4]Thiadiazol-2-Yl)-1H-Indole Derivatives Against Pancreatic Cancer Cells. *Anticancer Res.* **2019**, *39* (7), 3615–3620. https://doi.org/10.21873/anticanres.13509.

(29) Parrino, B.; Carbone, A.; Ciancimino, C.; Spanò, V.; Montalbano, A.; Barraja, P.; Cirrincione, G.; Diana, P.; Sissi, C.; Palumbo, M.; et al. Water-Soluble Isoindolo[2,1-a]Quinoxalin-6-Imines: In Vitro Antiproliferative Activity and Molecular Mechanism(s) of Action. *Eur J Med Chem* **2015**, *94*, 149–162. https://doi.org/10.1016/j.ejmech.2015.03.005.

(30) Parrino, B.; Ullo, S.; Attanzio, A.; Cascioferro, S.; Spanò, V.; Carbone, A.; Montalbano, A.; Barraja, P.; Cirrincione, G.; Tesoriere, L.; et al. Synthesis of 5H-Pyrido[3,2-b]Pyrrolizin-5-One Tripentone Analogs with Antitumor Activity. *Eur J Med Chem* **2018**, *158*, 236–246. https://doi.org/10.1016/j.ejmech.2018.09.017.

(31) Parrino, B.; Ullo, S.; Attanzio, A.; Spanò, V.; Cascioferro, S.; Montalbano, A.; Barraja, P.; Tesoriere, L.; Cirrincione, G.; Diana, P. New Tripentone Analogs with Antiproliferative Activity. *Molecules* **2017**, *22* (11). https://doi.org/10.3390/molecules22112005.

(32) Parrino, B.; Carbone, A.; Spanò, V.; Montalbano, A.; Giallombardo, D.; Barraja, P.; Attanzio, A.; Tesoriere, L.; Sissi, C.; Palumbo, M.; et al. Aza-Isoindolo and Isoindolo-Azaquinoxaline Derivatives with Antiproliferative Activity. *Eur J Med Chem* **2015**, *94*, 367–377. https://doi.org/10.1016/j.ejmech.2015.03.009.

(33) Parrino, B.; Carbone, A.; Muscarella, M.; Spanò, V.; Montalbano, A.; Barraja, P.; Salvador, A.; Vedaldi, D.; Cirrincione, G.; Diana, P. 11H-Pyrido[3′,2′:4,5]Pyrrolo[3,2-c]Cinnoline and Pyrido[3′,2′:4,5]Pyrrolo[1,2-c][1,2,3]Benzotriazine: Two New Ring Systems with Antitumor Activity. *J. Med. Chem.* **2014**, *57* (22), 9495–9511. https://doi.org/10.1021/jm501244f.

(34) Parrino, B.; Ciancimino, C.; Carbone, A.; Spano', V.; Montalbano, A.; Barraja, P.; Cirrincione, G.; Diana, P. Synthesis of Isoindolo[1,4]Benzoxazinone and Isoindolo[1,5]Benzoxazepine: Two New Ring Systems of Pharmaceutical Interest. **2015**, *71* (39), 7332–7338. https://doi.org/10.1016/j.tet.2015.04.083.

(35) Montalbano, A.; Parrino, B.; Diana, P.; Barraja, P.; Carbone, A.; Spanò, V.; Cirrincione, G. Synthesis of the New Oligopeptide Pyrrole Derivative Isonetropsin and Its One Pyrrole Unit Analogue. *Tetrahedron* **2013**, *69*, 2550–2554. https://doi.org/10.1016/j.tet.2013.01.076.

(36) Giovannetti, E.; van der Borden, C. L.; Frampton, A. E.; Ali, A.; Firuzi, O.; Peters, G. J. Never Let It Go: Stopping Key Mechanisms Underlying Metastasis to Fight Pancreatic Cancer. *Semin. Cancer Biol.* **2017**, *44*, 43–59. https://doi.org/10.1016/j.semcancer.2017.04.006.

(37) Nevala-Plagemann, C.; Hidalgo, M.; Garrido-Laguna, I. From State-of-the-Art Treatments to Novel Therapies for Advanced-Stage Pancreatic Cancer. *Nat Rev Clin Oncol* **2019**. https://doi.org/10.1038/s41571-019-0281-6.

(38) Razi, E.; Radak, M.; Mahjoubin-Tehran, M.; Talebi, S.; Shafiee, A.; Hajighadimi, S.; Moradizarmehri, S.; Sharifi, H.; Mousavi, N.; Sarvizadeh, M.; et al. Cancer Stem Cells as Therapeutic Targets of Pancreatic Cancer. *Fundam Clin Pharmacol* **2019**. https://doi.org/10.1111/fcp.12521.

(39) Mirzaei, H. R.; Sahebkar, A.; Salehi, R.; Nahand, J. S.; Karimi, E.; Jaafari, M. R.; Mirzaei, H. Boron Neutron Capture Therapy: Moving toward Targeted Cancer Therapy. *J Cancer Res Ther* **2016**, *12* (2), 520–525. https://doi.org/10.4103/0973-1482.176167.

(40) Mirzaei, H. R.; Mirzaei, H.; Lee, S. Y.; Hadjati, J.; Till, B. G. Prospects for Chimeric Antigen Receptor (CAR) Γδ T Cells: A Potential Game Changer for Adoptive T Cell Cancer Immunotherapy. *Cancer Lett.* **2016**, *380* (2), 413–423. https://doi.org/10.1016/j.canlet.2016.07.001.

(41) Amrutkar, M.; Gladhaug, I. P. Pancreatic Cancer Chemoresistance to Gemcitabine. *Cancers* **2017**, *9* (11), 157. https://doi.org/10.3390/cancers9110157.

(42) Sciarrillo, R.; Wojtuszkiewicz, A.; Kooi, I. E.; Gómez, V. E.; Boggi, U.; Jansen, G.; Kaspers, G.-J.; Cloos, J.; Giovannetti, E. Using RNA-Sequencing to Detect Novel Splice Variants Related to Drug Resistance in In Vitro Cancer Models. *J Vis Exp* **2016**, No. 118. https://doi.org/10.3791/54714.

(43) Le Large, T. Y. S.; El Hassouni, B.; Funel, N.; Kok, B.; Piersma, S. R.; Pham, T. V.; Olive, K. P.; Kazemier, G.; van Laarhoven, H. W. M.; Jimenez, C. R.; et al. Proteomic Analysis of Gemcitabine-Resistant Pancreatic Cancer Cells Reveals That Microtubule-Associated Protein 2 Upregulation Associates with Taxane Treatment. *Ther Adv Med Oncol* **2019**, *11*, 1758835919841233. https://doi.org/10.1177/1758835919841233.

(44) Avan, A.; Caretti, V.; Funel, N.; Galvani, E.; Maftouh, M.; Honeywell, R. J.; Lagerweij, T.; Van Tellingen, O.; Campani, D.; Fuchs, D.; et al. Crizotinib Inhibits Metabolic Inactivation of Gemcitabine in C-Met-Driven Pancreatic Carcinoma. *Cancer Res.* **2013**, *73* (22), 6745–6756. https://doi.org/10.1158/0008-5472.CAN-13-0837.

(45) Sant, S.; Johnston, P. A. The Production of 3D Tumor Spheroids for Cancer Drug Discovery. *Drug Discov Today Technol* **2017**, *23*, 27–36. https://doi.org/10.1016/j.ddtec.2017.03.002.

(46) Firuzi, O.; Che, P. P.; El Hassouni, B.; Buijs, M.; Coppola, S.; Löhr, M.; Funel, N.; Heuchel, R.; Carnevale, I.; Schmidt, T.; et al. Role of C-MET Inhibitors in Overcoming Drug Resistance in Spheroid Models of Primary Human Pancreatic Cancer and Stellate Cells. *Cancers (Basel)* **2019**, *11* (5). https://doi.org/10.3390/cancers11050638.

(47) Thiery, J. P.; Acloque, H.; Huang, R. Y. J.; Nieto, M. A. Epithelial-Mesenchymal Transitions in Development and Disease. *Cell* **2009**, *139* (5), 871–890. https://doi.org/10.1016/j.cell.2009.11.007.

(48) Puisieux, A.; Brabletz, T.; Caramel, J. Oncogenic Roles of EMT-Inducing Transcription Factors. *Nature Cell Biology* **2014**, *16* (6), 488–494. https://doi.org/10.1038/ncb2976.

(49) Valastyan, S.; Weinberg, R. A. Tumor Metastasis: Molecular Insights and Evolving Paradigms. *Cell* **2011**, *147* (2), 275–292. https://doi.org/10.1016/j.cell.2011.09.024.

(50) Batlle, E.; Sancho, E.; Francí, C.; Domínguez, D.; Monfar, M.; Baulida, J.; García de Herreros, A. The Transcription Factor Snail Is a Repressor of *E-Cadherin* Gene Expression in Epithelial Tumour Cells. *Nature Cell Biology* **2000**, *2* (2), 84–89. https://doi.org/10.1038/35000034.

(51) Cano, A.; Pérez-Moreno, M. A.; Rodrigo, I.; Locascio, A.; Blanco, M. J.; del Barrio, M. G.; Portillo, F.; Nieto, M. A. The Transcription Factor Snail Controls Epithelial–

Mesenchymal Transitions by Repressing E-Cadherin Expression. *Nature Cell Biology* **2000**, *2* (2), 76–83. https://doi.org/10.1038/35000025.

(52) Hajra, K. M.; Chen, D. Y.-S.; Fearon, E. R. The SLUG Zinc-Finger Protein Represses E-Cadherin in Breast Cancer. *Cancer Res* **2002**, *62* (6), 1613–1618.

(53) N-Cadherin Expression and Epithelial-Mesenchymal Transition in Pancreatic Carcinoma | Clinical Cancer Research http://clincancerres.aacrjournals.org/content/10/12/4125.long (accessed Mar 16, 2019).

(54) Wang, S.; Huang, S.; Sun, Y. L. Epithelial-Mesenchymal Transition in Pancreatic Cancer: A Review. *Biomed Res Int* **2017**, *2017*. https://doi.org/10.1155/2017/2646148.

(55) Meijer, L. L.; Garajová, I.; Caparello, C.; Le Large, T. Y. S.; Frampton, A. E.; Vasile, E.; Funel, N.; Kazemier, G.; Giovannetti, E. Plasma MiR-181a-5p Downregulation Predicts Response and Improved Survival After FOLFIRINOX in Pancreatic Ductal Adenocarcinoma. *Ann. Surg.* **2018**. https://doi.org/10.1097/SLA.0000000000003084.

(56) Hall, J. E.; Fu, W.; Schaller, M. D. Chapter Five - Focal Adhesion Kinase: Exploring FAK Structure to Gain Insight into Function. In *International Review of Cell and Molecular Biology*; Jeon, K. W., Ed.; Academic Press, 2011; Vol. 288, pp 185–225. https://doi.org/10.1016/B978-0-12-386041-5.00005-4.

(57) Zhou, J.; Yi, Q.; Tang, L. The Roles of Nuclear Focal Adhesion Kinase (FAK) on Cancer: A Focused Review. *J. Exp. Clin. Cancer Res.* **2019**, *38* (1), 250. https://doi.org/10.1186/s13046-019-1265-1.

(58) Kanteti, R.; Batra, S. K.; Lennon, F. E.; Salgia, R. FAK and Paxillin, Two Potential Targets in Pancreatic Cancer. *Oncotarget* **2016**, *7* (21), 31586–31601. https://doi.org/10.18632/oncotarget.8040.

(59) Ho, J.-N.; Jun, W.; Choue, R.; Lee, J. I3C and ICZ Inhibit Migration by Suppressing the EMT Process and FAK Expression in Breast Cancer Cells. *Mol Med Rep* **2013**, *7* (2), 384–388. https://doi.org/10.3892/mmr.2012.1198.

(60) Carbone, A.; Parrino, B.; Cusimano, M. G.; Spanò, V.; Montalbano, A.; Barraja, P.; Schillaci, D.; Cirrincione, G.; Diana, P.; Cascioferro, S. New Thiazole Nortopsentin Analogues Inhibit Bacterial Biofilm Formation. *Mar Drugs* **2018**, *16* (8). https://doi.org/10.3390/md16080274.

(61) Giovannetti, E.; Funel, N.; Peters, G. J.; Chiaro, M. D.; Erozenci, L. A.; Vasile, E.; Leon, L. G.; Pollina, L. E.; Groen, A.; Falcone, A.; et al. MicroRNA-21 in Pancreatic Cancer: Correlation with Clinical Outcome and Pharmacologic Aspects Underlying Its Role in

the Modulation of Gemcitabine Activity. *Cancer Res* **2010**, *70* (11), 4528–4538. https://doi.org/10.1158/0008-5472.CAN-09-4467.

(62) Massihnia, D.; Avan, A.; Funel, N.; Maftouh, M.; van Krieken, A.; Granchi, C.; Raktoe, R.; Boggi, U.; Aicher, B.; Minutolo, F.; et al. Phospho-Akt Overexpression Is Prognostic and Can Be Used to Tailor the Synergistic Interaction of Akt Inhibitors with Gemcitabine in Pancreatic Cancer. *Journal of Hematology & Oncology* **2017**, *10* (1), 9. https://doi.org/10.1186/s13045-016-0371-1.

(63) Sciarrillo, R.; Wojtuszkiewicz, A.; El Hassouni, B.; Funel, N.; Gandellini, P.; Lagerweij, T.; Buonamici, S.; Blijlevens, M.; Zeeuw van der Laan, E. A.; Zaffaroni, N.; et al. Splicing Modulation as Novel Therapeutic Strategy against Diffuse Malignant Peritoneal Mesothelioma. *EBioMedicine* **2019**, *39*, 215–225. https://doi.org/10.1016/j.ebiom.2018.12.025.

(64) Garajová, I.; Le Large, T. Y. S.; Giovannetti, E.; Kazemier, G.; Biasco, G.; Peters, G. J. The Role of MicroRNAs in Resistance to Current Pancreatic Cancer Treatment: Translational Studies and Basic Protocols for Extraction and PCR Analysis. In *Cancer Drug Resistance: Overviews and Methods*; Rueff, J., Rodrigues, A. S., Eds.; Methods in Molecular Biology; Springer New York: New York, NY, 2016; pp 163–187. https://doi.org/10.1007/978-1-4939-3347-1_10.

(65) La Monica, S.; Caffarra, C.; Saccani, F.; Galvani, E.; Galetti, M.; Fumarola, C.; Bonelli, M.; Cavazzoni, A.; Cretella, D.; Sirangelo, R.; et al. Gefitinib Inhibits Invasive Phenotype and Epithelial-Mesenchymal Transition in Drug-Resistant NSCLC Cells with MET Amplification. *PLoS ONE* **2013**, *8* (10), e78656. https://doi.org/10.1371/journal.pone.0078656.

(66) Giovannetti, E.; Labots, M.; Dekker, H.; Galvani, E.; Lind, J. S. W.; Sciarrillo, R.; Honeywell, R.; Smit, E. F.; Verheul, H. M.; Peters, G. J. Molecular Mechanisms and Modulation of Key Pathways Underlying the Synergistic Interaction of Sorafenib with Erlotinib in Non-Small-Cell-Lung Cancer (NSCLC) Cells. *Curr. Pharm. Des.* **2013**, *19* (5), 927–939.

(67) Steen, N. V. D.; Potze, L.; Giovannetti, E.; Cavazzoni, A.; Ruijtenbeek, R.; Rolfo, C.; Pauwels, P.; Peters, G. J. Molecular Mechanism Underlying the Pharmacological Interactions of the Protein Kinase C-β Inhibitor Enzastaurin and Erlotinib in Non-Small Cell Lung Cancer Cells. *Am J Cancer Res* **2017**, *7* (4), 816–830.

Supplementary data

Supplementary data

Physicochemical properties

The goal of pharmaceutical chemistry is the design and development of new drugs with a higher specificity for a target and the reduction of adverse drug reactions (ADRs). To date, many databases allow to predict the in silico behaviour of new chemical entities. For instance, SwissADME, a free web tool (http://www.swissadme.ch/), can predict the pharmacokinetics (PK) and pharmacodynamic (PD) properties of a designed compound. According to the Lipinski's rule of five (RO5), a drug-like compound should have the following physicochemical properties: molecular weight (MW) less than 500 Da, a logP values (hydrophobic characteristic) less than 5, hydrogen bond donors (HBD) no more than 5, hydrogen bond acceptor (HBA) no more than 1.[1] Furthermore, Veber and collaborators demonstrated that the reduction of rotatable bonds (RB) and the low polar surface area (PSA) contribute to the good oral bioavailability.[2] Other two parameters that have to be taken in consideration, include PSA less than or equal to 140 Å and RB less than 10.[2] Moreover, it is necessary to combine these values to the value of the ABS, A Bioavailability Score, that is defined as 'the probability that a compound will have >10% bioavailability in rat or measurable Caco-2 permeability'. This value takes into consideration the physical properties of the drug-like compound at pH 6-7. ABS value is 0.55 if compound passes the RO5 and 0.17 if it fails.[3] Finally, gastrointestinal (GI) absorption values and the ability to overcome the blood-brain barrier (BBB) were also calculated, according to the BOILED-egg (Brain Or IntestinaL EstimateD permeation predictive model). The physicochemical and ADME properties of the compounds **12a**,**b**,**h** and **13g** are summarized in the Table 1. All compounds complied with Lipinski's rule of five (RO5), showed PSA values below 140 Å and RB less than 10. Furthermore, they presented a high degree of GI and low brain penetration. Finally, three out of four compounds were not P-gp substrate. In the table 2 we reported the SMILES

(Simplified Molecular Input Line Entry Specification) codes that we used to calculate the physicochemical properties of the compounds **12a**,**b**,**h** and **13g.**

Supplementary Table 1. Physicochemical and ADME properties of compounds (comp) **12a**,**b**,**h** and **13g.**

Comp	MW (g/mol) <500	H-bond acceptors <10	H-bond donors <5	Log P o/w <5	Violation Lipinski Rule of 5	PSA[a] ($Å^2$) <140	RB <10[b]	BBB[c]	GI[d]	BS[e]
12a	403.32	3	2	-0.71	0	98.49	2	NO	high	0.55
12b	417.35	3	1	-0.47	0	87.63	2	NO	high	0.55
12h	435.34	4	1	-0.09	0	87.63	2	NO	high	0.55
13g	340.40	3	1	3.03	0	102.46	2	NO	high	0.55

a PSA: Polar surface area. **b** RB: Rotable bonds. **c** BBB: blood-brain barrier.

d GI: Gastrointestinal absorption. **e** BS: Bioavailability Score.

Supplementary Table 2. List of Simplified Molecular Input Line Entry Specification (SMILES) of compounds (comp) **12a,b,h** and **13g**

Comp	**SMILES**
12a	Br.C1NC2=C(C=CC=C2)C1C1=NN2C=C(N=C2S1)C1=CSC=C1
12b	Br.CN1C=C(C2=NN3C=C(N=C3S2)C2=CSC=C2)C2=C1C=CC=C2
13g	FC1=CC2=C(NC=C2C2=NN3C=C(N=C3S2)C2=CSC=C2)C=C1
12h	Br.FC1=CC2=C(NC=C2C2=NN3C=C(N=C3S2)C2=CSC=C2)C=C1

Supplementary Table 3. Antiproliferative activity of compounds **12a** and **12b** on PDAC-3 tumor cells and Hs27 normal fibroblast cells.

	IC_{50}[a] (µM) ± SEM[b]	
Cell line	**12a**	**12b**
PDAC-3	1.7 ± 0.39	1.7 ± 0.27
Hs27	7.7 ± 0.45	12.3 ± 0.84

[a]The values are means ± SEM of three separate experiments.
[b]SEM: Standard Error of the Mean.

Supplementary Figure 1. Effects of the migration events of compounds **12a** and **12b** on primary PDAC-3 cells. (**A**) Percentages of migration at T=0, 4, 8, 20 and 24 hours from the treatment of PDAC-3 cells treated with compound **12a** and **12b** at concentration 4x IC_{50}. *Points*, mean values obtained from the means of at least four different scratch areas. All the *P* values were determined Student's t-test. ****p<0.0001, ***p<0.001, **p<0.01, *p<0.05

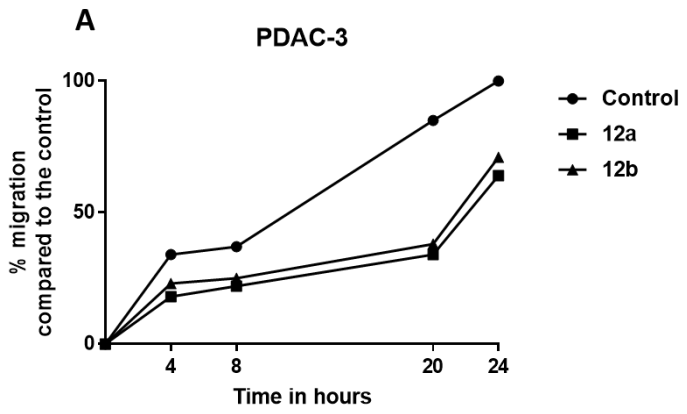

Table

	Compounds	
Time (h)	**12a**	**12b**
0	ns	ns
4	ns	*
8	ns	*
20	****	****
24	***	***

ns= not significant
****p<0.0001, ***p<0.001, **p<0.01, *p<0.05

Supplementary Figure 2. Modulation of protein levels expression key EMTs genes SNAIL-1, SNAIL-2, CDH1, CDH12, VIM and MMP2 in Panc-1 cells treated with compounds **12a** and **12b**. The protein levels were determined by western blot analysis after 24 hours of treatment at 5x IC_{50} value. All the *P* values were determined by Tukey's multiple comparisons test. ****p<0.0001, ***p<0.001, **p<0.01, *p<0.05

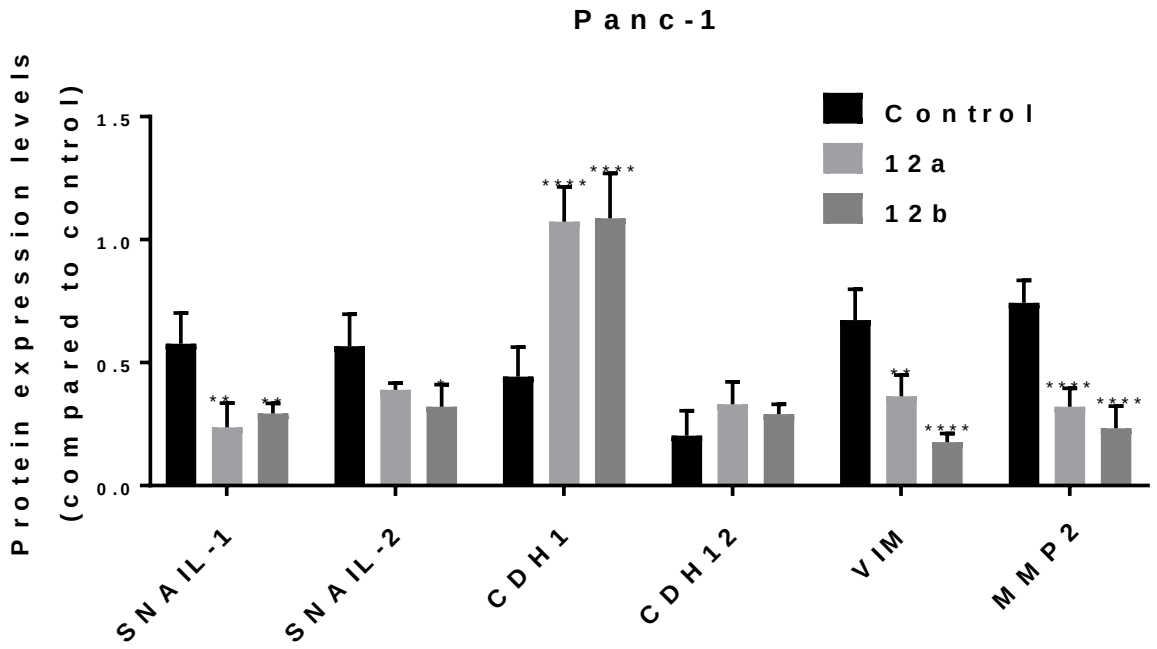

Supplementary Figure 3. Gelatine zymography analysis of media from Panc-1 cells incubated with serum-free medium for 24 hours. The enzymatic activity of MMP2 and MMP9 was determined by densitometric analysis. The cells are treated with the compounds **12a** and **12b** at concentration 5x IC_{50} value. All the P values were calculated with Tukey's multiple comparisons test. ****p<0.0001, *p<0.05.

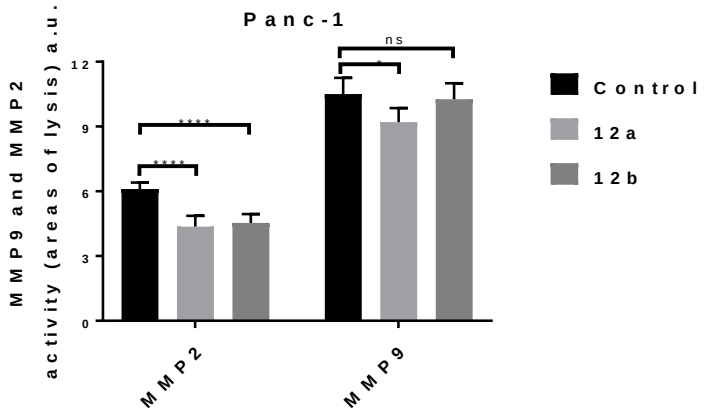

Supplementary Figure 4. Representative blots showing inhibition of FAK/PTK2 phosphorylation by compounds 12a and 12b in Capan-1 and SUIT-2 cells. The amount of pFAK was assessed in cell lysates after 24 h treatment with compounds 12a and 12b at 5x IC50s and compared to cell lysates from untreated cells (control). The blots shown are representative of 2 separate experiments, loading 20 μg protein. Loading control was GAPDH, as described previously [4].

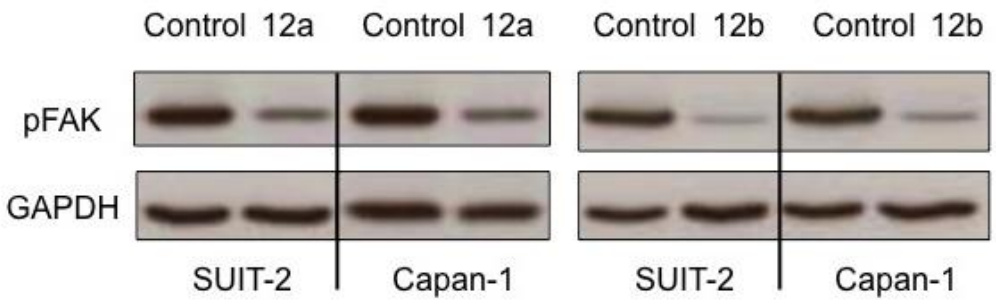

References

(1) Lipinski, C. A.; Lombardo, F.; Dominy, B. W.; Feeney, P. J. Experimental and Computational Approaches to Estimate Solubility and Permeability in Drug Discovery and Development Settings. *Adv. Drug Deliv. Rev.* **2001**, *46* (1–3), 3–26.

(2) Veber, D. F.; Johnson, S. R.; Cheng, H.-Y.; Smith, B. R.; Ward, K. W.; Kopple, K. D. Molecular Properties That Influence the Oral Bioavailability of Drug Candidates. *J. Med. Chem.* **2002**, *45* (12), 2615–2623.

(3) Martin, Y. C. A Bioavailability Score. *J. Med. Chem.* **2005**, *48* (9), 3164–3170. https://doi.org/10.1021/jm0492002.

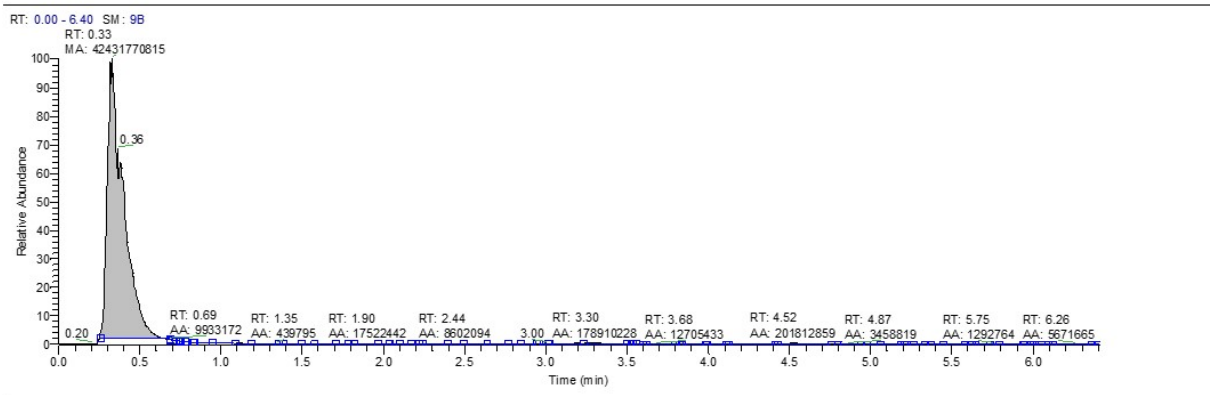

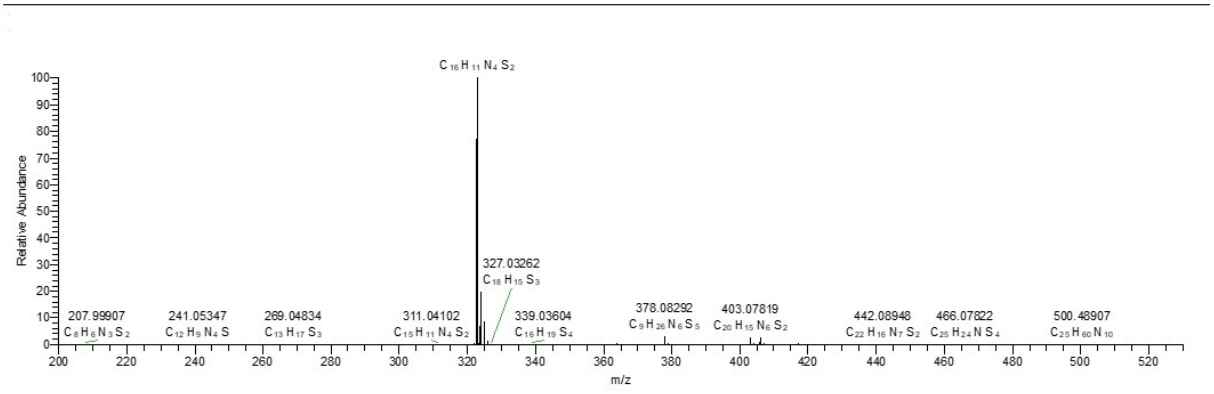

12a experimental mass -3.79 ppm with respect to theoretic mass

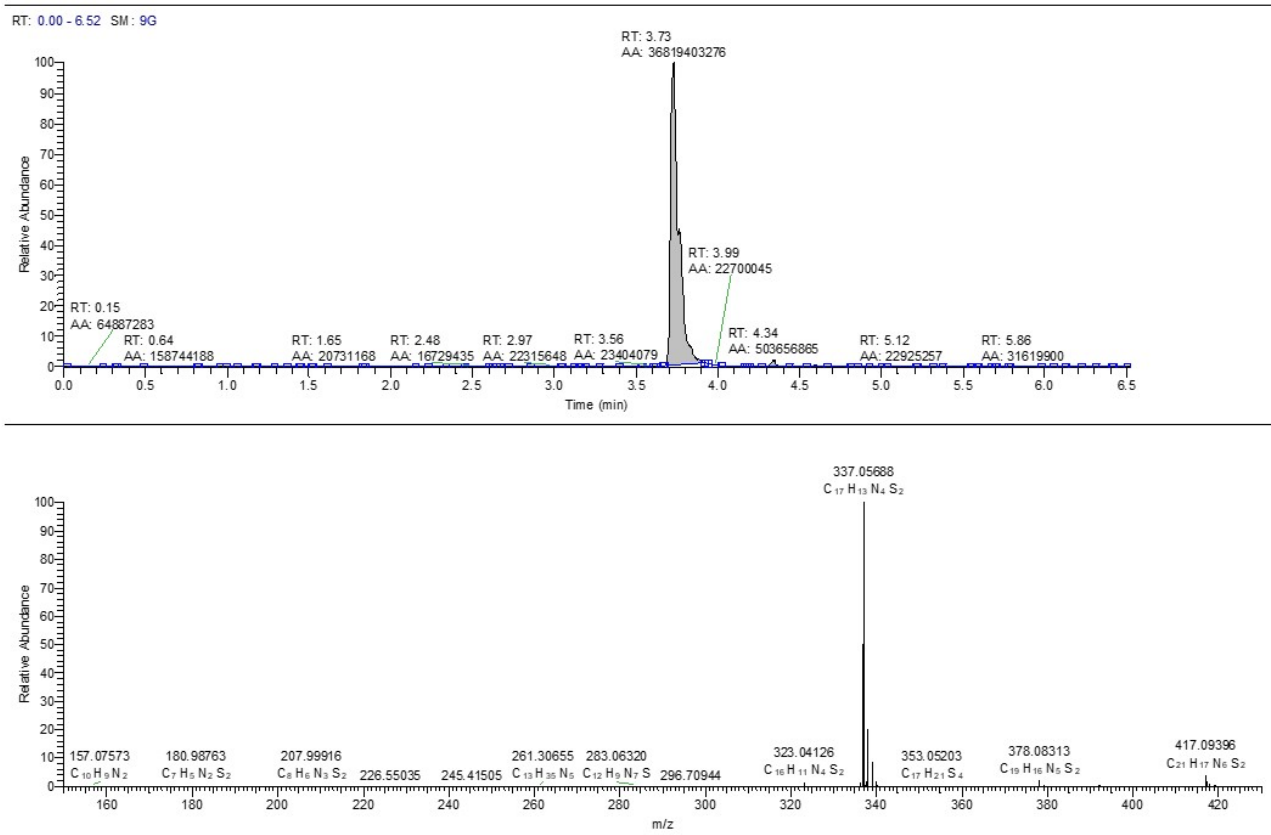

12b experimental mass -2.3ppm with respect to theoretic mass

Compound **12a** ^{1}H NMR

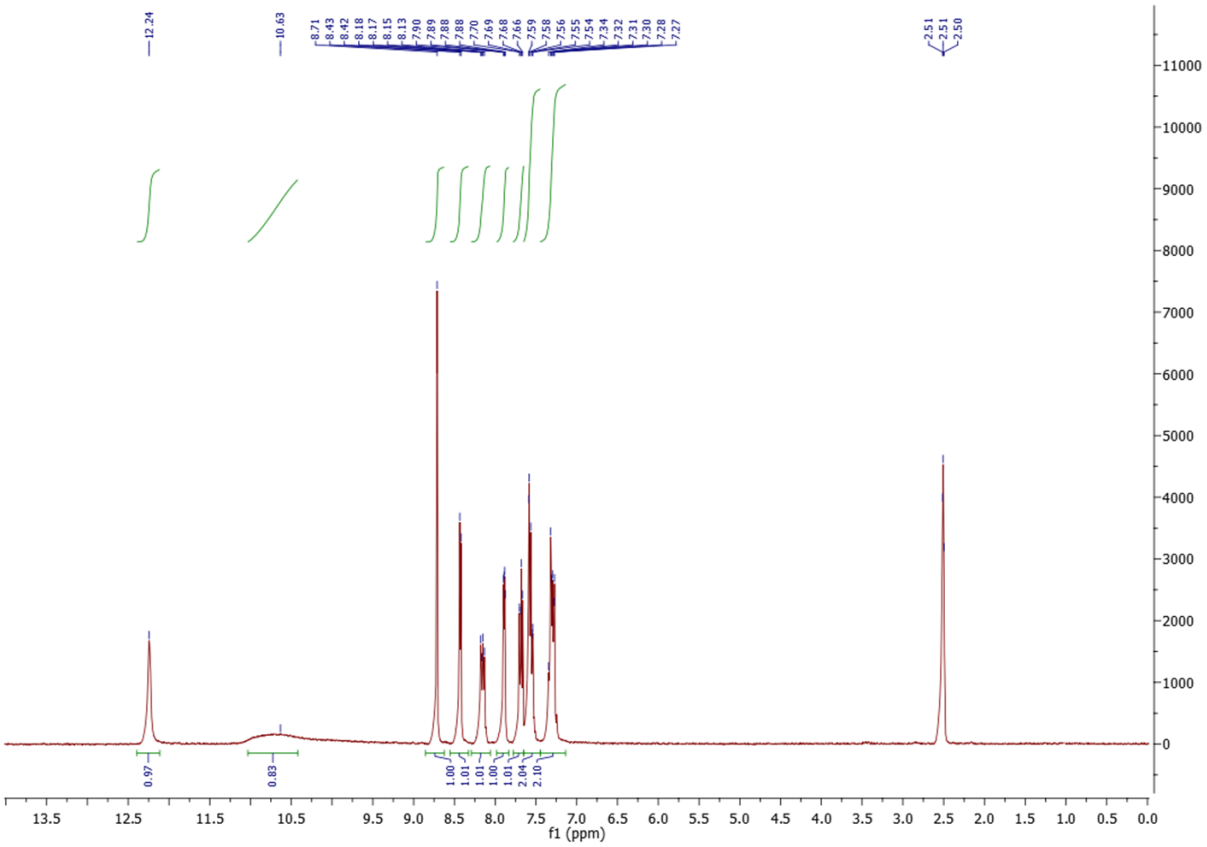

Compound **12a** ^{13}C NMR

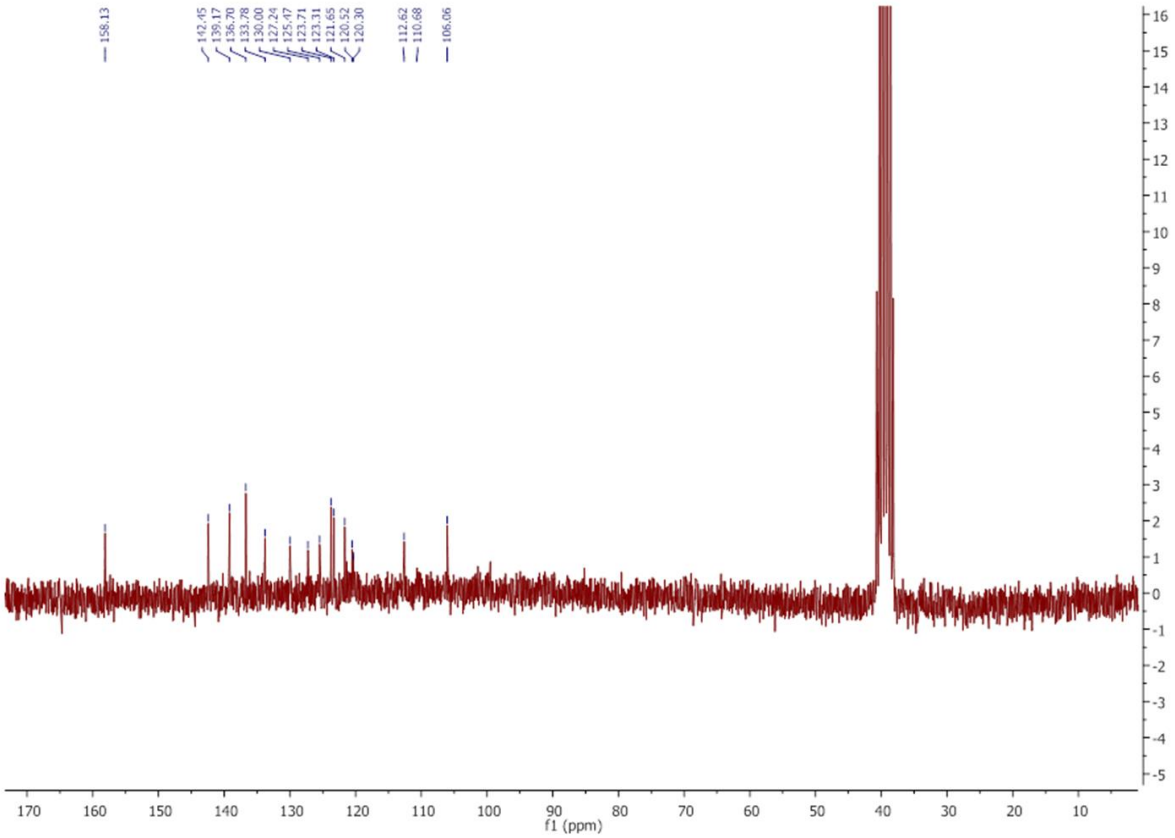

Compound **12b** ^{1}H NMR

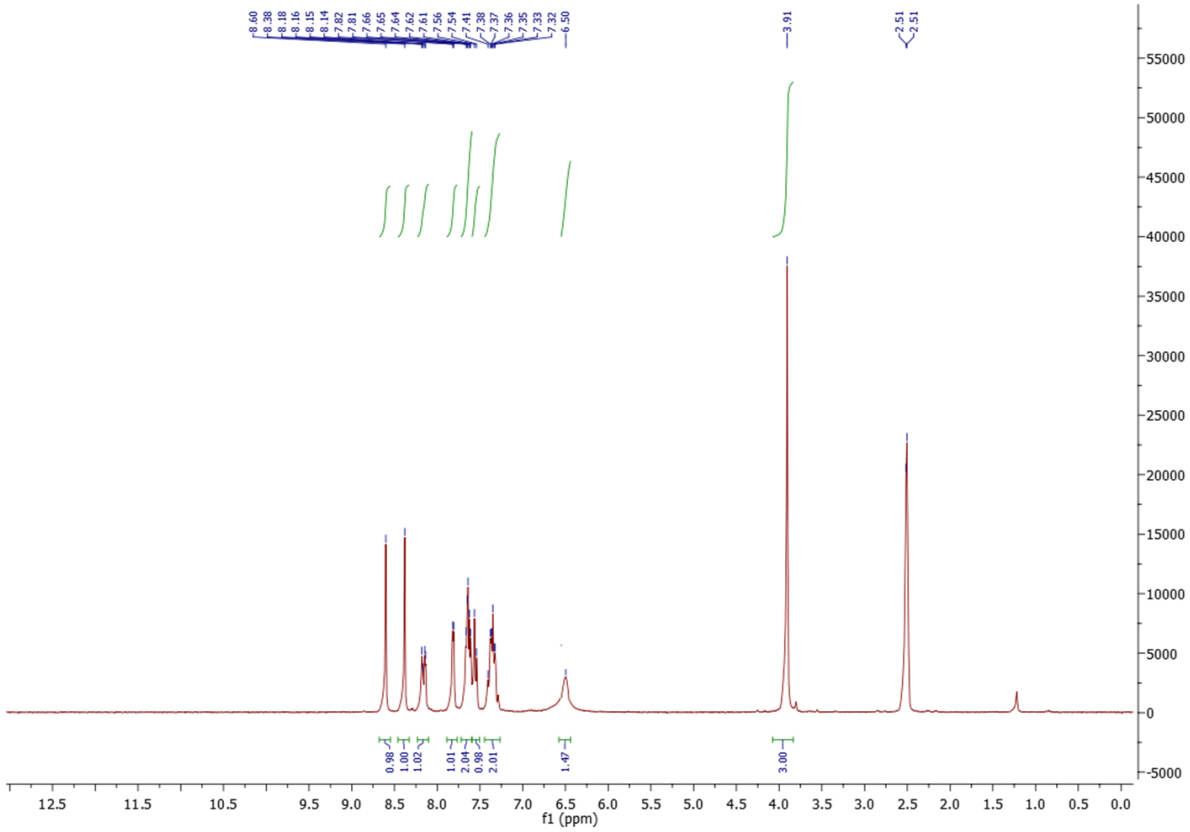

Compound **12b** ^{13}C NMR

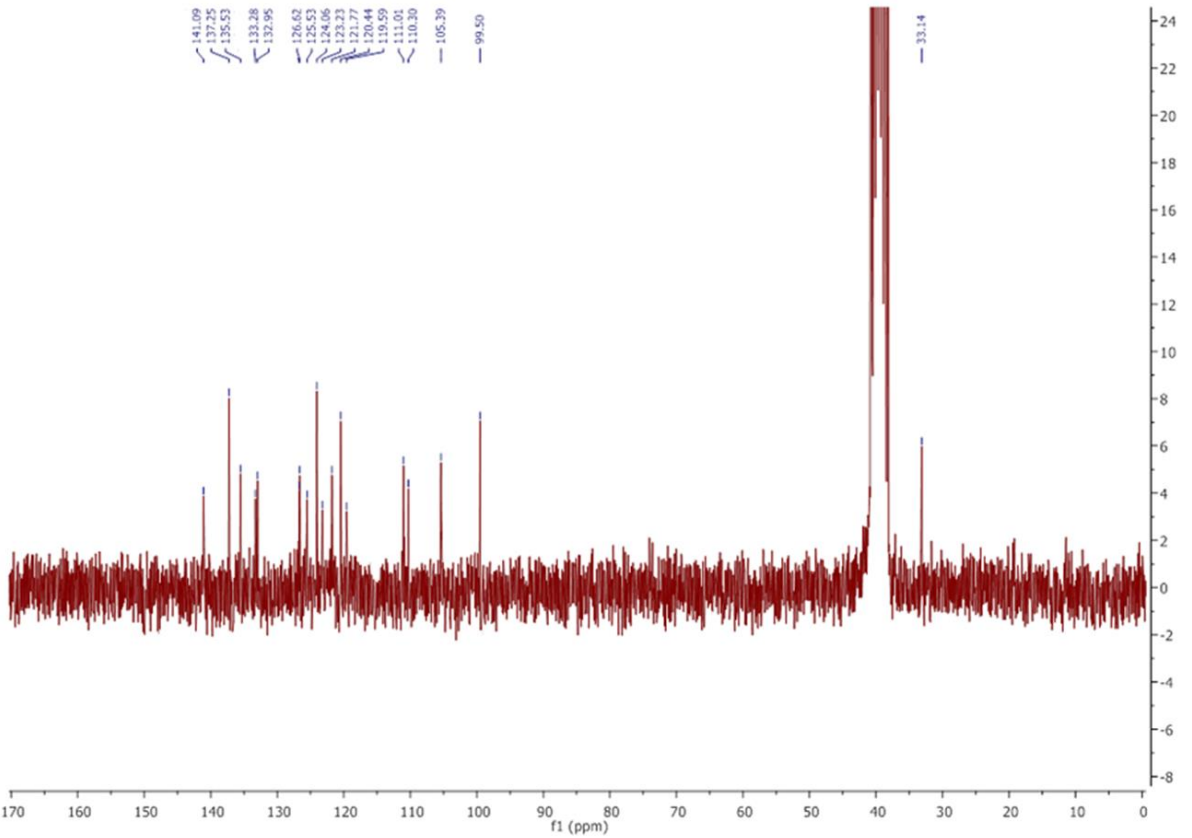

Compound **12h** ^{1}H NMR

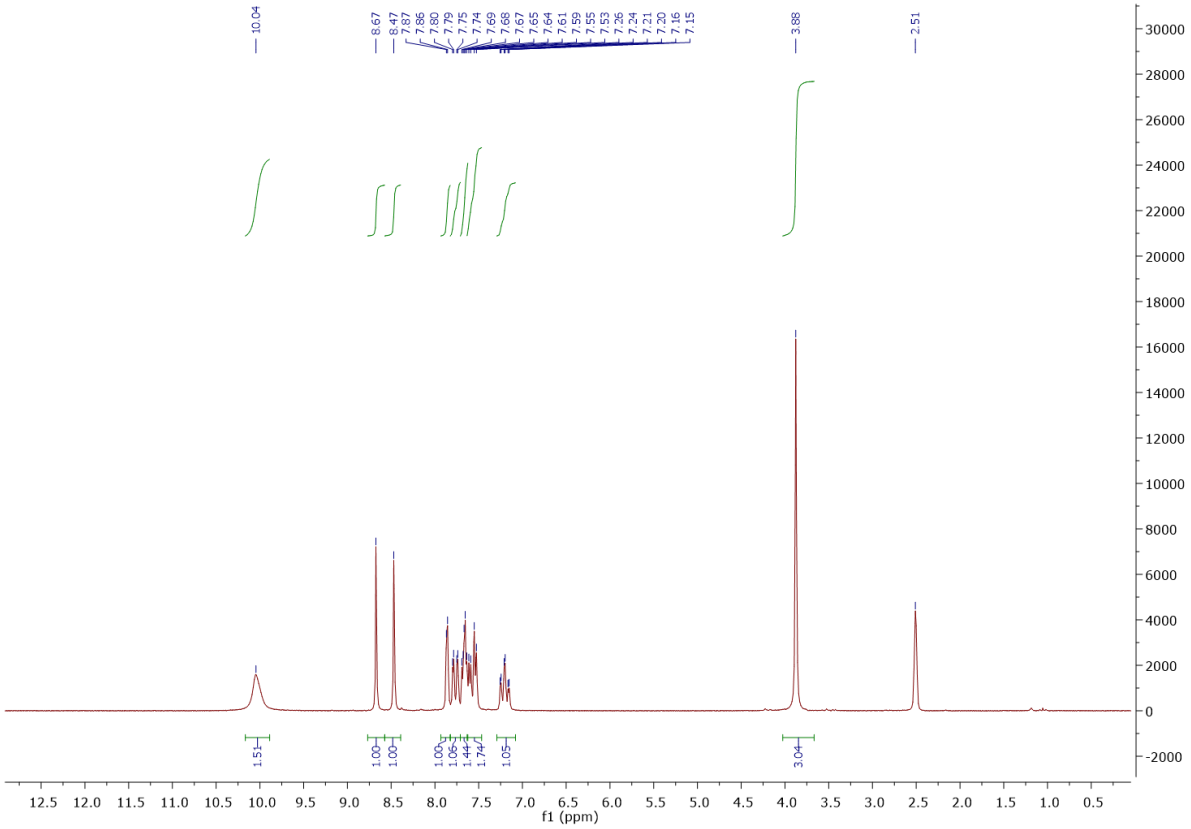

Compound **12h** ^{13}C NMR

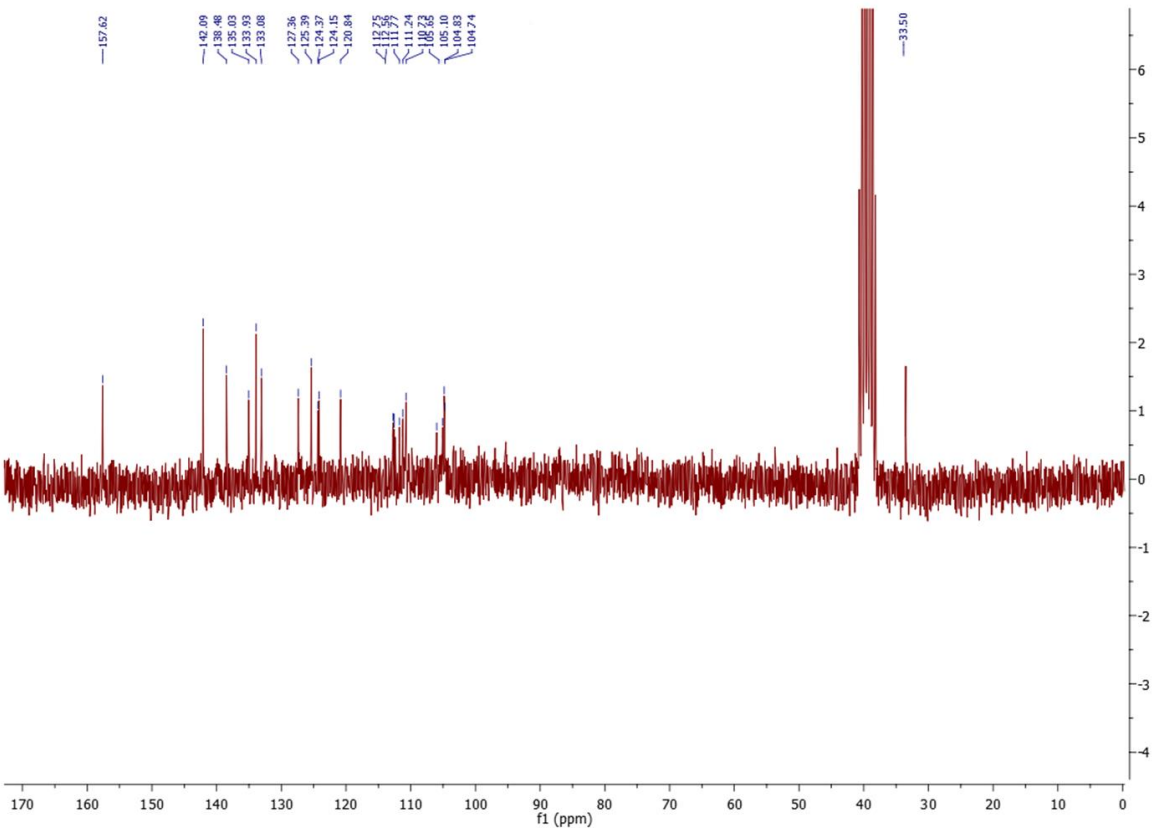

Compound **13g** ^{1}H NMR

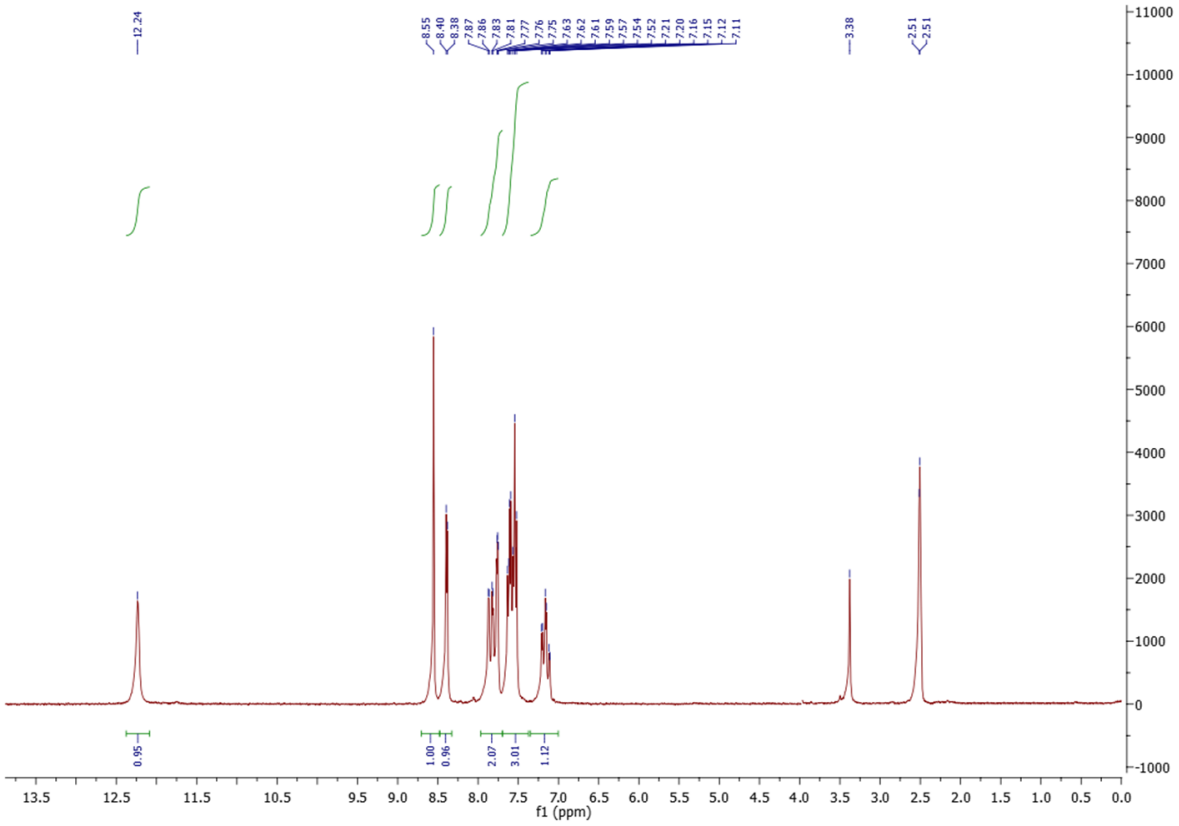

Compound **13g** ^{13}C NMR

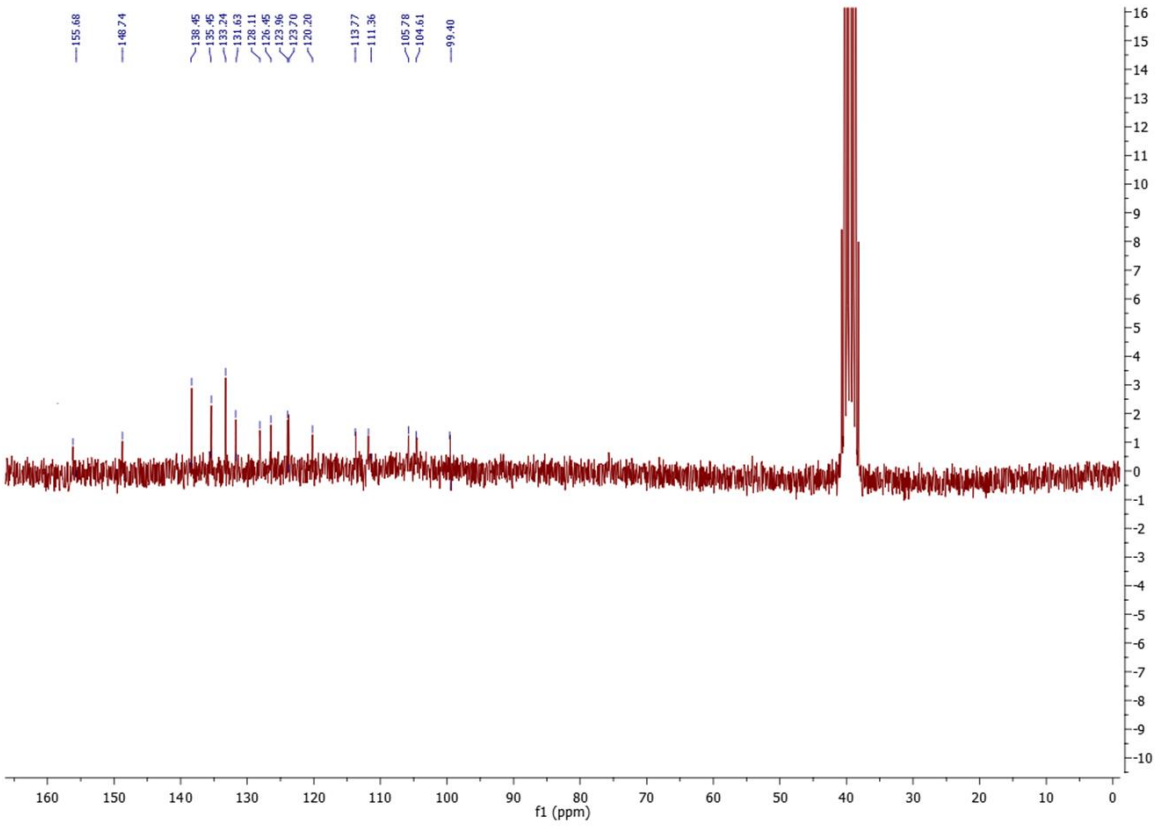

Compound **14k** ^{1}H NMR

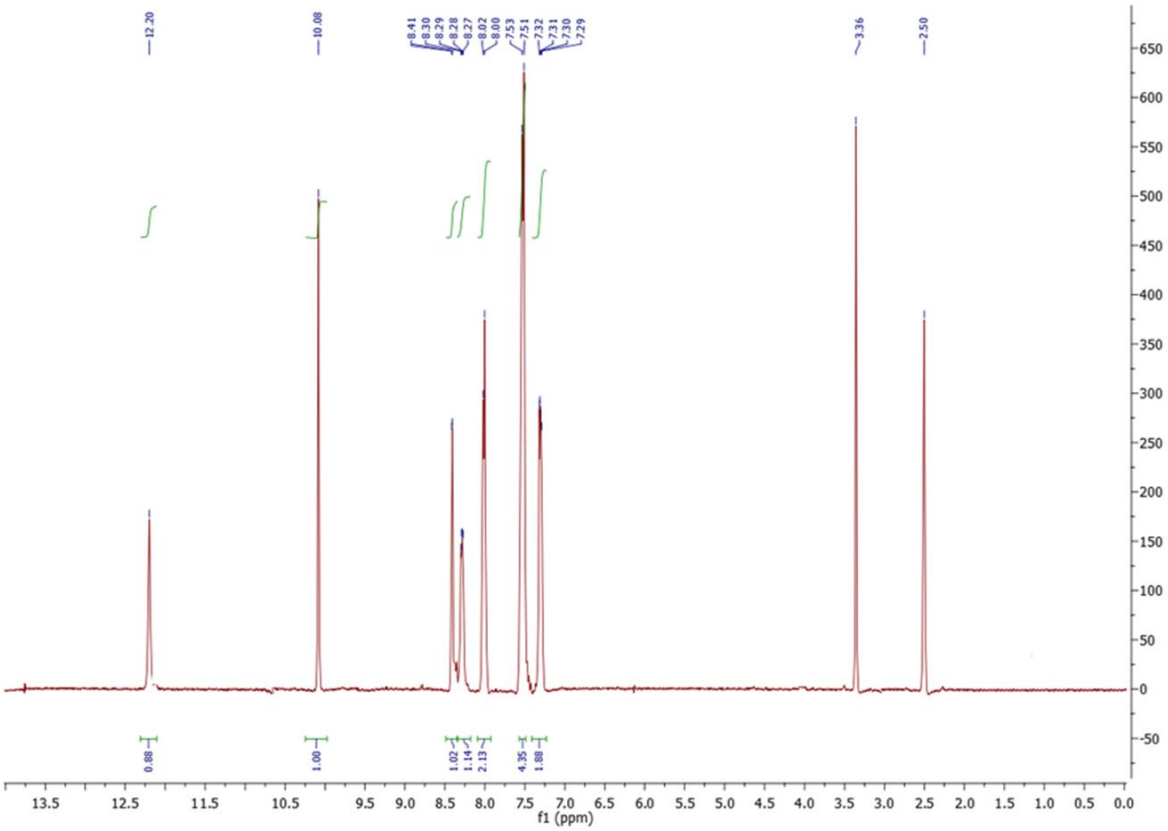

Compound **14k** ^{13}C NMR

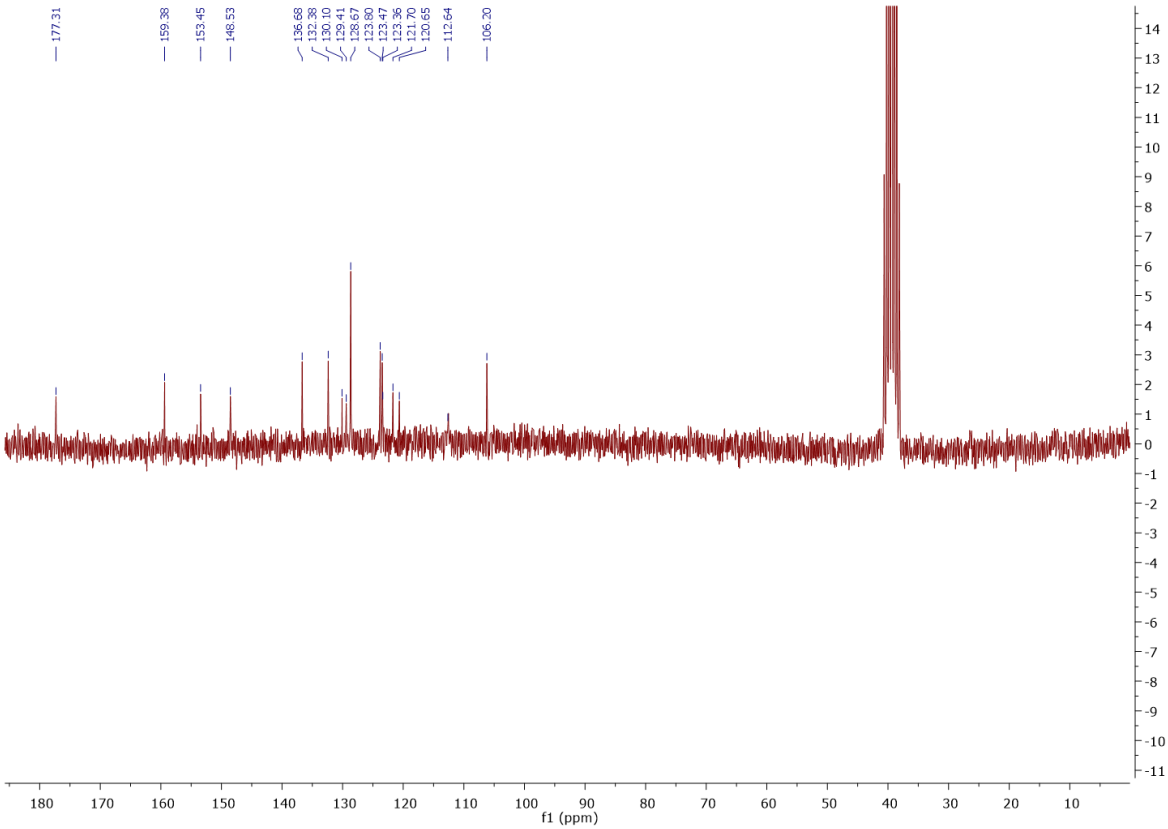

Compound **14p** ^{1}H NMR

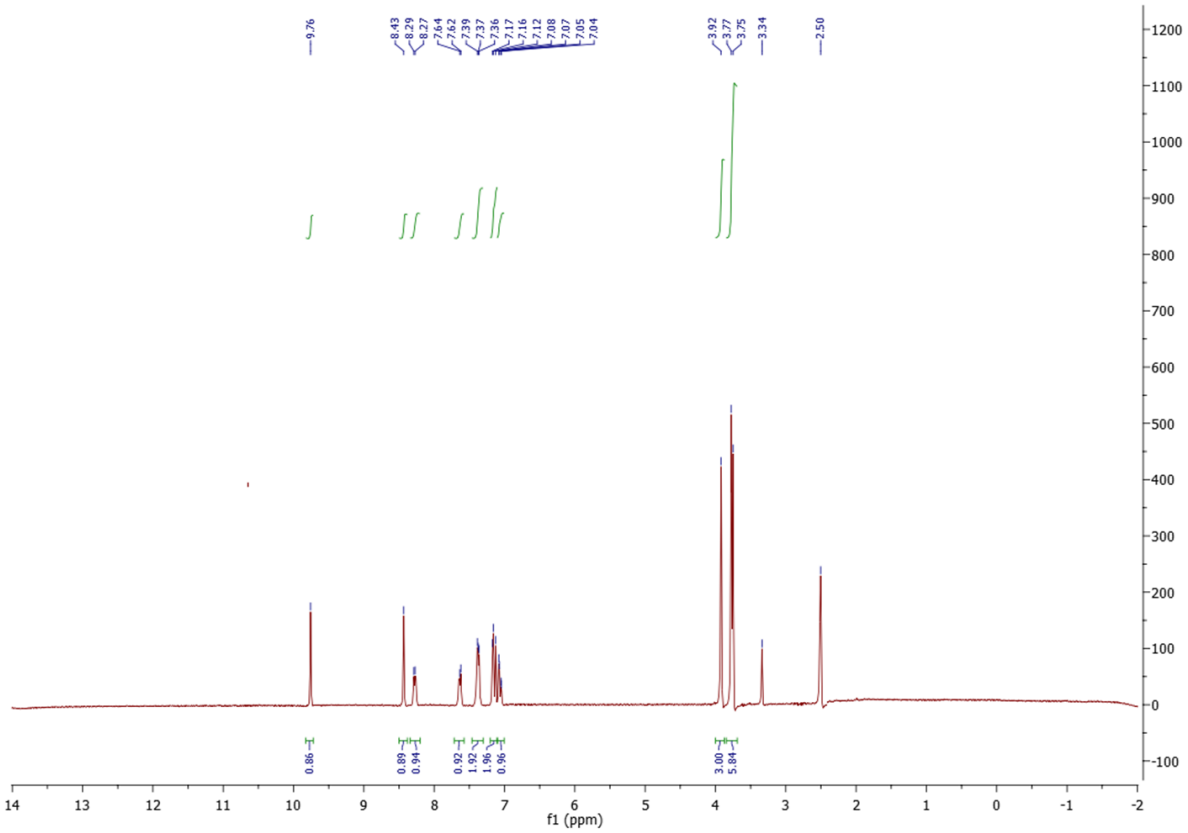

Compound **14p** ^{13}C NMR

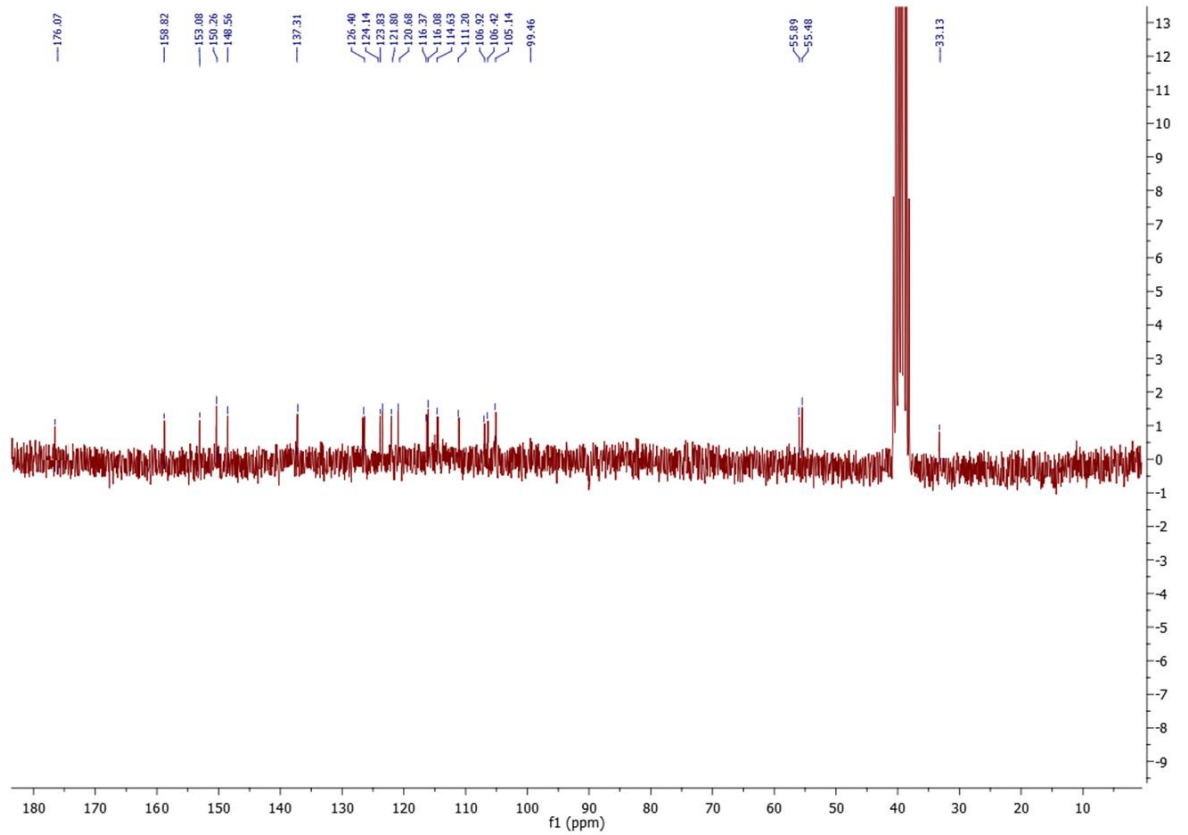

Compound **14q** ^{1}H NMR

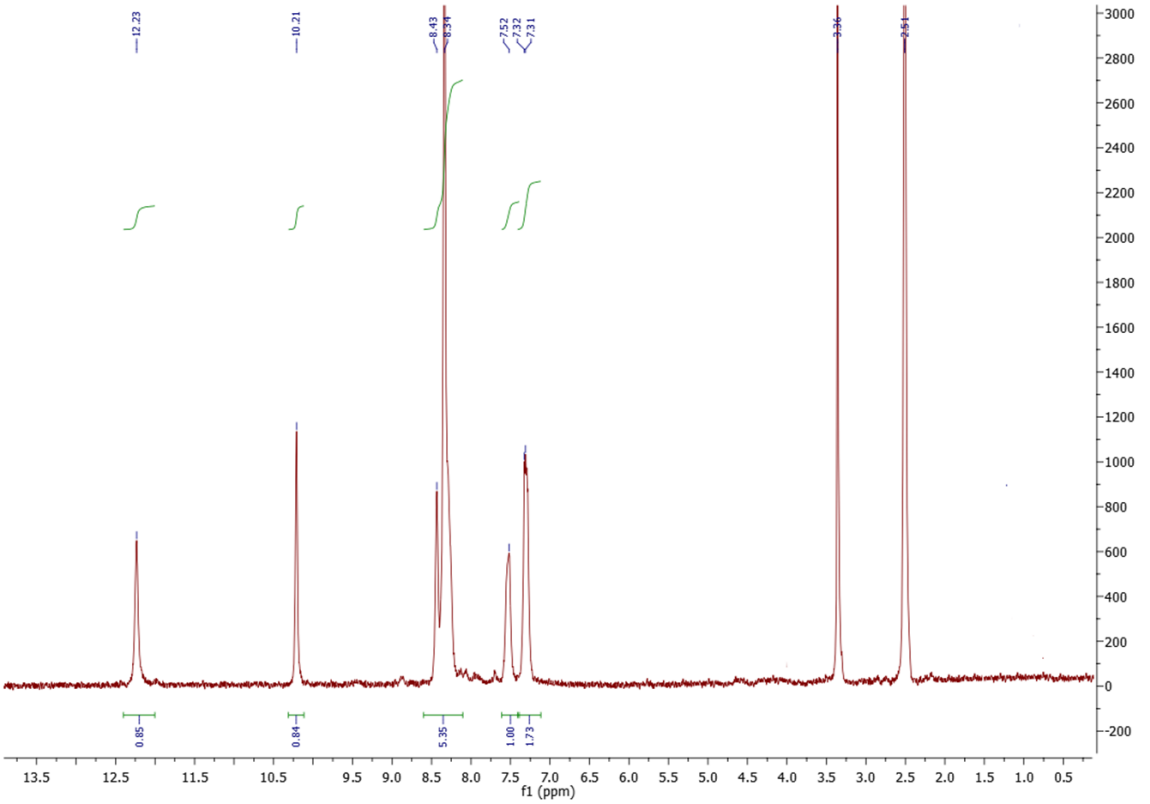

Compound **14r** ^{1}H NMR

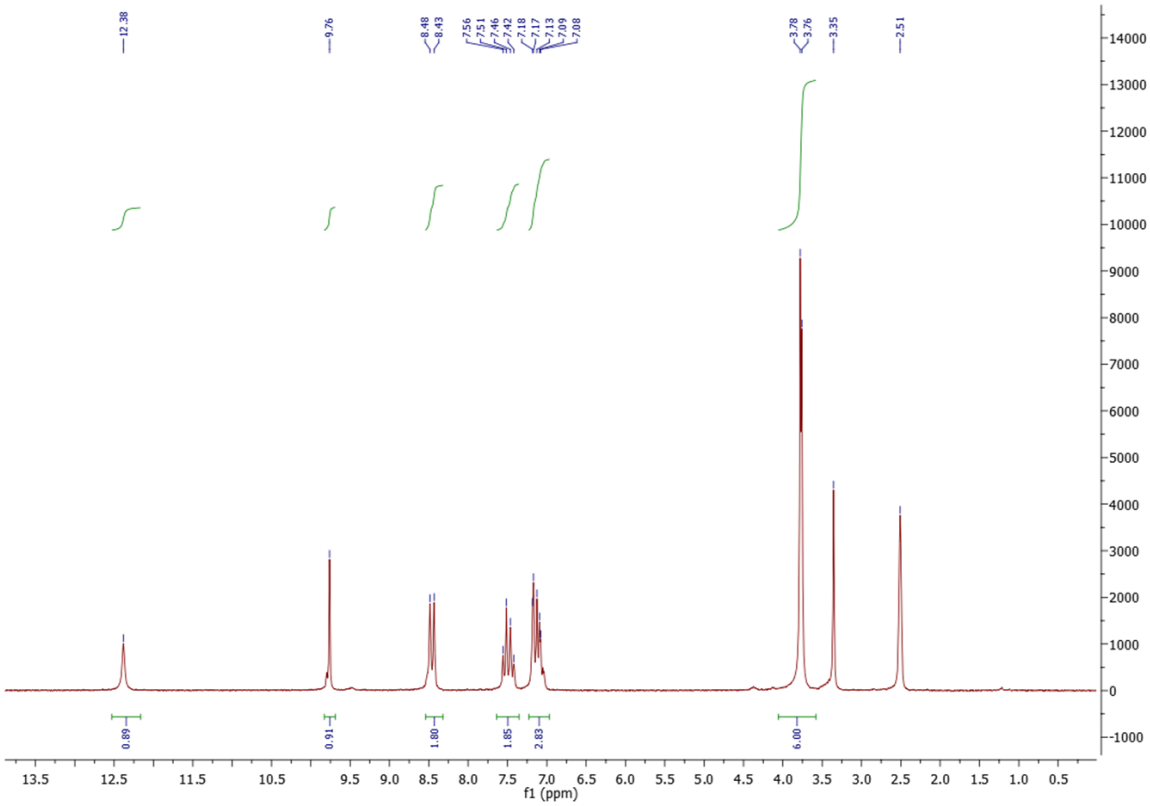

Compound **14r** ^{13}C NMR

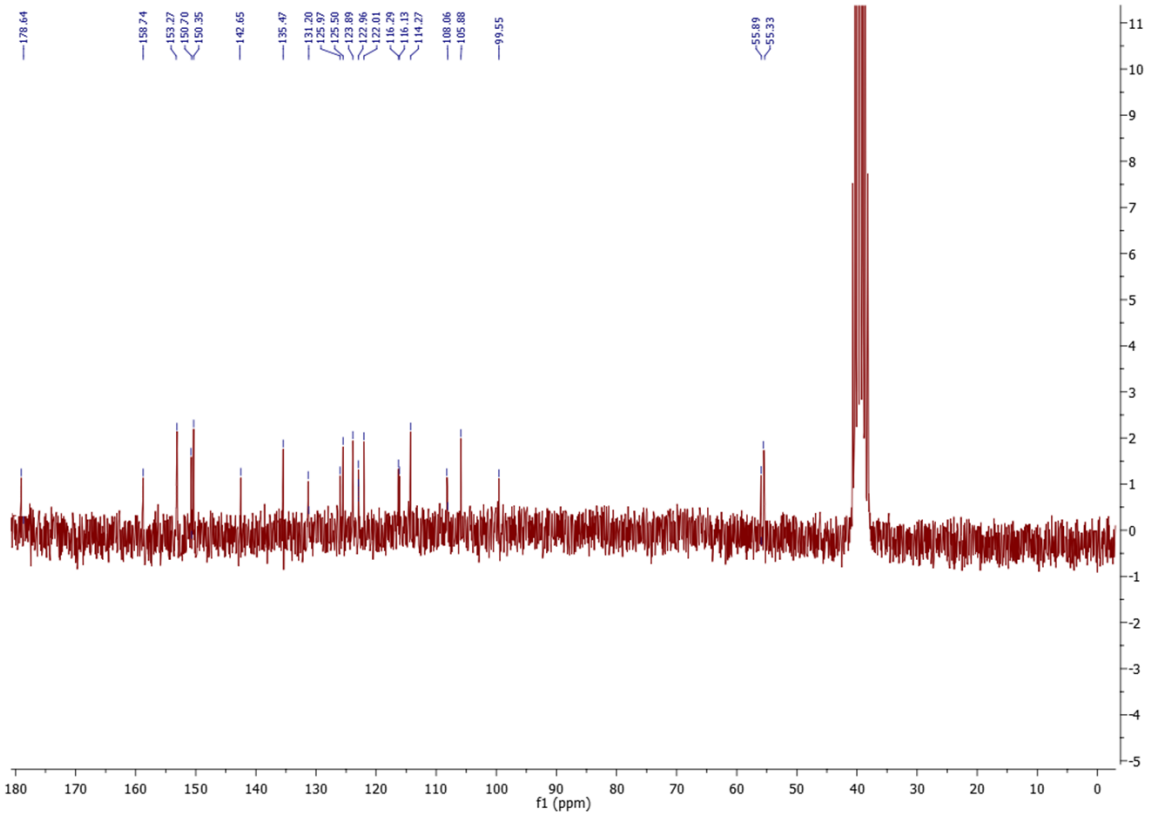

Chapter 8

2,6-Disubstituted imidazo[2,1-b][1,3,4]thiadiazole derivatives as potent staphylococcal biofilm inhibitors

Cascioferro S[1], Parrino B[1], **Li Petri G[1,3]**, Cusimano MG[1], Schillaci D[1], Di Sarno V[2], Musella S[2], Giovannetti E[3,4], Cirrincione G[1], Diana P[1*]

[*]Corresponding authors

1. *Dipartimento di Scienze e Tecnologie Biologiche Chimiche e Farmaceutiche (STEBICEF), Università degli Studi di Palermo, Via Archirafi 32, 90123 Palermo, Italy*
2. *Dipartimento di Farmacia, Università degli Studi di Salerno, Via G. Paolo II 132, 84084, Fisciano, Salerno, Italy*
3. *Department of Medical Oncology, VU University Medical Center, Cancer Center Amsterdam, De Boelelaan 1117, 1081HV, Amsterdam, the Netherlands*
4. *Cancer Pharmacology Lab, AIRC Start-Up Unit, University of Pisa and Fondazione Pisana per la Scienza, via Via Ferruccio Giovannini 13 - 56017 San Giuliano Terme, Pisa, Italy*

European Journal Medicinal Chemistry. 2019 Apr 1;167:200-210

doi: 10.1016/j.ejmech.2019.02.007. Epub 2019 Feb 10

2,6-Disubstituted imidazo[2,1-b][1,3,4]thiadiazole derivatives as potent staphylococcal biofilm inhibitors

Abstract

A class of 36 new 2-(6-phenylimidazo[2,-1-b][1,3,4]thiadiazol-2-yl)-1H-indoles was efficiently synthesized and evaluated for their anti-biofilm properties against the Gram-positive bacterial reference strains *Staphylococcus aureus* ATCC 25923, *S. aureus* ATCC 6538 and *Staphylococcus epidermidis* ATCC 12228, and the Gram-negative strains *Pseudomonas aeruginosa* ATCC 15442 and *Escherichia coli* ATCC 25922. Many of these new compounds, were able to inhibit biofilm formation of the tested staphylococcal strains showing BIC_{50} lower than 10 μg/mL. In particular, derivatives **9c** and **9h** showed remarkable anti-biofilm activity against *S. aureus* ATCC 25923 with BIC_{50} values of 0.5 and 0.8 μg/mL, respectively, whereas compound **9aa** was the most potent against *S. aureus* ATCC 6538, with a BIC_{50} of 0.3 μg/mL. Remarkably, these compounds showed effects in the early stages of the biofilm formation without affecting the mature biofilm of the same strains and the viability of the planktonic form. Their ability in counteracting a virulence factor (biofilm formation) without interfering with the bacterial growth in the free life form make them novel valuable anti-virulence agents.

Keywords: Anti-Biofilm agents; Anti-virulence agents; Staphylococcal biofilm inhibitors; imidazo[2,1-b][1,3,4]thiadiazole derivatives

Introduction

Antibiotic resistance, caused by the overuse/misuse of antibiotics and by the great evolutionary capacity of microorganisms, is currently considered a serious global threat.

Common pathogens including *Enterococcus faecium*, *Staphylococcus aureus*, *Klebsiella pneumoniae*, *Acinetobacter baumannii*, *Pseudomonas aeruginosa*, and *Enterobacter species*, known as ESKAPE pathogens (*e.g.*, capable of 'escaping' the biocidal action of antibiotics), are the leading cause of severe nosocomial infection which became resistant to various antibiotic therapies. As a counteracting measure, in the last decade, many efforts have been made for the development of new agents that target the virulence mechanisms of important pathogens without affecting their viability. These new therapeutic strategies aim indeed at imposing limited selective pressure in promoting the development of the antibiotic-resistance.[123]

According to current estimates by the National Institute of Health, a percentage ranging from 65 to 80% of all bacterial infections are biofilm-mediated.[4] The ability to grow as a biofilm is considered one of the main natural resistance mechanisms developed by pathogens as well as one of the most relevant virulence factor. This is indeed the main cause of nosocomial chronic infections which are difficult to treat with conventional antibiotics, including periodontitis, pneumonia in cystic fibrosis patients, and numerous infections associated with indwelling devices such as catheters, heart valves, and prostheses.[5,6] The biofilm is a stratified bacterial community that grows on a biological or artificial surface, characterized by a multifactorial tolerance to antibiotics. In addition to limiting the penetration of antibiotics, biofilms, contain, in the deepest layers, bacterial subpopulations (dormant cells) with low metabolic activity and proliferation rate that are intrinsically resistant to conventional antibiotics. In this bacterial community, single cells are embedded in a self-made polymeric matrix essentially composed by exopolysaccharides or other extracellular polymeric molecules, including extracellular DNA, amyloid fibers, etc., as well as molecules originating from the host, such as mucus and DNA.

Conventional antibiotic therapies effective on planktonic cells are usually inactive against biofilms. In the last few years, several attempts have been made to obtain new molecules able to interfere with the biofilm formation suitable for the treatment of biofilm-associated infections.[7–12]

Currently the main strategies to counteract biofilms involve prevention of their formation or the dispersing of mature biofilm. Inhibitors of biofilm formation are often compounds able to inhibit the microbial attachment to surfaces, interfering with the bacterial adhesion,

which is considered the initial step in bacterial pathogenesis. Other potential mechanisms of action for potential anti-biofilm therapeutics consist in: **i)** regulating the quorum sensing(QS) system which is the bacterial cell-to-cell signaling responsible for the coordination of many virulence factors, including biofilm formation; **ii)** interfering with regulatory mechanisms such as nucleotide second messenger signaling systems, and **iii)** disrupting the biofilm structure.[13]

Indole compounds are widely described for their therapeutical potential as anti-inflammatory, analgesic,[14] antiviral,[15] anti-cancer[16171819] and antibacterial agents. [20] Indole is produced by more than 85 species of pathogens as bacterial intercellular signal, which plays a key role in modulating *E. coli* biofilm formation and *P. aeruginosa* virulence by repressing motility, chemotaxis and bacterial adhesion. [1321 2223]

Lee et al. described the activity of indole-3-acetic acid, 3,30-methylene bis indole, indole-3-propioninc acid, indole-3-carbinol,indole-3-carboxyaldehyde and 3-indolylacetonitrile in inhibiting *E. coli* O157: H7 and *P. aeruginosa* biofilm formation without affecting microbial growth.[24]

Moreover the imidazo[2,1-b][1,3,4]thiadiazole ring system has been recognized as a privileged scaffold for obtaining molecules with a broad spectrum of biological activities, such as anticancer,[25] antioxidant,[26] antitubercolar,[27] anticonvulsivant,[28] analgesic,[29] and antibacterial.[30,31]

Despite the numerous therapeutic properties described for the imidazo[2,1-b][1,3,4]thiadiazole derivatives, the antibiofilm activity of this class of compounds has never been described.

However, the isosters triazolothiazole compounds **1**-**3** (Figure 1) were reported by Zhang et al.[32] as potent inhibitors of Sortase A(SrtA), a Gram-positive transpeptidase involved in the process of bacterial adhesion and, therefore, closely related to the biofilm formation process.[3334] Notably, compound **3** showed a significant *in vivo* anti-infective activity in preventing *S. aureus* blood-stream infections.

Our previous researches focused on nitrogen heterocyclic systems to counteract the global threat of the antibiotic resistance,[353637] and we then develop a special interest towards indole moiety.[38394041] Therefore, considering the interesting therapeutic potentials of the imidazo[2,1-*b*][1,3,4]thiadiazole scaffold, herein we report the synthesis of a new series of 2-(6-phenylimidazo[2,1-*b*][1,3,4]thiadiazol-2-yl)-1*H*-indole derivatives. These novel compounds were assayed for their preventive effect on biofilm formation of the Gram-positive bacterial reference strains *Staphylococcus aureus* ATCC 25923, *S. aureus* ATCC

6538 and *Staphylococcus epidermidis* ATCC 12228, and of the Gram-negative strains ATCC 15442 and *Escherichia coli* ATCC 25922.

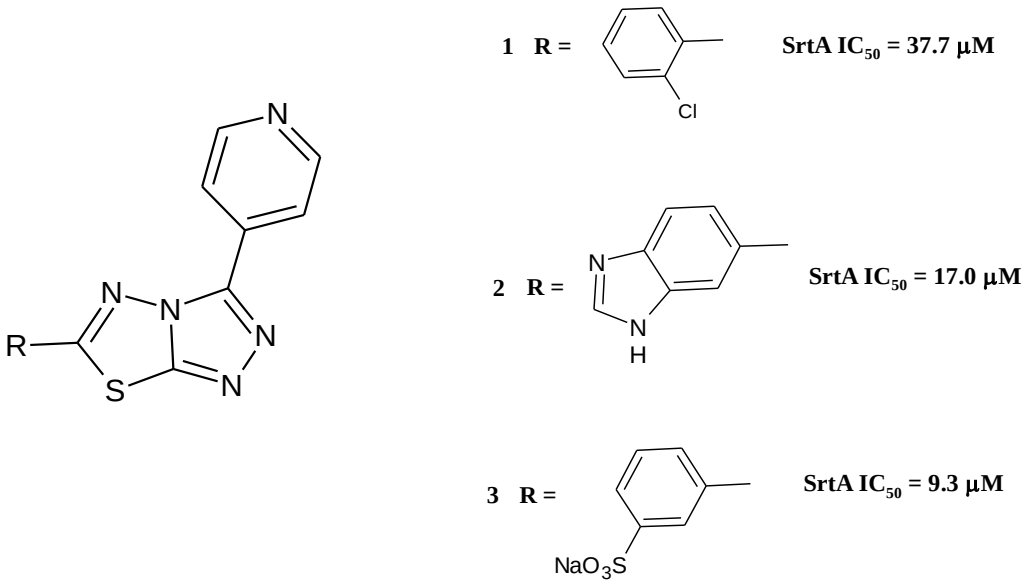

Figure 1. Chemical structures of triazolothiazole compounds **1-3.**

Chemistry

A series of 36 new imidazothiadiazole derivatives **9** and **10** was efficiently synthesized as described in **Scheme 1**.

Table 1. New 2-(6-phenylimidazo[2,1-*b*][1,3,4]thiadiazol-2-yl)-1*H*-indoles **9a-aj**.

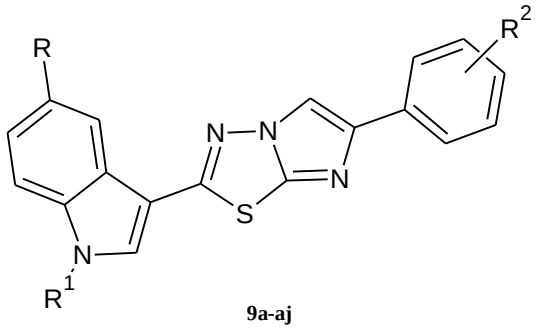

9a-aj

Comp	R	R^1	R^2	Yield(%)
9a	H	H	H	37
9b	H	H	3-OCH_3	33
9c	H	H	2,5-OCH_3	32
9d	H	H	4-F	32
9e	H	H	4-NO_2	42
9f	H	H	4-CF_3	40
9g	H	CH_3	H	40
9h	H	CH_3	3-OCH_3	42

9i	H	CH_3	2,5-OCH_3	48
9j	H	CH_3	4-F	40
9k	H	CH_3	4-NO_2	42
9l	H	CH_3	4-CF_3	30
9m	Br	H	H	40
9n	Br	H	3-OCH_3	40
9o	Br	H	2,5-OCH_3	33
9p	Br	H	4-F	42
9q	Br	H	4-NO_2	41
9r	Br	H	4-CF_3	35
9s	Br	CH_3	H	42
9t	Br	CH_3	3-OCH_3	35
9u	Br	CH_3	2,5-OCH_3	43
9v	Br	CH_3	4-F	38
9w	Br	CH_3	4-NO_2	46
9x	Br	CH_3	4-CF_3	40
9y	Cl	H	H	35
9z	Cl	H	3-OCH_3	36
9aa	Cl	H	2,5-OCH_3	46
9ab	Cl	H	4-F	45
9ac	Cl	H	4-NO_2	42
9ad	Cl	H	4-CF_3	36
9ae	Cl	CH_3	H	40
9af	Cl	CH_3	3-OCH_3	50
9ag	Cl	CH_3	2,5-OCH_3	55
9ah	Cl	CH_3	4-F	40
9ai	Cl	CH_3	4-NO_2	48
9aj	Cl	CH_3	4-CF_3	38

The 1*H*-indole-3-carbonitrile **5a** was commercially available, whereas carbonitriles **5b,c** were obtained by reaction of the corresponding 1*H*-indole **4** with the chlorosulfonyl isocyanate (CSI) in anhydrous acetonitrile at 0 °C in yield 98-100%. The methylation of derivatives **5** with dimethyl carbonate in anhydrous DMF under reflux at 130 °C, afforded the corresponding 1-methyl-1*H*-indole-3-carbonitrile **6** (yield 98%). The key intermediates **7a-f** were prepared by reaction of carbonitriles **5** and **6** thus obtained, with thiosemicarbazide in trifluoro acetic acid (TFA) at 60 °C for 3 h (yield 98-100%). Finally, the reaction between the appropriate 5-(1*H*-indol-3-yl)-1,3,4-thiadiazol-2-amine **7a-f** and the suitable α-

bromoacetyl compounds **8a-f** in ethanol under reflux for 24 h gave the desired new 2-(6-phenylimidazo[2,-1-*b*][1,3,4]thiadiazol-2-yl)-1*H*-indoles **9a-aj** as hydrobromide salts. Compounds **9e,f,k,l,q,r,ad,ae,ag-aj** were treated with saturated aqueous $NaHCO_3$ solution for obtaining the corresponding free bases **10** which were purified by silica gel column chromatography eluting by dichloromethane: ethyl acetate, 1:1 (42-55%) (Table 1). Reagents and conditions: **i**) CH_3CN, CSI, 0 °C, 2 h, then DMF, 0 °C, 1.5 h (98-100%); **ii**) DMF, $(CH_3O)_2CO$, K_2CO_3, 130 °C, 3.5 h; **iii**) trifluoroacetic acid, thiosemicarbazide, 60 °C, 3.5 h (98%); **iv**) anhydrous ethanol, 2-bromo-1-phenylethan-1-one **8**, reflux, 24 h (42-55%); **v**) $NaHCO_3$ saturated aqueous solution.

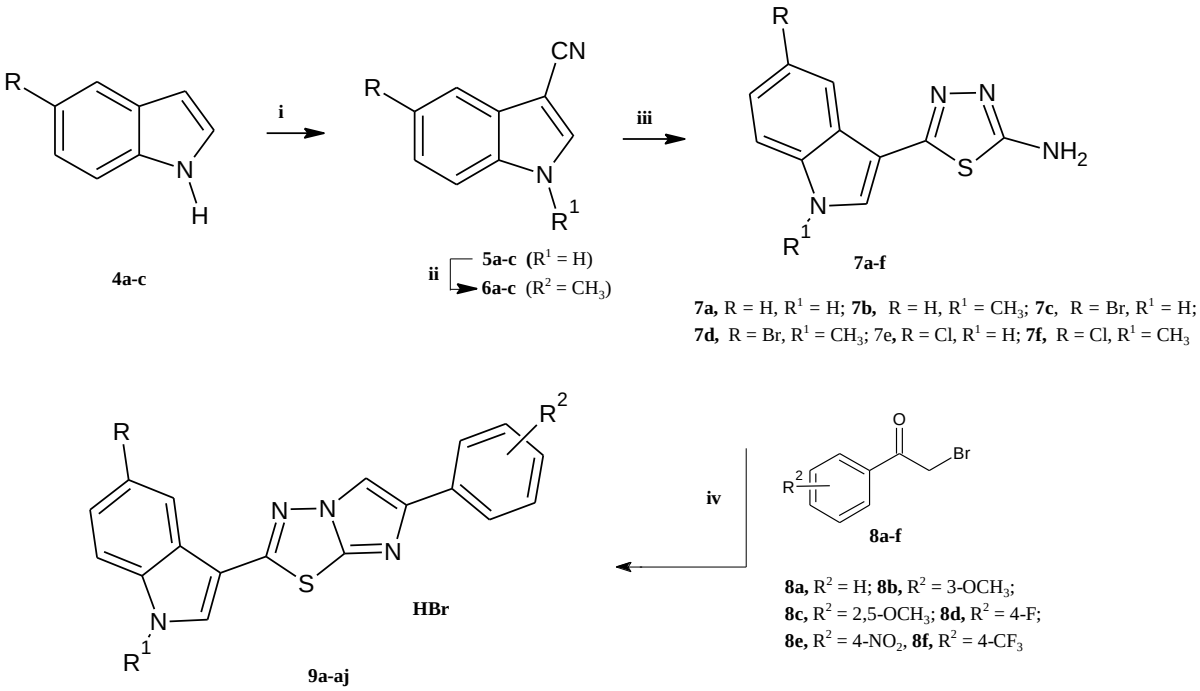

Scheme 1. Synthesis of new 2-(6-phenylimidazo[2,1-*b*][1,3,4]thiadiazol-2-yl)-1*H*-indoles **9a-aj**.

Results and discussion

Inhibition of biofilm formation

All the synthesized compounds **9a-d,g-j,m-p,s-ac,af** (hydrobromide salts) and **10e,f,k,l,q,r,ad,ae,ag-aj** (free bases) were primarily assayed *in vitro* for their antibacterial activity against the planktonic form of the Gram-positive bacterial reference strains *S. aureus* ATCC 25923, *S. aureus* ATCC 6538 and *S. epidermidis* ATCC12228, and of the Gram-negative strains *P. aeruginosa* ATCC 15442 and *E. coli* ATCC 25922. and the minimum inhibitory concentration (MIC) of the tested compounds was evaluated. The obtained results highlighted no interference by the imidazo[2,1-*b*][1,3,4]thiadiazoles **9** and **10** on the microbial planktonic growth (MIC>100mg/mL). This result was desirable from the perspective of obtaining derivatives with an anti-virulence profile, namely compounds able

to target key virulence factors rather than killing or inhibiting the growth of pathogens, which is advantageous for imposing limited selective pressure in promoting the development of the antibiotic-resistance mechanisms.

All the synthesized compounds **9** and **10** were then tested *in vitro* in order to evaluate their ability in inhibiting biofilm formation of the five tested strains. Compounds **9m,n,p,v,y,aj** and **10f,l**, showed no effect on the biofilm formation in the tested strains. For all the other synthesized derivatives the biofilm inhibitory concentration (BIC_{50}) values, that is the concentration at which the percentage of inhibition of biofilm formation is equal to 50% compared to the untreated growth control, were determined and reported in table 2. All compounds were able to interfere with the bacterial biofilm formation of the tested Gram-positive pathogens in a dose-dependent manner eliciting in many cases BIC_{50} values lower than 10 mg/mL. Interestingly, compounds **9c, 9h** and **9aa**, bearing one or two methoxy groups on the phenyl ring, displayed the best anti-biofilm activity against all tested Gram-positive strains with BIC_{50} values ranging from 0.5 to 18.5 mg/mL. In particular, derivatives **9c** and **9h** showed remarkable anti-biofilm activity against **S. aureus** ATCC 25923 with BIC_{50} values of 0.5 and 0.8 mg/mL, respectively, whereas compound **9aa** was the most potent against *S. aureus* ATCC 6538 with a BIC_{50} of 0.3 mg/mL. Noteworthy compounds **10k** and **9w**, which bring a nitro substituent in para position of the phenyl ring, significantly inhibited biofilm formation in all Gram-positive and Gram-negative tested strains showing BIC_{50} between 1.4 and 38.4 mg/mL. These results highlighted the influence of the substituents in the phenyl ring on the ability of this class of compounds in interfering with the biofilm formation. The presence of electron-donating methoxy groups was indeed advantageous for the anti-biofilm activity against Gram-positive pathogens, while the substitution on the phenyl ring with electron-withdrawing nitro groups improved the inhibitory activity against Gram-negative pathogens. Conversely, the structural modifications made at the indole nucleus, such as the introduction of a halogen atom at the 5 position or the methylation of the nitrogen atom, did not significantly influence the anti-biofilm activity of the compounds. The minimal concentrations required to inhibit 90% of biofilm formation (Table 3), as well as the concentration vs inhibition graph (Figure 2) were evaluated for the most active derivatives **9aa**, **9c** and **9h.**

The new derivatives **9c**, **9h** and **9aa** showed higher potency in inhibiting staphylococcal biofilm formation compared to the other indole derivatives so far described and elicited activity comparable to the most potent anti-biofilm compounds reported in literature.[13] Respect to the previous series of anti-biofilm compounds synthesized by us,[35–37] a significant

improvement in the inhibition of biofilm formation was observed. Among them, only the thiazole nortopsentin derivatives recently described[35] showed analogous inhibitory activity against staphylococcal biofilm with BIC_{50}, in some cases, in the low micromolar range, highlighting the importance of the indole scaffold for the anti-biofilm activity.

Table 2. Inhibition of biofilm formation, BIC_{50}, μg/mL (μM).

Comp	*S. aureus* ATCC 25923	*S. aureus* ATCC 6538	*S. epidermidis* ATCC 12228	*P. aeruginosa* 15442	*E. coli* 25922
9a	14.3 (35.9)	18.5 (46.5)	23.5 (59.1)	n.s.	n.s.
9b	34.3 (80.2)	16.1 (37.0)	14.3 (33.4)	34.3 (80.2)	29.8 (69.7)
9c	0.5 (1.2)	8.5 (18.5)	13.7 (29.9)	n.s.	n.s.
9d	6.5 (15.6)	5.6 (13.4)	12.8 (30.8)	19.7 (47.4)	n.s.
9e	17.2 (47.5)	7.3 (20.2)	14.9 (41.2)	n.s.	n.s.
9g	9.5 (23)	7.8 (18.9)	19.7 (47.9)	n.s.	n.s.
9h	0.8 (1.8)	12.4 (28.0)	18.5 (41.9)	n.s.	n.s.
9i	11.5 (24.3)	1.7 (3.6)	11.8 (25.0)	42.9 (91.0)	n.s.
9j	3.7 (8.6)	7.7 (17.9)	29.6 (68.9)	n.s.	n.s.
9k	7.9 (21.0)	1.4 (3.0)	7.9 (21.0)	11.3 (30.1)	12.9 (34.3)
9o	14.2 (26.4)	8.9 (16.5)	19.4 (36.1)	n.s.	n.s.
9q	12.5 (23.9)	14.1 (27.0)	9.9 (19.1)	22.6 (43.3)	n.s.
9r	7.8 (16.8)	6.2 (13.3)	8.9 (19.2)	n.s.	n.s.
9s	n.s.	n.s.	10.6 (21.6)	n.s.	n.s.
9t	8.5 (16.0)	6.5 (12.4)	33.2 (63.8)	13.7 (26.3)	n.s.
9u	50 (90.8)	4.9 (8.9)	28.8 (52.3)	15.7 (28.5)	n.s.
9w	11.2 (20.9)	1.7 (3.1)	38.4 (71.7)	20.7 (38.6)	10.5 (19.6)
9z	14.6 (31.6)	7.0 (15.1)	15.1 (32.7)	13.4 (29.0)	n.s.
9aa	11.9 (24.2)	0.28 (0.5)	9.3 (18.9)	n.s.	45 (91.5)
9ab	23.1 (51.3)	10.9 (24.2)	45.3 (100.7)	n.s.	n.s.
9ac	26.4 (55.3)	17.1 (35.8)	13.6 (28.5)	n.s.	n.s.
9ad	4.1 (9.7)	5.3 (12.6)	10.3 (24.5)	n.s.	n.s.
9ae	n.s.	n.s.	16.3 (36.5)	n.s.	n.s.
9af	n.s.	n.s.	11.4 (23.9)	n.s.	n.s.
9ag	82.5 (163.0)	35.1 (69.4)	4.1 (8.1)	n.s.	n.s.
9ah	n.s.	23.4 (50.4)	7.9 (17.0)	n.s.	n.s.
9ai	n.s.	16.2 (33.0)	38.3 (78.0)	n.s.	n.s.

n.s. not significant because lower than 15% of inhibition percentage at the screening concentration of 100 μg/mL

Table 3. Inhibition of biofilm formation expressed as BIC_{90}.

Compounds	BIC_{90}[μg/ml]
9c (*S.aureus* 25923)	36.5
9h (*S.aureus* 25923)	23.3
9aa (*S.aureus* 6538)	16.2

Compounds **9c,9h,9i,9w,9aa** and **10k**, which were the most potent against the *S. aureus* strains, were also tested with the aim to evaluate their dispersal activity against the 24 h preformed biofilm of the same strains. Among the tested compounds, only derivative **9c** showed a weak activity eliciting an IC_{50} value of 142.5mg/mL against *S. aureus* ATCC 25923. These results suggested a mechanism of anti-biofilm activity related to the

interference with adhesion or regulatory mechanisms involved in bacterial communication systems characterizing the first steps of biofilm formation, rather than an ability to disrupt mature biofilms. The selectivity showed by most of our compounds towards Gram-positive pathogens and their activity in the first stages of the biofilm formation without interferences on the microbial viability and on the preformed biofilm led us to hypothesize the inhibition of SrtA as possible mechanism of action.[33] To validate this hypothesis, compounds **9c**, **9h**, **9k** and **9aa**, which showed the highest anti-biofilm activity and the best selectivity towards the Gram-positive strains, were selected for evaluating their inhibitory activity against *S. aureus* SrtA. However, no compound proved to be effective at the maximum tested concentration of 100 mM against the transpeptidase. We therefore speculate that many other targets can be involved in the anti-biofilm activity of this class of compounds, including autoinducing peptides (AIPs), autoinducer-2 (AI-2), bacterial second messengers, such as c-di-GMP and c-di-AMP, and indole pathway.[13] In particular, indole plays a key role in the communication system employed by the bacteria to coordinate many processes involved in the antibiotic resistance including biofilm formation, bacterial virulence, motility and dormant cell formation. It was reported as indole-containing small molecules area able to decrease in *S. aureus* the production of staphyloxanthin, which is a virulence factor responsible for the oxidant and neutrophil resistance of the pathogen. Additionally, in *S. aureus*, the interference with the indole pathway inhibits the hemolytic activity of the bacterium against human red blood cells. Indole-signaling pathway is currently considered a valuable target to counteract bacterial virulence and biofilm formation. A recent study reported many indole-containing small molecules able to inhibit biofilm formation by interfering with the bacterial indole signalling.[42] Given the presence of the indole nucleus in these derivatives and considered that the anti-biofilm properties of most indole derivatives were due to the interference with the indole pathway, we hypothesize that our new compounds might act by this mechanism.

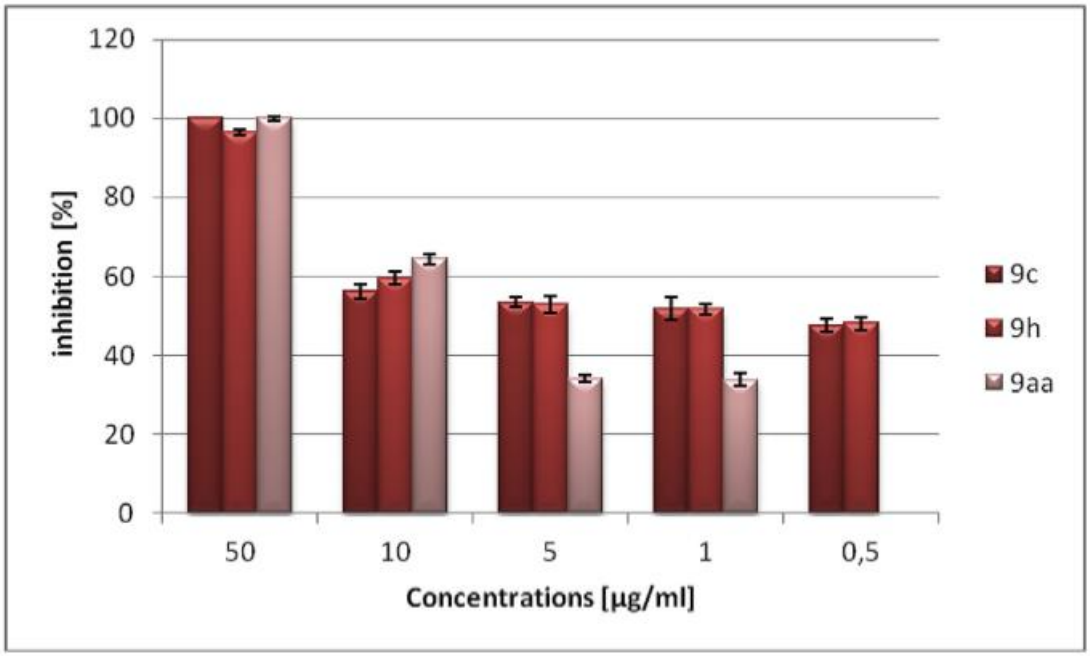

Figure 2. Concentration *versus* inhibition percentage graph, **9c** and **9h** towards *S. aureus* ATCC 25923, and 9aa towards *S. aureus* ATCC 6538.

Conclusions

A library of 36 new 2-(6-phenylimidazo[2,-1-*b*][1,3,4]thiadia-zol-2-yl)-1*H*-indoles **9** and **10** has been efficiently synthesized and evaluated for its anti-biofilm properties.

Despite the numerous biological properties described for the imidazo[2,1-*b*][1,3,4]thiadiazole scaffold, this is the first time that its anti-biofilm activity was reported. Among the synthesized compounds many derivatives were able to inhibit the biofilm formation of the tested staphylococcal strains showing BIC_{50} lower than 10 mg/mL, and in three cases (**9c**,**9h** and **9aa**) lower than 1 mg/mL. Remarkably, compounds **9c**,**9h**,**9i**,**9w**,**9aa** and **10k** showed the typical behaviour of anti-virulence agents, inhibiting the formation of the bacterial biofilm, which is considered one of the most important bacterial virulence factor, especially in the case of microorganisms once considered harmless such as *S. epidermidis*. The anti-virulence strategy, aimed to counteract virulence factors without interfering with the microbial growth, has attracted increasing interest in the fight against the antibiotic resistance. Therefore the derivatives **9c**,**9h** and **9aa** could be considered attractive lead compounds for developing a new class of potent inhibitors of staphylococcal biofilm formation. These innovative antibiofilm strategies warrant further studies, in order to obtain effective approaches that will be included in the therapeutic arsenals for use against difficult-to-treat infections, such as chronic and medical devices associated infections.

Experimental

Chemistry

All melting points were taken on a Büchi-Tottoly capillary apparatus and are uncorrected. IR spectra were determined in bromoform with a Shimadzu FT/IR 8400S spectrophotometer. ^{1}H and ^{13}C NMR spectra were measured at 200 and 50.0 MHz, respectively, in DMSO-d_6 solution, using a Bruker Avance II series 200 MHz spectrometer. Column chromatography was performed with Merk silica gel 230-400 mesh ASTM or with Büchi Sepacor chromatography module (prepacked cartridge system). Elemental analyses (C, H, N) were within ±0.4% of theoretical values and were performed with a VARIO EL III elemental analyzer. Purity of all the tested compounds was greater than 95%, determined by HPLC (Agilent 1100 Series).

General procedure for the synthesis of 1H-indole-3-carbonitriles (**5b-c)**

To a solution of the indole **4b,c** (5.10 mmol) in anhydrous acetonitrile (4.5 mL), chlorosulfonyl isocyanate (CSI) (0.44 mL, 5.10 mmol) was added dropwise. The reaction mixture was stirred at 0 °C for 2 h. Anhydrous dimethylformamide (DMF) (2.8 mL, 36.39 mmol) was slowly added and the mixture was maintained under stirring at 0 °C for 1.5 h. The reaction mixture was poured into crushed ice and the precipitate was filtered off and dried (Na_2SO_4) (yields 98-100%).

Analytical and spectroscopic data for compounds **5b,c** are in agreement with those previously reported.[43]

General procedure for the synthesis of 1-methylindole-3-carbonitriles (**6a-c)**

A mixture of the suitable 3-cyanoindole **5a-c** (7.03 mmol), 0.5 g of K_2CO_3, anhydrous DMF (10 mL) and dimethyl carbonate (1.8 mL, 21.4 mmol) was heated under reflux at 130 °C for 3.5 h. Then the reaction mixture was cooled to 3 °C and water and ice (25 mL) was slowly added under stirring. The oily suspension thus obtained was extracted with diethyl ether and the organic layer was washed with water and brine, dried over anhydrous Na_2SO_4 and evaporated under vacuum to obtain the 3-cyano-1-methylindole **6a-c** in excellent yields. Analytical and spectroscopic data are in accordance to those reported in literature.[44]

*General procedure for the synthesis of 5-(1H-indol-3-yl)-1,3,4-thiadiazol-2-amines (**7a-f**).*

A solution of the appropriate 1*H*-indole-3-carbonitriles **5a-c** or 1-methylindole-3-carbonitriles **6a-c** (5 mmol) and thiosemicarbazide (5mmol) in trifluoroacetic acid (5 mL)

was refluxed at 60 °C for 3.5 h. The reaction mixture was then poured into ice and slowly neutralized with $NaHCO_3$ saturated solution. The obtained precipitate was filtered off, washed with water, cyclohexane and diethyl ether.

*5-(1H-Indol-3-yl)-1,3,4-thiadiazol-2-amine (**7a**).*

Light yellow solid, yield: 98%, m.p. 210-211 °C, IR cm^{-1}: 3609 (NH), 3461-3210 (NH_2); ^{1}HNMR DMSO-*d6* (ppm): 7.15-7.24 (4H, m, Ar-H, NH_2), 7.45 (1H, d, *J* = 6.75 Hz, Ar-H), 7.85 (1H, d, *J* = 2.62 Hz, Ar-H), 8.11 (1H, d, *J* = 6.98 Hz, Ar-H), 11.64 (1H, s, NH); ^{13}C NMR DMSO-*d6* (ppm): 107.2 (s), 111.9 (d), 120.4 (d), 120.6 (d), 122.4 (d), 124.1 (s), 126.6 (d), 136.4 (s), 152.3 (s), 165.8 (s). Anal. Calcd for $C_{10}H_8N_4S$ (MW 216.26): C, 55.54%; H, 3.73%; N, 25.91%. Found: C, 55.71%; H, 3.68%; N, 25.75%.

*5-(1-Methyl-1H-indol-3-yl)-1,3,4-thiadiazol-2-amine (**7b**).*

Light yellow solid, yield: 98%, m.p. 124-125 °C, IR cm^{-1}: 3612 (NH), 3478-3228 (NH_2); ^{1}HNMR DMSO-*d6* (ppm): 3.85 (3H, s, CH3), 7.23-7.35 (2H, m, Ar-H), 7.55 (1H, d, *J* = 7.41 Hz, Ar-H), 8.06 (2H, d, *J* = 6.05 Hz, Ar-H), 8.57 (2H, bs, NH_2); ^{13}C NMR DMSO-*d6* (ppm): 33.3 (q), 107.5 (s), 110.6 (d), 120.6 (d), 121.2 (d), 122.8 (d), 124.2 (s), 131.8 (d), 136.2 (s), 152.4 (s), 166.8 (s). Anal. Calcd for $C_{11}H_{10}N_4S$ (MW 230.29): C, 57.37%; H, 4.38%; N, 24.33%. Found: C, 57.48%; H, 4.42%; N, 24.51%.

*5-(5-Bromo-1H-indol-3-yl)-1,3,4-thiadiazol-2-amine (**7c**).*

Yellow solid, yield: 92%, m.p. 232-233 °C. IR cm^{-1}: 3445 (NH), 4147 (NH_2); ^{1}HNMR (200 MHz, DMSO-*d6*) d: 7.19-7.46 (4H, m, ArH, NH_2), 7.91 (1H, s, Ar-H), 8.30 (1H, s, Ar-H), 11.83 (1H, bs, NH); ^{13}C NMR (50 MHz, DMSO-*d6*) d: 107.0 (s), 112.9 (s), 113.9 (d), 123.0 (d), 124.9 (d), 125.8 (s), 127.9 (d), 135.1 (s), 151.8 (s), 165.9 (s). Anal. Calcd for $C_{10}H_7BrN_4S$ (MW 295.16): C, 40.69%; H, 2.39%; N, 8.98%. Found: C, 40.72%; H, 2.36%; N, 8.95%.

*5-(5-Bromo-1-methyl-1H-indol-3-yl)-1,3,4-thiadiazol-2-amine (**7d**).*

Yellow solid, yield: 98%, m.p. 174-175 °C, IR cm^{-1}: 3558 (NH_2); ^{1}HNMR DMSO-*d6* (ppm): 3.84 (3H, s, CH_3), 7.51 (2H, dd, *J* = 1.92, 8.75 Hz, Ar-H), 8.08 (3H, m, Ar-H, NH_2), 8.23 (1H, s, Ar-H); ^{13}C NMR DMSO-*d6* (ppm): 32.9 (q), 105.4 (s), 112.7 (d), 113.5 (s), 123.0 (d), 125.1 (d), 125.9 (s), 132.3 (d), 135.7 (s), 151.3 (s), 166.2 (s). Anal. Calcd for

$C_{11}H_9BrN_4S$ (MW 309.19): C, 42.73%; H, 2.93%; N, 18.12%. Found: C, 42.82%; H, 3.01%; N, 18.24%.

*5-(5-Chloro-1H-indol-3-yl)-1,3,4-thiadiazol-2-amine (**7e**).*

Orange solid, yield: 98%, m.p. 234-235 °C, IR cm^{-1}: 3564 (NH), 3255 (NH_2); ^{1}HNMR DMSO-*d6* (ppm): 7.19-7.50 (4H, m, Ar-H, NH_2), 7.98 (1H, s, Ar-H), 8.14 (1H, s, Ar-H), 11.87 (1H, s, NH); ^{13}C NMR DMSO-*d6* (ppm): 106.9 (s), 113.6 (d), 119.9 (d), 122.5 (d), 125.0 (s), 125.1 (s), 128.4 (d), 134.9 (s), 151.8 (s), 166.0 (s). Anal. Calcd for $C_{10}H_7ClN_4S$ (MW 250.70): C, 47.91%; H, 2.81%; N, 22.35%. Found: C, 47.75%; H, 2.92%; N, 22.54%.

*5-(5-Chloro-1-methyl-1H-indol-3-yl)-1,3,4-thiadiazol-2-amine (**7f**).*

Yellow solid, yield: 100%, m.p. 95-96 °C, IR cm^{-1}: 3609 (NH^2); ^{1}HNMR DMSO-d6 (ppm): 3.84 (3H, s, CH3), 7.29 (1H, d, *J* = 8.77, Ar-H), 7.58 (1H, d, *J* = 8.76, Ar-H), 8.08 (4H, Ar-H, NH_2); ^{13}C NMR DMSO-*d6* (ppm): 33.0 (q), 105.2 (s), 112.3 (d), 119.9 (d), 122.7 (d), 125.2 (s), 125.7 (s), 132.7 (d), 135.5 (s), 166.4 (s). Anal. Calcd for $C_{11}H_9ClN_4S$ (MW 264.74): C, 49.91%; H, 3.43%; N, 21.16%. Found: C, 50.03%; H, 3.68%; N, 21.32%.

*General procedure for the synthesis of 3-(6-Phenylimidazo[2,1-b][1,3,4]thiadiazol-2-yl)-1H-indoles derivatives **9a-d**,**g-j**,**m-p**,**s-ac**,**af** and **10e**,**f**,**k**,**l**,**q**,**r**,**ad**,**ae**,**ag**,**ah**,**ai**,**aj***

A solution of the suitable 5-(1H-indol-3-yl)-1,3,4-thiadiazol-2-amine **7a-f** (0.92 mmol) and the appropriate 2-bromo-1-phenylethanone **8a-f** (0.92 mmol) in 40 mL of anhydrous ethanol was heated under reflux for 24 h. Upon cooling, the corresponding hydrobromide was filtered off and washed with ethanol. Derivatives **9a-d**,**g-j**,**m-p**,**s-ac**,**af** were isolated as pure compounds and were

characterized without further purifications. Instead, in the case of compounds **9e**,**f**,**k**,**l**,**q**,**r**,**ad**,**ae**,**ag-aj**. It was necessary the treatment with saturated aqueous $NaHCO_3$ solution for obtaining the corresponding free base **10** which was purified by silica gel column chromatography eluting by dichloromethane:ethyl acetate, 1:1. Derivatives **9k**,**q**,**w**,**ac**,**ai**,**v** were characterized only by 1HNMR spectra due to their poor solubility.

*3-(6-Phenylimidazo[2,1-b][1,3,4]thiadiazol-2-yl)-1H-indole hydrobromide (**9a**).*

Light yellow solid, yield: 47%, m.p. 305-306 °C, IR cm^{-1}: 2622 (NH), 3193 (NH); ^{1}HNMR (200 MHz, DMSO-*d6*) d: 7.27e7.58 (6H, m, Ar-H), 7.89 (2H, d, *J* = 8.4 Hz, Ar-H), 8.14-8.18 (1H, m, Ar-H), 8.41 (1H, d, *J* = 2.98 Hz, Ar-H), 8.83 (1H, s, Ar-H),12.24 (1H, s,

NH); ^{13}C NMR (50 MHz, DMSO-*d6*) d: 106.0 (s),110.9 (d),112.6 (d), 120.3 (d), 121.6 (d), 123.3 (d), 123.7 (s), 124.6 (2xd), 127.7 (d), 128.8 (2xd), 130.0 (d), 132.1 (s), 136.7 (s), 142.6 (s), 142.8 (s), 158.2 (s). Anal. Calcd for $C_{18}H_{13}BrN_4S$ (MW 397.28): C, 54.42%; H, 3.30%; N, 14.10%. Found: C, 54.61%; H, 3.15%; N, 14.18%.

*3-[6-(3-Methoxyphenyl)imidazo[2,1-b][1,3,4]thiadiazol-2-yl]-1H-indole hydrobromide (**9b**).*

Light yellow solid, yield: 43%, m.p. 284-285 °C, IR cm^{-1}: 2719 (NH), 3153 (NH); ^{1}HNMR (200 MHz, DMSO-*d6*) d: 3.82 (3H, s, OCH_3), 6.87-6.92 (1H, m, Ar-H), 7.27-7.58 (6H, m, Ar-H), 8.14-8.18 (1H, m, Ar-H), 8.40 (1H, d, *J* = 4.6 Hz, Ar-H), 8.84 (1H, s, Ar-H), 10.44 (1H, s, NH), 12.23 (1H, s, NH); ^{13}C NMR (50 MHz, DMSO-*d6*) d: 55.1 (q), 106.0 (s), 109.9 (d), 111.1 (d), 112.6 (d), 113.3 (d), 116.9 (d), 120.3 (d), 121.6 (d), 123.3 (d), 123.7 (s), 129.9 (d), 130.0 (d), 133.6 (s), 136.7 (s), 142.5 (s), 142.7 (s), 158.2 (s), 159.6 (s). Anal. Calcd for $C_{19}H_{15}BrN_4OS$ (MW 427.33): C, 53.40%; H, 3.54%; N, 13.11%. Found: C, 53.51%; H, 3.50%; N, 13.23%.

*3-[6-(2,5-Dimethoxyphenyl)imidazo[2,1-b][1,3,4]thiadiazol-2-yl]-1H-indole hydrobromide (**9c**).*

Light yellow solid, yield: 42%, m.p. 260-261 °C, IR cm^{-1}: 2735 (NH), 3124 (NH); ^{1}HNMR (200 MHz, DMSO-*d6*) d: 3.78 (3H, s, OCH_3), 3.94 (3H, s, OCH_3), 6.94-6.95 (1H, m, Ar-H), 7.09 (1H, d, *J* = 9.1 Hz, Ar-H), 7.28-7.32 (2H, m, Ar-H), 7.59-7.61 (2H, m, Ar-H), 8.15-8.20 (1H, m, Ar-H), 8.46 (1H, d, *J* = 3.15 Hz, Ar-H), 8.76 (2H, s, Ar-H, NH), 12.27 (1H, s, NH); ^{13}C NMR (50 MHz, DMSO-*d6*) d: 55.4 (q), 55.9 (q), 105.8 (s), 111.7 (d), 112.6 (d), 112.9 (d), 113.5 (d), 114.4 (d), 119.4 (s), 120.3 (d), 121.7 (d), 123.3 (d), 123.7 (s), 130.4 (d), 136.7 (s), 136.9 (s), 141.9 (s), 149.8 (s), 153.2 (s), 159.0 (s). Anal. Calcd for $C_{20}H_{17}BrN_4O_2S$ (MW 457.33): C, 52.52%; H, 3.75%; N, 12.25%. Found: C, 52.61%; H, 3.68%; N, 12.36%.

*3-[6-(4-Fluorophenyl)imidazo[2,1-b][1,3,4]thiadiazol-2-yl]-1H-indole hydrobromide (**9d**).*

Light yellow solid, yield: 42%, m.p. 318-319 °C, IR cm^{-1}: 2719 (NH), 3181 (NH); ^{1}HNMR (200 MHz, DMSO-*d6*) d: 7.25-7.34 (4H, m, 4xAr-H), 7.53-7.57 (1H, m, Ar-H), 7.87-7.94 (2H, m, 2xAr-H), 8.12-8.16 (1H, m, Ar-H, NH), 8.40 (1H, d, *J* = 2.98 Hz, Ar-H), 8.79 (1H, s, Ar-H); 12.03 (1H, s, NH), 12.24 (1H, s, NH); ^{13}C NMR (50 MHz, DMSO-*d6*) d: 106.0 (s), 110.7 (d), 112.6 (d), 115.5 (d), 115.9 (d), 120.2 (d), 121.6 (d), 123.2 (d), 123.7

(s), 126.6 (d), 126.7 (d), 128.6 (s), 133.0 (d), 136.6 (s), 141.5 (s), 142.8 (s), 158.3 (s), 159.2 (s). Anal. Calcd for $C_{18}H_{12}BrFN_4S$ (MW 415.27): C, 52.06%; H, 2.91%; N, 13.49%. Found: C, 52.15%; H, 2.78%; N, 13.40%.

*3-[6-(4-Nitrophenyl)imidazo[2,1-b][1,3,4]thiadiazol-2-yl]-1H-indole (**10e**).*

Orange solid, yield: 52%, m.p. 359-360 °C, IR cm^{-1}: 3324 (NH); ^{1}HNMR (200 MHz, DMSO-*d6*) d: 7.26-7.31 (2H, m, 2xAr-H), 7.51-7.56 (1H, m, Ar-H), 8.07-8.33 (6H, m, Ar-H), 8.93 (1H, s, Ar-H),12.16 (1H, s, NH); ^{13}C NMR (50 MHz, DMSO-*d6*) d: 106.4 (s), 112.5 (d), 113.1 (d), 120.3 (d), 121.5 (d), 123.2 (d), 123.7 (s), 124.1 (2xd), 124.9 (2xd), 129.8 (d), 136.7 (s), 140.6 (s), 142.4 (s), 144.2 (s), 145.7 (s), 158.0 (s). Anal. Calcd for $C_{18}H_{11}N_5O_2S$ (MW 361.37): C, 59.82%; H, 3.07%; N, 19.38%. Found: C, 59.97%; H, 3.25%; N, 19.51%.

*3-[6-(4-Trifluoromethylphenyl)imidazo[2,1-b][1,3,4]thiadiazol-2-yl]-1H-indole (**10f**).*

Light yellow solid, yield: 50%, m.p. 293-295 °C, IR cm^{-1}: 3678 (NH); ^{1}HNMR (200 MHz, DMSO-*d6*) d: 7.27-7.32 (2H, m, 2xAr-H), 7.53-7.57 (1H, m, Ar-H), 7.77 (2H, d, *J* = 8.37, Ar-H), 8.08-8.20 (3H, m, Ar-H), 8.35 (1H, s, Ar-H), 8.88 (1H, s, Ar-H), 12.16 (1H, s, NH); ^{13}C NMR (50 MHz, DMSO-*d6*) d: 106.3 (s), 112.0 (s), 112.5 (d), 120.3 (s), 120.3 (d), 121.5 (d), 123.2 (d), 123.7 (d), 124.8 (2xd),125.6 (2xd),129.7 (d),136.7 (s),137.9 (s),142.8 (s),143.6 (s), 157.8 (s). Anal. Calcd for $C_{19}H_{11}F_3N_4S$ (MW: 384.38): C, 59.37%; H, 2.88%; N, 14.58%. Found: C, 59.41%; H, 2.95%; N, 14.70%.

*1-Methyl-3-(6-phenylimidazo[2,1-b][1,3,4]thiadiazol-2-yl)-1H-indole hydrobromide (**9g**).*

Light yellow solid, yield: 50%, m.p. 282-283 °C, IR cm^{-1}: 2604 (NH); ^{1}HNMR (200 MHz, DMSO-*d6*) d: 3.90 (3H, s, CH_3), 7.32-7.45 (5H, m, Ar-H), 7.60-7.64 (1H, m, Ar-H), 7.88 (2H, d, *J* = 4.22 Hz; Ar-H), 8.13-8.18 (1H, m, Ar-H), 8.40 (1H, s, Ar-H), 8.78 (1H, s, Ar-H), 9.14 (1H, bs, NH); ^{13}C NMR (50 MHz, DMSO-*d6*) d: 33.1 (q), 100.0 (s), 110.8 (d), 111.1 (d), 120.4 (d), 121.9 (d),123.3 (d), 124.0 (s),124.6 (2xd),127.5 (d),128.7 (2xd),132.6 (s),133.3 (d),137.2 (s), 142.7 (s), 143.1 (s), 157.4 (s). Anal. Calcd for $C_{19}H_{15}BrN_4S$ (MW: 411.32): C, 55.48%; H, 3.68%; N, 13.62%. Found: C, 55.52%; H, 3.74%; N, 13.51%.

*3-[6-(3-methoxyphenyl)imidazo[2,1-b][1,3,4]thiadiazol-2-yl]-1-methyl-1H-indole hydrobromide (**9h**).*

Light yellow solid, yield: 52%, m.p. 266-267 °C, IR cm^{-1}: 2473 (NH); ^{1}HNMR (200 MHz, DMSO-*d6*) d: 3.82 (3H, s, OCH_3), 3.90 (3H, s, CH_3), 6.86-6.91 (1H, m, Ar-H), 7.35-7.46

(5H, m, Ar-H, NH), 7.63-7.64 (1H, m, Ar-H), 8.13-8.17 (1H, m, Ar-H), 8.40 (1H, s, Ar-H), 8.80 (1H, s, Ar-H), 10.45 (1H, bs, NH); ^{13}C NMR (50 MHz, DMSO-*d6*) d: 33.1 (q), 55.0 (q), 105.0 (s), 109.9 (d), 111.0 (d), 112.0 (d), 113.1 (d), 116.9 (d), 120.4 (d), 121.9 (d), 123.2 (d), 124.0 (s),129.8 (d), 133.3 (d), 134.0 (s), 137.2 (s), 142.6 (s), 143.1 (s), 157.4 (s), 159.6 (s). Anal. Calcd for $C_{20}H_{17}BrN_4OS$ (MW: 441.34): C, 54.43%; H, 3.88%; N, 12.69%. Found: C, 54.51%; H, 3.99%; N, 12.82%.

*3-[6-(2,5-Dimethoxyphenyl)imidazo[2,1-b][1,3,4]thiadiazol-2-yl]-1-methyl-1H-indole hydrobromide (**9i**).*

Light yellow solid, yield: 48%, m.p. 266-267 °C, IR cm^{-1}: 2607 (NH); ^{1}HNMR (200 MHz, DMSO-*d6*) d: 3.78 (3H, s, OCH_3), 3.89 (3H, s, OCH_3), 3.93 (3H, s, CH_3), 6.87-6.93 (1H, m, Ar-H), 7.02-7.10 (1H, m, Ar-H), 7.32-7.40 (2H, m, Ar-H), 7.61-7.64 (2H, m, Ar-H), 7.88 (1H, bs, NH), 8.14-8.18 (1H, m, Ar-H), 8.42 (1H, s, Ar-H), 8.67 (1H, s, Ar-H); ^{13}C NMR (50 MHz, DMSO-*d6*) d:33.1 (q), 55.4 (q), 55.9 (q), 105.7 (s), 111.7 (s), 112.6 (s), 112.9 (s), 113.5 (d), 114.3 (d), 119.4 (s), 120.2 (d), 121.7 (d), 123.3 (d), 123.6 (s), 130.4 (d), 136.7 (s), 136.9 (s), 141.9 (s), 149.8 (s), 153.2 (s), 159.0 (s). Anal. Calcd for $C_{21}H_{19}BrN_4O_2S$ (MW: 471.37): C, 53.51%; H, 4.06%; N, 11.89%. Found: C, 53.70%; H, 4.12%; N, 11.98%.

*3-[6-(4-fluorophenyl)imidazo[2,1-b][1,3,4]thiadiazol-2-yl]-1-methyl-1H-indole hydrobromide (**9j**).*

Light yellow solid, yield: 50%, m.p. 269-270 °C, IR cm^{-1}: 2610-2719 (NH); ^{1}HNMR (200 MHz, DMSO-*d6*) d: 3.89 (3H, s, CH_3), 7.23-7.37 (4H, m, Ar-H), 7.59e7.63 (1H, m, Ar-H), 7.86e7.93 (2H, m, Ar-H), 8.12e8.21 (2H, m, Ar-H, NH), 8.37 (1H, s, Ar-H), 8.73 (1H, s, Ar-H); ^{13}C NMR (50 MHz, DMSO-d6) d: 33.1 (q), 105.1 (s), 110.5 (d), 111.0 (d), 115.4 (d), 115.8 (d), 120.4 (d), 121.8 (d), 123.2 (d), 124.0 (s), 126.4 (d), 126.6 (d),129.5 (s),133.2 (d),137.2 (s),142.6 (2xs),142.7 (s),157.2 (s). Anal. Calcd for C19H14BrFN4S (MW: 429.31): C, 53.16%; H, 3.29%; N, 13.05%. Found: C, 53.08%; H, 3.88%; N, 12.72%.

*1-Methyl-3-[6-(4-nitrophenyl)imidazo[2,1-b][1,3,4]thiadiazol-2-yl]-1H-indole (**10k**).*

Orange solid, yield: 52%, m.p. 299-300 °C. ^{1}HNMR (200 MHz, DMSO-d6) d: 3.92 (3H, s, CH_3), 7.34-7.38 (2H, m, 2xAr-H), 7.62-7.65 (1H, m, Ar-H), 8.12-8.40 (6H, m, Ar-H), 9.00 (1H, s, Ar-H). Anal. Calcd for $C_{19}H_{13}N_5O_2S$ (MW: 375.40): C, 60.79%; H, 3.49%; N, 18.66%. Found: C, 60.92%; H, 3.32%; N, 18.79%.

5.1.4.12. *1-Methyl-3-{6-[4-(trifluoromethyl)phenyl]imidazo[2,1-b][1,3,4]thiadiazol-2-yl}-1H-indole (**10l**).* Light yellow solid, yield: 42% m.p. 242-243 °C. ^{1}HNMR (200 MHz, DMSO-*d6*) d: 3.88 (3H, s, CH_3), 7.30-7.39 (2H, m, Ar-H), 7.60 (1H, d, *J* = 8.37, Ar-H), 7.74 (2H, d, *J* = 8.4, Ar-H), 8.04-8.17 (3H, m, Ar-H), 8.32 (1H, s, Ar-H), 8.84 (1H, s, Ar-H); ^{13}C NMR (50 MHz, DMSO-d6) d: 33.1 (q), 105.2 (s), 111.0 (d), 112.0 (d), 112.1 (s), 120.4 (d), 120.6 (s), 121.8 (d), 123.2 (d), 124.0 (s), 124.8 (2xd), 125.5 (d), 125.6 (s), 133.2 (d), 137.2 (s), 137.7 (s), 142.8 (s), 143.4 (s), 157.3 (s). Anal. Calcd for $C_{20}H_{13}F_3N_4S$ (MW: 398.40): C, 60.29%; H, 3.29%; N, 14.06%. Found: C, 60.44%; H, 3.35%; N, 14.28%.

*5-Bromo-3-(6-phenylimidazo[2,1-b][1,3,4]thiadiazol-2-yl)-1H-indole hydrobromide (**9m**).*

Light yellow solid, yield: 50%, m.p. 303-304 °C, IR cm^{-1}: 2690-2804 (NH), 3553-3638 (NH); ^{1}HNMR (200 MHz, DMSO-*d6*) d: 7.29-7.55 (5H, m, Ar-H), 7.87 (2H, d, *J* = 7.6 Hz, Ar-H), 8.37 (2H, d, *J* = 18.81 Hz, Ar-H), 8.81 (1H, s, Ar-H), 12.33 (1H, s, NH); ^{13}C NMR (50 MHz, DMSO-*d6*) d: 106.0 (s),110.7 (d), 114.1 (s), 114.6 (d), 122.6 (d), 124.4 (2xd), 125.3 (s), 125.8 (d), 127.2 (d), 128.6 (2xd), 130.9 (d), 133.5 (s), 135.4 (s), 142.8 (s), 144.2 (s), 156.8 (s). Anal. Calcd for $C_{18}H_{12}Br_2N_4S$ (MW: 476.19): C, 45.40%; H, 2.54%; N, 11.77%. Found: C, 45.58%; H, 2.63%; N, 11.59%.

*5-Bromo-3-[6-(3-methoxyphenyl)imidazo[2,1-b][1,3,4]thiadiazol-2-yl]-1H-indole hydrobromide (**9n**).*

Light yellow solid, yield: 50%, m.p. 299-300 °C, IR cm^{-1}: 2629 (NH), 3113 (NH); ^{1}HNMR (200 MHz, DMSO-*d6*) d: 3.81 (3H, s, OCH_3), 6.85-6.90 (1H, m, Ar-H), 7.34-7.54 (5H, m, Ar-H), 8.30 (1H, d, *J* = 1.72 Hz, Ar-H), 8.43 (1H, d, *J* = 2.96 Hz, Ar-H), 8.86 (1H, s, Ar-H), 10.16 (1H, bs, NH), 12.37 (1H, s, NH); ^{13}C NMR (50 MHz, DMSO-*d6*) d: 55.0 (q), 106.0 (s), 109.8 (d), 111.1 (d), 113.1 (d), 114.6 (d), 116.8 (d), 120.3 (s), 122.6 (d), 125.8 (d), 123.7 (s), 129.8 (d), 131.1 (d), 133.6 (s), 136.7 (s), 142.5 (s), 142.7 (s), 158.2 (s), 159.6 (s). Anal. Calcd for $C_{19}H_{14}Br_2N_4OS$ (MW: 506.21): C, 45.08%; H, 2.79%; N, 11.07%. Found: C, 45.16%; H, 2.88%; N, 11.15%.

*5-Bromo-3-[6-(2,5-dimethoxyphenyl)imidazo[2,1-b][1,3,4]thiadiazol-2-yl]-1H-indole hydrobromide (**9o**).*

Light yellow solid, yield: 43%, m.p. 306-307 °C, IR cm^{-1}: 2565-2645 (NH), 3604 (NH); ^{1}HNMR (200 MHz, DMSO-*d6*) d: 3.77 (3H, s, OCH_3), 3.93 (3H, s, OCH_3), 6.89-6.91 (1H, m, Ar-H), 7.05 (1H, d, *J* = 9 Hz, Ar-H), 7.43-7.63 (3H, m, Ar-H), 8.32 (1H, d, *J* = 1.7 Hz,

Ar-H), 8.46 (1H, d, *J* = 2.98 Hz, Ar-H), 8.72 (1H, s, Ar-H), 12.38 (1H, s, NH); ^{13}C NMR (50 MHz, DMSO-*d6*) d: 55.4 (q), 55.8 (q),105.7 (s),111.6 (d),112.7 (d), 113.8 (d), 113.9 (s), 114.2 (d), 114.6 (s), 120.6 (s), 122.6 (d), 125.3 (d), 125.1 (d), 131.4 (d), 135.5 (s), 138.2 (s), 141.9 (s), 149.9 (s), 153.1 (s), 157.8 (s). Anal. Calcd for $C_{20}H_{16}Br_2N_4O_2S$ (MW: 536.24): C, 44.80%; H, 3.01%; N, 10.45%. Found: C, 44.71%; H, 3.20%, N, 10.56%.

*5-Bromo-3-[6-(4-fluorophenyl)imidazo[2,1-b][1,3,4]thiadiazol-2-yl]-1H-indole hydrobromide (**9p**).*

Light yellow solid, yield: 42%, m.p. 289-290 °C, IR cm^{-1}: 2868-2958 (NH), 3341-3484 (NH); ^{1}HNMR (200 MHz, DMSO-*d6*) d: 7.22-7.54 (4H, m, Ar-H), 7.85-7.92 (2H, m, Ar-H), 8.36 (2H, d, *J* = 26.23 Hz, Ar-H), 8.78 (1H, s, Ar-H), 12.34 (1H, s, NH); ^{13}C NMR (50 MHz, DMSO-*d6*) d: 105.9 (s), 110.5 (d), 114.0 (s), 114.6 (d), 115.3 (d), 115.7 (d), 122.6 (d), 125.3 (s), 125.8 (d), 126.2 (d), 126.4 (d), 127.9 (s), 130.4 (s), 130.8 (d), 131.2 (s), 135.4 (s), 142.9 (s), 156.7 (s). Anal. Calcd for C18H11Br2FN4S (MW: 494.18): C, 43.75%; H, 2.24%; N, 11.34%. Found: C, 43.82%; H, 2.18%; N, 11.51%.

*5-Bromo-3-[6-(4-nitrophenyl)imidazo[2,1-b][1,3,4]thiadiazol-2-yl]-1H-indole (**10q**).*

Orange solid, yield: 42%, m.p. 337-338 °C, IR cm^{-1}: 3609 (NH); ^{1}HNMR (200 MHz, DMSO-*d6*) d: 7.42-7.52 (2H, m, Ar-H), 8.10-8.34 (5H, m, Ar-H), 8.44 (1H, s, Ar-H), 9.09 (1H, s, Ar-H), 12.37 (1H, s, NH). Anal. Calcd for $C_{18}H_{10}BrN_5O_2S$ (MW: 440.27): C, 49.10%; H, 2.29%; N, 15.91%. Found: C, 49.25%; H, 2.03%; N, 15.79%.

*5-Bromo-3-[6-(4-trifluoromethylphenyl)imidazo[2,1-b][1,3,4]thiadiazol-2-yl]-1H-indole (**10r**).*

White solid, yield: 45%, m.p. 314-315 °C, IR cm^{-1}: 3609 (NH); ^{1}HNMR (200 MHz, DMSO-*d6*) d: 7.39-7.54 (2H, m, Ar-H), 7.76 (2H, d, *J* = 8.27 Hz, Ar-H), 8.02 (2H, d, *J* = 8.03 Hz, Ar-H), 8.35 (2H, dd, *J* = 1.56, 2.94 Hz, Ar-H), 8.94 (1H, s, Ar-H), 12.32 (1H, s, NH); ^{13}C NMR (50 MHz, DMSO-*d6*) d: 106.0 (s), 112.2 (d), 114.1 (s), 114.6 (s), 115.5 (d), 122.6 (d), 124.8 (2xd), 125.4 (s), 125.6 (s), 125.8 (d), 130.9 (d), 135.4 (s), 137.8 (s), 143.0 (s), 143.5 (s), 157.2 (s). Anal. Calcd for $C_{19}H_{10}BrF_3N_4S$ (MW: 463.27): C, 42.96%; H, 2.18%; N, 12.09%. Found: C, 43.12%; H, 2.35%; N, 12.28%.

*5-Bromo-1-methyl-3-(6-phenylimidazo[2,1-b][1,3,4]thiadiazol-2-yl)-1H-indole hydrobromide (**9s**).*

White solid, yield 52%, m.p. 219-220 °C, IR cm^{-1}: 2936 (NH); ^{1}HNMR (200 MHz, DMSO-*d6*) d: 3.87 (3H, s, CH_3), 7.27-7.61 (5H, m, Ar-H), 7.84 (2H, d, *J* = 7.19 Hz, Ar-H), 8.26 (1H, d, *J* = 1.81 Hz, Ar-H), 8.40 (1H, d, *J* = 5.2 Hz, Ar-H), 8.81 (1H, s, Ar-H), 8.91 (1H, bs, NH); ^{13}C NMR (50 MHz, DMSO-*d6*) d: 33.4 (q), 104.7 (s), 110.9 (s) 113.2 (d), 114.6 (s), 122.6 (d), 124.5 (d), 125.5 (s), 125.8 (d), 127.5 (d), 128.7 (d), 132.8 (s), 134.5 (d), 136.0 (s), 142.6 (s), 143.4 (s), 156.8 (s). Anal. Calcd for $C_{19}H_{14}Br_2N_4S$ (MW: 490.21): C, 46.55%; H, 2.88%; N, 11.43%. Found: C, 46.78%; H, 2.95%; N, 11.51%.

*5-Bromo-3-[6-(3-methoxyphenyl)imidazo[2,1-b][1,3,4]thiadiazol-2-yl]-1-methyl-1H-indole hydrobromide (**9t**).*

Light yellow solid, yield 45%, mp 285-286 °C. ^{1}HNMR (200 MHz, DMSO-*d6*) d: 3.80 (3H, s, CH_3), 3.86 (3H, s, OCH_3), 6.87 (1H, d, *J* = 7.86 Hz, Ar-H), 7.33-7.59 (5H, m, Ar-H), 8.24 (1H, d, *J* = 1.78 Hz, Ar-H), 8.41 (1H, s, Ar-H), 8.82 (1H, s, Ar-H), 9.50 (1H, bs, NH); ^{13}C NMR (50 MHz, DMSO-*d6*) d: 33.3 (q), 55.0 (q),104.7 (s), 109.7 (d), 113.1 (d),114.5 (s), 116.8 (d), 122.6 (d), 125.5 (s), 125.7 (d), 129.6 (d), 129.8 (d), 134.3 (d), 135.9 (s), 142.5 (s), 143.5 (s),156.7 (s), 159.2 (s), 159.5 (s). Anal. Calcd for $C_{10}H_{16}Br_2N_4OS$ (MW: 520.24): C, 46.17%; H, 3.10%; N, 10.77%. Found: C, 46.28%; H, 3.02%; N, 10.91%.

*5-Bromo-3-[6-(2,5-dimethoxyphenyl)imidazo[2,1-b][1,3,4]thiadiazol-2-yl]-1-methyl-1H-indole hydrobromide (**9u**).*

Light yellow solid, yield 53%, mp 290-291 °C, IR cm^{-1}: 2473-2610 (NH); ^{1}HNMR (200 MHz, DMSO-*d6*) d: 3.77 (3H, s, CH_3), 3.88 (3H, s, OCH_3), 3.92 (3H, s, OCH_3), 6.39 (1H, bs, NH), 6.83-7.07 (2H, m, Ar-H), 7.44-7.63 (3H, m, Ar-H), 8.28 (1H, d, *J* =1.68, Ar-H), 8.43 (1H, s, Ar-H), 8.66 (1H, s, Ar-H); ^{13}C NMR (50 MHz, DMSO-*d6*) d: 33.3 (q), 55.3 (q) 55.8 (q), 99.3 (s),100.7 (d),104.8 (s),106.5 (d),111.1 (s),111.6 (d), 112.5 (d), 114.6 (s), 122.8 (d), 125.7 (d), 130.6 (d), 134.0 (d), 134.4 (s), 138.0 (s), 139.4 (s), 149.9 (s), 153.1 (s), 157.0 (s). Anal. Calcd for $C_{21}H_{18}Br_2N_4O_2S$ (MW: 550.26): C, 45.84%; H, 3.30%; N, 10.18%. Found: C, 45.93%; H, 3.60%; N, 10.32%.

*5-Bromo-3-[6-(4-fluorophenyl)imidazo[2,1-b][1,3,4]thiadiazol-2-yl]-1-methyl-1H-indole hydrobromide (**9v**)*

White solid, yield 48%, mp 293-294 °C, IR cm^{-1}: 2588-2609 (NH); ^{1}HNMR (200 MHz, DMSO-*d6*) d: 3.88 (3H, s, CH_3), 7.21-7.30 (2H, t, Ar-H), 7.55 (2H, m, Ar-H), 7.87 (2H, dd, *J* = 1.9, 8.69 Hz, Ar-H), 8.28 (1H, d, *J* = 1.62, Ar-H), 8.39 (1H, s, Ar-H), 8.75 (1H, s, Ar-

H). Anal. Calcd for $C_{19}H_{13}Br_2FN_4S$ (MW: 508.20): C, 44.90%; H, 2.58%; N,11.02%. Found: C, 45.06%; H, 2.64%; N, 11.13%.

*5-Bromo-3-[6-(4-nitrophenyl)imidazo[2,1-b][1,3,4]thiadiazol-2-yl]-1-methyl-1H-indole hydrobromide (**9w**).*

Orange solid, yield 46%, mp 320-321 °C, IR cm^{-1}: 2925 (NH); ^{1}HNMR (200 MHz, DMSO-*d6*) d: 3.92 (3H, s, CH_3), 7.53 (1H, d, *J* = 2.08, Ar-H), 7.63-7.68 (1H, m, Ar-H), 8.12 (2H, d, *J* = 8.86, Ar-H), 8.28-8.33(3H, m, Ar-H), 8.47 (1H, s, Ar-H), 9.08 (1H, s, Ar-H). Anal. Calcd for $C_{19}H_{13}Br_2N_5O_2S$ (MW: 535.21): C, 42.64%; H, 2.45%; N, 13.08%. Found: C, 42.78%; H, 2.58%; N, 13.23%.

*5-Bromo-3-[6-(4-trifluoromethylphenyl)imidazo[2,1-b][1,3,4]thiadiazol-2-yl]-1-methyl-1H-indole (**10x**).*

Yellow solid, yield 42%, m.p. 254-255 °C. ^{1}HNMR (200 MHz, DMSO-*d6*) d: 3.84 (3H, s, CH_3), 7.41-7.57 (2H, m, 2xAr-H), 7.71 (2H, d, *J* = 8.38 Hz, Ar-H), 8.00 (2H, d, *J* = 8.09 Hz, Ar-H), 8.23 (1H, d, *J* = 1.72 Hz, Ar-H), 8.32 (1H, s, Ar-H), 8.85 (1H, s, Ar-H); ^{13}C NMR (50 MHz, DMSO-*d6*) d: 33.3 (q), 104.9 (s), 112.1 (d), 113.1 (d), 114.5 (s), 122.7 (2xd), 124.7 (d), 125.5 (d), 125.5 (d), 125.7 (d), 127.3 (s), 134.2 (d), 135.9 (s), 137.9 (s), 143.1 (s), 143.3 (s), 156.6 (s). Anal. Calcd for $C_{20}H_{12}BrF_3N_4S$ (MW: 477.30): C, 50.33%; H, 2.53%; N, 11.74%. Found: C, 50.54%; H, 2.72%; N, 11.88%.

*5-Chloro-3-(6-phenylimidazo[2,1-b][1,3,4]thiadiazol-2-yl)-1H-indole hydrobromide (**9y**).*

Light yellow solid, yield: 45%, m.p. 297-298 °C, IR cm^{-1}: 2890 (NH), 3445 (NH); ^{1}HNMR (200 MHz, DMSO-*d6*) d: 7.27-7.58 (5H, m, Ar-H), 7.87 (2H, d, *J* = 7.14 Hz, Ar-H), 8.17 (1H, d, *J* = 1.82 Hz, Ar-H), 8.40 (1H, d, *J* = 2.86 Hz, Ar-H), 8.76 (1H, s, Ar-H),12.31 (1H, s, NH); ^{13}C NMR (50 MHz, DMSO-*d6*) d: 106.3 (s), 110.6 (d), 114.8 (d), 119.6 (d), 123.2 (d), 124.4 (2xd), 124.8 (s), 126.1 (s), 127.0 (d), 128.6 (2xd), 130.9 (d), 134.0 (s), 135.2 (s), 142.9 (s), 144.8 (s), 156.6 (s). Anal. Calcd for $C_{18}H_{12}BrClN_4S$ (MW 558.21): C, 50.08%; H, 2.80%; N,12.98%. Found: C, 50.25%; H, 2.91%; N,12.90%.

*5-Chloro-3-[6-(3-methoxyphenyl)imidazo[2,1-b][1,3,4]thiadiazol-2-yl]-1H-indole hydrobromide (**9z**).*

White solid, yield: 46%, m.p. 291-292 °C, IR cm^{-1}: 3478 (NH), 2884 (NH); ^{1}HNMR (200 MHz, DMSO-*d6*) d: 3.81 (3H, s, OCH_3), 6.88 (1H, d, *J* = 6.84 Hz, Ar-H), 7.28-7.59 (5H, m,

Ar-H), 8.14 (1H, d, *J* = 1.82 Hz, Ar-H), 8.46 (1H, d, *J* = 2.90 Hz, Ar-H), 8.87 (1H, s, Ar-H), 10.19 (1H, bs, NH), 12.39 (1H, s, NH); ^{13}C NMR (50 MHz, DMSO-*d6*) d: 55.0 (q), 106.0 (s), 109.8 (d), 111.1 (s), 111.3 (s), 113.2 (d), 114.3 (2xd), 115.4 (s), 116.9 (d), 119.6 (s), 123.4 (d), 124.7 (s), 126.2 (s), 129.8 (d), 131.2 (s), 134.2 (s). Anal. Calcd for $C_{19}H_{14}BrClN_4OS$ (MW: 461.76): C, 49.42%; H, 3.06%; N, 12.13%. Found: C, 49.58%; H, 3.21%; N, 12.25%.

*5-Chloro-3-[6-(2,5-dimethoxyphenyl)imidazo[2,1-b][1,3,4]thiadiazol-2-yl]-1H-indole hydrobromide (**9aa**).*

White solid, yield: 46%, mp 265-266 °C, IR cm^{-1}: 3473 (NH), 2902 (NH); ^{1}HNMR (200 MHz, DMSO-*d6*) d: 3.77 (3H, s, OCH_3), 3.93 (3H, s, OCH_3), 6.86-6.92 (1H, m, Ar-H), 7.07 (1H, d, *J* = 9.05 Hz, Ar-H), 7.28-7.33 (1H, m, Ar-H), 7.57 (2H, m, Ar-H), 7.98 (1H, bs, NH), 8.15 (1H, s, Ar-H), 8.51 (1H, s, Ar-H), 8.76 (1H, s, Ar-H), 12.41 (1H, s, NH); ^{13}C NMR (50 MHz, DMSO-*d6*) d: 55.3 (q), 55.7 (q),106.1 (s), 112.7 (d), 114.2 (s), 114.8 (d), 116.3 (s), 119.5 (d), 123.3 (d), 124.8 (s), 126.9 (s), 131.4 (d), 135.2 (s), 150.6 (s), 152.7 (s), 152.9 (d), 153.1 (s), 157.3 (s). Anal. Calcd for $C_{20}H_{16}BrClN_4O_2S$ (MW: 491.79): C, 48.84%; H, 3.28%; N, 11.39%.
Found: C, 48.96%; H, 3.42%; N, 11.51%.

*5-Chloro-3-[6-(4-fluorophenyl)imidazo[2,1-b][1,3,4]thiadiazol-2-yl]-1H-indole hydrobromide (**9ab**).*

Light yellow solid, yield: 45%, m.p. 288-289 °C, IR cm^{-1}: 3484 (NH), 2890 (NH); ^{1}HNMR (200 MHz, DMSO-*d6*) d: 7.20 (1H, s, NH), 7.23-7.33 (3H, m, Ar-H), 7.57 (1H, d, *J* = 8.68 Hz, Ar-H), 7.59 (1H, s, Ar-H), 7.86-7.90 (2H, m, Ar-H), 8.15 (1H, d, *J* = 1.96 Hz, Ar-H), 8.43 (1H, d, *J* = 2.94, Ar-H), 8.78 (1H, s, Ar-H), 12.34 (1H, s, NH); ^{13}C NMR (50 MHz, DMSO-*d6*) d: 106.1 (s), 110.6 (d), 114.2 (d), 115.4 (d), 115.8 (d), 119.6 (d), 123.3 (d), 124.7 (s), 126.1 (s), 126.3 (d), 126.5 (d), 130.0 (s), 131.1 (d), 135.2 (s),142.9 (s),143.2 (s),157.0 (s). Anal. Calcd for $C_{18}H_{11}BrClFN_4S$ (MW: 449.73): C, 48.07%, H, 2.47%, N,12.46%. Found: C, 48.15%, H, 2.55%, N, 12.52%.

*5-Chloro-3-[6-(4-nitrophenyl)imidazo[2,1-b][1,3,4]thiadiazol-2-yl]-1H-indole hydrobromide (**9ac**).*

Yellow solid, yield: 42%, m.p. 342-343 °C, IR cm^{-1}: 3381 (NH), 2890 (NH); ^{1}HNMR (200 MHz, DMSO-*d6*) d: 7.35 (1H, s, Ar-H), 7.58 (1H, d, *J* = 8.84 Hz, Ar-H), 8.15-8.47

(7H, m, Ar-H), 9.07 (1H, s, NH), 12.37 (1H, s, NH). Anal. Calcd for $C_{18}H_{11}BrClN_5O_2S$ (MW: 476.73): C, 45.35%, H, 2.33%, N, 14.69%. Found: C, 45.45%, H, 2.38%, N, 14.75%.

*5-Chloro-3-[6-(4-trifluoromethylphenyl)imidazo[2,1-b][1,3,4]thiadiazol-2-yl]-1H-indole (**10ad**).*

White solid, yield: 46%, m.p. 312-313 °C, IR cm^{-1}: 2884 (NH); ^{1}HNMR (200 MHz, DMSO-*d6*) d: 7.28 (1H, d, *J* = 6.96 Hz, Ar-H), 7.55 (1H, d, *J* = 6.96 Hz, Ar-H), 7.74 (2H, d, *J* = 8.12 Hz, Ar-H), 8.02-8.14 (3H, m, Ar-H), 8.40 (1H, s, Ar-H), 8.92 (1H, s, Ar-H), 12.34 (1H, s, NH); ^{13}C NMR (50 MHz, DMSO-*d6*) d: 106.1 (s), 112.2 (d), 114.2 (d), 119.6 (d), 123.2 (d), 124.7 (s), 124.7 (s), 124.8 (2xd), 125.6 (d), 125.6 (d), 126.1 (s), 131.2 (d), 135.2 (s), 137.6 (s), 142.8 (s), 143.5 (s), 157.4 (s). Anal. Calcd for $C_{19}H_{10}ClF_3N_4S$ (MW: 418.82): C, 54.49%, H, 2.41%, N,13.38%. Found: C, 54.56%, H, 2.52%, N, 13.43%.

*5-Chloro-1-methyl-3-(6-phenylimidazo[2,1-b][1,3,4]thiadiazol-2-yl)-1H-indole (**10ae**).*

White solid, yield: 42%, m.p. 290-291 °C. ^{1}HNMR (200 MHz, DMSO-*d6*) d: 3.88 (3H, s, CH_3), 7.27-7.39 (4H, m, Ar-H), 7.43 (1H, d, *J* = 7.18 Hz, Ar-H), 7.64 (2H, d, *J* = 8.76 Hz, Ar-H), 8.13 (1H, s, Ar-H), 8.38 (1H, s, Ar-H), 8.72 (1H, s, Ar-H); ^{13}C NMR (50 MHz, DMSO-d6) d: 55.9 (q), 99.5 (s), 105.1 (s), 110.6 (d), 112.8 (d), 119.7 (d), 123.2 (d), 124.4 (d), 124.9 (d), 126.5 (s), 127.1 (2xd), 128.6 (d), 133.9 (s), 134.3 (d), 135.7 (s), 142.7 (s), 144.8 (s),156.1(s). Anal. Calcd for C19H13ClN4S (MW: 364.85): C, 62.55%, H, 3.59%, N, 15.36%. Found: C, 62.76%, H, 3.81%, N, 15.42%.

*5-Chloro-3-[6-(3-methoxyphenyl)imidazo[2,1-b][1,3,4]thiadiazol-2-yl]-1-methyl-1H-indole hydrobromide (**9af**).*

White solid, yield: 50%, m.p. 290-291 °C, IR cm^{-1}: 2970 (NH); ^{1}HNMR (200 MHz, DMSO-*d6)* d: 3.81 (3H, s, CH_3), 3.87 (3H, s, OCH_3), 6.87 (1H, d, *J* = 6.78 Hz, Ar-H), 7.33-7.41 (4H, m, Ar-H), 7.62 (1H, d, *J* = 8.77 Hz, Ar-H), 8.09 (1H, d, *J* = 2.00 Hz, Ar-H), 8.43 (1H, s, Ar-H), 8.81 (1H, s, Ar-H), 9.36 (1H, bs, NH); ^{13}C NMR (50 MHz, DMSO-*d6*) d: 33.4 (q), 55.0 (q), 104.8 (s), 109.8 (d), 111.1 (d), 112.8 (d), 113.2 (d), 116.9 (d), 119.6 (d), 123.2 (d), 124.9 (s), 126.6 (s), 129.8 (d), 134.0 (s), 134.6 (d),135.7 (s),142.5 (s),143.2 (s),156.9 (s),159.6 (s). Anal. Calcd for $C_{20}H_{16}BrClN_4OS$ (MW: 475.79): C, 50.49%; H, 3.39%; N, 11.78%. Found: C, 50.62%; H, 3.48%; N, 11.90%.

*5-Chloro-3-[6-(2,5-dimethoxyphenyl)imidazo[2,1-b][1,3,4]thiadiazol-2-yl]-1-methyl-1H-indole (**10ag**).*

White solid, yield: 55%, m.p. 289-290 °C. ^{1}HNMR (200 MHz, DMSO-*d6*) d: 3.76 (3H, s, CH_3), 3.91 (6H, s, 2xOCH_3), 6.80-6.86 (1H, m, Ar-H), 7.02 (1H, d, *J* = 8.97 Hz Ar-H), 7.36 (1H, dd, *J* = 2.06, 2.03 Hz, Ar-H), 7.63-7.72 (2H, m, Ar-H), 8.17 (1H, d, *J* = 1.94 Hz, Ar-H), 8.40 (1H, s, Ar-H), 8.52 (1H, s, Ar-H); ^{13}C NMR (50 MHz, DMSO-*d6*) d: 33.3 (q), 55.2 (q), 55.7 (q), 105.2 (s), 111.5 (d), 112.4 (d), 112.8 (d), 112.9 (d), 114.2 (d), 119.7 (d), 122.8 (s), 123.2 (d), 124.9 (s), 126.5 (s), 134.3 (d), 135.8 (s), 140.3 (s), 142.0 (s), 149.9 (s), 153.1 (s), 155.9 (s). Anal. Calcd for $C_{21}H_{17}ClN_4O_2S$ (MW: 424.90): C, 59.36%; H, 4.03%; N,13.19%. Found: C, 59.52%; H, 4.28%; N, 13.30%.

*5-Chloro-3-[6-(4-fluorophenyl)imidazo[2,1-b][1,3,4]thiadiazol-2-yl]-1-methyl-1H-indole (**10ah**).*

White solid, yield: 42%, m.p. 295-296 °C. ^{1}HNMR (200 MHz, DMSO-*d6*) d: 3.88 (3H, s, CH_3), 7.20-7.39 (3H, m, Ar-H), 7.64 (1H, d, *J* = 8.76 Hz, Ar-H), 7.84-7.91 (2H, m, Ar-H), 8.12 (1H, d, *J* = 1.76 Hz, Ar-H), 8.38 (1H, s, Ar-H), 8.70 (1H, s, Ar-H); ^{13}C NMR (50 MHz, DMSO-*d6*) d: 33.5 (q),105.1 (s),110.4 (d), 112.9 (d), 114.8 (s), 115.8 (d), 118.4 (d), 119.8 (d), 122.1 (d), 123.0 (d), 125.2 (s), 126.2 (d), 126.5 (s), 134.1 (d), 135.7 (s), 142.8 (s), 143.9 (s), 156.3 (s), 187.7 (s). Anal. Calcd for $C_{19}H_{12}ClFN_4S$ (MW: 382.84): C, 59.61%; H, 3.16%; N,14.63%. Found: C, 59.82%; H, 3.24%; N, 14.90%.

*5-Chloro-3-[6-(4-nitrophenyl)imidazo[2,1-b][1,3,4]thiadiazol-2-yl]-1-methyl-1H-indole (**10ai**).*

Yellow solid, yield 48%, m.p. 315-316 °C. ^{1}HNMR (200 MHz, DMSO-*d6*) d: 3.91 (3H, s, CH_3), 7.38-7.43 (1H, m, Ar-H), 7.69 (1H, d, *J* = 8.77, Ar-H), 8.09-8.17 (3H, m, Ar-H), 8.29 (2H, d, *J* = 8.79, Ar-H), 8.48 (1H, s, Ar-H), 9.05 (1H, s, Ar-H). Anal. Calcd for $C_{19}H_{12}ClN_5O_2S$ (MW: 409.85): C, 59.61%; H, 3.16%; N, 14.63%. Found: C, 59.82%; H, 3.24%; N, 14.90%.

*5-Chloro-3-[6-(4-trifluoromethylphenyl)imidazo[2,1-b][1,3,4]thiadiazol-2-yl]-1-methyl-1H-indole (**10aj**).*

White solid, yield: 43%, m.p. 245-246 °C. ^{1}HNMR (200 MHz, DMSO-*d6*) d: 3.87 (3H, s, CH_3), 7.32-7.38 (1H, m, Ar-H), 7.61 (1H, d, *J* = 8.77, Ar-H) 7.73 (2H, d, *J* = 8.34 Hz, Ar-H), 8.01-8.11 (3H, m, Ar-H), 8.37 (1H, s, Ar-H), 8.86 (1H, s, Ar-H); ^{13}C NMR (50 MHz,

DMSO-*d6*) d: 33.3 (q), 99.5 (s), 105.0 (s), 112.1 (d), 112.7 (d), 119.6 (d), 123.1 (d), 124.7 (2xd), 124.9 (s), 125.5 (2xd), 126.5 (s), 134.4 (d), 135.7 (s), 137.9 (s), 143.1 (s), 143.3 (s), 156.6 (s). Anal. Calcd for $C_{20}H_{12}ClF_3N_4S$ (MW: 432.85): C, 55.50%; H, 2.79%; N, 12.94%. Found: C, 55.71%; H, 2.90%; N, 12.88%.

Biology

Minimum inhibitory concentrations (MICs)

The following Gram-positive and Gram-negative bacterial reference strains were used: *S. aureus* ATCC 25923, *S. aureus* ATCC6538 and *S. epidermidis* ATCC 12228, *P. aeruginosa* ATCC 15442 and *E. coli* ATCC 25922. MICs were determined by a previously described micro method.[10] Briefly, a series of solutions were prepared with a range of concentrations from 100 to 0.75 mg/mL (obtained by two-fold serial dilution). The serial dilutions were made in tryptic soy broth (TSB, VWR International, Leuven) in a 96-wells plate, starting from a stock solution of 1 mg/mL in NaCl 0.9%w/v. A 10mL volume of a bacterial suspension from a 24 h culture containing ~106cfu/mL was added to each well. The plate was incubated at 37 °C for 24 h; after this time, the MICs were determined using a microplate reader (Glomax Multi detection SystemTM297 Promega, Milano, Italy) as the lowest concentrations of the studies compounds whose OD, read at 570 nm, was comparable with the negative control wells (broth only, without inoculum).Each assay was performed in triplicate and repeated at least twice.

Biofilm prevention assay

Above mentioned bacterial strains were incubated in test tubes with Tryptic Soy Broth (TSB) (5 mL) containing 2% w/v glucose at 37 °C for 24 h. The bacterial suspensions were then diluted to achieve a turbidity equivalent to a 0.5 McFarland standard. The diluted suspension (2.5mL) was added to each well of a single cell culture polystyrene sterile, flat-bottom 96-well plate filled with TSB (100mL) with 2% w/v glucose. A screening concentration of 100mg/mL of all compounds were directly added to the wells to assess inhibition percentages values, or in the case of determination of BIC_{50} (the concentration at which the percentage of inhibition of biofilm formation is equal to 50% compared to the untreated control), concentrations in the range among 100 and 0.1mg/mL. Plates were incubated at 37 °C for 24 h. After biofilm growth, the content of each well was removed, wells were washed twice with sterile PBS 1X and stained with 150mL of 0.1% w/v crystal violet solution for 30 min at room temperature. Excess solution was removed and the plate

was washed twice using tap water. A volume of 125mL of acetic acid of 33% v/v was added for 15 min to each stained well to solubilize the dye. The plate was read at 570 nm using a microplate reader (Glomax Multi detection System Promega). BIC_{50} were obtained by comparing the optical densities (ODs) of growth control wells with that of the sample wells, and the value was calculated by using a linear regression graph in Excel. Each assay was performed in triplicate and repeated at least twice. The percentage of inhibition was calculated through the following formula: % of inhibition= ((OD growth control OD sample)/OD growth control)X100

Anti-biofilm activity against preformed biofilm

A suspension of bacteria (0.5 McFarland standard) was obtained using the procedure described above for the inhibition of biofilm formation test. 2.5 mL of suspension was added to each well of a 96-weel plate containing TSB (100 mL) with 2% w/v glucose. After the growth of a biofilm (24 h old), the content of each well was removed, wells were washed up twice with sterile PBS and then filled with fresh TSB medium (200 mL). After that, different concentrations of compounds were added starting from a concentration equal or greater than MIC obtained against planktonic form of tested strains using TSB as medium. The microtiter plate was sealed and incubated at 37 °C for further 24 h. The content of each well was removed, wells were washed up twice with sterile PBS (100 mL to each well) and the 96-weel plate was placed at 60 °C for 1 h before staining with a 0.1% w/v crystal violet solution. After 30 min, plates were washed with tap water to remove any excess stain. Biofilm formation was determined by solubilizing crystal violet as above described and the absorbance was read at 540 nm using a microplate reader (Glomax Multi detection System Promega). The percentages of inhibition were calculated with the above-reported. Each assay was performed in triplicate and repeated at least twice.

Screening as sortase A (SrtA) inhibitors

The compounds **9c**,**9h** and **9ab**, showing the best activity in inhibiting biofilm formation of *S. aureus*, were tested at a screening concentration of 100 mM (1% DMSO) in black 96-well plates (Greiner Bio-One) as SrtA inhibitors. A known SrtA inhibitor, 4-(hydroxymercuri)benzoic acid, was used as positive control. The inhibitory activity of the three compounds was evaluated by quantifying the increase influorescence intensity upon cleavage of the Fluorescence Resonance Energy Transfer (FRET) peptide substrate into two separate fragments resulting in the release of 5-Fam fluorescence, which can be monitored

at excitation/emission=490/520 nm. A commercial kit (SensoLyte® 520 Sortase A Activity Assay Kit * Fluorimetric*) was used with slight modifica-tions. Briefly, the reactions were performed in a volume of 100 mL containing 1X assay buffer, 2.5mg/mL SrtA protease recombinant, 4Mm fluorescent peptide substrate, and the prescribed concentrations of the test compounds or positive control. The peptide substrate without the recombinant SrtA was incubated under the same conditions, and used as a negative control. The reactions were conducted adding both the test compounds and the diluted enzyme solution to the microplate wells. Then sortase substrate solution was added into each well. For kinetic reading, immediately start measuring fluorescence at Ex/Em=490/520 nm continuously recording data every 5 min for 60 min. All fluorescence-reading results are expressed in relative fluorescence units (RFU).

Appendix A. Supplementary data

Supplementary data to this article can be found online at https://doi.org/10.1016/j.ejmech.2019.02.007.

References

(1) Cascioferro, S. The Future of Antibiotic: From the Magic Bullet to the Smart Bullet. *Journal of Microbial & Biochemical Technology* **2014**, *06* (05). https://doi.org/10.4172/1948-5948.1000e118.

(2) Cascioferro, S.; Cusimano, M. G.; Schillaci, D. Antiadhesion Agents against Gram-Positive Pathogens. *Future Microbiol* **2014**, *9*, 1209–1220. https://doi.org/10.2217/fmb.14.56.

(3) Schillaci, D.; Spanò, V.; Parrino, B.; Carbone, A.; Montalbano, A.; Barraja, P.; Diana, P.; Cirrincione, G.; Cascioferro, S. Pharmaceutical Approaches to Target Antibiotic Resistance Mechanisms. *J. Med. Chem.* **2017**. https://doi.org/10.1021/acs.jmedchem.7b00215.

(4) Jamal, M.; Ahmad, W.; Andleeb, S.; Jalil, F.; Imran, M.; Nawaz, M. A.; Hussain, T.; Ali, M.; Rafiq, M.; Kamil, M. A. Bacterial Biofilm and Associated Infections. *J Chin Med Assoc* **2018**, *81* (1), 7–11. https://doi.org/10.1016/j.jcma.2017.07.012.

(5) Lynch, A. S.; Robertson, G. T. Bacterial and Fungal Biofilm Infections. *Annu. Rev. Med.* **2008**, *59*, 415–428. https://doi.org/10.1146/annurev.med.59.110106.132000.

(6) Parrino, B.; Diana, P.; Cirrincione, G.; Cascioferro, S. Bacterial Biofilm Inhibition in the Development of Effective Anti-Virulence Strategy. *Open Med Chem J* **2018**, *12*, 84–87. https://doi.org/10.2174/1874104501812010084.

(7) Raimondi, M. V.; Maggio, B.; Raffa, D.; Plescia, F.; Cascioferro, S.; Cancemi, G.; Schillaci, D.; Cusimano, M. G.; Vitale, M.; Daidone, G. Synthesis and Anti-Staphylococcal Activity of New 4-Diazopyrazole Derivatives. *Eur J Med Chem* **2012**, *58*, 64–71. https://doi.org/10.1016/j.ejmech.2012.09.041.

(8) Schillaci, D.; Petruso, S.; Raimondi, M. V.; Cusimano, M. G.; Cascioferro, S.; Scalisi, M.; La Giglia, M. A.; Vitale, M. Pyrrolomycins as Potential Anti-Staphylococcal Biofilms Agents. *Biofouling* **2010**, *26* (4), 433–438. https://doi.org/10.1080/08927011003718673.

(9) Schillaci, D.; Petruso, S.; Cascioferro, S.; Raimondi, M. V.; Haagensen, J. a. J.; Molin, S. In Vitro Anti-Gram-Positive and Antistaphylococcal Biofilm Activity of Newly Halogenated Pyrroles Related to Pyrrolomycins. *Int. J. Antimicrob. Agents* **2008**, *31* (4), 380–382. https://doi.org/10.1016/j.ijantimicag.2007.10.013.

(10) Schillaci, D.; Spinello, A.; Cusimano, M. G.; Cascioferro, S.; Barone, G.; Vitale, M.; Arizza, V. A Peptide from Human β Thymosin as a Platform for the Development of

New Anti-Biofilm Agents for Staphylococcus Spp. and Pseudomonas Aeruginosa. *World J. Microbiol. Biotechnol.* **2016**, *32* (8), 124. https://doi.org/10.1007/s11274-016-2096-2.

(11) Park, J. S.; Ryu, E.-J.; Li, L.; Choi, B.-K.; Kim, B. M. New Bicyclic Brominated Furanones as Potent Autoinducer-2 Quorum-Sensing Inhibitors against Bacterial Biofilm Formation. *Eur J Med Chem* **2017**, *137*, 76–87. https://doi.org/10.1016/j.ejmech.2017.05.037.

(12) Sambanthamoorthy, K.; Sloup, R. E.; Parashar, V.; Smith, J. M.; Kim, E. E.; Semmelhack, M. F.; Neiditch, M. B.; Waters, C. M. Identification of Small Molecules That Antagonize Diguanylate Cyclase Enzymes to Inhibit Biofilm Formation. *Antimicrob. Agents Chemother.* **2012**, *56* (10), 5202–5211. https://doi.org/10.1128/AAC.01396-12.

(13) Parrino, B.; Schillaci, D.; Carnevale, I.; Giovannetti, E.; Diana, P.; Cirrincione, G.; Cascioferro, S. Synthetic Small Molecules as Anti-Biofilm Agents in the Struggle against Antibiotic Resistance. *European Journal of Medicinal Chemistry* **2019**, *161*, 154–178. https://doi.org/10.1016/j.ejmech.2018.10.036.

(14) Radwan, M. A. A.; Ragab, E. A.; Sabry, N. M.; El-Shenawy, S. M. Synthesis and Biological Evaluation of New 3-Substituted Indole Derivatives as Potential Anti-Inflammatory and Analgesic Agents. *Bioorganic & Medicinal Chemistry* **2007**, *15* (11), 3832–3841. https://doi.org/10.1016/j.bmc.2007.03.024.

(15) Giampieri, M.; Balbi, A.; Mazzei, M.; La Colla, P.; Ibba, C.; Loddo, R. Antiviral Activity of Indole Derivatives. *Antiviral Research* **2009**, *83* (2), 179–185. https://doi.org/10.1016/j.antiviral.2009.05.001.

(16) Parrino, B.; Carbone, A.; Spanò, V.; Montalbano, A.; Giallombardo, D.; Barraja, P.; Attanzio, A.; Tesoriere, L.; Sissi, C.; Palumbo, M.; et al. Aza-Isoindolo and Isoindolo-Azaquinoxaline Derivatives with Antiproliferative Activity. *Eur J Med Chem* **2015**, *94*, 367–377. https://doi.org/10.1016/j.ejmech.2015.03.009.

(17) Spanò, V.; Attanzio, A.; Cascioferro, S.; Carbone, A.; Montalbano, A.; Barraja, P.; Tesoriere, L.; Cirrincione, G.; Diana, P.; Parrino, B. Synthesis and Antitumor Activity of New Thiazole Nortopsentin Analogs. *Mar Drugs* **2016**, *14* (12). https://doi.org/10.3390/md14120226.

(18) Parrino, B.; Attanzio, A.; Spanò, V.; Cascioferro, S.; Montalbano, A.; Barraja, P.; Tesoriere, L.; Diana, P.; Cirrincione, G.; Carbone, A. Synthesis, Antitumor Activity and CDK1 Inhibiton of New Thiazole Nortopsentin Analogues. *Eur J Med Chem* **2017**, *138*, 371–383. https://doi.org/10.1016/j.ejmech.2017.06.052.

(19) Parrino, B.; Carbone, A.; Ciancimino, C.; Spanò, V.; Montalbano, A.; Barraja, P.; Cirrincione, G.; Diana, P.; Sissi, C.; Palumbo, M.; et al. Water-Soluble Isoindolo[2,1-a]Quinoxalin-6-Imines: In Vitro Antiproliferative Activity and Molecular Mechanism(s) of Action. *Eur J Med Chem* **2015**, *94*, 149–162. https://doi.org/10.1016/j.ejmech.2015.03.005.

(20) Sharma, V.; Kumar, P.; Pathak, D. Biological Importance of the Indole Nucleus in Recent Years: A Comprehensive Review. *Journal of Heterocyclic Chemistry* **2010**, *47* (3), 491–502. https://doi.org/10.1002/jhet.349.

(21) Lee, J.-H.; Lee, J. Indole as an Intercellular Signal in Microbial Communities. *FEMS Microbiol. Rev.* **2010**, *34* (4), 426–444. https://doi.org/10.1111/j.1574-6976.2009.00204.x.

(22) Lee, J.; Attila, C.; Cirillo, S. L. G.; Cirillo, J. D.; Wood, T. K. Indole and 7-Hydroxyindole Diminish Pseudomonas Aeruginosa Virulence. *Microb Biotechnol* **2009**, *2* (1), 75–90. https://doi.org/10.1111/j.1751-7915.2008.00061.x.

(23) Lee, H. H.; Molla, M. N.; Cantor, C. R.; Collins, J. J. Bacterial Charity Work Leads to Population-Wide Resistance. *Nature* **2010**, *467* (7311), 82–85. https://doi.org/10.1038/nature09354.

(24) Lee, J.-H.; Cho, M. H.; Lee, J. 3-Indolylacetonitrile Decreases Escherichia Coli O157:H7 Biofilm Formation and Pseudomonas Aeruginosa Virulence. *Environ. Microbiol.* **2011**, *13* (1), 62–73. https://doi.org/10.1111/j.1462-2920.2010.02308.x.

(25) Romagnoli, R.; Baraldi, P. G.; Prencipe, F.; Balzarini, J.; Liekens, S.; Estévez, F. Design, Synthesis and Antiproliferative Activity of Novel Heterobivalent Hybrids Based on Imidazo[2,1-b][1,3,4]Thiadiazole and Imidazo[2,1-b][1,3]Thiazole Scaffolds. *Eur J Med Chem* **2015**, *101*, 205–217. https://doi.org/10.1016/j.ejmech.2015.06.042.

(26) Jakovljević, K.; Matić, I. Z.; Stanojković, T.; Krivokuća, A.; Marković, V.; Joksović, M. D.; Mihailović, N.; Nićiforović, M.; Joksović, L. Synthesis, Antioxidant and Antiproliferative Activities of 1,3,4-Thiadiazoles Derived from Phenolic Acids. *Bioorg. Med. Chem. Lett.* **2017**, *27* (16), 3709–3715. https://doi.org/10.1016/j.bmcl.2017.07.003.

(27) Alegaon, S. G.; Alagawadi, K. R.; Sonkusare, P. V.; Chaudhary, S. M.; Dadwe, D. H.; Shah, A. S. Novel Imidazo[2,1-b][1,3,4]Thiadiazole Carrying Rhodanine-3-Acetic Acid as Potential Antitubercular Agents. *Bioorg. Med. Chem. Lett.* **2012**, *22* (5), 1917–1921. https://doi.org/10.1016/j.bmcl.2012.01.052.

(28) Bhongade, B. A.; Talath, S.; Gadad, R. A.; Gadad, A. K. Biological Activities of Imidazo[2,1-b][1,3,4]Thiadiazole Derivatives: A Review. *Journal of Saudi Chemical*

Society **2016**, *20* (Supplement 1), S463–S475. https://doi.org/10.1016/j.jscs.2013.01.010.

(29) Jadhav, V. B.; Kulkarni, M. V.; Rasal, V. P.; Biradar, S. S.; Vinay, M. D. Synthesis and Anti-Inflammatory Evaluation of Methylene Bridged Benzofuranyl Imidazo[2,1-b][1,3,4]Thiadiazoles. *Eur J Med Chem* **2008**, *43* (8), 1721–1729. https://doi.org/10.1016/j.ejmech.2007.06.023.

(30) Chandrakantha, B.; Isloor, A. M.; Shetty, P.; Fun, H. K.; Hegde, G. Synthesis and Biological Evaluation of Novel Substituted 1,3,4-Thiadiazole and 2,6-Di Aryl Substituted Imidazo [2,1-b] [1,3,4] Thiadiazole Derivatives. *European Journal of Medicinal Chemistry* **2014**, *71* (Supplement C), 316–323. https://doi.org/10.1016/j.ejmech.2013.10.056.

(31) Tahtaci, H.; Karacık, H.; Ece, A.; Er, M.; Şeker, M. G. Design, Synthesis, SAR and Molecular Modeling Studies of Novel Imidazo[2,1-b][1,3,4]Thiadiazole Derivatives as Highly Potent Antimicrobial Agents. *Mol Inform* **2018**, *37* (3). https://doi.org/10.1002/minf.201700083.

(32) Zhang, J.; Liu, H.; Zhu, K.; Gong, S.; Dramsi, S.; Wang, Y.-T.; Li, J.; Chen, F.; Zhang, R.; Zhou, L.; et al. Antiinfective Therapy with a Small Molecule Inhibitor of Staphylococcus Aureus Sortase. *Proc. Natl. Acad. Sci. U.S.A.* **2014**, *111* (37), 13517–13522. https://doi.org/10.1073/pnas.1408601111.

(33) Cascioferro, S.; Totsika, M.; Schillaci, D. Sortase A: An Ideal Target for Anti-Virulence Drug Development. *Microb. Pathog.* **2014**, *77C*, 105–112. https://doi.org/10.1016/j.micpath.2014.10.007.

(34) Cascioferro, S.; Raffa, D.; Maggio, B.; Raimondi, M. V.; Schillaci, D.; Daidone, G. Sortase A Inhibitors: Recent Advances and Future Perspectives. *J. Med. Chem.* **2015**, *58* (23), 9108–9123. https://doi.org/10.1021/acs.jmedchem.5b00779.

(35) Carbone, A.; Parrino, B.; Cusimano, M. G.; Spanò, V.; Montalbano, A.; Barraja, P.; Schillaci, D.; Cirrincione, G.; Diana, P.; Cascioferro, S. New Thiazole Nortopsentin Analogues Inhibit Bacterial Biofilm Formation. *Mar Drugs* **2018**, *16* (8). https://doi.org/10.3390/md16080274.

(36) Cascioferro, S.; Maggio, B.; Raffa, D.; Raimondi, M. V.; Cusimano, M. G.; Schillaci, D.; Manachini, B.; Leonchiks, A.; Daidone, G. A New Class of Phenylhydrazinylidene Derivatives as Inhibitors of Staphylococcus Aureus Biofilm Formation. *Med Chem Res* **2016**, *25* (5), 870–878. https://doi.org/10.1007/s00044-016-1535-9.

(37) Cascioferro, S.; Maggio, B.; Raffa, D.; Raimondi, M. V.; Cusimano, M. G.; Schillaci, D.; Manachini, B.; Plescia, F.; Daidone, G. Synthesis and Biofilm Formation Reduction of Pyrazole-4-Carboxamide Derivatives in Some Staphylococcus Aureus Strains. *European Journal of Medicinal Chemistry* **2016**, *123*, 58–68. https://doi.org/10.1016/j.ejmech.2016.07.030.

(38) Carbone, A.; Parrino, B.; Di Vita, G.; Attanzio, A.; Spanò, V.; Montalbano, A.; Barraja, P.; Tesoriere, L.; Livrea, M. A.; Diana, P.; et al. Synthesis and Antiproliferative Activity of Thiazolyl-Bis-Pyrrolo[2,3-b]Pyridines and Indolyl-Thiazolyl-Pyrrolo[2,3-c]Pyridines, Nortopsentin Analogues. *Mar Drugs* **2015**, *13* (1), 460–492. https://doi.org/10.3390/md13010460.

(39) Parrino, B.; Carbone, A.; Di Vita, G.; Ciancimino, C.; Attanzio, A.; Spanò, V.; Montalbano, A.; Barraja, P.; Tesoriere, L.; Livrea, M. A.; et al. 3-[4-(1H-Indol-3-Yl)-1,3-Thiazol-2-Yl]-1H-Pyrrolo[2,3-b]Pyridines, Nortopsentin Analogues with Antiproliferative Activity. *Mar Drugs* **2015**, *13* (4), 1901–1924. https://doi.org/10.3390/md13041901.

(40) Parrino, B.; Ciancimino, C.; Carbone, A.; Spano', V.; Montalbano, A.; Barraja, P.; Cirrincione, G.; Diana, P. Synthesis of Isoindolo[1,4]Benzoxazinone and Isoindolo[1,5]Benzoxazepine: Two New Ring Systems of Pharmaceutical Interest. **2015**, *71* (39), 7332–7338. https://doi.org/10.1016/j.tet.2015.04.083.

(41) Parrino, B.; Ullo, S.; Attanzio, A.; Spanò, V.; Cascioferro, S.; Montalbano, A.; Barraja, P.; Tesoriere, L.; Cirrincione, G.; Diana, P. New Tripentone Analogs with Antiproliferative Activity. *Molecules* **2017**, *22* (11). https://doi.org/10.3390/molecules22112005.

(42) Melander, R. J.; Minvielle, M. J.; Melander, C. Controlling Bacterial Behavior with Indole-Containing Natural Products and Derivatives. *Tetrahedron* **2014**, *70* (37), 6363–6372. https://doi.org/10.1016/j.tet.2014.05.089.

(43) Adams, N. D.; Aquino, C. J.; Chaudhari, A. M.; Ghergurovich, J. M.; Kiesow, T. J.; Parrish, C. A.; Reif, A. J.; Wiggall, K. Triazolones as Fatty Acid Synthase Inhibitors. EP2538787A1, January 2, 2013.

(44) Xinglong Jiang, *; Ashish Tiwari, *; Maethonia Thompson; Zhihong Chen; Thomas P. Cleary, and; Lee, T. B. K. A Practical Method for N-Methylation of Indoles Using Dimethyl Carbonate https://pubs.acs.org/doi/full/10.1021/op0102215 (accessed Oct 25, 2018). https://doi.org/10.1021/op0102215.

Part III

In vitro and in vivo studies on Malignant Mesothelioma

(chapters 9-11)

Chapter 9

Proton-coupled folate transporter as a biomarker of outcome to treatment for pleural mesothelioma

Li Petri G[1,2], Cascioferro S[2], Parrino B[2], Peters GJ[1], Diana P[2], Giovannetti E[1,3*]

*Author for correspondence

1. *Department of Medical Oncology, VU University Medical Center, Cancer Center Amsterdam, De Boelelaan 1117, 1081HV Amsterdam, The Netherlands*
2. *Dipartimento di Scienze e Tecnologie Biologiche, Chimiche e Farmaceutiche, Sezione di Chimica e Tecnologie Farmaceutiche, Università degli Studi di Palermo, Via Archirafi 32, 90123 Palermo, Italy*
3. *Cancer Pharmacology Lab, AIRC Start-Up Unit, University of Pisa, via Paradisa, 56100, Pisa, Italy*

Pharmacogenomics. 2018 July 1;19(10): 811-814

doi: 10.2217/pgs-2018-0071. Epub 2018 June 19

"PCFT was not only identified as a new biomarker that can help predict pemetrexed's effectiveness or chemoresistance, but also a potential useful target to overcome such chemoresistance"

Proton-coupled folate transporter as a biomarker of outcome to treatment for pleural mesothelioma

Editorial

Keywords: chemoresistance, mesothelioma, PCFT, pemetrexed

The main objective of pharmacogenetics is the identification of genetic features involved in clinically meaningful variations in drug responsiveness. Therefore, pharmacogenetics may reduce the variation in individual response to drugs and for tailoring therapies according to genetic profile, fulfilling the promise of precision medicine.[1]

The problem of interindividual variability in drug response is particularly important in anticancer regimens, which are characterized by a narrow therapeutic window. Small alterations in the transport or metabolism of anticancer agents may indeed cause large changes in their pharmacological effects, both in terms of toxicity and efficacy.

As reported by the Pharmacology and Molecular Mechanisms group of the European Organization for the Research and Treatment of Cancer, the terms ‘pharmacogenetics’ and ‘pharmacogenomics’ are often used interchangeably and pharmacogenetics is considered as concerning the individual patient’s characteristics and pharmacogenomics those of the tumor.[2] However, according to this position paper as well as to the definition by the European agency for the evaluation of medicinal products ‘pharmacogenetics’ focuses on the association of one gene or several genes with drug activity, while ‘pharmacogenomics’ considers the whole genome, through the broader application of new genomic technologies.[3] Thus, in oncology, a pharmacogenetic approach aims to customize the chemotherapy treatment according to individual/somatic as well as tumor genetic characteristics. This represents a modern and intriguing challenge and pharmacogenetic tools are warranted to maximize the therapeutic efficacy and minimize useless treatments, especially in patients affected by solid tumors with limited therapeutic approaches, such as malignant pleural mesothelioma (MPM).

MPM is an aggressive tumor arising from the pleura, with grim prognosis. Its incidence is increasing throughout most of the world and it is predicted that it will rise in the next 10 years.[4] Most patients with MPM are not amenable to radical surgery and systemic therapy is the only potential treatment option. A number of prognostic factors have been described and are part of two prognostic scoring systems. In the European Organization for the Research and Treatment of Cancer score, poor prognosis is associated with a poor

performance status, a high white blood cell count, male gender and having sarcomatoid histologic subtype, while In the Cancer and Leukemia Group B scoring system pleural involvement, LDH >500 IU/l, poor PS, chest pain, platelets >400,000/µl, nonepithelial histology and age older than 75 years, jointly predict poor overall survival (OS).

Based on extensive genomic profiling, four MPM molecular subtypes were associated with OS.[5] However, up to now, there are no data about specific genetic biomarkers of response to chemotherapy in MPM patients.

The identification of such molecular predictors is urgently needed in order to select patients for optimal treatment strategies and to improve clinical outcome.

More than 14 years ago, US FDA approved the first ever (and the last so far) drug to be used in the first-line treatment of MPM in combination with cisplatin, pemetrexed. In fact, this combination significantly improved the response rate (41.3 vs 16.7%; $p < 0.0001$), time to progression (5.7 vs 3.9 months; $p = 0.001$), OS (12.1 vs 9.3 months; $p = 0.020$) and quality of life compared with cisplatin alone. The combination with carboplatin gave similar results.[6]

Pemetrexed is a multitargeted antifolate agent that enters the cancer cells through different transporters and is then converted to a series of analogous polyglutamate derivatives by the enzyme folylpolyglutamate synthetase. This polyglutamylation leads to extended intracellular retention, resulting in more prolonged efficacy. Active metabolites of pemetrexed inhibit several folate-dependent enzymes such as thymidylate synthase, dihydrofolate reductase, glycinamide ribonucleotide formyl transferase and to a lesser extent, aminoimidazole carboxamide ribonucleotide tranformylase and CI-tetrahydrofolate synthase, thereby inhibiting both pyrimidine and purine biosynthesis.[7]

In vitro studies demonstrated that several factors increase the antitumor activity of pemetrexed, including low expression levels of the main target TS, high activity of folylpolyglutamate synthetase and the rapid transport across the plasma membrane mediated by influx transporters for which pemetrexed has different affinities.[8] In agreement with previous data in non-squamous and squamous specimens from lung cancer patients treated with pemetrexed-based chemotherapy, as reviewed by Santarpia and collaborators,[9] high TS expression has also been associated with poor response, as well as significantly shorter median progression-free survival and OS in the two largest multicenter studies on pemetrexed-based regimens in MPM.[10,11]

In a more recent translational study, the efficacy of pemetrexed was associated with both low TS and high proton coupled folate transporter (PCFT/SLC46A1) expression

levels.[12] In fact, a high mRNA expression of *PCFT* and a low-mRNA expression of *TS* were associated with lower risk of developing a progressive disease compared with disease-control as well as with significantly longer progression-free survival and OS. Low-PCFT protein levels were also associated with shorter OS and multivariate analysis confirmed PCFT-independent prognostic role.

In mammalian cells, three distinct processes mediate membrane transport of folates and antifolates, including pemetrexed.[13] The reduced folate carrier (RFC) is a carrier-mediated anion exchanger, facilitating the translocation of a folate substrate across the cell membrane by the co-transport of another anion in the opposite direction. With a Ki for methotrexate influx ranging from 2 to 5 μmol/l in murine and human tumor cell lines, RFC has a higher affinity for methotrexate than for folic acid. Of note, the affinity for pemetrexed is twofold higher.[14] The folate receptors FR-α and FR-β are binding proteins anchored to the cell membranes by a glycosyl phosphatidylinositol tail that mediates transport by an endocytotic process. The maximum rate of transport into cells mediated by this mechanism is 100, the rate mediated by RFC. Hence, FR-mediated transport contributes little to the uptake of pemetrexed. The third folate transport system, characterized by a unique and distinct low-pH optimum that is present in the majority of human solid tumors, is mediated by PCFT. This transporter was initially characterized in mice, and only recently emerged as the main transporter mediating pemetrexed influx, with remarkable transport km values of 0.2–0.8 μM.[15]

The pivotal role of PCFT in the transport of folates and antifolates has been demonstrated in various models, showing that PCFT transfection in HeLa cells increased pemetrexed cytotoxicity,[16] while PCFT silencing increased IC_{50} values by fourfold and threefold in the MSTO-211H and H2452 MPM cells, respectively.[12] Of note, PCFT promoter can be silenced via DNA methylation,[17] resulting in reduced transcriptional activity. Indeed, H28 MPM cells, which displayed methylation of 85% of the CpG-islands of *PCFT* promoter had low expression levels of PCFT and were relatively more resistant to pemetrexed.[12] Additional experiments were then performed to evaluate PCFT expression and cell proliferation after DNA demethylation. These experiments were performed with 5-Aza-2´-deoxycytidine, which significantly reduced the methylation of the *PCFT* promoter, down to -70% in the H28 cells and subsequently increased them RNA expression of *PCFT* as well as the growth inhibitory activity of pemetrexed. This means that PCFT was not only identified as a new biomarker that can help predict pemetrexed's effectiveness or chemoresistance, but also a potential useful target to overcome such chemoresistance.

Where do we go from here? We suggest the following rational preclinical and clinical development strategies. First of all, additional preclinical studies in appropriate *in vivo* models of MPM should evaluate the key role of PCFT in the antitumor activity of pemetrexed and other potential molecular mechanisms underlying the differential PCFT expression, such as, for instance, the hypoxic/metabolic status of these tumors, which has also been correlated to pemetrexed resistance[18] and might suggest novel antiglycolitic therapeutic strategies.[19,20] Second, translational studies with prospectively collected samples, are essential for the validation of the previous retrospective data as well as for the identification of the best cut-off expression level for a validated pharmacogenetic test. Finally, a Phase I basket trial should test 5-Aza-2´-deoxycytidine, which is a well-tolerated compound currently used to treat myelodysplastic syndrome, in patients with different tumor types, such as mesothelioma and lung cancer, to be treated with pemetrexed and cisplatin and stratified according to PCFT expression. Subsequently, Phase II and Phase III trials could then select the best tumor type and establish the role of this new potential pharmacogenetic guided treatment *versus* the standard of care backbone chemotherapy, according to previously standardized and validated thresholds.

Hopefully, the results of these studies should enable oncologists to stratify patients based on PCFT before anticancer treatment, allowing the optimization of clinical outcomes through effective personalization of treatment.

Financial & competing interests disclosure

This work was partially supported by 'the Law Offices of Peter G Angelos Grant' from the Mesothelioma Applied Research Foundation (MARF), USA. The authors have no other relevant affiliations or financial involvement with any organization or entity with a financial interest in or financial conflict with the subject matter or materials discussed in the manuscript apart from those disclosed. No writing assistance was utilized in the production of this manuscript.

References

(1) Sánchez, N. S.; Mills, G. B.; Mills Shaw, K. R. Precision Oncology: Neither a Silver Bullet nor a Dream. *Pharmacogenomics* **2017**, *18* (16), 1525–1539. https://doi.org/10.2217/pgs-2017-0094.

(2) Robert, J.; Le Morvan, V.; Giovannetti, E.; Peters, G. J.; PAMM Group of EORTC. On the Use of Pharmacogenetics in Cancer Treatment and Clinical Trials. *Eur. J. Cancer* **2014**, *50* (15), 2532–2543. https://doi.org/10.1016/j.ejca.2014.07.013.

(3) European Medicines Agency - - Terminology in pharmacogenetics http://www.ema.europa.eu/ema/index.jsp?curl=pages/regulation/general/general_content_001405.jsp&mid= (accessed May 2, 2018).

(4) Carbone, M.; Kanodia, S.; Chao, A.; Miller, A.; Wali, A.; Weissman, D.; Adjei, A.; Baumann, F.; Boffetta, P.; Buck, B.; et al. Consensus Report of the 2015 Weinman International Conference on Mesothelioma. *J Thorac Oncol* **2016**, *11* (8), 1246–1262. https://doi.org/10.1016/j.jtho.2016.04.028.

(5) Bueno, R.; Stawiski, E. W.; Goldstein, L. D.; Durinck, S.; De Rienzo, A.; Modrusan, Z.; Gnad, F.; Nguyen, T. T.; Jaiswal, B. S.; Chirieac, L. R.; et al. Comprehensive Genomic Analysis of Malignant Pleural Mesothelioma Identifies Recurrent Mutations, Gene Fusions and Splicing Alterations. *Nat. Genet.* **2016**, *48* (4), 407–416. https://doi.org/10.1038/ng.3520.

(6) Ceresoli, G. L.; Zucali, P. A.; Favaretto, A. G.; Grossi, F.; Bidoli, P.; Del Conte, G.; Ceribelli, A.; Bearz, A.; Morenghi, E.; Cavina, R.; et al. Phase II Study of Pemetrexed plus Carboplatin in Malignant Pleural Mesothelioma. *J. Clin. Oncol.* **2006**, *24* (9), 1443–1448. https://doi.org/10.1200/JCO.2005.04.3190.

(7) Chattopadhyay, S.; Moran, R. G.; Goldman, I. D. Pemetrexed: Biochemical and Cellular Pharmacology, Mechanisms, and Clinical Applications. *Mol. Cancer Ther.* **2007**, *6* (2), 404–417. https://doi.org/10.1158/1535-7163.MCT-06-0343.

(8) Giovannetti, E.; Toffalorio, F.; De Pas, T.; Peters, G. J. Pharmacogenetics of Conventional Chemotherapy in Non-Small-Cell Lung Cancer: A Changing Landscape? *Pharmacogenomics* **2012**, *13* (9), 1073–1086. https://doi.org/10.2217/pgs.12.91.

(9) Santarpia, M.; Rolfo, C.; Peters, G. J.; Leon, L. G.; Giovannetti, E. On the Pharmacogenetics of Non-Small Cell Lung Cancer Treatment. *Expert Opin Drug Metab Toxicol* **2016**, *12* (3), 307–317. https://doi.org/10.1517/17425255.2016.1141894.

(10) Righi, L.; Papotti, M. G.; Ceppi, P.; Billè, A.; Bacillo, E.; Molinaro, L.; Ruffini, E.; Scagliotti, G. V.; Selvaggi, G. Thymidylate Synthase but Not Excision Repair Cross-

Complementation Group 1 Tumor Expression Predicts Outcome in Patients with Malignant Pleural Mesothelioma Treated with Pemetrexed-Based Chemotherapy. *J. Clin. Oncol.* **2010**, *28* (9), 1534–1539. https://doi.org/10.1200/JCO.2009.25.9275.

(11) Zucali, P. A.; Giovannetti, E.; Destro, A.; Mencoboni, M.; Ceresoli, G. L.; Gianoncelli, L.; Lorenzi, E.; De Vincenzo, F.; Simonelli, M.; Perrino, M.; et al. Thymidylate Synthase and Excision Repair Cross-Complementing Group-1 as Predictors of Responsiveness in Mesothelioma Patients Treated with Pemetrexed/Carboplatin. *Clin. Cancer Res.* **2011**, *17* (8), 2581–2590. https://doi.org/10.1158/1078-0432.CCR-10-2873.

(12) Giovannetti, E.; Zucali, P. A.; Assaraf, Y. G.; Funel, N.; Gemelli, M.; Stark, M.; Thunnissen, E.; Hou, Z.; Muller, I. B.; Struys, E. A.; et al. Role of Proton-Coupled Folate Transporter in Pemetrexed Resistance of Mesothelioma: Clinical Evidence and New Pharmacological Tools. *Ann. Oncol.* **2017**, *28* (11), 2725–2732. https://doi.org/10.1093/annonc/mdx499.

(13) Gonen, N.; Assaraf, Y. G. Antifolates in Cancer Therapy: Structure, Activity and Mechanisms of Drug Resistance. *Drug Resist. Updat.* **2012**, *15* (4), 183–210. https://doi.org/10.1016/j.drup.2012.07.002.

(14) Mauritz, R.; Peters, G. J.; Priest, D. G.; Assaraf, Y. G.; Drori, S.; Kathmann, I.; Noordhuis, P.; Bunni, M. A.; Rosowsky, A.; Schornagel, J. H.; et al. Multiple Mechanisms of Resistance to Methotrexate and Novel Antifolates in Human CCRF-CEM Leukemia Cells and Their Implications for Folate Homeostasis. *Biochem. Pharmacol.* **2002**, *63* (2), 105–115.

(15) Zhao, R.; Goldman, I. D. The Proton-Coupled Folate Transporter: Physiological and Pharmacological Roles. *Curr Opin Pharmacol* **2013**, *13* (6), 875–880.

(16) Diop-Bove, N. K.; Wu, J.; Zhao, R.; Locker, J.; Goldman, I. D. Hypermethylation of the Human Proton-Coupled Folate Transporter (SLC46A1) Minimal Transcriptional Regulatory Region in an Antifolate-Resistant HeLa Cell Line. *Mol. Cancer Ther.* **2009**, *8* (8), 2424–2431. https://doi.org/10.1158/1535-7163.MCT-08-0938.

(17) Gonen, N.; Bram, E. E.; Assaraf, Y. G. PCFT/SLC46A1 Promoter Methylation and Restoration of Gene Expression in Human Leukemia Cells. *Biochem. Biophys. Res. Commun.* **2008**, *376* (4), 787–792. https://doi.org/10.1016/j.bbrc.2008.09.074.

(18) Raz, S.; Sheban, D.; Gonen, N.; Stark, M.; Berman, B.; Assaraf, Y. G. Severe Hypoxia Induces Complete Antifolate Resistance in Carcinoma Cells Due to Cell Cycle Arrest. *Cell Death Dis* **2014**, *5*, e1067. https://doi.org/10.1038/cddis.2014.39.

(19) Nabavi, N.; Bennewith, K. L.; Churg, A.; Wang, Y.; Collins, C. C.; Mutti, L. Switching off Malignant Mesothelioma: Exploiting the Hypoxic Microenvironment. *Genes Cancer* **2016**, *7* (11–12), 340–354. https://doi.org/10.18632/genesandcancer.124.

(20) Giovannetti, E.; Leon, L. G.; Gómez, V. E.; Zucali, P. A.; Minutolo, F.; Peters, G. J. A Specific Inhibitor of Lactate Dehydrogenase Overcame the Resistance toward Gemcitabine in Hypoxic Mesothelioma Cells, and Modulated the Expression of the Human Equilibrative Transporter-1. *Nucleosides, Nucleotides and Nucleic Acids* **2016**, *35* (10–12), 643–651. https://doi.org/10.1080/15257770.2016.1149193.

Chapter 10

Impact of hypoxia on chemoresistance of mesothelioma mediated by the proton-coupled folate transporter, and preclinical activity of new anti-LDH-A compounds

Giovanna Li Petri[1,2*], Btissame El Hassouni[1*], Rocco Sciarrillo[1,3,4*],Niccola Funel[5], Giulia Mantini[1,6], Eveline A. Zeeuw van der Laan[1], Stella Cascioferro[2], Amir Avan[1,7], Paolo A. Zucali[8], Nadia Zaffaroni[9], Tonny Lagerweij[10], Barbara Parrino[2], Marcello Deraco[11], Carlotta Granchi[11], Alicia Bulinska[13], Ryszard T. Smolenski[12], Larry H. Matherly[13], Gerrit Jansen[14], Yehuda G. Assaraf[15], Patrizia Diana[2], Jacqueline Cloos[3,4], Godefridus J. Peters[1], Filippo Minutolo[11], Elisa Giovannetti[1,6]

*equal contributors

1. Department of Medical Oncology, Cancer Center Amsterdam, VU University Medical Center, Amsterdam, The Netherlands;
2. Dipartimento di Scienze e Tecnologie Biologiche Chimiche e Farmaceutiche (STEBICEF), Università degli Studi di Palermo, Palermo, Italy;
3. Department of Hematology, Cancer Center Amsterdam, VU University Medical Center, Amsterdam, The Netherlands;
4. Department of Pediatric Oncology, Cancer Center Amsterdam, VU University Medical Center, Amsterdam, The Netherlands;
5. Azienda Ospedaliera Universitaria Pisana, Pisa, Italy;
6. Cancer Pharmacology Lab, Fondazione Pisana per la Scienza, Pisa, Italy;
7. Metabolic syndrome Research center, Mashhad University of Medical Sciences, Mashhad, Iran;
8. Department of Oncology; Humanitas Clinical and Research Hospital, Rozzano (Milan), Italy;
9. Molecular Pharmacology Unit, Fondazione IRCCS Istituto Nazionale dei Tumori, Milano, Italy;
10. Department of Neurosurgery, Neuro-Oncology Research Group, Cancer Center Amsterdam, VU University Medical Center, Amsterdam, The Netherlands;
11. Peritoneal Malignancy Program, Fondazione IRCCS Istituto Nazionale dei Tumori, Milano, Italy;
12. Department of Pharmacy, University of Pisa, Pisa, Italy;
13. Department of Biochemistry, Medical University of Gdansk, Gdańsk, Poland;
14. Barbara Ann Karmanos Cancer Institute, Wayne State University School of Medicine, Detroit, USA;
15. Rheumatology and immunology Center, VU University Medical Center, Amsterdam, The Netherlands;

16. Fred Wyszkowski Cancer Research Laboratory, Department of Biology, Technion-Israel Institute of Technology, Haifa, Israel

Corresponding author:

Elisa Giovannetti, MD PhD

Notes: *Equal contributors

Provisionally accepted in British Journal of Cancer

Impact of hypoxia on chemoresistance of mesothelioma mediated by the proton-coupled folate transporter, and preclinical activity of new anti-LDH-A compounds

Abstract

BACKGROUND: Expression of proton-coupled folate-transporter (PCFT) is associated with survival of mesothelioma patients treated with pemetrexed, and is reduced by hypoxia, prompting studies to elucidate their correlation.

METHODS: Modulation of glycolytic gene expression was evaluated by PCR-arrays in tumor cells and primary cultures growing under hypoxia, in spheroids and after PCFT-silencing. Inhibitors of lactate dehydrogenase (LDH-A) were tested *in vitro* and *in vivo*. LDH-A expression was determined in tissue-microarrays of radically-resected malignant pleural mesothelioma (MPM, N=33) and diffuse peritoneal mesothelioma (DMPM, N=56) patients.

RESULTS: Overexpression of hypoxia marker CAIX was associated with low PCFT expression and decreased MPM cell growth inhibition by pemetrexed. Through integration of PCR-arrays in hypoxic cells and spheroids and following PCFT-silencing, we identified the up-regulation of LDH-A, which correlated with shorter survival of MPM and DMPM patients. Novel LDH-A inhibitors enhanced spheroid disintegration, and displayed synergistic effects with pemetrexed in MPM and gemcitabine in DMPM cells. Studies with bioluminescent hypoxic orthotopic and subcutaneous DMPM athymic-mice models revealed the marked antitumor activity of the LDH-A inhibitor NHI-Glc-2, alone or combined with gemcitabine.

CONCLUSIONS: This study provides novel insights on hypoxia/PCFT-dependent chemoresistance, unraveling the potential prognostic value of LDH-A, and demonstrating the preclinical activity of LDH-A inhibitors.

Keywords: malignant pleural and peritoneal mesothelioma, proton-coupled folate transporter, pemetrexed, chemoresistance, hypoxia, lactate dehydrogenase, spheroids, xenografts, prognosis

Background

Malignant pleural mesothelioma (MPM) and diffuse malignant peritoneal mesothelioma (DMPM) are rare but aggressive tumors arising from mesothelial cells lining the pleural and peritoneal cavity, respectively. The incidence of these malignancies is associated with exposure to asbestos and is increasing throughout the world, with a predicted peak in the next 15 years.[1] Both MPM and DMPM are typically diagnosed at an advanced stage and are extremely difficult to treat.

Systemic therapy is the only treatment option for the vast majority of MPM patients. The standard of care in the first line treatment is a combination of platinum-based chemotherapy with the third generation antifolate pemetrexed. This combination significantly improved the overall survival (OS, 12.1 vs 9.3 months; p=0.020), compared to cisplatin monotherapy.[2] Patients who do not qualify to receive cisplatin-based chemotherapy, are treated with alternative chemotherapy including pemetrexed alone, or in combination with carboplatin.[3] Systemic chemotherapy is also used for patients harboring DMPM, when patients cannot undergo cytoreductive surgery followed by hyperthermic perioperative chemotherapy.[4]

Coupled with a better understanding of the molecular mechanisms underlying drug resistance or sensitivity, the introduction of biomarkers into the pathologic analysis of both MPM and DMPM should drive the individualization of precision medicine, and improve the outcome of these malignancies. A few retrospective studies suggested the predictive role of the primary target of the activity of pemetrexed, thymidylate synthase (TS),[5,6] but further research on additional mechanisms of chemoresistance is warranted.[7,8]

The proton-coupled folate transporter (PCFT/SLC46A1) has recently emerged for its key role in folate and antifolate transport, which was demonstrated in various model systems, including MPM,[9] and in several human tissues.[10] Of note, the activities of the folate transporters reduced folate carrier (RFC/SLC19A1) and PCFT are significantly affected by the pH of the tumor microenvironment (TME). Whereas RFC displays optimal transport activity at physiological pH, PCFT-mediated transport is very low.[11] The optimal pH for PCFT-dependent transport is 5.5, with considerable transport activity detectable at pH 6.5 or 6.8, depending upon the tumor size, type and distance from blood vessels. Therefore, PCFT may be the sole route of delivery of folates and antifolates in the acidic microenvironment of solid tumors. Furthermore, PCFT exhibits a high transport affinity for pemetrexed[12] and PCFT transfection increases its folate and antifolate transport as well as antifolate cytotoxicity.[11] These findings support the unique role that PCFT plays in the transport and pharmacologic activity of pemetrexed; consistently, we recently demonstrated that low expression of the PCFT transporter, both at the

mRNA and protein levels, is associated with shorter survival of MPM patients treated with pemetrexed.[13] This enhanced our interest into additional key mechanisms associated with drug resistance underlying the modulation of PCFT expression in cancer cells. Interestingly, Raz and collaborators,[14] showed that severe hypoxia induced a complete antifolate-resistance and caused simultaneous suppression of key genes in folate homeostasis, including the influx transporters RFC and PCFT. This could be attributed, at least in part, to alterations in Sp1 activity or promoter methylation of these genes under hypoxic conditions. These data are in agreement with previous findings demonstrating that cells growing in three-dimensional (3D) systems, with increased hypoxic areas, showed diminished antifolate transport and decreased antifolate sensitivity.[15] The current study was aimed at evaluating the correlation between PCFT expression under hypoxic conditions with pemetrexed activity in MPM cells. Moreover, using a variety of *in vitro* models, including 3D spheroids, as well as targeted silencing and PCR-arrays, we sought to further elucidate key factors affecting drug resistance. These studies identified a significant up-regulation of the key glycolytic enzyme LDH-A. Our previous studies demonstrated that novel LDH-A inhibitors were especially effective and synergistic with gemcitabine against cells under hypoxic conditions, and gemcitabine displayed antitumor activity in both MPM and DMPM patients.[16–20] Moving from these premises, we investigated the role of LDH-A inhibition as a potential therapeutic strategy both in MPM and DMPM, using *in vitro* and *in vivo* orthotopic and subcutaneous models. Finally, we investigated whether the expression levels of LDH-A were associated with significantly worse clinical outcome, using tissue microarrays (TMA) with specimens from both MPM and DMPM patients. Our results provide novel mechanistic insights on mesothelioma chemoresistance that may contribute to the rational development of innovative prognostic biomarkers and therapeutic interventions for this devastating disease.

Methods

Patients and immunohistochemistry

Previous studies demonstrated that MPM is a hypoxic malignancy[21,22] and cells that survive hypoxia are more resistant to antifolates because of the down-regulation of several key enzymes and transporters.[14] Therefore, we evaluated by immunohistochemistry (IHC) the percentage and distribution of hypoxic cells by using the monoclonal antibody ab15086 (Abcam, Cambridge, MA) to detect the levels of Carbonic Anhydrase IX (CAIX), as described previously,[23] within areas with high and low PCFT levels that were assessed with PCFT polyclonal antibody.[13]
The expression levels of these proteins were evaluated in tissue microarrays (TMA) including tumors from 33 MPM patients enrolled at Humanitas Cancer Center (Milan, Italy) between 2008 and 2013, as described previously.[13] Further IHC studies were performed in order to assess the expression levels of LDH-A using both the TMA of MPM patient specimens and TMAs containing samples from 56 DMPM patients enrolled between 1995 and 2013 at National Cancer Institute (INT, Milan, Italy), as described previously.[24] Patients' characteristics are summarized in Supplemental Table 1. These studies were approved by the appropriate ethical review boards (Humanitas Cancer Center (ClinicalTrials.gov NCT00867711) and INT Review Board and Ethics Committees). Scoring for PCFT was described in our previous study.[13] Immunostaining intensity of CAIX was described in the Supplemental Table 2, while for LDH-A we used a previously proposed grading system with two LDH-A expression levels: strong cytoplasmic expression in >50% of cancer cells or nuclear expression in >10% of cancer cells was defined as high expression; otherwise, nuclear expression was considered low.[25] More details on TMA and IHC are reported in the Supplemental methods section.

Cells and drugs

Three human MPM cell lines (H28, H2452, MSTO-211H) were obtained from ATCC (Manassas, VA) and cultured as previously described.[26] Human primary DMPM cultures (MesoII and STO) were derived from tumor samples of patients who underwent surgery, and were maintained in DMEM/F12 (Gibco) under standard culture conditions for less than 20 passages.[24] Cells were routinely tested for mycoplasma. Analyses of mitochondrial function and glycolysis of MSTO-211H and H2452 cells were performed with the Seahorse XFp Metabolic Flux Analyzer (Agilent Technologies, Santa Clara, CA), showing that these cells have both a normal aerobic metabolism and aerobic glycolysis, though to different extent, as reported in the Supplemental methods and Supplemental Fig.S1.

Co-transduction of MesoII cells with luciferase vectors and Firefly-luciferase (F-luc) activity assessment were performed according to previously established methods.[23,24] Pemetrexed and gemcitabine were gifts from Eli Lilly (Indianapolis, IN), while the LDH-A inhibitors NHI-2 and NHI-Glc-2 were synthesized as described previously.[17,27] Drugs were dissolved in sterile water (gemcitabine) or dimethyl sulfoxide (DMSO, pemetrexed and LDH-A inhibitors) and diluted in culture medium immediately before use. In each experiment we did not use concentrations higher than 0.1% DMSO

Evaluation of the role of hypoxia on PCFT expression and pemetrexed activity

The impact of hypoxia on the sensitivity of MPM cells to pemetrexed was evaluated by growing cells at an O_2 tension of 1%, 5% (vol/vol) CO_2, and 94% (vol/vol) N_2 at 37°C, using a specific IncuSafe Jacomex Glove Box (Labo Equipment Sanyo, Loughborough, UK). The concentrations of pemetrexed that inhibited cell growth by 50% (IC_{50}) were determined using the sulforhodamine-B (SRB) assay, as described previously.[24] Cells exposed for 72 hours to hypoxic conditions were also used to explore the down-regulation of PCFT expression by quantitative real-time PCR (qRT-PCR), as well as after silencing with the specific anti-PCFT siRNA D#141241-siRNA (Thermofisher, Waltham, MA). The PCR reactions were performed using the Hs00560565_m1 Assay-on-Demand product (Applied Biosystems, Foster City, CA), with the ABI PRISM™ 3100 Genetic analyzer (Applied Biosystems). Further studies with qRT-PCR assessed the expression of LDH-A in MSTO and STO cells, using previously validated methods.[17] In addition, the influence of PCFT on pemetrexed-mediated cell growth inhibition was studied in parallel SRB experiments after 48 hours exposure to the anti-PCFT siRNA or its negative control.

Finally, since previous studies showed that 3D MPM models have hypoxic cores and are generally more chemoresistant than two-dimensional monolayer cell cultures,[17,24,28] we performed additional experiments using spheroids, that were also used for Western blot analysis of LDH-A levels, as well as an exploratory analysis using a sequential trypsin digestion of spheroids of H2452 cells, as reported in the Supplemental methods.

Analysis of pathways involved in pemetrexed resistance after PCFT silencing and under hypoxic conditions

The molecular events occurring after PCFT silencing and exposure to hypoxic conditions in cells growing as monolayers, as well as spheroids, were evaluated using Hypoxia RT2 Profiler™ PCR Arrays (Qiagen, Hilden, Germany), according to the manufacturers' protocol.

This array includes 84 key components of the molecular machinery that modulate cell metabolism in response to hypoxic signals. For this analysis we used H2452 cells growing as monolayers treated for 48 hours with the PCFT-specific siRNA, as well as cells exposed for 72 hours to hypoxic conditions, and spheroids, as described above.

Pharmacological interaction of NHI-2 and NHI-Glc-2 with pemetrexed and gemcitabine

The cell growth inhibitory effects of the combination of the LDH-A inhibitors NHI-2 and NHI-Glc-2 and pemetrexed were evaluated in spheroids of H2452 cells. These spheroids were treated simultaneously with 1 μM NHI-2 and 1 μM pemetrexed for 7 days. The cytotoxic effects were evaluated by determining the density and size of spheroids, as described previously.[17,24] Then, we evaluated the induction of apoptosis in H2452 cells growing as monolayer under hypoxic conditions and treated with 1 μM NHI-2 alone and 1 μM pemetrexed for 24 hours. The apoptotic index was calculated after bisbenzimide-HCl staining, as described previously.[29] Further studies evaluated the pharmacological interaction of NHI-Glc-2 with gemcitabine using cells growing either in monolayers, under normoxic and hypoxic conditions, or as spheroids.

***In vivo* experiments using orthotopic and subcutaneous mouse models and live imaging**

In vivo experiments were performed in nu/nu athymic female mice purchased from Harlan (Horst, The Netherlands). The working protocol was approved by the local committees on animal experimentation of the VU University Medical Center (VUmc, Amsterdam, The Netherlands) and of the University of Pisa (Pisa, Italy), according to the 2010/63/EU European Community Council Directive for laboratory animal care.

Orthotopic primary DMPM models (n=5 tumors per treatment group) were generated by injection of 3×10^6 Fm/GC primary cells into the peritoneal cavity of the mice. Mice were treated with NHI-Glc-2, solubilized in Polyethylene glycol 400 (PEG400, Sigma-Aldrich, St. Louis, MO), at 100 mg/kg, 5 days (1-5) for 2 weeks (formulation concentration: 25 mg/mL in PEG400, 100 μL i.p. injection for a 25 g mouse). Bioluminescence imaging (BLI) was evaluated with a Bruker In-Vivo Xtreme Capture System, using Molecular Imaging Software (Bruker Corporation, Billerica, MA). Additional imaging analyses to define tumor spatial characteristics and evaluate microenvironment structures, such as neovasculature and hypoxic status, were carried out by high-frequency-ultrasound including Power Doppler Mode (Vevo-2100, VisualSonics, Amsterdam, The Netherlands). Data normalization and image analysis were performed as described previously.[23,24]

Further experiments were performed on subcutaneous tumors, obtained by inoculation of 3×10^6 tumor cells. In these models we also tested drug combinations. Since 1) pemetrexed activity cannot be reliably evaluated in mouse models, because of the intrinsically high levels of folate and thymidine,[30] and 2) our previous experiments showed a synergistic interaction of LDH-A inhibitors with gemcitabine, we used LDH-A inhibitors in combination with gemcitabine.[17] When tumor volume reached an average size of 100 mm^3, the animals were randomly distributed into 4 groups (n=6 tumors per treatment group) as follows: 1) control/untreated mice; 2) mice treated with gemcitabine alone at 100 mg/kg, 2 days (day 1 and 4) for three weeks (formulation concentration: 25 mg/mL in PBS, 100 µL i.p. injection for a 25 g mouse); 3) mice treated with NHI-Glc-2, solubilized in PEG400, at 50 mg/kg, 5 days (day 1-5) for three weeks (formulation concentration: 12.5 mg/mL in PEG400); and 4) mice treated with a simultaneous combination of gemcitabine and NHI-Glc-2, at the doses mentioned above, for three weeks. Tumor xenografts were measured as described previously.[31]

Statistics

Clinical outcome was correlated with demographic/clinicopathological information parameters and CAIX and LDH-A expression by univariate analysis using the Chi-square test. Modified RECIST criteria to classify the MPM response to treatment as complete response (CR), partial response (PR), stable disease (SD), or progressive disease (PD). The patients who showed disease control (DC), including CR, PR, and SD, were compared with patients with PD, as described previously.[6] Survival curves (OS and progression-free survival, PFS) were analysed from the day of initiation of drug treatment to the end point (death or censoring) according to the Kaplan-Meier method, and compared by log-rank and Wilcoxon tests, using SPSS software Version 24 (IBM-SPSS, Chicago, IL). Significant prognostic variables identified by univariate analysis were included in the multivariate analysis, using Cox's proportional hazards model and the backward stepwise elimination (Wald) method, where hazard ratios (HRs) were calculated to estimate the magnitude and the direction of the effect. The *in vitro* experiments were performed in triplicates and repeated at least twice. Results reported in the figures are expressed as mean values ± standard error of the mean (SEM). Statistical analyses were carried out by two-way ANOVA followed by Bonferroni's post-test (to adjust for multiple comparisons), using GraphPad-Prism version 7 (Intuitive Software for Science, San Diego, CA). All analyses were two-sided and statistical significance was set at $P<0.05$. The *in vivo* experiments included as the primary and secondary experimental outcomes the assessment of tumor growth and of molecular markers (pO_2 and LDH-A). Statistical

analysis was conducted with ANOVA analysis with Bonferroni correction for post-hoc analysis to evaluate differences in tumor size in the different groups of animals. $P< 0.05$ was considered significant. Results were expressed as mean values ± standard deviation (SD).

Results

Role of hypoxia in modulation of PCFT expression and pemetrexed cytotoxicity

Since previous studies showed that hypoxia induces chemoresistance in different tumor types including MPM,[22,32] we evaluated the hypoxia marker CAIX in the TMA of primary MPM specimens. Most samples (84%; 28 out of 33) showed positive staining for this hypoxia marker, as previously reported.[21] Remarkably, a stronger and diffuse staining of CAIX was typically associated with reduced PCFT expression (Fig. 1A). These findings are in agreement with previous results in carcinoma cells exposed to severe hypoxic conditions.[14] When the tissues positive for CAIX staining were grouped into high- and low-expression according to the scoring system reported in Supplemental Table 2, we observed that high expression levels of CAIX were associated with low expression of PCFT (P=0.016, Fig. 1A), which was assessed as described previously.[18] These results are in agreement with the role of this folate/antifolate transporter in cells with acidic pH,[33] which commonly characterizes the TME. To further explore molecular mechanisms underlying the role of hypoxia in the modulation of PCFT and chemoresistance, we then evaluated PCFT expression in MPM cells cultured under hypoxic conditions. As shown in Fig. 1B, PCFT expression was downregulated under hypoxia in all the three MPM cell lines examined. This was accompanied by increased resistance to pemetrexed, compared to their counterparts grown under normoxia, with a significant inhibition of cell growth (as assessed by direct viable cell counting) upon exposure to 0.1, 1 and 10 μM pemetrexed (Fig. 1C and Supplemental Fig.S2). A similar reduction of PCFT expression was also detected in the MPM spheroids (Fig. 1B), and pemetrexed significantly affected the number of spheroids only at high concentrations, up to 1, 10 and 20 μM, in MSTO-211H, H2452 and H28 cells, respectively (Fig. 1D). We hypothesized that the reduction of PCFT expression was correlated to the hypoxic regions close to the core of these spheroids. Indeed, using a sequential trypsin digestion of spheroids of H2452 cells that had reached a diameter of approximately 500 μm, we observed that cells from perinecrotic region and necrotic core (PN+NC) were considerably less sensitive to drug activity compared to cells from the surface and intermediate regions (SR+IR), as reported in Fig. 1E.

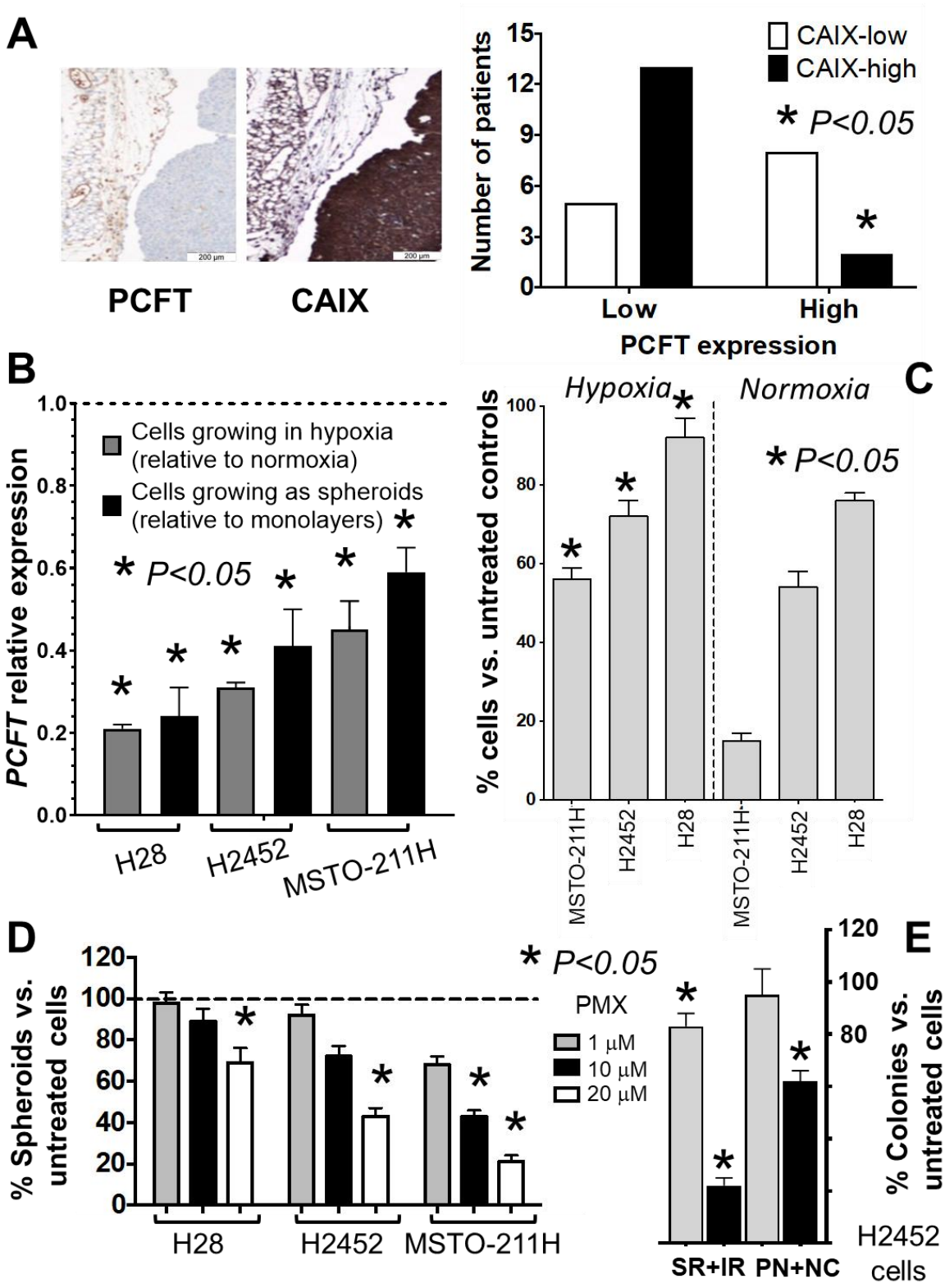

Figure 1. Hypoxia affects PCFT expression and pemetrexed activity. (A) Left panel: representative immunohistochemical pictures of two consecutive sections of an MPM tissue stained with anti-PCFT and anti-CAIX antibodies (left and right pictures, respectively, original magnification 20X). Right panel: analysis of the inverse/negative correlation of PCFT and CAIX staining in MPM patients (N=28). **(B)** Quantitative-RT-PCR analysis of PCFT mRNA expression in human MPM cell lines growing under hypoxic conditions or as spheroids. For each mesothelioma cell line, the results are presented relative to

the expression levels of PCFT in cells growing in normoxia as two-dimensional monolayer cell cultures, assigned a value of 1 (dashed line). *Columns*, mean values obtained from three independent experiments; *bars*, SEM. *Significantly different (P<0.05) compared to the untreated cells under normoxic conditions. **(C)** Cell growth inhibition performed with cells exposed to 1 μM pemetrexed (PMX) for 72 hours under hypoxic vs. normoxic conditions, as compared to compared to drug-free control cells. *Columns*, mean values obtained from three independent experiments; *bars*, SEM. *Significantly different (P<0.05) compared to the same treatments under normoxic conditions. **(D)** Relative number of spheroids originating from H2452 cells treated with PMX compared to spheroids originating from drug free cells, assigned a value of 100%. *Columns*, mean values obtained from three independent experiments; *bars*, SEM. *Significantly different (P<0.05) compared to spheroids growing from untreated cells. **(E)** Relative number of colonies originated from perinecrotic region and necrotic core (PN+NC) compared to the surface and intermediate regions (SR+IR) of 2452 spheroids treated with 1 or 10 μM PMX for 72 hours, compared to spheroids originating from untreated cells, assigned as a value of 100%. *Columns*, mean values obtained from three independent experiments; *bars*, SEM. *Significantly different (P<0.05) compared to untreated cells.

Role of LDH-A in the modulation of PCFT expression

To shed light on the molecular mechanisms underlying the chemoresistance of MPM cells to pemetrexed under hypoxia, as well as in cells growing as spheroids, and after specific down-regulation of PCFT expression, we performed a PCR array focusing on key regulators of hypoxia response. The volcano plot depicted in Fig. 2A arranged the genes according to the extent of differential expression (either up- or down-regulation, X-axis) and statistical significance with P values <0.01 (Y-axis) for both the up- or down-regulated genes in the H2452 spheroids, compared to cells growing in monolayers. Setting a 3-fold-change as the cut-off level, this analysis identified 25 significantly up-regulated genes (Supplemental Table 3). These include the hypoxia-inducible factor-1 (*HIF1*) and co-transcription factors *ARNT*, *HIF1A*, *HIF3A*, *HNF4A*, and *NCOA1*, as well as genes involved in glycolytic metabolism such as *LDH-A*, *ALDOA*, *ENO1*, *HK2*, *PDK1*, *PFKFB4*, *PGK1*, *PKM*, *SLC2A1*, and *SLC2A3*, but also the co-regulators of apoptosis and cell proliferation *ADM*, *BTG1* and *PIM1*. We also detected a marked increase in *MET* levels, as well as of the pleiotropic transcription factor *NFKB1*, both of which are frequently overexpressed in MPM and can suppress pro-apoptotic signalling pathways, promoting malignant behaviour and chemoresistance.[34–36] Finally, we observed a significant increase in *MMP9* levels, which has been linked to invasion/metastasis in several tumor types, including MPM.[37]

As depicted in the Venn diagram in Fig. 2B, only 9 of these significantly up-regulated genes in the H2452 spheroids were also among the 49 genes that were up-regulated under hypoxia, and there were only 4 common genes (i.e., *HIF1A*, *LDH-A*, *NFKB1* and *MMP9*) after *PCFT* silencing (Supplemental Table 3). Interestingly, the only up-regulated gene identified in all three conditions was *LDH-A*, which encodes for a key enzyme catalyzing the conversion of L-lactate and NAD to pyruvate and NADH in the final step of anaerobic glycolysis. Using the same conditions (i.e., spheroids, hypoxia exposure and PCFT silencing), we also observed a significant upregulation of *LDH-A* in H28 and MSTO-211H cells (Fig. 2C). The online database STRING, which allows the retrieval of the functional and physical interactions of proteins, did not identify a physical interaction between PCFT and LDH-A, as shown in Supplemental Fig.S3A. The only common node, creating a network with low stringency settings, was the ubiquitin C protein, which is involved in the post-transcriptional modification of both these target proteins. It is well known that hypoxia, through HIF-1α, triggers the up-regulation of genes that are critical for the promotion of glycolysis, including LDH-A.[32] In addition, three putative nuclear respiratory factor-1 (NRF-1) binding sites have been identified in the PCFT promoter, and compelling evidence established NRF-1 as a major inducible transcriptional regulator of PCFT, thereby linking folate transport with mitochondria biogenesis and cell metabolism.[38] However, the present study is the first to identify a relationship between PCFT-silencing and LDH-A overexpression. One may hypothesize that low PCFT expression could stimulate the increased expression of LDH-A as a feedback mechanism (Supplemental Fig.S3B). The increase in LDH-A activity, which catalyzes the reversible transformation of pyruvate into lactate, might lead to an extracellular acidification due to the lactate secretion and, consequently, would favour folate absorption through PCFT. We hypothesize that this increased PCFT activity would counteract the reduced expression of PCFT in hypoxic conditions. Of note, we also observed that LDH-A protein was overexpressed in MPM spheroids from all three MPM cell lines, compared to attached monolayer cells (Fig. 2D). However, the Western blot analyses of LDH-A in the spheroids were limited by the fact that we used the homogenates of the entire spheroids and could not estimate the spatial distribution of LDH-A, which was presumably differentially expressed in the peripheral and core regions of these spheroids. Since these spheroids were fragile we could not use our recently developed method with confocal microscopy,[39] in order to evaluate the localisation of LDH-A in terms of expression at the surface compared to the hypoxic regions close to the necrotic core.

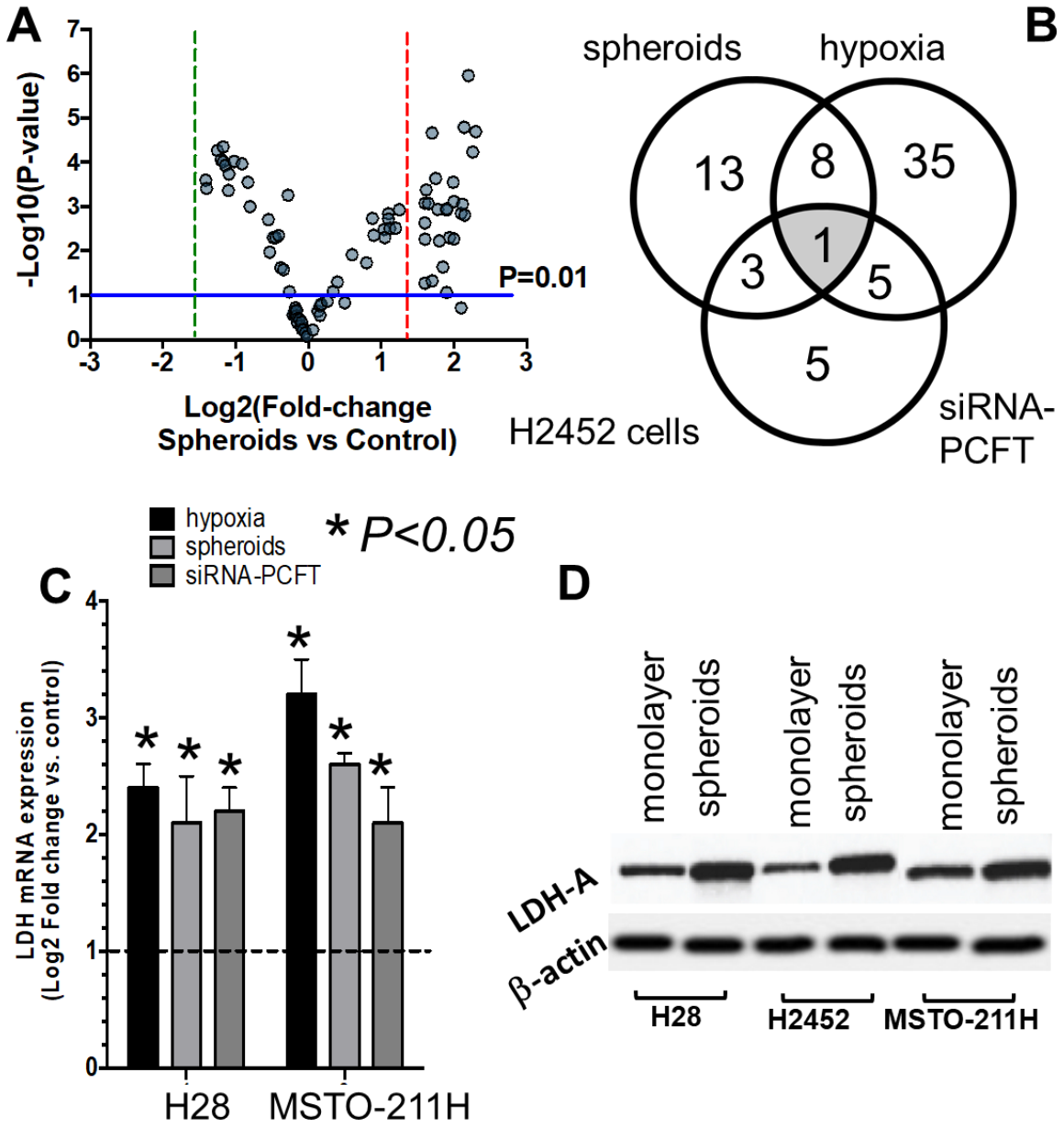

Figure 2. Correlation of hypoxia and PCFT silencing with LDH-A expression. (A) Volcano plot depicting the results of PCR arrays in H2452 spheroids compared to H2452 cells growing as monolayers. Horizontal blue line identifies the cut-off for genes which displayed a significantly different expression (P values were calculated with two-sided Student t-test); vertical red and green lines mark the cut-offs for the genes with 3-fold up- or downregulation, respectively. **(B)** Venn diagram of the overlap analysis of genes significantly upregulated in hypoxic cells, as well as in cells growing as spheroids and after specific downregulation of PCFT expression in H2452 cells. **(C)** Modulation of LDH-A expression in hypoxia, spheroids and after PCFT silencing. MPM cell lines showed a significant modulation of LDH-A mRNA expression when growing under hypoxic conditions, as spheroids or after PCFT silencing. *Columns*, mean values obtained from three independent experiments; *bars*, SEM. *Significantly different ($P<0.05$) from the respective control cells i.e., cells growing in normoxia for the cells growing in hypoxia, cells growing as monolayers for the cells growing as spheroids and cells exposed to siRNA

negative control for the cells exposed to siRNA PCFT silencing, respectively, exemplified by the dashed line, with expression values of 1. **(D)** Representative immunoblots illustrating the modulation of LDH-A protein expression in MPM cells growing as spheroids compared to cells growing as monolayers.

Preclinical activity of anti-LDH-A compounds in MPM cell lines and DMPM primary cultures growing as monolayers or as spheroids

To explore whether the increase in LDH-A expression is vital for cells with low-PCFT levels, we treated spheroids of H2452 cells with the specific LDH-A inhibitor NHI-2 and assessed the antitumor effects by determining the number and density/size of the spheroids. The total number of spheroids was not affected, but treatment with NHI-2 substantially increased the disintegration of the spheroids. In particular, NHI-2 significantly reduced the size of spheroids, indicated as spheroid aggregation in figure 3A, compared to the drug free control, and to the spheroids treated with pemetrexed alone. Moreover, NHI-2 enhanced both the pro-apoptotic (Supplemental Fig.S4A) and the cytotoxic effect of pemetrexed in these MPM models (Fig. 3A). Similar results were obtained with the glycoconjugated LDH-A inhibitor NHI-Glc-2 (Fig. 3A), which was synthesized to exploit the elevated glucose uptake of cancer cells and showed increased intracellular concentration compared to NHI-2.[27]

Since early passages of primary mesothelioma cells may better mimic the genetic characteristics of the disease, we extended our studies to two primary DMPM cell cultures, MesoII and STO. However, the percentages of cell growth of these cells were not affected by treatment with pemetrexed at concentrations until 10 μM, as shown in Figure 3B. This is in line with the lack of clinical activity of pemetrexed in DMPM. Thus, we did not perform further studies with pemetrexed in DMPM cells.

Since our previous study showed a synergistic interaction of LDH-A inhibitors with gemcitabine against pancreatic cancer cell lines in hypoxia,[17] we explored the cytotoxic effects of NHI-Glc-2 in combination with gemcitabine on MesoII and STO cells, cultured under normoxic and hypoxic conditions (1% O_2), as well as cells growing as adherent monolayers or spheroids. We initially treated cells growing under normoxic conditions with NHI-Glc-2 (0.5-50 μM) and observed a similar growth inhibitory effect in both tumor cell lines (IC_{50}= 20.1 in MesoII and 18.8 μM in STO cells, respectively). We then investigated the pharmacological interaction of this LDH-A inhibitor with an IC_{25} concentration of gemcitabine (i.e., 5.5 nM in MesoII and 1.9 nM in STO) in cells growing under normoxic and hypoxic conditions (Supplemental Fig. S4B). In both primary cell cultures, the combination index values (CI) indicated synergistic or strong synergistic effects which were mainly evident at 25 μM of NHI-Glc-2 in MesoII cells (Fig 3C).

Moreover, we evaluated the efficacy of this new combination on newly established 3D models of our primary cell cultures. Notably, in these models we observed an increase in LDH-A expression over time as detected by qRT-PCR (Supplemental Fig. S5), hence recapitulating the findings observed under hypoxia in different cells tissues.[32]

The spheroids were treated with 10 and 25 µM of NHI-Glc-2 for 7 days, and we observed a significant reduction in density compared to untreated spheroids, as assessed with ImageJ (Supplemental Fig. S6). In particular, the combination with gemcitabine (10 nM) was additive when NHI-Glc-2 was applied at a concentration of 10 µM (Fig 3D), while gemcitabine did not increase significantly the disaggregation of spheroids when NHI-Glc-2 was given at a concentration of 25 µM (data not shown). This is obviously due to the fact that this concentration would already greatly affect the structure of the spheroids and could not further synergize with gemcitabine.

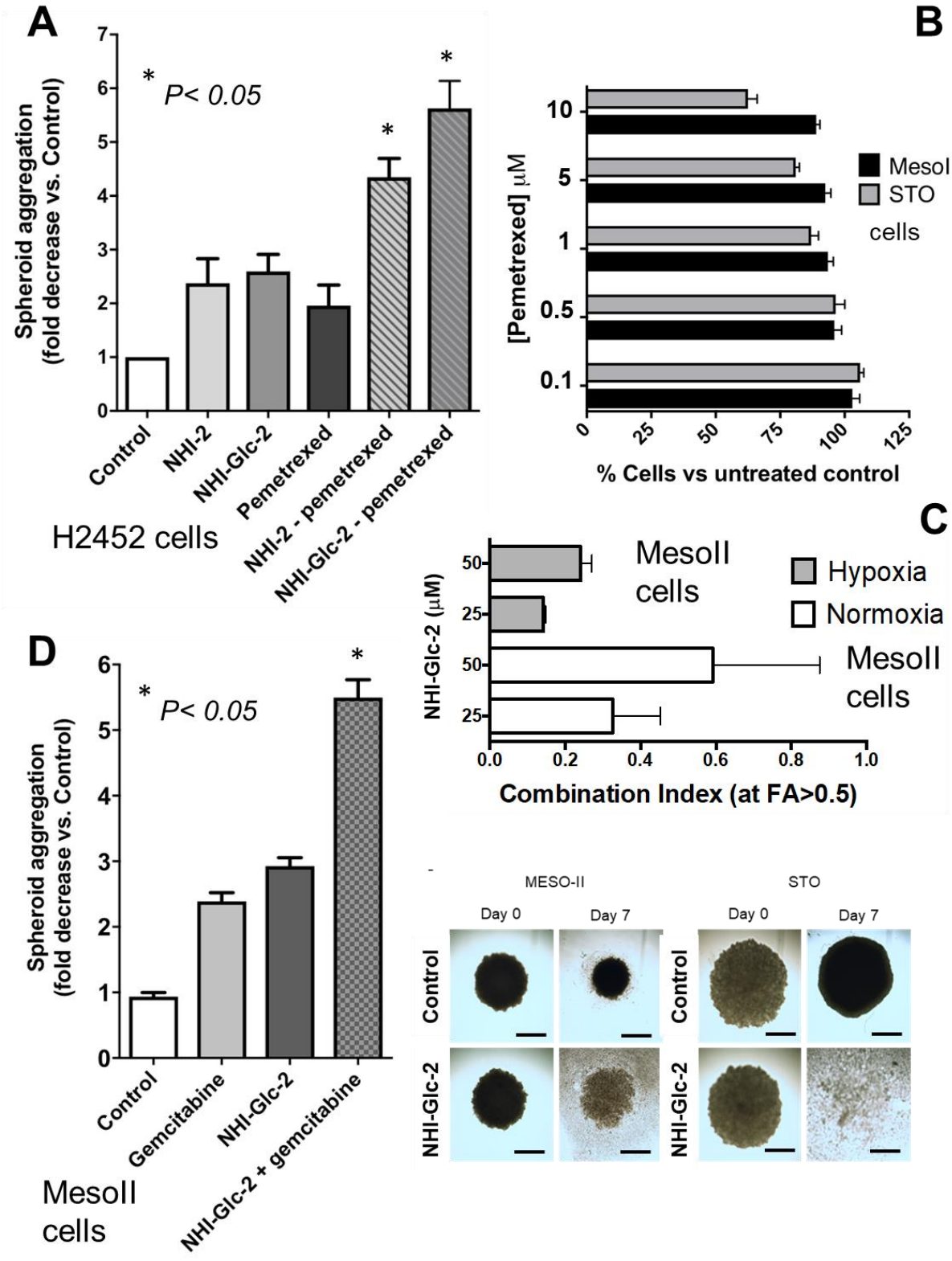

Figure 3. Cytotoxic effect of anti-LDH-A compounds alone and in combination with pemetrexed or gemcitabine on MPM and DMPM monolayers and spheroids. (A) Evaluation of the inhibition of the aggregation of the spheroids treated with pemetrexed (PMX), alone or in combination with 1 µM NHI-2, or NHI-Glc-2, compared to untreated spheroids originating from H2452 cells. The spheroids had similar volumes (below 500 μm^3) at the start of drug exposure, and the untreated spheroids were still

growing during the following 72 hours. *Columns*, mean values obtained from three independent experiments; *bars*, SEM. *Significantly different (P<0.05) from cells treated with PMX alone. **(B)** Cell viability bar graph of MesoII and STO cell lines treated with PMX. *Column*, mean values obtained from three independent experiments; *bars*, SEM. **(C)** Combination index values, calculated at FA>0.5, with Calcusyn software, as described in the Methods section. *Columns*, mean values obtained from three independent experiments; *bars*, SEM. **(D)** Evaluation of the inhibition of the aggregation of the spheroids treated with gemcitabine, alone or in combination with 10 μM NHI-Glc-2, compared to untreated spheroids originating from MesoII cells. *Columns*, mean values obtained from three independent experiments; *bars*, SEM. *Significantly different (P<0.05) from cells treated with gemcitabine alone. Right panel: representative images of DMPM spheroids. The spheroids had similar volumes (below 500 μm^3) and density at the start of drug exposure. However, after seven days, the volume of untreated spheroids was reduced while the density was significantly increased. In comparison with untreated spheroids (control), the treatment for 7 days with 25 μM of NHI-Glc-2 dramatically reduced the volume of STO spheroids, while in the MesoII spheroids showed about a 3-fold decrease in their aggregation (considering both the volume and density, as explained in the methods and Supplemental methods and Supplemental Fig.S6). Scale bar, 100 μm. *Column*, mean values obtained from three independent experiments; *bars*, SEM. *Significantly different (P<0.05) from cells untreated.

Anti-tumor activity of NHI-Glc-2 in DMPM xenografts

We recently developed two novel bioluminescent (BLI) orthotopic mouse models in order to monitor tumor growth of primary DMPM cells MesoII and STO over time.[24] The model with MesoII cells was selected for this study because of the higher level of LDH-A expression, as assessed by RNA sequencing, as described previously.[24] Moreover, the analysis of our RNA sequencing data (raw and normalized data were deposited at Gene Expression Omnibus; accession number: GSE112154) showed a significantly higher expression of genes in the LDH-A family in DMPM tissues compared to normal mesothelial cells (Supplemental Figure S7).

A rotational BLI analysis using the MARS system complemented with MRI and PET-CT showed tumor masses detectable in the whole abdominal cavity as multiple nodules,[17] thus reproducing the diffusion pattern of the clinical disease, as illustrated by the representative figures in mice after 3 weeks and at the time of sacrifice (Fig. 4A). The histopathological analysis demonstrated the presence of several neoplastic lesions, and IHC revealed a strong staining for LDH-A (Fig. 4B). In keeping with these findings, photoacoustic live imaging for deep tissue pO_2 measurement showed reduced oxygenation, suggesting the occurrence of hypoxia in many tumor nodules (Fig. 4C).

The mice were stratified into two groups, with comparable BLI signal, and then NHI-Glc-2 was administered i.p. at the maximum tolerated dose (MTD).[40] However, the analysis of the BLI

was performed only in 3 animals, and the results reported in Supplemental Fig. S8, showing a 70% reduction of tumor volumes (at day 15) in animals treated with NHI-Glc-2 compared to untreated animals, should be considered with caution. The histopathological studies performed on several samples from these models (including both peritoneal tumor plaques and tumor masses in the liver) showed a clear reduction in tumor volume in treated vs. untreated animals, as well as necrotic lesions. However, F-luc requires oxygen. Accordingly, bioluminescence imaging typically underestimates hypoxic tumors and the experiments were then repeated in groups of 6 animals after subcutaneous injection of 5×10^6 MesoII cells. In these models, IHC showed LDH-A levels that were comparable to those observed in the orthotopic tumors (Fig. 4D). The administration of NHI-Glc-2 resulted in a significant reduction in tumor growth (Fig. 4E). At the end of the 7th week of study, animals treated with 50 mg/kg NHI-Glc-2 showed a 49% reduction in tumor mass as compared to control animals (314 vs. 620 mm^3, $P < 0.001$). A similar decrease in tumor growth was detected in animals given gemcitabine, with a 47% reduction in tumor volume (331 vs. 620 mm^3, $P < 0.001$). Importantly, NHI-Glc-2 was well tolerated; no toxic deaths or signs of toxicity were observed and the body weight of animals given NHI-Glc-2 was similar to that of the drug free controls until the end of the 7th week (Supplemental Fig. S9), whereas that of mice given gemcitabine was slightly reduced (25 vs 28 g, $P=0.06$). Similarly, the combination of NHI-Glc-2 and gemcitabine was not toxic, and produced a significantly stronger shrinkage of the tumor mass. Indeed, statistical analyses revealed a mean reduction of 4-fold in tumor volume in the animals treated with the drug combination compared to controls (123 vs. 620 mm^3, $P < 0.001$) as well as a significant reduction compared both to animals treated with gemcitabine alone and to animals treated with NHI-Glc-2 monotherapy ($P<0.001$).

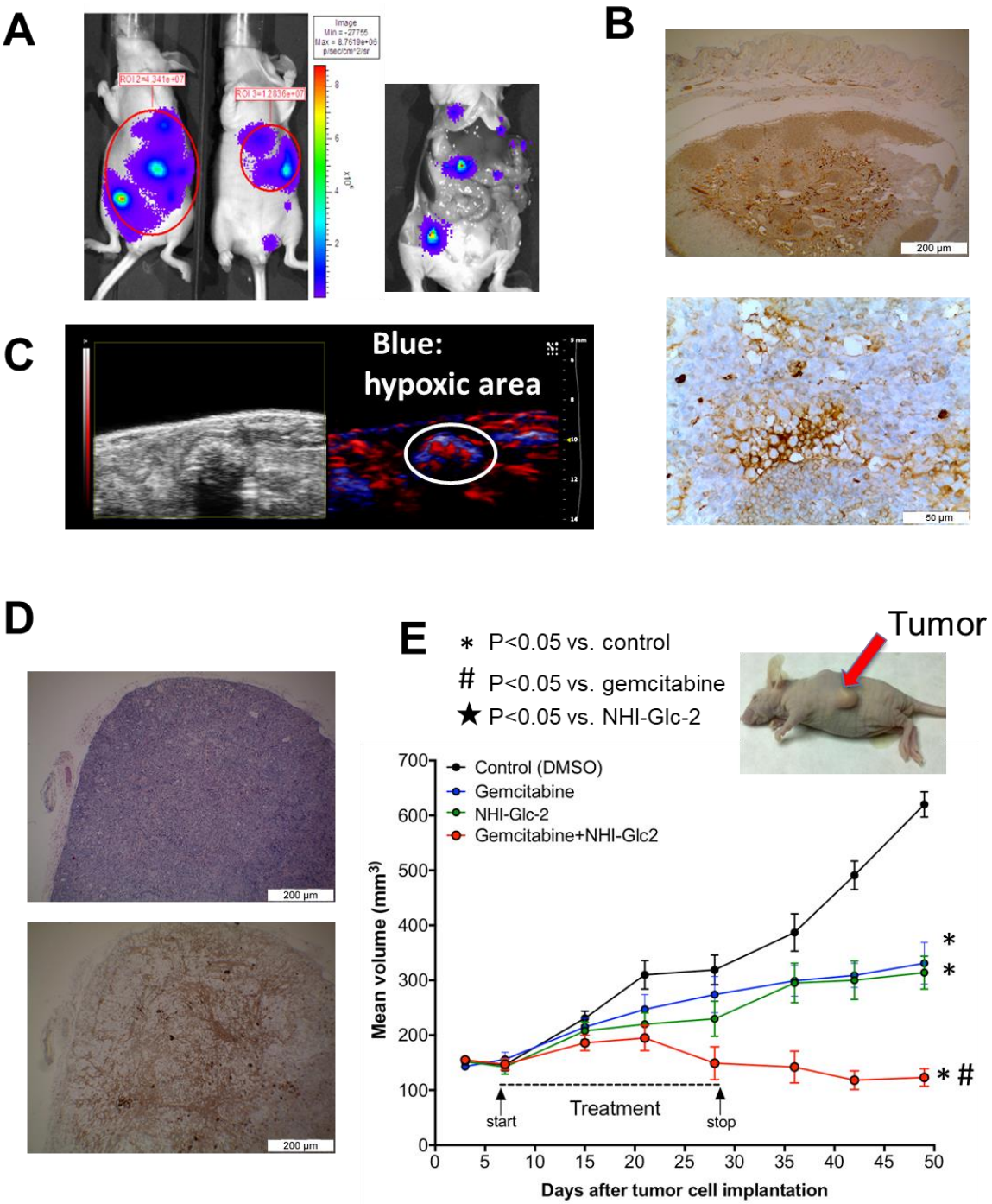

Figure 4. ***In vivo*** **activity of the new anti-LDH-A compound NHI-Glc-2 on orthotopic and subcutaneous DMPM models. (A)** Left panel: representative BLI images obtained with CCD camera of orthotopic models of primary DMPM cells transduced with F-luc. Right panel: representative images showing the multiple tumor masses in the whole abdominal cavity as nodules, thus reproducing the diffusion pattern of the clinical disease in a mouse sacrificed after 2 weeks from inoculation of MesoII cells. (**B**) Representative immunohistochemical pictures (upper panel 4X, lower panel 40X magnification) showing LHD-A overexpression in DMPM tissues obtained after orthotopic implantation of MesoII cells in mice. **(C)** Representative images of photoacoustic live imaging providing both a non-invasive anatomical image of tumors (up to 40 µm resolution) and the

measurement of deep tissue pO_2. The latter showed reduced oxygenation (in blue), suggesting that tumor nodules were characterized by hypoxic regions. **(D)** Representative H&E (upper panel), and immunohistochemical (lower panel) pictures (4X magnification) demonstrating LDH-A overexpression which characterized subcutaneous tumors obtained by inoculation of MesoII cells in mice. **(E)** Volumes of subcutaneous tumors of mice, as shown in the representative picture, treated with gemcitabine (100 mg/kg, i.p., 2 days a week), NHI-Glc-2 (solubilized in PEG400, 50 mg/kg, 5 days a week), or their combination compared to untreated mice. *Points*, mean values obtained from six mice; *bars*, SEM. *Significantly different ($P<0.05$) from untreated animal. # and ★Significantly different from animals treated with gemcitabine or NHI-Glc-2 monotherapy, respectively.

Correlation of LDH-A overexpression with shorter survival of MPM and DMPM patients.

LDH-A protein levels were analyzed by IHC on TMAs including tumor specimens from MPM and DMPM patients (Suppl. Fig.S10 and Fig. 5A). IHC staining was assessed by two independent pathologists under blinded conditions and any discrepancies were resolved by consensus. The concordance between scores from different paraffin cores of the same tumor was greater than 90%.

These analyses showed a variable LDH-A protein expression among specimens, ranging from a few scattered positive cells with a weak cytoplasmic staining to tissues with diffuse and strong cytoplasmic reactivity, in some cases accompanied by nuclear expression. Previous studies demonstrated the hypoxic microenvironment of mesothelioma[21,22] and that LDH-A overexpression correlated with hypoxia in different solid tumors.[41] In the present study, 20 out of 33 MPM cases (60%) and 36 out of the 56 DMPM (64%) displayed high LDH-A expression. Though the statistical analyses were performed on small cohorts of patients, we found a significant correlation between low LDH-A protein expression and DC after pemetrexed-based chemotherapy in MPM patients. In particular, DC was achieved in 92% of the patients with low LDH-A expression, while only 43% of patients with high LDH-A experienced DC ($P=0.03$, Fig. 5B). The univariate analysis revealed a significant correlation between high expression levels of LDH-A and significantly shorter OS ($P<0.001$, Fig. 5B. upper panel), and PFS ($P=0.02$, Fig. 5B lower panel) in MPM patients. Patients with high LDH-A expression had a median OS of 10.4 months (95% CI, 7.1-13.7) and a median PFS of 6.9 months (95% CI, 2.7-11.2), whereas patients with low expression levels of LDH-A had a median OS of 36.7 months (95% CI, 27.4-46.6) and a median PFS of 12.1 months (95% CI, 7.9-16.3). LDH-A expression levels were not associated with age, sex, histology or EORTC/PS grade. Among these clinicopathological parameters, the non-epithelioid (i.e. sarcomatoid or biphasic) histology, correlated with significantly shorter OS and PFS (Supplemental Table 4), as reported

previously.[1] However, only three patients had a non-epithelioid histology and we did not perform a multivariate analysis because of the very limited sample size.

The prognostic role of LDH-A was validated by IHC in an independent cohort of DMPM patients (Fig. 5C upper panel). Patients with low LDH-A expression had OS of 35.0 months (95%CI, 30.7-39.3), whereas the remaining patients had an OS of 12.0 months (95%CI, 5.3-18.7, P=0.01). A trend towards a significant correlation was reported for LDH-A and gender, but the latter was not correlated to survival (Supplemental Table 5). Conversely, LDH-A expression levels were not correlated with other clinicopathological parameters, including performance status (PS) and histology, which showed a correlation with both OS and PFS (Supplemental Table 5), as reported previously.[1]

A similar correlation was found for PFS. In particular, patients with low LDH-A expression had significantly longer PFS (22.0 months, 95%CI, 7.0-36.9), whereas patients with high LDH-A levels had PFS of 10.0 months (95%CI, 6.5-13.5, P<0.01, Fig. 5C, lower panel). Moreover, both epithelioid subtype and good PS were associated with significantly longer PFS (Supplemental Table 5).

The Cox proportional hazards regression model used for multivariate analysis in DMPM patients confirmed LDH-A expression as an independent prognostic factor for progression and survival (Table 1). In particular, high expression levels of LDH-A were associated with an increased risk of relapse (HR=2.4, 95%CI, 1.2-2.6, P=0.01) and death (HR=2.7, 95%CI, 1.7-3.6, P=0.02).

Collectively, these findings demonstrate that both MPM and DMPM are characterized by elevated expression of LDH-A, which is associated with dismal prognosis. Therefore, targeting LDH-A in these patients could constitute an attractive therapeutic avenue.

Table 1. Factors that affect the overall survival (OS) and progression-free survival (PFS) in the multivariate analysis of DMPM patients.

Covariates for overall survival (OS)	HR (95% CI)	*Wald P*
LDH: high vs. low	2.74 (1.72-3.66)	*0.02*
PS: 1-2 vs. 0	3.21 (1.91-3.82)	*0.02*
Histology: non-epithelioid vs. epithelioid	2.04 (1.13-3.14)	*0.07*
Covariates for progression-free survival (PFS)	HR (95% CI)	*Wald P*
LDH: high vs. low	2.41 (1.23-2.62)	*0.01*
PS: 1-2 vs. 0	3.63 (1.73-4.11)	*0.02*
Histology: non-epithelioid vs. epithelioid	2.27 (1.12-3.74)	*0.29*
Abbreviations: HR, Hazard Ratio, PS, Performance status		

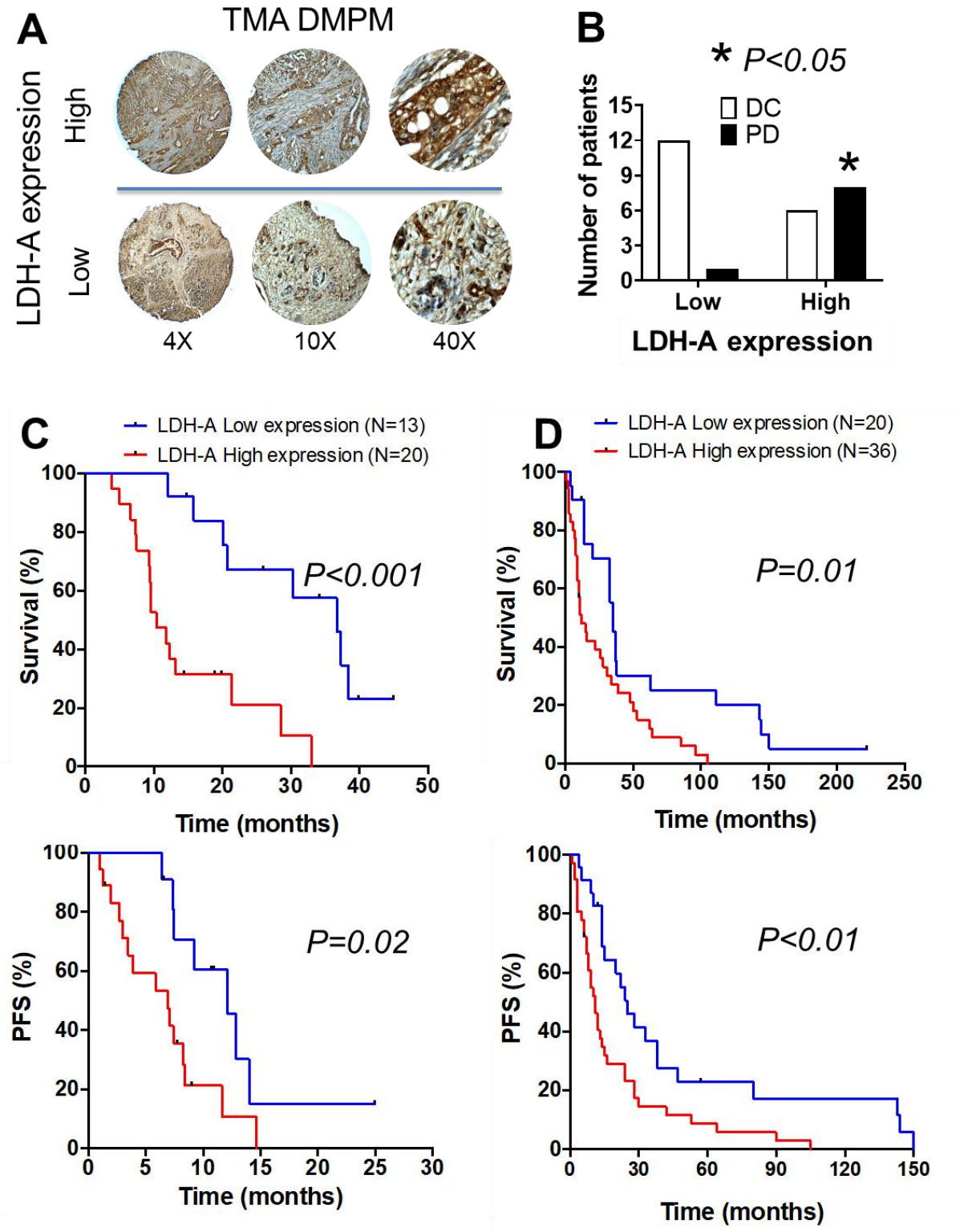

Figure 5. High expression of LDH-A correlates with significantly shorter overall survival (OS) and progression-free survival (PFS) in both MPM and DMPM patients. (A) Representative pictures of immunohistochemical analyses of tissue microarrays (TMAs) cores in the cohorts of DMPM patients, illustrating cases with high (upper panels) and low (lower panels) LDH-A expression (at 4X, 10X and 40X original magnification). **(B)** Kaplan-Meier curves of OS (upper panel) and PFS (lower panel) in MPM patients according to LDH-A high vs. low expression levels, as described above. **(C)** Kaplan-

Meier curves of OS (upper panel) and PFS (lower panel) in DMPM patients according to LDH-A high vs. low expression levels, as described above. *P-values* were determined with the Log-rank test.

Discussion

The current study revealed for the first time that low levels of PCFT in MPM specimens were associated with hypoxia as detected by high expression of the hypoxic marker CAIX. Moreover, we established that hypoxic and PCFT-silenced cells are characterized by up-regulation of LDH-A

We then explored the clinical relevance of this discovery and reported the key prognostic value of LDH-A in both MPM and DMPM patients. Furthermore, we used innovative *in vitro* and *in vivo* models to characterize the anti-proliferative capacity of LDH-A inhibitors, in order to provide mechanistic insights regarding the aggressive behaviour of mesothelioma and in an attempt to contribute to the rational development of new prognostic and therapeutic approaches.

PCFT has recently emerged as a predictive parameter in MPM patients treated with pemetrexed-based chemotherapeutic regimens, since low PCFT expression was associated with shorter PFS and OS.[13] PCFT is the main transporter mediating pemetrexed influx, with remarkable transport Km values of 0.2–0.8 μM at acidic pH,[42] and its expression has been linked to growth inhibitory activity of pemetrexed after transfection into a folate transporter-null cell variant.[43] We consistently observed that PCFT silencing increased the IC_{50} values of pemetrexed in our MPM cell lines.

We have previously shown the regulation of PCFT gene expression by NRF-1,[38] the dominant transcription factor orchestrating mitochondrial biogenesis and respiration, which acts as a key repressor of HIF-1α under hypoxic conditions.[44] Similarly, we previously found that hypoxia downregulated gene expression of both RFC and PCFT, as well as other key enzymes in folate metabolism, and rendered HeLa cells refractory to both pemetrexed and other hydrophilic and lipophilic antifolates.[14] However, the present study is the first to demonstrate the role of PCFT suppression and hypoxia as causative of pemetrexed resistance in MPM. Indeed, we observed in MPM specimens that low/intermediate levels of expression of the hypoxic marker CAIX were associated with intermediate expression levels of PCFT, while specimens with the highest levels of CAIX showed reduced PCFT expression. In line with these results, *in vitro* studies under hypoxic conditions and in mesothelioma spheroids showed that the levels of PCFT expression were reduced, accompanied by decreased pemetrexed activity. Using these *in vitro*

models of hypoxia, along with PCFT-silenced cells, and a specific PCR array, we found that LDH-A was the only significantly up-regulated gene in all three models.

The oxidoreductase LDH-A is a key enzyme in aerobic glycolysis as well as major checkpoint for the switch from aerobic to anaerobic glycolysis, which catalyzes the reduction of pyruvate to lactate and constitutes a fundamental metabolic adaptation of cancer cells to a relatively hostile environment, facilitating tumor growth.[32,45] Serum, plasma and tissue levels of LDH-A are prognostic factors in several tumor types, and the ratio of pleural fluid to serum LDH>1.0 was a significant predictor for OS in 71 MPM patients.[46] Moreover, gene expression analysis of 16 MPM specimens compared to 4 control pleural tissue samples using cDNA microarray filters with 4132 clones showed that LDH-A was among the 166 significantly up-regulated genes.[47] In particular, the expression of LDH-A showed a 5.5-fold change (P=0.00001), which was validated by RT-PCR. Interestingly, the analysis of our microarray data showed a significantly higher expression of LDHAL6A in DMPM tissues compared to normal mesothelial tissues, and this protein has all the biological functions of LDH-A according to KEGG and REACTOME databases.

Lactate production also contributes to extracellular acidosis, thus supporting tumor invasiveness and exerting immunosuppressive effects.[45] This has raised interest regarding the mechanisms underlying regulation of LDH-A in cancer cells, including critical post-transcriptional modifications.[48,49] Importantly, the results of the present study also suggest that low PCFT expression levels might directly or indirectly stimulate the enhanced expression of LDH-A, though the mechanism by which this occurs remains unclear. Increased acidity caused by LDH-A could in principle favour folate transport via PCFT, even when the latter is expressed at decreased levels and this should enhance pemetrexed uptake.

Notably, in the current study LDH-A emerges also as an attractive druggable target for therapeutic interventions. Previous studies with the LDH inhibitor oxamate on glioma spheroids have shown the changed metabolism with drastic changes in radiation sensitivity.[50] In the present study the specific LDH-A inhibitor NHI-2 was cytotoxic to H2452 MPM spheroids under conditions where pemetrexed was ineffective. Similarly, a glycoconjugated analogue of NHI-2 (NHI-Glc-2) was active against MPM and DMPM primary cells, growing both as monolayers and as spheroids. Because of its enhanced uptake into tumor cells, likely mediated by glucose transporters (GLUTs),[27] NHI-Glc-2 was also selected for *in vivo* studies. Several studies suggested that early passages of primary tumor cells and “avatar” mice can mimic the genetic diversity that characterizes the human disease and represent the best preclinical platform to study drug activity in different tumor types, including mesothelioma.[51,52] However, there is

still a need for experimental models coupled to in-depth molecular profiling in order to decipher the genetic alterations that drive drug sensitivity/resistance, and only a few studies evaluated DMPM models. Therefore, in a proof-of-principle pharmacological study, we used our recently established mouse models, obtained by orthotopic or subcutaneous inoculation of primary DMPM cells, genetically engineered to express the F-luc luciferase, providing an ease-of-use, low cost, non-invasive and high-throughput imaging tool to monitor tumor growth.[24] These models recapitulated the main histological and genetic features of the primary tumors, including hypoxic tumor domains, overexpression of LDH-A;[21,47] remarkably, NHI-Glc-2 caused a significant reduction in tumor growth, when compared to untreated animals. Moreover, the *in vivo* studies on the combination of NHI-Glc-2 with gemcitabine reflected the synergistic effects observed *in vitro*, revealing a significant reduction compared to animals treated with either gemcitabine or NHI-Glc-2. These results are consistent with our previous findings on the synergistic interaction of gemcitabine with other LDH-A inhibitors in preclinical models of pancreatic cancer and MPM.[17,18] Further studies are warranted to unravel the molecular mechanisms underlying this synergistic interaction. However, one may speculate that hypoxia can affect gemcitabine activity, as was found in other 3D models.[53] The synthesis of active gemcitabine deoxynucleotides was possibly decreased through downregulation, genomic deletions and frame-shift mutations of the rate-limiting enzyme deoxycytidine kinase, as reported recently for acute myeloid leukemia and pancreatic cancer cells,[17,54,55] or downregulation of the equilibrative nucleoside transporter 1, as reported previously in MPM cells.[18] However, since hypoxic cells represent only a subpopulation in most tumors, and anti-hypoxia agents require a long residence time in tumors in order to exploit fluctuating hypoxia and cause efficient, long-range, bystander killing,[56] these synergistic activity is extremely important. Moreover, in agreement with the hypothesis that inhibition of molecular targets in hypoxic cells should offer a more benign toxicity profile, which is distinctly different from that of conventional cytotoxic therapy, we indeed did not observe untoward toxicity in animals treated with a combination of gemcitabine and NHI-Glc-2. These results prompt further studies on the combination of our new anti-LDH-A agents with current standard cytotoxic agents in clinical trials.

Another important step we undertook towards the evaluation of the role of LDH-A in the clinical setting was the analysis of the correlation of its expression with clinical outcome. A recent meta-analysis showed that elevated serum LDH-A levels prior to chemotherapeutic treatment, is a significant prognostic factor in malignant mesothelioma.[57] However, to the best

of our knowledge the current research is the first study to demonstrate the prognostic role of LDH-A protein expression in tumor tissues from both MPM and DMPM patients.

Our current study is inarguably not a long-term follow up and prolonged longitudinal study of the impact of treatment. On the other hand, in other animal models it has already been shown that tumor growth in the first 7-10 days post-engraftment, can reliably predict the effect of treatment and overall survival.[58] In addition, this non-long term follow up in our models would alleviate significant genetic alterations as compared to the original tumors.

An important limitation of our study is that LDH-A expression was tested retrospectively in relatively small cohorts of MPM and DMPM patients, treated with different therapies with and without pemetrexed, and on a small number of mesothelioma cell lines and primary cells. However, bench-to-bedside research on hundreds of samples, which clearly improved prognostic capabilities in several tumor types, such as lung or breast cancer, are extremely difficult to achieve in mesotheliomas, which are rare tumors.[1] Indeed, most previous candidate biomarkers are based solely on mRNA evidence and our findings with protein levels in two cohorts of patients, indicate the value of the prognostic value of LDH-A and should prompt prospective studies for further validation. Moreover, our data showed that high expression levels of LDH-A are detectable in more than 50% of specimens from both MPM and DMPM patients. Thus, these findings might be relevant to a large number of mesothelioma patients.

A large number of compounds with LDH-A inhibitory activity have been discovered and studied pre-clinically as anticancer agents,[45] none of which is currently approved for clinical use. In addition, many trials with new, targeted agents resulted in clinical failures in mesothelioma patients.[59,60] However, a combined approach of chemical biology, preclinical pharmacology, bioinformatics and appropriate models and biobanks, as reported in this study, should create new opportunities for the development of more effective inhibitors as drug-like candidates.

In conclusion, our clinical data, combined with our *in vitro* and *in vivo* findings, strongly suggest that mesothelioma are more aggressive if they have high expression of LDH-A, which can be targeted by specific LDH-A inhibitors, therefore representing a promising new avenue for prognostic and therapeutic purposes.

Acknowledgements

The authors would like to thank Naomi Peterson (VUmc, Amsterdam, The Netherlands), Claudio Ricci, Luca Pollina (AOUP, Pisa, Italy) for their work on the mouse models and TMA stainings. We extend our gratitude to Maria Gemelli (Cancer Center Humanitas, Milano, Italy) for her work on the clinical database, Paolo Gandellini (Molecular Pharmacology Unit, Fondazione IRCCS Istituto Nazionale dei Tumori, Milano, Italy) for his work on the microarray data, Leticia G. Leon (Cancer Pharmacology Lab, Pisa, Italy) for preliminary *in vitro* studies, and to Zhanjun Hou (Barbara Ann Karmanos Cancer Institute, Wayne State University School of Medicine, Detroit, MI, USA) who provided the anti-PCFT antibody.

Funding

This work was partially supported in the collections and analysis of data by the following grants: "the Law Offices of Peter G. Angelos Grant" from the Mesothelioma Applied Research Foundation (MARF), United States (Elisa Giovannetti, Paolo A Zucali, Filippo Minutolo and Godefridus J. Peters), Fondazione Humanitas, Milano, Italy (Elisa Giovannetti, Paolo A Zucali,), CCA Foundation 2012 (Elisa Giovannetti, Godefridus J Peters, Amir Avan), 2013 (Jacqueline Cloos, Elisa Giovannetti) 2015 and 2016 (Elisa Giovannetti) grants, KWF Dutch Cancer Society grants (KWF project#10401 and #11957, Elisa Giovannetti), Polish National Science Center project 2018/31/B/NZ7/02909 (Godefridus J. Peters, Elisa Giovannetti, Filippo Minutolo, Ryszard T. Smolenski), University of Pisa (Intramural Funds, Carlotta Granchi, Elisa Giovannetti and Filippo Minutolo), Italian Association for Cancer Research AIRC/Start-Up grant and (Elisa Giovannetti), R01 CA53535 (Larry Matherly) from the National Institutes of Health and the Eunice and Milton Ring Endowed Chair for Cancer Research (Larry Matherly).

Availability of data and materials

All data generated or analysed during this study are included in this published article (and in supplementary information files).

Authors' contributions

EG, FM and GJP designed and coordinated the study. GLP, BEH and RS were the principal investigators and take primary responsibility for the experiments; NF, EAZ, AA, TL and GM performed additional experimental work and prepared some of the figures, NF and EG performed the studies on TMA, SC, NZ, BP, MD, CG, LHM and PAZ provided essential material, NZ, JC, GJ, YGA, PD, and RTS participated in the research design; GLP and EG wrote the paper; GJP, YGA and EG edited the paper. All authors read and approved the final manuscript.

Competing interests

The authors have no conflict of interest to disclose.

Consent for publication

Consent to publish has been obtained from all the participants (or legal parent or guardian for children) to report individual patient data.

Ethics approval and consent to participate

This study was approved by the Local Ethics Committee of the Humanitas Cancer Center (Rozzano, Milano, Italy) and National Cancer Center (Milano, Italy). Patients who provided tissues and primary cell cultures have provided a written informed consent.

References

(1) Carbone M, Adusumilli PS, Alexander HR, Baas P, Bardelli F, Bononi A *et al.* Mesothelioma: Scientific clues for prevention, diagnosis, and therapy. *CA Cancer J Clin* 2019. doi:10.3322/caac.21572.

(2) Vogelzang NJ, Rusthoven JJ, Symanowski J, Denham C, Kaukel E, Ruffie P *et al.* Phase III study of pemetrexed in combination with cisplatin versus cisplatin alone in patients with malignant pleural mesothelioma. *J Clin Oncol* 2003; **21**: 2636–2644.

(3) Ceresoli GL, Zucali PA, Favaretto AG, Grossi F, Bidoli P, Del Conte G *et al.* Phase II study of pemetrexed plus carboplatin in malignant pleural mesothelioma. *J Clin Oncol* 2006; **24**: 1443–1448.

(4) Sugarbaker PH. Update on the management of malignant peritoneal mesothelioma. *Transl Lung Cancer Res* 2018; **7**: 599–608.

(5) Righi L, Papotti MG, Ceppi P, Billè A, Bacillo E, Molinaro L *et al.* Thymidylate synthase but not excision repair cross-complementation group 1 tumor expression predicts outcome in patients with malignant pleural mesothelioma treated with pemetrexed-based chemotherapy. *J Clin Oncol* 2010; **28**: 1534–1539.

(6) Zucali PA, Giovannetti E, Destro A, Mencoboni M, Ceresoli GL, Gianoncelli L *et al.* Thymidylate synthase and excision repair cross-complementing group-1 as predictors of responsiveness in mesothelioma patients treated with pemetrexed/carboplatin. *Clin Cancer Res* 2011; **17**: 2581–2590.

(7) Lustgarten DES, Deshpande C, Aggarwal C, Wang L-C, Saloura V, Vachani A *et al.* Thymidylate synthase and folyl-polyglutamate synthase are not clinically useful markers of response to pemetrexed in patients with malignant pleural mesothelioma. *J Thorac Oncol* 2013; **8**: 469–477.

(8) Mairinger F, Vollbrecht C, Halbwedl I, Hatz M, Stacher E, Gülly C *et al.* Reduced folate carrier and folylpolyglutamate synthetase, but not thymidylate synthase predict survival in pemetrexed-treated patients suffering from malignant pleural mesothelioma. *J Thorac Oncol* 2013; **8**: 644–653.

(9) Matherly LH, Hou Z, Gangjee A. The promise and challenges of exploiting the proton-coupled folate transporter for selective therapeutic targeting of cancer. *Cancer Chemother Pharmacol* 2018; **81**: 1–15.

(10) Cherian C, Kugel Desmoulin S, Wang L, Polin L, White K, Kushner J *et al.* Therapeutic targeting malignant mesothelioma with a novel 6-substituted pyrrolo[2,3-d]pyrimidine

thienoyl antifolate via its selective uptake by the proton-coupled folate transporter. *Cancer Chemother Pharmacol* 2013; **71**: 999–1011.

(11) Zhao R, Goldman ID. The molecular identity and characterization of a Proton-coupled Folate Transporter--PCFT; biological ramifications and impact on the activity of pemetrexed. *Cancer Metastasis Rev* 2007; **26**: 129–139.

(12) Gonen N, Bram EE, Assaraf YG. PCFT/SLC46A1 promoter methylation and restoration of gene expression in human leukemia cells. *Biochem Biophys Res Commun* 2008; **376**: 787–792.

(13) Giovannetti E, Zucali PA, Assaraf YG, Funel N, Gemelli M, Stark M *et al.* Role of proton-coupled folate transporter in pemetrexed resistance of mesothelioma: clinical evidence and new pharmacological tools. *Ann Oncol* 2017; **28**: 2725–2732.

(14) Raz S, Sheban D, Gonen N, Stark M, Berman B, Assaraf YG. Severe hypoxia induces complete antifolate resistance in carcinoma cells due to cell cycle arrest. *Cell Death Dis* 2014; **5**: e1067.

(15) Peters GJ, Smitskamp-Wilms E, Smid K, Pinedo HM, Jansen G. Determinants of activity of the antifolate thymidylate synthase inhibitors Tomudex (ZD1694) and GW1843U89 against mono- and multilayered colon cancer cell lines under folate-restricted conditions. *Cancer Res* 1999; **59**: 5529–5535.

(16) Klabatsa A, Sheaff MT, Steele JPC, Evans MT, Rudd RM, Fennell DA. Expression and prognostic significance of hypoxia-inducible factor 1α (HIF-1α) in malignant pleural mesothelioma (MPM). *Lung Cancer* 2006; **51**: 53–59.

(17) Maftouh M, Avan A, Sciarrillo R, Granchi C, Leon LG, Rani R *et al.* Synergistic interaction of novel lactate dehydrogenase inhibitors with gemcitabine against pancreatic cancer cells in hypoxia. *Br J Cancer* 2014; **110**: 172–182.

(18) Giovannetti E, Leon LG, Gómez VE, Zucali PA, Minutolo F, Peters GJ. A specific inhibitor of lactate dehydrogenase overcame the resistance toward gemcitabine in hypoxic mesothelioma cells, and modulated the expression of the human equilibrative transporter-1. *Nucleosides, Nucleotides and Nucleic Acids* 2016; **35**: 643–651.

(19) Simon GR, Verschraegen CF, Jänne PA, Langer CJ, Dowlati A, Gadgeel SM *et al.* Pemetrexed plus gemcitabine as first-line chemotherapy for patients with peritoneal mesothelioma: final report of a phase II trial. *J Clin Oncol* 2008; **26**: 3567–3572.

(20) Burt BM, Richards WG, Lee H-S, Bartel S, Dasilva MC, Gill RR *et al.* A Phase I Trial of Surgical Resection and Intraoperative Hyperthermic Cisplatin and Gemcitabine for Pleural Mesothelioma. *J Thorac Oncol* 2018; **13**: 1400–1409.

(21) Capkova L, Koubkova L, Kodet R. Expression of carbonic anhydrase IX (CAIX) in malignant mesothelioma. An immunohistochemical and immunocytochemical study. *Neoplasma* 2014; **61**: 161–169.

(22) Nabavi N, Bennewith KL, Churg A, Wang Y, Collins CC, Mutti L. Switching off malignant mesothelioma: exploiting the hypoxic microenvironment. *Genes Cancer* 2016; **7**: 340–354.

(23) Avan A, Caretti V, Funel N, Galvani E, Maftouh M, Honeywell RJ *et al.* Crizotinib inhibits metabolic inactivation of gemcitabine in c-Met-driven pancreatic carcinoma. *Cancer Res* 2013; **73**: 6745–6756.

(24) Sciarrillo R, Wojtuszkiewicz A, El Hassouni B, Funel N, Gandellini P, Lagerweij T *et al.* Splicing modulation as novel therapeutic strategy against diffuse malignant peritoneal mesothelioma. *EBioMedicine* 2019; **39**: 215–225.

(25) Koukourakis MI, Giatromanolaki A, Sivridis E, Gatter KC, Harris AL, Tumour Angiogenesis Research Group. Lactate dehydrogenase 5 expression in operable colorectal cancer: strong association with survival and activated vascular endothelial growth factor pathway--a report of the Tumour Angiogenesis Research Group. *J Clin Oncol* 2006; **24**: 4301–4308.

(26) Giovannetti E, Zucali PA, Assaraf YG, Leon LG, Smid K, Alecci C *et al.* Preclinical emergence of vandetanib as a potent antitumour agent in mesothelioma: molecular mechanisms underlying its synergistic interaction with pemetrexed and carboplatin. *Br J Cancer* 2011; **105**: 1542–1553.

(27) Calvaresi EC, Granchi C, Tuccinardi T, Di Bussolo V, Huigens RW, Lee HY *et al.* Dual targeting of the Warburg effect with a glucose-conjugated lactate dehydrogenase inhibitor. *Chembiochem* 2013; **14**: 2263–2267.

(28) Barbone D, Ryan JA, Kolhatkar N, Chacko AD, Jablons DM, Sugarbaker DJ *et al.* The Bcl-2 repertoire of mesothelioma spheroids underlies acquired apoptotic multicellular resistance. *Cell Death Dis* 2011; **2**: e174.

(29) Massihnia D, Avan A, Funel N, Maftouh M, van Krieken A, Granchi C *et al.* Phospho-Akt overexpression is prognostic and can be used to tailor the synergistic interaction of Akt inhibitors with gemcitabine in pancreatic cancer. *Journal of Hematology & Oncology* 2017; **10**: 9.

(30) van der Wilt CL, Backus HH, Smid K, Comijn L, Veerman G, Wouters D *et al.* Modulation of both endogenous folates and thymidine enhance the therapeutic efficacy of thymidylate synthase inhibitors. *Cancer Res* 2001; **61**: 3675–3681.

(31) Cavazzoni A, La Monica S, Alfieri R, Ravelli A, Van Der Steen N, Sciarrillo R *et al.* Enhanced efficacy of AKT and FAK kinase combined inhibition in squamous cell lung carcinomas with stable reduction in PTEN. *Oncotarget* 2017; **8**: 53068–53083.

(32) Grasso C, Jansen G, Giovannetti E. Drug resistance in pancreatic cancer: Impact of altered energy metabolism. *Crit Rev Oncol Hematol* 2017; **114**: 139–152.

(33) Matherly LH, Wilson MR, Hou Z. The Major Facilitative Folate Transporters Solute Carrier 19A1 and Solute Carrier 46A1: Biology and Role in Antifolate Chemotherapy of Cancer. *Drug Metab Dispos* 2014; **42**: 632–649.

(34) Leon LG, Gemelli M, Sciarrillo R, Avan A, Funel N, Giovannetti E. Synergistic activity of the c-Met and tubulin inhibitor tivantinib (ARQ197) with pemetrexed in mesothelioma cells. *Curr Drug Targets* 2014; **15**: 1331–1340.

(35) Yang H, Bocchetta M, Kroczynska B, Elmishad AG, Chen Y, Liu Z *et al.* TNF-alpha inhibits asbestos-induced cytotoxicity via a NF-kappaB-dependent pathway, a possible mechanism for asbestos-induced oncogenesis. *Proc Natl Acad Sci USA* 2006; **103**: 10397–10402.

(36) Goparaju CM, Blasberg JD, Volinia S, Palatini J, Ivanov S, Donington JS *et al.* Onconase Mediated NFKβ Down-Regulation in Malignant Pleural Mesothelioma. *Oncogene* 2011; **30**: 2767–2777.

(37) Servais EL, Colovos C, Rodriguez L, Bograd AJ, Nitadori J, Sima C *et al.* Mesothelin overexpression promotes mesothelioma cell invasion and MMP-9 secretion in an orthotopic mouse model and in epithelioid pleural mesothelioma patients. *Clin Cancer Res* 2012; **18**: 2478–2489.

(38) Gonen N, Assaraf YG. The obligatory intestinal folate transporter PCFT (SLC46A1) is regulated by nuclear respiratory factor 1. *J Biol Chem* 2010; **285**: 33602–33613.

(39) Firuzi O, Che PP, El Hassouni B, Buijs M, Coppola S, Löhr M *et al.* Role of c-MET Inhibitors in Overcoming Drug Resistance in Spheroid Models of Primary Human Pancreatic Cancer and Stellate Cells. *Cancers (Basel)* 2019; **11**. doi:10.3390/cancers11050638.

(40) El Hassouni B, Sciarrillo R, Gómez V, Maftouh M, Mantini G, Vonk C *et al.* Abstract 3082: Targeting hypoxic pancreatic cancer cells with glucose conjugated lactate dehydrogenase inhibitor NHI-Glc-2. 2019, pp 3082–3082.

(41) Koch A, Ebert EV, Seitz T, Dietrich P, Berneburg M, Bosserhoff A *et al.* Characterization of glycolysis-related gene expression in malignant melanoma. *Pathology - Research and Practice* 2020; **216**: 152752.

(42) Zhao R, Najmi M, Aluri S, Spray DC, Goldman ID. Concentrative Transport of Antifolates Mediated by the Proton-Coupled Folate Transporter (SLC46A1); Augmentation by a HEPES Buffer. *Mol Pharmacol* 2018; **93**: 208–215.

(43) Zhao R, Qiu A, Tsai E, Jansen M, Akabas MH, Goldman ID. The proton-coupled folate transporter: impact on pemetrexed transport and on antifolates activities compared with the reduced folate carrier. *Mol Pharmacol* 2008; **74**: 854–862.

(44) Wang D, Zhang J, Lu Y, Luo Q, Zhu L. Nuclear respiratory factor-1 (NRF-1) regulated hypoxia-inducible factor-1α (HIF-1α) under hypoxia in HEK293T. *IUBMB Life* 2016; **68**: 748–755.

(45) El Hassouni B, Granchi C, Vallés-Martí A, Supadmanaba IGP, Bononi G, Tuccinardi T *et al.* The dichotomous role of the glycolytic metabolism pathway in cancer metastasis: Interplay with the complex tumor microenvironment and novel therapeutic strategies. *Seminars in Cancer Biology* 2019. doi:10.1016/j.semcancer.2019.08.025.

(46) Gonlugur TE, Gonlugur U. Pleural fluid findings as prognostic factors for malignant pleural mesothelioma. *J Clin Lab Anal* 2008; **22**: 334–336.

(47) Singhal S, Wiewrodt R, Malden LD, Amin KM, Matzie K, Friedberg J *et al.* Gene expression profiling of malignant mesothelioma. *Clin Cancer Res* 2003; **9**: 3080–3097.

(48) Zhao D, Zou S-W, Liu Y, Zhou X, Mo Y, Wang P *et al.* Lysine-5 acetylation negatively regulates lactate dehydrogenase A and is decreased in pancreatic cancer. *Cancer Cell* 2013; **23**: 464–476.

(49) Sciarrillo R, Minutolo F, Peters GJ, Giovannetti E. Lactate dehydrogenase acetylation adds another piece to the puzzle of metabolic reprogramming in pancreatic cancer. *Translational Gastrointestinal Cancer* 2014; **3**: 64-66–66.

(50) Gorlach A, Bolling B, Holtermann G, Schwachofer J, Carlsson J, Acker H. Changes in growth, po(2) and ph after exposure to oxamate - studies of 2 human tumor-cell lines growing as multicellular spheroids. *International journal of oncology* 1995; **7**: 831–9.

(51) Oehl K, Kresoja-Rakic J, Opitz I, Vrugt B, Weder W, Stahel R *et al.* Live-Cell Mesothelioma Biobank to Explore Mechanisms of Tumor Progression. *Front Oncol* 2018; **8**. doi:10.3389/fonc.2018.00040.

(52) Wu L, Allo G, John T, Li M, Tagawa T, Opitz I *et al.* Patient-Derived Xenograft Establishment from Human Malignant Pleural Mesothelioma. *Clin Cancer Res* 2017; **23**: 1060–1067.

(53) Smitskamp-Wilms E, Pinedo HM, Veerman G, Ruiz van Haperen VW, Peters GJ. Postconfluent multilayered cell line cultures for selective screening of gemcitabine. *Eur J Cancer* 1998; **34**: 921–926.

(54) Levin M, Stark M, Berman B, Assaraf YG. Surmounting Cytarabine-resistance in acute myeloblastic leukemia cells and specimens with a synergistic combination of hydroxyurea and azidothymidine. *Cell Death & Disease* 2019; **10**: 1–14.

(55) Degwert N, Latuske E, Vohwinkel G, Stamm H, Klokow M, Bokemeyer C *et al.* Deoxycytidine kinase is downregulated under hypoxic conditions and confers resistance against cytarabine in acute myeloid leukaemia. *Eur J Haematol* 2016; **97**: 239–244.

(56) Wilson WR, Hay MP. Targeting hypoxia in cancer therapy. *Nat Rev Cancer* 2011; **11**: 393–410.

(57) Zhuo Y, Lin L, Wei S, Zhang M. Pretreatment elevated serum lactate dehydrogenase as a significant prognostic factor in malignant mesothelioma: A meta-analysis. *Medicine (Baltimore)* 2016; **95**: e5706.

(58) Pergolini I, Morales-Oyarvide V, Mino-Kenudson M, Honselmann KC, Rosenbaum MW, Nahar S *et al.* Tumor engraftment in patient-derived xenografts of pancreatic ductal adenocarcinoma is associated with adverse clinicopathological features and poor survival. *PLoS ONE* 2017; **12**: e0182855.

(59) Bronte G, Incorvaia L, Rizzo S, Passiglia F, Galvano A, Rizzo F *et al.* The resistance related to targeted therapy in malignant pleural mesothelioma: Why has not the target been hit yet? *Crit Rev Oncol Hematol* 2016; **107**: 20–32.

(60) Zucali PA. Target therapy: new drugs or new combinations of drugs in malignant pleural mesothelioma. *J Thorac Dis* 2018; **10**: S311–S321.

Supplemental methods

Patients, TMAs and Immunohistochemistry (IHC). Patient selection for the tissue-microarrays (TMAs) was based on the following inclusion criteria: a histological diagnosis of MPM or DMPM, and the availability of tumor tissue and clinicopathological data, which were recorded in prospectively maintained databases and anonymized after inclusion.

The study protocols were approved by the institutional review boards and the ethics committees of the Humanitas Research Hospital, Rozzano, Milan, Italy and National Cancer Institute, Milan, Italy, in accordance with the ethical guidelines of the Declaration of Helsinki. All participants provided written informed consent for sample collection and subsequent analysis.

For the TMA with MPM samples, the paraffin-embedded surgical or biopsy specimens (slides of 10 µm) were collected from the pathology files of the Humanitas Research Hospital, Rozzano, Milan, Italy (from January 2008 to December 2013). All these samples were collected before chemotherapy. All patients received pemetrexed at 500 mg/m^2 and a carboplatin infusion with a target area under the plasma concentration–time curve of 5 mg/mL*minutes (AUC5), administered intravenously every 21 days. All patients received folic acid and vitamin B12 supplementation. Patient characteristics were described in terms of number and percentage, or median and range, when appropriate, according to a recent prognostic study on a cohort of unresectable MPM patients who received pemetrexed-based chemotherapy [Bille' et al., 2017].

For the TMA with DMPM samples, tumor tissues of 56 DMPM patients treated with CRS and HIPEC in the National Cancer Institute, Milan, Italy (from August 1995 to October 2013) were selected for pathological examination. TMAs were constructed by using a tissue-arraying instrument (Beecher Instruments, Silver Springs, MD, USA).

IHC staining of paraffin-embedded tissues from MPM patients for proton-coupled folate transporter (PCFT), carbonic anhydrase IX (CAIX) and lactate dehydrogenase (LDH-A) were performed as described previously. Before staining with specific polyclonal rabbit anti-human antibody for PCFT [Hou et al, 2012], or with the commercial anti-CAIX (dilution 1:500; monoclonal antibody ab15086, Abcam, Cambridge, MA) and anti-LDH-A LDH-A (dilution 1:100; ab9002, Abcam) antibodies, the TMA slides were deparaffinized using xylene, rehydrated in alcohol and microwaved at 400W (2 times, for 5 minutes). Immunostaining was performed by the avidin-biotin peroxidase complex technique. Negative controls were obtained by replacement of primary antibody with phosphate-buffered saline (PBS), while positive controls were obtained using sections of colorectal cancer. Immunoreactivity was enhanced by antigen retrieval for 30 minutes in 10 mM sodium citrate, pH 6.0. The sections were washed

three times in PBS and blocked with Super Block (Skytek Laboratories, Logan, UT) and 3% hydrogen peroxide for 10 minutes prior to overnight incubation at 4°C with the primary antibody (dilution, 1:40). After overnight incubation with the primary antibodies, the sections were washed two times for 3 minutes in PBS and incubated with the appropriate kit containing the secondary antibody tagged with avidin-biotinylated horseradish peroxidase (Cell Marque revelation Kit, Sigma). Finally, the colorimetric reaction obtained with 3'-3' diaminobenzidine was counterstained with hematoxylin, and slides were permanently fixed with synthetic mounting. The sections were scored by two researchers blinded to clinical outcome, who also evaluated the extent of tissue loss, background staining and overall interpretability. Scoring for PCFT was described in our previous study [Giovannetti et al., 2017]

Immunostaining intensity of CAIX was described in the supplemental table 1, while for LDH-A we used a previously proposed grading system with two LDH-A expression levels: strong cytoplasmic expression in >50% of cancer cells or nuclear expression in >10% of cancer cells was defined as high expression; otherwise, nuclear expression was considered low [Koukourakis et al., 2006].

Neoplastic cells were always uniformly stained and counting all the tumor cells in each spot made positivity assessment. To further implement the reproducibly of our technical procedures, as discussed previously for other biomarkers in MPM samples [Li Petri et al., 2018], all stained TMA sections were also digitally imaged at 40X, using a computerized high-resolution acquisition system (D-Sight, Menarini, Florence, Italy), equipped with the automated quantitative image analysis software algorithm DSight software 2.1.0. Multipreview of the images allowed editing of the area of interests.

Determination of Mitochondrial Function and Glycolysis in Mesothelioma cells

Oxygen Consumption Rate (OCR) and ECAR (Extracellular Acidification Rate) were measured in the mesothelioma cell lines MSTO and H2452 by using the Seahorse XFp Metabolic Flux Analyzer (Agilent Technologies, Inc, Santa Clara, Ca, USA). One day before the assay, cells were seeded at a density of 40,000 per well in a final volume of 80 µl in a Seahorse plate. The mitochondrial stress test was performed according to manufacturer's instructions. Before the analysis, medium was changed with Seahorse XFp RPMI medium, enriched with 1 mM pyruvate, 2 mM glutamine and 10 mM glucose and then incubated for 45 minutes. After three baseline measurements, Oligomycin (inhibitor of V Complex), Carbonyl cyanide-4 (trifluoromethoxy) phenylhydrazone (FCCP, mitochondrial uncoupler) and a mix of Rotenon and Antimycin A (inhibitors of Complexes I and III) were sequentially injected into

each well to final concentrations of 1.5 µM, 0.5 µM 0.5 µM. The obtained data allowed for calculations of ATP-linked Respiration, Maximal Respiration, Spare Capacity, Proton Leak and Non-Mitochondrial Oxygen Consumption. The Glycolysis Stress Test was conducted with similar seeding conditions. At the day of analysis, the Seahorse XFp RPMI medium was enriched with 2 mM glutamine and adjusted to pH 7.4. Glucose (substrate for glycolysis), Oligomycin (inhibitor of mitochondrial ATP production) and 2-deoxyglucose (inhibitor of hexokinase) were consecutively added into wells to final concentrations of 10 mM, 5 µM and 100 mM, respectively. The Glycolytic capacity, Glycolytic reserve, Glycolysis and Non-Glycolytic Acidification were estimated and normalized to mg of protein.

Quantitative-RT-PCR (qRT-PCR). PCR reactions were performed in triplicate with 5 µL of cDNA, 12.5 µL of TaqMan Universal PCR Master Mix, and 5 µL of probe, and forward and reverse primers in a final volume of 25 µL. Samples were amplified by the following thermal profile: an initial incubation at 50°C for 5 minutes to prevent the reamplification of carry-over PCR products by AmpErase uracil-N-glycosylase, followed by incubation at 95°C for 10 minutes to supress AmpErase UNG activity and denature the DNA, 50 cycles of denaturation at 95°C for 15 seconds, followed by annealing and extension at 60°C for 1 minute. Specific forward and reverse primers and probes were obtained from Applied Biosystems Assay-on-Demand products. All the samples were amplified in triplicate with appropriate non-template controls, and the coefficient of variation was less than 2%.

Analysis of *PCFT* gene expression modulation by siRNA. For the analysis of PCFT modulation, MPM cells were plated in triplicate at a density of 2×10^5 cells/well in 6-well plates. After 24 hours, the cells were treated with siRNA anti-PCFT or negative control (Silencer® Select Negative Control #1 siRNA, Ambion) in a final RNA concentration of 25 nmol/L. Lipofectamine™ was used as transfection solution, according to the manufacturer's instructions. The modulation of *PCFT* expression by this siRNA was investigated by q-RT-PCR, after 48 and 72 hours, as described previously [Maftouh et al., 2015].

Cell growth inhibition assays. For sulforhodamine-B (SRB) assays, cells were plated at $5x10^4$ cells per well, using 96-well plates, and growth inhibition was expressed as the percentage of control (vehicle treated cells) absorbance (corrected for absorbance before drug addition). After 72 hours, optical density was measured at 540 nm using the Tecan SpectraFluor (Tecan, San Diego, CA, USA). The 50% inhibitory concentration of cell growth (IC50) was calculated by

non-linear least squares curve fitting (GraphPad PRISM version 5.0, Intuitive Software for Science, San Diego, CA, USA). To investigate whether the modulation of PCFT expression affected pemetrexed cytotoxicity, we performed the same SRB experiments in cells treated for 48 hours with the siRNA anti-PCFT or its negative control, in a final RNA concentration of 25 nmol/L.

Spheroids. MPM spheroids were established by seeding 1000 MPM cells per ml in DMEM/F12 GlutaMAX-I (1:1, Invitrogen), in ultra-low attachment plates (Corning Incorporated, Corning, NY). These spheroids were generated for 7-10 days, and then harvested for RNA isolation and analysis of PCFT expression, as described above. Spheroid volume (V) was calculated from the geometric mean of the perpendicular diameters D = (Dmax + Dmin)/2, as follows: $V = (4/3) * \pi(D/2)3$).

We also performed an exploratory analysis using a sequential trypsin digestion of spheroids of H2452 that had reached a diameter of approximately 500 μm. These serial trypsin treatments, enabled the segregation into four heterogeneous populations comprising proliferating cells from the surface (SL), an intermediate region (IR), nonproliferating hypoxic cells from the predominantly hypoxic perinecrotic region (PN), and a necrotic core (NC), as described previously [McMahon et al., 2012]. Aliquots containing cells in suspension derived from pooled NC/PN versus SL/IR regions were segregated and 10^5 viable (trypan blue excluding) cells were plated into 6-well culture dishes and treated with PMX 1 and 10 □M. After 7 days incubation at 37 °C, the drug-treated colonies of greater than 50 cells were counted and plating efficiency determined as the number of colonies formed/number of cells plated expressed as a percentage of untreated colonies.

In parallel experiments we also evaluated whether pemetrexed was able to affect spheroid formation by counting the number of spheroids created in cells exposed immediately after seeding to 0.1, 1, 10 and 20 μM pemetrexed for 72 hours, compared to untreated cells.

MESO II and STO spheroids with a diameter of approximately 300 μm were created in 96-well flat bottom plates coated with 1.5% agarose. DMEM/F12 medium was replaced with drug-free medium or medium containing gemcitabine or PI-FLY161 (6 wells per condition). Images of spheroids were taken with an automated phase-contrast microscope (Universal Grab software,

Digital Cell Imaging Labs). To detect the amount of light passing through the spheroids, pixel intensities of 8-bit black/white-converted images were calculated using ImageJ Software (U.S. National Institutes of Health, Bethesda, Maryland, USA) and expressed as Mean Grey value (= sum of all Grey values of the spheroid selection divided by the pixels of that selection). Inhibition of cell aggregation for each drug-treated spheroid after 7 days ("treated" in the formula below) was calculated by normalizing for the Mean Grey values of the sum control spheroids (Σ control, where "n" is the number of replicates in the formula below) as follows:

Inhibition of cell aggregation = $|((1 - treated)/(\Sigma control / n))|$

Western blot of LDH-A. In order to evaluate the modulation of LDH-A protein expression in MPM cells growing as a monolayers or as spheroids, the H28, H2452 and MSTO-211H cells were cultured for 72 h and western blotting was performed, as described earlier [Maftouh et al, 2012]. Briefly, 30 30 µg of proteins was separated on a 10% SDS- polyacrylamide gel and transferred onto PVDF membrane (Immobilion-FL, Millipore, Billerica, MA). The membrane was blocked with Rockland (Rockland Inc., Boyertown, PA), and incubated overnight with anti-LDH-A antibody (Abcam, Cambridge, UK, at 1:1000 dilution), and mouse anti-β-actin (1:10000 dilution; Sigma).

***In vivo* experiments using orthotopic and subcutaneous mouse models and live imaging**

In vivo experiments were performed in nu/nu athymic female mice 4 weeks old with average 23 g of weight (range, 22-24 g) at the arrival, while the weight during the experiment is reported in the Supplemental Figure S8). The animals were purchased purchased from Harlan (Horst, The Netherlands).

The working protocol was approved by the local ethical committees on animal experimentation of the VU University Medical Center (VUmc, Amsterdam, The Netherlands) and of the University of Pisa (Comitato di Ateneo per la Sperimentazione Animale, Pisa, Italy), according to the 2010/63/EU European Community Council Directive for laboratory animal care.

In the study design and report we followed the ARRIVE reporting guideline and provide a completed ARRIVE checklist as a supplemental file specifying where in the manuscript each item is reported.

In particular, we undertook the following steps to minimise the effects of subjective bias when allocating animals to treatment: randomisation procedure (matching for tumor volume and animal weight) and blinding assessment of the results by the pathologists. The animals were hosted in cages (3 animals/cage), under pathogen free [SPF] condition, with standard light/dark

cycle, and temperature conditions, and free access to food and water, environmental enrichment). Welfare-related assessments and interventions were carried out prior to, and during the experiment.

Orthotopic primary DMPM models (n=5 tumors per treatment group) were generated by injection of 3×10^6 Fm/GC primary cells into the peritoneal cavity of the mice. Postoperative pain was counteracted by administering temgesic (0.05-0.1 mg/kg SC), which was already demonstrated to be an effective anaesthetic [Giovannetti et al., 2014]. Mice were treated with NHI-Glc-2, solubilized in Polyethylene glycol 400 (PEG400, Sigma-Aldrich, St. Louis, MO), at 100 mg/kg, 5 days (1-5) for 2 weeks (formulation concentration: 25 mg/mL in PEG400, 100 µL i.p. injection for a 25 g mouse). The drug was administered in the morning, in the mouse facility laboratory. the animals in the different experimental groups were treated and assessed always in the same order. Lidocaine was used as local anesthetic on the skin of the mouse.

Bioluminescence imaging (BLI) was evaluated with a Bruker In-Vivo Xtreme Capture System, using Molecular Imaging Software (Bruker Corporation, Billerica, MA).

Additional imaging analyses to define tumor spatial characteristics and evaluate microenvironment structures, such as neovasculature and hypoxic status, were carried out by high-frequency-ultrasound including Power Doppler Mode (Vevo-2100, VisualSonics, Amsterdam, The Netherlands).

Further experiments were performed on subcutaneous tumors, obtained by inoculation of 3×10^6 tumor cells. When tumor volume reached an average size of 100 mm^3, the animals were randomly distributed into 4 groups (n=6 tumors per treatment group) as follows: 1) control/untreated mice; 2) mice treated with gemcitabine alone at 100 mg/kg, 2 days (day 1 and 4) for three weeks (formulation concentration: 25 mg/mL in PBS, 100 µL i.p. injection for a 25 g mouse); 3) mice treated with NHI-Glc-2, solubilized in PEG400, at 50 mg/kg, 5 days (day 1-5) for three weeks (formulation concentration: 12.5 mg/mL in PEG400); and 4) mice treated with a simultaneous combination of gemcitabine and NHI-Glc-2, at the doses mentioned above, for three weeks. Tumor xenografts were measured as described previously [Cavazzoni et al., 2017]. No deaths and 100% tumor take-rate are reported in the literature for mesothelioma models obtained by IP injection of mesothelioma cells. Research papers report mouse death essentially due to tumor and metastasis development. However, our mice were sacrificed before MM primary tumors and metastases can cause severe symptoms, via cervical dislocation. Since previous studies showed that orthotopic administration of cancer cell lines gives tumor growth in 100% [Pinton et al., 2014] we used a number of 3 mice per group (+two extra mouse in case of sudden death) to test if a primary cell culture results in tumor formation. The number of

animals for the analysis of drug activity in the subcutaneous models was based on previous studies in which a standard error of 34% was reported in the number of proliferating cancer cells [Shah et al, 2011]. With this standard error, a group size of 6 animals is sufficient to detect a treatment effect of 55%.

Regarding the implications of our experimental methods or findings for the replacement, refinement or reduction (the "3Rs") of the use of animals in research we declared in our research protocol that "The development of a mouse model with mesothelioma (MM) primary cultures is of crucial importance to gain a better understanding of the biology of this devastating tumor. Furthermore, such models will allow preclinical research into new therapeutic strategies. The MM animal models will be used to test the effects of drugs potentially effective in treating patients affected by this devastating disease. So far, many trials have been initiated in the clinic without supporting evidence from pre-clinical research or using traditional preclinical models that deviate from their originator tumor. The lack of such pre-clinical studies with appropriate mice models may be one of the causes of the lack of positive results in clinical trials, and ultimately for the lack of improvement in survival expectancy in these patients. The use of animals and the moderate/severe distress that will be caused to them is acceptable in the light of the extreme need for research into the biology of MM. Furthermore, we strongly believe that our experiments will allow us to develop novel effective therapeutic strategies for patients affected by this aggressive and lethal tumor." Moreover, our scientific findings, based on appropriately designed and analysed animal experiments, should further accelerate the development and use of models and tools, based on the latest science and technologies, to address important scientific questions and have impact of welfare minimising the use of animals in future studies.

Supplementary References (in alphabetic order)

- Billé A, Krug LM, Woo KM, Rusch VW, Zauderer MG. Contemporary Analysis of Prognostic Factors in Patients with Unresectable Malignant Pleural Mesothelioma. J Thorac Oncol. 2016;11:249–55.
- Enhanced efficacy of AKT and FAK kinase combined inhibition in squamous cell lung carcinomas with stable reduction in PTEN.
- Cavazzoni A, La Monica S, Alfieri R, Ravelli A, Van Der Steen N, Sciarrillo R, et al. Oncotarget. 2017;8(32):53068-53083.

- Giovannetti E, Wang Q, Avan A, Funel N, Lagerweij T, Lee JH, et al. Role of CYB5A in pancreatic cancer prognosis and autophagy modulation. J Natl Cancer Inst. 2014;106(1):djt346.
- Giovannetti E, Zucali PA, Assaraf YG, Funel N, Gemelli M, Stark M, et al. Role of proton-coupled folate transporter in pemetrexed resistance of mesothelioma: clinical evidence and new pharmacological tools. Ann Oncol 2017;28:2725–32.
- Hou Z, Kugel Desmoulin S, Etnyre E, Olive M, Hsiung B, Cherian C, Wloszczynski PA, Moin K, Matherly LH. Identification and functional impact of homo-oligomers of the human proton-coupled folate transporter. J Biol Chem. 2012;287:4982-95.
- Koukourakis MI, Giatromanolaki A, Sivridis E, Gatter KC, Harris AL; Tumour Angiogenesis Research Group. Lactate dehydrogenase 5 expression in operable colorectal cancer: strong association with survival and activated vascular endothelial growth factor pathway--a report of the Tumour Angiogenesis Research Group. J Clin Oncol. 2006;24(26):4301-8.
- Li Petri, Cascioferro S, Parrino B, Peters GJ, Diana P, Giovannetti E. Proton-coupled folate transporter as a biomarker of outcome to treatment for pleural mesothelioma. Pharmacogenomics. 2018;19(10):811-814.
- Maftouh M, Avan A, Sciarrillo R, Granchi C, Leon LG, Rani R, et al. Synergistic interaction of novel lactate dehydrogenase inhibitors with gemcitabine against pancreatic cancer cells in hypoxia. Br J Cancer. 2014;110(1):172-82.
- McMahon KM, Volpato M, Chi HY, Musiwaro P, Poterlowicz K, Peng Y, et al. Characterization of changes in the proteome in different regions of 3D multicell tumor spheroids. J Proteome Res. 2012;11(5):2863-75.
- Pinton G, Manente AG, Daga A, Cilli M, Rinaldi M, Nilsson S, Moro L. Agonist activation of estrogen receptor beta (ERŒ≤) sensitizes malignant pleural mesothelioma cells to cisplatin cytotoxicity. Mol Cancer. 2014;13:227.
- Shah N, Zhai G, Knowles JA, Stockard CR, Grizzle WE, Fineberg N, et al. 18)F-FDG PET/CT imaging detects therapy efficacy of anti-EMMPRIN antibody and gemcitabine in orthotopic pancreatic tumor xenografts. Mol Imaging Biol. 2012;14(2):237-44.

Supplemental figures

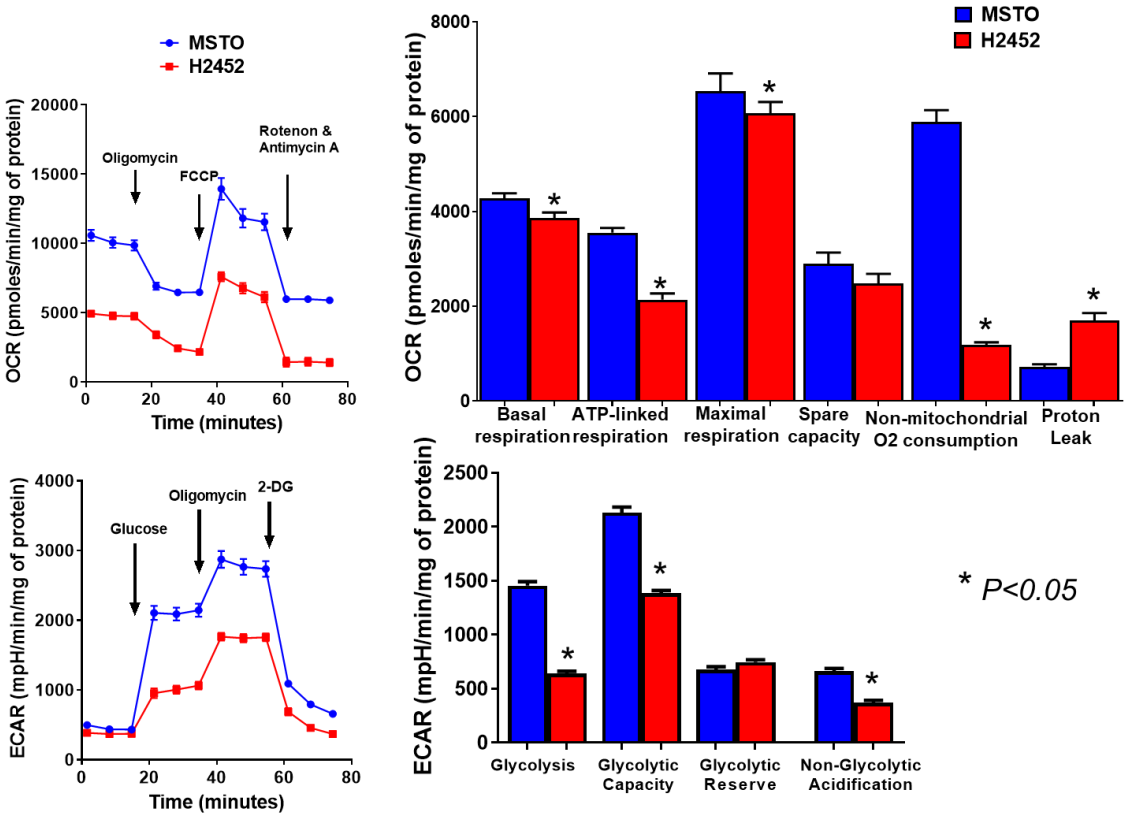

Figure S1: Differential profiles in the metabolism of MPM cells. The MSTO-211H and H2452 mesothelioma cells showed different profiles in their basal energy metabolism as assessed by using Seahorse XF24 Extracellular Flux analyser, as described previously. Specifically, this machine measures glycolysis by analysing the extracellular acidification rate (ECAR) and measures mitochondrial oxidative phosphorylation on the basis of the oxygen consumption rate (OCR), through real-time and live cell analysis. The OCR of MSTO-211H and H2452 mesothelioma cells was measured after Seahorse XFp Cell Mito Stress Test over time (minutes), and resulting data calculated for ATP-linked basal Respiration, maximal respiration, spare capacity, non-mitochondrial oxygen consumption and proton leak are reported in the left and right upper panel, respectively. The ECAR was measured after Seahorse XFp Glycolysis Stress Test, and resulting data calculated for Glycolytic capacity, Glycolytic reserve, Glycolysis and Non-Glycolytic Acidification are reported in the left and right lower panel, respectively. Columns, mean values obtained from three different independent experiments, bars, SEM. *Significant difference ($P<0.05$) between the two cell lines.

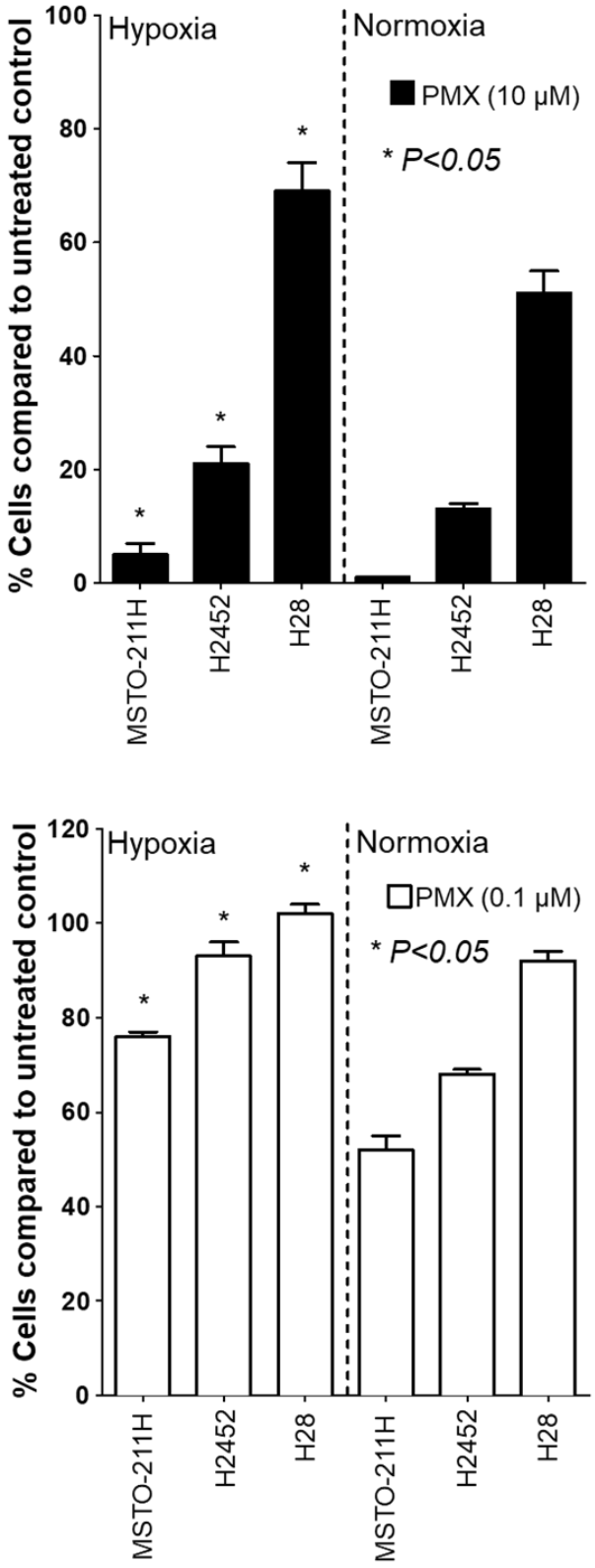

Figure S2: Hypoxia affects pemetrexed activity. Cell growth inhibition was performed in cells exposed to pemetrexed 10 µM PMX (upper panel) or 0.1 µM PMX (lower panel) for 72 hours under hypoxic vs. normoxic conditions, as compared to drug-free control cells. Columns, mean values obtained from three independent experiments; bars, SEM. *Significantly different (P<0.05) when compared to the same treatments under normoxic conditions.

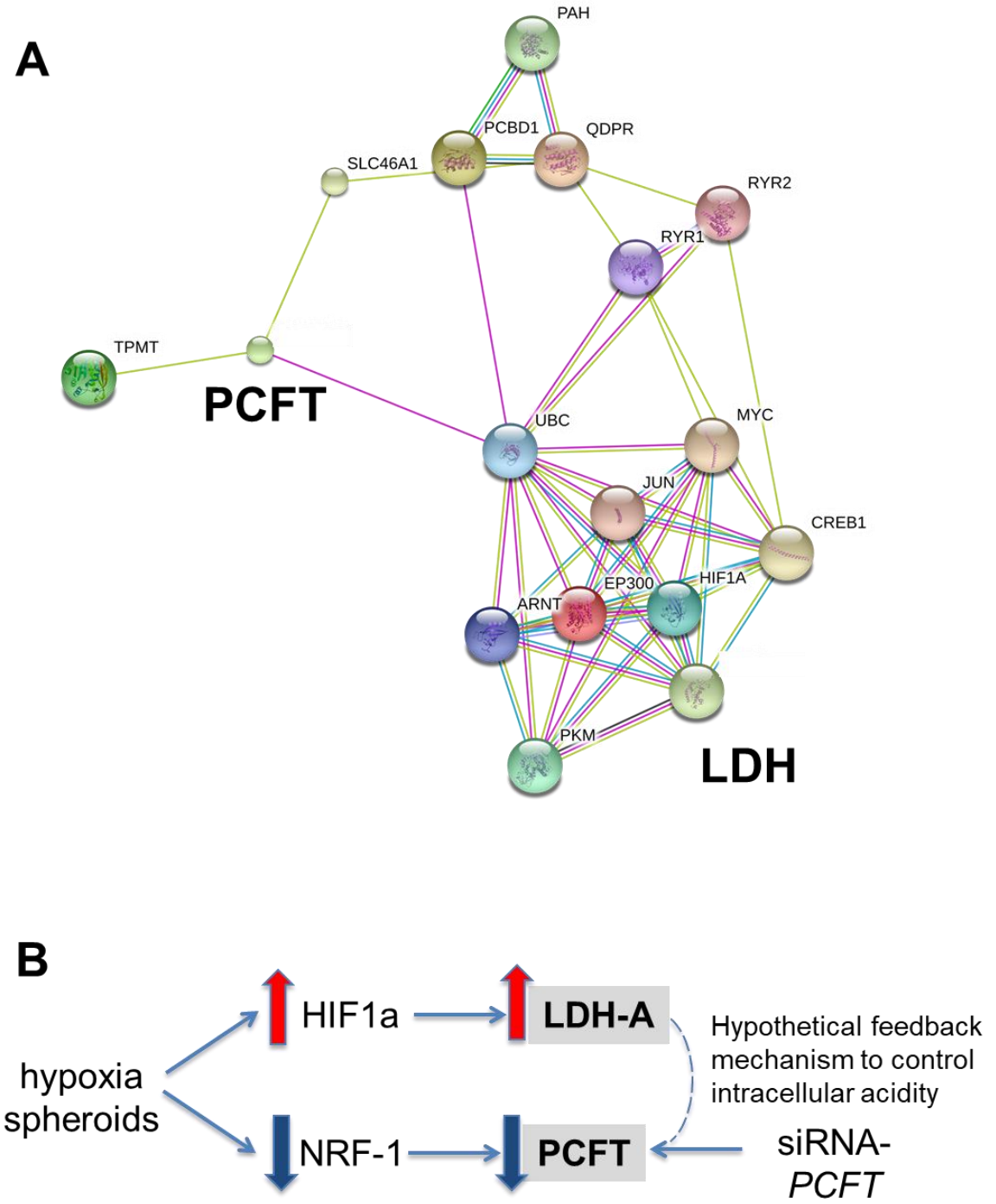

Figure S3. Interaction between PCFT and LDH-A. (A) Protein network visualization from the STRING website. The online database STRING (http://string-db.org), which allows retrieving the functional and physical interactions of proteins, did not reveal a direct physical interaction between PCFT and LDH-A. **(B)** Proposed hypothetical model of PCFT and LDH-A modulation in cells growing in hypoxia and as spheroids and after targeted downregulation of PCFT expression.

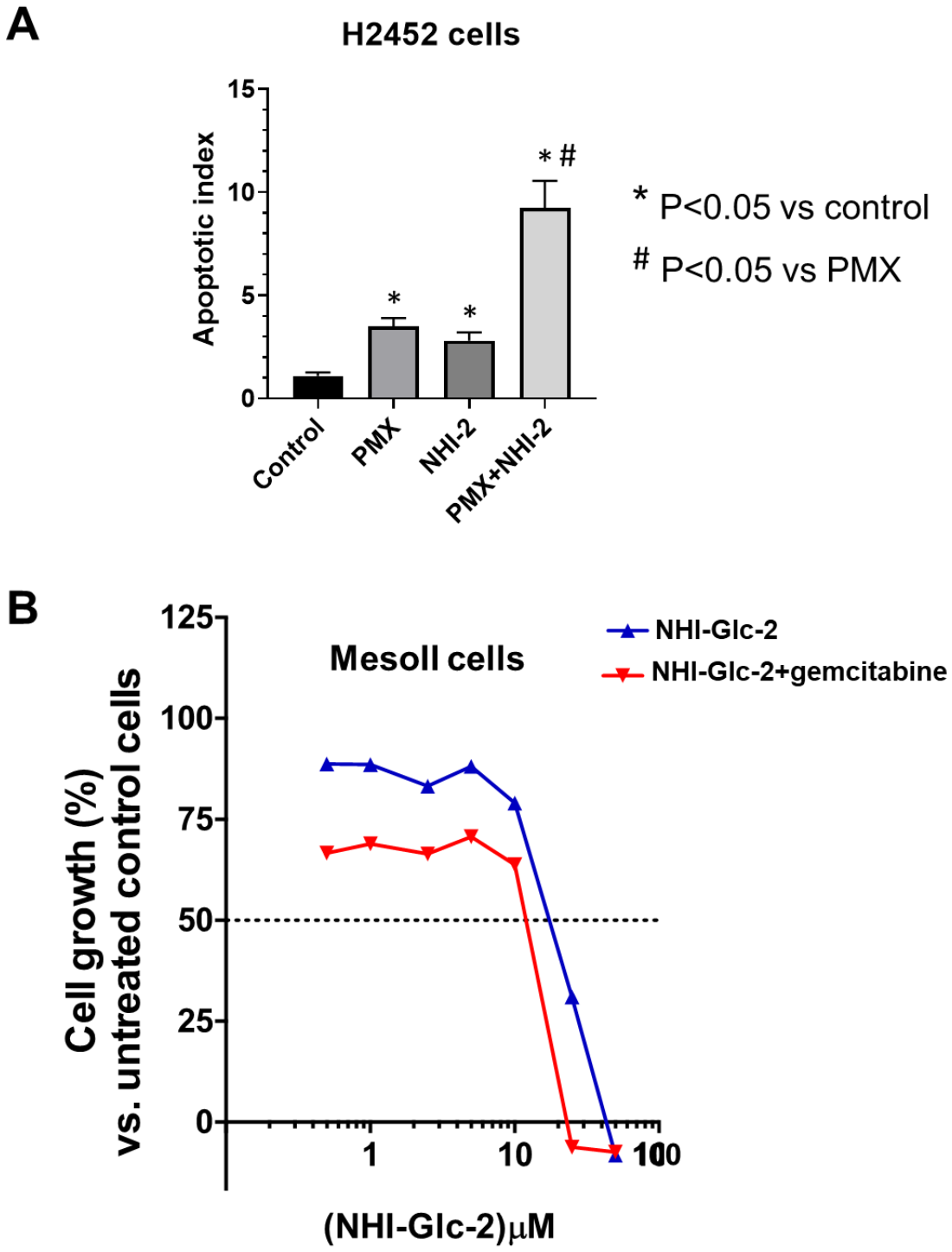

Figure S4. Interaction between chemotherapeutic drugs and LDH-A inhibitors. (A) Apoptosis induction by 1 μM NHI-2 and 1 μM pemetrexed (PMX) and their combination for 24 hours pemetrexed in H2452 cells growing as monolayer under hypoxic conditions. The apoptotic index was calculated after bisbenzimide-HCl staining, as described previously [Massihnia et al., J Hematol Oncol 2017]. **(B)** Cell growth inhibition by NHI-Glc-2 alone, and in combination with gemcitabine at IC_{25}. Growth inhibition curves of MesoII cells of a representative experiment with NHI-Glc-2 alone, and in combination with gemcitabine, under hypoxic conditions. *Points*, mean values obtained from three independent experiments; *bars*, SEM.

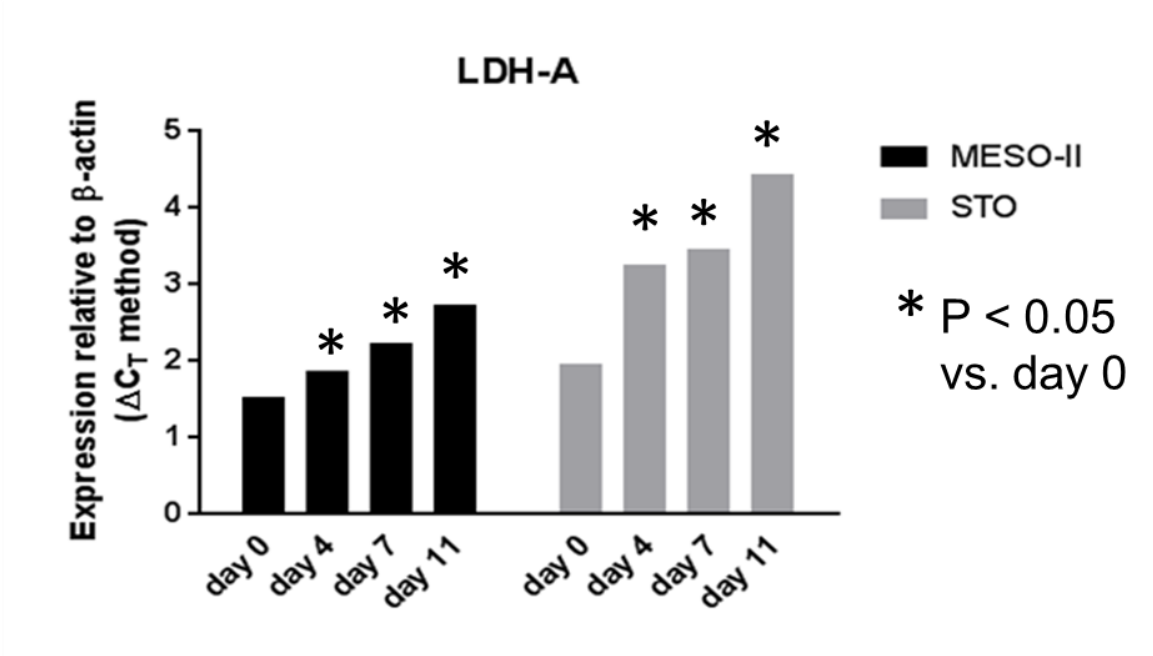

Figure S5. Increased LDH-A mRNA levels in spheroids. Modulation of LDH-A expression as assessed in MesoII and STO spheroids by qRT-PCR. *Columns*, mean values obtained from three independent experiments (the SEM values were not reported since they were always below 5%).

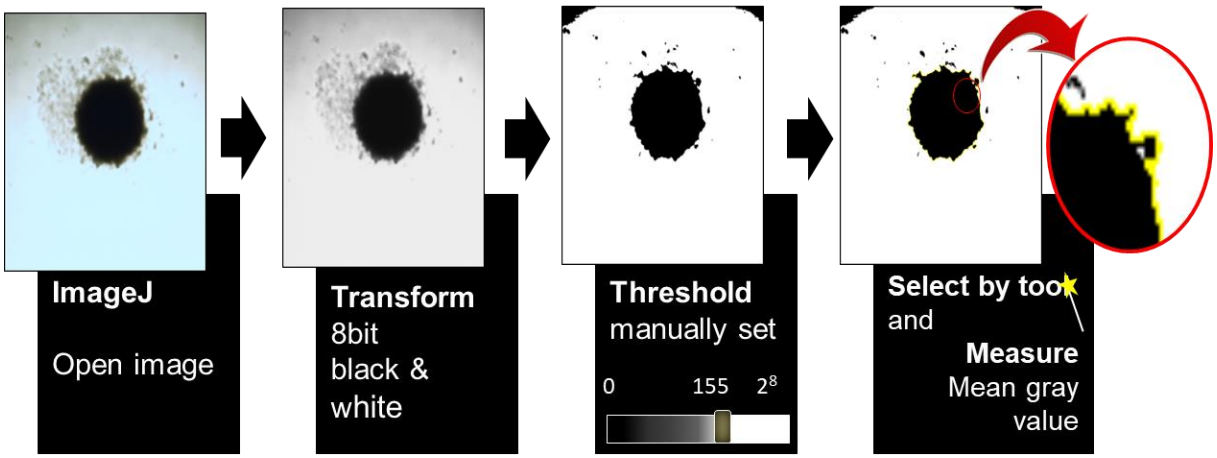

Figure S6. Scheme describing the analysis of spheroid aggregation. To detect the light passing through the spheroids, pixel intensities of 8-bit black/white-converted images were calculated using ImageJ Software (U.S. National Institutes of Health, Bethesda, MD, USA), as described in the supplemental methods.

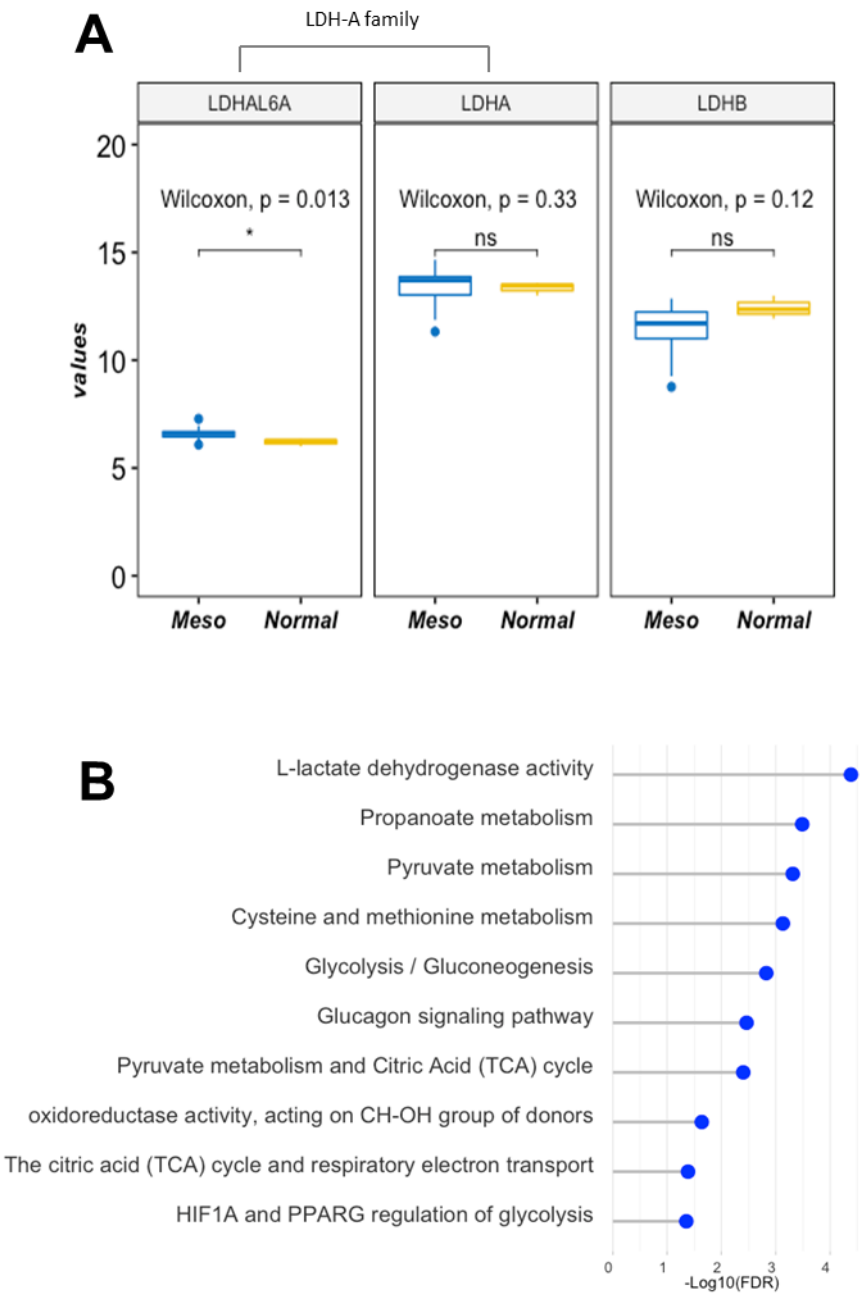

Figure S7. Microarray data analyses showing higher LDHAL6A expression in DMPM tissues compared to normal mesothelium tissues. (A) Differential analysis of mRNA expression of LDHA, LDHAL6A, LDHB in Mesothelioma and Normal tissues. LDHAL6A, a protein belonging to the LDHA family, is significantly overexpressed in mesothelioma tissues in the GSE112154 dataset. **(B)** Analysis of shared processes between LDHA and LDHAL6A.

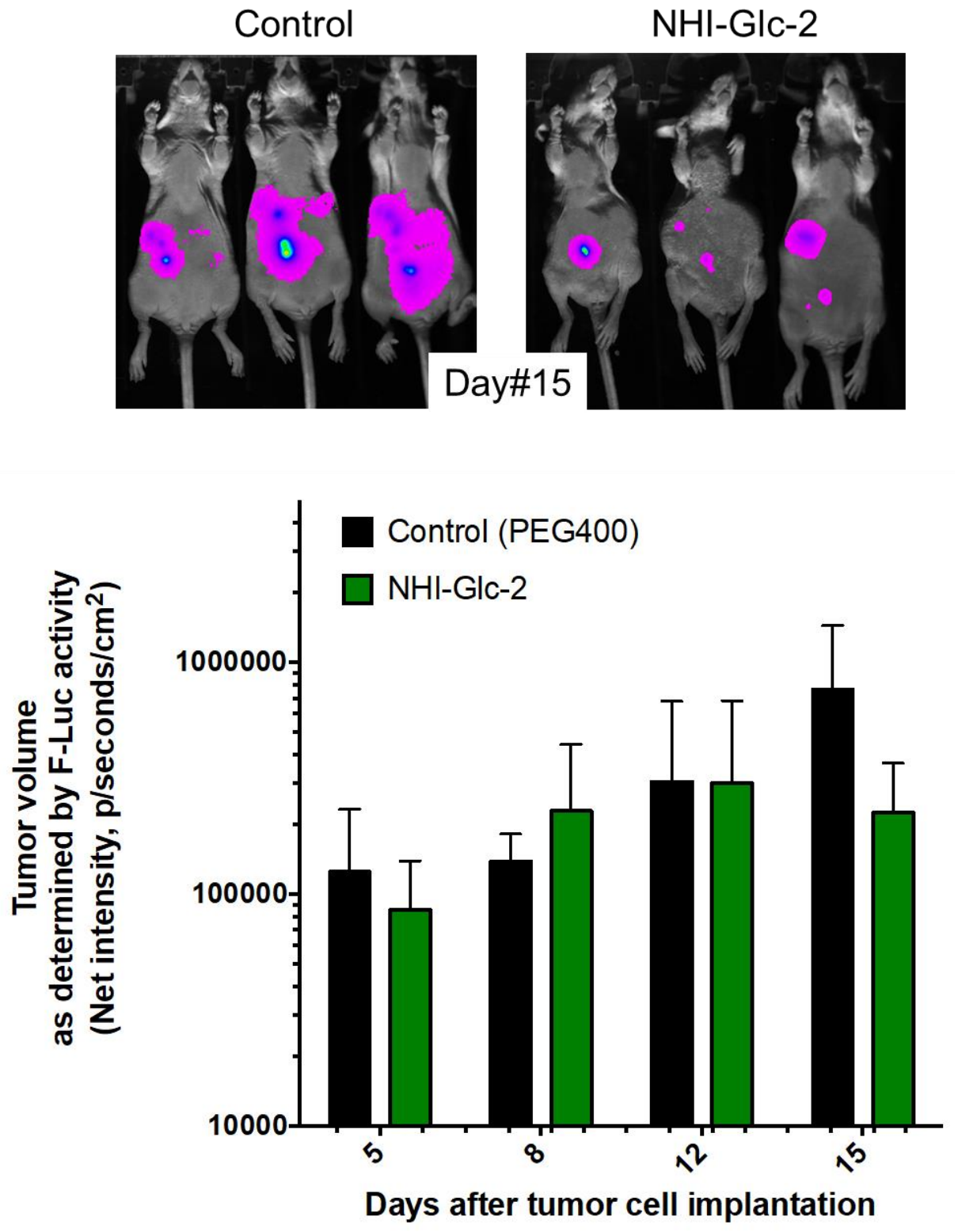

Figure S8. Modulation of tumor volume in orthotopic DMPM tumors. Upper panel: Representative BLI images of mice harbouring orthotopic DMPM tumors. At the start of the experiment, mice were stratified into groups with comparable BLI signal, and then treated with NHI-GLC-2 administered i.p. for 2 weeks. Lower panel: Tumor growth as detected by BLI analysis. *Columns*, mean values obtained from the measurements in three mice; *bars*, SD.

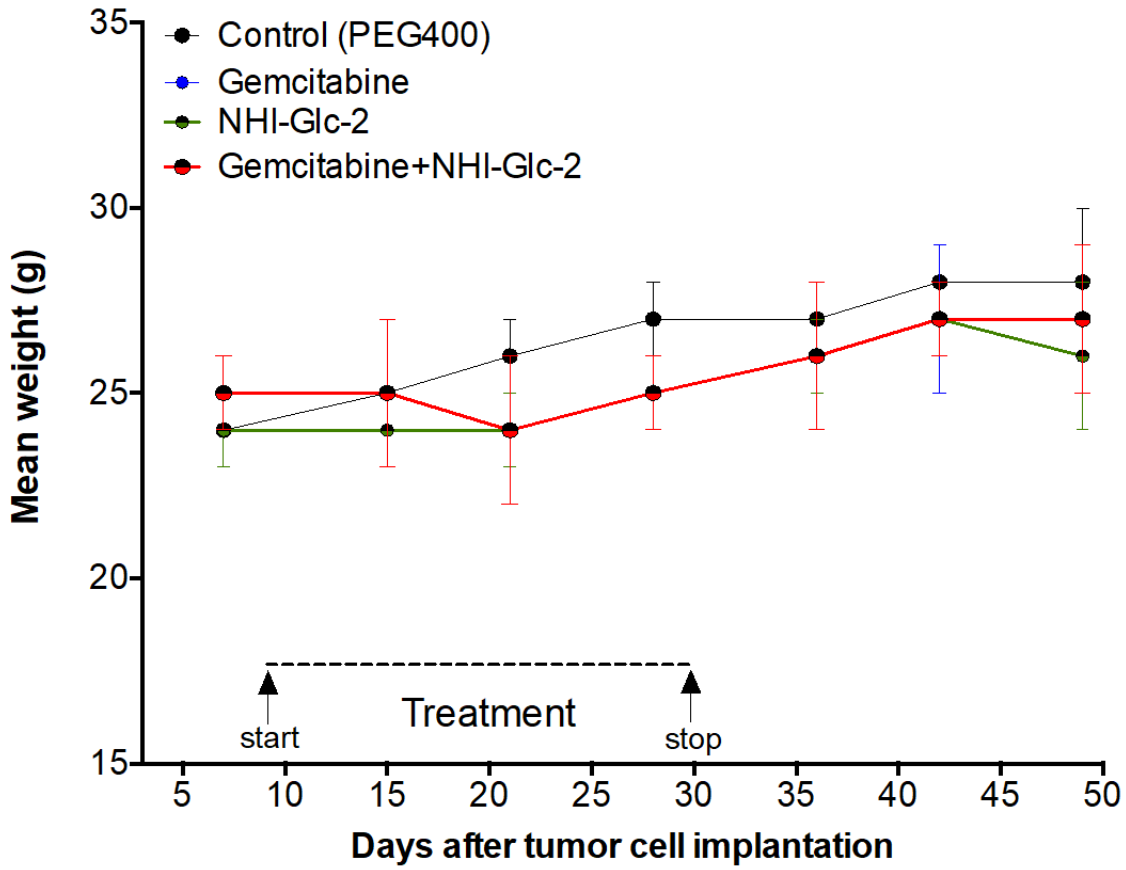

Figure S9. Body weight of animals inoculated subcutaneously with DMPM cells. Median weight loss was always <10%, without toxic deaths. These results support the conclusion that the gemcitabine/NHI-Glc-2 combination displays a safe antitumor activity against *in vivo* models of DMPM.

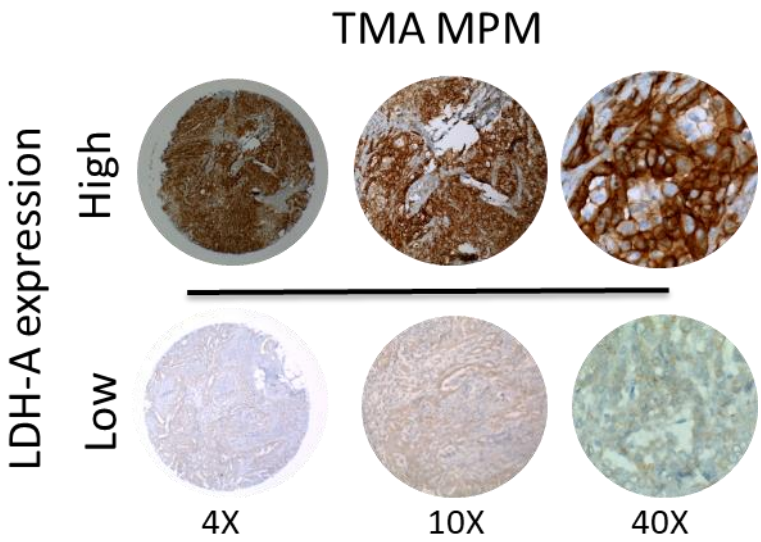

Figure S10. LDH-A immunohistochemical analyses of MPM tissue microarrays (TMAs). Representative TMA cores in the cohorts of MPM patients, illustrating cases with high (upper panels) and low (lower panels) LDH-A expression (at 4X, 10X and 40X original magnification). Of note, at 40X the LDH-A staining seems membrane-bound. However, this is an artefact. As clearly detected at the other magnification the staining is indeed cytoplasmatic. As clearly detected at the other magnifications the staining is indeed cytoplasmatic. Since these cells have very big nuclei, these nuclei are taking most of the space in the cytoplasm and the staining seems located near to the membrane at 40X. However, this staining is not a "membrane staining", also in comparison to our previous staining of EGFR in MPM tissues [Giovannetti et al., Br J Cancer 2011].

Supplemental Table 1

Baseline characteristics of MPM and DMPM patients

Clinical characteristics	*n* of patients (%)	
	MPM (N=33)	**DMPM (N=56)**
Age, years [median, range]	68 [47-82]	73 [51-85]
Age		
≤65	13 (39)	28 (50)
>65	20 (61)	28 (50)
Gender		
Male	16 (48)	17 (30)
Female	17 (52)	39 (70)
EORTC prognostic score / PS		
Good / 0	28 (85)	44 (78)
Poor /1-2	5 (15)	12 (22)
Histologic subtype		
Epithelial	30 (90)	47 (84)
Non-epithelial	3 (10)	9 (16)
PFS, months (median, 95%CI)	7.5 (6.2-8.8)	13.0 (10.2-15.7)
OS, months (median, 95%CI)	20.1 (8.5-31.7)	26.0 (11.9-40.1)

Notes: Survival and PFS data were available for all patients. Abbreviations: OS, Overall survival; PFS, progression-Free survival; PS, performance status

Supplemental Table 2

Scoring of CAIX protein expression staining

Intensity of staning			**Weak**	**Middle**	**Strong**
	Range	**Score**	**1**	**2**	**3**
Positive cells %	**X=0**	**0**	**NO CAIX**	**NO CAIX**	**NO CAIX**
	0<x<25	**1**	**Low CAIX**	**Low CAIX**	**High CAIX**
	25<x<	**2**	**Low CAIX**	**High CAIX**	**High CAIX**
	x>75	**3**	**High CAIX**	**High CAIX**	**High CAIX**
"High CAIX" include the scores 4,5 and 6 "Low CAIX" includes the scores 2 and 3					

Supplemental Table 3

List of genes significantly up-regulated in cells growing as monolayers or spheroids, after exposure to hypoxic conditions as well as after PCFT silencing (showing a PCFT reduction of 80% at RT-PCR) and, using the Hypoxia RT2 ProfilerTM array. The genes are reported in alphabetic order (NC, negative control, genes in blue are in common between the "Spheroids vs. monolayers" and the "Hypoxia vs. Normoxia" groups, genes in green are in common between the "Spheroids vs. monolayers" and the "PCFT siRNA vs. NC siRNA" groups, genes in red are in common between the "Hypoxia vs. Normoxia" and the "PCFT siRNA vs. NC siRNA" groups, **LDH-A** is the only gene in common among all these three groups).

P values <0.01; Fold change= 3		
Spheroids vs. monolayers N=25	Hypoxia vs. Normoxia N=49	PCFT siRNA vs. NC siRNA N=14
ADM	*ADORA2B*	*ATR*
ALDOA	*ANGPTL4*	*BLM*
ARNT	*ANKRD37*	*BHLHE40*
BTG1	*ANXA2*	*BNIP3*
ENO1	*APEX1*	*CA9*
HIF1A	*ARNT*	*EGLN1*
HIF3A	*ATR*	*FOS*
HK2	*BNIP3*	*HIF1A*
HNF4A	*BNIP3L*	*IGFBP3*
LDH-A	*BTG1*	***LDH-A***
LGALS3	*CA9*	*MMP9*
LOX	*CCNG2*	*MET*
MAP3K1	*COPS5*	*NFKB1*
MET	*CTSA*	*PFKP*
MIF	*DDIT4*	
MMP9	*DNAJC5*	
NCOA1	*EDN1*	
NFKB1	*EGLN2*	
PDK1	*EGR1*	
PFKFB4	*EPO*	
PGK1	*GBE1*	
PGK1	*GBE1*	
PIM1	*HIF3A*	

PKM2	*HNF4A*	
SLC2A1	*IER3*	
SLC2A3	*IGFBP3*	
	JMJD6	
	LDH-A	
	LOX	
	MIF	
	MXI1	
	NDRG1	
	NOS3	
	ODC1	
	P4HA1	
	P4HB	
	PKM2	
	PLAU	
	RBPJ	
	RUVBL2	
	SERPINE1	
	SLC2A1	
	SLC2A3	
	TFRC	
	TPI1	
	TXNIP	
	USF2	
	VDAC1	
	VEGFA	

Supplemental Table 4

Outcome of the patients in the MPM patients according to clinicopathological characteristics.

Characteristics	**LDH-A expression**		**PFS (Months)**	**OS (Months)**
	Low	***High***	***Median (95%CI)***	***Median (95%CI)***
			7.5 (6.2-8.8)	20.1 (8.5-31.7)
Age				
≤ 65	6	7	8.4 (5.2-11.6)	21.4 (2.2-40.6)
> 65	7	13	7.5 (6.2-8.8)	13.1 (8.4-31.7)
p-value	*0.52*		*0.91*	*0.32*
Gender				
Female	6	10	8.2 (7.0-9.4)	15.8 (4.9-26.7)
Male	7	10	7.4 (4.7-10.1)	20.1 (3.5-36.7)
p-value	*0.83*		*0.61*	*0.84*
EORTC *prognostic score*				
Good	*13*	*15*	7.7	20.6
Poor	*0*	*5*	6.8	19.1
p-value	*0.14*		*0.91*	*0.32*
Histology				
Epithelioid	13	17	8.4 (6.0-10.8)	20.7 (12.8-28.7)
Non-epithelioid	0	3	5.9 (0.8-11.0)	6.6 (2.3-10.9)
p-value	*0.40*		*0.02*	*0.04*

Abbreviations: EORTC, European Organization for Research and Treatment of Cancer; PFS, progression-free survival; OS, overall survival (Survival data were available for all patients and the minimum follow-up at the time of analysis was 27 months).

Notes: The potential association of LDH-A expression with clinicopathological characteristics was compared between groups using the chi-square test, with continuity correction when cells had expected count less than 5, while the correlation with PFS and OS was evaluated using the log-rank test

Supplemental Table 5

Outcome of the patients in the DMPM patients according to clinicopathological characteristics

Characteristics	**LDH-A expression**		**PFS (Months)**	**OS (Months)**
	Low	***High***	***Median (95%CI)***	***Median (95%CI)***
			13.0 (10.2-15.7)	26.0 (11.9-40.1)
Age				
≤ 65	9	19	10.0 (4.8-15.2)	14.0 (11.9-36.0)
> 65	12	16	14.0 (10.1-17.9)	31.0 (15.2-46.8)
p-value	*0.41*		*0.49*	*0.57*
Gender				
Female	18	21	14.0 (12.0-16.0)	26.0 (9.6-42.4)
Male	3	14	10.0 (7.3-12.7)	22.0 (3.8-40.2)
p-value	*0.08*		*0.52*	*0.53*
PS				
0	*17*	*27*	14.0 (5.3-22.7)	31.0 (19.6-42.4)
1-2	*4*	*8*	8.0 (4.8-15.9)	8.0 (6.9-18.2)
p-value	*0.74*		*<0.01*	*<0.01*
Histology				
Epithelioid	19	25	14.0 (11.8-16.2)	31.0 (17.0-45.0)
Non-epithelioid	2	7	8.0 (4.0-16.8)	9.0 (6.1-11.9)
p-value	*0.43*		*0.07*	*0.02*

Abbreviations: PFS, progression-free survival; PS, Performance Status; OS, overall survival.

Notes: The potential association of LDH-A expression with clinicopathological characteristics was compared between groups using the chi-square test, with continuity correction when cells had expected count less than 5, while the correlation with PFS and OS was evaluated using the log-rank test

Chapter 11

Biological Evaluation of a series of imidazo[2,1-b][1,3,4]thiadiazole derivatives against Diffuse Malignant Peritoneal Mesothelioma

Li Petri G[1,2], El Hassouni B[1], Zoppi S[1], Cascioferro S[2], Zaffaroni N[3], Peters GJ[1], Cirrincione G[2], Diana P[2], Giovannetti E[1,4]

1. *Department of Medical Oncology, Cancer Center Amsterdam, VU University Medical Center, Amsterdam, The Netherlands;*
2. *Dipartimento di Scienze e Tecnologie Biologiche Chimiche e Farmaceutiche (STEBICEF), Università degli Studi di Palermo, Palermo, Italy;*
3. *Molecular Pharmacology Unit, Fondazione IRCCS Istituto Nazionale dei Tumori, Milano, Italy;*
4. *Cancer Pharmacology Lab, Fondazione Pisana per la Scienza, Pisa, Italy;*

Unpublished results

Biological Evaluation of a series of imidazo[2,1-b][1,3,4]thiadiazole derivatives against Diffuse Malignant Peritoneal Mesothelioma.

Abstract

A new class of our imidazo[2,1-*b*][1,3,4]thiadiazole compounds have recently been evaluated as inhibitors of tyrosine phosphorylation of focal adhesion kinase (FAK) in pancreatic carcinoma models. FAK is overexpressed in malignant mesothelioma and has recently emerged as an interesting target for the treatment of this disease. Therefore, 10 imidazo[2,1-*b*][1,3,4]thiadiazole compounds characterized by the indole bicycle and a thiophene ring, were evaluated for the cytotoxic activity on two primary cell cultures of diffuse malignant peritoneal mesothelioma, MesoII and STO cells. Compounds **1a** and **1b** showed promising antitumor activity with IC_{50} values in the range from 0.59 to 2.81 μM in both cell lines cultured as monolayer. In 3D models, the compounds reduced the areas of spheroids approximately 2 times compared to the control after seventeen days of treatment. In addition, antimigratory activity was found by scratch wound healing assays in STO cells. These promising results prompt us to continue the research for future mechanistic studies of the antitumor activity.

Introduction

Malignant mesothelioma (MM) refers to a rare but aggressive tumor derived from mesothelial cells. They form a monolayer that covers the body' serous cavities and whose main function is to provide a protective membrane for the lung (pleural), the intestine (peritoneum), the heart (pericardium) and the *tunica vaginalis*. The thorax and abdominal cavity are the primary sites for the development of cancer, with a rate of 80-90% and 10-15%, respectively, instead pericardium (1%) and *tunica vaginalis* (<1%) are rarely affected.[1] The World Health Organization (WHO) has characterized three main histological types of mesothelioma, as well as their frequency rates: epithelioid (60-70%), sarcomatoid (10-15%) and biphasic (25-30%), this latter is a combination of the first two.[2] It is well documented that the main cause for the onset of the disease is the ingestion and/or inhalation of asbestos, particularly due to occupational exposure. Other mineral fibres such as thorium, talc, mica or erionite, as well as radiation or simian virus 40 (SV40) contribute to the development of the disease.[3–5] The incidence rate is closely associated to the etiology and although the use of asbestos has been banned for more than 30 years, its reduction has not been recorded in recent epidemiological data.[6–9] It is almost always a fatal disease due to advanced stage at diagnosis, usually after 30-40 years of latency period, with a median survival time after diagnosis of 9–12 months,[10] only 12% of patients live longer than one year.[11] Most patients receive benefit from a multimodal treatment that include the combination of surgery, chemotherapy and radiation; singly, these modalities did not give positive outcomes or advantages in terms of survival.[12–14] Anyway, not all patients can undergo surgery and consequently, systemic chemotherapy becomes the best optional route. Though mesotheliomas originate in different serous membranes, the efficacy of conventional chemotherapy varies with the location.[15]

Like many other solid tumors, mesotheliomas develop as result of different molecular disorders. The understanding of these events pushes the researcher on two fronts: **1-** to identify new molecules with antitumor activity; **2-** assess the activity of compounds already known for their mechanism of action and used for the treatment of various diseases alone or in combination with other drugs. Recently, we reported the antitumor activity of a new class of imidazo[2,1-*b*][1,3,4]thiadiazole compounds on pancreatic ductal adenocarcinoma (PDAC), highlighting their ability to reduce FAK phosphorylation on tyrosine residue [Y-397] (unpublished results). Therefore, encouraged by the strategies of 'drug repositioning' in drug discovery,[16] we decided to study the antitumor activity of ten imidazo[2,1-*b*][1,3,4]tiadiazole compounds (Figure 1) on two diffuse malignant peritoneal mesothelioma (DMPM) cells, STO and MesoII.

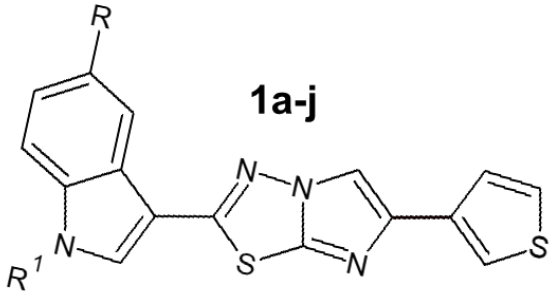

Compounds	R	R^1
1a	H	H
1b	H	CH_3
1c	Br	CH_3
1d	Cl	H
1e	Cl	CH_3
1f	F	CH_3
1g	Br	H
1h	F	H
1i	OCH_3	H
1j	OCH_3	CH_3

Figure 1. *Upper panel:* Chemical backbone structure of compounds **1a-j**. *Lower panel:* Table listing the chemical structure of the R and R^1 substituents for each compound

Materials and Methods

Drugs and chemical

The imidazo[1,2-*b*][1,3,4]thiadiazole compounds were synthesized at the Department of Pharmacy, University of Palermo, Italy (unpublished results). The drugs were dissolved in dimethyl sulfoxide (DMSO). The medium, foetal bovine serum (FBS), penicillin (50 IU mL^{-1}) and streptomycin (50 µg mL^{-1}) were from Gibco (Gaithersburg, MD,USA). All other chemicals were from Sigma (Zwijndrecht, the Netherlands).

Cell cultures

Human DMPM primary cultures (STO and MesoII) were derived from samples of patients who underwent surgery.[17] The cells were maintained in DMEM/F12 (Dulbecco's Modified Eagle's Medium: Nutrient Mixture F12) for less than 20 passages, supplemented with 10% heat-inactivated FBS, 1% penicillin/streptomycin. Cells were routinely tested for mycoplasma.

Cell growth inhibition

The cell growth inhibitory effect of imidazo[1,2-*b*][1,3,4]thiadiazole compounds was evaluated by sulforhodamine-B (SRB) assay following the protocol as previously described.[18] Cells were seeded into a 96-well flat-bottom plates in triplicate in a volume of 100 µL ($5x10^3$

cells/ well for both cell lines, MesoII and STO) and incubate for 24 hours at 37 °C to create a confluent monolayer. Thereafter, the cells were treated with 100 µL of the compounds at eight different concentrations (from 312.5 to 40000 nM) for 72 hours and maintained at 37 °C, 5% CO_2 and 100% humidity. Thereafter, the cells were fixed with 25 µL of trichloroacetic acid (TCA) (5.5% final concentration; Merck, Darmstadt, Germany) and incubated for at least 1 hour at 4°C. Then, the plates were gently washed with deionized water and let dry at room temperature (RT). Once dried, the cells were stained with 50 µL of 0.4% SRB solution in 1% acetic acid for 15 minutes at RT. The excess of SRB stain was removed on dry paper and the plates were washed with a 1% acetic acid solution and let dry at RT overnight. The SRB stain was dissolve in 150 µL of tris(hydroxymethyl)aminomethane solution pH= 8.8 (TRIS base), and the absorbance was measured at a wavelength of 490 nm and 540 nm. Cell growth inhibition was calculated as the percentage of drug treated cells *versus* vehicle-treated cells ("negative control") OD (corrected for OD before drug addiction, "day-0"). Finally, the half maximal inhibitory concentration values (IC_{50}) were calculated with GraphPad Prism 7 (Intuitive Software for Science).

Wound healing assay

The *in vitro* scratch wound-healing assay was performed as previously described.[19] MesoII and STO cells were seeded in the 96-well flat-bottom plates at the density of $5x10^4$ cells/well in 100 µL in order to reach a confluent layer. After 24 hours of pre-incubation at 37 °C, 5% CO_2 and 100% humidity, the cell monolayer was scratched with a needle to create a scratch of constant width and subsequently washed with PBS to get rid of detached cells. Thereafter, the medium was replaced in the control wells and medium added with the compounds of interest to the experimental wells. The wound confluence was monitored by phase-contrast microscopy (Universal Grab 6.3 software) (DCILabs) integrated to the Leica DMI300B (Leica) migration station and the pictures were captured immediately after scratch (T = 0), and 4, 8 and 20 hours from the treatment. The results were analyzed with the Scratch Assay 6.2 software (Digital Cell Imaging Labs).

Spheroids formation assay

MesoII and STO spheroids were created following the protocols as reported previously.[20] Cells were seeded at a density of $7x10^4$ cells/well for MesoII and $5x10^4$ cells/well for STO, in a volume of 100 µL in CELLSTAR®96-well cell repellent U-bottom plates (Greiner Bio-One, Cat No. 650970, Kremsmünster, Austria). Spheroids were generated for three days, and then treated with compounds **1a** and **1b** at two different concentrations equal to IC_{50} found by previous SRB assays and $5xIC_{50}$. Pictures of the plate were taken every two days after changing

the only medium for the control wells and medium added with compounds for experimental wells and the experiment lasted seventeen days. The reduction in size of spheroids were monitored by phase-contrast microscopy (Universal Grab 6.3 software) (DCILabs) integrated to the Leica DMI300B (Leica) station. Finally, pictures were analysed with ImageJ Software (U.S. National Institute of Health, Bethesda, Maryland, USA) to determine the area of the spheroids treated and compare it to the area of the untreated spheroids, as described previously.[21]

Statistical analysis

All SRB assays were carried out in triplicate and repeated at least three times, whereas the percentages of cell migration were calculated taking into account at least ten scratch areas. The area of spheroids were determined by ImageJ software. The data were evaluated using the GraphPad Prism version 7 software (GraphPad Software, San Diego, CA, USA). IC_{50s} of cytotoxic assays are expressed as mean values ± SEM. The scratch areas were analyzed by Universal Grab 6.3 software. Statistical analysis results for migration assays were obtained by the Student's t-test, whereas for spheroids assays by Tukey's multiple comparisons test. *P* values: ****p<0.0001, ***p<0.001, **p<0.01, *p<0.05.

Results and discussions

Antiproliferative activity

The cytotoxic activity of ten imidazo[1,2-*b*][1,3,4]thiadiazole compounds was evaluated on two DMPM cell lines, MesoII and STO, by SRB assay. Preliminary screening tests were conducted with all compounds at three fixed concentrations of 0.1, 1 and 10 µM. Only four out of ten compounds (**1a,b,g** and **j**), showed more than 50% inhibition of growth at 10 µM. Therefore, they were chosen for further screenings at eight different concentrations in the range from 312.5 to 40000 nM, in order to determine reliable half maximal inhibitory concentration values (IC_{50s}). The table in the Figure 2 summarizes the IC_{50s} of MesoII and STO cells treated with the aforementioned compounds; all four compounds showed relevant antiproliferative activity with IC_{50s} ranging from 5.9 to 0.59 µM. Notably, the lowest IC_{50s} were found in STO cells exposed to **1a** and **1b** (0.81 and 0.59 µM, respectively) (Figure 2A), whereas in MesoII cells the same compounds showed IC_{50s} slightly higher, approximately 2.8 and 2.6 µM, respectively (Figure 2B). Conversely, the IC_{50s} of compounds **1c-f,i** and **j** were above of 10 µM. The results found with the compounds **1a** and **1b**, prompted us to investigate their cytotoxic activity on 3D models.

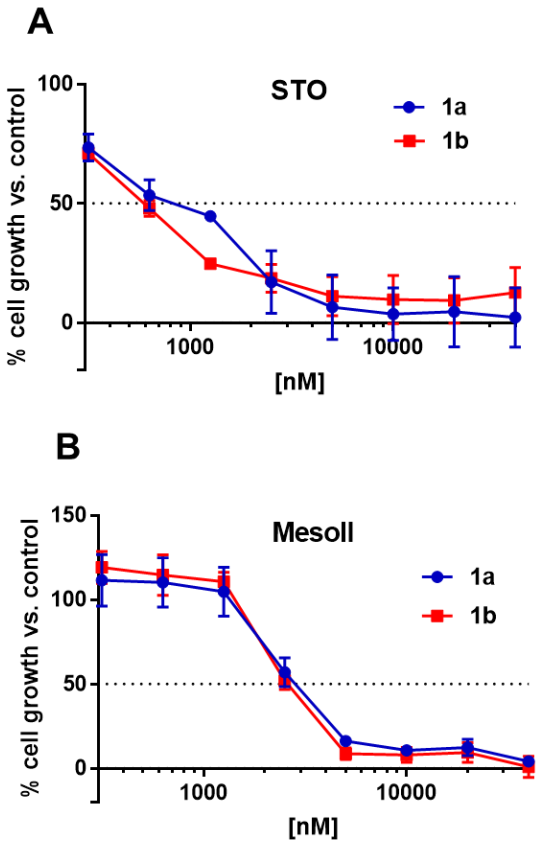

[a]IC_{50} (μM) ± SEM[b]		
Compounds	**MesoII**	**STO**
1a	2.81 ± 0.39	0.81 ± 0.35
1b	2.58 ± 0.12	0.59 ± 0.11
1c	>10	>10
1d	>10	>10
1e	>10	>10
1f	>10	>10
1g	5.9 ± 1.53	3.65 ± 1.03
1h	3.4 ± 0.29	1.14 ± 0.11
1i	>10	>10
1j	>10	>10

[a]The values are means ± SEM of three separated experiments
[b]SEM: Standard Error of the Mean

Figure 2. Representative growth curves of STO (**A**) and MesoII (**B**) cells after 72 hours of exposure to increased concentrations of compounds **1a** and **1b** (from 0.3125 to 40000 nM). *Points*, mean values obtained from three independent experiments; *bars*, SEM. *Right table:* list of the half maximal inhibitory concentrations values (IC_{50}) in μM of each compound against the DMPM cell lines. Values are reported as the Means ± Standard Error of the Mean of three separate experiments.

Volume reduction of MesoII- and STO-derived tumor spheres

Earlier studies reported that the drug activity found in the two-dimensional monolayer cell model is different when tested in the three-dimension cell culture,[22] supporting the use of these models for drug testing. Additionally, the 3D model offers a more realistic representation of the tumor microenvironment including the physical and mechanical properties of the extracellular matrix, the oxygen gradient, extracellular pH and gradient of nutrients, as well as drug transport.[23] Therefore, in order to obtain proper cytotoxic activity, we evaluated the ability of compounds **1a** and **1b** to affect the size of spheroids of MesoII and STO cells. Briefly, we seeded MesoII and STO cells in 96-well cell-repellent plates and we allowed them to form spheroids for three days. Thereafter, the spheroids were exposed to the compounds **1a** and **1b** for seventeen days. As shown in Figures 3A and 3B, the size of spheroids were reduced over time in both cell lines. Notably, after 17 days of treatment, we found about 2-fold reduction,

compared to the untreated spheroids. Moreover, statistical analyses revealed that the results were significant (P<0.0001).

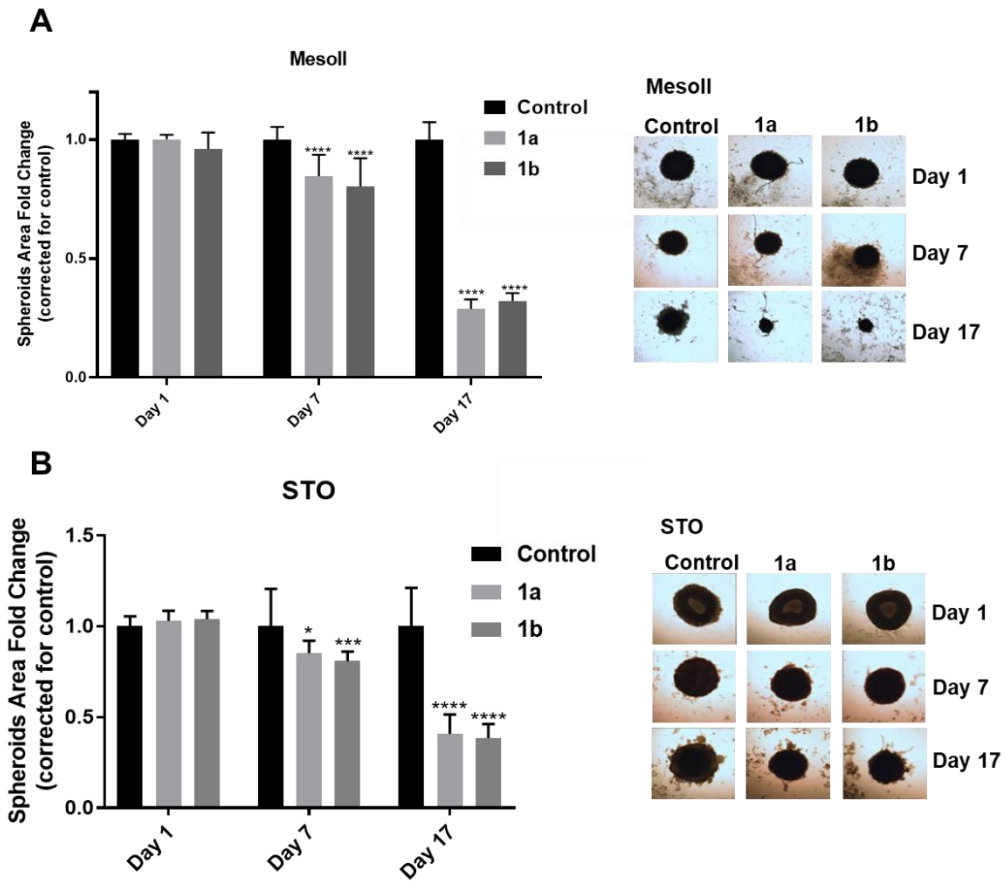

Figure 3. Size reduction of MesoII and STO spheroids treated with compounds **1a** and **1b** at 5-times the IC_{50}. **A:** *Left plot:* Fold-change corrected for control, of the MesoII spheroids size at day 1, day 7 and day 17. *Right pictures:* representative images of MesoII spheroids exposed to the compounds **1a** and **1b**, taken with the automated phase-contrast microscope at day 1 of treatment, and after 7 and 17 days. **B:** *Left plot:* Fold-change corrected for control of the STO spheroids size at day 1, day 7 and day 17. *Right pictures:* representative images of STO spheroids exposed to the compounds **1a** and **1b**, taken at day 1 of treatment, and after 7 and 17 days. All p-values were determined by Two-way ANOVA followed by Tukey's multiple comparisons test, **** = p<0.0001. The values were obtained taking into account the mean values of the areas of at least ten different spheroids.

Compounds 1a and 1b inhibited cell migration in STO cells

Secondary lesions that originate from DMPM primary site are very uncommon. However, localized and/or regional metastasis with the involvement of lymph nodes have been found.[24–26] Furthermore, the spread of tumor cells to form new metastasis *loci* on distant organs has been reported; particularly, pancreas and kidneys are the organs mainly involved, whereas lung, heart and brain are less commonly compromised.[27,28] The interesting antiproliferative activity of

compounds **1a** and **1b**, prompted us to investigate their anti-migratory activity on MesoII and STO cells by scratch wound-healing assay. Briefly, the cells were treated with the compounds **1a** and **1b** at concentration 3x IC_{50s}. After the treatments, the migration was monitored over time within 20 hours and images of wound closure were captured at different timepoints (T=0, 4, 8, and 20 hours). Notably, in order to exclude that the wound track could be covered by cell proliferation, we calculated the doubling time of each cell line which was more than 24 hours. As shown in Figure 4A-B, MesoII cells are characterized by a more aggressive migratory behaviour. Indeed, as shown in Figure 4B, after 20 hours from the treatment, the cells showed a complete closure of the wound both in controls and treated wells. The anti-migratory activity of the same compounds was more evident in STO cells where we observed a reduction of migration rates by 25.81% and 20%, after 20 hours from the treatment, compared to control (set at 100%) (Figure 4B). Statistical analyses revealed that the reduction of migration in STO cells treated with compounds **1a** was significant, compared to the control (i.e., untreated cells).

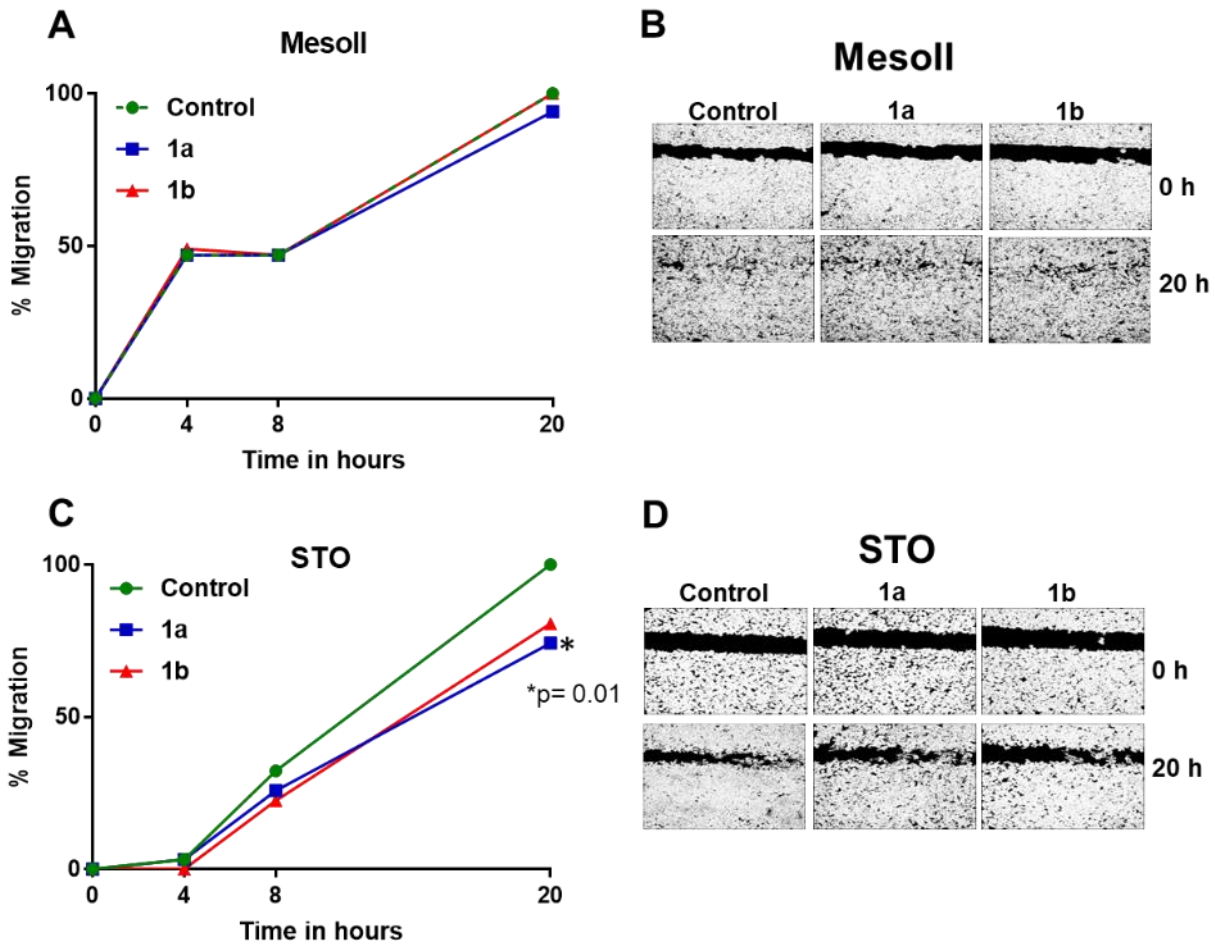

Figure 4. Modulation of the migration rate in MesoII and STO cells treated with the compounds **1a** and **1b** at concentration of 3x IC_{50}. **A,C:** Percentages of migration monitored over time (0, 4, 8 and 20 hours) in MesoII (**A**) and STO (**B**) cells treated with compound **1a** and **1b**. *Points*, mean values obtained from

the means of at least six different scratch areas. *P* values were calculated with Student's t-test. *p<0.05. **B,D:** Representative images of the wounds closure captured with the microscope at 0 and 24 hours on MesoII (**B**) and STO (**D**) cells. Original magnification 5X.

Conclusions

Ten imidazo[1,2-*b*][1,3,4]thiadiazole compounds were tested for their antiproliferative activity on two primary cell cultures of diffuse malignant peritoneal mesothelioma, namely MesoII and STO. Four compounds **1a,b,g** and **h** showed promising antitumor activity with IC_{50s} in the range from 5.9 to 0.59 µM. Notably, compounds **1a** and **1b** displayed lowest IC_{50s} in both cell lines. These results also reflected the sensitivity to the drugs when the cells had grown up as spheroids, inhibiting their formation and thus their area approximately 2 times compared to the controls. The lowest IC_{50S} values were found in the treatment of STO cells were also associated with the ability of compounds **1a** and **1b** to reduce cell migration by 25.81% and 20%, respectively. These results lead us to learn more about the mechanism of action and investigate the ability of these compounds to inhibit FAK phosphorylation.

References

(1) Tischoff, I.; Neid, M.; Neumann, V.; Tannapfel, A. Pathohistological Diagnosis and Differential Diagnosis. In *Malignant Mesothelioma*; Tannapfel, A., Ed.; Springer Berlin Heidelberg: Berlin, Heidelberg, 2011; Vol. 189, pp 57–78. https://doi.org/10.1007/978-3-642-10862-4_5.

(2) Galateau-Salle, F.; Churg, A.; Roggli, V.; Travis, W. D. The 2015 World Health Organization Classification of Tumors of the Pleura: Advances since the 2004 Classification. *Journal of Thoracic Oncology* **2016**, *11* (2), 142–154. https://doi.org/10.1016/j.jtho.2015.11.005.

(3) Luberto, F.; Ferrante, D.; Silvestri, S.; Angelini, A.; Cuccaro, F.; Nannavecchia, A. M.; Oddone, E.; Vicentini, M.; Barone-Adesi, F.; Cena, T.; et al. Cumulative Asbestos Exposure and Mortality from Asbestos Related Diseases in a Pooled Analysis of 21 Asbestos Cement Cohorts in Italy. *Environmental Health* **2019**, *18* (1), 71. https://doi.org/10.1186/s12940-019-0510-6.

(4) Baas, P.; Fennell, D.; Kerr, K. M.; Van Schil, P. E.; Haas, R. L.; Peters, S.; ESMO Guidelines Committee. Malignant Pleural Mesothelioma: ESMO Clinical Practice Guidelines for Diagnosis, Treatment and Follow-Up. *Ann. Oncol.* **2015**, *26 Suppl 5*, v31-39. https://doi.org/10.1093/annonc/mdv199.

(5) Carbone, M.; Ly, B. H.; Dodson, R. F.; Pagano, I.; Morris, P. T.; Dogan, U. A.; Gazdar, A. F.; Pass, H. I.; Yang, H. Malignant Mesothelioma: Facts, Myths, and Hypotheses. *Journal of Cellular Physiology* **2012**, *227* (1), 44–58. https://doi.org/10.1002/jcp.22724.

(6) Carbone, M.; Adusumilli, P. S.; Alexander, H. R.; Baas, P.; Bardelli, F.; Bononi, A.; Bueno, R.; Felley-Bosco, E.; Galateau-Salle, F.; Jablons, D.; et al. Mesothelioma: Scientific Clues for Prevention, Diagnosis, and Therapy. *CA Cancer J Clin* **2019**. https://doi.org/10.3322/caac.21572.

(7) Tomasson, K.; Gudmundsson, G.; Briem, H.; Rafnsson, V. Malignant Mesothelioma Incidence by Nation-Wide Cancer Registry: A Population-Based Study. *J Occup Med Toxicol* **2016**, *11*. https://doi.org/10.1186/s12995-016-0127-4.

(8) Keshava, H. B.; Tang, A.; Siddiqui, H. U.; Raja, S.; Raymond, D. P.; Bribriesco, A.; Stevenson, J.; Murthy, S. C.; Ahmad, U. Largely Unchanged Annual Incidence and Overall Survival of Pleural Mesothelioma in the USA. *World J Surg* **2019**. https://doi.org/10.1007/s00268-019-05132-6.

(9) Le Stang, N.; Bouvier, V.; Glehen, O.; Villeneuve, L.; FRANCIM network; MESOPATH Referent National Center; Galateau-Sallé, F.; Clin, B. Incidence and

Survival of Peritoneal Malignant Mesothelioma between 1989 and 2015: A Population-Based Study. *Cancer Epidemiol* **2019**, *60*, 106–111. https://doi.org/10.1016/j.canep.2019.03.014.

(10) Delgermaa, V.; Takahashi, K.; Park, E.-K.; Le, G. V.; Hara, T.; Sorahan, T. Global Mesothelioma Deaths Reported to the World Health Organization between 1994 and 2008. *Bull World Health Organ* **2011**, *89* (10), 716-724C. https://doi.org/10.2471/BLT.11.086678.

(11) Neumann, V.; Löseke, S.; Nowak, D.; Herth, F. J. F.; Tannapfel, A. Malignant Pleural Mesothelioma: Incidence, Etiology, Diagnosis, Treatment, and Occupational Health. *Dtsch Arztebl Int* **2013**, *110* (18), 319–326. https://doi.org/10.3238/arztebl.2013.0319.

(12) Kim, J.; Bhagwandin, S.; Labow, D. M. Malignant Peritoneal Mesothelioma: A Review. *Ann Transl Med* **2017**, *5* (11). https://doi.org/10.21037/atm.2017.03.96.

(13) Archer, M. A.; Bueno, R. Surgery for Malignant Pleural Mesothelioma. *Lung Cancer Management* **2015**, *4* (5), 231–241. https://doi.org/10.2217/lmt.15.26.

(14) Batirel, H. F.; Metintas, M.; Caglar, H. B.; Yildizeli, B.; Lacin, T.; Bostanci, K.; Akgul, A. G.; Evman, S.; Yuksel, M. Trimodality Treatment of Malignant Pleural Mesothelioma. *J Thorac Oncol* **2008**, *3* (5), 499–504. https://doi.org/10.1097/JTO.0b013e31816fca1b.

(15) Garcia-Carbonero, R.; Paz-Ares, L. Systemic Chemotherapy in the Management of Malignant Peritoneal Mesothelioma. *Eur J Surg Oncol* **2006**, *32* (6), 676–681. https://doi.org/10.1016/j.ejso.2006.03.009.

(16) Xue, H.; Li, J.; Xie, H.; Wang, Y. Review of Drug Repositioning Approaches and Resources. *Int J Biol Sci* **2018**, *14* (10), 1232–1244. https://doi.org/10.7150/ijbs.24612.

(17) De Cesare, M.; Cominetti, D.; Doldi, V.; Lopergolo, A.; Deraco, M.; Gandellini, P.; Friedlander, S.; Landesman, Y.; Kauffman, M. G.; Shacham, S.; et al. Anti-Tumor Activity of Selective Inhibitors of XPO1/CRM1-Mediated Nuclear Export in Diffuse Malignant Peritoneal Mesothelioma: The Role of Survivin. *Oncotarget* **2015**, *6* (15), 13119–13132. https://doi.org/10.18632/oncotarget.3761.

(18) Sciarrillo, R.; Wojtuszkiewicz, A.; Kooi, I. E.; Gómez, V. E.; Boggi, U.; Jansen, G.; Kaspers, G.-J.; Cloos, J.; Giovannetti, E. Using RNA-Sequencing to Detect Novel Splice Variants Related to Drug Resistance in In Vitro Cancer Models. *J Vis Exp* **2016**, No. 118. https://doi.org/10.3791/54714.

(19) Massihnia, D.; Avan, A.; Funel, N.; Maftouh, M.; van Krieken, A.; Granchi, C.; Raktoe, R.; Boggi, U.; Aicher, B.; Minutolo, F.; et al. Phospho-Akt Overexpression Is Prognostic

and Can Be Used to Tailor the Synergistic Interaction of Akt Inhibitors with Gemcitabine in Pancreatic Cancer. *Journal of Hematology & Oncology* **2017**, *10* (1), 9. https://doi.org/10.1186/s13045-016-0371-1.

(20) Maftouh, M.; Avan, A.; Sciarrillo, R.; Granchi, C.; Leon, L. G.; Rani, R.; Funel, N.; Smid, K.; Honeywell, R.; Boggi, U.; et al. Synergistic Interaction of Novel Lactate Dehydrogenase Inhibitors with Gemcitabine against Pancreatic Cancer Cells in Hypoxia. *Br. J. Cancer* **2014**, *110* (1), 172–182. https://doi.org/10.1038/bjc.2013.681.

(21) Sciarrillo, R.; Wojtuszkiewicz, A.; El Hassouni, B.; Funel, N.; Gandellini, P.; Lagerweij, T.; Buonamici, S.; Blijlevens, M.; Zeeuw van der Laan, E. A.; Zaffaroni, N.; et al. Splicing Modulation as Novel Therapeutic Strategy against Diffuse Malignant Peritoneal Mesothelioma. *EBioMedicine* **2019**, *39*, 215–225. https://doi.org/10.1016/j.ebiom.2018.12.025.

(22) Riedl, A.; Schlederer, M.; Pudelko, K.; Stadler, M.; Walter, S.; Unterleuthner, D.; Unger, C.; Kramer, N.; Hengstschläger, M.; Kenner, L.; et al. Comparison of Cancer Cells in 2D vs 3D Culture Reveals Differences in AKT–MTOR–S6K Signaling and Drug Responses. *J Cell Sci* **2017**, *130* (1), 203–218. https://doi.org/10.1242/jcs.188102.

(23) Langhans, S. A. Three-Dimensional in Vitro Cell Culture Models in Drug Discovery and Drug Repositioning. *Front. Pharmacol.* **2018**, *9*. https://doi.org/10.3389/fphar.2018.00006.

(24) Boussios, S.; Moschetta, M.; Karathanasi, A.; Tsiouris, A. K.; Kanellos, F. S.; Tatsi, K.; Katsanos, K. H.; Christodoulou, D. K. Malignant Peritoneal Mesothelioma: Clinical Aspects, and Therapeutic Perspectives. *Ann Gastroenterol* **2018**, *31* (6), 659–669. https://doi.org/10.20524/aog.2018.0305.

(25) Yan, T. D.; Deraco, M.; Elias, D.; Glehen, O.; Levine, E. A.; Moran, B. J.; Morris, D. L.; Chua, T. C.; Piso, P.; Sugarbaker, P. H. A Novel Tumor-Node-Metastasis (TNM) Staging System of Diffuse Malignant Peritoneal Mesothelioma Using Outcome Analysis of a Multi-Institutional Database*. *Cancer* **2011**, *117* (9), 1855–1863. https://doi.org/10.1002/cncr.25640.

(26) Sugarbaker, P. H. Intra-Abdominal Manifestations of Pleural Mesothelioma. *Ann Transl Med* **2017**, *5* (11). https://doi.org/10.21037/atm.2016.11.44.

(27) Tertemiz, K. C.; Ozgen Alpaydin, A.; Gurel, D.; Savas, R.; Gulcu, A.; Akkoclu, A. Multiple Distant Metastases in a Case of Malignant Pleural Mesothelioma. *Respir Med Case Rep* **2014**, *13*, 16–18. https://doi.org/10.1016/j.rmcr.2014.07.003.

(28) Finn, R. S.; Brims, F. J. H.; Gandhi, A.; Olsen, N.; Musk, A. W.; Maskell, N. A.; Lee, Y. C. G. Postmortem Findings of Malignant Pleural Mesothelioma: A Two-Center Study of 318 Patients. *Chest* **2012**, *142* (5), 1267–1273. https://doi.org/10.1378/chest.11-3204.

Chapter 12

Discussion & Conclusions

Discussion

According to the World Health Organization (WHO) about 1 in 6 deaths is due to cancer, thus representing the second leading cause of death globally, only after cardiovascular disease. In 2019, in the United States (US), approximately 1.8 million new cancer cases are estimated to occur in both sexes, one third of which will be death cases (approximately 600.000 cases),[1] while in Europe, in 2018, 3.91 million new cases were registered (excluding non-melanoma skin cancers) and 1.93 million deaths.[2] These extremely high numbers encourage the research for new therapeutic strategies for cancer treatment that remains a major challenge in medicinal chemistry. Several approaches have been used to treat cancers, including surgery, radiotherapy, hormone therapy, chemotherapy and immunotherapy[3] and, mostly in the last years, researchers are increasingly focusing on targeted therapy. In fact, compared to traditional chemotherapy that aims at the processes needed for cancer cells to grow and divide, targeted therapy works by targeting specific cancer genes or proteins involved in the growth and spread of cancer. Furthermore, ideally targeted therapy acts as a cytostatic, blocking tumor proliferation, while chemotherapy is cytotoxic, killing fast-growing cells, also causing damage to healthy cells.[4] In practice, most so-called targeted therapies also cause substantial toxicities often necessitating discontinuation of treatment.

The first step in the search for potential drug-like compounds, which generally occurs in academia, is the preclinical investigation of their *in vitro* cytotoxic activity. Therefore, the use of adequate cellular models and chemosensitivity assays is needed to identify new therapeutic agents in a library of compounds. In **chapter 2** we briefly summarized the main criteria to be used in planning *in vitro* cytotoxic studies in order to obtain reliable results. The most representative example of large-scale *in vitro* drug screening is the high-throughput test in multi-well plates in which the dose-response results of drugs screening are easily calculable and reproducible. *In vitro* monolayer assays(2D) are the best low-cost strategy for assessing the cellular sensitivity to new drug candidates. Among these, trypan blue exclusion, sulforhodamine-B (SRB), tetrazolium (MTT) or resazurine reduction, and ATP content are the most widely used and are based on the ability of cells to bind, exclude or metabolize some dyes. Of course, these tests do not take into consideration the complexity of the tumor microenvironment which plays a fundamental role in the spread of cancer cells and drugs resistance. Therefore, multicellular spheroids and organoids also represent valuable models in cellular pharmacology studies, exploitable even in co-culture approaches. These 3D models reproduce the *in vivo* environment of tumors and take into account some features such as cell-cell or cell-extracellular matrix contacts, the activity of drugs in a context of the low oxygen

gradient, especially in the core of spheroids, the high hydrogen ion concentration (pH) and different gradient of nutrients. In this Thesis we focused on the assays based on 2D cultures. Various factors must be carefully evaluated before performing the tests. These include:

- an appropriate drug solvent that guarantees stability to the drug and is not toxic to the cells;
- selection of the best pharmacological drug concentrations both for established drugs and novel compounds;
- time of exposure of the drug that mimics the *in vivo* situation (*e.g.* reflecting time of plasma peaks and drug persistence);
- optimizing cell-seeding density and assay timing based on cell-doubling time.

Finally, cell proliferation and survival in monolayer (2D) cultures is calculated taking into consideration the product of two parameters: concentration of drugs (C), and time to exposure (T).

The colony-forming assay is another *in vitro* test through which the ability of cell to form colonies during the treatment is evaluated. The two parameters that indicate the ability of drugs to completely reduce or cancel the formation of colonies are the plating efficiency (PE), namely the ratio between the number of colonies and the number of seeded cells, and the surviving fraction (SF), that is the number of colonies after the treatment of cells expressed in terms of PE.

It is extremely important that during the execution of the *in vitro* test there is a constant control of cell cultures to exclude contaminations, indeed, a lack of quality control causes a lack of reproducibility. The main types of contaminants are: Bacteria, Fungi, Mycoplasma and Viruses. Bacteria and Fungi are easily detected thank to the turbidity and colour change of the culture medium due to the change in pH, or by microscope. Instead, Mycoplasma is the smallest prokaryotes with 0.3-0.8 μm in diameter that represents the main threat of the cultures, through metabolic effects or DNA degradation, thus inducing altered growth rate and morphological changes of the cells, as well as chromosome aberrations.[5] Different techniques have been developed to detect Mycoplasma contamination, including growth in broth, staining, (*e.g.*, 4′,6-diamidino-2-phenylindole, DAPI), polymerase chain reaction, and ATP luminescence.[6]

Clinical therapies based on drug combinations have been widely used for over 50 years, when the combination of mechlorethamine, vincristine, procarbazine and prednisone (MOPP) showed promising results in the treatment of childhood leukemia.[7] The choice to combine two or more drugs depends mainly on the mechanism of action of each drug and the goal is to achieve better treatment efficacy, evade increasing toxicity, targeting different cellular and

acellular subpopulations in a heterogeneous tumor, avoiding the development of resistance, and finally, adding a drug that protects against toxicity. In **chapter 3** we briefly describe the types of analyses generally used to calculate the efficacy of drug combinations, as well as their advantages and disadvantages. In addition we evaluated the software that helps to interpret the results, and finally we discussed the application of machine learning methods applied in biomedical sciences.

The mathematical equations used to calculate the effects of the combination in cell-free systems are based on either the Loewe Additivity (in which it was hypothesized that drug A combined with itself, would give a final effect given by the sum of: A+A=2A. When another drug was used, the reference state would be A+B=2A),[8] Bliss Independence model (in which the additivity is the product of the fractional response, in which 0.5 x 0.5=0.25),[9] or a combination of both, such as Chou and Talalay's median-drug-effect.

Finally, application of cell-free models to cellular systems assumed a sigmoid dose-response curve based on the Hill equations that allows:

a) *the fractional effect analysis;* this analysis determines the additive theoretical effects of a combination, given to the product of the fractional effect of each drug of the combination. For instance, the fractional effect of a drug with 50% growth inhibition activity is 0.5. Consequently the theorical fractional effect of two drugs with the same growth inhibition activity, *e.g.* of 50%; is 0.5 x 0.5=0.25. Therefore, synergism is obtained when the fractional effects detected are less than 0.25, while antagonism occurs when values are higher than 0.25. The disadvantage of this model is the inability to calculate a confidence interval within each experiment. Furthermore, there are no negative fractional values, so it is not possible to calculate killed cells.

b) *The isobolograms plot*[10] is based on a straight line connecting the concentrations of two drugs on the X and Y axes, when the combination is additive. The synergistic or antagonistic effects are represented by curves to the left or right of this, respectively. Unfortunately, this model does not allow us to quantify these effects, just as cell killing cannot be evaluated.

c) *The response surface area model*[11–13] is based on mixed Loewe-Bliss equations and allows the quantification of synergism or additive affects, as well as calculating the confidence interval and evaluating the effects of more than two drugs. Unfortunately, this model requires statistical expertise for the interpretation of the results obtained.

d) *The median effect analysis* was developed by Chou and Talalay based on Loewe and Bliss models. The effect of drug combinations is represented by sigmoidal curves coming out

of an equation formulated taking into account the Henderson-Hasselbach, Michaelis-Menten, Hill and Scatchard equations. The diagrams showing the effects of the combination are the results of Fa value (fraction affected) and CI (Combination Index) and evaluates synergy in the whole interval Fa from 0 to 1.However, when Fa is above of 0.95, CI values are usually not reliable, while CI values obtained at Fa<0.5 are not relevant, since Fa<0.5 represent clinically not relevant growth inhibition.

Calcusyn (or Compusyn by a different manufacturer) and Combenefit are two software program used to calculate the effects of combination treatments, based on the median drug effect analysis and response surface area, respectively. Calcusyn was widely used to evaluate the combination of conventional antitumor drugs. However, Calcusyn can also be used to calculate the combination of conventional and targeted anticancer drugs, (*e.g.* pemetrexed or gemcitabine with tyrosine kinase inhibitors-TKI) taking into consideration genetic alterations and concentration of TKI, or the combination of two or more TKIs.[14–16] Of course, when we translate these results into *in vivo* models, we need to considered additional parameters, as well as pharmacokinetics and pharmacodynamics characteristics of the drugs and their interactions. These aspects are increasingly improved and predicted by models based on artificial intelligence.

Combination treatments form the mainstay for curative treatments of many cancers (e.g. breast cancer, childhood cancer, lymphomas). However, the outcome of combination-based treatment, can be different for each patient mainly due to individual and tumor genetic profiles. Therefore, in order to achieve better efficacy of cancer treatments, one needs to identify molecular or genetic determinants that characterize each patient. This is possible through a careful research and individualization of prognostic tumor biomarkers useful for the clinical management to guide therapeutic decisions that should identify the subgroups of patients who would benefit from specific treatments. In **chapter 4** we describe dysregulations both at germinal and tumor level potentially affecting the standard treatment modalities in pancreatic ductal adenocarcinoma (PDAC). In particular, we focused on polymorphisms and -omics profiles related to the response to a single chemotherapeutic or pharmacological combinations, including gemcitabine, FOLFIRINOX and nab-paclitaxel combinations, as well as limitations of targeted therapies.

Currently, no biomarker has been identified to improve the treatment with gemcitabine since application of preclinical or clinical investigations on potential biomarkers have yielded controversial results. For instance, several studies highlighted the correlation between high expression of the human equilibrative nucleoside transporter 1 (hENT1), which is usually

associated with polymorphisms, and longer overall survival (OS) of patients treated with gemcitabine.[17,18] Unfortunately, studies with unvalidated antibodies such as SP120 obscured the data. E.g. one immunohistochemical study on hENT1 expression using this rabbit monoclonal antibody SP120 showed no correlation between hENT1 levels and OS.[19] In addition, since gemcitabine resistance is also due to the complex microenvironment of PDAC, it is possible to have a lack of correlation between clinical outcomes and pharmacogenetics of tumor biomarkers.[20] Further studies have evaluated the polymorphisms in the enzymes involved in the metabolism of gemcitabine such as deoxycytidine kinase and cytidine deaminase and, therefore, their role as biomarkers.[21] Also these evaluations did not give representative results due to the use of different methodologies in the conduct of the studies.

The first-line treatment of patients with metastatic PDAC is the combination of different chemotherapeutic drugs including 5-flourouracil (5-FU), leucovorin, irinotecan and oxaliplatin, under the name FOLFIRINOX. This protocol was introduced when in Phase III clinical trials better overall survival (OS) and progression-free survival (PFS) was observed compared to gemcitabine monotherapy.[22] Unfortunately, there are currently no reliable biomarkers to predict its efficacy and safety. Recently, a retrospective study reported a positive correlation between mutations in five genes involved in the DNA damage repair (*BRCA1*, *BRCA2*, *PALB2*, *MSH2*, and *FANCF*) and longer OS of patients treated with FOLFIRINOX.[23] Two additional studies supported the potential role of genes involved in DNA repair as biomarkers of FOLFIRINOX activity; the first revealed a PFS greater than 2 years in two patients with inactivating genetic mutations related to HRR (homologous recombination repair) while the second showed downregulation of microRNA-181a-5p.[24] Contrary to what is reported in the literature on the correlation between the expression of excision repair cross-complementing (ERCC) proteins (in particular, ERCC-1, -2, -3 and -4) and glutathione S-transferase Pi (GSTPi) with the response to platinum-based chemotherapy, there are not statistically significant associations between patients with unresectable PDAC treated with FOLFIRINOX and tumor expression of the previously mentioned proteins.[25] Further studies should be conducted to compare the efficacy of treatment with FOLFIRINOX and polymorphisms of the NER system (nucleotide excision repair), such as XPD-Lys751Gln, which are generally associated with greater resistance to cisplatin-induced damage. Finally, dihydropyrimidine dehydrogenase (DPD) and thymidylate synthase (TS) have been subject of investigation in a regimen treatment with 5-fluorouracil (5-FU) as potential prognostic biomarkers. In a preclinical study with 15 PDAC cell lines and two 5-FU-resistant sub-clones, higher mRNA expression levels of both DPD and TS were correlated with reduced 5-FU sensitivity,[26] and this correlation was also found in a

study 68 resected pancreatic cancer tissues treated with adjuvant 5-FU liver perfusion chemotherapy in which DPD protein expression was high.[27] Other data on correlation between TS protein expression and outcome of PDAC patients treated with 5-FU are controversial. Indeed, high TS protein levels were correlated with longer OS in resectable patients and not in patients with advanced PDAC.[28] Finally, with regards on the search for biomarkers of irinotecan treatments, there are only a few questionable results. One study showed that irinotecan-resistant cells had a low expression of topoisomerase 1 (TOP1), the main target of irinotecan, while another showed that the expression of TOP1 was not associated with the sensitivity of irinotecan.[29,30] In addition, catabolic enzymes CYP3A4, CYP3A5, UGT1A10, or the expression of the export transporters ABCB1 and ABCC2 have also been studied as a biomarkers of irinotecan activity, but there was not any correlation.[31] Finally, further analysis of the *in vivo* models genetic databases, proteomics and tissue microarrays (TMAs) showed a high expression of carboxyl esterase-2 (CES2), which activates irinotecan, associated with a better prognosis in 22 resectable and borderline resectable patients treated with FOLFIRINOX in the neoadjuvant setting.

The activity of the secreted protein acidic and rich in cysteine (SPARC), also known as osteonectin (ON), has been correlated to PDAC cells proliferation and metastasis. Because this protein binds the albumin of nab-paclitaxel, it has been studied as its biomarker of response.[32] The results obtained by immunohistochemical analysis, engineered mouse and patients derived xenografts, showed that SPARC did not play a role in the internalization of nab-paclitaxel in tumor cells.[33–35] The positive clinical outcomes of the combination of nab-paclitaxel with gemcitabine are due to the ability of the first to inactivate the enzyme cytidine deaminase (CDA) and consequently, increasing gemcitabine concentration. Nevertheless, the use of specific CDA inhibitor administered with the aim to increase gemcitabine concentration, did not lead an increase in cancer cell death, thus suggesting other factors involved in cytotoxic activity.[36]

It is well know that paclitaxel induces cell death through the disruption of mitosis by binding to the microtubule protein beta-tubulin (TUBB3). Even in PDAC patients with unresectable disease and lacking of TUBB3, treated with paclitaxel, immunohistochemical analysis showed a longer PSF, thus suggesting it as a new biomarker.[37,38] However, preclinical studies highlighted that in cells resistant to paclitaxel, the activity of TUBB3 was restored by the FOXO3a-dependent regulation of ABCB1, which further induced cross-resistance to different chemotherapeutics such as 5-FU, docetaxel, and cisplatin.[39] In conclusion, there are not effective biomarkers that help to stratify PDAC patients and optimize cancer treatment.

Although improving the understanding of PDAC tumor biology, 'actionable' therapeutic targets have not yet been identified.[40] Indeed, target therapy approach has often led to clinical failure, as found in many literature sources and which we reported in Chapter 4. Probably, these drawbacks are due to the important role plaid by tumor microenvironment of PDAC which contribute to metastasis and drug resistance.[41,42]

Chemotherapy offers only small advantages to patients and most efforts to improve existing regimes have failed in advanced clinical studies. Therefore, not only the identification of new targets is necessary, but also the discovery of new therapies for the treatment of cancer and the overcoming of resistance to current therapies to improve the patient's prognosis.

The use of heterocyclic systems in the development of new anticancer drugs has always been a milestone in medicinal chemistry.[43] Their incorporation into the molecules is a useful tool for modifying some pharmacological properties such as lipophilicity, polarity and aqueous solubility, and in addition, potency and selectivity toward specific targets. Indeed, heterocycles allow to obtain compounds with ideal biological and physicochemical features. As a result, many marketed molecules have structural units composed of heterocycles. Furthermore, the basic units of biological molecules such as DNA and proteins, or essential elements such as vitamins or carbohydrates, consist of one or more fused or linked heterocycles.

These premises led us to continue the studies on heterocyclic systems and, based on molecular hybridization knowledge as new strategy in drug design, we synthesized a new series of seventy 3-(imidazo[2,1-*b*][1,3,4]thiadiazol-2-yl)-1*H* indole analogues (Table 1) characterized by two interesting biological scaffolds, the indole and imidazothiadiazole heterocycles. The variability of substituents aimed to evaluate how structural modifications on the indole or phenyl nucleus, the introduction of an aldehyde group at the position 5 of the imidazothiadiazole scaffold or the replacement of the phenyl ring with a thiophene could influence the anticancer activity of this class of compounds. Particularly, we investigated the antitumor activity of this class of molecules on PDAC and diffuse malignant peritoneal mesothelioma (DMPM) as we reported in **chapters 5,6,7** and **11**. In addition, based on the recent concept of drug repositioning[44] and literature data on antibacterial activity of imidazo[2,1-*b*][1,3,4]thiadiazole derivatives,[45-46] we evaluated the antibiofilm activity of thirty-six compounds synthesized, as reported in the **chapter 8**. In the **chapters 6,7** and **8** we reported the chemical synthesis of the compounds.

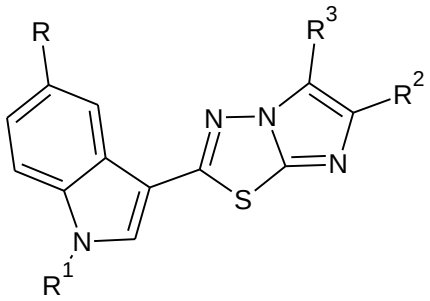

Comp	R	R^1	R^2	R^3
1	H	H	tiophen-3-yl	H
2	H	CH_3	tiophen-3-yl	H
3	Br	CH_3	tiophen-3-yl	H
4	Cl	H	tiophen-3-yl	H
5	Cl	CH_3	tiophen-3-yl	H
6	F	CH_3	tiophen-3-yl	H
7	Br	H	tiophen-3-yl	H
8	F	H	tiophen-3-yl	H
9	OCH_3	H	tiophen-3-yl	H
10	OCH_3	CH_3	tiophen-3-yl	H
11	H	H	C_6H_5	H
12	H	CH_3	C_6H_5	H
13	H	H	4-F-C_6H_4	H
14	H	CH_3	4-F-C_6H_4	H
15	H	H	4-CF_3-C_6H_4	H
16	H	CH_3	4-CF_3-C_6H_4	H
17	H	H	3-OCH_3-C_6H_4	H
18	H	CH_3	3-OCH_3-C_6H_4	H
19	H	H	2,5-OCH_3-C_6H_4	H
20	H	CH_3	2,5-OCH_3-C_6H_4	H
21	H	H	4-NO_2-C_6H_4	H
22	H	CH_3	4-NO_2-C_6H_4	H
23	Br	H	C_6H_5	H
24	Br	CH_3	C_6H_5	H
25	Br	H	4-F-C_6H_4	H
26	Br	CH_3	4-F-C_6H_4	H
27	Br	H	4-CF_3-C_6H_4	H
28	Br	CH_3	4-CF_3-C_6H_4	H
29	Br	H	3-OCH_3-C_6H_4	H
30	Br	CH_3	3-OCH_3-C_6H_4	H
31	Br	H	2,5-OCH_3-C_6H_4	H
32	Br	CH_3	2,5-OCH_3-C_6H_4	H
33	Br	H	4-NO_2-C_6H_4	H
34	Br	CH_3	4-NO_2-C_6H_4	H
35	Cl	H	C_6H_5	H
36	Cl	CH_3	C_6H_5	H
37	Cl	H	4-F-C_6H_4	H
38	Cl	CH_3	4-F-C_6H_4	H
39	Cl	H	4-CF_3-C_6H_4	H
40	Cl	CH_3	4-CF_3-C_6H_4	H
41	Cl	H	3-OCH_3-C_6H_4	H
42	Cl	CH_3	3-OCH_3-C_6H_4	H
43	Cl	H	2,5-OCH_3-C_6H_4	H
44	Cl	CH_3	2,5-OCH_3-C_6H_4	H
45	Cl	H	4-NO_2-C_6H_4	H

46	Cl	CH_3	4-NO_2-C_6H_4	H
47	OCH_3	H	C_6H_5	H
48	OCH_3	CH_3	C_6H_5	H
49	OCH_3	H	4-F-C_6H_4	H
50	OCH_3	CH_3	4-F-C_6H_4	H
51	OCH_3	H	4-CF_3-C_6H_4	H
52	OCH_3	CH_3	4-CF_3-C_6H_4	H
53	OCH_3	H	3-OCH_3-C_6H_4	H
54	OCH_3	CH_3	3-OCH_3-C_6H_4	H
55	OCH_3	H	2,5-OCH_3-C_6H_4	H
56	OCH_3	CH_3	2,5-OCH_3-C_6H_4	H
57	OCH_3	H	4-NO_2-C_6H_4	H
58	F	H	C_6H_5	H
59	F	H	4-CF_3-C_6H_4	H
60	F	CH_3	4-CF_3-C_6H_4	H
61	F	H	3-OCH_3-C_6H_4	H
62	F	H	2,5-OCH_3-C_6H_4	H
63	H	H	C_6H_5	CHO
64	H	CH_3	C_6H_5	CHO
65	H	H	4-F-C_6H_4	CHO
66	H	H	3OCH_3-C_6H_4	CHO
67	H	H	2,5-OCH_3-C_6H_3	CHO
68	H	CH_3	2,5-OCH_3-C_6H_3	CHO
69	H	H	4-NO_2-C_6H_4	CHO
70	Br	H	2,5-OCH_3-C_6H_3	CHO

Table 1. All imidazo[2,1-*b*][1,3,4]thiadiazole synthesized

Thirty-six 2-(6-phenylimidazo[2,-1-*b*][1,3,4]thiadiazol-2-yl)-1*H*-indoles derivatives **11-46**, were tested for their *in vitro* antibiofilm activity against the Gram-positive bacterial reference strains *Staphylococcus aureus* ATCC 25923, *Staphylococcus aureus* ATCC 6538 and *Staphylococcus epidermidis* ATCC 12228, and the Gram-negative strains *Pseudomonas aeruginosa* ATCC 15442 and *Escherichia coli* ATCC 25922, and the minimum inhibitory concentrations (MIC) were evaluated. Notably, against Gram-positive pathogens, all compounds showed the ability to inhibit bacterial biofilm formation in a dose-dependent manner, eliciting in many cases the biofilm inhibitory concentration (BIC_{50}) values lower than 24.5 μM, (concentration at which the percentage of inhibition of biofilm formation is equal to 50% compared to the untreated growth control). Interestingly, compounds characterized by one or two methoxy groups on the phenyl ring, displayed better activity with BIC_{50} values ranging from 0.5 to 46.5 μM, whereas compounds with nitro substituent in para position of the phenyl ring, significantly inhibited biofilm formation in all Gram-positive and Gram-negative tested strains showing BIC_{50} between 3 and 71.7 μM. These results allowed us to draw conclusions about the structure activity relationship (SAR). Certainly, the substituents in the phenyl ring affected the activity; in particular, electron-withdrawing, like nitro group substituents, are advantageous for the activity against both Gram-positive and Gram-negative pathogens, whereas electron-donating substituents are advantageous only for the activity against Gram-

positive pathogens. Instead, different substituents on the indole nucleus, as well as its N-methylation, did not affect the antibiofilm activity. Six of the most promising compounds **18-20,22,34,43** showed lower BIC_{50} values against *S. aureus* strains, therefore an additional assay was performed in order to investigate the potential mechanism of action. In particular, we evaluated the dispersal activity against the 24 h preformed biofilm of the same strains. Only one out of six compounds, derivative **18**, showed weak activity eliciting an IC_{50} value of 322 µM against *S. aureus* ATCC 25923. Altogether, these results suggested a mechanism of antibiofilm activity related to the interference with adhesion or regulatory mechanisms involved in bacterial communication systems characterizing the first steps of biofilm formation, rather than an ability to disrupt mature biofilms. Therefore, we investigated the inhibition of Sortase A enzyme (SrtA) as possible mechanism of action. Unfortunately, no compound was effective at the maximum tested concentration of 100 µM against the transpeptidase.

Forty out of seventy compounds were submitted to the National Cancer Institute (NCI) and selected to evaluate their antitumor activity against a panel of sixty human cancer cells derived from 9 cancer cell types and grouped into disease subpanels including leukemia, non-small cell lung, colon, central nervous system, melanoma, ovarian, renal, prostate, and breast cancers. They were initially tested according to the NCI protocol at one-dose of 10 µM. Three compounds **1,6** and **31** exhibited significant growth inhibition in this first step and they were selected for further screening at five concentrations (from 10^{-4}-10^{-8} M). Finally, they showed interesting *in vitro* anticancer activity with GI_{50} values ranging from micromolar to sub-micromolar level, i.e., 10.3-1.67 µM (compound **31**), 11.4-0.23 µM (compound **1**) and 12.2-0.29 µM (compound **6**), respectively.

In order to expand the NCI panel, we further evaluated the *in vitro* antitumor activity of the synthesized imidazo[2,1-*b*][1,3,4]thiadiazole derivatives on PDAC (except for compounds **21,33,34,45** and **46** that, due to the poor solubility in dimethyl sulfoxide (DMSO), have not been tested), while compounds **1-10** characterized by a thiophen nucleus were also tested on DMPM primary cell lines.

Among the tested compounds, derivatives **1,2,6** and **8** showed remarkable antiproliferative activity against three preclinical PDAC cell lines, SUIT-2, Capan-1 and Panc-1 with the half-maximal inhibitory concentration (IC_{50}) values in the range from 0.85 to 4.86 µM (as shown in **chapter 7**). Compounds **1** and **2** displayed better cytotoxic activity in all the cell lines with IC_{50S} in the range of 0.85 and 1.7 µM. Notably, on SUIT-2 cells the IC_{50s} were 0.85 and 0.99 µM, respectively. As evidenced by the cytotoxic results, the most promising compounds were of type *2-(1H-indol-3-yl)-6-(thiophen-3-yl)imidazo[2,1-b][1,3,4]thiadiazole*. Evaluation of

SAR, led us to observe that the presence of the halogens chlorine (-Cl) and bromine (-Br) on the indole scaffold is disadvantageous, while F-analogues, similarly to the hydrogen (-H) analogues, probably due to the small atomic ray of fluorine (-F), showed better cytotoxicity activity. Not even the methoxy group ($-OCH_3$) on indole scaffold improved antitumor activity. Instead, N-methylation of indole did not affect the activity. These observations have highlighted the irrelevant function of phenyl ring on antitumor activity, both substituted or not. Finally, the presence of aldehyde (-CHO) group at position five of imidazothiadiazole, compounds **63-70**, did not improve the activity compared the analogues without it, compounds **10-12,17,19-21,31** which did not show cytotoxic activity.

One of the main cause of clinical failure is the development of resistance to chemotherapy. Gemcitabine was the first agent approved by the Food and Drug Administration (FDA) for the treatment of advanced and metastatic pancreatic cancer, but its clinical effects has been limited by the chemoresistance.[47] Therefore, we investigated whether cell growth of Panc-1R, a subclone of Panc-1 cells made resistant to gemcitabine, was influenced by our compounds **1,2,6** and **8**. Surprisingly, all compounds maintained their ability to reduce cell growth with IC_{50s} of 2.7, 2.2, 2.8 and 3.9 μM, respectively. In addition, the same compounds showed cytotoxic activity also on primary culture, PDAC-3, with IC_{50S} ranging from 1.7 (compound **1** and **2**) to 3.9 (compound **8**) and 5.1 μM (compounds **6**). In order to provide more realistic cytotoxic results, we created 3D models of PDAC-3, which compared to 2D monolayer assays, mimic the tumor tissues environment including the physical and mechanical properties of the extracellular matrix, the oxygen gradient, extracellular pH and gradient of nutrients, as well as drug transport.[48] In particular, we treated spheroids with compounds **1** and **2** for eight days during which we observed their shrinkage. Finally, we calculated the area of treated spheroids which were approximately the half compared to the control for both compounds.

The high metastatic profile of PDAC led us to investigate the ability of compounds **1** and **2** to inhibit the migratory behaviour of SUIT-2, Capan-1, Panc-1, Panc-1R and PDAC-3 cell lines, by scratch wound-healing assay, which provides a useful method for screening compounds with high-throughput efficiency. The best results were found on SUIT-2 and Panc-1R cells treated with the compounds **1** and **2,** in which, after 24 h of treatment, the areas of the wound, compared the controls set to 100%, were of 33.3% and 32%, respectively, in Panc-1R, while in SUIT-2 they were 34.9% and 41%, respectively. The anti-migratory activity was less evident in Capan-1 and Panc-1 cells treated with the same compounds, for which we observed the migration rates approximately between 50 and 60%. Finally, in PDAC-3 treated with compounds **1** and **2**, the migration rates were 64% and 71%, respectively.

The results shown above might be explained by the modulation of key regulators of epithelial-to-mesenchymal transition (EMT) events, including the zinc-finger transcription factors, SNAIL1 and SNAIL2 both potent epithelial repressors, E-cadherin and N-cadherin (also called CDH1 and CDH12, respectively) calcium-dependent cell adhesion molecules, vimentin (VIM), type III intermediate filament (IF) protein typically expressed in mesenchymal cells, and finally, the matrix metalloproteinases (MMPs), especially the metalloproteinase-2/-9. In particular, we evaluated their expression both at mRNA and proteins levels, by RT-qPCR, Western blot and gelatine zymography analyses, in SUIT-2, Capan-1 and Panc-1 cells treated with compounds **1** and **2** for 24 h. In SUIT-2 and Capan-1 cell lines the mRNA levels of SNAIL1 and SNAIL2, normalized with GAPDH expression, were increased from 1.5 to approximately 1.9 fold, suggesting a low amount of protein expression due to a feedback mechanism of control. Indeed, Western blot analysis confirmed the low protein expression of SNAIL-1 and -2 that are not sufficient to inhibit CDH1 mRNA transcription.[49–51] Indeed we evaluated the downregulation of CDH1 mRNA and high protein levels. Instead, protein expression of VIM and MMP2 were significantly reduced. Finally, CDH12 protein expression did not noticeably change compared to the control. Compounds **1** and **2** induced a significant decrease, approximately by 50%, of the proteolytic activity of MMP2 and MMP9 isolated from SUIT-2 and Capan-1 cells and detected by using specific gelatine zymography assays, whereas the areas of lysis created by the proteolytic activities of both enzymes isolated from Panc-1 cells were not significantly wider compared to the control.

Several studies reported in the literature have demonstrated that the indole and imidazothiadiazole derivatives can be a versatile structures to discover drug-like kinase inhibitor able to act through the inhibition of different protein kinases.[52–54] Therefore, we investigated the potential mechanism of action of our compounds as inhibitor of tyrosine kinases by tyrosine kinase peptide substrate array. The results of these analyses highlighted the ability of compounds **2** to inhibit the phosphorylation of 45 peptide substrates in SUIT-2 cells and we visualized on Cytoscape a network of interactions between proteins containing the phosphorylated peptides. Notably, PTK2/FAK emerged as an important hub between those proteins. The treatment with compounds **2** inhibited the phosphorylation of PTK2/FAK more than 2-fold compared to the control, with FDR < 0.01. Therefore, we assessed the inhibition of phosphorylation of PTK2/FAK at tyrosine residue 397 (FAK [pY397]) as one of the possible mechanisms of action of our compound, using a quantitative ELISA assay. This assay validated a reduction of p-FAK in SUIT-2, Capan-1 and Panc-1 cells treated with compounds **1** and **2** with fold-change values ranging from 0.4 to 0.5. These results suggested FAK as target of our

compounds and may explain how they can suppress FAK-driven migration and growth in PDAC cells.

The interesting antitumor activity shown by compounds of type *2-(1H-indol-3-yl)-6-(thiophen-3-yl)imidazo[2,1-b][1,3,4]thiadiazole*, prompted us to investigate their antitumor activity also on DMPM, as reported in **chapter 11**. In detail, we tested the *in vitro* antiproliferative activity of derivatives **1-10** on two primary DMPM cells, MesoII and STO by SRB assay. As in PDAC cells, the results showed that compounds **1,2,6** and **8** have a higher cytotoxic activity, inducing the inhibition of cell growth with low IC_{50} values in the range from 5.9-0.59 µM, in both cell lines. The most relevant results were found in STO cells in which we found IC_{50S} of 0.81 and 0.59 µM after treatment with compounds **1** and **2**, respectively. Conversely, MesoII cells were more resistant and the IC_{50s} were slightly higher, approximately 2.8 and 2.6 µM, respectively. The IC_{50} values of the others eight compounds were above 10 µM, therefore we continued to investigate the cytotoxic activity of the first two compounds using the 3D models of MesoII and STO cells. In both cell lines, after seventeen days of treatment, we observed a statistically significant reduction of the size of spheroids with approximate 2 fold-change, compared to those not treated.

Although mesothelioma cells rarely spread to distant organs, some cases of metastasis have been detected, mainly in the pancreas, kidneys, lung, heart and brain.[55,56] Therefore, compounds **1** and **2** were selected to investigate their antimigratory activity in MesoII and STO cells by scratch wound-healing assays. The results highlighted the low tendency to the migration of STO cells, in fact, after 20 hours of the treatment, we observed that in the control cells the area of wound remained large while, in the experimental wells there was a reduction of migration rates by 25.81% and 20%, respectively for compounds **1** and **2** compared to control (set at 100%). Instead, after 20 hours of treatment, MesoII cells showed a complete closure of the wound both in the treated and untreated cells, with only a slightly ability of our compounds to reduce migration.

We concluded that our imidazo[2,1-*b*][1,3,4]thiadiazole derivatives showed relevant *in vitro* antitumor activity but they had no antimigratory activity. Further investigation are warranted to deeper the mechanism of action underlying their antitumor activity.

Because of the increased understanding of the genomic landscape of tumor biology, personalized therapy can improve the treatment of malignant tumors, in particular those with limited therapeutic approaches, such as malignant pleural mesothelioma (MPM).

MPM is an aggressive tumor arising from the pleura, with a poor prognosis. Often, systemic therapy is the only route to treat this devastating disease and pemetrexed in

combination with cisplatin or carboplatin, is the only first-line treatment option, which improved the response rate, time to progression, overall survival and quality of life compared to cisplatin alone.[57] The uptake of pemetrexed into cells can be mediated by three influx membrane transporters, specific for both folates and antifolates. These include: i) the reduced folate carrier (RFC), a carrier-mediated anion exchanger; ii) the folate receptors FR-α and FR-β, that mediate transport by endocytotic processes; iii) the proton-coupled folate transporters (PCFT), the main transporter of pemetrexed which is optimal at low pH. Expression levels of PCFT are correlated with the activity of pemetrexed. Moreover, when the promoter of *PCFT* is methylated , protein expression is decreased leading to resistance to pemetrexed. Conversely, the use of the demethylation agent such as 5-Aza-2´-deoxycytidine, increased the expression of mRNA and protein levels, leading to an sensitivity to pemetrexed. Therefore, PCFT might be used as a biomarker to predict the efficacy of therapy with pemetrexed and, in addition, it might targeted to overcome chemoresistance. In **Chapter 9** we suggest preclinical and clinical studies as useful tools to allow the oncologists to stratify patients based on the PCFT levels and personalize the treatment to achieve positive outcomes:

- **i)** preclinical studies *in vivo* model to clarify the role of PCFT in pemetrexed activity and understanding the role of hypoxia on PFCT expression and pemetrexed resistance;
- **i)** translational studies to establish best cut-off of PCFT expression level for a validated pharmacogenetic test and validate previous retrospective analyses;
- **ii)** finally, performing a Phase I trial in which demethylation agent 5-Aza-2´-deoxycytidine is used in patients with different tumor type.

In **chapter 10** we describe a correlation between hypoxia and the low expression of PCFT transporter. High levels of hypoxic marker CAIX were associated with low expression of PCFT. We observed that MPM cells grown under hypoxic conditions and as spheroids showed resistance to pemetrexed. In addition, by PCR array performed on these previous *in vitro* models and in PCFT-silenced cells, we found that LDH-A was the only significantly up-regulated gene in all three models. Therefore, LDH-A emerged as an attractive druggable target for therapeutic interventions. Specific inhibitors designed against LDH-A, such as NHI-2 and its glycoconjugated analogue NHI-Glc-2, showed cytotoxic activity against MPM and DMPM cells, grown both as monolayers and as spheroids. Moreover, in mouse models obtained by orthotopic or subcutaneous inoculation of primary DMPM cells, NHI-Glc-2 caused a significant reduction of tumor growth, that was more evident after combination with gemcitabine compared to animals treated with either gemcitabine or NHI-Glc-2. Moreover, we demonstrated a prognostic role of LDH-A protein expression in small cohorts of MPM and

DMPM patients in which high expression levels of LDH-A were found in more than 50% of specimens. Our *in vitro* and *in vivo* findings and clinical data suggest that the aggressiveness of mesothelioma is correlated with the high expression of LDH-A, which can be targeted by specific LDH-A inhibitors, therefore representing a promising new avenue for prognostic and therapeutic purposes.

Conclusions

There is a growing need to understand the molecular mechanisms underlying the dysregulation of signalling pathways in cancer cells, as well as new drugs to overcome the resistance to the conventional therapies. This Thesis was focused on the search for new treatments for pancreatic cancer and mesothelioma and is the result of a joint PhD (Palermo/Amsterdam) which integrates pharmaceutical/medicinal chemistry/oncological research. In particular, we reported the synthesis of a library of seventy imidazo[2,1-*b*][1,3,4]thiadiazole derivatives bearing the indole scaffold, which were designed as hybrid potential MTDLs. These compounds were tested for their *in vitro* antiproliferative activity on a panel of PDAC cell lines (SUIT-2, Capan-1, Panc-1, Panc-1R, and a primary cell line PDAC-3) and four of them, compounds **1,2,6** and **8**, showed interesting antitumor activity with IC_{50S} ranging from micromolar to sub-micromolar level, associated with significant reduction of cell-migration and spheroids shrinkage. These results can be explained by the modulation of key regulators of epithelial-to-mesenchymal transition (EMT) and the inhibition of the phosphorylation of tyrosine PTK2/FAK as potential mechanism of action. It should be noted that the most promising compounds are characterized by the thiophene ring instead of the phenyl ring, which led us to hypothesize a key role for thiophene for interaction with the target. Therefore, the same subclass of compounds were also chosen to evaluate their antitumor activity on DMPM culture cells, MesoII and STO. As in PDAC, both primary cell lines showed greater sensitivity to the same four compounds, with IC_{50s} in the range from 0.59 to 5.9 μM and the ability to induce the shrinkage of spheroids more than half compared to the control after seventeen days. Unfortunately, they did not show interesting antimigratory activity, and this can be explained by the low capacity of mesothelioma cells to spread from primary tumor to distant sites. Considered that these compounds reduced the phosphorylation of FAK in PDAC cells, further studies will be carried out to evaluate their ability to inhibit it also in DMPM cells. This is supported by the literature data which have reported the constitutive activation of FAK in several mesothelioma cells as responsible of cancer growth.

Thirty-six imidazo[2,1-*b*][1,3,4]thiadiazole derivatives were further tested for the antibiofilm activity against Gram-positive and Gram-negative bacteria and many compounds showed biofilm inhibitory concentration (BIC_{50}) values lower than 24.5 μM. In addition, the investigation of the mechanism of action showed that the compounds influenced the early stages of biofilm formation without affecting the mature biofilm.

The last part of the Thesis focused on the mesothelium diseases. Specifically, we studied the most frequent malignant mesotheliomas, namely the pleural and the peritoneal. We showed a

correlation of hypoxia with the low expression of PCFT transporter in MPM and the chemoresistance to the traditional drug, pemetrexed, and furthermore, we demonstrated highest levels of LDH-A in hypoxic and PCFT-silenced cells. Therefore, we unraveled the potential prognostic value of LDH-A, also demonstrating the preclinical activity of LDH-A inhibitors in *in vitro* and in *in vivo* models of MPM and DMPM. In mouse models obtained by orthotopic or subcutaneous inoculation of primary DMPM cells, the combination of LDH-A inhibitor with gemcitabine reduced tumor volume. In addition, by IHC on TMAs in small cohorts of MPM and DMPM patients we found high expression levels of LDH-A in more than 50% of specimens that were inversely related with the OS.

References

(1) Siegel, R. L.; Miller, K. D.; Jemal, A. Cancer Statistics, 2019. *CA: A Cancer Journal for Clinicians* **2019**, *69* (1), 7–34. https://doi.org/10.3322/caac.21551.

(2) Ferlay, J.; Colombet, M.; Soerjomataram, I.; Dyba, T.; Randi, G.; Bettio, M.; Gavin, A.; Visser, O.; Bray, F. Cancer Incidence and Mortality Patterns in Europe: Estimates for 40 Countries and 25 Major Cancers in 2018. *Eur. J. Cancer* **2018**, *103*, 356–387. https://doi.org/10.1016/j.ejca.2018.07.005.

(3) Yildizhan, H.; Barkan, N. P.; Karahisar Turan, S.; Demiralp, Ö.; Özel Demiralp, F. D.; Uslu, B.; Ōzkan, S. A. Chapter 1 - Treatment Strategies in Cancer from Past to Present. In *Drug Targeting and Stimuli Sensitive Drug Delivery Systems*; Grumezescu, A. M., Ed.; William Andrew Publishing, 2018; pp 1–37. https://doi.org/10.1016/B978-0-12-813689-8.00001-X.

(4) Targeted Cancer Therapies Fact Sheet https://www.cancer.gov/about-cancer/treatment/types/targeted-therapies/targeted-therapies-fact-sheet (accessed Sep 29, 2019).

(5) Effects of Mycoplasma Contamination on Research https://www.news-medical.net/life-sciences/Effects-of-Mycoplasma-Contamination-on-Research.aspx (accessed Nov 5, 2019).

(6) Molla Kazemiha, V.; Amanzadeh, A.; Memarnejadian, A.; Azari, S.; Shokrgozar, M. A.; Mahdian, R.; Bonakdar, S. Sensitivity of Biochemical Test in Comparison with Other Methods for the Detection of Mycoplasma Contamination in Human and Animal Cell Lines Stored in the National Cell Bank of Iran. *Cytotechnology* **2014**, *66* (5), 861–873. https://doi.org/10.1007/s10616-013-9640-9.

(7) DeVita, V. T.; Chu, E. A History of Cancer Chemotherapy. *Cancer Res* **2008**, *68* (21), 8643–8653. https://doi.org/10.1158/0008-5472.CAN-07-6611.

(8) Loewe, S.; Muischnek, H. Effect of combinations: Mathematical basis of problem. Arch. Exp. Pathol. Pharmacol 1926, 114, 313–326. - Open Access Library http://www.oalib.com/references/8794422 (accessed Nov 5, 2019).

(9) Bliss, C. I. The Toxicity of Poisons Applied Jointly1. *Annals of Applied Biology* **1939**, *26* (3), 585–615. https://doi.org/10.1111/j.1744-7348.1939.tb06990.x.

(10) Elion, G. B.; Singer, S.; Hitchings, G. H. Antagonists of Nucleic Acid Derivatives. VIII. Synergism in Combinations of Biochemically Related Antimetabolites. *J. Biol. Chem.* **1954**, *208* (2), 477–488.

(11) Steel, G. G.; Peckham, M. J. Exploitable Mechanisms in Combined Radiotherapy-Chemotherapy: The Concept of Additivity. *Int. J. Radiat. Oncol. Biol. Phys.* **1979**, *5* (1), 85–91. https://doi.org/10.1016/0360-3016(79)90044-0.

(12) Chou, T. C.; Talalay, P. Quantitative Analysis of Dose-Effect Relationships: The Combined Effects of Multiple Drugs or Enzyme Inhibitors. *Adv. Enzyme Regul.* **1984**, *22*, 27–55.

(13) Berenbaum, M. C. What Is Synergy? *Pharmacol. Rev.* **1989**, *41* (2), 93–141.

(14) Giovannetti, E.; Lemos, C.; Tekle, C.; Smid, K.; Nannizzi, S.; Rodriguez, J. A.; Ricciardi, S.; Danesi, R.; Giaccone, G.; Peters, G. J. Molecular Mechanisms Underlying the Synergistic Interaction of Erlotinib, an Epidermal Growth Factor Receptor Tyrosine Kinase Inhibitor, with the Multitargeted Antifolate Pemetrexed in Non-Small-Cell Lung Cancer Cells. *Mol. Pharmacol.* **2008**, *73* (4), 1290–1300. https://doi.org/10.1124/mol.107.042382.

(15) Avan, A.; Caretti, V.; Funel, N.; Galvani, E.; Maftouh, M.; Honeywell, R. J.; Lagerweij, T.; Van Tellingen, O.; Campani, D.; Fuchs, D.; et al. Crizotinib Inhibits Metabolic Inactivation of Gemcitabine in C-Met-Driven Pancreatic Carcinoma. *Cancer Res.* **2013**, *73* (22), 6745–6756. https://doi.org/10.1158/0008-5472.CAN-13-0837.

(16) Van Der Steen, N.; Leonetti, A.; Keller, K.; Dekker, H.; Funel, N.; Lardon, F.; Ruijtenbeek, R.; Tiseo, M.; Rolfo, C.; Pauwels, P.; et al. Decrease in Phospho-PRAS40 Plays a Role in the Synergy between Erlotinib and Crizotinib in an EGFR and CMET Wild-Type Squamous Non-Small Cell Lung Cancer Cell Line. *Biochem. Pharmacol.* **2019**, *166*, 128–138. https://doi.org/10.1016/j.bcp.2019.05.014.

(17) Farrell, J. J.; Elsaleh, H.; Garcia, M.; Lai, R.; Ammar, A.; Regine, W. F.; Abrams, R.; Benson, A. B.; Macdonald, J.; Cass, C. E.; et al. Human Equilibrative Nucleoside Transporter 1 Levels Predict Response to Gemcitabine in Patients with Pancreatic Cancer. *Gastroenterology* **2009**, *136* (1), 187–195. https://doi.org/10.1053/j.gastro.2008.09.067.

(18) Greenhalf, W.; Ghaneh, P.; Neoptolemos, J. P.; Palmer, D. H.; Cox, T. F.; Lamb, R. F.; Garner, E.; Campbell, F.; Mackey, J. R.; Costello, E.; et al. Pancreatic Cancer HENT1 Expression and Survival from Gemcitabine in Patients from the ESPAC-3 Trial. *J. Natl. Cancer Inst.* **2014**, *106* (1), djt347. https://doi.org/10.1093/jnci/djt347.

(19) Sinn, M.; Riess, H.; Sinn, B. V.; Stieler, J. M.; Pelzer, U.; Striefler, J. K.; Oettle, H.; Bahra, M.; Denkert, C.; Bläker, H.; et al. Human Equilibrative Nucleoside Transporter 1 Expression Analysed by the Clone SP 120 Rabbit Antibody Is Not Predictive in Patients

with Pancreatic Cancer Treated with Adjuvant Gemcitabine - Results from the CONKO-001 Trial. *Eur. J. Cancer* **2015**, *51* (12), 1546–1554. https://doi.org/10.1016/j.ejca.2015.05.005.

(20) Erkan, M.; Reiser-Erkan, C.; Michalski, C. W.; Kong, B.; Esposito, I.; Friess, H.; Kleeff, J. The Impact of the Activated Stroma on Pancreatic Ductal Adenocarcinoma Biology and Therapy Resistance. *Curr. Mol. Med.* **2012**, *12* (3), 288–303. https://doi.org/10.2174/156652412799218921.

(21) Elnaggar, M.; Giovannetti, E.; Peters, G. J. Molecular Targets of Gemcitabine Action: Rationale for Development of Novel Drugs and Drug Combinations. *Curr. Pharm. Des.* **2012**, *18* (19), 2811–2829. https://doi.org/10.2174/138161212800626175.

(22) Conroy, T.; Desseigne, F.; Ychou, M.; Bouché, O.; Guimbaud, R.; Bécouarn, Y.; Adenis, A.; Raoul, J.-L.; Gourgou-Bourgade, S.; de la Fouchardière, C.; et al. FOLFIRINOX versus Gemcitabine for Metastatic Pancreatic Cancer. *N. Engl. J. Med.* **2011**, *364* (19), 1817–1825. https://doi.org/10.1056/NEJMoa1011923.

(23) Sehdev, A.; Gbolahan, O.; Hancock, B. A.; Stanley, M.; Shahda, S.; Wan, J.; Wu, H. H.; Radovich, M.; O'Neil, B. H. Germline and Somatic DNA Damage Repair Gene Mutations and Overall Survival in Metastatic Pancreatic Adenocarcinoma Patients Treated with FOLFIRINOX. *Clin. Cancer Res.* **2018**, *24* (24), 6204–6211. https://doi.org/10.1158/1078-0432.CCR-18-1472.

(24) Meijer, L. L.; Garajová, I.; Caparello, C.; Le Large, T. Y. S.; Frampton, A. E.; Vasile, E.; Funel, N.; Kazemier, G.; Giovannetti, E. Plasma MiR-181a-5p Downregulation Predicts Response and Improved Survival After FOLFIRINOX in Pancreatic Ductal Adenocarcinoma. *Ann. Surg.* **2018**. https://doi.org/10.1097/SLA.0000000000003084.

(25) Tezuka, S.; Ueno, M.; Kobayashi, S.; Morimoto, M.; Ohkawa, S.; Hirotani, A.; Tozuka, Y.; Moriya, S.; Nakamura, Y.; Miyagi, Y.; et al. Predictive Value of ERCC1, ERCC2, ERCC4, and Glutathione S-Transferase Pi Expression for the Efficacy and Safety of FOLFIRINOX in Patients with Unresectable Pancreatic Cancer. *Am J Cancer Res* **2018**, *8* (10), 2096–2105.

(26) Kurata, N.; Fujita, H.; Ohuchida, K.; Mizumoto, K.; Mahawithitwong, P.; Sakai, H.; Onimaru, M.; Manabe, T.; Ohtsuka, T.; Tanaka, M. Predicting the Chemosensitivity of Pancreatic Cancer Cells by Quantifying the Expression Levels of Genes Associated with the Metabolism of Gemcitabine and 5-Fluorouracil. *Int. J. Oncol.* **2011**, *39* (2), 473–482. https://doi.org/10.3892/ijo.2011.1058.

(27) Nakayama, S.; Takeda, S.; Kawase, Y.; Inoue, S.; Kaneko, T.; Nakao, A. Clinical Significance of Dihydropyrimidine Dehydrogenase in Adjuvant 5-Fluorouracil Liver Perfusion Chemotherapy for Pancreatic Cancer. *Ann Surg* **2004**, *240* (5), 840–844. https://doi.org/10.1097/01.sla.0000143300.49878.51.

(28) Zandomeni, R.; Mittleman, B.; Bunick, D.; Ackerman, S.; Weinmann, R. Mechanism of Action of Dichloro-Beta-D-Ribofuranosylbenzimidazole: Effect on in Vitro Transcription. *PNAS* **1982**, *79* (10), 3167–3170. https://doi.org/10.1073/pnas.79.10.3167.

(29) Takeda, S.; Shimazoe, T.; Sato, K.; Sugimoto, Y.; Tsuruo, T.; Kono, A. Differential Expression of DNA Topoisomerase I Gene between CPT-11 Acquired- and Native-Resistant Human Pancreatic Tumor Cell Lines: Detected by RNA/PCR-Based Quantitation Assay. *Biochem. Biophys. Res. Commun.* **1992**, *184* (2), 618–625. https://doi.org/10.1016/0006-291x(92)90634-w.

(30) Grunnet, M.; Calatayud, D.; Schultz, N. A. A.; Hasselby, J. P.; Mau-Sørensen, M.; Brünner, N.; Stenvang, J. TOP1 Gene Copy Numbers Are Increased in Cancers of the Bile Duct and Pancreas. *Scand. J. Gastroenterol.* **2015**, *50* (4), 485–494. https://doi.org/10.3109/00365521.2014.980318.

(31) Capello, M.; Lee, M.; Wang, H.; Babel, I.; Katz, M. H.; Fleming, J. B.; Maitra, A.; Wang, H.; Tian, W.; Taguchi, A.; et al. Carboxylesterase 2 as a Determinant of Response to Irinotecan and Neoadjuvant FOLFIRINOX Therapy in Pancreatic Ductal Adenocarcinoma. *J. Natl. Cancer Inst.* **2015**, *107* (8). https://doi.org/10.1093/jnci/djv132.

(32) Desai, N.; Pnsldent, V. Nab Technology : A Drug Delivery Platform Utilising Endothelial Gp 60 Receptor-Based Transport and Tumour-Derived SPARC for Targeting I; 2009.

(33) Neesse, A.; Frese, K. K.; Chan, D. S.; Bapiro, T. E.; Howat, W. J.; Richards, F. M.; Ellenrieder, V.; Jodrell, D. I.; Tuveson, D. A. SPARC Independent Drug Delivery and Antitumour Effects of Nab-Paclitaxel in Genetically Engineered Mice. *Gut* **2014**, *63* (6), 974–983. https://doi.org/10.1136/gutjnl-2013-305559.

(34) Kim, H.; Samuel, S.; Lopez-Casas, P.; Grizzle, W.; Hidalgo, M.; Kovar, J.; Oelschlager, D.; Zinn, K.; Warram, J.; Buchsbaum, D. SPARC-Independent Delivery of Nab-Paclitaxel without Depleting Tumor Stroma in Patient-Derived Pancreatic Cancer Xenografts. *Mol. Cancer Ther.* **2016**, *15* (4), 680–688. https://doi.org/10.1158/1535-7163.MCT-15-0764.

(35) Hidalgo, M.; Plaza, C.; Musteanu, M.; Illei, P.; Brachmann, C. B.; Heise, C.; Pierce, D.; Lopez-Casas, P. P.; Menendez, C.; Tabernero, J.; et al. SPARC Expression Did Not Predict Efficacy of Nab-Paclitaxel plus Gemcitabine or Gemcitabine Alone for Metastatic Pancreatic Cancer in an Exploratory Analysis of the Phase III MPACT Trial. *Clin. Cancer Res.* **2015**, *21* (21), 4811–4818. https://doi.org/10.1158/1078-0432.CCR-14-3222.

(36) Neesse, A.; Frese, K. K.; Bapiro, T. E.; Nakagawa, T.; Sternlicht, M. D.; Seeley, T. W.; Pilarsky, C.; Jodrell, D. I.; Spong, S. M.; Tuveson, D. A. CTGF Antagonism with MAb FG-3019 Enhances Chemotherapy Response without Increasing Drug Delivery in Murine Ductal Pancreas Cancer. *Proc Natl Acad Sci U S A* **2013**, *110* (30), 12325–12330. https://doi.org/10.1073/pnas.1300415110.

(37) Hwang, J.-E.; Hong, J.-Y.; Kim, K.; Kim, S.-H.; Choi, W.-Y.; Kim, M.-J.; Jung, S.-H.; Shim, H.-J.; Bae, W.-K.; Hwang, E.-C.; et al. Class III β-Tubulin Is a Predictive Marker for Taxane-Based Chemotherapy in Recurrent and Metastatic Gastric Cancer. *BMC Cancer* **2013**, *13*, 431. https://doi.org/10.1186/1471-2407-13-431.

(38) Kato, A.; Naiki-Ito, A.; Naitoh, I.; Hayashi, K.; Nakazawa, T.; Shimizu, S.; Nishi, Y.; Okumura, F.; Inoue, T.; Takada, H.; et al. The Absence of Class III β-Tubulin Is Predictive of a Favorable Response to Nab-Paclitaxel and Gemcitabine in Patients with Unresectable Pancreatic Ductal Adenocarcinoma. *Hum. Pathol.* **2018**, *74*, 92–98. https://doi.org/10.1016/j.humpath.2018.01.009.

(39) Aldonza, M. B. D.; Hong, J.-Y.; Alinsug, M. V.; Song, J.; Lee, S. K. Multiplicity of Acquired Cross-Resistance in Paclitaxel-Resistant Cancer Cells Is Associated with Feedback Control of TUBB3 via FOXO3a-Mediated ABCB1 Regulation. *Oncotarget* **2016**, *7* (23), 34395–34419. https://doi.org/10.18632/oncotarget.9118.

(40) Caparello, C.; Meijer, L. L.; Garajova, I.; Falcone, A.; Le Large, T. Y.; Funel, N.; Kazemier, G.; Peters, G. J.; Vasile, E.; Giovannetti, E. FOLFIRINOX and Translational Studies: Towards Personalized Therapy in Pancreatic Cancer. *World J. Gastroenterol.* **2016**, *22* (31), 6987–7005. https://doi.org/10.3748/wjg.v22.i31.6987.

(41) Neesse, A.; Bauer, C. A.; Öhlund, D.; Lauth, M.; Buchholz, M.; Michl, P.; Tuveson, D. A.; Gress, T. M. Stromal Biology and Therapy in Pancreatic Cancer: Ready for Clinical Translation? *Gut* **2019**, *68* (1), 159–171. https://doi.org/10.1136/gutjnl-2018-316451.

(42) Grasso, C.; Jansen, G.; Giovannetti, E. Drug Resistance in Pancreatic Cancer: Impact of Altered Energy Metabolism. *Crit. Rev. Oncol. Hematol.* **2017**, *114*, 139–152. https://doi.org/10.1016/j.critrevonc.2017.03.026.

(43) Martins, P.; Jesus, J.; Santos, S.; Raposo, L. R.; Roma-Rodrigues, C.; Baptista, P. V.; Fernandes, A. R. Heterocyclic Anticancer Compounds: Recent Advances and the Paradigm Shift towards the Use of Nanomedicine's Tool Box. *Molecules* **2015**, *20* (9), 16852–16891. https://doi.org/10.3390/molecules200916852.

(44) Ashburn, T. T.; Thor, K. B. Drug Repositioning: Identifying and Developing New Uses for Existing Drugs. *Nature Reviews Drug Discovery* **2004**, *3* (8), 673–683. https://doi.org/10.1038/nrd1468.

(45) Schillaci, D.; Spanò, V.; Parrino, B.; Carbone, A.; Montalbano, A.; Barraja, P.; Diana, P.; Cirrincione, G.; Cascioferro, S. Pharmaceutical Approaches to Target Antibiotic Resistance Mechanisms. *J. Med. Chem.* **2017**, *60* (20), 8268–8297. https://doi.org/10.1021/acs.jmedchem.7b00215.

(46) Cascioferro, S.; Parrino, B.; Petri, G. L.; Cusimano, M. G.; Schillaci, D.; Di Sarno, V.; Musella, S.; Giovannetti, E.; Cirrincione, G.; Diana, P. 2,6-Disubstituted Imidazo[2,1-b][1,3,4]Thiadiazole Derivatives as Potent Staphylococcal Biofilm Inhibitors. *European Journal of Medicinal Chemistry* **2019**, *167*, 200–210. https://doi.org/10.1016/j.ejmech.2019.02.007.

(47) Amrutkar, M.; Gladhaug, I. P. Pancreatic Cancer Chemoresistance to Gemcitabine. *Cancers* **2017**, *9* (11), 157. https://doi.org/10.3390/cancers9110157.

(48) 2D Versus 3D Cell Cultures | Mimetas https://mimetas.com/article/2d-versus-3d-cell-cultures (accessed Oct 5, 2019).

(49) Batlle, E.; Sancho, E.; Francí, C.; Domínguez, D.; Monfar, M.; Baulida, J.; García de Herreros, A. The Transcription Factor Snail Is a Repressor of *E-Cadherin* Gene Expression in Epithelial Tumour Cells. *Nature Cell Biology* **2000**, *2* (2), 84–89. https://doi.org/10.1038/35000034.

(50) Cano, A.; Pérez-Moreno, M. A.; Rodrigo, I.; Locascio, A.; Blanco, M. J.; del Barrio, M. G.; Portillo, F.; Nieto, M. A. The Transcription Factor Snail Controls Epithelial–Mesenchymal Transitions by Repressing E-Cadherin Expression. *Nature Cell Biology* **2000**, *2* (2), 76–83. https://doi.org/10.1038/35000025.

(51) Hajra, K. M.; Chen, D. Y.-S.; Fearon, E. R. The SLUG Zinc-Finger Protein Represses E-Cadherin in Breast Cancer. *Cancer Res* **2002**, *62* (6), 1613–1618.

(52) Rathi, A. K.; Syed, R.; Singh, V.; Shin, H.-S.; Patel, R. V. Kinase Inhibitor Indole Derivatives as Anticancer Agents: A Patent Review. *Recent Pat Anticancer Drug Discov* **2017**, *12* (1), 55–72. https://doi.org/10.2174/1574892811666161003112119.

(53) Patel, H.; Sing, B.; Bhardwaj, V.; Palkar, M.; Shaikh, H.; Rane, R.; Alwan, W.; Gadad, A.; Noolvi, M.; Karpoormath, R. Design, Synthesis and Evaluation of Small Molecule Imidazo[2,1-b][1,3,4]Thiadiazoles as Inhibitors of Transforming Growth Factor-β Type-I Receptor Kinase (ALK5). *European journal of medicinal chemistry* **2014**, *93*. https://doi.org/10.1016/j.ejmech.2014.09.002.

(54) Bramson, H. N.; Corona, J.; Davis, S. T.; Dickerson, S. H.; Edelstein, M.; Frye, S. V.; Gampe, R. T.; Harris, P. A.; Hassell, A.; Holmes, W. D.; et al. Oxindole-Based Inhibitors of Cyclin-Dependent Kinase 2 (CDK2): Design, Synthesis, Enzymatic Activities, and X-Ray Crystallographic Analysis. *J. Med. Chem.* **2001**, *44* (25), 4339–4358. https://doi.org/10.1021/jm010117d.

(55) Tertemiz, K. C.; Ozgen Alpaydin, A.; Gurel, D.; Savas, R.; Gulcu, A.; Akkoclu, A. Multiple Distant Metastases in a Case of Malignant Pleural Mesothelioma. *Respir Med Case Rep* **2014**, *13*, 16–18. https://doi.org/10.1016/j.rmcr.2014.07.003.

(56) Finn, R. S.; Brims, F. J. H.; Gandhi, A.; Olsen, N.; Musk, A. W.; Maskell, N. A.; Lee, Y. C. G. Postmortem Findings of Malignant Pleural Mesothelioma: A Two-Center Study of 318 Patients. *Chest* **2012**, *142* (5), 1267–1273. https://doi.org/10.1378/chest.11-3204.

(57) Ceresoli, G. L.; Zucali, P. A.; Favaretto, A. G.; Grossi, F.; Bidoli, P.; Del Conte, G.; Ceribelli, A.; Bearz, A.; Morenghi, E.; Cavina, R.; et al. Phase II Study of Pemetrexed plus Carboplatin in Malignant Pleural Mesothelioma. *J. Clin. Oncol.* **2006**, *24* (9), 1443–1448. https://doi.org/10.1200/JCO.2005.04.3190.

Chapter 13

English Summary

The union of medical and pharmaceutical disciplines has led to great results in the understanding of tumor biology and, thereby, in the fight against this disease. Unfortunately, as shown by high mortality rates, clinical outcomes are still unsatisfactory. The researchers have to continue their studies on several fronts, starting with the identification of biomarkers as useful tools for early diagnosis, disease prevention, drug monitoring and personalized therapy, as well as new targets and drugs for the treatment of these devastating diseases. The study reported in the current Thesis is mainly based on the search for new therapeutics in the treatment of pancreatic and mesothelioma cancers. PDAC is a lethal malignant neoplasm that cause thousands deaths every year and despite the advancement for its detection and managements, the overall survival of 5-years continues to be still of 8%,[1] and germline and somatic mutations, as well as the strongly desmoplastic reaction are the main responsible of chemoresistance.[2] To that goal, a critical review was made to highlight the polymorphisms underlying the different PDAC responses to traditional treatments. On the other hands, malignant mesothelioma is a fatal disease and most patients living only one year after diagnosis, mainly due to a long latency period.[3,4]

Therefore, a new class of potential MTDLs was efficiently synthesized and tested for their antitumor activity on a panel of pancreatic cancer and diffuse malignant peritoneal mesothelioma. In addition, we provided new insights on hypoxia and PCFT expression which was inversely related with that LDH-A. Thereby, we demonstrated the effectiveness of LDH-A inhibitors for the malignant mesothelioma treatment.

Overall the Thesis is articulated in three main parts:

Part I: ***In vitro pharmacological studies as important tools in large-scale drug discovery, and approaches to the combination therapy with special focus on PDAC cancer (chapters 2-4)***

In **chapter 2** we provided an overview about the available cytotoxic *in vitro* tests for the high-throughput screening in drug-discovery, and we suggested the main criteria to consider when designing and performing *in vitro* cell-based assays in order to obtain reliable and reproducible results.

Because resistance to chemotherapy has become the main cause of clinical failure in treatments based on the mono-therapeutic approach, in **chapter 3** we summarized the main mathematical equations to evaluate the synergistic, additive or antagonistic effects of drug combinations; furthermore, we briefly discussed how computational approach helps to evaluate combined drug therapy.

Combination therapy is widely used for the treatment of PDAC that compared to monotherapy, has shown improvement in the overall survival. Unfortunately, most patients

with PDAC do not benefit from chemotherapy. Although the advances in pharmacogenetics knowledge have reduced the individual variability of drug response, there are still many pitfalls. In the **chapter 4** we described the main findings on PDAC pharmacogenetics, critically reappraising the studies on polymorphisms and -omics profiles correlated to the response to gemcitabine, FOLFIRINOX and nab-paclitaxel combinations, as well as limitations of targeted therapy.

Part II: ***Preclinical evaluation of the new class of imidazo[2,1-b][1,3,4]thiadiazole compounds as antitumor and their repurposing as antibiofilm agents (chapters 5-8)***

In **chapters 5** and **6**, we described the cytotoxic activity of derivatives of type *2-(6-phenylimidazo[2,1-b][1,3,4]thiadiazol-2-yl)-1H-indoles* against three PDAC cell lines, SUIT-2, Capan-1 and Panc-1. Many of these compounds inhibited cell growth with IC_{50} values lower than 10 µM in one or more cell lines. In addition, the most promising compounds have been object of study to evaluate their anti-migratory activity. In particularly, compound *5-methoxy-3-[6-(4-nitrophenyl)imidazo[2,1-b][1,3,4]thiadiazol-2-yl]-1H-indole,* that showed IC_{50} approximately 5 µM in all cell lines, reduced cell migration by 41 and 73%, respectively in SUIT-2 and Capan-1 cells.

In **chapter 7** we investigated the antitumoral activity of derivatives of type *2-(1H-indol-3-yl)-6-(thiophen-3-yl)imidazo[2,1-b][1,3,4]thiadiazole* and of *2-(1H-indol-3-yl)-6-phenylimidazo[2,1-b][1,3,4]thiadiazole-5-carbaldehyde* on a panel of PDAC cells, including SUIT-2, Capan-1, Panc-1, Panc-1R (immortalized cancer cells) and PDAC-3 (primary cell line). Four out of eighteen compounds tested, belonging to the class of *2-(1H-indol-3-yl)-6-(thiophen-3-yl)imidazo[2,1-b][1,3,4]thiadiazole,* showed cytotoxic activity with IC_{50S} in the range of 0.85 and 4.85 µM, as well as their ability to induce spheroids shrinkage. Mostly in PDAC immortalized cell lines, these same compounds reduced cell migration approximately three and four times compared to the control. These results were explained with the modulation of key determinants of EMT events and the inhibition of the phosphorylation of focal adhesion kinase FAK/PTK2 on tyrosine residue Y-397.

In **chapter 8** we investigated the antibiofilm properties of compounds reported in **chapter 5** and **6** against Gram-positive bacterial (reference strains *Staphylococcus aureus* ATCC 25923, *S. aureus* ATCC 6538 and *Staphylococcus epidermidis* ATCC 12228) and Gram negative (strains *Pseudomonas aeruginosa* ATCC 15442 and *Escherichia coli* ATCC 25922). Two compounds *3-[6-(2,5-dimethoxyphenyl)imidazo[2,1-b][1,3,4]thiadiazol-2-yl]-1H-indole* and *3-[6-(3-methoxyphenyl)imidazo[2,1-b][1,3,4]thiadiazol-2-yl]-1-methyl-1H-indole* showed remarkable anti-biofilm activity against *S. aureus* ATCC 25923 with BIC_{50} values of 0.5 and

0.8 μg/mL, respectively, whereas compound *5-chloro-3-[6-(2,5-dimethoxyphenyl)imidazo[2,1-b][1,3,4]thiadiazol-2-yl]-1H-indole* was the most potent against *S. aureus* ATCC 6538, with a BIC_{50} of 0.3 μg/mL. Remarkably, these compounds showed effects in the early stages of the biofilm formation without affecting the mature biofilm of the same strains and the viability of the planktonic form.

Part III: ***In vitro and in vivo studies on malignant mesothelioma (chapters 9-11)***

In **chapter 9** we reported the role of PCFT in the response to the treatment with pemetrexed, thus underlying its role as biomarker to predict the effectiveness of the treatment, as well as to consider it as new target to overcome drug resistance. The differential expression levels of PCFT is the main cause of treatment failure, therefore, to improve clinical outcome of patients with malignant mesothelioma, we suggested a series of preclinical and clinical strategies in order to realize personalized therapies and useful to the oncologists to select the patients before anticancer treatment.

In **chapter 10** we identified the correlation between hypoxia and the downregulated expression of PCFT with higher LDH-A levels. The *in vitro* cytotoxic effects, as well as the significant reduction of tumor growth in *in vivo* models after treatment with a specific inhibitor of LDH-A combined with pemetrexed or gemcitabine on MPM and DMPM tumors, respectively, highlighted the potential prognostic and therapeutic role of LDH-A. These findings prompt to the rational development of new LDH-A inhibitors as therapeutic strategies against mesothelioma.

In **chapter 11** we investigated the *in vitro* antitumor activity of ten *2-(1H-indol-3-yl)-6-(thiophen-3-yl)imidazo[2,1-b][1,3,4]thiadiazole* derivatives against two DMPM primary cell lines, MesoII and STO, grown as monolayers and as spheroids, as well as their ability to affect the migratory behaviour of cells. The results showed that four compounds reduced cell growth with IC_{50s} in the range of 0.59 and 5.9 μM in both cell lines, and in 3D models we observed the shrinkage of spheroids approximately three times compared to the control. Instead the same compounds did not affect cell migration. Based on the *in vitro* and *in vivo* studies reported in the literature on the role of FAK and its inhibitors for the treatment of mesothelioma, further studies will be carried out to investigate the mechanism of action as potential inhibitors of FAK.

Chapter 14

CV and list of publications

Personal information

Born: 20.04.1991, **Nationality:** Italian

email: giovanna-lipetri@libero.it

Current position: PhD candidate in Molecular and Biomolecular Science

Education

November 2016 - October 2019: PhD Student (joint PhD) in pharmaceutical/medicinal chemistry and oncological research. Title of the dissertation: *Synthesis and biological evaluation of new imidazo[2,1-b][1,3,4]thiadiazole derivatives as anticancer and antibiofilm agents, and preclinical investigation of anti-LDH-A compounds against malignant mesothelioma*

-Department of Biological, Chemical and Pharmaceutical Sciences and Technologies (STEBICEF), University of Palermo, Palermo, Italy. Promotors: Prof. Patrizia Diana, Prof. Girolamo Cirrincione;

-Department of Medical Oncology, VU University Medical Center, Amsterdam, The Netherlands. Promotors: Prof. Dr. Godefridus J Peters, Prof. Dr Elisa Giovannetti.

December 2016: Qualification examination for the profession of Pharmacist, Second Session of 2016, Palermo (Italy).

November 2010 - July 2016: Master's degree in Pharmacy, Department of Biological, Chemical and Pharmaceutical Sciences and Technologies (STEBICEF), University of Palermo, Palermo, Italy.

Vote: 110/110 *cum laude*. Thesis Title: *Synthesis of a 3,5-dimethyl-6-phenyl-8-(trifluoromethyl)-5,6-dihydropyrazole[3,4-f][1,2,3,5]tetrazepin-4(3H)-one with potential biological activity.* Promotor: Dr. Maria Valeria Raimondi.

Experiences

November 2017 - June2018: Tutor for students enrolled in bachelor's and master's degree at the University of Palermo.

November 2016 - November 2019: tutor for bachelor's and master's students as part of their experimental thesis in Medicinal Chemistry/Biochemistry

June 2015 - November 2015: Practical and professional curricular internship. Main activities and responsibilities: technical-administrative conduct of the pharmacy; economic-fiscal management; dispensation and storage of drugs, drug management, galenical preparations, information and health education of the population through the distribution aimed at the correct use of medicines and prevention, products other than drugs or similar and in any case with health value

Awards

Poster Prize: PAMM-PHARMACOLOGY & MOLECULAR MECHANISMS GROUP. 40th EORTC-PAMM WINTER MEETING, Verona, Italy, 6th-9th February 2019.

List of publications

- ***Proton-coupled folate transporter as a biomarker of outcome to treatment for pleural mesothelioma***

  Giovanna Li Petri , Stella Cascioferro, Barbara Parrino, Godefridus J Peters, Patrizia Diana and Elisa Giovannetti

  Pharmacogenomics Vol. 19, No. 10

- ***2,6-Disubstituted imidazo[2,1-b][1,3,4]thiadiazole derivatives as potent staphylococcal biofilm inhibitors***

  Stella Cascioferro, Barbara Parrino, **Giovanna Li Petri**, Maria G Cusimano, Domenico Schillaci, Valentina Di Sarno, Simona Musella, Elisa Giovannetti, Girolamo Cirrincione, Patrizia Diana

  European Journal of Medicinal Chemistry, Volume 167, 1 April 2019, Pages 200-210

- ***Pharmacogenetics of treatments for pancreatic cancer***

  Btissame El Hassouni, **Giovanna Li Petri**, Daniel SK Liu , Stella Cascioferro, Barbara Parrino, Waqar Hassan, Patrizia, Asif Ali, Adam E Frampton, Elisa Giovannetti

  Expert Opinion on Drug Metabolism & Toxicology. 2019 May 17

- ***A Brief Guide to Performing Pharmacological Studies In Vitro: Reflections from the EORTC-PAMM Course "Preclinical and Early-phase Clinical Pharmacology"***

  Mjriam Capula, Cristina Corno, Btissame El Hassouni, **Giovanna Li Petri**, Sandra Aranđelović; EORTC PAMM Group

  Anticancer Research 2019 July

- ***To Combine or Not Combine: Drug Interactions and Tools for Their Analysis. Reflections from the EORTC-PAMM Course on Preclinical and Early-phase Clinical Pharmacology***

  Btissame El Hassouni, Giulia Mantini, **Giovanna Li Petri,** Mjriam Capula, Lenka Boyd, Hannah NV Weinstein, Andrea Vallés-Marti, Mathilde CM Kouwenhoven, Elisa Giovannetti, Bart A Westerman, Godefridus J Peters; EORTC PAMM Group

  Anticancer Research. 2019 July

- ***Biological Evaluation of the Antiproliferative and Anti-migratory Activity of a Series of 3-(6-Phenylimidazo[2,1-b][1,3,4]thiadiazol-2-yl)-1H-indole Derivatives Against Pancreatic Cancer Cells***

Giovanna Li Petri, Stella Cascioferro, Btissame El Hassouni, Daniela Carbone, Barbara Parrino, Girolamo Cirrincione, Godefridus J Peters, Patrizia Diana, Elisa Giovannetti

Anticancer Research. 2019 July

- ***3-(6-Phenylimidazo [2,1-b][1,3,4]thiadiazol-2-yl)-1H-Indole Derivatives as New Anticancer Agents in the Treatment of Pancreatic Ductal Adenocarcinoma***

  Stella Cascioferro[a], **Giovanna Li Petri**[a], Barbara Parrino, Btissame El Hassouni[a], Daniela Carbone, Vincenzo Arizza, Ugo Perricone, Alessandro Padova, Niccola Funel, Godefridus J Peters, Girolamo Cirrincione, Elisa Giovannetti[*], Patrizia Diana[*]

  [a]equal contributors

  [*]Corresponding authors

  Molecules. 2020 January

- ***Imidazo[2,1-b][1,3,4]thiadiazoles with antiproliferative activity against primary and gemcitabine-resistant pancreatic cancer cells***

  Stella Cascioferro[a], **Giovanna Li Petri[a]**, Barbara Parrino, Daniela Carbone, Niccola Funel, Cecilia Bergonzini, Giulia Mantini, Henk Dekker, Daan Geerke, Godefridus J Peters, Girolamo Cirrincione, Elisa Giovannetti[*], Patrizia Diana[*]

  [a]equal contributors

  [*]Corresponding authors

  European Journal of Medicinal Chemistry

Provisionally accepted

- ***Impact of hypoxia on chemoresistance of mesothelioma mediated by the proton-coupled folate transporter, and preclinical activity of new anti-LDH-A compounds***
  Giovanna Li Petri[*], Btissame El Hassouni[*], Rocco Sciarrillo[*], Niccola Funel, Giulia Mantini, Eveline A Zeeuw van der Laan, Stella Cascioferro, Amir Avan, Paolo A Zucali, Nadia Zaffaroni, Tonny Lagerweij, Barbara Parrino, Marcello Deraco, Carlotta Granchi, Alicia Bulinska, Ryszard T Smolenski, Larry H Matherly, Gerrit Jansen, Yehuda G Assaraf, Patrizia Diana, Jacqueline Cloos, Godefridus J Peters, Filippo Minutolo, Elisa Giovannetti
  [*]equal contributors

In preparation

- ***Biological Evaluation of a series of imidazo[2,1-b][1,3,4]tiadiazole derivatives against Diffuse Malignant Peritoneal Mesothelioma tumor***
  Giovanna Li Petri, Btissame El Hassouni, Silvia Zoppi, Stella Cascioferro, Nadia Zaffaroni, Godefridus J Peters, Girolamo Cirrincione, Patrizia Diana, Elisa Giovannetti

Conference abstracts and poster presentations

- **Novel lactate dehydrogenase-A (LDH-A) inhibitors overcome chemoresistance of mesothelioma mediated by hypoxia**
  Giovanna Li Petri, Carlotta Granchi, Rocco Sciarrillo, Niccola Funel, Paolo A Zucali, Stella Cascioferro, Nadia Zaffaroni, Godefridus J Peters, Patrizia Diana, Filippo Minutolo, Elisa Giovannetti
  40th EORTC-PAMM Winter Meeting, 06 Feb - 9 Feb 2019, Verona, Italy
- **Preclinical activity of new imidazo[2,1-*b*][1,3,4]thiadiazoles derivatives on pancreatic cancer cells**
  Stella Cascioferro, **Giovanna Li Petri**, Barbara Parrino, Ugo Perricone, Alessandro Padova, Girolamo Cirrincione, Godefridus J Peters, Patrizia Diana, Elisa Giovannetti.
  40th EORTC-PAMM Winter Meeting, 06 Feb - 9 Feb 2019, Verona, Italy
- **New Imidazo[2,1-*b*][1,3,4]thiadiazoles with anticancer activity**
  Giovanna Li Petri, Stella Cascioferro, Barbara Parrino, Godefridus J Peters, Girolamo Cirrincione, Patrizia Diana, Elisa Giovannetti.
  3th annual retreat (CCA), 14-15 February 2019, Amsterdam. The Netherlands
- **Role of hypoxia in pemetrexed-resistance of mesothelioma mediated by proton-coupled folate transporter, and preclinical activity of new anti-LDH compounds**
  Giovanna Li Petri, Carlotta Granchi, Rocco Sciarrillo, Niccola Funel, Paolo A Zucali, Yehuda G Assaraf, Stella Cascioferro, Barbara Parrino, Gerrit Jansen, Larry H. Matherly, Nadia Zaffaroni, Filippo Minutolo, Patrizia Diana, Godefridus J Peters, Elisa Giovannetti.
  Science Exchange Day (SED), 27 September 2019, Amsterdam, The Netherlands
- **New Imidazo[2,1-*b*][1,3,4]thiadiazoles with anticancer activity**

Stella Cascioferro, **Giovanna Li Petri**, Barbara Parrino, Ugo Perricone, Alessandro Padova, Elisa Giovannetti, Godefridus J Peters, Girolamo Cirrincione, Patrizia Diana. Med Chem Sicily, 17-20 July 2018, Palermo, Italy

- **Role of hypoxia in pemetrexed-resistance of mesothelioma mediated by proton-coupled folate transporter, and preclinical activity of new anti-LDH compounds**
  Giovanna Li Petri, Carlotta Granchi, Rocco Sciarrillo, Niccola Funel, Paolo A Zucali, Yehuda G Assaraf, Stella Cascioferro, Barbara Parrino, Gerrit Jansen, Larry H Matherly, Nadia Zaffaroni, Filippo Minutolo, Patrizia Diana, Godefridus J Peters, Elisa Giovannetti.
  39th EORTC-PAMM Winter Meeting, 07 Feb - 10 Feb 2018, Rome, Italy
- **Sintesi e valutazione biologica di nuovi nitroderivati analoghi della pirrolomicina D attivi su Pseudomonas aeruginosa**
  Agnese Ribaudo, Maria G Cusimano, Fabiana Plescia, Benedetta Maggio, Giuseppe Daidone, Demetrio Raffa, Mery La Franca, **Giovanna Li Petri**, Ornella Randazzo, Roberta Listro, Giampaolo Barone, Domenico Schillaci, Maria V Raimondi (2018). In: Atti del Congresso della Società Chimica Italiana - Congresso Congiunto delle Sezioni Sicilia e Calabria 2018. p. 61, Catania, 9-10/2/2018
- **Progettazione e sintesi di nuovi derivati 4-chinazolinonici potenziali inibitori della diidrofolato reduttasi**
  Mery La Franca, Ornella Randazzo, Fabiana Plescia, Benedetta Maggio, Giuseppe Daidone, Demetrio Raffa, **Giovanna Li Petri**, Roberta Listro, Agnese Ribaudo, Giampaolo Barone, Maria V Raimondi (2018).
  In: Atti del Congresso della Società Chimica Italiana - Congresso Congiunto delle Sezioni Sicilia e Calabria 2018. p. 62, Catania, 9-10/2/2018
- **Sintesi di un isostero del 3,5-dimetil-6-fenil-8-(trifluorometil)-5,6-diidropirazolo[3,4-*f*][1,2,3,5]tetrazepin-4(3H)-one (CF3-TZP) con potenziale attività biologica**
  Ornella Randazzo, **Giovanna Li Petri**, Fabiana Plescia, Benedetta Maggio, Giuseppe Daidone, Demetrio Raffa, La Franca, Mery, Roberta Listro, Agnese Ribaudo, Giampaolo Barone, Maria V Raimondi (2018).
  In: Atti del Congresso della Società Chimica Italiana. p. 60, Catania, 9-10/2/2018
- **Pirrolomicine che inibiscono la Sortasi A nelle infezioni sostenute da batteri Gram-positivi**

Roberta Listro, Maria Grazia Cusimano, Fabiana Plescia, Benedetta maggio, Giuseppe Daidone, Demetrio Raffa, Mery La Franca, **Giovanna Li Petri**, Agnese Ribaudo, Ornella Randazzo, Giampaolo Barone, Domenico Schillaci, Maria V Raimondi (2018). In: Atti del Congresso della Società Chimica Italiana - Congresso Congiunto delle Sezioni Sicilia e Calabria 2018. p. 63, Catania, 9-10/2/2018